Department of Chemistry
UNIVERSITY OF DELHI

M.Sc Chemistry

Inorganic Special Paper
Semester IV

Course – 4101 B
Course Title – Spectral Techniques in Inorganic Chemistry

By – Dr. Vartika Tomar

Quadrupolar Nuclei

A quadrupolar nucleus is one that has a quantum spin number greater than ½. Such nuclei have a lower symmetry than spin-½ nuclei. The quadrupole moment that varies between nuclei is a measure of this asymmetry.

Their energies split upon the application of a magnetic field into multiple levels (fig. 1). By comparison, spin-½ nuclei split into only two levels. The number of levels is given by 2n + 1 where is the spin number. The different splitting patterns can be seen in their coupling with other nuclei.

The NMR signals of quadrupolar nuclear are usually wider than those of spin-½ nuclei due to rapid quadrupolar relaxation. The line-width increases with the line-width factor that is related to the quadrupole moment of the nucleus, the size and asymmetry of the molecule. For example, deuterium has a small line-width factor of 0.41 fm^4 with a quadrupole moment of 0.286 fm^2 and yields a line-width in HOD of 1.7 Hz while ^{17}O has a line-width factor of 2.1 fm^4 with a quadrupole moment of -2.56 and yields a line-width in $H_2{}^{17}O$ of 69 Hz. Some nuclei such as ^{197}Au and ^{201}Hg yield signals too broad to be observed with a high-resolution NMR spectrometer.

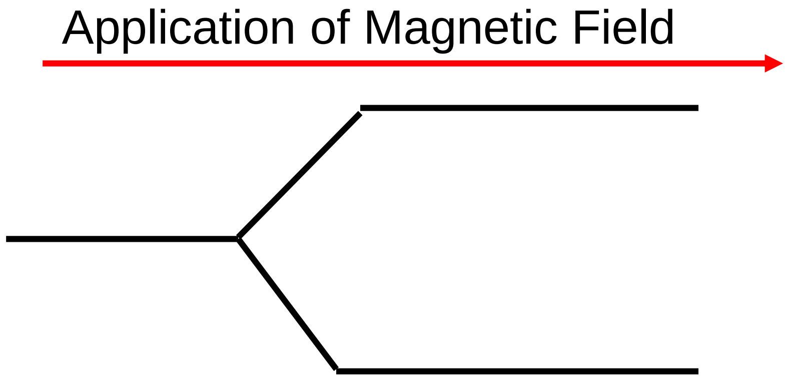

Spin ½: ^{1}H, ^{13}C, ^{15}N, ^{31}P etc.

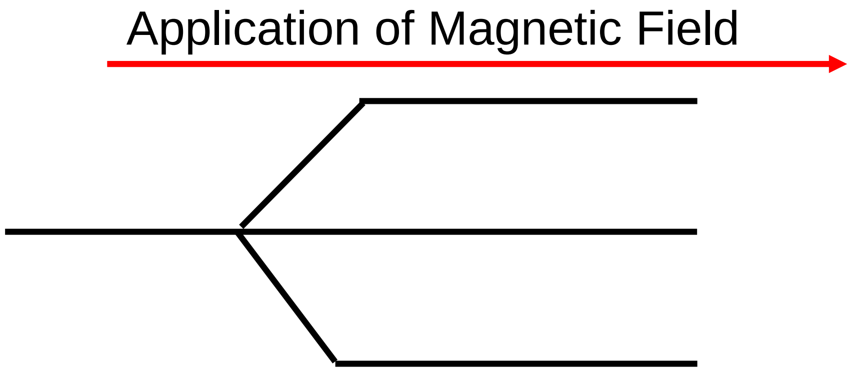

Spin 1: ^{2}H, ^{6}Li, ^{14}N, etc.

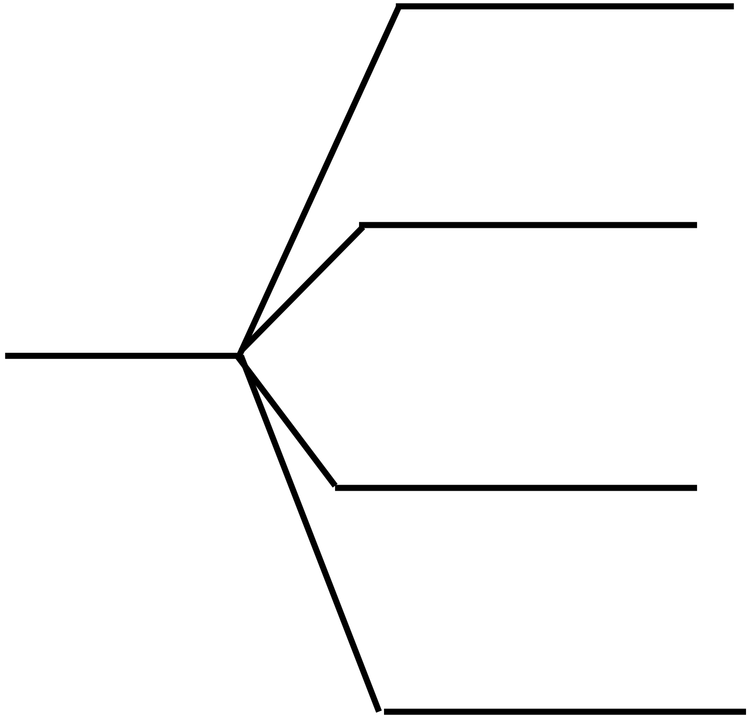

Spin 3/2: ^{7}Li, ^{11}B, ^{23}Na, ^{33}S, ^{35}Cl, ^{37}Cl, ^{39}K etc.

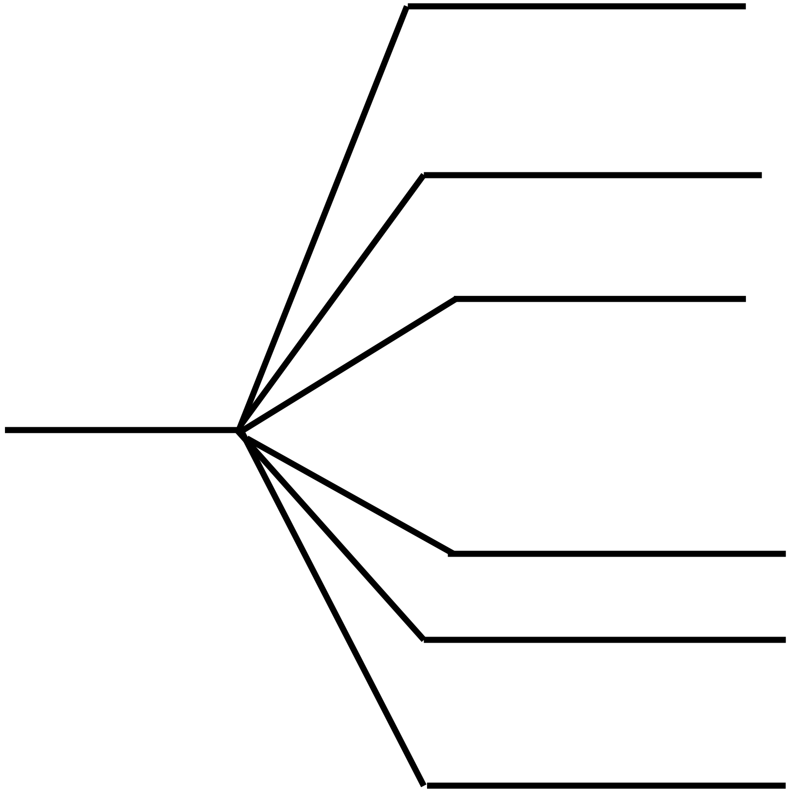

Spin 5/2: ^{17}O, ^{25}Mg, ^{27}Al, ^{55}Mn, etc.

Fig: Energy level diagram for nuclei of different spins

Consequences of Nuclei with Quadrupole Moment on NMR

Nuclei with quadrupole moments undergo spin-lattice relaxation readily and have very small values for T_1.

When the nucleus with a quadrupole moment is attached to another atom whose spectrum is being measured, it is observed that rather extensive broadening occurs. When one attempts to obtain an NMR spectrum on a nucleus with a quadrupole moment that undergoes relaxation readily, the signals are sometimes broadened so extensively that no spectrum is obtained. This is the case for most halogen (except fluorine) compounds.

The effectiveness of the quadrupole relaxation process depends upon the interaction of the quadrupole moment with the electric field gradient at the nucleus. The field gradient is caused by the asymmetry of the electronic environment. Sharp signals have been obtained for the halide ions and symmetric compounds of the halogens (e.g., ClO_4^-), where the spherical charge distribution gives rise to only small field gradients at the nucleus, leading to large values of T_1.

Solution of I^-, (I^{127}, I = 3/2) give rise to an NMR signal. When iodine is added, the triiodide ion, I_3^-, is formed, destroying the cubic symmetry of iodide ion so that quadrupole broadening becomes effective and the signal disappears. Small amount of iodine result in a broadening of the iodide resonance and the rate constant for the reaction $I^- + I_2 \longrightarrow I_3^-$ can be calculated from the broadening.

Fluorine NMR Spectrum of NF_3

The changes in a series of spectra obtained as a function of temperature are opposite to those normally obtained for exchange processes. At -205^0 C a sharp single peak is obtained for NF_3 and as the temperature is raised the line broadens and a spectrum consisting of a sharp triplet (I = 1 for N^{14}) results at 20^0 C. It is proposed that at low temperature the slow molecular motions are most effective for quadrupole relaxation of N^{14}, and as a result, a single line is obtained. At higher temperatures, relaxation is not as effective and the lifetime of a given state for the N^{14} nucleus is sufficient to cause spin-spin splitting. A similar effect is observed for pyrrole.

N^{14} resonance of azoxybenzene

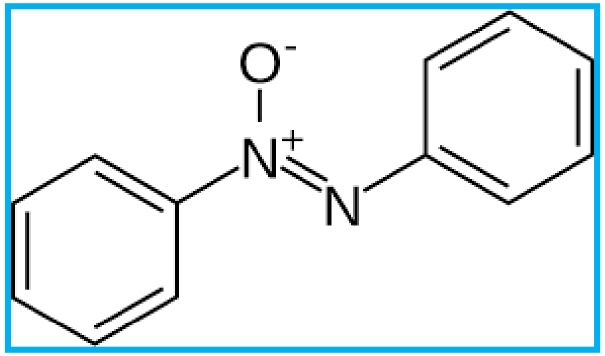

It exhibits only a singlet. The nitrogens are not equivalent and it is proposed that the field gradient at the N-O nitrogen is so large as to make this resonance unobservable.

The Double Resonance Technique

- Used to simplify complex spectra.
- Involves application of second strong rf field whose frequency is adjusted to cause saturation of a second nucleus which is splitting the nucleus being measured.
- This saturation causes the second nucleus to undergo frequent transitions so that the effect from spin-spin splitting caused by this nucleus disappears. The second nucleus is, in effect, decoupled from the rest of the system.
- In details, it simplify proton spectra by saturating a set of proton nuclei which differ in chemical shift from another set and which are splitting that set (i.e., A or B of ABX, AB_2, etc.)
- The chemical shift is evaluated from the frequency of the audio side band on the strong rf field which is most effective for decoupling.
- The doble resonance technique has been successfully employed to determine the relative sign of coupling constants.
- This method is applicable to chemically nonequivalent groups of hydrogen nuclei to simplify the interpretation of high resolution proton magnetic resonance spectra

Proton NMR Spectrum of Diboarne

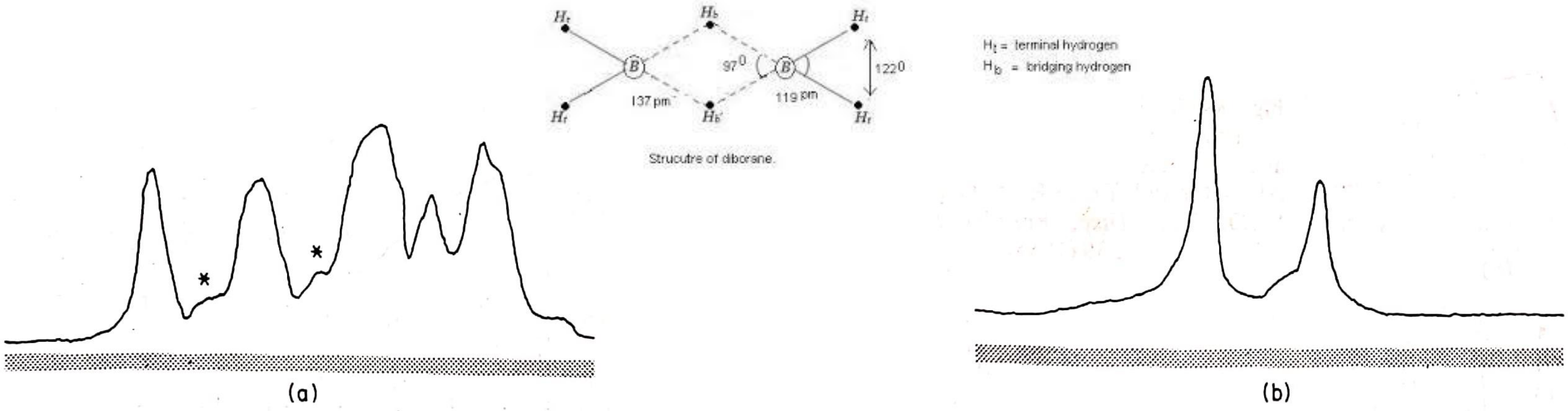

Fig: Proton NMR Spectrum of Diborane (a) Proton NMR with B^{11} and B^{10} splitting. (b) Proton NMR with B^{11} nucleus saturated

In fig (a), the spectrum results from two sets of nonequivalent protons (bridge and terminal protons) being split by the B11 nucleus. The asterisk denotes fine structure arising from the smaller abundance of protons on B10 nuclei (B10 has a natural abundance of 18.83% and I = 3 compared to 81.17% for B11 with I = 3/2).

In fig (b), the splitting caused by B11 has been removed by saturation of the boron nucleus by the double resonance technique.

Two peak intensity ration 2:1 are obtained, corresponding to the four terminal and two bridged protons.

Proton NMR Spectra of Al(BH$_4$)$_3$

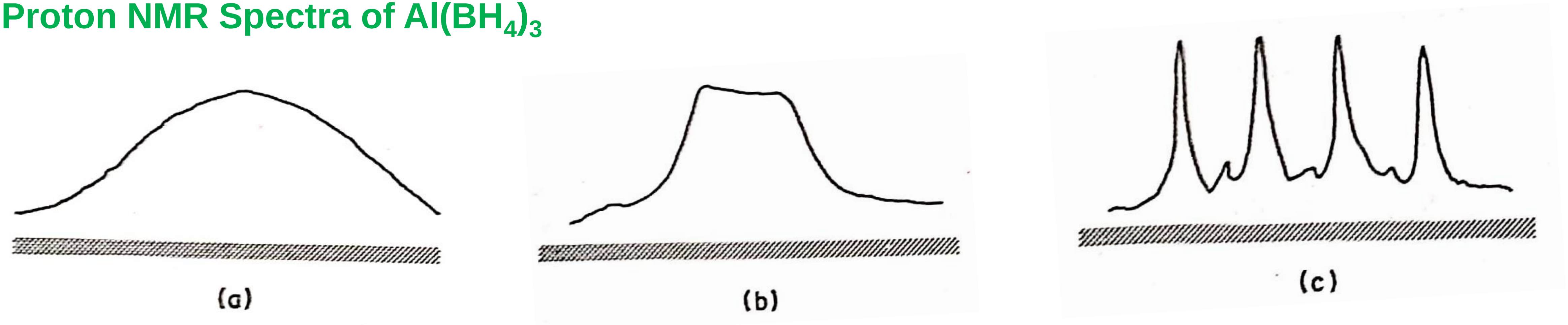

Fig. Proton NMR of Al(BH$_4$)$_2$ (a) Proton resonance (b) Proton resonance, B^{11} saturated (c) Proton resonance, Al^{27} saturated

This molecule contains six Al-H-B bridge bonds. Both B and Al^{27} (I = 5/2) has quadrupole moments. The proton NMR at 30 mc sec^{-1} consists of a single broad line (Figure (a)). When the B^{11} nucleus is saturated, the proton resonance spectrum in figure (b) results. Examination of the proton resonance while saturating B^{11} is symbolically designed as H^1-{B^{11}}. Figure (c) represents the proton NMR spectrum when the sample is irradiated with frequency corresponding to that of Al^{27}(H^1-{Al^{27}}). The four large peaks arise from B^{11} splitting of the proton and the smaller peak from B^{11} splitting. The bridging and terminal hydrogens are not distinguished because of a rapid proton exchange reaction which makes all hydrogens equivalent.

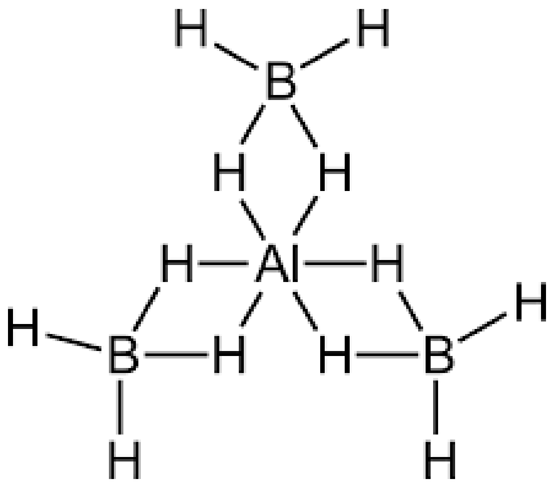

N_2F_2

Two isomers have been obtained in the preparation of N_2F_2. One definitely has a trans structure with fluorine on each nitrogen. In conflicting reports, the structure of the second isomer has been reported to be the cis isomer and also $F_2N{=}N$. An excellent discussion of the results obtained by employing several different physical methods in an attempt to resolve this problem has been reported along with fluorine NMR spectrum and results from a double resonance experiment. Saturation of the N^{14} nucleus in this second isomer with a string rf field causes collapse of all nitrogen splitting. It is concluded that the chemical shift of the two nitrogens must be equivalent and this eliminates the $F_2N{=}N$ structure. Additional evidence is obtained for this structure from a complete spectral interpretation. The value for $J_{N\text{-}F}$ calculated in this study for a cis structure is reasonable when compared to $J_{N\text{-}F}$ for NF_3

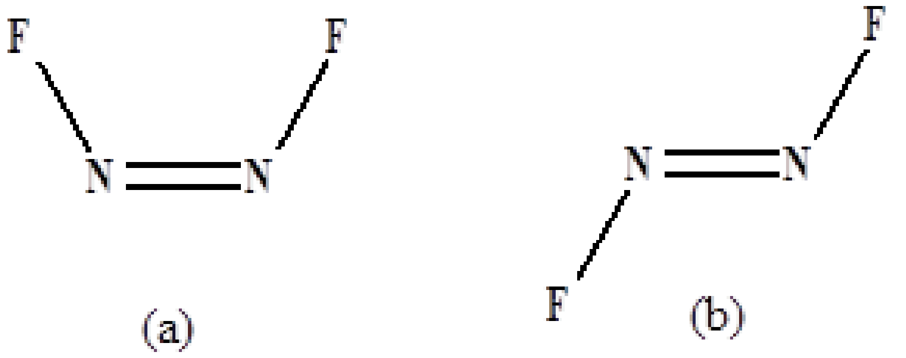

NMR spectrum of $(C_2H_5)_2Tl^+$

Loosely coupled spin systems can often be regarded as giving a number of subspectra, each associated with a different spin orientation of a particular nucleus or group of equivalent nuclei. It may be possible to perform double resonance experiments that perturb only one of these subspectra and thus determine which lines belong to a particular subspectrum. The two naturally occurring isotopes of Thallium, ^{203}Tl and ^{205}Tl, both have spin ½ and such similar magnetogyric ratios that difference between the splittings that they produce in the proton spectrum of this species are not resolved.

Consider the NMR spectrum of $(C_2H_5)_2Tl^+$ in figure (I for Tl = ½). If $J_{Tl\text{-}CH3}$ and $J_{Tl\text{-}CH2}$ are both positive, both low field peaks correspond to interaction with positive nuclear magnetic quantum numbers of Tl. If the signs of J are different, one low field peak corresponds to interaction with the moment from thallium nuclei where m = +½ and the other is -½, By irradiation at the center of gravity of each of the multiplets, it was shown that each CH_3 triplet was coupled to the distant methylene quartet and vice versa. For example, irradiation with a frequency corresponding to the low field triplet resulted in the disappearance of the fine structure of the high field methylene signal. This result indicates that $J_{Tl\text{-}CH3}$ and $J_{Tl\text{-}CH2}$ have opposite signs, for if the sign were the same, the two field multiplets would be coupled together as would the two high field multiplets and saturation of the low field triplet would cause collapse of the fine structure in the low field methylene signal.

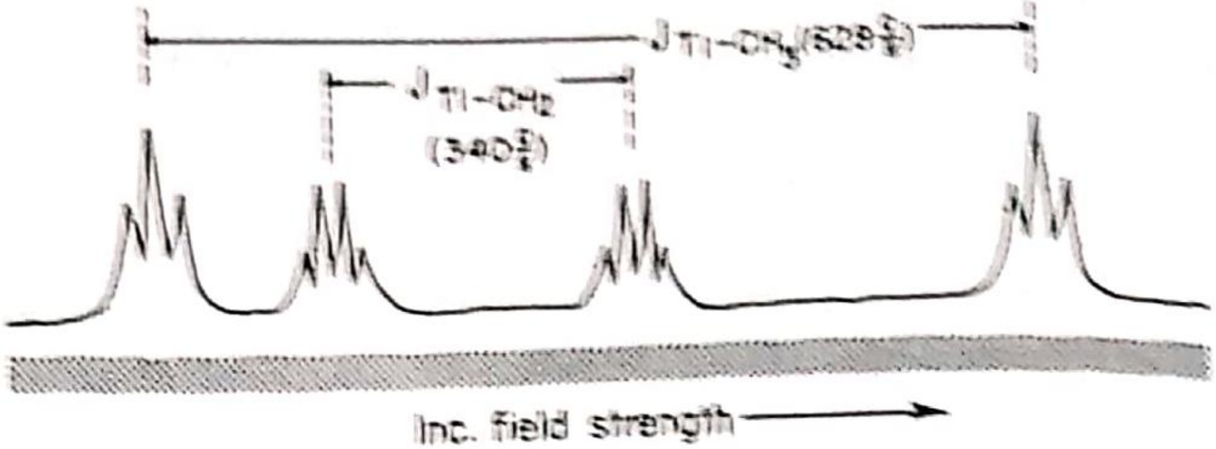

NMR Spectrum of $(C_2H_5)_2Tl^+$

PDFs for Further Studies and Reference

AIP | The Journal of Chemical Physics

Exchange of iodide ion with triiodide ion studied by nuclear magnetic resonance

Edward E. Genser and Robert E. Connick

Citation: The Journal of Chemical Physics **58**, 990 (1973); doi: 10.1063/1.1679356
View online: http://dx.doi.org/10.1063/1.1679356
View Table of Contents: http://scitation.aip.org/content/aip/journal/jcp/58/3?ver=pdfcov
Published by the AIP Publishing

THE JOURNAL OF CHEMICAL PHYSICS VOLUME 58, NUMBER 3 1 FEBRUARY 1973

Exchange of iodide ion with triiodide ion studied by nuclear magnetic resonance

Edward E. Genser* and Robert E. Connick

Inorganic Materials Research Division, Lawrence Berkeley Laboratory and Department of Chemistry, University of California, Berkeley, California 94720

(Received 13 July 1972)

Previous studies of NMR line broadening of the iodide resonance in aqueous solutions of triiodide have been interpreted in terms of the rate of dissociation and formation of triiodide, with the result that the derived rate constant appeared to exceed the diffusion limiting value. The present study has resolved this anomaly and shows the exchange to be described instead by the reactions $I^{*-}+I_3^-=I_3^{*-}+I^-$ at iodide concentrations greater than $0.05M$. Several mechanisms of exchange are considered based on both symmetrical and unsymmetrical forms of triiodide ion, the latter of which is supported by Raman data in the literature. The interpretation makes use of nuclear quadrupole coupling constants reported for solid salts of triiodide. The data are fitted to the exchange modified Bloch equations to obtain a value of the rotational correlation time, τ_r, for each of the mechanisms; τ_r is then compared to a theoretical value of τ_r calculated for triiodide ion. Although the data do not permit a unique mechanism to be established, it appears that at least two of the iodines in triiodide must be involved in exchange. The results are compatible with an attack on an end iodine of triiodide with the formation of the intermediate I_4^{2-}.

Myers[1] has used the measurement of the linewidth of the nuclear magnetic resonance of iodine-127 in iodide solutions containing triiodide ion to yield information on the rate of exchange of iodine nuclei between the two species. The ^{127}I nucleus, when present as I^- in an aqueous solution, undergoes transverse relaxation through quadrupole coupling with the surrounding water molecules at a rate which produces a conveniently measurable resonance linewidth. The same nucleus, when present in I_3^-, relaxes much more rapidly because of the much stronger quadrupole coupling. Therefore, the presence of a small amount of triiodide ion causes measurable broadening of the I^- resonance linewidth through chemical exchange.

Myers interpreted the concentration dependence of the line broadening in terms of the rapid formation and dissociation of triiodide ion:

$$I^- + I_2 \underset{k_b}{\overset{k_f}{\rightleftharpoons}} I_3^-. \tag{1}$$

From the results of his study he deduced a value for k_f of $4.7\times10^{10}\ M^{-1}\cdot\text{sec}^{-1}$ at 35°C. However, estimates[2,3] of the diffusion controlled bimolecular rate constant[4] for this reaction at the same temperature give a value for k_f of only $1.8\times10^{10}\ M^{-1}\cdot\text{sec}^{-1}$. The work reported here was undertaken with the hope of resolving this discrepancy. Our initial measurements at 27°C appeared to be consistent with Myers' rate law and moreover yielded an even larger value of k_f. Further measurements, however, of the concentration and temperature dependences of the line broadening revealed a more complicated exchange mechanism.

EXPERIMENTAL

The techniques and theory of the measurement of rapid rate processes through NMR line broadening have been amply treated elsewhere.[5–7] The experiments were performed on a Varian V4200B spectrometer at 8.00 MHz which corresponds, for ^{127}I, to a field of 9.4 kG. The iodide ion linewidths are peak-to-peak separations of the absorption derivative. For solutions of potassium iodide at $2M$ (moles per liter) and below, the linewidth was constant at 1.15 G. The line shapes were Lorentzian to a good approximation, for which the expression $1/T_2=(\sqrt{3}/2)\gamma\Delta H$ applies, where γ is the nuclear gyromagnetic ratio, ΔH is the linewidth in gauss, and T_2 is the transverse relaxation time. Field sweeps were calibrated using the sidebands impressed on water protons at 40 MHz. The amplitudes of the modulation and radiofrequency fields were set well below the levels which produce observable broadening.

The iodide salt was weighed out directly and the triiodide concentrations were measured spectrophotometrically by using the molar extinction coefficient of I_3^- at the absorption maximum at 3530 Å.[8] The pure iodide solutions were made $10^{-3}M$ in $Na_2S_2O_3$ to prevent oxidation. The linewidths were independent of ionic strength below $2M$ apart from the small effects attributed to ion pairing with the specific alkali metal cation.[9] All solutions containing 0.1, 0.4, 1.0, and $2.0M$ I^- were at a constant ionic strength of $2.00M$, achieved by adding $NaNO_3$ to the KI and I_2. All other solutions had an ionic strength equal to the iodide concentration (KI). The temperature dependences were studied with an apparatus described elsewhere,[7] consisting of a Pyrex cell with a glass coil immersed in the sample, through which a gas was passed for heat exchange.

The spectrophotometric measurement of the I_3^- concentration requires further comment. Chia[10] and French and Effenberger[11] have shown that the apparent molar absorptivity of I_3^- varies with the iodide concentration. Chia's data interpolated to 3530 Å and combined with the data of Awtrey and Connick[8] for low iodide concentrations gives for the molar absorptivity

$$\epsilon^{3530}=2.64\times10^4(1+0.164[\mathrm{I}^-]) \qquad (2)$$

up to $1M$ I^-. We define the apparent triiodide concentration $[\mathrm{I}_3^-]_{\mathrm{app}}$ as

$$[\mathrm{I}_3^-]_{\mathrm{app}}=A^{3530}/2.64\times10^4 b \qquad (3a)$$

and the "stoichiometric triiodide" symbol $[\mathrm{I}_3^-]'$ as

$$[\mathrm{I}_3^-]'=A^{3530}/2.64\times10^4 b(1+0.164[\mathrm{I}^-])$$

$$=[\mathrm{I}_3^-]_{\mathrm{app}}/1+0.164[\mathrm{I}^-], \qquad (3b)$$

where A is the absorbance and b the cell length.

French and Effenberger have analyzed their data in terms of higher polyiodides and give for the equilibrium quotient for the formation of I_4^{2-}, the next most important species for the conditions used here, at ionic strength $2M(\mathrm{KNO}_3)$ and 25°:

$$\mathrm{I}_3^-+\mathrm{I}^-=\mathrm{I}_4^{2-}, \qquad Q=0.184. \qquad (4)$$

If one accepts their interpretation,

$$[\mathrm{I}_3^-]'=[\mathrm{I}_3^-]+[\mathrm{I}_4^{2-}]. \qquad (5)$$

RESULTS AND DISCUSSION

In Fig. 1 a plot of the line broadening δ(in gauss) vs $[\mathrm{I}_3^-]_{\mathrm{app}}$ at $2M$ iodide concentration is shown. The value of the contribution from the pure iodide ion linewidth was subtracted from the measured over-all linewidth to obtain δ. Linear plots of this type were also obtained at several other iodide ion concentrations. The linearity establishes that the observed increase in rate of relaxation of I^- arising from the presence of I_3^- is proportional to $[\mathrm{I}_3^-]_{\mathrm{app}}$ and therefore to $[\mathrm{I}_3^-]'$ and also $[\mathrm{I}_3^-]$ at a given iodide concentration. The slopes of the linear plots, such as Fig. 1, were measured and multiplied by $(\sqrt{3}/2)\gamma$ to give the second-order rate constants for the enhanced I^- relaxation, shown in Table I, according to:

$$(\sqrt{3}/2)\gamma\delta=[\mathrm{I}^{*-}]^{-1}(d[\mathrm{I}^{*-}]/dt)=k_1[\mathrm{I}_3^-]'=k_2[\mathrm{I}_3^-]$$

$$=k_0[\mathrm{I}_3^-]_{\mathrm{app}}. \qquad (6)$$

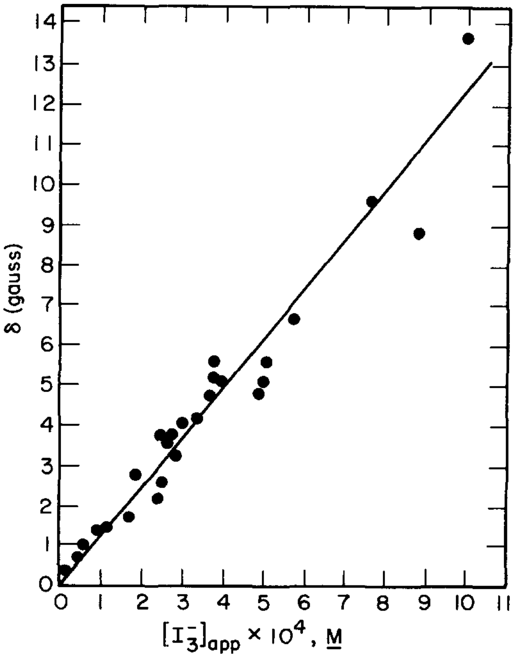

FIG. 1. Variation of line broadening with triiodide concentration for $2.0M$ iodide solutions at 27°C.

TABLE I. Relaxation data for I^- in solutions containing I_3^- at 27°C.

$[\mathrm{I}^-]$, M	μ^{a}, M	$1/k_0$, $M\cdot$sec	$1/k_1$, $M\cdot$sec	$1/k_2$, $M\cdot$sec
0.050	0.05	0.85×10^{-9}	0.84×10^{-9}	0.83×10^{-9}
0.100	2.00	0.92	0.90	0.89
0.400	2.00	2.65	2.49	2.32
1.00	2.00	7.25	6.23	5.26
2.00	2.00	17.4	13.6[b]	10.0
3.00	3.00	25.1		
4.00	4.00	34.0		
5.00	5.00	43.		
6.00	6.00	48.		

[a] Ionic strength.

[b] Equation (2) is a first-order empirical correction to the molar absorptivity for the presence of higher polyiodides, valid up to $1M$ iodide. A more exact treatment based on the assumed presence of I_4^{2-} was used to calculate ϵ^{3530} at $2M$ I^-, resulting in a 4% higher value of $[\mathrm{I}_3^-]'$ than given by Eq. (3b).

The evaluation of k_2 requires the additional assumption of the presence of the I_4^{2-} species and the applicability of French and Effenberger's equilibrium quotient for Eq. (4) to the present system: $k_2=k_1(1+0.184[\mathrm{I}^-])$ at room temperature. At low (I^-), k_2 approaches k_1.

Obviously k_1 and k_2 are not constant. Values of the reciprocal of each plotted against $[\mathrm{I}^-]$ in Fig. 2 indicates that to a first approximation they are inversely proportional to the iodide concentration. Thus the simplest approximate rate law for the enhanced relaxation of I^- is

$$-d[\mathrm{I}^{*-}]/dt=k_3([\mathrm{I}^{*-}][\mathrm{I}_3^-]'/[\mathrm{I}^-])$$

$$=k_4([\mathrm{I}^{*-}][\mathrm{I}_3^-]/[\mathrm{I}^-])$$

$$=k_4Q_{\mathrm{I}_3^-}[\mathrm{I}^{*-}][\mathrm{I}_2], \qquad (7)$$

where $Q_{\mathrm{I}_3^-}$ is the equilibrium quotient for the formation of I_3^-. This is exactly the rate law for the relaxation found by Myers[1] and interpreted by him as the rate of dissociation and formation of triiodide ion.

The key to the problem was revealed by a study of the temperature dependence of the relaxation. In Fig. 3 is shown a plot of $\log([\mathrm{I}^-]\delta/[\mathrm{I}_3^-]_{\mathrm{app}})$ vs $1/T$

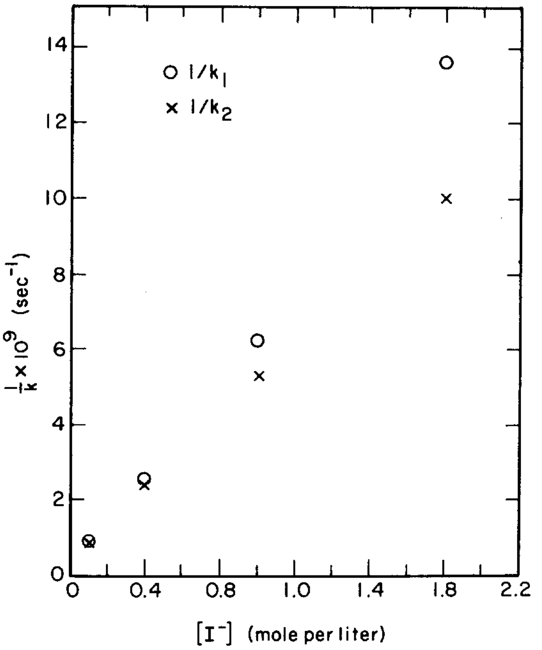

FIG. 2. Plot of $1/k_1$ (O) and $1/k_2$ (×) [see Eq. (6)] vs the iodide concentration.

for several iodide concentrations at and above 0.4*M*. The contribution from the pure iodide ion linewidth—the temperature dependence of which is shown in Fig. 4—has been subtracted from the over-all linewidth to obtain the value of δ.

In Fig. 3, if the rate of relaxation depended on the rate of dissociation of triiodide ion, the plot would be of the usual Arrhenius type with the rate constant increasing with increasing temperature. Exactly the opposite trend is found with $\Delta E \simeq -4.3$ kcal.

In a two environment system with a small difference in chemical shift, the enhancement of relaxation of the first environment by the presence of the second is controlled by the slower of the two steps: (1) chemical exchange and (2) relaxation in the second environment. The temperature dependence data show unequivocally that the former is not controlling under the conditions in Fig. 3.

If relaxation is the controlling step, the rate is proportional to the rate of relaxation in the second environment:

$$-d[I^{*-}]/dt = k'[I_3^{*-}] = k''Q_{I_3^-}[I^{*-}][I_2], \qquad (8)$$

which is just the form found experimentally, to a good approximation. With relaxation control dominating at 0.4*M* I$^-$ and higher, chemical exchange must be faster than the relaxation. The triiodide dissociation and recombination mechanism for the exchange becomes even more impossible with this new interpretation. The system must effect an exchange of iodide atoms between I_3^- and I^- considerably more rapidly than the diffusion controlled bimolecular reaction rate limit for Eq. (1). The only reasonable possibility appears to be the direct bimolecular reaction:

$$I^{*-} + I_3^- \overset{k_5}{\rightleftharpoons} I_3^{*-} + I^-. \qquad (9)$$

At the diffusion limit this reaction theoretically could produce exchange at approximately $Q_{I_3^-}[I^-]$ times the rate of exchange through $I^- + I_2$. This would correspond to a rate which is 714 times greater for a 1*M* iodide solution at 25°C.

By a suitable change in the experimental conditions it should be possible to make chemical exchange the controlling factor. The above mechanism for such a situation gives

$$-d[I^{*-}]/dt = k_5[I^{*-}][I_3^-]. \qquad (10)$$

It will be shown below [Eq. (13)] that chemical exchange control will be favored (low relative rate) by low iodide concentration. Consideration of the temperature dependence shows that low temperature will also favor chemical exchange control since decreasing the temperature will decrease the rate of chemical exchange but increase the quadrupole relaxation of I_3^- because of the longer correlation time from tumbling.

Attempts to gain evidence of chemical exchange control were carried out as follows: measurements were made at 27°C with decreasing concentrations of iodide ion down to 0.05*M* at which point the small

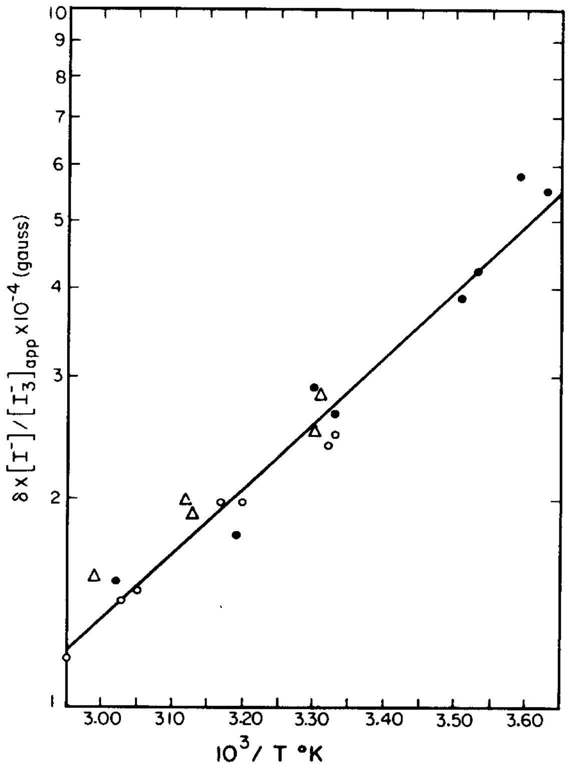

FIG. 3. Temperature dependence of $[I^-]\delta/[I_3^-]_{app}$ for triiodide solutions: 0.4*M* iodide, ○; 1.0*M* iodide, ●; 2.0*M* iodide, △.

signal-to-noise ratio precluded further decrease. As will be explained later, chemical exchange control according to Eq. (10) should manifest itself in Fig. 2 as a finite intercept on the ordinate axis. Such a result was obtained although the accuracy is not high.

Second, the temperature dependence was measured at low iodide ion concentration (0.05*M*), as shown in Fig. 5. The sign of the temperature dependence is now reversed from that found at 0.4*M* and higher iodide concentrations, thus confirming the presence of chemical exchange control. The low value of the activation energy indicates, as would be expected, that exchange control is only slightly more important than relaxation control under the conditions of the experiment.

We now wish to establish an explicit relationship between the resonance linewidth of the iodide ion and the pertinent rate and relaxation parameters. We consider the special solution of the exchange modified Bloch equations for two site exchange with one component in low abundance. The quantity $1/T_{2_p}$ is given in terms of the line broadening, δ, by[7]:

$$T_{2_p}^{-1}=(\tfrac{1}{2}\sqrt{3})\gamma\delta=\tau_c^{-1}\left(\frac{(T_{2_d}^{2})^{-1}+(T_{2_d}\tau_d)^{-1}+\Delta\omega_d^{2}}{(T_{2_d}^{-1}+\tau_d^{-1})^{2}+\Delta\omega_d^{2}}\right), \tag{11}$$

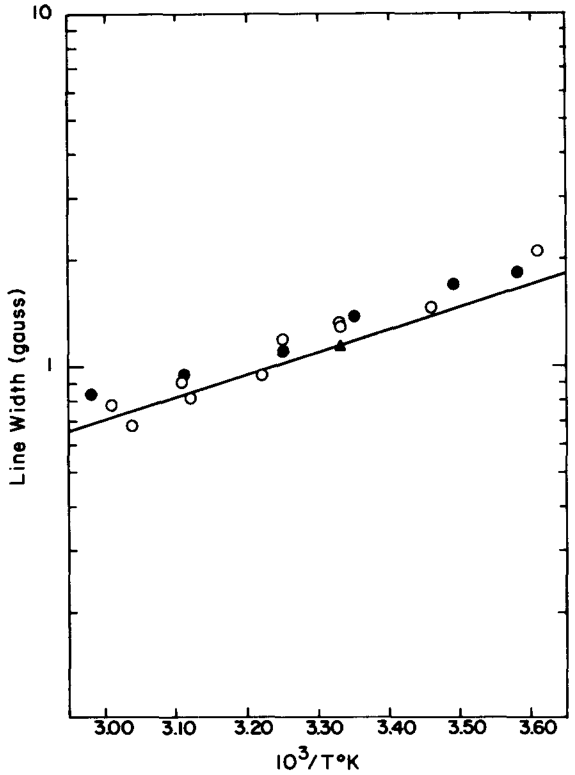

FIG. 4. Temperature dependence of peak-to-peak linewidth of iodide ion in the absence of triiodide: 0.1*M* KI, ○; 2.0*M* ●. The activation energies for the iodide linewidth are the same within experimental error for the 0.1*M* and 2*M* KI solutions. The slope is fixed by the experimental points and the line is drawn through the accurately known value of the linewidth at 27°C, i.e., 1.15±0.03 G.

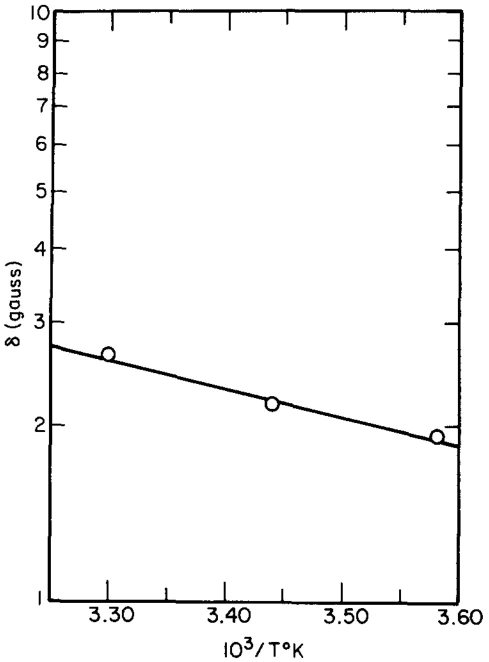

FIG. 5. Temperature dependence of line broadening for a solution 0.05*M* in iodide and $1.07\times10^{-5}M$ in triiodide.

where τ_d, T_{2_d}, and $\Delta\omega_d$ are, respectively, the chemical lifetime, transverse relaxation time, and chemical shift of the iodine in species *d*. We make the identification of the species *c* with iodide, whose resonance we are observing, and *d* with triiodide. The specific processes are:

$$I^{*-}\xrightarrow{1/T_{2_c}}I^{-}, \tag{12a}$$

$$I^{*-}+I_3^{-}\underset{k_6}{\overset{k_5}{\rightleftharpoons}}I_3^{*-}+I^{-}, \tag{12b}$$

$$I_3^{*-}\xrightarrow{1/T_{2_d}}I_3^{-}, \tag{12c}$$

with $1/\tau_c=k_5[I_3^-]$ and $1/\tau_d=k_6[I^-]$.

We can simplify Eq. (11) by noting that the chemical shift $\Delta\omega_d$ is an ordinary diamagnetic shift which is small in comparison to the relaxation and exchange rates, and may therefore be ignored, i.e., the chemical shift is much less than the line broadening. Then Eq. (11) becomes

$$T_{2_p}^{-1}=\tau_c^{-1}[\tau_d/(T_{2_d}+\tau_d)]=k_5[I_3^-]/(k_6[I^-]T_{2_d}+1). \tag{13}$$

Equation (13) displays, very simply, the line broadening as a function of the chemical and magnetic lifetimes of an ^{127}I nucleus in triiodide. For very rapid chemical exchange one has a relaxation controlled width, i.e., for $(\tau_d/T_{2d})\ll1$,

$$T_{2_p}^{-1}=(\tau_d/\tau_c)T_{2_d}^{-1}=T_{2_d}^{-1}(k_5/k_6)([I_3^-]/[I^-]). \tag{14}$$

In the limit of slow exchange the line broadening is

TABLE II. Possible mechanisms for exchange of I^- with I_3^-.

Mechanism	k_5/k_6	ν_q^2
A. Attack on center iodine of I_3^-		
1. Symmetrical I_3^-	2	ν_{ab}^{2} [c]
2. Unsymmetrical I_3^-		
a. No inversion	1	ν_a^2
b. Rapid inversion	2	$[\frac{1}{2}(\nu_a+\nu_b)]^2$ or $\frac{1}{2}(\nu_a^2+\nu_b^2)$
B. Attack on end iodine of I_3^-		
1. Symmetrical I_3^-	Kinetics more complex[a]	$[\frac{1}{3}(2\nu_{ab}+\nu_c)]^2$ or $\frac{1}{3}(2\nu_{ab}^2+\nu_c^2)$ [c]
2. Unsymmetrical I_3^-		
a. No inversion	1	ν_a^2
b. Rapid inversion	Kinetics more complex[b]	$[\frac{1}{3}(\nu_a+\nu_b+\nu_c)]^2$ or $[\frac{1}{2}(\nu_a+\nu_b)]^2+\nu_c^2$

[a] See text and Eq. (19).

[b] See text.

[c] ν_{ab} is the quadrupole coupling constant for the end iodines in symmetrical I_3^-.

controlled by the exchange rate, i.e., for $\tau_d/T_{2_d} \gg 1$,

$$T_{2_p}^{-1} = \tau_c^{-1} = k_5[I_3^-]. \tag{15}$$

The experimental data are qualitatively consistent with this description. To proceed further, it is necessary to examine more carefully both the relaxation and the chemical exchange processes.

The nuclear magnetic relaxation of ^{127}I occurs by quadrupole coupling. For liquids the expression for $T_{2_d}^{-1}$ is of the form[12]:

$$T_{2_d}^{-1} = 4\pi^2\alpha\nu_q^2\tau_{\mathrm{eff}} = \beta\tau_{\mathrm{eff}}, \tag{16}$$

where $\nu_q = e^2qQ/h$ is the conventional quadrupole coupling constant in which q is the electric field gradient at the nucleus whose quadrupole moment is Q. The value of α for a nuclear spin of $\frac{5}{2}$ (i.e., ^{127}I) is 2.4×10^{-2}. The expression is exact for axial symmetry (which we shall assume), and a very good approximation for small departures therefrom. The quantity τ_{eff} is an "effective" correlation time for the quadrupole coupling given by the expression

$$\tau_{\mathrm{eff}}^{-1} = \tau_r^{-1} + k_6[I^-]. \tag{17}$$

Here, τ_r^{-1} and $k_6[I^-]$ are the rates at which the quadrupole coupling is interrupted through rotational motion and chemical exchange, respectively.

The value of τ_r is often estimated from the Debye–Bloembergen model of a randomly rotating sphere embedded in a viscous liquid. Shimizu[13] has derived the quadrupole relaxation formula for the tumbling of a symmetrical ellipsoid. It has the same form as Eqs. (16) and (17), but the rotational part of τ_{eff} is more complex. On estimating major and minor axes of the ellipsoid from interatomic distances of triiodide ion and the van der Waals radius of iodine, one calculates from Shimizu's work a value of τ_r of approximately 4.4×10^{-11} sec at 25°C. The value is uncertain because the hydrodynamic basis of the model is highly questionable at molecular dimensions[14]; a factor of 2 error would not be surprising. Since only rotation about the minor axes is effective in decorrelating the quadrupole coupling of linear I_3^-, the hydrodynamic theory may actually be more appropriate here than for a sphere.[15]

Taking the inverse of Eq. (13) and substituting for T_{2_d} from Eq. (16) yields

$$T_{2_p}[I_3^-] = k_5^{-1} + (k_6[I^-]/k_5\beta)(\tau_r^{-1} + k_6[I^-]). \tag{18}$$

Equation (18) oversimplifies the chemical exchange and relaxation processes. There are three iodine atoms in I_3^-. It is most unlikely that they all exchange at the same rate. Each may have a different quadrupole coupling constant. There is strong evidence that I_3^- in aqueous solution is not symmetrical, although it is probably linear or very nearly so. X-ray structure determinations[16] of solid triiodides have shown I_3^- to be sometimes symmetrical and sometimes asymmetrical with the two different distances from the center to the end iodines, ranging from 2.82 to 2.91 Å for the short distance and 3.10 to 2.95 Å for the long distance. Recent Raman measurements in aqueous solution[17,18] also indicate two active stretching frequencies, which would only be the case if the I_3^- were unsymmetrical and retained a given asymmetrical configuration for the order of 2×10^{-12} sec or longer.

Of great interest here are the quadrupole coupling measurements of Sasane, Nakamura, and Kubo[19] on solid NH_4I_3, RbI_3, and CsI_3. Three distinct coupling constants were observed for each substance, averaging 710, 1490, and 2480 MHz, although the individual values varied appreciably. These are assigned in order to ν_a, ν_b, and ν_c of the atoms indicated in unsymmetrical I_3^-, with the a–c bond longer than the c–b bond:

$$\underset{a}{\mathrm{I}}—\underset{c}{\mathrm{I}}\text{–}\underset{b}{\mathrm{I}}^-.$$

TABLE III. Kinetic parameters calculated for different mechanisms.

Mechanism (See Table II)	Based on $[I_3^-]'$ [b]		Based on $[I_3^-]$ [b]	
	k_5	$1/\tau_r$	k_5	$1/\tau_r$
A, 1 A, 2, b[a]	2.7×10^9	1.2×10^{10}	2.2×10^9	1.0×10^{10}
A, 2, a B, 2, a	1.6×10^9	1.1×10^9	1.4×10^9	0.75×10^9
B, 1 B, 2, b[a]	4.1×10^9	4.3×10^{10}	3.3×10^9	3.6×10^{10}

[a] Inversion rate assumed to be much greater than $1/\tau_r$.

[b] The interpretations based on $[I_3^-]'$ and $[I_3^-]$ correspond to substitution of the k_5 and k_6 data of Table I, respectively, into Eqs. (18) and (19), along with the assumption in the $[I_3^-]'$ interpretation that $[I_3^-]$ in these two equations may be replaced by $[I_3^-]'$.

The sum of the three frequencies for each solid is remarkably constant and nearly equal to twice that of the iodine atom,[20] as could be expected if only *p* orbitals are used in bonding, i.e., the molecular orbital model proposed by Pimentel,[21] and if the theory of Townes and Dailey[22] is applied.

The exchange process can proceed by attack of the incoming I^- on either the central or one of the end iodines of triiodide. In the first process the incoming I^- replaces an end iodine, without change of the relative positions of the other two. In the second case the incoming iodide attaches to one of the end iodines, which in turn becomes the new center iodine, while the other end iodine is lost as I^-. In addition to the two methods of attack there are other complexities. Both the unsymmetrical and symmetrical structures for I_3^- must be considered. The symmetry of the activated complex (or an intermediate) can affect the exchange. If the triiodide is unsymmetrical, the rate of inversion of the asymmetry can affect the results. Further, when two or more sites are involved in relaxation the appropriate combination of quadrupole coupling constants must be chosen.

The results of consideration of a number of the more plausible of these alternatives is presented in Table II. Here the cases are classified first by mode of attack and second by symmetry of the I_3^-, with the possibility of rapid inversion for the unsymmetrical case. The second column lists the appropriate ratio for k_5/k_6 in Eq. (18), except where indicated, and the last column gives appropriate expressions for ν_q in Eq. (16), except where indicated; when alternative expressions are given the first corresponds to rapid exchange between the sites relative to tumbling and the latter case the opposite.

The equation for the transverse relaxation time involving relaxation and exchange can be derived readily using classical kinetic methods of the steady state as long as the chemical shift is small enough not to contribute to the linewidth,[2] which is the case here. In addition, it is necessary that exchange not be rapid compared to the randomizing process, i.e., tumbling in the present case. When this latter condition does not hold, the derivation is more complex.

For attack on the end iodine of symmetrical triiodide the relaxation equation is

$$T_{2_p}[I_3^-]=k_5^{-1}+[I^-]\Bigg/\left(\frac{k_5\beta_{ab}}{k_6(\tau_r^{-1}+2k_6[I^-])}+\frac{1}{(k_5[I^-])^{-1}+(\tau_r^{-1}+k_5[I^-])\beta_c^{-1}}\right), \tag{19}$$

where β_i corresponds to the β of Eq. (16) for the atom indicated by the subscript. This form is only valid when $k_5[I^-]$ is appreciably smaller than $1/\tau_r$, which turns out to be the case up to $1M$ I^-. For the unsymmetrical I_3^- with attack on the end iodine, a similar equation is obtained if the rate of inversion of the asymmetry is rapid compared to the sum of the relaxation rates in the tightly bound and center positions.

Because of the many possible mechanistic paths, indicated only incompletely in Table I, it is not feasible to use the NMR results to determine uniquely the mechanism of relaxation. To simplify the problem the average quadrupole coupling values of Sasane, Nakamura, and Kubo[19] will be used to fix the ν_q parameters in the equation for T_{2_p}. Fortunately, the two possible averages—the average of the squares and the square of the averages (in Table II)—do not differ greatly. As judged by its constancy in Ref. 19, $(\nu_a+\nu_b)/2$ should be a good measure of the quadrupole coupling frequency of the end iodines of symmetrical I_3^-, and is so used in Table II.

Using the above parameters, the data at $0.1M$ and $1M$ I^- were used to calculate k_5 and $1/\tau_r$ for the various paths in Table II with the results shown in Table III. The first set of results labeled, Based on $[I_3^-]'$, corresponds to assuming approximately that the species forming at higher iodide (presumably I_4^{2-}) contributes to the relaxation in the same degree that an I_3^- does, at $1M$ iodide. The second set, labeled, Based on $[I_3^-]$, corresponds to assuming that the species forming at higher iodide contributes nothing to the relaxation.

The test to be applied to the calculations of Table III is the reasonableness of the $1/\tau_r$ values. The value estimated from hydrodynamic theory, as discussed earlier, is $1/\tau_r = 2.3\times10^{10}$ sec^{-1} at 25°, with considerable uncertainty. This value is in severe disagreement (20 fold) with cases A.2.a and B.2.a, and, therefore, it is concluded that the exchange process is not restricted to the weakly bound end iodine of an unsymmetrical I_3^-.

The hydrodynamic estimate of $1/\tau_r$ is about equally close to the derived values for the other two pairs of mechanisms for exchange, with no significant basis for favoring one set over the other.

Although only the data for the $0.1M$ and $1M$ I^- solutions at ionic strength $2.0M$ have been used in the above interpretation, the values in Table I at $0.4M$ and $2.0M$ I^- are reasonably consistent. The precise shape of the curves of Fig. 2 was not believed to be definitive in the fitting because of uncertainties about the amount of I_4^{2-} and its relaxation behavior. The point at $0.05M$ I^-, when placed on Fig. 1, lies above the other data, as would be expected from a sizeable activity coefficient correction to the rate of exchange at the much lower ionic strength.

At the $1M$ iodide point the I_4^{2-} concentration is calculated from Eq. (4) to be 0.184 times the I_3^- concentration; therefore, the correction for the presence of I_4^{2-} is not trivial. The assumption made for the second set of k_5 and $1/\tau_r$ values of Table III, that the I_4^{2-} does not contribute to the relaxation, seems unrealistic from the following argument. Bonding considerations point to a linear structure for I_4^{2-}. A simple molecular orbital picture of a symmetrical, linear structure places a "p" electron deficiency of $\frac{1}{2}$ electron on each iodide, leading to an over-all quadrupole relaxation parameter which is $\frac{3}{4}$ that of triiodide when averaged over the four and the three positions, respectively. With a somewhat slower tumbling rate for I_4^{2-}, the net result is a predicted relaxation rate per I_4^{2-} roughly equal to that for an I_3^- in the relaxation controlled region. Therefore, one might expect the parameters from the interpretation based on $[I_3^-]'$ to be closer to the actual situation.

It seems likely that the I_4^{2-} is an intermediate in the exchange process between I^- and I_3^-. If so, the mechanism consists of attack by the I^- on the end of the I_3^-, i.e., the second group of mechanisms in Table II. If I_3^- is symmetrical or inverts any asymmetry rapidly relative to relaxation, all three positions of I_3^- become available for relaxation in the relaxation controlled limit. Such a situation corresponds to cases B.1 and B.2.b, respectively, of Table II. These would seem to be the most likely mechanisms. In either case the bimolecular rate constant k_5 is near, but within, the diffusion limit.

Very recently Turner, Flynn, Sutin, and Beitz[23] have measured to formation and dissociation of triiodide by means of a laser temperature-jump apparatus. Their data show that the exchange of I^- with I_3^- by the mechanism of Eq. (1) is unimportant relative to that by Eq. (9) in the present study.

---

[1] O. E. Myers, J. Chem. Phys. **28**, 1027 (1958).

[2] E. E. Genser, Thesis, Lawrence Radiation Laboratory Report UCRL-9846, University of California, January 1962.

[3] M. Eigen and K. Kustin, J. Am. Chem. Soc. **84**, 1355 (1962).

[4] A. A. Frost and R. G. Pearson, *Kinetics and Mechanism* (Wiley, New York, 1961), 2nd ed., Chap. 11.

[5] H. S. Gutowsky and A. Saika, J. Chem. Phys. **21**, 1688 (1953).

[6] H. M. McConnell, J. Chem. Phys. **28**, 430 (1958).

[7] T. J. Swift and R. E. Connick, J. Chem. Phys. **37**, 307 (1962); J. Chem. Phys. **41**, 2553 (1964).

[8] A. D. Awtrey and R. E. Connick, J. Am. Chem. Soc. **73**, 1842 (1951).

[9] H. G. Hertz, Z. Electrochem. **65**, 36 (1961).

[10] Y.-T. Chia, Thesis, University of California Radiation Laboratory Report UCRL-8311, 2 June 1958.

[11] D. French and J. A. Effenberger, abstracts of papers, 140th Meeting of the American Chemical Society, Chicago, Illinois, September 1961, abstracts of papers 25T.

[12] A Abragam, *The Principles of Nuclear Magnetism* (Oxford U.P., London, 1961), Chap. VIII.

[13] H. Shimizu, J. Chem. Phys. **40**, 754 (1964). A correction has been noted by T. T. Bopp, J. Chem. Phys. **47**, 3621 (1967).

[14] W. Kauzman, Rev. Mod. Phys. **14**, 12 (1942).

[15] W. A. Steele, J. Chem. Phys. **38**, 2404 (1963), J. Chem. Phys. **38**, 2411 (1963).

[16] T. Migchelsen and A. Vos, Acta Crystallogr. **23**, 796 (1967), and references therein.

[17] A. G. Maki and R. Forneris, Spectrochim. Acta A **23**, 867 (1967).

[18] K. R. Loos, private communication, Shell Development Co., Emeryville, California

[19] A. Sasane, D. Nakamura, and M. Kubo, J. Chem. Phys. **71**, 3249 (1967).

[20] V. Jaccarino, J. G. King, R. H. Satten, and H. H. Stroke, Phys. Rev. **94**, 1798 (1954); T. P. Das and E. L. Hahn, *Nuclear Quadrupole Resonance Spectroscopy, Supplement 1* (Academic, New York, 1958).

[21] G. C. Pimentel, J. Chem. Phys. **19**, 446 (1951).

[22] C. H. Townes and B. P. Dailey, J. Chem. Phys. **23**, 118 (1955).

[23] D. H. Turner, G. W. Flynn, N. Sutin, and J. V. Beitz, J. Am. Chem. Soc. **94**, 1554 (1972).

Quadrupolar Nuclei in Solid-state Nuclear Magnetic Resonance

Dieter Freude

in
Encyclopedia of Analytical Chemistry
R.A. Meyers (Ed.)
pp. 12188–12224

Quadrupolar Nuclei in Solid-state Nuclear Magnetic Resonance

Dieter Freude
Universität Leipzig, Leipzig, Germany

Solid-state nuclear magnetic resonance (NMR) spectroscopy is mostly applied to ^{1}H or ^{13}C nuclei with the nuclear spin $I = \frac{1}{2}$, but about 100 of 130 NMR isotopes have $I > \frac{1}{2}$, and the electric quadrupole interaction strongly broadens the NMR signal in the solid-state powder spectra. The perturbing effect of the electric quadrupole interaction is reduced at the higher magnetic fields which are available at present. In addition, approaches of the solid-state NMR traditionally used in the study of spin-$\frac{1}{2}$ nuclei have been adapted for use with quadrupolar nuclei, and some techniques, e.g. double-rotation (DOR) and multiple-quantum transition in combination with fast spinning [multiple-quantum magic-angle spinning (MQMAS)], were recently developed for quadrupolar nuclei with half-integer spins.

This article describes the basic theory, the line shape for first- and second-order quadrupole broadened spectra with and without magic-angle spinning (MAS) of the powder, the most important experimental techniques for the study of quadrupolar nuclei with half-integer spins such as DOR, dynamic-angle spinning (DAS), MQMAS, echo and nutation techniques, and some recent developments in deuterium NMR. Electric field gradient and chemical shift data for the most commonly studied quadrupolar nuclei with half-integer spins, ^{27}Al, ^{23}Na, and ^{17}O, and a few references to recent solid-state NMR studies of some other quadrupolar nuclei are given.

1 INTRODUCTION

The applicability of the NMR technique continues to expand in physics, chemistry, materials science, geology, biology, and medicine for either spectroscopic studies or imaging purposes. The majority of the recent applications can be found in the field of analytical chemistry. In 1998, *Current Contents (Physical, Chemical and Earth Sciences)* referred to about 8500 NMR studies, including 1800 studies of solids. Solid-state NMR, for which some special techniques must be used in order to obtain highly resolved spectra, is mostly applied to ^{1}H or ^{13}C nuclei with spin $I = \frac{1}{2}$. About 100 of 130 NMR isotopes have $I > \frac{1}{2}$, and the electric quadrupole interaction strongly broadens the NMR signal in the solid-state powder spectra. However, more than 400 references to solid-state NMR studies of quadrupolar nuclei in *Current Contents* in 1998 demonstrate that this problem could be overcome.

The demand for the characterization of inorganic materials and some recently developed experimental techniques have led to growing interest in high-resolution solid-state NMR spectroscopy of quadrupolar nuclei in powder samples. In addition, the perturbing effect of the electric quadrupole interaction is reduced at higher magnetic fields, which are now commercially available up to 21 T also for solid-state NMR spectrometers. In addition, approaches of the solid-state NMR traditionally used in the study of spin-$\frac{1}{2}$ nuclei have been adapted for use with quadrupolar nuclei, e.g. echo methods, sample spinning about the magic angle (MAS), multiple-dimensional spectroscopy, double resonance and adiabatic transfer. Some techniques, e.g. DOR and multiple-quantum transition in combination with fast spinning (MQMAS), were developed for quadrupolar nuclei with half-integer spins.

This article describes the basic theory, the line shape for first- and second-order quadrupole broadened spectra with and without MAS of the powder, the most important experimental techniques for the study of quadrupolar nuclei with half-integer spins such as DOR, DAS, MQMAS, echo and nutation techniques, and finally some recent developments of the deuterium NMR. Since single-crystal studies are not considered in this article,

Encyclopedia of Analytical Chemistry
R.A. Meyers (Ed.)

we refer to recent papers by Vosegaard et al.,(1,2) which describe the up-to-date experimental techniques, and the review by Kanert and Mehring, 'Static Quadrupole Effects in Disordered Cubic Solids'.(3) The classical papers of Volkoff et al., 'Nuclear Electric Quadrupole Interaction in Single Crystals',(4,5) of Das and Saha, 'Electric Quadrupole Interaction and Spin Echoes in Crystals',(6) and the classical review by Cohen and Reif, 'Quadrupole Effects in NMR Studies of Solids',(7) should also be mentioned.

Some other reviews on solid-state NMR of quadrupolar nuclei include mainly powder studies. They are, in chronological order, Spiess, 'Deuteron NMR – A New Tool for Studying Chain Mobility and Orientation in Polymers',(8) Freude and Haase, 'Quadrupole Effects in Solid-state NMR',(9) Jäger, 'Satellite Transition Spectroscopy of Quadrupolar Nuclei',(10) Hoatson and Vold, '^{2}H-NMR Spectroscopy of Solids and Liquid Crystals',(11) Chmelka and Zwanziger, 'Solid-state NMR Line Narrowing Methods for Quadrupolar Nuclei – Double Rotation and Dynamic-angle Spinning',(12) Chandrakumar, 'Spin-1 NMR',(13) Ulrich and Grage, 'H-2 NMR (Solid-state NMR of Polymers)',(14) and Smith and van Eck, 'Recent Advances in Experimental Solid-state NMR Methodology for Half-integer Spin Quadrupolar Nuclei'.(15)

For the spin–lattice relaxation of quadrupole spins, which is not considered in the present article, we refer to Chapter 7 in Freude and Haase.(9) A survey of nuclear quadrupole frequency data published before the end of 1982 is given by Chihara and Nakamura in *Landolt-Börnstein*, Vol. 20.(16) Values of the chemical shift of quadrupolar nuclei in solids can be found in books such as *Multinuclear NMR* edited by Mason.(17) For ^{2}H NMR we refer to other publications.(11,13,14,18) In section 10 we present as a continuation of Freude and Haase(9) some electric field gradient and chemical shift data for the most commonly studied quadrupolar nuclei with half-integer spins ^{27}Al, ^{23}Na and ^{17}O. A few references to recent solid-state NMR studies of some other quadrupolar nuclei are also given.

2 BASIC THEORY

At least three Cartesian coordinate systems were used for the description of the NMR interactions: the external magnetic field in the z-direction and the radiofrequency (RF) coil in the x-direction determine the laboratory axis system (LAB) with the coordinates (x, y, z). The interaction representation is based on the coordinates $x_\mathrm{i} = x\cos wt$, $y_\mathrm{i} = \pm y\cos wt$, $z_\mathrm{i} = z$. This system rotates around the direction of the external magnetic field with the applied RF $w = 2\pi\nu$. The microscopic properties of the complex under study such as the dipolar interactions, the anisotropy of the chemical shift or the electric field gradient are described in the principal axis system (PAS). The principal axes (X, Y, Z) are related to the structure of the complex, e.g. for the dipolar interaction the Z-direction is parallel to the internuclear vector.

The various interactions of the nuclear spin $\boldsymbol{I}$ can be described by the corresponding Hamiltonians. In the following we use I for the spin number and $\boldsymbol{I}$ for the spin angular momentum vector and also for the corresponding vector operator (Hamiltonian). The interaction of a nuclear spin with an external magnetic field $\boldsymbol{B}$ gives the Hamiltonian (Equation 1)

$$\mathcal{H} = \boldsymbol{IZB} \tag{1}$$

$\boldsymbol{Z} = -\gamma\hbar\boldsymbol{1}$ includes the unity matrix $\boldsymbol{1}$, the gyromagnetic ratio γ of the nuclear spins and Planck's constant, $h = 2\pi\hbar$.(19) For the case of a static external magnetic field B_0 pointing in the z-direction and the application of an RF field $B_x(t) = 2B_\mathrm{rf}\cos(wt)$ in the x-direction, we have for the external interactions Equation (2):

$$\mathcal{H}_0 + \mathcal{H}_\mathrm{rf} = \hbar w_\mathrm{L} I_z + 2\hbar w_\mathrm{rf}\cos(wt) I_x \tag{2}$$

where $w_\mathrm{L} = 2\pi\nu_\mathrm{L} = -\gamma B_0$ denotes the Larmor frequency and the nutation frequency w_rf is defined as $w_\mathrm{rf} = -\gamma B_\mathrm{rf}$. The transformation from the laboratory frame to the rotating frame gives, by neglecting the part which oscillates with twice the RF, Equation (3):

$$\mathcal{H}_{0,\mathrm{i}} + \mathcal{H}_{\mathrm{rf,i}} = \hbar\Delta w I_z + \hbar w_\mathrm{rf} I_x \tag{3}$$

where $\Delta w = w_\mathrm{L} - w$ denotes the resonance offset.

In addition to the external interactions there exist internal interactions of a nuclear spin, which can be efficiently expressed in the notation of irreducible tensor operators.(20) The definition and the most important feature (coordinate rotation) of an irreducible tensor operator of rank k with $(2k + 1)$ components is given by Equation (4):

$$P_R T_q^{(k)} P_R^{-1} = \sum_{q'=-k}^{+k} T_{q'}^{(k)} D_{q'q}^{(k)}(R) \tag{4}$$

where $D_{q'q}^{(k)}(R)$ denote the matrix elements of the irreducible representation of the group $\mathrm{O}^+(3)$ of the ordinary three-dimensional rotations. The transformation operator P_R is defined as $P_R = \exp\{\mathrm{i}\Omega\boldsymbol{e}_\mathrm{r}\boldsymbol{J}\}$, where $\boldsymbol{J}$ is the total angular momentum operator, $\boldsymbol{e}_\mathrm{r}$ is the unit vector pointing in the direction of rotation and Ω represents the angle of rotation. The rotation transforms the eigenfunctions, $|Im\rangle$, of the angular momentum operator

I_z as Equation (5):

$$P_R|Im\rangle = \sum_{m'} |Im'\rangle D^{(k)}_{m'm}(R) \qquad (5)$$

The matrix elements $D^{(k)}_{q'q}(R)$ (Wigner matrices) can be written as Equation (6):

$$D^{(k)}_{m'm}(\alpha, \beta, \gamma) = \exp\{\mathrm{i}\alpha m'\} d^{(k)}_{m'm}(\beta) \exp\{\mathrm{i}\gamma m\} \qquad (6)$$

with the Euler angles α, β and γ. The elements $d^{(k)}_{m'm}(\beta)$ of the reduced Wigner matrices depend on the angle β only. They are given in Table 1 for rank 2; values for rank 4 can be found in Zheng et al.(21) As presented in Figure 1, a positive rotation to a frame (x, y, z) about the Euler angles includes the rotation α about the original z axis, the rotation β about the obtained y' axis and the rotation γ about the final z'' axis [cf. Rose(22)].

Table 1 Reduced Wigner matrix $d^{(k)}_{qq'}(\beta)$ for rank 2[a]

q'/q	-2	-1	0	1	2
-2	a^4	$-\sqrt{2}a^2c$	$\sqrt{\frac{3}{2}}c^2$	$-\sqrt{2}b^2c$	b^4
-1	$\sqrt{2}a^2c$	$a^2(2d-1)$	$-\sqrt{3}cd$	$b^2(2d+1)$	$-\sqrt{2}b^2c$
0	$\sqrt{\frac{3}{2}}c^2$	$\sqrt{3}cd$	$\frac{1}{2}(3d^2-1)$	$-\sqrt{3}cd$	$\sqrt{\frac{3}{2}}c^2$
1	$\sqrt{2}b^2c$	$b^2(2d+1)$	$\sqrt{3}cd$	$a^2(2d-1)$	$-\sqrt{2}a^2c$
2	b^4	$\sqrt{2}b^2c$	$\sqrt{\frac{3}{2}}c^2$	$\sqrt{2}a^2c$	a^4

[a] The following abbreviations are used: $a = \cos\frac{\beta}{2}$, $b = \sin\frac{\beta}{2}$, $c = \sqrt{2}ab = \frac{1}{\sqrt{2}}\sin\beta$ and $d = a^2 - b^2 = \cos\beta$.

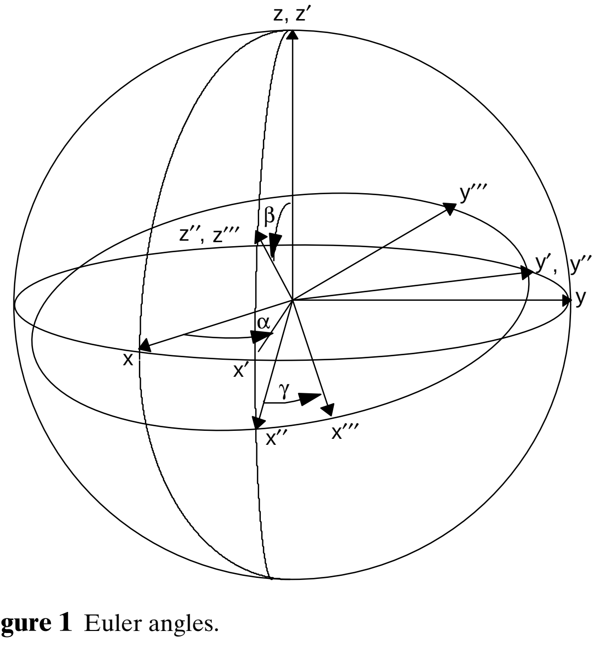

Figure 1 Euler angles.

The commutator shows another important feature of an irreducible tensor operator (Equations 7–9):(20)

$$[I_z, T^{(k)}_q] = qT^{(k)}_q \qquad (7)$$

and

$$[I_{\pm1}, T^{(k)}_q] = \mp\sqrt{\tfrac{1}{2}\{k(k+1) - q(q\pm1)\}}\,T^{(k)}_{q\pm1} \qquad (8)$$

with

$$I_{\pm1} = \mp\tfrac{1}{\sqrt{2}}(I_x \pm \mathrm{i}I_y) \qquad (9)$$

The tensor product $\boldsymbol{U}^{(\boldsymbol{K})}_{\boldsymbol{Q}}$ of two operators $T^{(k)}_q$ and $V^{(k)}_q$ is defined according to Equation (10):(20)

$$\boldsymbol{U}^{(\boldsymbol{K})}_{\boldsymbol{Q}} = \sum_{qq'} T^{(k)}_q V^{(k')}_{q'} \langle kk'qq'|kk'KQ\rangle \qquad (10)$$

where $\langle kk'qq'|kk'KQ\rangle$ are Clebsch–Gordan coefficients.(20) The scalar product of the operators $T^{(k)}_q$ and $V^{(k)}_q$ is simpler (Equation 11):

$$T^{(k)}_q \cdot V^{(k)}_q = \sum_{q=-k}^{+k} (-1)^q T^{(k)}_q V^{(k)}_{-q} \qquad (11)$$

Fortunately, most internal interactions in the NMR can be written in this form.(23) In the following the operators $T^{(k)}_q$ and $V^{(k)}_q$ act on two noninteracting systems, the nuclear spin coordinates and the spatial coordinates (lattice parameters), respectively.

In the strong external magnetic field it holds for the internal interactions by neglecting the nonsecular part of the corresponding Hamiltonian that (Equation 12)

$$[\mathcal{H}_0, \mathcal{H}_{\mathrm{internal}}] = 0 \qquad (12)$$

Comparison of Equation (12) with Equation (7) shows that only tensor elements with $q = 0$ contribute to the secular part of the internal Hamiltonians in a strong external magnetic field, if the system is described in the laboratory frame (LAB). However, the microscopic properties of the system are described in the PAS and a rotation of the coordinates from the PAS to the LAB by means of the Wigner matrix elements $D^{(k)}_{q'0}(R)$ must be performed. For example, the element $q = 0$ of the tensor $V^{(k)}$ is obtained by Equation (13):

$$V^{(k)}_0(\mathrm{LAB}) = \sum_{q'=-k}^{k} V^{(k)}_{q'}(\mathrm{PAS}) D^{(k)}_{q'0}(R) \qquad (13)$$

Operators of rank 0 are invariant with respect to rotations. For the chemical shift we have (Equations 14–16)

$$T^{(0)}_0 = \tfrac{-1}{\sqrt{3}} I_z B_0 \qquad (14)$$

$$V^{(0)}_0 = \sqrt{3}\sigma_{\mathrm{iso}} \qquad (15)$$

and

$$\mathcal{H}^{\text{isotropic}}_{\text{chemical shift}} = -\gamma\hbar\sigma_{\text{iso}} I_z B_0 \tag{16}$$

where σ_{iso} is the isotropic part of the shielding tensor (Equation 17):

$$\sigma_{\text{iso}} = \frac{\sigma_{XX} + \sigma_{YY} + \sigma_{ZZ}}{3} \tag{17}$$

Rank 0 operators do not contribute to dipolar interactions or quadrupolar interaction in first order. The contribution of the rank 1 operators can be neglected for all considered interactions. Therefore, anisotropy of the chemical shift, dipolar interactions and quadrupolar interactions in first order can be described by rank 2 operators in the form of Equation (18):

$$\mathcal{H} = C \sum_{q=-2}^{+2} (-1)^q T_q^{(2)} V_{-q}^{(2)} \tag{18}$$

Several contributions as described in Table 2 can be superimposed. The elements of the shielding tensor σ (trace $3\sigma_{\text{iso}}$) and of the traceless tensor of the electric field gradient $\boldsymbol{V}$ [which must not confused with the operator $V^{(k)}$] are given in the PAS. Parameters of the anisotropy are $\delta = \sigma_{ZZ} - \sigma_{\text{iso}}$ for the chemical shift and $V_{ZZ} = eq$ for the electric field gradient, where e denotes the elementary charge and the value q alone has no physical meaning in SI units. Q is the quadrupolar moment and eQ is called the electric quadrupolar moment. The asymmetry parameter η is in the range $0 \le \eta \le 1$. With the convention $|V_{ZZ}| \ge |V_{YY}| \ge |V_{XX}|$ or $|\sigma_{ZZ} - \sigma_{\text{iso}}| \ge |\sigma_{YY} - \sigma_{\text{iso}}| \ge |\sigma_{XX} - \sigma_{\text{iso}}|$, we obtain (Equations 19 and 20)

$$\eta = \frac{V_{XX} - V_{YY}}{V_{ZZ}} \tag{19}$$

or

$$\eta = \frac{\sigma_{XX} - \sigma_{YY}}{\sigma_{ZZ} - \sigma_{\text{iso}}} \tag{20}$$

Equation (21):

$$I_{\pm 1} = \mp \tfrac{1}{\sqrt{2}} (I_x \pm \mathrm{i} I_y) \tag{21}$$

and Equation (22):

$$F(\alpha, \beta, \eta) = \left(\frac{3\cos^2\beta - 1}{2} + \frac{\eta}{2} \sin^2\beta \cos 2\alpha \right) \tag{22}$$

are used in Table 2. The last row in Table 2 gives components which were transformed from the PAS into the LAB by the Euler angles α and β using Equation (13) for rank 2. With Equation (18) we obtain for the secular part of the Hamiltonian in the LAB for quadrupolar interaction in the first order (Equation 23)

$$\mathcal{H}_{\text{Q}} = \frac{eQV_{ZZ}}{4I(2I-1)} [3I_z^2 - I(I+1)] \times \left(\frac{3\cos^2\beta - 1}{2} + \frac{\eta}{2} \sin^2\beta \cos 2\alpha \right) \tag{23}$$

The quadrupolar coupling constant C_{qcc} is commonly defined according to Equation (24):

$$C_{\text{qcc}} = \frac{e^2 qQ}{h} \tag{24}$$

Table 2 Some contributions to the Hamiltonian[a]

Parameter	Chemical shift	Dipolar interaction between $\boldsymbol{I_i}$ and $\boldsymbol{I_k}$	Quadrupole interaction
C	$\hbar\gamma$	$-2\gamma_i\gamma_k\hbar^2 \frac{\mu_0}{4\pi}$	$\frac{eQ}{2I(2I-1)}$
$T_0^{(2)}$	$\sqrt{\frac{2}{3}} I_z B_0$	$\sqrt{\frac{1}{6}} (3I_{zi}I_{zk} - \boldsymbol{I}_i\boldsymbol{I}_k)$	$\sqrt{\frac{1}{6}} [3I_z^2 - I(I+1)]$
$T_{\pm 1}^{(2)}$	$\sqrt{\frac{1}{2}} I_{\pm 1} B_0$	$\sqrt{\frac{1}{2}} (I_{\pm 1i}I_{zk} + I_{zi}I_{\pm 1k})$	$\sqrt{\frac{1}{2}} (I_{\pm 1}I_z + I_{-z}I_{\pm 1})$
$T_{\pm 2}^{(2)}$	0	$I_{\pm 1i}I_{\pm 1k}$	$I_{\pm 1}^2$
$V_0^{(2)\text{PAS}}$	$\sqrt{\frac{3}{2}} (\sigma_{ZZ} - \sigma_{\text{iso}}) = \sqrt{\frac{3}{2}}\delta$	$\sqrt{\frac{3}{2}} r_{ik}^{-3}$	$\sqrt{\frac{3}{2}} V_{ZZ} = \sqrt{\frac{3}{2}} eq$
$V_{\pm 1}^{(2)\text{PAS}}$	0	0	0
$V_{\pm 2}^{(2)\text{PAS}}$	$\frac{1}{2}(\sigma_{XX} - \sigma_{YY}) = \frac{1}{2}\eta\delta$	0	$\frac{1}{2}(V_{XX} - V_{YY}) = \frac{1}{2}\eta eq$
$V_0^{(2)\text{LAB}}$	$\sqrt{\frac{3}{2}}\delta F(\alpha, \beta, \eta)$	$\sqrt{\frac{3}{2}} \frac{1}{r_{ik}^3} \left(\frac{3\cos^2\theta_{ik} - 1}{2} \right)$	$\sqrt{\frac{3}{2}} eqF(\alpha, \beta, \eta)$

[a] The dipolar interaction is the homonuclear one. For heteronuclear dipolar interactions $T_0^{(2)}$ must be substituted by $\sqrt{1/6} I_{zi}I_{zk}$.

However, for the quadrupolar frequency, ν_{Q} or w_{Q}, different definitions exist in the literature. We use the values according to Equation (25):

$$\nu_{\mathrm{Q}} = \frac{3e^2qQ}{2I(2I-1)h} = \frac{3C_{\mathrm{qcc}}}{2I(2I-1)} \qquad (25)$$

or Equation (26):

$$w_{\mathrm{Q}} = \frac{3e^2qQ}{2I(2I-1)\hbar} \qquad (26)$$

which were introduced for half-integer spin nuclei in the field of nuclear quadrupolar resonance (NQR) by Das and Hahn,(24) and established by Abragam(19) also for NMR. For different definitions in the case of half-integer spin nuclei, see Freude and Haase(9) (p. 33) and some papers following Frydman and Harwood.(25) For integer spins even less notational consistency exists, cf. Hoatson and Vold(11) (pp. 5 and 8). Equation (24) is still valid, but the definition of the quadrupolar frequency after Equation (26) is seldom used for spin-1 nuclei.

By substituting $V_{ZZ} = eq$ and using the angular dependent quadrupole frequency (Equation 27)

$$\nu'_{\mathrm{Q}} = \nu_{\mathrm{Q}}\left(\frac{3\cos^2\beta - 1}{2} + \frac{\eta}{2}\sin^2\beta\cos 2\alpha\right) \qquad (27)$$

one can write (Equation 28)

$$\mathcal{H}_{\mathrm{Q}}^{\text{first-order}} = \frac{h\nu'_{\mathrm{Q}}}{6}[3I_z^2 - I(I+1)] \qquad (28)$$

Equation (28) represents the first-order contribution of the quadrupolar interaction in the strong external magnetic field. From the second-order contribution the secular part with respect to I_z is given by Equation (29):

$$\mathcal{H}_{\mathrm{Q}}^{\text{second-order}} = \frac{h\nu_{\mathrm{Q}}^2}{9\nu_{\mathrm{L}}}\left\{2I_{\mathrm{Z}}\left[2I_{\mathrm{Z}}^2 - I(I+1) + \frac{1}{4}\right]V_{-1}V_1 + I_{\mathrm{Z}}\left[I_{\mathrm{Z}}^2 - I(I+1) + \frac{1}{2}\right]V_{-2}V_2\right\} \qquad (29)$$

The components $V_{p,p'}$ in Equation (29) correspond to the LAB. They can be obtained from the components in the PAS by means of Equation (13).

The homonuclear dipolar interaction of a pair (i, k) of spins with the distance r_{ik} and an angle θ between the internuclear vector and the direction of the external magnetic field is described by the Hamiltonian (Equation 30)

$$\mathcal{H}_{\mathrm{D}} = \frac{\mu_0}{4\pi}\gamma_i\gamma_k\hbar^2\left(\frac{3\cos^2\theta_{ik} - 1}{2r_{ik}^3}\right)(3I_{z,i}I_{z,k} - \boldsymbol{I}_i\boldsymbol{I}_k) \qquad (30)$$

and it holds that $\gamma_i = \gamma_k$. For heteronuclear dipolar interactions we have $\gamma_i \neq \gamma_k$ and $(3I_{z,i}I_{z,k} - \boldsymbol{I}_i\boldsymbol{I}_k)$ in Equation (30) must be substituted by $(I_{z,i}I_{z,k})$.

The Hamiltonian of the chemical shift is the sum of the isotropic and the anisotropic contributions (Equation 31):

$$\mathcal{H}_{\mathrm{CS}} = \gamma\hbar B_0 I_z\left[\sigma_{\mathrm{iso}} + \delta\left(\frac{3\cos^2\beta - 1}{2} + \frac{\eta}{2}\sin^2\beta\cos 2\alpha\right)\right] \qquad (31)$$

3 EXCITATION

The energy of a spin interaction can be described by the size of the corresponding Hamiltonian $\|\mathcal{H}\|$. For NMR the usual sequence is $\|\mathcal{H}_0\| \gg \|\mathcal{H}_{\mathrm{rf}}\| \gg \|\mathcal{H}_{\mathrm{Q}}\|$, $\|\mathcal{H}_{\mathrm{D}}\|$, $\|\mathcal{H}_{\mathrm{CSA}}\|$. Expressed in frequencies: the Larmor frequency ($\|\mathcal{H}_0\|$), cf. Equation (2), is of the order of magnitude of 10–1000 MHz, the nutation frequency ($\|\mathcal{H}_{\mathrm{rf}}\|$), cf. Equation (2), is of the order of magnitude of 1–400 kHz and the internal interactions are smaller than the RF field strength. However, the latter is sometimes not correct for quadrupolar nuclei in solids. We can assume the relation $\|\mathcal{H}_0\| \gg \|\mathcal{H}_{\mathrm{Q}}\| \gg \|\mathcal{H}_{\mathrm{D}}\|$, $\|\mathcal{H}_{\mathrm{CSA}}\|$ and have to distinguish the well-defined cases $\|\mathcal{H}_{\mathrm{rf}}\| \gg \|\mathcal{H}_{\mathrm{Q}}\|$ (*) or $\|\mathcal{H}_{\mathrm{rf}}\| \ll \|\mathcal{H}_{\mathrm{Q}}\|$ (**) and the ill-defined intermediate case (***). A so-called hard pulse can perform a nonselective excitation of the whole quadrupolar broadened spectrum, if the RF field strength meets (*). The soft pulse (**) excitation is limited to any single transition ($m = -I, -I+1, \ldots, I-1$) in a single crystal or to the central transition ($m = -\frac{1}{2}$) for powdered materials. Here the transition m denotes the transition between the magnetic quantum numbers $m \longleftrightarrow m+1$.

The excitation of quadrupolar nuclei with half-integer spins is discussed in detail by Freude and Haase.(9) For a short description of the problem of excitation of any NMR transition, we start from the basic equation for the frequency spectrum of a rectangular pulse with the duration τ and the carrier frequency ν_0 with $\delta\nu = \nu - \nu_0$ (Equation 32):

$$f(\delta\nu) = \frac{1}{\tau}\int_{-\tau/2}^{+\tau/2}\cos(2\pi\delta\nu t)\,\mathrm{d}t = \frac{\sin(\pi\delta\nu\tau)}{\pi\delta\nu\tau} \qquad (32)$$

It has its maximum $f(\delta\nu) = 1$ for $\nu = \nu_0$ and the first nodes in the frequency spectrum occur at $\delta\nu = \pm 1/\tau$. The spectral energy density E is proportional to the square of the RF field strength which includes the offset dependence of Equation (32). If we define the usable bandwidth of excitation $\delta\nu_{1/2}$ in analogy to electronics by Equation (33):

$$E\left(\nu = \pm\delta\nu_{1/2}\right) = \tfrac{1}{2}E(\nu = \nu_0) \qquad (33)$$

or Equation (34):

$$f^2(\nu = \pm\delta\nu_{1/2}) = \tfrac{1}{2}f^2(\nu = \nu_0) \qquad (34)$$

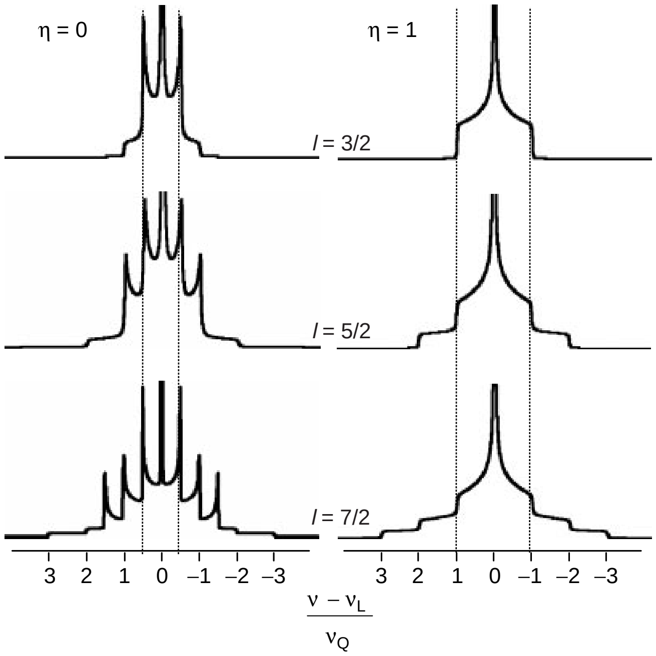

Figure 2 Examples of the static line shape (without MAS) of first-order quadrupolar broadened powder spectra for nonselective excitation. The central line is not fully represented (cut off). The theoretical line shapes are slightly Gaussian broadened.

the bandwidth of excitation $\delta\nu_{1/2} \approx 0.886/\tau$ follows from Equation (32). It should be noted that also the quality factor of the probe, $Q = \nu/\delta\nu_{\text{probe}}$, limits the bandwidth of excitation independently of the applied RF field strength or pulse duration. A superposition of the free induction decay (FID) of the NMR signals (liquid sample excited by a very short pulse) for some equidistant values of the resonance offset (without retuning the probe) shows easily the bandwidth $\delta\nu_{\text{probe}}$ of the probe. The spectral range of resonances for first-order quadrupolar shifts, which should be excited, amounts to $\nu_Q(2I-1)$ or $3C_{\text{qcc}}/2I$ (cf. Figure 2). The superposition of both limitations gives the conditions in Equation (35):

$$\frac{1}{\tau} > 1.13\nu_Q(2I-1) \approx \frac{1.4C_{\text{qcc}}}{2I} \tag{35}$$

and Equation (36):

$$\delta\nu_{\text{probe}} > \nu_Q(2I-1) = \frac{3C_{\text{qcc}}}{2I} \tag{36}$$

for a "nonselective" excitation of the spectrum. For increasing pulse width τ or decreasing bandwidth $\delta\nu_{\text{probe}}$ of the probe, a "partly selective", i.e. nonuniform, excitation of the transitions or a "selective" excitation of one transition only takes place.

If the single pulse is substituted by a composite pulse, a designed broadband or narrowband excitation can be achieved.(26)

The intensity of the FID $G(t=0)$ after the pulse with the RF field strength w_{rf} and the duration τ is, for nonselective excitation of all transitions $m \leftrightarrow m+1$, given by Equation (37):(9)

$$G_{m,m+1}^{\text{nonselective}}(0) = \frac{3[I(I+1) - m(m+1)]}{2I(I+1)(2I+1)} \sin w_{\text{rf}}\tau \tag{37}$$

Equation (37) gives also the relative intensities of all transitions, e.g. 12/30, 9/35 and 4/21 for the central lines in the case of nonselective excitation of the $I = \frac{3}{2}$, $\frac{5}{2}$ and $\frac{7}{2}$ nuclei, respectively. The selective excitation of a single transition can be described by Equation (38):(9)

$$G_{m,m+1}^{\text{selective}}(0) = \frac{3\sqrt{I(I+1) - m(m+1)}}{2I(I+1)(2I+1)} \times \sin\left(\sqrt{I(I+1) - m(m+1)}\,w_{\text{rf}}\tau\right) \tag{38}$$

Comparison with Equation (37) reveals that the maximum observed intensity is reduced by $\sqrt{I(I+1) - m(m+1)}$, but the effective nutation frequency is enhanced by the same value. For the central transition, $m = -\frac{1}{2}$, we obtain Equation (39):

$$\nu_{\text{rf}}^{\text{eff}} = (I + \tfrac{1}{2})\nu_{\text{rf}} \tag{39}$$

Thus, for the selective excitation of the central transition, the optimum pulse duration is equal to the duration of a nonselective $\pi/2$ pulse divided by $I + \frac{1}{2}$. The RF power should be as low as possible. Second-order quadrupolar broadening, the chemical shift anisotropy and dipole broadening give the lower limit for the RF power which should be applied, in order to excite the full central transition in powder spectra. Then, only a small portion of the satellite powder spectra is also excited. The partly selective excitation of more than one transition can be treated only numerically.(9)

The problem of ill-defined excitation in cases of strong quadrupolar interaction can be overcome by adiabatic frequency sweeps. Adiabatic passages are well known in NMR.(19) Kentgens(27) established in 1991 the quantitative excitation of a half-integer spin system by a frequency-stepped adiabatic half-passage (FSAHP) on the basis of an approach of Sindorf and Bartuska(28) and introduced in 1999 double-frequency sweeps (DFS) in static, MAS and MQMAS NMR experiments on the basis of an appropriate time-dependent amplitude modulation to the carrier frequency, which was applied before by Fu et al.(29) to integer spin systems in single crystals.

In the FSAHP, the spin system is far off-resonance at the beginning of the irradiation. The frequency is then stepped through the region of resonances slowly enough that the density operator can follow the Hamiltonian. Switching off the RF power at the resonance position of the central transition creates a single-quantum coherence like a $\pi/2$ pulse applied to a spin-$\frac{1}{2}$ system. A full passage would be comparable to a nonselective π pulse. A frequency sweep that adiabatically inverts the satellite transitions, in order to transfer magnetization to the central levels and increase the intensity of the corresponding signal, was introduced by Haase and Conradi.(30) The combination of this population enhancement with cross-polarization (CP) from ^{27}Al to ^{17}O was demonstrated.(31) A DFS can be generated by an amplitude modulation of the RF which causes two sidebands that are swept from a start frequency to a final frequency during the pulsing.(32) The authors claim that the DFS technique enhances the signal intensity also in MQMAS experiments.

The exclusive detection of the $\pm\frac{1}{2} \leftrightarrow \pm\frac{3}{2}$ transitions, which is based on a central-transition signal enhancement by means of an adiabatic RF sweep was introduced by McDowell et al.(33) in order to simplify the spectra and increase the sensitivity. Another approach to resolution enhancement by population transfer between Zeeman levels of the quadrupolar spin system with selective pulses and adiabatic frequency sweeps was first applied to ^{63}Cu in superconductors by Haase et al.(34)

Another NMR technique that uses adiabatic passage in combination with rotational echo and double resonance was introduced by Gullion.(35) He combined the principles of rotational-echo double resonance (REDOR),(36) with the transfer-of-populations double-resonance (TRAPDOR) developed by Grey et al.(37) The so-called REAPDOR NMR technique allows first, like TRAPDOR, the indirect detection of signals which are too broad to be directly observable for the single-resonance observation of the quadrupolar nucleus and second, like REDOR, the measurement of distances between spin pairs.(35)

CP excites a spin system by polarization transfer from another spin system. CP was introduced by Hartmann and Hahn(38) and is described in detail in the textbook by Slichter.(39) S. Vega(40) first applied static CP to half-integer nuclei and A.J. Vega(41,42) considered the spin dynamics of cross-polarization magic-angle spinning (CPMAS) NMR as a function of the ratio $\nu_{\mathrm{rf}}^2/\nu_{\mathrm{Q}}\nu_{\mathrm{rot}}$. Applications until 1992 are reviewed in Chapter 6.2 of Freude and Haase.(9) Recent discussions about the spin-locking efficiency of the CPMAS NMR of half-integer quadrupolar nuclei were presented by Hayashi,(43,44) Ding and McDowell(45,46) and Sun et al.(47) The combination of CP with other NMR techniques will be considered in sections 5–7.

4 LINE SHAPE OF STATIC AND MAGIC-ANGLE SPINNING NUCLEAR MAGNETIC RESONANCE SPECTRA

The following considerations concern the angular dependent quadrupolar shift. Assuming the resonance offset to be zero, the quadrupolar shift should be given as $\nu - \nu_{\mathrm{L}}$. For simplicity, we omit $-\nu_{\mathrm{L}}$, the subtraction of the Larmor frequency. The conventions $\nu_{m,m+1}$ and $\nu_{m,-m}$ for single-quantum transitions and symmetric transitions, respectively, are used here in agreement with the majority of the literature. For the central transition $\nu_{-1/2,+1/2}$ we have $m = -\frac{1}{2}$. Then, the first-order quadrupolar shift becomes, with ν'_{Q} from Equation (27), Equation (40):

$$\nu_{m,m+1} = \nu'_{\mathrm{Q}}(m + \tfrac{1}{2}) \qquad (40)$$

for single-quantum transitions, which means zero for the central transition $m = -\frac{1}{2}$. The first-order quadrupolar contribution is zero for all symmetric transitions $m \leftrightarrow -m$. See Equation (28) and note that $I_z \equiv m$ is a number in this case.

The second-order quadrupolar shift can be obtained by means of Equation (29) as Equation (41):

$$\nu_{m,m+1} = -\frac{\nu_{\mathrm{Q}}^2}{18\nu_{\mathrm{L}}}\{[24m(m+1) - 4I(I+1) + 9]V_1V_{-1} + [6m(m+1) - 2I(I+1) + 3]V_2V_{-2}\} \qquad (41)$$

or Equation (42):

$$\nu_{m,-m} = -\frac{m\nu_{\mathrm{Q}}^2}{18\nu_{\mathrm{L}}}\{[4I(I+1) - 8m^2 - 1]V_1V_{-1} + [2I(I+1) - 2m^2 - 1]V_2V_{-2}\} \qquad (42)$$

for single or symmetric quantum transitions, respectively. The components V_j are given in the LAB and can be described, with the Wigner matrices of rank 2, as functions of corresponding values in the PAS, which are given in Table 2. The V_jV_{-j} terms in Equations (41) and (42), therefore, can be written also as Wigner matrices for which the rank goes up to 4. Amoureux(48) gave a corresponding equation with the coefficients for the transformation of Equation (42) from the LAB into the PAS.

The second-order quadrupolar shift of the central transition can also be obtained with $m = -\frac{1}{2}$ from Equations (41) and (42) (Equation 43):

$$\nu_{-1/2,+1/2} = -\frac{\nu_{\mathrm{Q}}^2}{6\nu_{\mathrm{L}}}\left[I(I+1) - \frac{3}{4}\right] \times (A\cos^4\beta + B\cos^2\beta + C) \qquad (43)$$

Table 3 Functions A, B and C for the second-order static and MAS line shapes of the central transition (cf. Equation 43)

Function	Static	MAS
A	$-\frac{27}{8}-\frac{9}{4}\eta\cos 2\alpha-\frac{3}{8}\eta^2\cos^2 2\alpha$	$+\frac{21}{16}-\frac{7}{8}\eta\cos 2\alpha-\frac{7}{48}\eta^2\cos^2 2\alpha$
B	$+\frac{15}{4}-\frac{1}{2}\eta^2+2\eta\cos 2\alpha+\frac{3}{4}\eta^2\cos^2 2\alpha$	$-\frac{9}{8}-\frac{1}{12}\eta^2+\eta\cos 2\alpha-\frac{7}{24}\eta^2\cos^2 2\alpha$
C	$-\frac{3}{8}+\frac{1}{3}\eta^2+\frac{1}{4}\eta\cos 2\alpha-\frac{3}{8}\eta^2\cos^2 2\alpha$	$+\frac{5}{16}-\frac{1}{8}\eta\cos 2\alpha+\frac{7}{48}\eta^2\cos^2 2\alpha$

The components V_pV_{-p} are substituted now by functions depending on the Euler angles α and β and the asymmetry parameter η. The functions A, B, C (Table 3, static) were first used by Narita et al.(49) in order to calculate the second-order powder pattern of the central transition for a static (nonrotating) sample. Müller(50) showed that in the case of very fast MAS of the samples Equation (43) holds with other functions A, B, C (Table 3, MAS).

In order to deduce quadrupole parameters from experimentally obtained spectra, it is usual to fit the experimental spectrum with calculated spectra using a utility program of the spectrometer software. Figures 2 and 3 show spectra, which were obtained with the program WINFIT from Bruker. If the spinning speed is not large compared with the second-order shift, the average Hamiltonian can be used for numerical calculations.

Equation (43) allows an analytical determination of the center of gravity $\nu_{\mathrm{cg}} \equiv \nu_{\mathrm{iso}}$ for the powder pattern, which is called the isotropic quadrupolar shift of the signal of the central transition. This shift is not influenced by a rotation of the sample. We denote it as $\nu_{\mathrm{iso\,Q}}$ (Equation 44):

$$\nu_{\mathrm{iso\,Q}} = -\frac{\nu_Q^2}{30\nu_L}\left[I(I+1)-\frac{3}{4}\right]\left(1+\frac{\eta^2}{3}\right) \tag{44}$$

An important parameter of the powder line shape $f(\nu)$ is the second moment defined by Equation (45):

$$M_2 = \int (\nu-\nu_{\mathrm{iso}})^2 f(\nu)\,\mathrm{d}\nu \tag{45}$$

with $\int f(\nu)\,\mathrm{d}\nu = 1$. The dimension Hz^2 of M_2 changes to s^{-2} or T^2 if the line shape is given as $f(w)$ or $f(B)$, respectively. The square root of M_2 characterizes the second-order broadening of the signal. Equations (46–48) give the second moments as a function of ν_{iso} for the static and for the MAS spectrum and in addition the narrowing factor, which can be achieved by the application of MAS to the second-order quadrupolar broadening of the central transition:

$$M_2^{\mathrm{static}} = \nu_{\mathrm{iso}}^2\frac{23}{7} \tag{46}$$

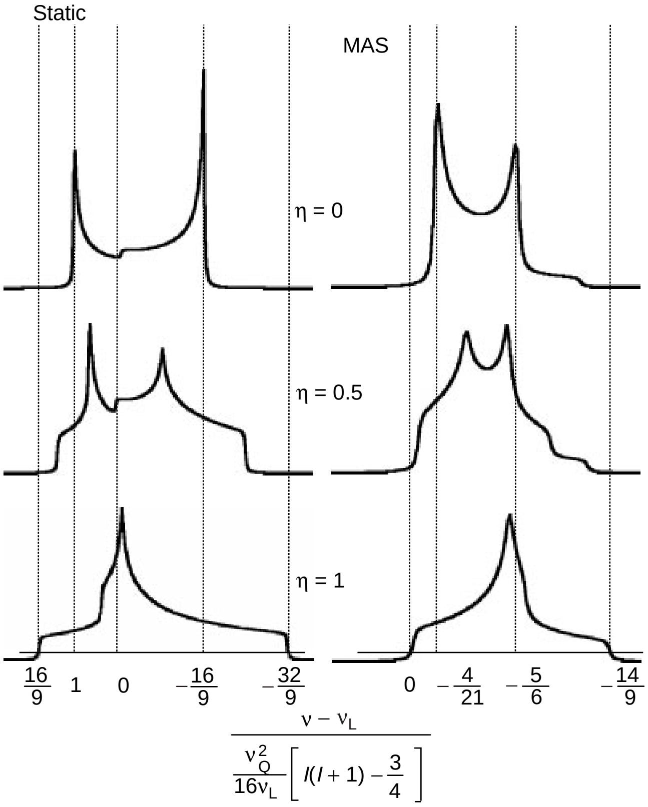

Figure 3 Examples of the line shapes, without and with MAS, of second-order quadrupolar broadened powder spectra of the central transition. The theoretical line shapes are slightly Gaussian broadened.

$$M_2^{\mathrm{MAS}} = \nu_{\mathrm{iso}}^2\frac{1}{4} \tag{47}$$

$$\sqrt{\frac{M_2^{\mathrm{static}}}{M_2^{\mathrm{MAS}}}} = \sqrt{\frac{92}{7}} \approx 3.6 \tag{48}$$

Equations (46–48) in combination with Equation (44) allow the determination of $\nu_Q\sqrt{1+\eta^2/3}$ from the second moment of the line shape, if the latter is exclusively broadened by second-order quadrupolar interaction. However, other contributions to the second moment of the static line shape should also be considered. The anisotropy of the chemical shift gives Equation (49):

$$M_2^{\mathrm{csa}} = \frac{4}{9}\frac{(\Delta\sigma\nu_{\mathrm{L}})^2}{5}\left(1+\frac{\eta^2}{3}\right) \tag{49}$$

where $\Delta\sigma = \sigma_{ZZ} - (\sigma_{XX} - \sigma_{YY})/2$ denotes the total anisotropy and η is the asymmetry parameter (cf. Equations 20 and 21) and ν_{iso} in Equation (45) must be taken as the isotropic value of the chemical shift.

If the dipolar interaction is small compared with the quadrupolar interaction, the spin flipping between different transitions is prohibited, and the second moment due to the dipolar interaction is modified.(9,19) We will give here only the equations for dominating dipolar interaction. The dipolar second moment of a spin system consisting of N resonant spins of type I (homonuclear interaction) and M nonresonant spins of type S (heteronuclear interaction) can be determined by the dimensionless Equation (50):

$$\frac{M_2/\mathrm{Hz}^2}{(\gamma_{\mathrm{I}}/2\pi)^2} = \frac{M_2/\mathrm{s}^{-2}}{\gamma_{\mathrm{I}}^2} = M_2/\mathrm{T}^2 = \frac{C_{\mathrm{I}}}{r_{\mathrm{I}}^6/\mathrm{m}^6} + \frac{C_{\mathrm{S}}}{r_{\mathrm{S}}^6/\mathrm{m}^6} \tag{50}$$

with (Equations 51–54)

$$C_{\mathrm{I}} = \frac{3}{5}I(I+1)\left(\frac{\mu_0}{4\pi}\right)^2\gamma_{\mathrm{I}}^2\hbar^2 \tag{51}$$

$$C_{\mathrm{S}} = \frac{4}{15}S(S+1)\left(\frac{\mu_0}{4\pi}\right)^2\gamma_{\mathrm{S}}^2\hbar^2 \tag{52}$$

$$\frac{1}{r_{\mathrm{I}}^6} = \frac{1}{N}\sum_{i=1}^{N}\sum_{k\neq i}^{N}\frac{1}{r_{ik}^6} \tag{53}$$

$$\frac{1}{r_{\mathrm{S}}^6} = \frac{1}{N}\sum_{i=1}^{N}\sum_{k=1}^{M}\frac{1}{r_{ik}^6} \tag{54}$$

The value C_{S} of a nonresonant nucleus can be easily calculated from the value of the same resonant nucleus C_{I} by $C_{\mathrm{S}} = C_{\mathrm{I}} \times 4/9$. If in Equation (50) the unit of the magnetic flux density T is substituted by 10^{-4} T (this corresponds to the old cgs unit gauss) and the unit m is substituted by the old unit Å, then the values C_{I} can be taken from Table 4.

Another dimensionless equation is very helpful in order to correlate the second moment of a line, which is broadened by any interaction, to the line width, which is commonly described by the full width at half-maximum (fwhm $\equiv \delta\nu_{1/2}$). Under the assumption of a gaussian line shape we obtain, for $M_2/\mathrm{s}^{-2} = \gamma_{\mathrm{I}}^2 M_2/\mathrm{T}^2 = (\gamma_{\mathrm{I}}/2\pi)^2 M_2/\mathrm{Hz}^2$, cf. Equation (50), with T_2 as the transversal relaxation time and the line width $\delta\nu$ given in hertz, Equation (55):

$$M_2/\mathrm{s}^{-2} = \frac{2}{(T_2/\mathrm{s})^2} = (\delta\nu_{1/2}/\mathrm{Hz})^2\frac{\pi^2}{\ln 4} \approx 7.12(\delta\nu_{1/2}/\mathrm{Hz})^2 \tag{55}$$

Table 4 Values of C_{I} in the equation $M_2/10^{-8}\mathrm{T}^2 = \left(\frac{C_{\mathrm{I}}}{r_{\mathrm{I}}^6/\text{Å}^6} + \frac{C_{\mathrm{S}}}{r_{\mathrm{S}}^6/\text{Å}^6}\right)^{\mathrm{a}}$

^{1}H	358.1	^{19}F	316.9	^{63}Cu	125.8	^{121}Sb	239.2
^{2}H	22.50	^{23}Na	125.3	^{65}Cu	144.3	^{127}I	167.2
^{7}Li	270.4	^{27}Al	283.6	^{75}As	52.52	^{133}Cs	129.4
^{9}Be	35.36	^{29}Si	14.13	^{77}Se	13.02	^{195}Pt	16.55
^{10}B	66.16	^{31}P	58.68	^{79}Br	112.4	^{199}Hg	11.38
^{11}B	184.3	^{35}Cl	17.19	^{81}Br	130.6	^{201}Hg	7.798
^{13}C	22.64	^{37}Cl	11.91	^{87}Rb	191.7	^{203}Tl	116.9
^{14}N	4.983	^{51}V	519.3	^{93}Nb	706.0	^{205}Tl	119.2
^{15}N	3.677	^{55}Mn	254.1	^{117}Sn	45.45	^{207}Pb	15.67
^{17}O	76.81	^{59}Co	419.3	^{119}Sn	49.74	^{209}Bi	305.1

[a] Values of C_{S} are given by $C_{\mathrm{S}} = C_{\mathrm{I}} \times 4/9$. The distances r_{I} and r_{S} denote in a simple model the internuclear distances of one resonant spin to another resonant spin and to a nonresonant spin, respectively. For the general case, see the definitions of r_{I} and r_{S} in Equations (53) and (54).

Now we go back to Equation (41) and consider the MAS spectra of the satellite transitions in addition to the central transition. Samoson(51) has shown that the second-order quadrupolar shift of the $m \leftrightarrow m+1$ transition can be split into an isotropic part describing the center of gravity of the quadrupolar shift and an angular-dependent part (Equation 56):

$$\begin{aligned}\nu_{m,m+1} = &-\frac{\nu_{\mathrm{Q}}^2}{30\nu_{\mathrm{L}}}[I(I+1) - 9m(m+1) - 3]\left[1+\frac{\eta^2}{3}\right] \\ &-\left(\frac{\nu_{\mathrm{Q}}^2}{30\nu_{\mathrm{L}}}\left[I(I+1) - \frac{17}{3}m(m+1) - \frac{13}{6}\right]\right) \\ &\times\left(\left[A\cos^4\beta + B\cos^2\beta + C\right]\right)\end{aligned} \tag{56}$$

with (Equations 57–59)

$$A = \frac{105}{16} - \frac{35}{8}\eta\cos 2\alpha + \frac{35}{48}\eta^2\cos^2 2\alpha \tag{57}$$

$$B = -\frac{45}{8} + \frac{5}{12}\eta^2 + 5\eta\cos 2\alpha - \frac{35}{24}\eta^2\cos^2 2\alpha \tag{58}$$

$$C = +\frac{9}{16} + \frac{1}{3}\eta^2 - \frac{5}{8}\eta\cos 2\alpha + \frac{35}{48}\eta^2\cos^2 2\alpha \tag{59}$$

For the central transition, $m = -\frac{1}{2}$, Equation (56) corresponds to Equation (43) and the isotropic, upper part in Equation (56) corresponds to Equation (44). The true value of the isotropic chemical shift can be determined from the experimentally obtained isotropic shift (center of gravity of the signal), if the isotropic quadrupolar shift can be determined as shown below.(10,51,52) For nonselective excitation, or at least partially selective excitation, MAS sidebands can be observed which are just outside of the spectral range of the static spectrum of the central transition. Their main intensity results from the $\pm\frac{1}{2} \leftrightarrow \pm\frac{3}{2}$ transitions, whereas the center band results mainly from the $+\frac{1}{2} \leftrightarrow -\frac{1}{2}$ transition. The average resonance position of two equal-order sidebands can be obtained experimentally as the center of gravity of the corresponding sidebands. Thus, the difference $\Delta = \nu_{\mathrm{iso\ Q}\pm 1/2,\pm 3/2} - \nu_{\mathrm{iso\ Q}-1/2,+1/2}$ of the average resonance position of two first satellite sidebands to the center of gravity of the center band (central transition) can be measured and compared with the corresponding difference derived from Equation (56) (Equation 60):

$$\Delta = -\frac{\nu_{\mathrm{Q}}^2}{30\nu_{\mathrm{L}}} 9 \left(1 + \frac{\eta^2}{3}\right) \tag{60}$$

Finally, the combination of Equations (56) and (60) gives the isotropic quadrupolar shift of the center band, which for $I = \frac{5}{2}$ is equal to $\nu_{\mathrm{iso\ Q}-1/2,+1/2} = \Delta 8/9$.

This procedure for the determination of the quadrupolar shift or other quadrupolar parameters was introduced by Samoson.(51) It is convenient for $I = \frac{5}{2}$ nuclei, because the linewidth of their $\pm\frac{1}{2} \leftrightarrow \pm\frac{3}{2}$ satellites is decreased by a factor of 0.3 with respect to the central line. Jäger used this sideband analysis for the study of various inorganic compounds(10) and denoted it SATRAS (satellite-transition spectroscopy).

Now we go back to Equation (42) and use the representation of Amoureux(48) for the shift of a symmetric transition in the case of very fast sample rotation around the magic angle $\theta = \arccos 3^{-1/2} \approx 54.74°$. Then, the contributions from the rank 2 components disappear and we obtain(53) Equation (61):

$$\begin{aligned}
\nu_{p/2,-p/2} &= \nu_{\mathrm{iso\ Q}(p)} + \nu_{\mathrm{aniso\ Q}(p)} \\
&= \frac{p\nu_{\mathrm{Q}}^2(3+\eta^2)}{90\nu_{\mathrm{L}}} \left\{ I(I+1) - \frac{3}{4}p^2 \right\} \\
&\quad - \left\{ \frac{p\nu_{\mathrm{Q}}^2}{12960\nu_{\mathrm{L}}} \right\} \left\{ (18+\eta^2) d_{0,0}^{(4)} \right. \\
&\quad \left. + \sqrt{360}\,\eta\, d_{2,0}^{(4)} \cos 2\alpha + \sqrt{70}\,\eta^2\, d_{4,0}^{(4)} \cos 4\alpha \right\} \\
&\quad \times \left\{ 36I(I+1) - 17p^2 - 10 \right\} \left\{ \left(-\frac{9}{28}\right) \right. \\
&\quad \left. \times \left(35\cos^4\theta - 30\cos^2\theta + 3\right) \right\}
\end{aligned} \tag{61}$$

where p denotes the quantum level pQ and symmetric coherences with the notation $p/2 \leftrightarrow -p/2$ instead of $m \leftrightarrow -m$ are considered. The Euler angles (α, β) describe the spinner axis with respect to the PAS. The elements d of the reduced Wigner matrices are related to β by Equations (62–64):

$$d_{0,0}^{(4)} = \frac{1}{8}(35\cos^4\beta - 30\cos^2\beta + 3) \tag{62}$$

$$d_{2,0}^{(4)} = \frac{\sqrt{10}}{8}(7\cos^2\beta - 1)\sin^2\beta \tag{63}$$

$$d_{4,0}^{(4)} = \frac{\sqrt{70}}{16}\sin^4\beta \tag{64}$$

Equation (61) still contains a function of the rotor angle θ in the last brackets, in order to give one basic equation for MQMAS and DOR as well: if we insert the magic angle $\theta = \arccos\sqrt{1/3} \approx 54.74°$, then the value of the last brackets is equal to one and Equation (61) can be used as the basic equation for MQMAS NMR (cf. section 6). If we consider a DOR and the second rotor angle is fixed to $\arccos\sqrt{(6 \pm \sqrt{96/5})/14} \approx 30.56°$ or $70.12°$, then the value of the last brackets in Equation (61) is equal to zero and the total anisotropic part of Equation (61) disappears. For the central transition, $p = -1$, only the isotropic quadrupolar shift remains, which can be directly observed by DOR NMR. The isotropic contribution in Equation (61) is identical with Equation (44) and with the isotropic part of Equation (56), if the central transition is considered ($p = -1$ and $m = -\frac{1}{2}$).

5 DOUBLE-ROTATION AND DYNAMIC-ANGLE SPINNING

Samoson et al.(54) succeeded in 1988 in building a double-rotor probe. The outer rotor, inclined by $\beta_2 = 54.74°$ with respect to the external field, rotated at about 400 Hz, and had a diameter of 20 mm. The sample in the inner rotor, 5 mm diameter, rotated at about 2 kHz, and the angle between both axes of rotation was $\beta_1 = 30.56°$.(54)

A torque-free rotation can be achieved only for a certain ratio of $k = w_1/w_2$. The two contributions to the inner-rotor angular velocity are w_1 and the angular velocity w_2 imposed by the outer rotor. The latter can be decomposed into one component $w_2\cos\beta_1$ along the z-axis of the inner rotor and another component $w_2\sin\beta_1$ perpendicular to this axis in y-direction, so that y-direction, axis z of the inner rotor, and axis Z of the outer rotor are in one plane. Thus, $w_x = 0$, $w_y = w_2\sin\beta_1$, $w_z = w_1 + w_2\cos\beta_1$, and the resulting angular momentum $\boldsymbol{L}$ must be in the Z-direction in order to be torque-free(55) (cf. Figure 4) (Equation 65):

$$\tan\beta_1 = \frac{J_y w_2 \sin\beta_1}{J_z(w_1 + w_2\cos\beta_1)} \tag{65}$$

For $\beta_1 = \arccos\sqrt{(6 + \sqrt{96/5})/14} \approx 30.56°$, we obtain Equation (66):

$$\begin{aligned}
\frac{w_1}{w_2} \equiv \frac{\nu_{\mathrm{inner}}}{\nu_{\mathrm{outer}}} = k &= \sqrt{\frac{6 + \sqrt{96/5}}{14}} \left(\frac{J_y}{J_z} - 1\right) \\
&\approx 0.86 \left(\frac{J_y}{J_z} - 1\right)
\end{aligned} \tag{66}$$

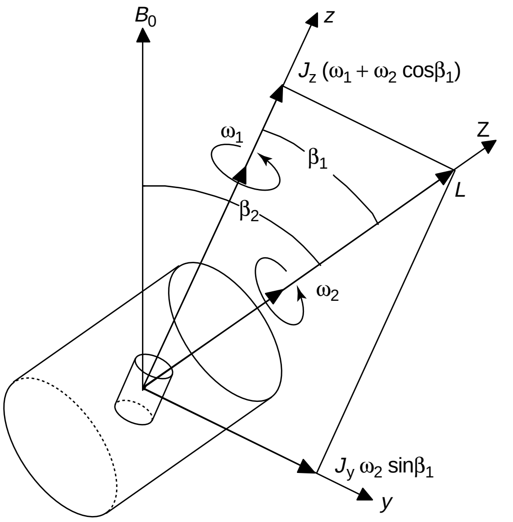

Figure 4 Moments of inertia for DOR after Wu et al.(55) By adjusting the ratio of moments, J_y/J_x, the addition of the two vector components of the angular momentum along the inner-rotor axis z and the y-axis can be made to point along the outer-rotor axis Z, so that spinning the outer rotor will not affect the orientation of the total angular momentum of the inner rotor.

and the usual design of the inner rotor gives values of J_y/J_z so that $5 < k < 6$. Wu et al.(55) explained that the spinning system is in a stable state when the torque-free condition, which is given by Equation (66), is slightly violated and the frequencies obey Equation (67):

$$\nu_{\text{inner}} = k\nu_{\text{outer}} + \Delta\nu_{\text{inner}} \tag{67}$$

where the excess of the inner frequency $\Delta\nu_{\text{inner}}$ is about 1 kHz.

The application of rotation-synchronized pulses has been shown to be effective in eliminating half of the DOR sidebands.(56) The total suppression of sidebands can be achieved by the application of additional pulses(57) and by application of the magic-angle turning technique.(58) A theoretical consideration of the DOR sidebands can be found in the literature.(59–61)

DOR NMR gives accurate values of the isotropic shift, δ_{iso}, of the NMR of a quadrupolar nucleus. Two shift effects are superimposed: the isotropic quadrupolar shift, which is described in Equation (44), and the isotropic value of the chemical shift, which was introduced in Equation (16). We substitute σ_{iso}, the isotropic part of the shielding tensor, by the value of the chemical shift $\delta_{\text{CS iso}} = \sigma_{\text{ref}} - \sigma_{\text{iso}}$ (with respect to a given isotropic chemical shift of a reference compound). Then we substitute the second-order quadrupolar shift $\nu_{\text{iso Q}}$ in Equation (44) by the dimensionless value $\delta_{\text{Q iso}} = (\nu_{\text{iso Q}})/\nu_{\text{L}}$. In this notation we obtain for the observed isotropic shift in the DOR experiment Equation (68):

$$\begin{aligned}\delta_{\text{DOR}} &= \delta_{\text{CS iso}} + \delta_{\text{Q iso}} \\ &= \delta_{\text{CS iso}} - \frac{\nu_{\text{Q}}^2}{30\nu_{\text{L}}^2}\left[I(I+1) - \frac{3}{4}\right]\left(1 + \frac{\eta^2}{3}\right)\end{aligned} \tag{68}$$

For common use the shifts can be expressed in parts per million (ppm) by multiplying the right-hand side of Equation (68) by 10^6. Equation (68) reflects the fact that the value of the isotropic chemical shift cannot be obtained from *one* DOR experiment if the quadrupolar shift is unknown. However, two DOR experiments at different external field strengths, which means at different Larmor frequencies, give the value of the chemical shift $\delta_{\text{CS iso}}$ and also the quadrupolar parameter $\nu_{\text{Q}}\sqrt{1 + \eta^2/3}$.

The DOR technique has been applied, first, to the ^{23}Na resonance in sodium oxalate(54,56,62) and later to NaNO$_2$(56,63) to the ^{17}O resonance in diopside(64) and silicates(65) and to the ^{27}Al resonance of YAG.(63) The majority of the DOR NMR studies was devoted to zeolites of faujasite type(66–75) and to zeolite-like materials such as aluminophosphates,(47,66,76–86) zincosilicates(87) or sodalite.(88,89) Other materials studied included aluminas(90) and aluminum borate(91) (^{27}Al), gallium phosphate(92) (^{71}Ga) and boron nitride(93) (^{11}B). CP effects have been studied.(47,79) Amoureux(94) proposed a combination of DOR and variable-angle spinning (VAS) in which the quadrupolar shift of DOR NMR can be deduced with a simulation of the second-dimension spectra obtained with stepped values of the angle of the outer rotor with respect to the external magnetic field.

The rotation frequencies of the inner and outer rotor at present do not exceed $\nu_{\text{inner}} = 12$ kHz and $\nu_{\text{outer}} = 2$ kHz, respectively. A pneumatic unit, which is controlled by a computer, simplifies the experimental set-up and makes it safer. However, compared with the MAS technique, a more complicated set-up and stronger wear of the rotors must still be accepted for DOR experiments.

A DAS experiment was first performed independently by Chmelka et al.(64) and Llor and Virlet.(95) The DAS technique uses a time-dependent angle of the rotor axis, which toggles in the simple experiment between 37.38° and 79.19° for two equal periods of time. During the hopping time, necessary for switching the angle (>30 ms), the evolution of the magnetization can be reduced by means of a selective $\pi/2$ pulse pair applied at a time t_1 after the preparation pulse. The signal consists of a second-order quadrupolar echo with a maximum at the time t_1 after the last pulse. The data acquisition of the FID starting at the echo maximum gives the data in the t_2 domain. The two-dimensional (2-D) spectrum is obtained after a 2-D Fourier transformation with respect to t_1 and t_2. An advanced concept introduces a fourth $\pi/2$ pulse in order to retain two pathways from the t_1 evolution yielding a pure absorption-phase spectrum and introduces a third angle of rotation of 54.74°, in order to correlate in two dimensions the DAS spectra with MAS spectra.(96,97) A sideband pattern emerges if the evolution period of the 2-D DAS experiment is divided into unequal parts by RF pulses or spinner reorientation, as shown by Grandinetti et al.(98) Fyfe et al.(99) found that the switch to the magic angle after the CP step is useful for obtaining high-resolution spectra of slowly relaxing spin species. A 2-D heteronuclear correlation DAS NMR experiment with CP from ^{23}Na to ^{31}P was applied by Jarvie et al.(100) in order to find connectivities between the nuclei. Wenslow and Mueller(101) demonstrated the increased information of this so-called DAS/CP/MAS NMR experiment for the study of cation sites in glasses. Medek et al.(102) introduced the three-dimensional dynamic-angle correlation spectroscopy (DACSY), which is based on the acquisition of DAS NMR signals as a function of different initial and final spinning axes.

Two drastic limitations for the application of the DAS technique compared with the DOR technique should be noted. First, the spin–lattice relaxation time T_1, which is often short for quadrupolar nuclei, has to be larger than the time period necessary for flipping the rotor axis. Second, the spin exchange due to dipolar interactions, which cannot be eliminated during the relatively long flipping time of the rotor axis, has to be sufficiently small.

6 MULTIPLE-QUANTUM MAGIC-ANGLE SPINNING TECHNIQUE

In 1995, Frydman and Harwood(25) proved the feasibility of a 2-D NMR experiment that makes use of invisible multiple-quantum transitions combined with MAS to remove the anisotropy of the quadrupolar interaction. Symmetric $p/2 \leftrightarrow -p/2$ coherences with the quantum level pQ were selected, since the corresponding powder resonances are devoid of first-order quadrupolar effects.

The phase development $\varphi(t)$ of the single or multiple-quantum coherence can be written as Equation (69):

$$\begin{aligned}\frac{\varphi(t)}{2\pi t} &= \Delta\nu p + \nu_{p/2,-p/2} \\ &= \Delta\nu p + \frac{p\nu_Q^2(3+\eta^2)[4I(I+1)-3p^2]}{360\nu_L} \\ &\quad - \frac{p\nu_Q^2\{36I(I+1)-17p^2-10\}}{12960\nu_L}\{(18+\eta^2)d_{0,0}^{(4)} \\ &\quad + \sqrt{360}\,\eta d_{2,0}^{(4)}\cos 2\alpha + \sqrt{70}\,\eta^2 d_{4,0}^{(4)}\cos 4\alpha\} \qquad (69)\end{aligned}$$

with $\nu_{p/2,-p/2}$ from Equation (61), which is reduced under MAS conditions. The contributions from the chemical shift and from the resonance offset are included in $\Delta\nu = \sigma_{\mathrm{iso}}\nu_L - \nu_{\mathrm{offset}}$. Equation (69) shows that by going from the multiple-quantum level pQ to the −1Q level of observation, the sign of the phase development can be inverted. Thus, the influence of the anisotropy of the second-order quadrupolar interaction is averaged out, if the times t_1 and t_2 spent on the quantum levels pQ and −1Q, respectively, fulfill the condition in Equation (70):

$$t_2 = p\frac{36I(I+1)-17p^2-10}{36I(I+1)-27}t_1 = R(I,p)t_1 \qquad (70)$$

This relation describes the appearance of the isotropic echo, and thus gives the slope $R(I,p)$ of the anisotropic axis in the 2-D spectrum, which is obtained after the 2-D Fourier transformation with respect to t_2 and t_1.

Several pulse sequences were used in order to excite a multiple-quantum coherence and convert it to the observable single-quantum coherence after the evolution time. The pulse sequence, which is shown in Figure 5, is mostly applied now. The highest possible RF power should be used for the first and second pulse, which excites the triple- (or quintuple-) quantum coherence and converts it back to zero-quantum coherence, respectively. The third pulse (z-filter) should be much weaker, in order to excite the central transition only. It converts nonobservable zero-quantum coherence and populations ($p = 0$) into observable single-quantum coherences ($p = -1$).

The symmetric 3Q coherence pathway in Figure 5 is ($0 \rightarrow \pm 3 \rightarrow 0 \rightarrow -1$). The symmetric quintuple-quantum

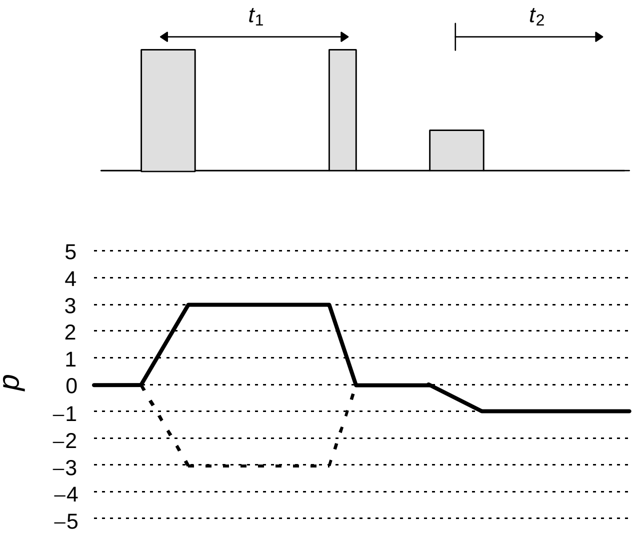

Figure 5 Pulse sequence and coherence transfer pathway for the echo (upper way) and antiecho (lower way) consisting of two strong pulses and a weak z-filter pulse. The triple-quantum MAS pathway is shown on the lines for the nuclear spin $I = \frac{5}{2}$.

(5Q) pathway is ($0 \rightarrow \pm 5 \rightarrow 0 \rightarrow -1$). Two-pulse sequences (without z-filter) can be described by the notation ($0 \rightarrow \pm p \rightarrow -1$). Although only one sign of p (cf. Equation 70) yields an echo which can be observed, it is needed to acquire both $\pm p$ coherence transfer pathways when trying to produce 2-D MQMAS spectra that are free from dispersive distortions.(103) Equally strong signals from both pathways must be collected, in order to obtain pure adsorptive spectra. This is more difficult if a two-pulse sequence is used, which includes the different transitions $+p \rightarrow -1$ and $-p \rightarrow -1$ for the last step in the echo and antiecho coherence transfer pathway, respectively. However, both pathways are completely symmetrical when considering the coherence jumps in the z-filter pulse sequence.(104,105)

The flip angles of the first and second pulses should be optimized with respect to the best signal amplitude. In principle, this can be done by numerical calculations,(106) e.g. by the program PULSAR.(107) The result depends on the nuclear spin I and its Larmor frequency ν_L, the chosen coherence pQ and the ratio between the nutation frequency $\nu_{rf} = \gamma B_{rf}/2\pi$ and the quadrupolar frequency ν_Q. One conclusion is that the MQMAS NMR spectra, which are obtained by strong pulses, do not present quantitative results with respect to the concentration of species, since the multiple-quantum transition efficiency is different for nuclei with different quadrupolar frequency ν_Q.

The calculations need a full set of NMR parameters including the quadrupolar parameters and do not take into consideration second-order and spinning effects. Therefore, the optimization of the pulse duration should be performed at the beginning of the NMR experiment by variation of the pulse duration; and only the initial flip angles for this procedure should be taken from the numerical calculations. Nonselective flip angles of about 180° and 50° for the first and second pulse, respectively, can be used for any I and pQ, if the Larmor frequency is about 100 MHz and the ratio between the quadrupolar frequency ν_Q and the nonselective nutation frequency is $\nu_Q/\nu_{rf} \approx 10$. More precise flip angles are given in the literature(106,108) as a function of I and pQ. (Note that definition of the quadrupolar frequency in the literature(25,106,108) is different to the definition of Abragam;(19) cf. Equation (25), which is used here: $\nu_Q^{\text{Frydman}} = \nu_Q^{\text{Abragam}}/6$.)

An alternative approach to the generation of multiple-quantum transitions by strong pulses is to use the adiabatic transfer by the interchange between the eigenstates 3Q and 1Q undergoing MAS.(42) Wu et al.(109) introduced a triple-quantum magic-angle spinning (3QMAS) experiment by rotation-induced adiabatic coherence transfer (RIACT) for $I = \frac{3}{2}$ nuclei and applied it to the study of sodium sites in inorganic salts. They claimed that this method gives quantitative MQMAS NMR spectra, since the adiabatic coherence transfer is independent of the strength of the quadrupolar interaction. However, theoretical calculations(108) showed that, compared with the nonadiabatic excitation, the disturbing off-resonance effects are more extensive for RIACT. Lim and Grey(110) performed numerical simulations of the RIACT experiment as a function of asymmetry parameter and pulse spacings and discussed the effect of very fast sample spinning. Mildner et al.(111) demonstrated by means of ^{17}O studies of silicates that RIACT can be applied to $I = \frac{5}{2}$ spins at the moderate RF field strength of $\nu_{rf} \approx 30$ kHz.

Ding and McDowell(112,113) claimed that a shaped first excitation pulse would also achieve quantitative results in nonadiabatic 3QMAS NMR experiments and that properly shaped pulses can also reduce the requirements on the RF power and sample spinning speeds. The superior excitation of triple-quantum coherences by composite pulse schemes was also shown by Marinelli et al.(114)

Kentgens and Verhagen(32) showed that DFSs are very efficient for the conversion of triple- to single-quantum coherence in MQMAS spectroscopy. Goldbourt et al.(115) used instead fast radiofrequency amplitude modulation (FAM) in the version FAM and FAM1 for $I = \frac{3}{2}$ and $I = \frac{5}{2}$ nuclei, respectively, and obtained a substantial intensity and resolution enhancement of the signal over the commonly used MQMAS pulse schemes. A very strong RF field, no resonance offset and a high spinning rate, if possible 30 kHz as shown by Rocha,(116) are still the requirements for most MQMAS experiments.

For both the nonadiabatic and adiabatic MQMAS experiments described above, the selection of desired multiple-quantum coherences is done by phase cycling.(111,117) Methods of hypercomplex or time-proportional phase increment (TPPI) 2-D Fourier transformation [cf. Ernst et al.(118)] are used for the acquisition of real and imaginary part with respect to the t_1/ν_1 dimension. Fyfe et al.(119) used pulsed field gradients instead of phase cycling. The advantage is the simplification of the MQMAS pulse program, which allows the implementation of correlation experiments. However, the insertion of the field gradient coil reduces the maximum achievable RF power.

A shearing transform of the experimentally obtained 2-D spectrum, which aligns anisotropic ridges parallel to the ν_2 axis in such a way that the isotropic dimension can be displayed along the ν_1 axis, is described below. Brown et al.(104,120,121) introduced an experiment with an additional pulse called split-t_1 MQMAS that is pure adsorptive and includes the shearing ratio into the pulse program so that anisotropic ridges

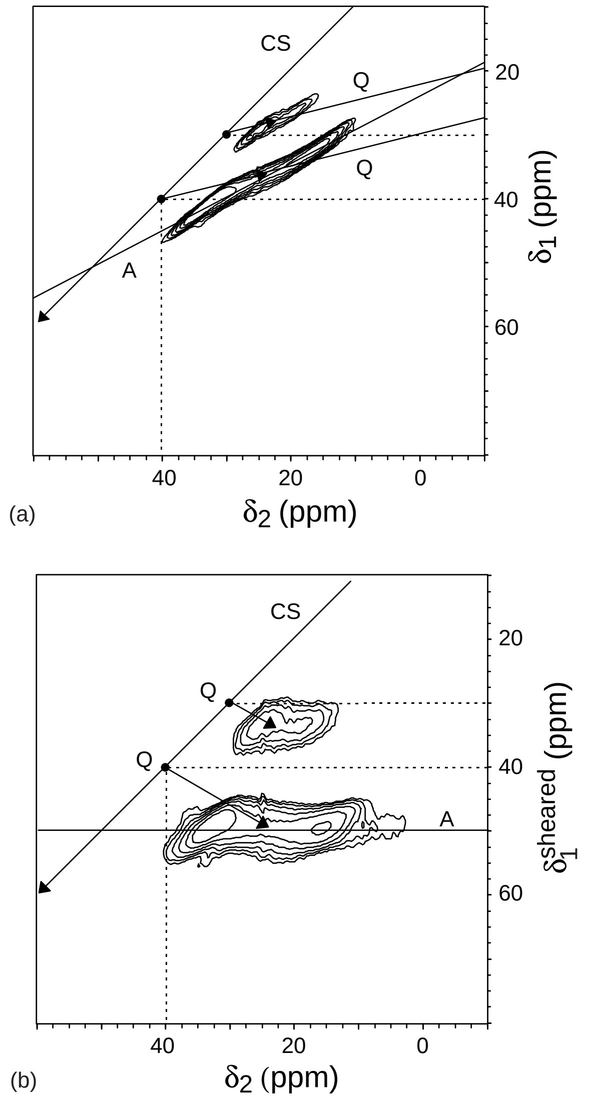

Figure 6 2-D ^{17}O 3QMAS NMR spectra of the zeolite Na-ZSM-5 (a) after the 2-D Fourier transformation and (b) after the following shearing transformation. The two signals were assigned to SiOSi and SiOAl fragments with concentrations of 80 and 20%, $\delta = 40$ and 30 ppm, $C_{\text{qcc}} = 5.3$ and 3.5 MHz, $\eta = 0.12$ and 0.29, respectively.(53) (The figure was provided by Ulf Pingel.)

are parallel to the ν_2 axis after the 2-D Fourier transformation.

Figure 6(a) and (b) shows the 2-D ^{17}O 3QMAS NMR spectra of the zeolite Na-ZSM-5 before and after the shearing procedure. The two signals in the spectra are due to Si–O–Si and Si–O–Al bonds.(53) The spectra demonstrate how the projection on the ν_1 axis is changed by the shearing. The analytical treatment starts from the isotropic part of Equation (69). Without resonance offset, the total shift is a superposition of the isotropic part of the chemical shift, $\sigma_{\text{iso}}\nu_{\text{L}}$, and the isotropic part of the quadrupolar shift, $\nu_{\text{iso Q}}$ (Equation 71):

$$\begin{aligned}\nu_{\text{iso}} &= \sigma_{\text{iso}}\nu_{\text{L}}p + \nu_{\text{iso Q}} \\ &= \sigma_{\text{iso}}\nu_{\text{L}}p + \frac{p\nu_{\text{Q}}^2(3+\eta^2)[4I(I+1)-3p^2]}{360\nu_{\text{L}}}\end{aligned} \tag{71}$$

Equation (71) can be transformed into relative units (ppm) by multiplication by $10^6/(-p\nu_{\text{L}})$. The value $-p\nu_{\text{L}}$ describes the apparent Larmor frequency and includes the real Larmor frequency for $p = -1$. For the ν_1 axis (before shearing) and for the ν_2 axis, we have Equations (72) and (73), respectively:

$$\begin{aligned}\delta_1 &= \delta_{\text{CS iso}} + \delta_{\text{Q iso}} \\ &= \delta_{\text{CS iso}} - \frac{\nu_{\text{Q}}^2(3+\eta^2)[4I(I+1)-3p^2]}{360\nu_{\text{L}}^2}\end{aligned} \tag{72}$$

$$\begin{aligned}\delta_2 &= \delta_{\text{CS iso}} + \delta_{\text{Q iso}} \\ &= \delta_{\text{CS iso}} - \frac{\nu_{\text{Q}}^2(3+\eta^2)[4I(I+1)-3]}{360\nu_{\text{L}}^2}\end{aligned} \tag{73}$$

Equation (73) describes the shift δ_2 of the center of gravity of the anisotropic ridge, which is not influenced by the shearing transformation. The coordinate $\delta_1^{\text{shearing}}$ after the transformation is given by(108) Equation (74):

$$\begin{aligned}\delta_1^{\text{shearing}} &= \delta_{\text{CS iso}} + \delta_{\text{Q iso}}^{\text{shearing}} \\ &= \delta_{\text{CS iso}} + \frac{\nu_{\text{Q}}^2(3+\eta^2)[4I(I+1)-3]}{612\nu_{\text{L}}^2}\end{aligned} \tag{74}$$

It can be seen that after shearing the quadrupolar shift becomes always positive and independent of p. Comparison of Equation (74) with Equation (73) gives the slope of two special lines in the sheared 2-D spectrum. One line with slope 1, which is denoted CS in Figure 6, describes the variable isotropic chemical shift in the case of zero quadrupolar shift. Only one line CS exists and crosses the coordinates (0, 0). Lines Q with slope $-10/17$ describe variable quadrupolar shifts at one value $\delta_{\text{CS iso}}$, which is given by the crossing of line Q with line CS. The shift difference between this crossing point and the center of gravity of a signal gives the corresponding quadrupolar shift $\delta_{\text{Q iso}}^{\text{shearing}}$. One-dimensional anisotropic slices A are obtained from the 2-D spectrum. These slices can be fit by a line-shape simulation, which gives values for ν_{Q} and η, whereas $\delta_{\text{Q iso}}$ is a measure of $\nu_{\text{Q}}\sqrt{1+\eta/3}$. The quadrupolar parameter obtained from the 2-D spectrum can then be used for a simulation of the single-quantum MAS NMR spectrum. This procedure yields correct information about the relative concentration of the various species giving rise to the corresponding signals. The program REGULAR, which was developed by Delevoye,(122) takes full advantage of the information included in the 2-D MQMAS NMR spectrum and thereby quantifies the distribution of nucleus surroundings also in badly crystallized and amorphous materials. A 2-D result is obtained which represents quadrupolar constants versus isotropic chemical shifts with correct relative intensities. Scaling and labeling of the isotropic axis (ν_1 axis after shearing) was considered in detail by Man.(123)

The residual line width of the MQMAS NMR spectra is a matter of current research. Wu and Wasylishen(124) showed that the heteronuclear dipolar interaction between two nuclei does not cause residual dipolar couplings in MQMAS NMR experiments.

The spinning sidebands in the multiple-quantum dimension are a common feature of dipolar-coupled spin $I = \frac{1}{2}$ and half-integer quadrupolar systems. Both cases were considered by Friedrich et al.(125) The case of half-integer spins is the subject of various studies.(126–129) Spinning sidebands arise even in the absence of explicit time modulations of any spin interactions, due to orientation and time dependence characterizing the multiple- to single-quantum conversion process, as shown by Marinelli and Frydman.(126) The sidebands cause signal loss and misinterpretation of spectra. Rotor synchronization, which means setting the evolution dwell time equal to the rotation period, is useful for suppressing these spinning sidebands.(130) However, it limits the spectral width of the multiple-quantum dimension to the rotation frequency. This drawback increases on going from triple- to quintuple-quantum transitions.

Several combinations of MQMAS with other NMR techniques have been successfully applied. Vosegaard et al.(131) added the Carr–Purcell–Meiboom–Gill (CPMG) pulse sequence to the MQMAS pulse program, in order to improve the sensitivity by splitting the line shape in the ν_2 dimension into manifolds of spin-echo sidebands. High-power ^{1}H decoupling improves the resolution in both dimensions.(132,133) Lacassagne et al.(134) demonstrated improved resolution for strong heteronuclear coupling by applying composite decoupling schemes during the evolution and acquisition time. Wang et al.(135) provided chemical shift anisotropy data by multiple-quantum variable-angle spinning (MQVAS). CP provides information about connectivities.(136–139) REDOR(139–141) and heteronuclear chemical shift correlation (HETCOR)(138,142) were also applied in addition to MQMAS. The most difficult combination, DOR in addition to MQMAS, was presented by Samoson et al.(143,144) The advantage of multiple-quantum double-rotation (MQDOR) compared with MQMAS is that the need for simulations is avoided.(143) However, although in principle most informative, experimental difficulties and low multi-quantum conversion efficiency make the applicability of the MQDOR technique currently relatively limited.(144)

MQMAS NMR studies have been carried out on all half-integer quadrupolar spins from $I = \frac{3}{2}$ to $I = \frac{9}{2}$ [^{93}Nb(106)]. The nucleus ^{59}Co ($I = \frac{7}{2}$) in nitrogen compounds was studied to show the interplay between the chemical shift anisotropy and the quadrupolar interaction. However, the majority of the studies were focused on the two nuclei ^{27}Al ($I = \frac{5}{2}$) and ^{23}Na ($I = \frac{3}{2}$). Two examples are the study of the aluminum coordination in $SrAl_{12}O_{19}$ by Jansen et al.(145) and the study of sodium cations in dehydrated zeolites by Hunger et al.(146) Zeolites, zeolite-like materials and glasses(147,148) have been investigated in many studies.

7 NUTATION TECHNIQUE

Nutation NMR spectroscopy represents a 2-D experiment: a strong RF field is irradiated during the evolution period t_1, and the FID is observed during the detection period t_2. In the rotating frame, the spins *nutate* (precess) around the strong RF field with specific nutation frequencies w_1; here the subscript 1 denotes the frequency axis w_1 in the 2-D spectrum corresponding to the Fourier transform with respect to t_1 and should not be confused with $w_{\mathrm{rf}} = \gamma B_{\mathrm{rf}}$ which is a constant for the 2-D experiment. The original one-dimensional nutation experiment of Torrey(149) uses only one point of the FID.

Samoson and Lippmaa(150,151) introduced 2-D nutation NMR studies of half-integer quadrupolar nuclei. A corresponding one-dimensional experiment was performed by Fenzke et al.(152) For quadrupolar nuclei, the effective nutation frequencies w_1 depend on the strength of the quadrupolar interaction, as has been shown in section 3. If $w_Q \ll w_{\mathrm{rf}}$, then the transverse magnetization responds to the RF pulse like spin-$\frac{1}{2}$ nuclei, thus $w_1 = w_{\mathrm{rf}}$. If $w_Q \gg 10w_{\mathrm{rf}}$, the central transition can be treated as a two-level system and an effective nutation frequency is expected, that is, increased by a factor $I + \frac{1}{2}$, i.e. $w_1 = (I + \frac{1}{2})w_{\mathrm{rf}}$ (cf. Equation 39). For the intermediate case, $0.1 < w_Q/w_{\mathrm{rf}} < 100$, the nutation spectra are complicated because of the influence of the partly excited outer satellite transitions.

Nutation spectra can be calculated using numerical procedures or by means of an analytical description which is the more complicated the larger the spin quantum number. The powder average, which produces complicated nutation spectra, is necessary, in order to deduce quadrupolar parameters from the spectra and to compare the experimental spectrum with a set of calculated spectra. An analytical approach was found for $I = \frac{3}{2}$,(153–156) for $I = \frac{5}{2}$,(157,158) and for $I = \frac{7}{2}$(159,160) yielding $(I + \frac{1}{2})^2$ different nutation frequencies of the central transition. Each frequency gives rise to a powder pattern, and $2I$ of the $(I+\frac{1}{2})^2$ frequencies are dominant. Calculated line shapes of nutation spectra can be found in papers by Kentgens et al.(161,162) and in a review by Freude and Haase.(9) The latter reviews the quadrupolar nutation literature from 1983 to 1992 (about 40 papers), including experimental aspects such as inhomogeneity of the RF field, resonance offset, influence of MAS, spin–lattice relaxation, spin–spin relaxation in the rotating frame and some advanced concepts in nutation spectroscopy. Since 1993, another 15 papers were published, among them recent work about nutation MAS NMR by Ding and McDowell.(46,163)

The most advanced concept, the off-resonance nutation NMR of half-integer nuclei, was introduced by Kentgens.(164) The large resonance offset, $\nu_{\text{offset}} \gg \nu_{\text{rf}}$, during the irradiation causes an evolution of the spin system in the effective field, $\boldsymbol{B}_{\text{eff}} = \boldsymbol{B}_{\text{offset}} + \boldsymbol{B}_{\text{rf}}$, whereas the signal is as usually observed in resonance. The off-resonance technique extends the range of applicability at given $\boldsymbol{B}_0$ and $\boldsymbol{B}_{\text{rf}}$ to larger values of C_{qcc}. The acquisition of several spectra with different ν_{offset} improves the reliability of the fitting process, which is essential for obtaining information from nutation spectra. A loss of signal intensity due to the uninformative zero-frequency peak, which is typical for off-resonance irradiation, can be avoided by a soft selective pulse or by using an FSAHP (cf. section 3), for the preparation of the central transition magnetization only. A recent review including the perspectives of the nutation NMR of half-integer quadrupolar nuclei was given by Kentgens.(162) He proposed a combination of MQMAS, off-resonance nutation and echo techniques for sites with very large C_{qcc}.

8 ECHO TECHNIQUES

Echo techniques provide two data sets in the NMR time domain. First, the echo decay dependence on the time t_2 starting from zero at the maximum of the echo gives similar information to the initial FID after the preparation pulse, but the loss of signal during the ring down of the probe and the recovery of the receiver immediately after the pulse is overcome in the echo technique. Second, by varying the pulse distance t_1 between the preparation pulse and the refocusing second pulse, the resulting envelope of the echo decay gives additional information about the spin system. The refocusing effect of a second pulse after a preceding $\pi/2$ pulse for an interaction that is proportional to I_z is called the Hahn echo. The original experiment by Hahn(165) was performed with identical phase incoherent pulses in an inhomogeneous external magnetic field. The term Hahn echo is now in use for the spin-echo (after $\pi/2 - t_1 - \pi - t_1$) of spin-$\frac{1}{2}$ nuclei or of quadrupolar nuclei with half-integer spins, if the central transition is selectively excited.

However, the quadrupolar interaction strongly influences the formation of an echo: homonuclear dipolar interactions which mainly cause the decay of the spin-echo amplitude become less effective since spin-flipping between different transitions is forbidden. Owing to the nature of the quadrupolar coupling, which is to first order proportional to I_z^2, refocusing is not complete. Also, the limited range of excitation for very broad lines of powder samples causes complicated spin-echo behavior.

Echo studies on quadrupolar nuclei with half-integer spin (for integer spin, see section 9) were reviewed by Freude and Haase,(9) beginning with the pioneering work of Das and Saha(6) in 1955 up to the publications in 1993, e.g. Haase and Oldfield.(166) Several cases, which can be mainly divided into nonselective and selective excitation, were considered, as follows.(9)

Nonselective and hard pulses without dipole interaction cause several echoes at times $k \times t_1$ with $k = \frac{1}{2}, 1, \frac{3}{2}$ and $k = \frac{1}{2}, 1, \frac{3}{2}, 2, 3$ for $I = \frac{3}{2}$ and $I = \frac{5}{2}$, respectively. Some of these are forbidden echoes: $k = \frac{1}{2}, \frac{3}{2}$ and $k = \frac{3}{2}, 3$ for $I = \frac{3}{2}$ and $I = \frac{5}{2}$, respectively. On going from hard to soft pulses (cf. section 3), the influence of the quadrupolar interaction during the pulse has to be considered and the selection rule is changed. Then also the forbidden echoes can be observed. The consideration of dipole interaction for first-order quadrupolar echoes can be divided into two parts. First, the heteronuclear dipole interaction, which is proportional to I_zS_z, can generally be removed by the application of a second π-pulse. However, strong coupling among the S spins, and also a short spin–lattice relaxation time of the S spins, can destroy the formation of the I spin echo. Second, if the homonuclear dipolar interaction is large compared with the quadrupolar interaction, $\|\mathcal{H}_{\text{D}}\| \gg \|\mathcal{H}_{\text{Q}}\|$, its influence is essentially the same as for spin-$\frac{1}{2}$ nuclei. If the quadrupolar interaction is large compared with the dipolar interaction, $\|\mathcal{H}_{\text{Q}}\| \gg \|\mathcal{H}_{\text{D}}\|$, spin exchange due to homonuclear dipole interaction between adjacent levels can be considered as being suppressed completely and the echo decay can be investigated by selective excitation of each transition, separately.

$\|\mathcal{H}_{\text{Q}}\| \gg \|\mathcal{H}_{\text{rf}}\| \gg \|\mathcal{H}_{\text{D}}\|$ and $\|\mathcal{H}_{\text{Q}}\| \gg \|\mathcal{H}_{\text{rf}}\| \approx \|\mathcal{H}_{\text{D}}\|$ denote the cases of selective excitation of a single transition without and with dipole interaction, respectively. For powder we can mainly excite the central transition, and for single crystals we can tune to any transition and describe it by the reduced spin-$\frac{1}{2}$ formalism.(19) Without the dipole interaction an echo is observed at the time t_1 after the π pulse in full analogy with spin-$\frac{1}{2}$ nuclei subjected to an inhomogeneous interaction. Since the calculation of the spin-echo amplitude in the presence of dipolar interactions can be complicated, the spin-echo decay has been discussed by Haase and Oldfield(166) in terms of the second moment spin-echo decay (cf. section 5.2.5 in Freude and Haase(9)).

Echo techniques in combination with coherence selection (multiple-quantum filter) reduce the overlap of signals of quadrupolar nuclei in anisotropic soft matter, as demonstrated by Furo and Halle.(167,168) Recent progress in this field was presented by Eliav et al.(169–172) The use of echoes for the editing of ^{27}Al MAS NMR spectra of zeolite catalysts was shown by Schmitt et al.(173) The connection between all NMR interactions (except the homonuclear dipole interaction) and the optimum experimental conditions for the avoidance of spectral distortions was described by Dumazy et al.(174)

The leading authority in the field of quadrupolar echoes is Pascal Man, who has published more than 10 papers on this topic during the last decade. Most of them are discussed in recent publications.(175–177)

The CPMG(178,179) pulse sequence $\pi/2_x$, $(t_1, \pi_y, t_1)_n$ can be considered as an advanced concept of the Hahn echo. Larsen et al. reconsidered the quadrupolar version of CPMG (QCPMG) without MAS(180) and with MAS.(181) For MQMAS NMR and ^{2}H NMR, see sections 6 and 9, respectively. More than one order of magnitude can be gained in sensitivity by the application of this QCPMG technique.

9 ^{2}H NUCLEAR MAGNETIC RESONANCE SPECTROSCOPY

^{2}H is the most important NMR isotope with an integer nuclear spin $I = 1$, rather seldom ^{6}Li and ^{14}N NMR studies can be found in the literature. About 10% of the solid-state NMR studies of quadrupolar nuclei concern deuteron magnetic resonance spectroscopy, which is a powerful technique for investigating molecular structure and dynamics. This small section does not correspond to the importance of the deuterium NMR, especially for the study of dynamics. The textbook by Schmidt-Rohr and Spiess, *Multidimensional Solid-state NMR and Polymers*(18) and the reviews by Hoatson and Vold, '^{2}H-NMR Spectroscopy of Solids and Liquid Crystals',(11) and Ulrich and Grage, '^{2}H NMR (Solid-state NMR of Polymers)',(14) demonstrate the wealth of modern applications of solid-state ^{2}H NMR.

The experimental techniques for nuclei with the spin $I = 1$ are different to the techniques for nuclei having half-integer spins mainly for one reason, that no central transition exists. There are only two transitions for the magnetic quantum number m: $-1 \leftrightarrow 0$ and $0 \leftrightarrow 1$. They cause a line splitting that is symmetric with respect to the Larmor frequency if the quadrupolar interaction is considered in first-order perturbation theory with respect to the Zeeman interaction (cf. Equation 40). From Equation (41) it follows that the second-order shifts for both transitions are identical. Thus, the splitting between the two lines (difference frequency), which is the experimentally observed parameter in studies of single crystals, is not influenced by the second-order quadrupolar interaction.

Equations (40) and (41) can be used for nuclei with the spin $I = 1$, but the quadrupolar frequency should be substituted by the quadrupolar coupling constant using $\nu_Q = 3C_{qcc}/2$. The definition of the quadrupolar frequency for half-integer spins in Equations (25) and (26) is rather unusual for integer spins. The use of the quadrupolar coupling constant C_{qcc} after Equation (24) is commonly accepted, but for integer spins no notational consistency exists with respect to the quadrupolar frequency ν_Q.

The asymmetry parameter η (cf. Equations 19 and 20), is relatively small for the majority of the ^{2}H NMR studies due to a rotation symmetry of the hydrogen bonding. The theoretical powder line shape of nuclei with $I = 1$ and $\eta = 0$ is equal to the line shape of isolated pairs of nuclei with the spin $I = \frac{1}{2}$. Therefore, the typical ^{2}H NMR pattern of the so-called static powder (no sample rotation and no internal rotation) is often referred to as the Pake powder pattern. Pake in 1948 studied the ^{1}H NMR spectra of gypsum and discussed the angular dependence of the doublets in the spectra of a single crystal and the powder pattern in the spectrum of a powder sample as well.(182)

The splitting of lines of single crystals or the full width of powder patterns reach values up to 300 kHz. From $\delta\nu_{1/2} \approx 0.886/\tau$ (cf. Equations 32–34), it follows that a duration $\tau \leq 2\,\mu$s for the $\pi/2$ pulse is necessary, in order to obtain a quite uniform excitation of the whole spectrum. In addition to the need for high RF power, an echo pulse sequence must be applied in order to overcome the dead time problem of the receiver. A simple pulse sequence consisting of two $\pi/2$ pulses with a pulse duration of $2\,\mu$s and a pulse separation of $20\,\mu$s with phase cycling (the phase of the first pulse is cycled with respect to the synthesizer, and in addition the phase of the second pulse is cycled with respect to the first pulse) is the standard for solid-state ^{2}H NMR experiments. The pulse separation must be adjusted to one rotation period if MAS is applied. Hoatson discussed the broadband composite excitation sequences(183) and the Hadamard pulse excitation(184,185) for detecting quadrupolar order in ^{2}H NMR. Noise spectroscopy provides broad-bandwidth excitation with minimal applied RF field strengths. The state-of-the-art for applications to the ^{2}H solid-state NMR was described by Yang et al.(186,187) More detailed consideration of the quadrupolar echo in ^{2}H NMR can be found in the review by Hoatson and Vold,(11) Chapter 2.2, and the references therein. (The NMR echo for nuclei with half-integer spin is discussed in section 8 of this article.) The excitation with symmetric quadrupolar-shaped (SQUASH)(188) and time-asymmetric-shaped (QUASH) pulses(189) improves the excitation bandwidth.

Deuterium labels are introduced synthetically or by a postsynthesis treatment of the material. The labeled hydrogen segment can be investigated in terms of its specific structural and dynamic properties. The natural abundance of ^{2}H is only 150 ppm. The relative sensitivity of naturally abundant ^{2}H with respect to the ^{1}H NMR sensitivity at constant external field is only 1.5 ppm. Nevertheless, natural abundance high-resolution solid-state ^{2}H NMR investigations can be performed if MAS, high-power ^{1}H decoupling and ^{1}H–^{2}H CP are used.(190,191)

^{1}H–^{2}H CP effects in single- and double-quantum (DQ) transitions of the ^{2}H NMR were theoretically and experimentally investigated by Vega et al.(192) in 1980. There are two reasons why CP is rarely used in the solid-state ^{2}H NMR: the maximum increase in the ^{2}H NMR intensity due to the CP from ^{1}H spins is given by the gyromagnetic ratio $\gamma_H/\gamma_D \approx 6.5$ for infinitely diluted ^{2}H nuclei. This value decreases if the concentration of ^{2}H nuclei increases with the deuteron enrichment. However, the increasing level of deuteration increases the ^{2}H NMR intensity more effectively. The second point is that the high-power decoupling of the protons close to the deuterons causes some problems. However, ^{1}H–^{2}H CP is invaluable for the investigation of the interfaces of the deuterated segments, e.g. in polymer blends. Ba et al.(193) proposed a quadrupolar echo double resonance (QEDOR) and a solid echo double resonance (SOLEDOR) NMR experiment in order to provide information about deuteron–proton distances. A new theoretical model that describes CPMAS experiments for abundant $I = \frac{1}{2}$ spins coupled to a single spin $S = 1$ was presented by Marks et al.(194) Gan and Robyr(195) described a new 2-D CPMAS experiment with a three-pulse sequence for the determination of the relative orientation between ^{2}H quadrupolar coupling tensors.

The MAS technique for powder materials offers a more sensitive technique (compared with the quadrupolar echo technique) and the opportunity for an accurate measurement of the chemical shift.(196) A simple variation of the processing procedure of the FID, which is obtained in a one-pulse experiment, gives a 2-D spectrum with quadrupolar pattern in one dimension and the isotropic chemical shift in the other dimension.(197,198) The 2-D data set in the time domain can be constructed from the one-dimensional set, which should be acquired with a dwell time τ_{dwell} and a rotation frequency ν_{rot} in the order of magnitude of 1 µs and 5 kHz, respectively. $N = (2\nu_{rot}\tau_{dwell})^{-1}$ points with the time distance of $2\tau_{dwell}$ starting at the top of each rotational echo define the t_2 domain, and the increments of t_1 as the rotation period $1/\nu_{rot}$ give the t_1 domain. Spaniol et al.(199) recently used a 2-D ^{2}H MAS NMR experiment for the separation of paramagnetic and quadrupolar interactions.

Quadrupolar effects do not shift (or broaden in the case of powder) the signals arising from DQ transitions. Therefore, 2-D ^{2}H DQ NMR spectra provide information about the chemical shift of the deuterons.(200) Advantages of the MAS NMR technique compared with the DQ NMR technique are the higher sensitivity of the single-quantum compared with the DQ transition and the higher sensitivity of the MAS technique compared with the static echo technique. Multiple-quantum effects in combination with MAS are less often used for ^{2}H nuclei(201–203) compared with nuclei with half-integer spin (cf. section 6). Chandrakumar et al.(203) use a four-pulse experiment (QUADSHIFT) with a t_1 interval in the middle (which is incremented by the rotation period) in order to obtain chemical shift values and quadrupolar parameters from DQ coherences under MAS conditions [see also Chandrakumar(13)]. ^{2}H MAS NMR imaging experiments were described by Blümich.(185)

Deuterium NMR spectroscopy of single-crystal systems is an active field of research. The original approach of Volkoff et al.(4,5) is still in use, in order to obtain the quadrupolar parameters from the angular dependence of the line splitting, and new aspects were found and applied by Haeberlen et al.(204,205) The work up until 1994 is reviewed by Chandrakumar(13) and recent results are also available(204,205) The ordering behavior at the phase transition in single crystals of betaine phosphate and betaine phosphite has also been studied by one-dimensional and 2-D ^{2}H NMR.(206)

The majority of ^{2}H NMR studies concern molecular dynamics. Many polymer systems are studied, because ^{2}H NMR is ideally suited to explore molecular motions in polymers.(14) There is a wide range of timescales for the correlation times that are accessible by various methods: 10^2–10^{-4} s (2-D exchange spectroscopy), 10^2–10^{-5} s (selective inversion), 10^{-4}–10^{-8} s (line-shape analysis), 10^2–10^{-4} s (T_2 anisotropy), 10^{-8}–10^{-12} s (T_{1Z} anisotropy) and 10–10^{-12} s (T_{1Q} anisotropy).(11) For exchange spectroscopy we refer to the textbook by Schmidt-Rohr and Spiess.(18) The introduction of multi-dimensional exchange experiments by Spiess et al. gave rise to strong developments in this field. Kubo et al.(207) recently combined deuterium selective-excitation exchange spectroscopy with the Hadamard method for the measurement of reorientation rates. The technique of selective inversion is based on the selective excitation or the so-called hole burning that has been well known in NMR from the very beginning.(208) Recent applications to ^{2}H NMR have been reviewed by Hoatson and Vold.(11)

Table 5 Quadrupolar coupling constant $C_{qcc} = e^2qQ/h$, the asymmetry parameter η and the isotropic value of the chemical shift δ (referred to 1.0 M $AlCl_3\cdot 6H_2O$) for the ^{27}Al NMR of powder compounds at ambient temperature[a]

Compound	Site	C_{qcc} (MHz)	η	δ (ppm)	Refs.
Aluminates					
$CaO\cdot 6Al_2O_3$	AlO_4	2.0	$0_{assumed}$	65	261
	AlO_5	6.7	$0_{assumed}$	27.5	262
	AlO_6-I	1.5	$0_{assumed}$	9	261
	AlO_6-II	<1	$0_{assumed}$	16	261
$CaO\cdot 2Al_2O_3$	AlO_4-I	6.7	0.8	78	261
	AlO_4-II	13	0.1	~60	261
$CaO\cdot Al_2O_3$	AlO_4-I	2.7	0.85	80	261
	AlO_4-II	2.7	0.85	83	261
$4CaO\cdot 3Al_2O_3$	AlO_4	2.4	0.95	80	261
$12CaO\cdot 7Al_2O_3$	AlO_4-I	3.7	0.9	79	261
	AlO_4-II	11	0.2	85	263
$3CaO\cdot Al_2O_3$	AlO_4	9.7	0.3	85	263
	AlO_4-I	8.69	0.32	79.5	264
	AlO_4-II	9.3	0.54	78.25	264
$4CaO\cdot 3Al_2O_3\cdot 3H_2O$	AlO_4-I	1.8	0.5	78	261
	AlO_4-II	5.4	0.45	79	261
$KAlO_2$	AlO_4	1.1	0.7	76	263
$KAlO_2\cdot 0.5H_2O$	AlO_4	5.6	0.0	77	263
$KAlO_2\cdot H_2O$	AlO_4	6.5	0.6	83	263
$KAlO_2\cdot 1.5H_2O$	AlO_4	5.0	0.25	81	263
$5BaO\cdot Al_2O_3$	AlO_4	2.3	0.8	80	263
$BaO\cdot Al_2O_3$	AlO_4	2.4	0.4	78	263
$\alpha BaO\cdot Al_2O_3\cdot 2H_2O$	AlO_4-I	3.4	0.5	81	263
	AlO_4-II	5.1	0.9	80	263
α-$LiAlO_2$	AlO_6	2.8	0.05	16	265
β-$LiAlO_2$	AlO_4	1.8	0.55	82	265
	AlO_4	1.86	0.56	83.0	266
γ-$LiAlO_2$	AlO_4	3.2	0.7	81	265
β-$NaAlO_2$	AlO_4	1.4	0.5	80	263
α-Al_2O_3	AlO_6	2.40	0.01	18.8	267
γ-Al_2O_3	AlO_4	>5.0	~0	>67	268, 269
	AlO_6	4.5	~0	>9	268, 269
γ-Al_2O_3 (rehydrated)	AlO_4	5.1	–	71.5	270
	AlO_5	5.1	–	44.0	270
	AlO_6	3.55	–	10.0	270
κ-Al_2O_3	AlO_4	7.6	0.3	81.5	271
	AlO_6-(1)	5.0	–	ca. 13	271
	AlO_6-(4)	8.5	–	18	271
χ-Al_2O_3	AlO_4	5.0	0.3	71.5	272
	AlO_5	2.7	0.3	38.5	272
	AlO_6	4.5	0.3	11.5	272
$Cd_8(AlO_2)_{12}S_2$ (sodalite)	AlO_4	2.00	<0.1	80.4	273
$Ca_8(AlO_2)_{12}S_2$ (sodalite)	AlO_4	3.55	<0.1	79.1	273
$Cd_8(AlO_2)_{12}Se_2$ (sodalite)	AlO_4	3.95	<0.1	78.7	273
$Cd_8(AlO_2)_{12}(SO_4)_2$ (sodalite)	AlO_4	3.24	<0.1	79.1	273
$Sr_8(AlO_2)_{12}S_2$ (sodalite)	AlO_4	4.65	<0.1	76.9	273
$Sr_8(AlO_2)_{12}Se_2$ (sodalite)	AlO_4	5.10	<0.1	76.6	273
$Sr_8(AlO_2)_{12}(CrO_4)_2$ (sodalite)	AlO_4	6.75	<0.1	75.5	273
$SrAl_{12}O_{19}$	AlO_4	3.45	0.1	68.0	145
	AlO_5	2.1	0.7	18.0	145
	AlO_6-(1)	0.6	1	17.1	145
	AlO_6-(2)	1.3	1	9.6	145
	AlO_6-(3)	4.9	0.63	21.7	145
Alumoborates					
$2SrO\cdot Al_2O_3\cdot B_2O_3$	AlO_4	4.3	0.65	83.5	91
$2CaO\cdot Al_2O_3\cdot B_2O_3$	AlO_4	6.25	0.45	79.5	91

(*continued overleaf*)

Table 5 (*continued*)

Compound	Site	C_{qcc} (MHz)	η	δ (ppm)	Refs.
$2Li_2O{\cdot}Al_2O_3{\cdot}B_2O_3$	AlO_4	6.0	0.45	76	91
$3Li_2O{\cdot}Al_2O_3{\cdot}2B_2O_3$	AlO_4	6.7	0.83	70	91
$9Al_2O_3{\cdot}2B_2O_3$	AlO_4	6.8	0.1	53	91
	AlO_5	4.8	0.3	31	91
	AlO_6	6.2	0.4	10.5	91
Aluminumphosphates					
$AlPO_4$ (quartz)	AlO_4	4.2	0.35	44.8	274
$AlPO_4$ (tridimite)	AlO_4	0.75	0.95	39.8	274
$AlPO_4$ (cristobalite)	AlO_4	1.2	0.75	42.5	274
$Al_2PO_4(OH)_3$ (augelite)	AlO_5	5.5	0.78	30	275
	AlO_6	4.7	0.2	−3	275
$Al_2PO_4(OH)_3{\cdot}H_2O$ (senegalite)	AlO_5	2.87	0_{assumed}	30	275
	AlO_6	4.09	0_{assumed}	1.7	275
$KAlP_2O_7$	AlO_6	1.2	0.25	−16	276
$AlPO_4$-5 (molecular sieve)	AlO_4	2.3	0.95	40.4	274
$AlPO_4$-8 (dehydrated sieve)	AlO_4-(1)	3.9	0.5_{assumed}	40.1	84
	AlO_4-(2)	3.6	0.5_{assumed}	40.6	84
	AlO_4-(3)	3.6	0.5_{assumed}	47.0	84
	AlO_4-(4)	3.0	0.5_{assumed}	42.9	84
	AlO_4-(5)	3.4	0.5_{assumed}	42.6	84
$AlPO_4$-14 (molecular sieve)	AlO_4-(3)	1.75/1.74	0.70/0.63	43.2/42.9	83/277
	AlO_4-(2)	4.15/4.08	0.82/0.82	44.0/43.5	83/277
	AlO_5-(1)	5.66/5.58	0.89/0.97	27.2/27.1	83/277
	AlO_6-(4)	2.60/2.57	0.68/0.70	−0.9/−1.3	83/277
$AlPO_4$-21 (molecular sieve)	AlO_4	3.7	0.15	47.3	78
	AlO_5-I	5.9	0.68	14.6	78
	AlO_5-II	7.4	0.52	15.7	78
$AlPO_4$-25 (molecular sieve)	AlO_4-I	1.9	0.67_{assumed}	40.8	78
	AlO_4-II	0.8	0.67_{assumed}	39.5	78
$AlPO_4$-25 (dehydrated molecular sieve)	AlO_4-I	2.3	0.67_{assumed}	39.2	78
	AlO_4-II	1.1	0.67_{assumed}	37.5	78
Alumosilicates					
Al_2SiO_5 (sillimanite)	AlO_4	6.77	0.53	64.5	278
	AlO_6	8.93	0.46	4.0	278
Al_2SiO_5 (andalusite)	AlO_5	5.73	0.7	35	279
	AlO_6	15.5	0.0	10	279
Al_2SiO_5 (kyanite)	AlO_6-(1)	10.1	0.27	13.0	280
	AlO_6-(2)	3.8	0.85	4.0	280
	AlO_6-(3)	6.4	0.70	5.7	280
	AlO_6-(4)	9.2	0.38	5.9	280
Mullite ($\sim 3Al_2O_3{\cdot}1SiO_2$)	AlO_6	7.3	0	6.3	281
	AlO_4(T)	7.3	0	68	281
	AlO_4(T′)	6	0.5	53	281
	AlO_4(T*)	4	0.5	45	281
Pennine	AlO_4	2.8	–	72	278
	AlO_6	1.4	–	10	278
$KAlSi_2O_6$ (leucite)	T1-T3	2.1–2.3	0_{assumed}	61–69	282
$CaAl_2Si_2O_8$ (anorthite)	T1-T6	2.7–8.2	0.45–0.70	61–66	282
$KAl_2\{(OH,F)_2/AlSi_3O_{10}\}$	AlO_4	2.1	–	72	278
(muscovite)	AlO_6	2.2	–	5	278
$CaAl_2\{(OH)_2/Al_2Si_2O_{10}\}$	AlO_4	4.2	–	76	278
(margarite)	AlO_6	6.3	–	11	278
Xantophyllite	AlO_4	2.8	–	76	278
	AlO_6	2.0	–	11	278
$Na_8Al_2Be_2Si_8O_{24}Cl_2$ (tugtupide)	AlO_4	1.36	0.08	63.4	218

Table 5 (*continued*)

Compound	Site	C_{qcc} (MHz)	η	δ (ppm)	Refs.
$NaAlSi_3O_8$ (low albite)	AlO_4	3.29	0.62	62.7	283
$KAlSi_3O_8$ (microcline)	AlO_4	3.22	0.21	58.5	283
(Mg, Fe)Al_3SiBO_9 (grandidierite)	AlO_5	8.7	0.95	41.0	284
	AlO_6-(1)	3.5	0.5	9.0	284
	AlO_6-(2)	8.6	0.95	11.0	284
Natrolite	AlO_4	1.67	0.50	64	278
LiCl-sodalite	AlO_4	0.98	0.59	71.9	217
LiBr-sodalite	AlO_4	0.71	0.61	70.9	217
NaCl-sodalite	AlO_4	0.94	0.32	62.9	217
NaBr-sodalite	AlO_4	0.81	0.29	61.8	217
NaI-sodalite	AlO_4	0.57	0.34	60.4	217
Na-A, hydrated zeolite	AlO_4	1.1	0.75	59.2	278
Na-Y, hydrated zeolite	AlO_4	2.0	0.5	62.8	278
Na-Y, dehydrated zeolite	AlO_4	5.5	0.3	ca. 60	285
H-Y, dehydrated zeolite	AlO_3	13.1	0.75	105 ± 20	285
	AlO_3	13.5	0.4	–	286
	AlO_3	15.3	0.4	60	287
	AlO_4	6.0	0.7	–	286
H-Y, dealuminated, dehydr.	AlO_3	13.7	0.5	–	286
	AlO_4	7.0	0.7	–	286
USY	AlO_4	2.8	–	60.0	270
	AlO_5	4.1	–	34.5	270
	AlO_6	2.9	–	4.0	270
HMOR, dehydrated zeolite	AlO_3	15.0	0.35	–	286
	AlO_4	6.8	0.7	–	286
Na-ZSM-5, dehydrated zeolite	AlO_4	4.7	0.5	ca. 60	285
H-ZSM-5, dehydrated zeolite	AlO_3	16.0/15.5	0.1/0.5	82 ± 20/–	285/286
	AlO_4	7.3	0.7	–	286
H, Al-MCM-41 (as synthesized)	AlO_4	2.3	0_{assumed}	52.6	288
Fluoroaluminates					
$H_3AlF_6 \cdot 6H_2O$	AlF_6	0.3	0.0	−2.8	289
$K_2AlF_5 \cdot H_2O$	AlF_6	12	0.0	0	289
$Rb_2AlF_5 \cdot H_2O$	AlF_6	13	0.0	0	289
$CsAlF_5 \cdot H_2O$	AlF_6	7.5	0.15	−10	289
NH_4AlF_4	AlF_6	10	0.1	−6	289
$KAlF_4$	AlF_6	12	0.0	−5	289
$RbAlF_4$	AlF_6	13	0.1	−4	289
$Al_2SiO_4F_2$ (topas)	AlF_6	1.7	0.4	0.3	289
Others					
$Al(acac)_3$	AlO_6	3.03	0.15	0.0	290
$Al(trop)_3$		4.43	0.08	36.6	290
$Al(TMHD)_3$	AlO_6	3.23	0.10	1.5	290
$AlCl_3 \cdot 3Al(OH)_3 \cdot 6H_2O$	AlO_6	6.9	0.4	7	291
$AlCl_3 \cdot 4Al(OH)_3 \cdot 7H_2O$	AlO_6	5.7	0.7	3	291
$AlCl_3 \cdot OPCl_3$	$AlCl_3O$	6.0	0.15	88	292
$Al_2Ge_2O_7$	AlO_5	8.8	0.4	36	293
$AlLaGe_2O_7$	AlO_5	7.2	0.37	36	293
$Al_2(MoO_4)_3$	AlO_6-(1)	1.12	0.65	−12.4	272
	AlO_6-(2)	0.88	0.95	−13.4	272
	AlO_6-(3)	1.21	1.0	−10.3	272
	AlO_6-(1)	0.78	0.8	−11.1	272
$Al_2(OH)_2(H_2O)_8(SO_4)_2 \cdot 2H_2O$	AlO_6	4.6	0.4	3	291
$Al_2(OH)_4SO_4 \cdot 7H_2O$ (aluminite)	AlO_6-I	10.1	0.1	6.9	291
	AlO_6-II	11.6	0.15	6.4	291
$KAl(SO_4)_2 \cdot 12H_2O$	AlO_6	0.400	0.00	−4.1	266
$NH_4Al(SO_4)_2 \cdot 12H_2O$	AlO_6	0.456	0.00	−0.4	266

---

[a] The data published in 1983–92 were compiled by Dirk Müller.

Table 6 Quadrupolar coupling constant $C_{qcc} = e^2qQ/h$, the asymmetry parameter η and the isotropic value of the chemical shift δ (refered to 1.0 M NaCl) for the ^{23}Na NMR of powdered substances at ambient temperature[a]

Compound	Site	C_{qcc} (MHz)	η	δ (ppm)	Ref.
Sodium–nitrogen compounds					
$NaNO_3$		0.337	0.00	−8.0	266
$NaNO_2$		1.09	0.11	−0.1	266
NaN_3		0.297	0.12	−3.8	266
Aluminosilicates					
NaX (Si/Al = 1.0)	I	1.1	0.5	5.2*	294
	I′	5.8	0.0	−12.8*	294
	II	5.0	0.0	−8.8*	294
	III′(1,2)	2.2	0.7	−10.8*	294
	III′(3)	1.2	0.9	−22.8*	294
NaX (Si/Al = 1.23)	I	0.0	0.0	1.2*	74
	I′	5.2	0.0	−11.8*	74
	II	4.6	0.0	−7.8*	74
	III′(1,2)	2.6	0.7	−5.8*	74
	III′(3)	1.6	0.9	−21.8*	74
NaY (Si/Al = 2.5)	I	1.2	0_{assumed}	2.2*	146
	I′	4.8	0.0	3.2*	74
	II	3.9	0.0	−4.8*	74
EMT (Si/Al = 3.7)	I	1.0	0_{assumed}	0.7*	146
	I′ + II	4.1	0.3	0.2*	146
NaMOR (Si/Al = 7.1)	12-ring	2.0	0_{assumed}	−6.8*	146
	Sidepockets	3.1	0_{assumed}	−16.8*	146
NaZSM-5 (Si/Al = 18)		2.0	0_{assumed}	−10.8*	146
$NaAlSi_3O_8$ (albite)		2.69	0.25	−7.1	295
$Na_8Al_2Be_2Si_8O_{24}Cl_2$ (tugtupide)		1.41	0.44	7.7	218
Amphibole HSMC	M(4)	3.9	0.49	9.3	296
	A	2.9	0.26	5.5	296
NaCl-sodalite, dehydrated		0–0.5	–	−8.8	217
		~0	0.67_{assumed}	6.3	71
NaCl-sodalite, hydrated		≤0.1	–	–	297
NaBr-sodalite, dehydrated		0.72	0.12	−9.9	217
		1	0.67_{assumed}	8.5	71
NaBr-sodalite, hydrated		0.6–0.8	–	–	297
NaI-sodalite, dehydrated		1.73	0.06	−20.6	217
		1.9	0.67_{assumed}	9.3	71
NaI-sodalite, hydrated		1.5–1.8	0	–	297
Na-hydroxosodalite		2.00	0.10	3.2*	298
Na-nitride sodalite		1.00	0.18	0.4*	298
Silicates					
$Na_2H_2SiO_4{\cdot}8H_2O$		1.11	0.72	3.8*	298
$Na_2H_2SiO_4{\cdot}5H_2O$	I	1.35	0.45	5.7*	298
	II	2.01	0.70	0.0*	298
$Na_2H_2SiO_4{\cdot}4H_2O$	I	1.80	0.75	9.0*	298
	II	2.83	0.17	9.5*	298
Others					
NaOH		3.5	0.00	19.4*	298
$Na_3P_3O_9$	I	1.57	0.55	1.6*	298
	II	2.20	0.70	−7.6*	298
$Na_2(OOCCH)_2{\cdot}H_2O$	I	1.34	0.80	−2.2*	298
	II	0.80	0.75	0.9*	298
$Na_2C_2O_4$		2.50	0.74	17.9	266
$CH_3COONa{\cdot}3H_2O$		0.779	0.38	2.1	266
Na_2SO_4		2.60	0.58	−1.3*	298

[a] An asterisk denotes values of the chemical shift which were originally referred to solid NaCl and transformed by $\delta(1\text{ M NaCl}) = \delta(\text{solid NaCl}) + 7.2$ ppm. Zeolite samples listed in this table were dehydrated.

Table 7 Quadrupolar coupling constant $C_{qcc} = e^2qQ/h$, the asymmetry parameter η and the isotropic value of the chemical shift δ (referred to H_2O) for the ^{17}O NMR of powder compounds at ambient temperature[a]

Compound	Site	C_{qcc} (MHz)	η	δ (ppm)	Ref.
Aluminum oxides and hydroxides					
α-Al_2O_3 (corundum)	OAl_4	2.17	0.55	75	299
AlO(OH) (boehmite)	OAl_4	1.20	0.1	70	299
	OAl_4	1.15	0.13	70.0	266
	Al_2OH	5.0	0.5	40	299
$Al(OH)_3$ (bayerite)	Al_2OH	6.0	0.3	40	299
γ-Al_2O_3	OAl_4	1.8	$0_{assumed}$	73	299
η-Al_2O_3	OAl_4	1.6	$0_{assumed}$	73	299
δ-Al_2O_3	OAl_4	1.6	$0_{assumed}$	72	299
θ-Al_2O_3	OAl_4	1.2	$0_{assumed}$	72	299
	OAl_3	4.0	0.6	79	299
$Al_{13}O_{40}$ cluster	AlOAl	1.2	0	50	300
Microporous materials					
$AlPO_4$-5	AlOP	5.7	0.0	63	301
$AlPO_4$-11	AlOP	5.7	0.0	64	301
$AlPO_4$-17	AlOP	5.6	0.1	67	301
Ga-sodalite	SiOGa	4.0	0.3	29	301
	SiOSi	5.1	0.0	52	301
NaBa-Ga-sodalite	SiOGa	4.0	0.3	29	301
	SiOSi	5.1	0.0	52	301
Ga-X	SiOGa	4.0	0.3	28	301
	SiOSi	5.0	0.0	50	301
Na-Y	SiOAl	3.1	0.2	31	302
	SiOSi	4.6	0.2	46	302
Ba, Na-Y	SiOAl	3.4	0.2	45	302
	SiOSi	5.1	0.1	57	302
NH_4-Y	SiOAl	3.2	0.2	31	302
	SiOSi	5.0	0.1	47	302
Na-Y, dealuminated	SiOSi	5.2	0.1	47	302
Sil-Y, dehydrated	SiOSi O1	5.1	0.3	42.3	85
	SiOSi O4	5.28	0.2	34.8	85
	SiOSi O3	5.14	0.1	47.3	85
	SiOSi O2	5.39	0.2	37.2	85
Na-A, dehydrated	SiOAl	3.2	0.2	33	302
Na-A, hydrated	SiOAl O1	3.4	0	43.6	86
	SiOAl O3	3.4	0.25	40.5	86
	SiOAl O2	3.4	0	31.0	86
Na-LSX, hydrated	SiOAl O1	3.2	0.4	50.3	86
	SiOAl O3	3.4	0.3	45.0	86
	SiOAl O2	3.3	0.3	41.7	86
	SiOAl O4	3.6	0.15	36.9	86
Na-ZSM-5, hydrated	SiOSi	5.3	0.12	40.0	53
	SiOAl	3.5	0.29	30.0	53
Stilbite	SiOSi	5.1	0.18	43	303
	SiOAl	3.5	0.28	33	303
Silicates					
SiO_2 (low cristobalite)	SiOSi	5.3	0.0	46	302
SiO_2 (cristobalite)	SiOSi	5.3	0.125	40	304
SiO_2 (amorphous)	SiOSi	5.8	0.0	50	305
	SiOH	4.0	0.3	20	305
SiO_2 (stishovite)	SiOSi	6.5	0.125	109	306
SiO_2 (coesite)	SiOSi O5	5.16	0.292	58	307
	SiOSi O2	5.43	0.166	41	307
	SiOSi O3	5.45	0.168	57	307
	SiOSi O4	5.52	0.169	53	307
	SiOSi O1	6.05	0.000	29	307

(*continued overleaf*)

Table 7 (*continued*)

Compound	Site	C_{qcc} (MHz)	η	δ (ppm)	Ref.
Mg_2SiO_4 (forsterite)	SiOMg-I	2.35	0.2	61	308
	SiOMg-II	2.35	1.0	62	308
	SiOMg-III	2.70	0.3	47	308
	SiOMg-I	2.8	0_{assumed}	64	309
	SiOMg-II	3.3	0_{assumed}	72	309
	SiOMg-III	3.0	0_{assumed}	49	309
$MgSiO_3$ (clinoenstatite)	SiOMg-I	3.2	0.0	60	310
	SiOMg-II	3.2	0.0	42	310
	SiOSi	5.1	0.3	62	310
	SiO-?	2.9–5.2	0_{assumed}	57–70	309
$CaMgSi_2O_6$ (diopside)	SiOCa	2.7	0.0	84	310
	SiOMg	2.7	0.1	63	310
	SiOSi	4.4	0.3	69	310
	SiOCa	2.8	0_{assumed}	86	309
	SiOMg	2.7	0_{assumed}	64	309
	SiOSi	4.5	0_{assumed}	69	309
$Mg_3Si_4O_{10}(OH)_2$ (talc)	SiOMg	3.2	0.0	40	305
	SiOSi	5.8	0.0	50	305
	MgOH	7.3	0.0	0	305
$Li_2Si_2O_5$	br O1	5.6	0.55	108	311
	br O2	4.05	0.05	35	311
	nb O3	2.45	0.1	38	311
α-$Na_2Si_2O_5$	br O1	5.74	0.2	52	311
	br O2	4.67	0.3	74	311
	nb O3	2.4	0.2	36	311
$K_2Si_2O_5$	br O1	5.1	0.1	114	311
	br O2	4.7	0.2	69	311
	nb O3	2.1	0.5	72	311
$Rb_2Si_2O_5$	br O1	4.4	0.1	124	311
	br O2	4.7	0.5	59	311
	nb O3	1.9	0.5	93	311
$K_2Si_4O_9$ (wadeite)	br O1	4.45	0.35	62.5	306
	SiOSi O2	4.9	0.2	97	306
$BaSiO_3$	br O	3.7	0.4	87	310
α-$SrSiO_3$	br O	4.1	0.4	80	310
α-$CaSiO_3$	br O	3.8	0.2	75	310
$CaSiO_3$ (wollastonite)	SiO-?	2.3–4.7	0_{assumed}	115–167	309
Ca_2SiO_4 (larnite)	SiO-?	2.5–2.8	0_{assumed}	122–134	309
Na-ilerite (RUB-18)	SiOSi	5.1	0	42.6	312
	SiOH	3.1	0	61.2	312
Aluminosilicate glasses					
YAS	br O	3.1	–	54	313
	nb O			143	313
	nb O			210	313
LAS	br O	3.1	–	58	313
	nb O			178	313
$NaAlSi_3O_8$	SiOSi	5.1	0.15	49	314
	SiOAl	3.2	0.05	33	314
$NaAlSi_3O_8$	SiOSi	5.2	0.2	40	315
	SiOAl	3.8	0.2	25	315
Analcime	H_2O	7.6	0	18	316
Silicate glasses					
$Na_2Si_4O_9$	SiOSi	5.2	0.22	51	315
	nb O	2.7	0.25	40	315
	H_2O	6.0	0.7	20	315
$Na_2Si_2O_5$	br O	4.9	0.1	69	311
	nb O	2.35	0.2	37	311

Table 7 (*continued*)

Compound	Site	C_{qcc} (MHz)	η	δ (ppm)	Ref.
$Na_2Si_3O_7$	br O	5.0	0	60	306
	nb O	2.3	0	39	306
$Li_2Si_2O_5$	br O	5.0	0.15	68	311
	nb O	2.55	0.2	42	311
$K_2Si_2O_5$	br O	4.7	0.25	60	311
	nb O	2.5	0.45	84	311
$K_2Si_4O_9$	br O	4.9	0	52	306
	nb O	2.3	0	76	306
$Cs_2Si_2O_5$	br O	4.55	0.3	68	311
	nb O	3.1	0.55	145	311
Ba Si glass	br O	4.0	0.3	78	317
Ba Ca Si glass	br O	4.1	0.3	68	317
Ca Si glass	br O	4.7	0.3	59	317
	br O	4.6	0.0	66	318
	nb O	2.1	0.2	110	318
Na_2O–GeO_2 crystals and glasses					
GeO_2 (quartz)	GeO_4	7.3	0.48	70	319
GeO_2 (rutile)	GeO_6	7.5	0.10	160	319
Na_2GeO_3 (crystal)	GeO_4	5.2	0.5	70	319
	NBO	2.5	0.5	47	
$Na_2O{\cdot}9GeO_2$	GeO_4	7.0	0.5	165	319
	GeO_6				
2 $Na_2O{\cdot}9GeO_2$	GeO_4	6.0	0.5	80	319
Others					
TiO_2 (rutile)	TiOTi	1.5	0.87	596.5	249
$HfGeO_4$	HfOGe	5.2	0.65	185	320
$Mg(OH)_2$ (brucite)	MgOH	6.8	0	20	321
$Mg(OH)_2$ polycristalline	MgOH	6.8	0.0	25	305
$Mg(OH)_x(OCH_3)_{2-x}$	MgOH	7.25	0	−25	321
Hydroxyapatite $Ca_5(P^{17}O_4)_3(OH)$		4.0/4.1	0.0/0.1	108/115	322
$CaHP^{17}O_4{\cdot}2H_2O$		4.2/4.3	0/0	98/96	322
KH_2PO_4		5.2	0.55	92	322
$NH_4H_2PO_4$		5.1	0.55	93	322
$Ba(ClO_3)_2{\cdot}H_2{}^{17}O$	H_2O	6.8	1.00	22	322
$Ca(OH)_2$		6.5	0.00	62	322
$CaCO_3$		6.97	1	204	323

[a] The data published after 1989 were compiled by Ulf Pingel. A site nb O and br O denotes nonbridging and bridging oxygen, respectively.

If the quadrupolar echo decay $(\pi/2, t_1, \pi/2, t_1, t_2)$ is monitored as a 2-D data set, the doubly Fourier transformed 2-D spectrum can be influenced by a slow motion. Schleicher et al.(209) applied this technique for the observation of dynamics in alanine. Müller et al.(210) used a multiple-pulse quadrupolar echo sequence, in order to obtain information about the chemical exchange. For other examples, including the influence of dynamics on the longitudinal relaxation time in the Zeeman reservoir T_{1Z} or the relaxation time in the quadrupolar reservoir T_{1Q}, see Vold et al.(11,211)

Larsen et al.(212) applied the CPMG experiment to deuterons (^{2}H QCPMG) and thereby enhanced the sensitivity by about one order of magnitude and the dynamic range by two orders of magnitude.

Dynamic experiments were mainly performed with nonrotating samples. However, dynamic ^{2}H MAS NMR is now in progress. Weintraub and Vega(213) studied dimethyl sulfone by MAS and off-MAS techniques. Kristensen et al. investigated multiaxial dynamics(214) and effects of restricted rotational diffusion.(215)

10 SURVEY OF NUCLEAR MAGNETIC RESONANCE PARAMETERS FOR SELECTED COMPOUNDS

Collections of electric field gradient and chemical shift data for the most commonly studied quadrupolar nuclei with half-integer spins ^{27}Al, ^{23}Na and ^{17}O are presented in Tables 5, 6 and 7, respectively. For solid-state NMR studies of other quadrupolar nuclei we give only a few references to recent publications: lithium-6,(216) lithium-7,(74,217) beryllium-9,(218) boron-11,(219–221) nitrogen-14,(222) magnesium-25,(223) sulfur-33,(224,225) chlorine-35/37,(226) potassium-39,(227,228) calcium-43,(229–231) scandium-45,(232) titanium-47/49,(233,234) vanadium-51,(235,236) chromium-53,(237) cobalt-59,(236,238,239) copper-65,(240) zinc-67,(241,242) gallium-69/71,(243–245) bromine-81,(246) rubidium-85/87,(247,248) zirconium-91,(249) niobium-93,(33,249) molybdenum-95,(250) indium-115,(251) antimony-121,(252) iodine-127,(253,254) cesium-133,(255,256) barium-137,(257,258) lanthanum-139(73,259) and lutetium-175.(260)

ACKNOWLEDGMENTS

I am grateful to Jean-Paul Amoureux, Horst Ernst, Jürgen Haase, Michael Hunger, Christian Jäger, Dieter Michel, Toralf Mildner, Dirk Müller, Ulf Pingel, Dagmar Prager, Ago Samoson, Mark E. Smith, Daniel Prochnow, and Ingo Wolf for contributions and advice. This work was supported by the Deutsche Forschungsgemeinschaft, SFB 294, project Fr 902/9, and the Graduiertenkolleg Physikalische Chemie der Grenzflächen.

ABBREVIATIONS AND ACRONYMS

CP	Cross-polarization
CPMAS	Cross-polarization Magic-angle Spinning
CPMG	Carr–Purcell–Meiboom–Gill
DACSY	Dynamic-angle Correlation Spectroscopy
DAS	Dynamic-angle Spinning
DFS	Double-frequency Sweeps
DOR	Double-rotation
DQ	Double-quantum
FAM	Fast Radiofrequency Amplitude Modulation
FID	Free Induction Decay
FSAHP	Frequency-stepped Adiabatic Half-passage
fwhm	Full Width at Half-maximum
HETCOR	Heteronuclear Chemical Shift Correlation
LAB	Laboratory Axis System
MAS	Magic-angle Spinning
MQDOR	Multiple-quantum Double-rotation
MQMAS	Multiple-quantum Magic-angle Spinning
MQVAS	Multiple-quantum Variable-angle Spinning
NMR	Nuclear Magnetic Resonance
NQR	Nuclear Quadrupolar Resonance
PAS	Principal Axis System
QEDOR	Quadrupolar Echo Double Resonance
REDOR	Rotational-echo Double Resonance
RF	Radiofrequency
RIACT	Rotation-induced Adiabatic Coherence Transfer
SATRAS	Satellite-transition Spectroscopy
SOLEDOR	Solid Echo Double Resonance
TPPI	Time-proportional Phase Increment
TRAPDOR	Transfer-of-populations Double-resonance
VAS	Variable-angle Spinning
2-D	Two-dimensional
3QMAS	Triple-quantum Magic-angle Spinning

RELATED ARTICLES

Nuclear Magnetic Resonance and Electron Spin Resonance Spectroscopy **(Volume 13)**
Nuclear Magnetic Resonance and Electron Spin Resonance Spectroscopy: Introduction • Chemical Shifts in Nuclear Magnetic Resonance

Nuclear Magnetic Resonance and Electron Spin Resonance Spectroscopy cont'd **(Volume 14)**
Nuclear Magnetic Resonance Instrumentation • Parameters, Calculation of Nuclear Magnetic Resonance • Quadrupole Couplings in Nuclear Magnetic Resonance, General

REFERENCES

1. T. Vosegaard, E. Hald, V. Langer, H. Skov, P. Daugaard, H. Bildsoe, H. Jakobsen, 'Improved Hardware and Software for Single-crystal NMR Spectroscopy', *J. Magn. Reson.*, **135**, 126–132 (1998).
2. T. Vosegaard, E. Hald, P. Daugaard, H.J. Jakobsen, 'A Two-axis Goniometer for Sensitivity Enhancement in Single-crystal NMR Spectroscopy', *Rev. Sci. Instrum.*, **70**, 1771–1779 (1999).
3. O. Kanert, M. Mehring, 'Static Quadrupole Effects in Disordered Cubic Solids', *NMR Basic Principles Prog.*, **3**, 1–81 (1971).

4. B.V.G. Volkoff, H.E. Petch, D.W.I. Smellie, 'Nuclear Electric Quadrupole Interaction in Single Crystals', *Can. J. Phys.*, **30**, 270–289 (1952).
5. B.G.M. Volkoff, 'Second Order Nuclear Quadrupole Effects in Single Crystals', *Can. J. Phys.*, **31**, 820–836 (1953).
6. T.P. Das, A.K. Saha, 'Electric Quadrupole Interaction and Spin Echoes in Crystals', *Phys. Rev.*, **98**, 516–524 (1955).
7. M.H. Cohen, F. Reif, 'Quadrupole Effects in Nuclear Magnetic Resonance Studies of Solids', *Solid State Phys.*, **5**, 321–438 (1957).
8. H.W. Spiess, 'Deuteron NMR – A New Tool for Studying Chain Mobility and Orientation in Polymers', *Adv. Polym. Sci.*, **66**, 23–58 (1985).
9. D. Freude, J. Haase, 'Quadrupole Effects in Solid-state NMR', *NMR Basic Principles Prog.*, **29**, 1–90 (1993).
10. C. Jäger, 'Satellite Transition Spectroscopy of Quadrupolar Nuclei', *NMR Basic Principles Prog.*, **31**, 133–170 (1994).
11. G.L. Hoatson, R.L. Vold, '^{2}H-NMR Spectroscopy of Solids and Liquid Crystals', *NMR Basic Principles Prog.*, **32**, 1–67 (1994).
12. B.F. Chmelka, J.W. Zwanziger, 'Solid-state NMR Line Narrowing Methods for Quadrupole Nuclei – Double Rotation and Dynamic-angle Spinning', *NMR Basic Principles Prog.*, **33**, 79–124 (1994).
13. N. Chandrakumar, 'Spin-1 NMR', *NMR Basic Principles Prog.*, **34**, 1–117 (1996).
14. A.S. Ulrich, S.L. Grage, 'H-2 NMR (Solid-state NMR of Polymers)', *Stud. Phys. Theor. Chem.*, **84**, 190–211 (1998).
15. M.E. Smith, E.R.H. van Eck, 'Recent Advances in Experimental Solid State NMR Methodology for Half-integer Spin Quadrupole Nuclei [Review]', *Prog. Nucl. Magn. Reson. Spectrosc.*, **34**, 159–201 (1999).
16. H. Chihara, N. Nakamura, *Nuclear Quadrupole Resonance Spectroscopy Data, Landold-Börnstein, New Series, Group III*, Springer, Berlin, Vol. 20, 1988.
17. J. Mason, *Multinuclear NMR*, Plenum Press, New York, 1989.
18. K. Schmidt-Rohr, H.W. Spiess, *Multidimensional Solid-state NMR and Polymers*, Academic Press, London, 1994.
19. A. Abragam, *Principles of Nuclear Magnetism*, Oxford University Press, Oxford, 1961.
20. M. Weissbluth, *Atoms and Molecules*, Academic Press, New York, London, 1978.
21. Z.W. Zheng, Z.H. Gan, N.K. Sethi, D.W. Alderman, D.M. Grant, 'An Efficient Simulation of Variable-angle Spinning Lineshapes for the Quadrupole Nuclei with Half-integer Spin', *J. Magn. Reson.*, **95**, 509–522 (1991).
22. M.E. Rose, *Elementary Theory of Angular Momentum*, John Wiley, New York, 1967.
23. U. Haeberlen, *High Resolution NMR in Solids, Selective Averaging*, Academic Press, New York, 1976.
24. T.P. Das, E.L. Hahn, 'Nuclear Quadrupole Resonance Spectroscopy', *Solid State Phys., Suppl.*, **1**, 1–223 (1958).
25. L. Frydman, J.S. Harwood, 'Isotropic Spectra of Half-integer Quadrupole Spins from Bidimensional Magic-angle Spinning NMR', *J. Am. Chem. Soc.*, **117**, 5367–5368 (1995).
26. S. Wimperis, 'Broadband and Narrowband Composite Excitation Sequences', *J. Magn. Reson.*, **86**, 46–59 (1990).
27. A.P.M. Kentgens, 'Quantitative Excitation of Half-integer Quadrupole Nuclei by a Frequency-stepped Adiabatic Half-passage', *J. Magn. Reson.*, **95**, 619–625 (1991).
28. D.W. Sindorf, V.J. Bartuska, 'Wide-line NMR Spectroscopy in Solids Using Variable Frequency Pulses', *J. Magn. Reson.*, **85**, 581–585 (1989).
29. R.Q. Fu, V.L. Ermakov, G. Bodenhausen, 'Divergent Double Chirp Pulses for Refocusing Quadrupole Interactions', *Solid State NMR*, **7**, 1–10 (1996).
30. J. Haase, M.S. Conradi, 'Sensitivity Enhancement for NMR of the Central Transition of Quadrupole Nuclei', *Chem. Phys. Lett.*, **209**, 287–291 (1993).
31. J. Haase, E. Oldfield, 'Aluminum to Oxygen Cross-polarization in Alpha-Al_2O_3 (Corundum)', *Solid State NMR*, **3**, 171–175 (1994).
32. A.P.M. Kentgens, R. Verhagen, 'Advantages of Double Frequency Sweeps in Static, MAS and MQMAS NMR of Spin $I = \frac{3}{2}$ Nuclei', *Chem. Phys. Lett.*, **300**, 435–443 (1999).
33. A.F. McDowell, M.S. Conradi, J. Haase, 'First-satellite Spectroscopy, a New Method for Quadrupole Spins', *J. Magn. Reson. A*, **119**, 211–218 (1996).
34. J. Haase, N.J. Curro, R. Stern, C.P. Slichter, 'New Double Resonance Technique for Quadrupole Nuclei', *Mol. Phys.*, **95**, 891–896 (1998).
35. T. Gullion, 'Measurement of Dipolar Interactions Between Spin-$\frac{1}{2}$ and Quadrupole Nuclei by Rotational-echo, Adiabatic-passage, Double-resonance NMR', *Chem. Phys. Lett.*, **246**, 25–330 (1995).
36. T. Gullion, 'Introduction to Rotational-echo, Double Resonance NMR', *Concepts in Magn. Reson.*, **10**, 277–289 (1998).
37. C.P. Grey, W.S. Veeman, A.J. Vega, 'Referenz', *J. Chem. Phys.*, **98**, 7711 (1993).
38. S.R. Hartmann, E.L. Hahn, 'Nuclear Double Resonance in the Rotating Frame', *Phys. Rev.*, **128**, 2042–2053 (1962).
39. C.P. Slichter, *Principles of Magnetic Resonance*, Springer, Berlin, 1990.
40. S. Vega, 'Multiple-quantum Cross-polarization NMR on Spin Systems with $I = \frac{1}{2}$ and $S = \frac{3}{2}$ in Solids', *Phys. Rev. A*, **23**, 3152–3173 (1981).
41. A.J. Vega, 'CP/MAS of Quadrupole $S = \frac{3}{2}$ Nuclei', *Solid State NMR*, **1**, 17–32 (1992).
42. A.J. Vega, 'MAS NMR Spin Locking of Half-integer Quadrupole Nuclei', *J. Magn. Reson.*, **96**, 50–68 (1992).

43. S. Hayashi, K. Hayamizu., 'Line Shapes in CP/MAS NMR Spectra of Half-integer Quadrupole Nuclei', *Chem. Phys. Lett.*, **203**, 319–324 and **205**, 597 (1993).

44. S. Hayashi, 'MAS NMR of Half-integer Quadrupole Nuclei – Effect of Spin-locking Efficiency on Powder Lineshapes', *Solid State NMR*, **3**, 93–101 (1994).

45. S.W. Ding, C.A. McDowell, 'Theoretical Calculations of the CPMAS Spectral Lineshapes of Half-integer Quadrupole Systems', *J. Magn. Reson. A*, **114**, 80–87 (1995).

46. S.W. Ding, C.A. McDowell, 'Application of Floquet Theory to Quadrupole Nuclear Spin-$\frac{5}{2}$ Nuclei in Solids Undergoing Sample Rotation', *Mol. Phys.*, **95**, 841–848 (1998).

47. W. Sun, J.T. Stephen, L.D. Potter, Y. Wu, 'Rotation-induced Resonance and Second-order Quadrupole Effects on Spin Locking of Half-integer Quadrupole Nuclei', *J. Magn. Reson. A*, **116**, 181–188 (1995).

48. J.P. Amoureux, 'High-resolution Solid-state NMR for Spin $\frac{3}{2}$ and $\frac{9}{2}$: The Multi-quantum Transitions Method', *Solid State NMR*, **2**, 83–88 (1993).

49. K. Narita, J.J. Umeda, H. Kusumoto, 'NMR Powder Patterns of the Second-order Nuclear-Quadrupole Interaction on the Central Line in Solids with Asymmetric Field Gradient', *J. Chem. Phys.*, **44**, 2719–2723 (1966).

50. D. Müller, 'Zur Bestimmung Chemischer Verschiebungen der NMR-Frequenzen bei Quadrupolkernen aus den MAS NMR-Spektren', *Ann. Phys.*, **39**, 451–460 (1982).

51. A. Samoson, 'Satellite Transition High-resolution NMR of Quadrupole Nuclei in Powders', *Chem. Phys. Lett.*, **119**, 29–32 (1985).

52. H.J. Jakobsen, J. Skibsted, H. Bildsoe, N.C. Nielsen, 'Magic-angle Spinning NMR Spectra of Satellite Transitions for Quadrupole Nuclei in Solids', *J. Magn. Reson.*, **85**, 173–180 (1989).

53. J.-P. Amoureux, F. Bauer, H. Ernst, C. Fernandez, D. Freude, D. Michel, U.-T. Pingel, 'O-17 Multiple-quantum and ^{1}H MAS NMR Studies of Zeolite ZSM-5', *Chem. Phys. Lett.*, **285**, 10–14 (1998).

54. A. Samoson, E. Lippmaa, A. Pines, 'High Resolution Solid State NMR Averaging of Second-order Effects by Means of a Double-rotor', *Mol. Phys.*, **65**, 1013–1018 (1988).

55. Y. Wu, B.Q. Sun, A. Pines, A. Samoson, E. Lippmaa, 'NMR Experiments with a New Double Rotor', *J. Magn. Reson.*, **89**, 297–309 (1990).

56. A. Samoson, E. Lippmaa, 'Synchronized Double-rotation NMR Spectroscopy', *J. Magn. Reson.*, **84**, 410–416 (1989).

57. A. Samoson, J. Tegenfeldt, 'Suppression of DOR Sidebands', *J. Magn. Reson. A*, **110**, 238–244 (1994).

58. D. Kuwahara, T. Nakai, 'Spinning-sideband Suppression in DOR NMR Spectra Using a Magic-angle-turning Technique', *Chem. Phys. Lett.*, **260**, 249–252 (1996).

59. B.Q. Sun, J.H. Baltisberger, Y. Wu, A. Samoson, A. Pines, 'Sidebands in Dynamic Angle Spinning (DAS) and Double Rotation (DOR) NMR', *Solid State NMR*, **1**, 267–295 (1992).

60. E. Cochon, J.P. Amoureux, 'Sideband Analysis in DOR NMR Spectra. 1. 'Infinite' Inner-rotor Speed', *Solid State NMR*, **2**, 205–222 (1993).

61. J.P. Amoureux, E. Cochon, 'Sideband Analysis in DOR NMR Spectra. 2. Real Finite Inner-rotor Speed', *Solid State NMR*, **2**, 223–234 (1993).

62. A. Samoson, A. Pines, 'Double Rotor for Solid-state NMR', *Rev. Sci. Instrum.*, **60**, 3239–3241 (1989).

63. D. Müller, M. Smith, L. Wunsch, 'NMR at More Than One Magic Angle', Bruker Report, Bruker, Karlsruhe, 31–32, 1990.

64. B.F. Chmelka, K.T. Mueller, A. Pines, J. Stebbins, Y. Wu, J.W. Zwanziger, 'Oxygen-17 NMR in Solids by Dynamic-angle Spinning and Double Rotation', *Nature*, **339**, 42–43 (1989).

65. K.T. Mueller, Y. Wu, B.F. Chmelka, J. Stebbins, A. Pines, 'High-resolution Oxygen-17 NMR of Solid Silicates', *J.Am. Chem. Soc.*, **113**, 32–38 (1991).

66. R. Jelinek, B.F. Chmelka, Y. Wu, M.E. Davis, J.G. Ulan, R. Gronsky, A. Pines, 'Adsorption Effects in Aluminophosphate Molecular Sieves Studied by Al-27 Double-rotation NMR', *Catal. Lett.*, **15**, 65–73 (1992).

67. G.J. Ray, A. Samoson, 'Double Rotation and Variable Field Al-27 NMR Study of Dealuminated Y-Zeolites', *Zeolites*, **13**, 410–413 (1993).

68. M. Hunger, G. Engelhardt, H. Koller, J. Weitkamp, 'Characterization of Sodium Cations in Dehydrated Faujasites and Zeolite EMT by Na-23 DOR, 2D-Nutation, and MAS NMR', *Solid State NMR*, **2**, 111–120 (1993).

69. H.A.M. Verhulst, W.J.J. Welters, G. Vorbeck, L.J.M. Vandeven, V.H.J. Debeer, R.A. Vansanten, J.W. Dehaan, 'New Assignment of the Signals in Na-23 DOR NMR to Sodium Sites in Dehydrated NaY Zeolite', *J. Phys. Chem.*, **98**, 7056–7062 (1994).

70. G.W. Haddix, M. Narayana, S.C. Tang, Y. Wu, 'Double-rotation NMR, Magic Angle Spinning NMR, and X-ray Diffraction Study of the Structure of Aluminum Molybdate', *J. Phys. Chem.*, **97**, 4624–4627 (1993).

71. R. Jelinek, S. Özkar, G.A. Ozin., 'Extraframework Sodium Cation Sites in Sodium Zeolite Y Probed by 23-Na Double-rotation NMR', *J. Am. Chem. Soc.*, **114**, 4907–4908 (1992).

72. R. Jelinek, S. Ozkar, G.A. Ozin, 'Intrazeolite Topotaxy – Na-23 Double-rotation NMR Study of Transition-metal Hexacarbonyls and Oxides Encapsulated in Sodium Zeolite-Y', *J. Phys. Chem.*, **96**, 5949–5953 (1992).

73. M. Hunger, G. Engelhardt, J. Weitkamp, 'Solid-state Na-23, La-139, Al-27 and Si-29 NMR Spectroscopic Investigations of Cation Location and Migration in

Zeolites LaNaY', *Microporous Mater.*, **3**, 497–510 (1995).

74. M. Feuerstein, M. Hunger, G. Engelhardt, J. Amoureux, 'Characterisation of Sodium Cations in Dehydrated Zeolite NaX by Na-23 NMR Spectroscopy', *Solid State NMR*, **7**, 95–103 (1996).
75. H. Koller, E. Meijer, R. Vansanten, 'Al-27 Quadrupole Interaction in Zeolites Loaded with Probe Molecules – A Quantum-chemical Study of Trends in Electric Field Gradients and Chemical Bonds in Clusters', *Solid State NMR*, **9**, 165–175 (1997).
76. Y. Wu, B. Chmelka, A. Pines, M.E. Davis, P.J. Grobet, P.A. Jacobs, 'High-resolution Al-27 NMR Spectroscopy for the Aluminophosphate Molecular Sieve VPI-5', *Nature*, **346**, 550–552 (1990).
77. P.J. Grobet, A. Samoson, H. Geerts, J.A. Martens, P.A. Jacobs, 'Crystallographic Site Discrimination in Aluminophosphate Molecular Sieves by Solid-state NMR – Influence of the Field-dependent Isotropic 2nd-order Quadrupole Shift', *J. Phys. Chem.*, **95**, 9620–9622 (1991).
78. R. Jelinek, B.F. Chmelka, Y. Wu, P.J. Grandinetti, A. Pines, P.J. Barrie, J. Klinowski, 'Study of the Aluminophosphates $AlPO_4$-21 and $AlPO_4$-25 by ^{27}Al Double-rotation NMR', *J. Am. Chem. Soc.*, **113**, 4097–4101 (1991).
79. Y. Wu, D. Lewis, J.S. Frye, A.R. Palmer, R.A. Wind, 'Cross-polarization Double-rotation NMR', *J. Magn. Reson.*, **100**, 425–430 (1992).
80. J. Jänchen, M.P.J. Peeters, J.W. Dehaan, L.J.M. Vandeven, J.H.C. Vanhooff, I. Girnus, U. Lohse, 'Adsorption Calorimetric Measurements and Al-27 DOR NMR Studies on the Molecular Sieve $AlPO_4$-18', *J. Phys. Chem.*, **97**, 12042–12046 (1993).
81. G.J. Kennedy, J.B. Higgins, C.F. Ridenour, H.X. Li, M.E. Davis, 'Multifield MAS and DOR NMR Studies of a Hydrated Aluminophosphate Molecular Sieve – $AlPO_4$-H_2', *Solid State NMR*, **4**, 173–178 (1995).
82. M. Kovalakova, P. Grobet, 'Double Rotation Al-27 NMR in Molecular Sieves', *Appl. Magn. Reson.*, **10**, 447–476 (1996).
83. C.A. Fyfe, H.M.Z. Altenschildesche, K.C. Wong-Moon, H. Grondey, J.M. Chezeau, '1D and 2D Solid State NMR Investigations of the Framework Structure of As-synthesized $AlPO_4$-14', *Solid State NMR*, **9**, 97–106 (1997).
84. M. Kovalakova, P. Grobet, 'The Al-27 DOR NMR Characterization of the Molecular Sieve $AlPO_4$-8', *Solid State NMR*, **9**, 107–113 (1997).
85. L. Bull, A. Cheetham, T. Anupold, A. Reinhold, A. Samoson, J. Sauer, B. Bussemer, Y. Lee, S. Gann, J. Shore, A. Pines, R. Dupree, 'A High-resolution O-17 NMR Study of Siliceous Zeolite Faujasite', *J. Am. Chem. Soc.*, **120**, 3510–3511 (1998).
86. U.T. Pingel, J.P. Amoureux, T. Anupold, F. Bauer, H. Ernst, C. Fernandez, D. Freude, A. Samoson, 'High-field O-17 NMR Studies of the SiOAl Bond in Solids', *Chem. Phys. Lett.*, **194**, 345–350 (1998).
87. C. Rohrig, I. Dierdorf, H. Gies, 'X-ray Powder Diffraction and NMR-spectroscopic Investigations on a Porous Zincosilicate Related to the Zeolite VPI-7 (VSV)', *J. Phys. Chem. Solids.*, **56**, 1369–1376 (1995).
88. R. Jelinek, B.F. Chmelka, A. Stein, G.A. Ozin, 'Multinuclear Magic-angle Spinning and Double-rotation NMR Study of the Synthesis and Assembly of a Sodalite Semiconductor Supralattice', *J. Phys. Chem.*, **96**, 6744–6752 (1992).
89. G. Engelhardt, P. Sieger, J. Felsche, 'Multinuclear Solid State NMR of Host–Guest Systems with TO_2 (T = Si, Al) Host-frameworks – A Case Study on Sodalites', *Anal. Chim. Acta*, **283**, 967–985 (1993).
90. T.J. Bastow, J.S. Hall, M.E. Smith, S. Steuernagel, 'Characterisation of Hydrated Aluminas by MAS and DOR Al-27 NMR', *Mater. Lett.*, **18**, 197–200 (1994).
91. D. Massiot, D. Müller, T. Hubert, M. Schneider, A.P.M. Kentgens, B. Cote, J.P. Coutures, W. Gessner, 'Double Rotation and Magic-angle Spinning Nuclear Magnetic Resonance Study of Al-27: Reexamination of the Aluminum Borate $9Al_2O_3{\cdot}2B_2O_3$', *Solid State NMR*, **5**, 175–180 (1995).
92. F. Taulelle, A. Samoson, T. Loiseau, G. Ferey, 'ULM-18, a Fluorinated Gallium Phosphate with Perforated Layers: XRD and NMR, Structure Determination, and HF Localization in a D4R', *J. Phys. Chem. B*, **102**, 8588–8598 (1998).
93. G. Jeschke, 'Spin Locking of $I = \frac{3}{2}$ Nuclei in Static and Spinning Samples – A Description by Abstract Spins and Floquet Formalism', *J. Chem. Phys.*, **108**, 907–917 (1998).
94. J.P. Amoureux, 'Variable-angle Double Rotation Technique: A New Two-dimensional High-resolution Technique for Quadrupole Nuclei', *Solid State NMR*, **4**, 229–239 (1995).
95. A. Llor, J. Virlet, 'Towards High-resolution NMR of More Nuclei in Solids: Sample Spinning with Time-dependent Spinner Axis Angle', *Chem. Phys. Lett.*, **152**, 248–253 (1988).
96. K.T. Mueller, E.W. Wooten, A. Pines, 'Pure-absorption-phase Dynamic-angle Spinning', *J. Magn. Reson.*, **92**, 620–627 (1991).
97. P.J. Grandinetti, J.H. Baltisberger, A. Llor, Y.K. Lee, U. Werner, M.A. Eastman, A. Pines, 'Pure-absorption-mode Lineshapes and Sensitivity in 2-Dimensional Dynamic-angle Spinning NMR', *J. Magn. Reson. A*, **103**, 72–81 (1993).
98. P.J. Grandinetti, Y.K. Lee, J.H. Baltisberger, B.Q. Sun, A. Pines, 'Sideband Patterns in Dynamic-angle-spinning NMR', *J. Magn. Reson. A*, **102**, 195–204 (1993).
99. C.A. Fyfe, K.C. Wongmoon, H. Grondey, K.T. Mueller, 'Increased Efficiency of Coherence Transfer in Cross-polarization NMR from Quadrupole

Nuclei – Dynamic-angle Cross-polarization', *J. Phys. Chem.*, **98**, 2139–2142 (1994).

100. T.P. Jarvie, R.M. Wenslow, K.T. Mueller, 'High-resolution Solid-state Heteronuclear Correlation NMR for Quadrupolar and Spin-$\frac{1}{2}$ Nuclei', *J. Am. Chem. Soc.*, **117**, 570–571 (1995).
101. R.M. Wenslow, K.T. Mueller, 'Cation Sites in Mixed-alkali Phosphate Glasses', *J. Non-Cryst. Solids*, **231**, 78–88 (1998).
102. A. Medek, J.R. Sachleben, P. Beverwyk, L. Frydman, 'Multi-rank Nuclear Magnetic Resonance Studies of Half-integer Quadrupole Nuclei in Solids by Three-dimensional Dynamic-angle Correlation Spectroscopy', *J. Chem. Phys.*, **104**, 5374–5382 (1996).
103. C. Fernandez, J.P. Amoureux, 'Triple-quantum MAS-NMR of Quadrupole Nuclei', *Solid State NMR*, **5**, 315–321 (1996).
104. S.P. Brown, S. Wimperis, 'Two-dimensional Multiple-quantum MAS NMR of Quadrupole Nuclei: A Comparison of Methods', *J. Magn. Reson.*, **128**, 42–61 (1997).
105. J.P. Amoureux, C. Fernandez, S. Steuernagel, 'Z Filtering in MQMAS NMR', *J. Magn. Reson. A*, **123**, 116–118 (1996).
106. J.P. Amoureux, C. Fernandez, L. Frydman, 'Optimized Multiple-quantum Magic-angle Spinning NMR Experiments on Half-integer Quadrupoles', *Chem. Phys. Lett.*, **259**, 347–355 (1996).
107. J.P. Amoureux, C. Fernandez, Y. Dumazy, 'A Useful Tool for the Elaboration of New Solid-state NMR Experiments: PULSAR', *J. Chim. Phys.*, **92**, 1939–1942 (1995).
108. J.P. Amoureux, C. Fernandez, 'Triple, Quintuple and Higher Orders Multiple Quantum MAS NMR of Quadrupole Nuclei', *Solid State NMR*, **10**, 211–224 (1998).
109. G. Wu, D. Rovnyak, R.G. Griffin, 'Quantitative Multiple-quantum Magic-angle-spinning NMR Spectroscopy of Quadrupole Nuclei in Solids', *J. Am. Chem. Soc.*, **118**, 9326–9332 (1996).
110. K.H. Lim, C.P. Grey, 'Analysis of the Anisotropic Dimension in the RIACT (II) Multiple Quantum MAS NMR Experiment for $I = \frac{3}{2}$ Nuclei', *Solid State NMR*, **13**, 101–112 (1998).
111. T. Mildner, M.E. Smith, R. Dupree, 'Rotationally Induced Triple Quantum Coherence Excitation in MAS NMR Spectroscopy of $I = \frac{5}{2}$ Spins', *Chem. Phys. Lett.*, **301**, 389–394 (1999).
112. S. Ding, C.A. McDowell, 'Shaped Pulse Excitation in Multi-quantum Magic-angle Spinning Spectroscopy of Half-integer Quadrupole Spin Systems', *Chem. Phys. Lett.*, **270**, 81–86 (1997).
113. S.W. Ding, C.A. McDowell, 'Multiple-quantum MAS NMR Spectroscopy of Spin-$\frac{3}{2}$ Quadrupole Spin Systems Using Shaped Pulses', *J. Magn. Reson.*, **135**, 61–69 (1998).
114. L. Marinelli, A. Medek, L. Frydman, 'Composite Pulse Excitation Schemes for MQMAS NMR of Half-integer Quadrupole Spins', *J. Magn. Reson.*, **132**, 88–95 (1998).
115. A. Goldbourt, P.K. Madhu, L. Frydman, S. Vega, 'Fast RF Amplitude Modulation in MQMAS NMR Spectroscopy', in *Abstracts of the 41st Rocky Mountain Conference*, 97–98, 1999.
116. J. Rocha, 'Direct Observation of Highly Distorted Hexacoordinated Aluminum in Andalusite by Very Fast Al-27 MAS NMR', *Chem. Commun.*, 2489 (1998).
117. D. Massiot, B. Touzo, D. Trumeau, J.P. Coutures, J. Virlet, P. Florian, P.J. Grandinetti, 'Two-dimensional Magic-angle Spinning Isotropic Reconstruction Sequences for Quadrupole Nuclei', *Solid State NMR*, **6**, 73–83 (1996).
118. R.R. Ernst, G. Bodenhausen, A. Wokaun, *Principles of Nuclear Magnetic Resonance in One and Two Dimensions*, Oxford University Press, London, 1987.
119. C.A. Fyfe, J. Skibsted, H. Grondey, H. Meyer zu Altenschildesche, 'Pulsed Field Gradient Multiple-quantum MAS NMR Spectroscopy of Half-integer Spin Quadrupolar Nuclei', *Chem. Phys. Lett.*, **281**, 44–48 (1997).
120. S.P. Brown, S.J. Heyes, S. Wimperis, 'Two-dimensional MAS Multiple-quantum NMR of Quadrupole Nuclei, Removal of Inhomogeneous Second-order Broadening', *J. Magn. Reson. A*, **119**, 280–284 (1996).
121. S.P. Brown, S.E. Ashbrook, S. Wimperis, 'Al-27 Multiple-quantum Magic Angle Spinning NMR Study of the Thermal Transformation Between the Microporous Aluminum Methylphosphonates AlMePO-beta and AlMePO-alpha', *J. Phys. Chem. B*, **103**, 812–817 (1999).
122. L. Delevoye, 'Quantification des Spectres MQMAS et Application a l'Etude des Materiaux Microporeux', Thesis, Lille, 1988.
123. P.P. Man, 'Scaling and Labeling the High-resolution Isotropic Axis of Two-dimensional Multiple-quantum Magic-angle-spinning Spectra of Half-integer Quadrupole Spins', *Phys. Rev. B*, **58**, 2764 (1998).
124. G. Wu, R.E. Wasylishen, 'The Influence of the Heteronuclear Dipolar Interaction on NMR Spectra of Quadrupole Nuclei', *Mol. Phys.*, **95**, 1177–1183 (1998).
125. U. Friedrich, I. Schnell, S.P. Brown, A. Lupulescu, D.E. Demco, H.W. Spiess, 'Spinning-sideband Patterns in Multiple-quantum Magic-angle Spinning NMR Spectroscopy', *Mol. Phys.*, **95**, 1209–1227 (1998).
126. L. Marinelli, L. Frydman, 'On the Origin of Spinning Side Bands in MQMAS NMR Experiments', *Chem. Phys. Lett.*, **275**, 188–198 (1997).
127. T. Charpentier, C. Fermon, J. Virlet, 'Efficient Time Propagation Technique for MAS NMR Simulation – Application to Quadrupole Nuclei', *J. Magn. Reson.*, **132**, 181–190 (1998).
128. T. Charpentier, C. Fermon, J. Virlet, 'Numerical and Theoretical Analysis of Multiquantum Magic-angle

Spinning Experiments', *J. Chem. Phys.*, **109**, 3116–3130 (1998).

129. J.P. Amoureux, M. Pruski, D.P. Lang, C. Fernandez, 'The Effect of RF Power and Spinning Speed on MQMAS NMR', *J. Magn. Reson.*, **131**, 170–175 (1998).
130. D. Massiot, 'Sensitivity and Lineshape Improvements of MQMAS by Rotor-synchronized Data Acquisition', *J. Magn. Reson. A*, **122**, 240–244 (1996).
131. T. Vosegaard, F.H. Larsen, H.J. Jakobsen, P.D. Ellis, N.C. Nielsen, 'Sensitivity-enhanced Multiple-quantum MAS NMR of Half-integer Quadrupole Nuclei', *J. Am. Chem. Soc.*, **119**, 9055–9056 (1997).
132. G. Wu, D. Rovnyank, B. Sun, R.G. Griffin, 'High-resolution Multiple Quantum MAS NMR Spectroscopy of Half-integer Quadrupole Nuclei', *Chem. Phys. Lett.*, **249**, 210–217 (1996).
133. M. Hanaya, R.K. Harris, 'Effect of ^{1}H-decoupling in Two-dimensional Multiple-quantum MAS NMR Spectroscopy of Na-23 in a Hydrous Layered Silicate', *Solid State NMR*, **8**, 147–151 (1997).
134. V. Lacassagne, P. Florian, V. Montoullout, C. Gervais, F. Babonneau, D. Massiot, 'Resolution Enhancement in Solid-state MQMAS Experiments Achieved by Composite Decoupling', *Magn. Reson. Chem.*, **36**, 956–959 (1998).
135. S.H. Wang, Z. Xu, J.H. Baltisberger, L.M. Bull, J.F. Stebbins, A. Pines, 'Multiple-quantum Magic-angle Spinning and Dynamic-angle Spinning NMR Spectroscopy of Quadrupolar Nuclei', *Solid State NMR*, **8**, 1–16 (1997).
136. M. Pruski, D.P. Lang, C. Fernandez, J.P. Amoureux, 'Multiple-quantum Magic-angle Spinning NMR with Cross-polarization: Spectral Editing of High-resolution Spectra of Quadrupole Nuclei', *Solid State NMR*, **7**, 327–331 (1997).
137. C. Fernandez, L. Delevoye, J.P. Amoureux, '^{27}Al{^{1}H} Cross Polarization Triple Quantum Magic Angle Spinning NMR', *J. Am. Chem. Soc.*, **119**, 6858–6862 (1997).
138. S.H. Wang, S.M. De Paul, L.M. Bull, 'High-resolution Heteronuclear Correlation Between Quadrupole and Spin-$\frac{1}{2}$ Nuclei Using Multiple-quantum Magic-angle Spinning', *J. Magn. Reson.*, **125**, 364–368 (1997).
139. C. Magnenet, D. Massiot, I. Klur, J.P. Coutures, 'Characterization of TiO_2 pigments by Al-27 NMR', *J. Chim. Phys.*, **95**, 310–316 (1998).
140. C. Fernandez, D.P. Lang, J.P. Amoureux, M. Pruski, 'Measurement of Heteronuclear Dipolar Interactions Between Quadrupole and Spin-$\frac{1}{2}$ Nuclei in Solids by Multiple-quantum REDOR NMR', *J. Am. Chem. Soc.*, **120**, 2672–2673 (1998).
141. M. Pruski, C. Fernandez, D.P. Lang, J.P. Amoureux, 'Measurement of Interatomic Connectivities in Molecular Sieves Using MQMAS-based Methods', *Catal. Today*, **10**, 401–409 (1999).
142. S. Steuernagel, 'A New Sequence for the MQMAS/HETCOR Experiment', *Solid State NMR*, **11**, 197–201 (1998).
143. A. Samoson, 'Two-dimensional Isotropic NMR of Quadrupole Nuclei in Solids', *J. Magn. Reson.*, **121**, 209–211 (1996).
144. T. Anupold, A. Reinhold, P. Sarv, A. Samoson, 'A Comparison of Double Rotation and Multi-quantum Magic Angle Spinning Spectra', *Solid State NMR*, **13**, 87–91 (1998).
145. S.R. Jansen, H.T. Hintzen, R. Metselaar, J.W. de Haan, L.J.M. van de Ven, A.P.M. Kentgens, G.H. Nachtegaal, 'Multiple Quantum Al-27 Magic-angle-spinning Nuclear Magnetic Resonance Spectroscopic Study of $SrAl_{12}O_{19}$: Identification of an Al-27 Resonance from a Well-defined AlO_5 Site', *J. Phys. Chem.*, **102**, 5969–5976 (1998).
146. M. Hunger, P. Sarv, A. Samoson, 'Two-dimensional Triple-quantum Na-23 MAS NMR Spectroscopy of Sodium Cations in Dehydrated Zeolites', *Solid State NMR*, **9**, 115–120 (1997).
147. C. Jäger, P. Hartmann, G. Kunath-Fandrei, O. Hirsch, P. Rehak, J. Vogel, M. Feike, H.W. Spiess, K. Herzog, B. Thomas, 'Novel Opportunities of Structural Investigations of Glasses by 2D NMR', *Ber. Bunsenges. Phys. Chem.*, **100**, 1560–1562 (1996).
148. L. Zuchner, J.C.C. Chan, W. Müller-Warmuth, H. Eckert, 'Short-range Order and Site Connectivities in Sodium Aluminoborate Glasses: I. Quantification of Local Environments by High-resolution B-11, Na-23, and Al-27 Solid-state NMR', *J. Phys. Chem. B*, **102**, 4495 (1998).
149. H.C. Torrey, 'Transient Nutations in NMR', *Phys. Rev.*, **76**, 1059–1068 (1949).
150. A. Samoson, E. Lippmaa, 'Excitation Phenomena and Line Intensities in High-resolution NMR Spectra of Half-integer Quadrupole Nuclei', *Phys. Rev. B*, **28**, 6567 (1983).
151. A. Samoson, E. Lippmaa, 'Central Transition NMR Excitation Spectra of Half-integer Quadrupole Nuclei', *Chem. Phys. Lett.*, **100**, 205–208 (1983).
152. D. Fenzke, D. Freude, T. Fröhlich, J. Haase, 'NMR Intensity Measurements of Half-integer Quadrupole Nuclei', *Chem. Phys. Lett.*, **111**, 171–175 (1984).
153. A. Wokaun, R.R. Ernst, 'Selective Excitation and Detection in Multilevel Spin Systems: Application of Single Transition Operators', *J. Chem. Phys.*, **67**, 1752 (1977).
154. L. Pandey, S. Towta, D.G. Hughes, 'NMR Pulse Response and Measurement of the Quadrupole of $I = \frac{3}{2}$ Nuclei', *J. Chem. Phys.*, **85**, 6923–6927 (1986).
155. P.P. Man, 'Investigation of the Central Line of Mn-55 in $KMnO_4$ by a Two-dimensional NMR Method', *J. Magn. Reson.*, **67**, 78–90 (1986).
156. R. Janssen, W.S. Veeman, 'Quadrupole Nutation NMR in Solids', *J. Chem. Soc., Faraday Trans.*, **184**, 3747–3759 (1988).

157. J.A.M.v.d. Mijden, R. Janssen, W.S. Veeman, 'Analytical Description of the $I = \frac{5}{2}$ Quadrupole Nutation Experiment', *Mol. Phys.*, **69**, 53–64 (1990).
158. P.P. Man, 'Analytical Expression for the Spin-$\frac{5}{2}$ Line Intensities', *Mol. Phys.*, **78**, 307–318 (1993).
159. P.P. Man, P. Tougne, 'Exact Expression for the Spin-$\frac{7}{2}$ Line Intensities: Application to Solid State Co-59(III) NMR', *Mol. Phys.*, **83**, 997–1009 (1994).
160. S.Z. Ageev, B.C. Sanctuary, 'Analytical Solutions for Spin-$\frac{7}{2}$ Line Intensities in Solid State NMR', *Mol. Phys.*, **84**, 835–844 (1995).
161. A.P.M. Kentgens, J.J.M. Lemmens, F.M.M. Geurts, W.S. Veeman, 'Two-dimensional Solid-state Nutation NMR of Half-integer Quadrupole Nuclei', *J. Magn. Reson.*, **71**, 62–74 (1987).
162. A.P.M. Kentgens, 'Off-resonance Nutation NMR Spectroscopy of Half-integer Quadrupole Nuclei', *Prog. Nucl. Magn. Reson. Spectrosc.*, **32**, 141–164 (1998).
163. S.W. Ding, C.A. McDowell, 'Nutation Magic-angle Spinning Spectra of Half-integer Quadrupole Spin Systems', *J. Magn. Reson. A*, **112**, 36–42 (1995).
164. A.P.M. Kentgens, 'Off-resonance Nutation NMR Spectroscopy of Half-integer Quadrupole Nuclei', *J. Magn. Reson. A*, **114**, 302–309 (1993).
165. E.L. Hahn, 'Spin Echoes', *Phys. Rev.*, **80**, 580–594 (1950).
166. J. Haase, E. Oldfield, 'Spin-echo Behavior of Nonintegral Spin Quadrupole Nuclei in Inorganic Solids', *J. Magn. Reson. A*, **101**, 30–40 (1993).
167. I. Furo, B. Halle, 'Multiple Quantum NMR Spectroscopy on $I > 1$ Nuclei in Anisotropic Systems', *Mol. Phys.*, **76**, 1169–1197 (1992).
168. I. Furo, B. Halle, '2-D Quadrupole-echo Spectroscopy with Coherence Selection and Optimized Pulse Angle', *J. Magn. Reson.*, **98**, 388–407 (1992).
169. U. Eliav, G. Navon, 'A Study of Dipolar Interactions and Dynamic Processes of Water Molecules in Tendon by H-1 and H-2 Homonuclear and Heteronuclear Multiple-quantum-filtered NMR Spectroscopy', *J. Magn. Reson.*, **137**, 295–310 (1999).
170. U. Eliav, G. Navon, 'Corrections and Additions To "Quadrupole-echo Techniques in Multiple-quantum-filtered NMR Spectroscopy of Heterogeneous Systems", JMR 1995', *J. Magn. Reson.*, **128**, 98 (1997).
171. U. Eliav, G. Navon, 'Quadrupole-echo Techniques in Multiple-quantum-filtered NMR Spectroscopy of Heterogeneous Systems', *J. Magn. Reson. A*, **115**, 241–253 (1995).
172. U. Eliav, T. Kushnir, T. Knubovets, Y. Itzchak, G. Navon, 'The Effect of Magnetic Field Inhomogeneity on the Transverse Relaxation of Quadrupole Nuclei Measured by Multiple Quantum Filtered NMR', *J. Magn. Reson.*, **128**, 82–86 (1997).
173. K.D. Schmitt, J. Haase, E. Oldfield, 'Spectral Editing: A Quantitative Application of Spin-echo-nuclear Magnetic Resonance Spectroscopy to the Study of Zeolite Catalysts', *Zeolites*, **14**, 89 (1994).
174. Y. Dumazy, J.P. Amoureux, C. Fernandez, 'Theoretical and Experimental Study of Quadrupole Echoes in Solid State NMR', *Mol. Phys.*, **90**, 959–970 (1997).
175. P. Man, 'Second-order Quadrupole Effects on Hahn Echoes in Fast-rotating Solids at the Magic Angle [Review]', *Phys. Rev. B*, **55**, 8406–8424 (1997).
176. P. Man, 'Numerical Analysis of Solomon Echo Amplitudes in Static Solids', *J. Chem. Phys.*, **105**, 3908–3919 (1997).
177. S.Z. Ageev, P.P. Man, J. Fraissard, B.C. Sanctuary, 'Determination of Quadrupole Spin Coupling for Spin-$\frac{7}{2}$ Using Two Pulse Sequences', *Mol. Phys.*, **91**, 75–80 (1997).
178. H.Y. Carr, E.M. Purcell, 'Effects of Diffusion on Free Precession in Nuclear Magnetic Resonance Experiments', *Phys. Rev.*, **80**, 630–638 (1954).
179. S. Meiboom, D. Gill, 'Modified Spin-echo Method for Measuring Nuclear Relaxation Times', *Rev. Sci. Instrum.*, **29**, 688–691 (1958).
180. F.H. Larsen, H.J. Jakobsen, P.D. Ellis, N.C. Nielsen, 'Sensivity-enhanced Quadrupole-echo NMR of Half-integer Quadrupole Nuclei. Magnitudes and Relative Orientation of Chemical Shielding and Quadrupole Coupling Tensors', *J. Phys. Chem.*, **101**, 8597–8606 (1997).
181. F.H. Larsen, H.J. Jakobsen, P.D. Ellis, N.C. Nielsen, 'High-field QCPMG-MAS NMR of Half-integer Quadrupolar Nuclei with Large Quadrupole Couplings', *Mol. Phys.*, **95**, 1185–1195 (1998).
182. G.E. Pake, 'Nuclear Resonance Adsorption in Hydrated Crystals: Fine Structure of the Proton Line', *J. Chem. Phys.*, **16**, 327–336 (1948).
183. G. Hoatson, 'Broadband Composite Excitation Sequences for Creating Quadrupole Order in H-2 NMR', *J. Magn. Reson.*, **94**, 152–159 (1991).
184. G.L. Hoatson, B. Blümich, 'Deuteron Hadamard NMR of Solids and Liquid Crystals', *J. Magn. Reson.*, **95**, 446–451 (1991).
185. B. Blümich, 'Wideline ^{2}H-NMR Spectroscopy and Imaging of Solids', *Z. Naturforsch., Teil A*, **49**, 19–26 (1994).
186. D.-K. Yang, J.E. Atkins, C.C. Lester, D.B. Zax, 'New Developments in NMR Using Noise Spectroscopy', *Mol. Phys.*, **95**, 747–757 (1998).
187. D.-K. Yang, D.B. Zax, 'Bandwidth Extension in Noise Spectroscopy', *J. Magn. Reson.*, **135**, 267–270 (1998).
188. S. Habot, D.L. Lu, N.J. Tagg, G.R. Gall, D.J. Siminovitch, 'Time Symmetry – An Application to Shaped Pulse Excitation of Spin-1 Systems', *Solid State NMR*, **10**, 137–150 (1998).
189. M.A. McCoy, W.S. Warren, 'Pulse Shaping in Quadrupole-echo NMR', *J. Magn. Reson.*, **98**, 24–35 (1992).
190. A.E. Aliev, K.D.M. Harris, D.C. Apperley, 'Natural Abundance High-resolution Solid State H-2 NMR Spectroscopy', *Chem. Phys. Lett.*, **226**, 193–198 (1994).

191. R. Poupko, Z. Olender, D. Reichert, Z. Luz, 'Deuterium MAS NMR in Natural Abundance', *J. Magn. Reson. A*, **106**, 113–115 (1994).

192. S. Vega, T.W. Shattuck, A. Pines, 'Double-quantum Cross-polarization NMR in Solids', *Phys. Rev. A*, **22**, 638–661 (1980).

193. Y. Ba, C.I. Ratcliffe, J.A. Ripmeester, 'Quadrupole Echo Double Resonance (QEDOR) and Solid Echo Double Resonance (SOLEDOR) NMR', *Chem. Phys. Lett.*, **299**, 201–206 (1999).

194. D. Marks, N. Zumbulyadis, S. Vega, 'Deuterium Cross-polarization Magic-angle Spinning', *J. Magn. Reson. A*, **122**, 16–36 (1996).

195. Z. Gan, P. Robyr, 'Deuterium Polarization Transfer in Rotating Solids and Its Application in Structural Investigation', *Mol. Phys.*, **95**, 1143–1152 (1998).

196. J.H. Kristensen, H. Bildsoe, H.J. Jakobsen, N.C. Nielsen, 'Deuterium Quadrupole Couplings from Least-squares Computer Simulations of ^{2}H MAS NMR Spectra', *J. Magn. Reson.*, **92**, 443–453 (1991).

197. B. Blümich, P. Blümler, J. Jansen, 'Presentation of Sideband Envelopes by Two-dimensional One Pulse (TOP) Spectroscopy', *Solid State NMR*, **1**, 111–113 (1992).

198. H. Ernst, D. Freude, I. Wolf, 'Multinuclear Solid-state NMR Studies of Brönsted Sites in Zeolites', *Chem. Phys. Lett.*, **212**, 588–596 (1993).

199. T.P. Spaniol, A. Kubo, T. Terao, 'Two-dimensional Deuterium MAS NMR of Paramagnetic Compounds – Separation of Paramagnetic and Quadrupole Interactions', *J. Chem. Phys.*, **106**, 5393–5405 (1997).

200. S. Vega, A. Pines, 'Operator Formalism for Double Quantum NMR', *J. Chem. Phys.*, **66**, 5624–5644 (1977).

201. R. Eckman, L. Mueller, A. Pines, 'Deuterium Double-quantum NMR with MAS', *Chem. Phys. Lett.*, **74**, 376–378 (1980).

202. Y. Yang, M. Schuster, B. Blümich, H.W. Spiess, 'Dynamic Magic-angle Spinning NMR Spectroscopy: Exchange Induced Sidebands', *Chem. Phys. Lett.*, **139**, 239–243 (1987).

203. N. Chandrakumar, G.v. Fircks, H. Günther, 'The 2-D Quadshift Experiment. Separation of Deuterium Chemical Shifts and Quadrupole Couplings by Two-dimensional Solid-state MAS NMR Spectroscopy', *Magn. Reson. Chem.*, **32**, 433–435 (1994).

204. A. Detken, H. Zimmermann, U. Haeberlen, Z. Luz, 'Dynamic Hydrogen Disorder in Solid Tropolone. A Single-crystal NMR Study of Hydroxyl Deuterons', *J. Magn. Reson.*, **126**, 95–102 (1997).

205. P. Speier, H. Zimmermann, U. Haeberlen, Z. Luz, 'Dynamic Disorder in 2,3-Dimethylnaphthalene: A Single Crystal Deuteron Nuclear Magnetic Resonance Study', *Mol. Phys.*, **95**, 1153–1167 (1998).

206. P. Freude, D. Michel, J. Totz, K.A, 'Ordering Behavior at the Antiferrodistortive Phase Transition in Betaine Phosphate and Betaine Phosphite', *Ferroelectrics*, **208**, 93–103 (1998).

207. A. Kubo, A. Yogo, F. Imashiro, T. Terao, 'Deuterium NMR Study of the Glassy Crystal Pentachlorotoluene – Hadamard Quadrupole-order Exchange NMR', *J. Phys. Chem.*, **100**, 15 933–15 941 (1996).

208. N. Bloembergen, E.M. Purcell, R.V. Pound, 'Relaxation Effects in NMR Absorption', *Phys. Rev.*, **102**, 679–712 (1948).

209. A. Schleicher, K. Müller, G. Kothe, '2-D NMR Relaxation Spectroscopy of Solids', *J. Chem. Phys.*, **92**, 6432 (1990).

210. K. Müller, R. Poupko, Z. Luz, '2-D Presentation of the Quadrupole-echo Modulation in Chemically Exchanging Systems of Spin $I = 1$', *J. Magn. Reson.*, **93**, 291–298 (1991).

211. R.R. Vold, R.L. Vold, 'Deuterium Relaxation in Molecular Solids', *Adv. Magn. Opt. Reson.*, **16**, 85–171 (1991).

212. F.H. Larsen, H.J. Jakobsen, P.D. Ellis, N.C. Nielsen, 'Molecular Dynamics from H-2 Quadrupole Carr–Purcell–Meiboom–Gill Solid-state NMR Spectroscopy', *Chem. Phys. Lett.*, **292**, 467–473 (1998).

213. O. Weintraub, S. Vega, 'Dynamic H-2 NMR of Rotating Solids', *Solid State NMR*, **4**, 341–351 (1995).

214. J.H. Kristensen, G.L. Hoatson, R.L. Vold, 'Investigation of Multiaxial Molecular Dynamics by H-2 MAS NMR Spectroscopy', *Solid State NMR*, **13**, 1–37 (1998).

215. J.H. Kristensen, G.L. Hoatson, R.L. Vold, 'Effect of Restricted Rotational Diffusion on H-2 MAS NMR Spectra', *J. Chem. Phys.*, **110**, 4533–4553 (1999).

216. Y.J. Lee, F. Wang, C.P. Grey, 'Li-6 and Li-7 MAS NMR Studies of Lithium Manganate Cathode Materials', *J. Am. Chem. Soc.*, **120**, 12601–12613 (1998).

217. N.C. Nielsen, H. Bildsoe, H.J. Jakobsen, P. Norby, 'Li-7, Na-23, and Al-27 Quadrupole Interactions in Some Aluminosilicate Sodalites from MAS NMR Spectra of Satellite Transitions', *Zeolites*, **11**, 622–633 (1991).

218. J. Skibsted, P. Norby, H. Bildsoe, H.J. Jakobsen, 'Line Shapes and Widths of MAS Sidebands for Al-27 Satellite Transitions – Multinuclear MAS NMR of Tugtupite $Na_8Al_2Be_2Si_8O_{24}Cl_2$', *Solid State NMR*, **5**, 239–255 (1995).

219. P.J. Bray, S.J. Gravina, P.E. Stallworth, S.P. Szu, J. Zhong, 'NMR Studies of the Structure of Glasses', *Exp. Tech. Phys.*, **36**, 397–413 (1988).

220. W. Müller-Warmuth, 'The Structure of Glasses Studied by MAS-NMR Spectroscopy of Quadrupole Nuclei', *Z. Naturforsch., Teil A*, **51**, 585–590 (1996).

221. S.J. Hwang, C. Fernandez, J.P. Amoureux, J. Cho, S.W. Martin, M. Pruski, 'Quantitative Study of the Short Range Order in B_2O_3 and B_2S_3 by MAS and Two-dimensional Triple-quantum MAS ^{11}B NMR', *Solid State NMR*, **8**, 109–121 (1997).

222. T.J. Bastow, D. Massiot, J.P. Coutures, 'N-14 NMR in AlN and BN', *Solid State Nucl. Magn. Reson.*, **10**, 241–245 (1998).

223. K.J.D. Mackenzie, R.H. Meinhold, 'MAS NMR Study of Pentacoordinated Magnesium in Grandidierite', *Am. Mineral.*, **82**, 479–482 (1997).

224. T.J. Bastow, S.N. Stuart, 'NMR Study of the Zinc Chalcogenides (ZnX, X = 0, S, Se, Te)', *Phys. Status Solidi B*, **145**, 719–728 (1988).

225. W.A. Daunch, P.L. Rinaldi, 'Natural-abundance Solid-state S-33 NMR with High-speed Magic-angle Spinning', *J. Magn. Reson. A*, **123**, 219–221 (1996).

226. M.A. Fedotov, O.L. Malkina, V.G. Malkin, 'Cl-35/37 NMR Chemical Shifts and Nuclear Quadrupole Couplings for Some Small Chlorine Compounds – Experimental and Theoretical Study of Chemical Shifts and Nuclear Quadrupole Couplings for Some Small Chlorine Compounds', *Chem. Phys. Lett.*, **258**, 330–335 (1996).

227. T.J. Bastow, S.L. Segel, K.R. Jeffrey, 'Antiferroelectric Transition in KOH(D) – A H-2 and K-39 NMR Study', *Solid State Commun.*, **78**, 565–568 (1991).

228. R. Blinc, J. Dolinsek, T. Apih, W. Schranz, A. Fuith, H. Warhanek, '2D K-39 NMR Study of the Phase Transition in KSCN', *Solid State Commun.*, **93**, 609–611 (1995).

229. P.V. Bellot, A. Trokiner, Y. Zhdanov, A. Yakubovskii, 'Ca-43 NMR in Solid State', *J. Chim. Phys.*, **95**, 280–288 (1998).

230. R. Dupree, A.P. Howes, S.C. Kohn, 'Natural Abundance Solid State Ca-43 NMR', *Chem. Phys. Lett.*, **276**, 399–404 (1997).

231. R.G. Bryant, S. Ganapathy, S.D. Kennedy, 'High-resolution Ca-43 NMR in Solids', *J. Magn. Reson.*, **72**, 376–378 (1987).

232. A.R. Thompson, E. Oldfield, 'Solid-state Scandium-45, Yttrium-89, and Lanthanum-139 NMR Spectroscopy', *J. Chem. Soc., Chem. Commun.*, 27–29 (1987).

233. A. Labouriau, W.L. Earl, 'Titanium Solid-state NMR in Anatase, Brookite and Rutile', *Chem. Phys. Lett.*, **270**, 278–284 (1997).

234. S.F. Dec, M.F. Davis, G.E. Maciel, C.E. Bronnimann, J.J. Fitzgerald, S.S. Han, 'Solid-state Multinuclear NMR Studies of Ferroelectric, Piezoelectric, and Related Materials', *Inorg. Chem.*, **32**, 955–959 (1993).

235. J. Skibsted, N.C. Nielsen, H. Bildsoe, H.J. Jakobsen, 'Magnitudes and Relative Orientation of V-51 Quadrupole Coupling and Anisotropic Shielding Tensors in Metavanadates and KV_3O_8 from V-51 MAS NMR Spectra – Na-23', *J. Am. Chem. Soc.*, **115**, 7351–7362 (1993).

236. S. Hayashi, 'V-51 and CO-59 Off-MAS NMR Spectra – Determination of Quadrupole Coupling, Chemical Shift Anisotropy and Their Relative Orientation', *Magn. Reson. Chem.*, **34**, 791–798 (1996).

237. G.N. Abelyashev, V.N. Berzhanskiii, S.N. Polulyah, N.A. Sergeev, 'Pecularities of the Formation of a Two Pulse Echo in Spin-$\frac{3}{2}$ Systems', *Fiz. Tverd. Tela*, **34**, 676–678 (1992) (in Russian).

238. F.H. Larsen, H.J. Jakobsen, P.D. Ellis, N.C. Nielsen, 'QCPMG-MAS NMR of Half-integer Quadrupole Nuclei', *J. Magn. Reson.*, **131**, 144–147 (1998).

239. T. Charpentier, J. Virlet, 'Triple Quantum MQMAS Spectroscopy of Co-59 ($I = \frac{7}{2}$) in $Na_3Co(NO_2)_6$ and *trans*-$Co[(en_2)(NO_2))_2]NO_3$ Interplay Between the Quadrupole Coupling and Anisotropic Shielding Tensors', *Solid State NMR*, **12**, 227–242 (1998).

240. S.L. Hu, J.A. Reimer, A.T. Bell, 'Cu-65 NMR Spectroscopy of Cu-exchanged ZSM-5 Catalysts', *J. Phys. Chem. B*, **101**, 1869–1871 (1997).

241. G. Wu, 'Zinc-67 NMR Spectroscopy of Solids', *Chem. Phys. Lett.*, **298**, 375–380 (1998).

242. T.J. Bastow, 'Zn-67 NMR in Zinc Metal', *J. Phys. Condens. Matter*, **8**, 11309–11315 (1996).

243. D. Massiot, V. Montouillout, F. Fayon, F.P.C. Bessada, 'QPASS – Towards Higher Resolution in NMR of Half Integer Quadrupole Nuclei with High Quadrupole Couplings', *J. Chim. Phys.*, **95**, 270–279 (1998).

244. T. Vosegaard, D. Massiot, N. Gautier, H.J. Jakobsen, 'Ga-71 Chemical Shielding and Quadrupole Coupling Tensors of the Garnet $Y_3Ga_5O_{12}$ from Single-crystal Ga-71 NMR', *Inorg. Chem.*, **36**, 2446–2450 (1997).

245. R. Klik, V. Bosacek, L. Kubelkova, D. Freude, D. Michel, 'Coordination State of Gallium in MFI Structures Prepared by Direct Synthesis and by Postsynthetic Modification of Boralites', *Zeolites*, **19**, 343–348 (1997).

246. R. Jelinek, A. Stein, G.A. Ozin, 'Br-81 and Cl-35 NMR Investigation of Sodium, Silver, Halo Sodalite Semiconductor Supralattices', *J. Am. Chem. Soc.*, **115**, 2390–2396 (1993).

247. T. Vosegaard, J. Skibsted, H. Bildsoe, H.J. Jakobsen, 'Combined Effect of Second-order Quadrupole Coupling and Chemical Shielding Anisotropy on the Central Transition in MAS NMR of Quadrupole Nuclei. Rb-87 MAS NMR', *J. Phys. Chem.*, **99**, 10 731–10 735 (1995).

248. T. Vosegaard, I.P. Byriel, H.J. Jakobsen, T. Vosegaard, I.P. Byriel, H.J. Jakobsen, 'Characterization of the Two Rubidium Sites in Rb_2CrO_4 by Rb-87 Single-crystal NMR', *J. Phys. Chem. B*, **101**, 8955–8958 (1997).

249. T.J. Bastow, 'Materials Characterisation by Nuclear Quadrupole Interaction', *Z. Naturforsch., Teil A*, **49**, 320–328 (1994).

250. V.M. Mastikhin, O.B. Lapina, R.I. Maximovskaya, 'Mo-95 Solid-state NMR Spectra of Molybdates', *Chem. Phys. Lett.*, **148**, 413–416 (1988).

251. O.H. Han, H.K.C. Timken, E. Oldfield, 'Solid-state MAS NMR Spectroscopic Study of Group III–V Semiconductors', *J. Chem. Phys.*, **89**, 6046–6052 (1988).

252. T. Ueda, N. Nakamura, 'Sb-121 NMR and SCF-MS-X-alpha Studies of Quadrupole Interaction and the Electronic Structure of Mixed-valence Compound, Cs_2SbC_{16}', *Z. Naturforsch., Teil A*, **51**, 672–676 (1996).

253. N. Lee, B.C. Sanctuary, T.K. Halstead, 'I-127 NMR Study of Quadrupole Echoes in KI', *J. Magn. Reson.*, **98**, 534–555 (1992).

254. G. Hinze, R. Bohmer, B. Zalar, R. Blinc, 'The Orientational Glass $(KI)_{(0.56)}(NH_4I)_{(0.44)}$ studied by I-127 NMR', *J. Phys. Condens. Matter*, **9**, 117–125 (1997).

255. S. Kroeker, K. Eichele, R. Wasylishen, J. Britten, 'Cesium-133 NMR Study of CsCD(SCN)(3) – Relative Orientation of the Chemical Shift and Electric Field Gradient Tensors', *J. Phys. Chem. B*, **101**, 3727–3733 (1997).

256. J. Skibsted, T. Vosegaard, H. Bildsoe, H.J. Jakobsen, 'Cs-133 Chemical Shielding Anisotropies and Quadrupole Couplings from MAS NMR of Cesium Salts', *J. Phys. Chem.*, **100**, 14 872–14 881 (1996).

257. K. Kumagai, Y.V. Piskunov, A.Y. Yakubovskii, S.V. Verkhovskii, A.P. Gerashenko, Y.I. Zhdanov, K.N. Mikhalev, I.V. Sagaradze, E.Y. Medvedev, S.M. Cheshnitskii, R.N. Pletnev, 'Local Distortions in the BiO_6-octahedra Sublattice $BaPb_XBi_{1-X}O_3$ as seen by Ba-137 NMR/NQR', *Physica C*, **247**, 209–220 (1997).

258. T.J. Bastow, 'An NMR Study of Ba-137 and Ti-47, 49 in Ferroelectric $BaTiO_3$', *J. Phys. Condens. Matter*, **1**, 4985–4991 (1989).

259. T.J. Bastow, 'La-139 Nuclear Magnetic Resonance Characterisation of La_2O_3 and $La_{1-x}Sr_xMO_3$ Where M = Cr, Mn or Co', *Solid State NMR*, **3**, 17–22 (1994).

260. P.J. Chu, B.C. Gerstein, H.D. Tang, R.N. Shelton, 'Studies of the Electronic Phase Transition in $Lu_5Ir_4Si_{10}$ and $Lu_5Rh_4Si_{10}$ by Lu-175 NMR', *Phys. Rev. B*, **37**, 1796–1806 (1988).

261. D. Müller, W. Gessner, A. Samoson, E. Lippmaa, G. Scheler, 'Solid-state Al-27 NMR Studies on Polycrystalline Aluminates of the Systems $CaO{\cdot}Al_2O_3$', *Polyhedron*, **5**, 779 (1986).

262. W.S. Veeman, 'Quadrupole Nutation NMR in Solids', *Z. Naturforsch., Teil A*, **47**, 353–360 (1992).

263. D. Müller, W. Gessner, A. Samoson, E. Lippmaa, G. Scheler, 'Solid-state Aluminum-27 Nuclear Magnetic Resonance Chemical Shift and Quadrupole Coupling Data for Condensed AlO_4 Tetrahedra', *J. Chem. Soc., Dalton Trans*, 1277–1281 (1986).

264. J. Skibsted, H. Bildsoe, H.J. Jakobsen, 'High-speed Spinning Versus High Magnetic Field in MAS NMR of Quadrupole Nuclei. Al-27 MAS NMR of $3Ca\ Al_2O_3$', *J. Magn. Reson.*, **92**, 669–676 (1991).

265. D. Müller, W. Gessner, G. Scheler, 'Chemical Shift and Quadrupole Coupling of the Al-27 NMR Spectra of $LiAlO_2$ Polymorphs', *Polyhedron*, **2**, 1195–1200 (1984).

266. J. Skibsted, N.C. Nielsen, H. Bildsöe, H.J. Jacobsen, 'Satellite Transitions in MAS NMR Spectra of Quadrupolar Nuclei', *J. Magn. Reson.*, **95**, 88–117 (1991).

267. T. Vosegaard, H.J. Jakobsen, 'Al-27 Chemical Shielding Anisotropy', *J. Magn. Reson.*, **128**, 135–137 (1997).

268. H. Kraus, R. Prins, A.P.M. Kentgens, 'A Al-27 MQMAS and Off-resonance Nutation NMR Investigation of Mo-P/gamma-Al_2O_3 Hydrotreating Catalyst Precursors', *J. Phys. Chem.*, **100**, 16 336–164 345 (1996).

269. H. Kraus, M. Muller, R. Prins, A.P.M. Kentgens, 'Comments on the Al-27 NMR Visibility of Aluminas', *J. Phys. Chem. B*, **102**, 3862–3865 (1998).

270. D. Coster, A.L. Blumenfeld, J.J. Fripiat, 'Lewis Acid Sites and Surface Aluminum in Aluminas and Zeolites: A High-resolution NMR Study', *J. Phys. Chem.*, **98**, 6201–6211 (1994).

271. B. Ollivier, R. Retoux, P. Lacorre, D. Massiot, G. Ferey, 'Crystal Structure of kappa-Alumina – An X-ray Powder Diffraction, TEM and NMR Study', *J. Mater. Chem.*, **7**, 1049–1056 (1997).

272. G. Kunathfandrei, T.J. Bastow, J.S. Hall, C. Jäger, M.E. Smith, 'Quantification of Aluminum Coordinations in Amorphous Aluminas by Combined Central and Satellite Transition Magic Angle Spinning NMR Spectroscopy', *J. Phys. Chem.*, **99**, 15 138–15 141 (1995).

273. M.T. Weller, M.E. Brenchley, D.C. Apperley, N.A. Davies, 'Correlations Between Al-27 MAS NMR Spectra and the Coordination Geometry of Framework Aluminates', *Solid State NMR*, **3**, 103–106 (1994).

274. D. Müller, E. Jahn, G. Ladwig, U. Haubenreisser, 'High-resolution Solid-state 27-Al and 31P NMR: Correlation Between Chemical Shift and Mean Al–O–P angle in $AlPO_4$ Polymorphs', *Chem. Phys. Lett.*, **109**, 332–336 (1984).

275. W.F. Bleam, S.F. Dec, J.S. Frye, 'Al-27 Solid-state NMR Study of Five-coordinate Aluminum in Augelite and Senegalite', *Phys. Chem. Miner.*, **16**, 817–820 (1989).

276. D. Müller, I. Grunze, E. Hallas, G. Ladwig, 'Hochfeld-Al-27-NMR-Untersuchungen zur Aluminiumkoordination in kristallinen Aluminiumpohosphaten', *Z. Anorg. Allg. Chem.*, **500**, 80–88 (1983).

277. C. Fernandez, J.P. Amoureux, J.M. Chezeau, L. Delmotte, H. Kessler, 'Al-27 MAS NMR Characterization of $AlPO_4$-14. Enhanced Resolution and Information by MQMAS', *Microporous Mater.*, **6**, 331–340 (1996).

278. E. Lippmaa, A. Samoson, M. Mägi, 'High-resolution Al-27 NMR of Aluminosilicates', *J. Am. Chem. Soc.*, **108**, 1730–1735 (1986).

279. L.B. Alemany, D. Massiot, B.L. Sheriff, M.E. Smith, F. Taulelle, 'Observation and Accurate Quantification of Al-27 MAS NMR Spectra of Some Al_2SiO_5 Polymorphs Containing Sites with Large Quadrupole Interactions', *Chem. Phys. Lett.*, **177**, 301–306 (1991).

280. L.B. Alemany, S. Steuernagel, J.P. Amoureux, R.L. Callender, A.R. Barron, 'Very Fast MAS and MQMAS NMR Studies of the Spectroscopically Challenging Minerals Kyanite and Andalusite on 400, 500, 800 MHz Spectrometers', *Solid State NMR*, **14**, 1–18 (1999).

281. G. Kunathfandrei, P. Rehak, S. Steuernagel, H. Schneider, C. Jäger, 'Quantitative Structural Analysis of Mullite by Al-27 Nuclear Magnetic Resonance Satellite Transition Spectroscopy', *Solid State NMR*, **3**, 241–248 (1994).

282. J.H. Baltisberger, Z. Xu, J.F. Stebbins, S.H. Wang, A. Pines, 'Triple-quantum Two-dimensional Al-27 MAS

NMR Spectroscopic Study of Aluminosilicate and Aluminate Crystals and Glasses', *J. Am. Chem. Soc.*, **118**, 7209–7214 (1996).

283. R.J. Kirkpatrick, R.A. Kinsey, K.A. Smith, D.M. Henderson, E. Oldfield, 'High Resolution Solid-state Sodium-23, Aluminum-27, and Silicon-29 Nuclear Magnetic Resonance Spectroscopic Reconnaissance of Alkali and Plagioclase Feldspars', *Am. Mineral.*, **70**, 106–123 (1985).
284. M.E. Smith, S. Steuernagel, 'A Multinuclear Magnetic Resonance Examination of the Mineral Grandidierite', *Solid State NMR*, **1**, 175–183 (1992).
285. D. Freude, H. Ernst, I. Wolf, 'Solid-state NMR Studies of Acid Sites in Zeolites', *Solid State NMR*, **3**, 271–286 (1994).
286. M. Hunger, T. Horvath, 'Multi-nuclear Solid-state NMR Study of the Local Structure of SiOHAl Groups and Their Interaction with Probe-molecules in Dehydrated Faujasite, Mordenite and Zeolite ZSM-5', *Ber. Bunsenges. Phys. Chem.*, **99**, 1316–1320 (1995).
287. C.P. Grey, A.J. Vega, 'Determination of the Quadrupole of the Invisible Aluminum Spins in Zeolite HY with H-1/Al-27 TRAPDOR NMR', *J. Am. Chem. Soc.*, **117**, 8232–8242 (1995).
288. H. Kosslick, G. Lischke, G. Walther, W. Storek, A. Martin, R. Fricke, 'Physico-chemical and Catalytic Properties of Al-, Ga- and Fe-substituted Mesoporous Materials Related to MCM-41', *Microporous Mater.*, **9**, 13–33 (1997).
289. D. Müller, U. Bentrup, 'Al-27 NMR Studies on Alkali Fluoroaluminates', *Z. Anorg. Allg. Chem.*, **575**, 17–25 (1989).
290. R.W. Schurko, R.E. Wasylishen, H. Foerster, 'Characterization of Anisotropic Aluminum Magnetic Shielding Tensors. Distorted Octahedral Complexes and Linear Molecules', *J. Phys. Chem. A*, **102**, 9750–9760 (1998).
291. D. Müller, personal communication, 1992.
292. R.W. Schurko, R.E. Wasylishen, A.D. Phillips, 'A Definitive Example of Aluminum-27 Chemical Shielding Anisotropy', *J. Magn. Reson.*, **133**, 388–394 (1998).
293. D. Massiot, A. Kahn-Harari, D. Michel, D. Müller, F. Taulelle, 'Aluminum-27 MAS NMR of $Al_2Ge_2O_7$ and $LaAlGe_2O_7$: Two Pentacoordinated Aluminum Environments', *Magn. Reson. Chem.*, **28**, 82–88 (1990).
294. M. Feuerstein, G. Engelhardt, P.L. McDaniel, J.E. MacDougall, T.R. Gaffney, 'Solid-state Nuclear Magnetic Resonance Investigation of Cation Siting in LiNaLSX Zeolites', *Microporous Mater.*, **16**, 27–35 (1998).
295. A.M. George, J.F. Stebbins, 'High-temperature Na-23 MAS NMR Data for Albite – Comparison to Chemical-shift Models', *Am. Mineral.*, **80**, 878–884 (1995).
296. L. Delevoye, S.X. Liu, M.D. Welch, C. Fernandez, J.P. Amoureux, J. Klinowski, 'Triple-quantum Al-27 and Na-23 MAS NMR Study of Amphiboles', *J. Chem. Soc., Faraday Trans.*, **93**, 2591–2595 (1997).
297. R. Janssen, G.A.H. Tijink, W.S. Veeman, T.L.M. Maesen, J.F.v. Lent, 'High-temperature NMR Study of Zeolite Na-A: Detection of a Phase Transition', *J. Phys. Chem.*, **93**, 899–904 (1989).
298. G. Engelhardt, H. Koller, 'A Simple Procedure for the Determination of the Quadrupole Interaction Parameters and Isotropic Chemical Shifts from MAS NMR Spectra of Half-integer Spins in Solids', *Magn. Reson. Chem.*, **29**, 941–945 (1991).
299. T.H. Walter, E. Oldfield, 'Magic-angle Spinning Oxygen-17 NMR of Aluminum Oxides and Hydroxides', *J. Phys. Chem.*, **93**, 6744–6751 (1989).
300. A.R. Thompson, A.C. Kunwar, H.S. Gutowsky, E. Oldfield, 'Oxygen-17 and Aluminum-27 NMR Spectroscopic Investigations of Aluminum(III) Hydrolysis Products', *J. Chem. Soc., Dalton Trans.*, 2317–2322 (1987).
301. H.K.C. Timken, N. James, G.L. Turner, S.L. Lambert, L.B. Welsh, E. Oldfield, 'Solid-state Oxygen-17 NMR Spectroscopic Studies of Zeolites and Related Systems. Part 2', *J. Am. Chem. Soc.*, **108**, 7236–7241 (1986).
302. H.K.C. Timken, G.L. Turner, J.P. Gilson, L.B. Welsh, E. Oldfield, 'Solid-state Oxygen-17 NMR Spectroscopic Studies of Zeolites and Related Systems. Part 1', *J. Am. Chem. Soc.*, **108**, 7231–7235 (1986).
303. Z. Xu, J.F. Stebbins, 'Oxygen Sites in the Zeolite Stilbite: A Comparison of Static, MAS, VAS, DAS and Triple Quantum MAS NMR Techniques', *Solid State NMR*, **11**, 243–251 (1998).
304. D.R. Spearing, I. Farnan, J.F. Stebbins, 'Dynamics of the Alpha–Beta Phase Transitions in Quartz and Cristobalite as Observed by In Situ High Temperature Si-29 NMR and O-17 NMR', *Phys. Chem. Miner.*, **19**, 307–321 (1992).
305. T.H. Walter, G.L. Turner, E. Oldfield, 'Oxygen-17 Cross-polarization NMR Spectroscopy of Inorganic Solids', *J. Magn. Reson.*, **76**, 106–120 (1988).
306. X. Xue, J.F. Stebbins, M. Kanzaki, 'Correlations Between O-17 NMR Parameters and Local Structure Around Oxygen in High-pressure Silicates: Implications for the Structure of Silicate Melts at High Pressure', *Am. Mineral.*, **79**, 31–42 (1994).
307. P.J. Grandinetti, J.H. Baltisberger, I. Farnan, J.F. Stebbins, U. Werner, A. Pines, 'Solid-state O-17 Magic-angle and Dynamic-angle Spinning NMR Study of the SiO_2 Polymorph Coesite', *J. Phys. Chem.*, **99**, 12 341–12 348 (1995).
308. S. Schramm, E. Oldfield, 'High-resolution Oxygen-17 NMR of Solids', *J. Am. Chem. Soc.*, **106**, 2502–2506 (1984).
309. K.T. Mueller, J.H. Baltisberger, E.W. Woote, A. Pines., 'Isotropic Chemical Shifts and Quadrupole Parameters for Oxygen-17 Using Dynamic-angle Spinning NMR', *J. Phys. Chem.*, **96**, 7001–7004 (1992).
310. H.K.C. Timken, S.E. Schramm, R.J. Kirkpatrick, E. Oldfield, 'Solid-state Oxygen-17 NMR Spectroscopic Studies of Alkaline Earth Metasilicates', *J. Phys. Chem.*, **91**, 1054–1058 (1987).

311. H. Maekawa, P. Florian, D. Massiot, H. Kiyono, M. Nakamura, 'Effect of Alkali Metal Oxide on O-17 NMR Parameters and Si−O−Si Angles of Alkali Metal Disilicate', *J. Phys. Chem.*, **100**, 5525–5532 (1996).
312. U. Pingel, 'O-17 NMR of Porous Solids', Thesis, Universität Leipzig, 1999.
313. T. Schaller, J.F. Stebbins, 'The Structural Role of Lanthanum and Yttrium in Aluminosilicate Glasses: A Al-27 and O-17 MAS NMR Study', *J. Phys. Chem. B*, **102**, 10 690–10 697 (1998).
314. P.J. Dirken, S.C. Kohn, M.E. Smith, E.R.H. van Eck, 'Complete Resolution of Si−O−Si and Si−O−Al Fragments in an Aluminosilicate Glass by O-17 Multiple Quantum Magic Angle Spinning NMR Spectroscopy', *Chem. Phys. Lett.*, **266**, 568–574 (1997).
315. H. Maekawa, T. Saito, T. Yokokawa, 'Water in Silicate Glass: O-17 NMR of Hydrous Silica, Albite, and $Na_2Si_4O_9$ Glasses', *J. Phys. Chem. B*, **102**, 7523–7529 (1998).
316. Z. Xu, H. Maekawa, J.V. Oglesby, J.F. Stebbins, 'Oxygen Speciation in Hydrous Silicate Glasses: An Oxygen-17 NMR Study', *J. Am. Chem. Soc.*, **120**, 9894 (1998).
317. J.F. Stebbins, J.V. Oglesby, Z. Xu, 'Disorder Among Network-modifier Cations in Silicate Glasses – New Constraints from Triple-quantum O-17 NMR', *Am. Mineral.*, **82**, 1116–1124 (1997).
318. X. Cong, R.J. Kirkpatrick, 'O-17 MAS NMR Investigation of the Structure of Calcium Silicate Hydrate Gel', *J. Am. Ceram. Soc.*, **79**, 1585–1592 (1996).
319. R. Hussin, D. Holland, R. Dupree, 'Does Six-coordinate Germanium Exist in Na_2O-GeO_2 glasses – O-17 NMR Measurements', *J. Non-cryst. Solids*, **234**, 440–445 (1998).
320. T.J. Bastow, M.E. Smith, H.J. Whitfield, 'O-17 NMR Investigation of Hafnia and Ternary Hafnium Oxides', *J. Mater. Chem.*, **6**, 1951–1955 (1996).
321. E.R.H. Van Eck, M.E. Smith, 'Orientation of the Quadrupole and Dipole Tensors of Hydroxyl Groups by O-17 Quadrupole Separated Local Field NMR', *J. Chem. Phys.*, **108**, 5904–5912 (1998).
322. G. Wu, D. Rovnyak, P.C. Huang, R.G. Griffin, 'High-resolution Oxygen-17 NMR Spectroscopy of Solids by Multiple-quantum Magic-angle-spinning', *Chem. Phys. Lett.*, **277**, 79–83 (1997).
323. M.E. Smith, S. Steuernagel, H.J. Whitfield, 'O-17 Magic-angle Spinning Nuclear Magnetic Resonance of $CaCO_3$', *Solid State NMR*, **4**, 313–316 (1995).

Solid State Nuclear Magnetic Resonance, 2 (1993) 325–334
Elsevier Science Publishers B.V., Amsterdam

Quadrupole effects of spin-3/2 nuclei on the solid-state magic-angle spinning nuclear magnetic resonance spectra of spin-1/2 nuclei

Deviations from first-order theory and implications concerning the sign of the indirect coupling constant

Sergio H. Alarcón [a], Alejandro C. Olivieri [a,*] and Robin K. Harris [b]

[a] *Departamento de Química Analítica, Facultad de Ciencias Bioquímicas y Farmacéuticas, Suipacha 531, Rosario 2000, Argentina*
[b] *Department of Chemistry, University of Durham, South Road, Durham DH1 3LE, UK*

(Received 29 July 1993; accepted 4 October 1993)

Abstract

The effect of the interaction between spin-3/2 and spin-1/2 nuclei on solid-state magic-angle spinning nuclear magnetic resonance (MAS NMR) spectra of the latter is studied in cases where deviations from first-order theory are expected. A comparison is made between the exact and first-order perturbation approaches. Both dipolar and indirect (iso- and anisotropic) coupling interactions are considered. Implications regarding $^{13}C,^{35,37}Cl$, $^{31}P,^{63,65}Cu$ and $^{119}Sn,^{35,37}Cl$ cases are discussed. It is shown that in the latter two cases the sign of the indirect coupling constant J can be derived.

Keywords: spin-3/2 nuclei; spin-1/2 nuclei; first-order theory; coupling constant

Introduction

The effects transmitted by quadrupolar nuclei to MAS NMR resonances of spin-1/2 nuclei in the solid state have attracted considerable attention in recent years. Many cases of both dipolar and combined dipolar–indirect coupling interactions between quadrupolar and spin-1/2 nuclei have been reported for a variety of materials. These involve organic and inorganic compounds, zeolites, surface-immobilized substrates, silicon ceramics, etc. The topic has been reviewed recently [1]. Further spin pairs not covered in this review are $^{31}P,^{99,101}Ru$ [2] and $^{113}Cd,^{14}N$ [3]. First-order perturbation theory (valid when the ratio of quadrupolar to Zeeman energy for the quadrupolar nucleus is small) is found to be applicable in many cases. This approach has been shown to be able to provide a simple connection between the relevant data involved, namely quadrupole parameters, bond distances and angles, and iso- and anisotropic indirect (scalar) coupling interactions [4–6]. Recently, perturbation theory has been applied to the inverse case (*i.e.*, for large quadrupole coupling constants), and both dipolar and indirect coupling interactions were taken into account [7,8]. One outcome of this body of work is the possibility of estimating the anisotropy of the scalar coupling interac-

---

* Corresponding author.

tion (ΔJ), a parameter of somewhat elusive experimental accessibility [1].

The general, first-order perturbative equation for the "high-field" case, when both dipolar and indirect coupling interactions to a spin-3/2 nucleus occur is [5]:

$$\begin{aligned}\Delta\nu_m &= -mJ + (3\chi D'/20\nu_S)\left[5/4 - m^2\right]\\ &\quad\times(3\cos^2\beta^D - 1)\\ &= -mJ - d(5/4 - m^2) \qquad (1)\end{aligned}$$

where $\Delta\nu_m$ is the shift (relative to the unperturbed, isotropic I frequency) produced by $|m\rangle$ eigenstates of quadrupolar nuclei S ($m = 3/2$, $1/2$, $-1/2$, $-3/2$), J is the isotropic I,S indirect coupling constant ($I = 1/2$, $S = 3/2$), D' is the "effective" dipolar coupling constant [$D' = D - (\Delta J)/3$], D is the I,S dipolar coupling constant [$D = (\mu_0/4\pi)\gamma_I\gamma_S h/4\pi^2 r^3$], χ is the S quadrupole coupling constant [$\chi = e^2 q_{zz} Q/h$, the electric field gradient (EFG) at S is assumed to be axially symmetric], ν_S is the Zeeman frequency of S, β^D is the angle between the I,S internuclear vector and the principal axis of the quadrupolar tensor, ΔJ is the anisotropy in the J tensor ($\Delta J = J_{\parallel} - J_{\perp}$; J is considered to be axially symmetric and coaxial with $\mathbf{D}$), and $d = -(3\chi D'/20\nu_S)(3\cos^2\beta^D - 1)$. This latter factor has been called "the second-order shift" itself [1], due to the fact that first-order perturbations on the eigenstates of S leads to second-order effects on the I lines. Eqn. 1 applies to the intensity-weighted average of each of the four resonances, which are in principle powder patterns. A careful analysis of the signs of the relevant magnitudes involved in eqn. 1 shows that, for all possibilities of signs of the gyromagnetic ratios γ_I and γ_S, the term D'/ν_S may be written as $D'/\nu_S = |D/\nu_S| - (1/3)\Delta K\,|\gamma_I\gamma_S/\nu_S|$ (where $\Delta K = \Delta J/\gamma_I\gamma_S$). This means that, if ν_S is always taken as positive, D' can be written as $D' = |D| - (1/3)\Delta K\,|\gamma_I\gamma_S|$. Thus the sense of the distortion d depends on the combined signs of D', χ and the angular factor ($3\cos^2\beta^D - 1$). Furthermore, the first term in eqn. 1 should be $-mJ\gamma_I/|\gamma_I|$, which also accounts for a negative γ_I.

Relevant examples of this are ^{119}Sn spectra affected by ^{35,37}Cl nuclei in chlorostannic compounds [9–11], and ^{31}P spectra of ^{63,65}Cu-containing phosphine–copper–halide complexes [12–22]. In both of these cases, information on ΔJ effects have been gathered, though in certain cases the quadrupole coupling constants are not smaller than the resonance ν_S frequencies [22]. When there are reasons to expect both J and ΔJ to be negligible in comparison with D, eqn. 1 predicts two spin-1/2 signals at $\pm(3\chi D/20\nu_S)(3\cos^2\beta^D - 1)$, *i.e.*, a symmetric doublet with a splitting given by:

$$\begin{aligned}s &= \Delta\nu_{\pm 1/2} - \Delta\nu_{\pm 3/2}\\ &= (3\chi D/10\nu_S)(3\cos^2\beta^D - 1) \qquad (2)\end{aligned}$$

Notice that in contrast to the ^{13}C,^{14}N case (where $S = 1$ and 2:1 asymmetric doublets result) [4] the fact that the doublet is symmetric makes it insensitive to the sign of χ.

For the ^{13}C,^{35,37}Cl spin pair, both J and ΔJ are expected to be small compared with D [23,24]. In this case, since it is reasonable to assume that $\beta^D = 0$, first-order theory predicts symmetric splittings given by:

$$s = \Delta\nu_{\pm 1/2} - \Delta\nu_{\pm 3/2} = (6\chi D/10\nu_S) \qquad (3)$$

Very recently, symmetric doublets have been observed in high-field MAS NMR spectra of solid chlorine-containing organic compounds [24–26]. It seems clear that in these latter cases perturbation theory is not strictly applicable, since χ is actually larger than ν_S. Experimentally this is verified by the fact that the splitting is not inversely proportional to the field strength of the spectrometer. The deviations from the first-order regime are such that s becomes smaller than the value predicted by eqn. 3, which is contrary to the implications of figures in ref. 12.

In the present report, we compare the results predicted by first-order theory in the case of spin-1/2,spin-3/2 coupling with those obtained by full-matrix diagonalization of the complete Zeeman–quadrupole Hamiltonian for S nuclei. Equations are derived which can be used to predict the appearance of the spin-1/2 lines up to $(\chi/\nu_S) = 3$, both including indirect (iso- and anisotropic) and dipolar contributions. Additionally, the possibility of determining the sign of J is discussed when substantial indirect coupling effects are involved.

Theory

When first-order theory is no longer applicable, the S eigenstates are calculated by numerical methods, with diagonalization of the complete Zeeman–quadrupole Hamiltonian [12]. We consider here the approach of Menger and Veeman [12], but for a general value of the angle β^D. An axially symmetric EFG tensor is assumed, with its unique z axis inclined an angle θ with respect to the magnetic field $\boldsymbol{B}_0$ (Fig. 1a). The diagonalization renders the S eigenstates as an expansion of Zeeman states $|n\rangle$:

$$|\psi_m(\theta)\rangle = \sum_{-S}^{S} a_{mn}(\theta)\,|n\rangle \tag{4}$$

All coefficients $a_{mn}(\theta)$ are real and depend on the orientation θ. Once they are available, the

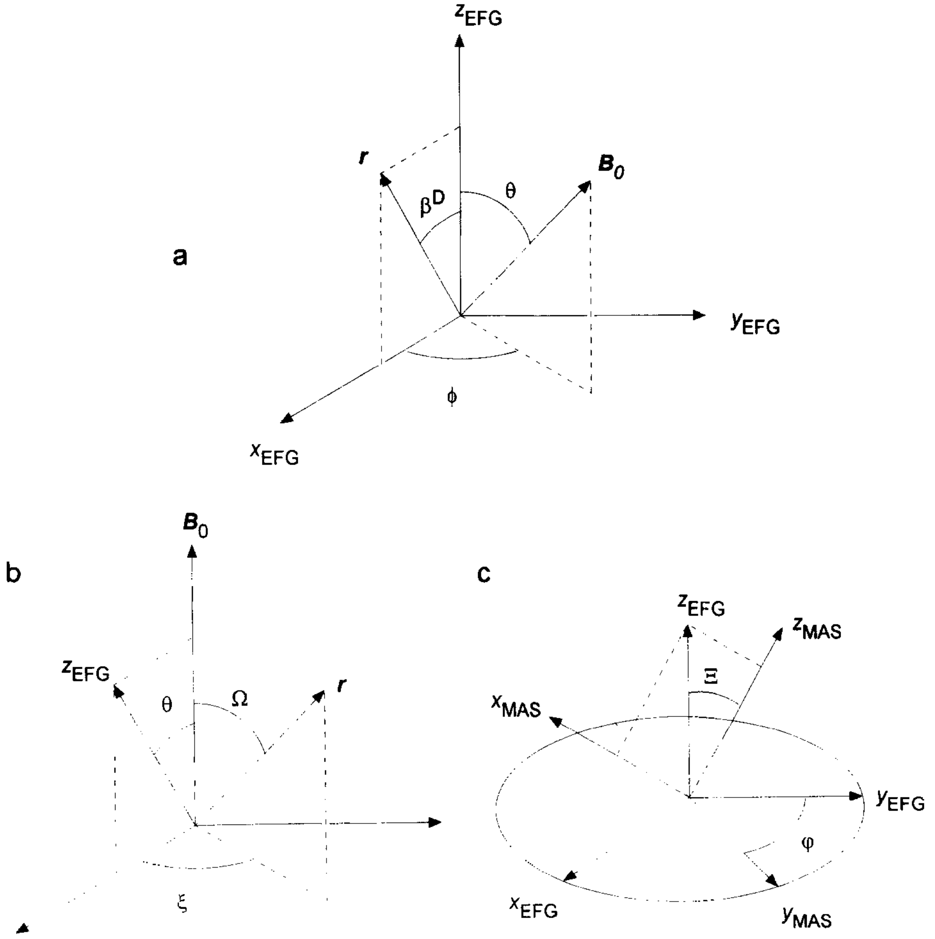

Fig. 1. Different reference frames used to study the MAS NMR lines of spin-1/2 nuclei coupled to spin-3/2 quadrupolar nuclei. (a) Location of the magnetic field $\boldsymbol{B}_0$ and the internuclear vector $\boldsymbol{r}$ in the EFG frame. (b) Location of the main z_{EFG} axis and the vector $\boldsymbol{r}$ in the Zeeman frame. (c) Relative orientation of MAS and EFG frames.

dipolar I,S coupling can be included:

$$\begin{aligned}\Delta\nu_m(\theta) = -D\Big\{&(1-3\cos^2\Omega)\sum n a_{mn}^2(\theta)\\ &-3\sin\Omega\cos\Omega\cos\xi\\ &\times\sum\big[\sqrt{[S(S+1)-m(m+1)]}\\ &\times a_{m,n+1}(\theta)a_{mn}(\theta)\\ &+\sqrt{[S(S+1)-m(m-1)]}\\ &\times a_{m,n-1}(\theta)a_{mn}(\theta)\big]\Big\} \qquad (5)\end{aligned}$$

where the angles Ω and ξ locate the internuclear vector $\boldsymbol{r}$ in the Zeeman frame (Fig. 1b). If $\boldsymbol{r}$ is further positioned in the xz plane of the EFG tensor (Fig. 1a), then $\cos\Omega = \cos\beta^D\cos\theta + \sin\beta^D\sin\theta\cos\phi$, and $(\sin\Omega\cos\xi) = \cos\beta^D\sin\theta - \sin\beta^D\cos\theta\cos\phi$. On the other hand, under MAS conditions, the following relations are valid (Fig. 1c):

$$\begin{aligned}\cos\theta = {}&\cos(54.7°)\cos\Xi\\ &+\sin(54.7°)\sin\Xi\cos(\omega t) \qquad (6)\\ \sin\theta\cos\phi = {}&-\cos(54.7°)\sin\Xi\cos\varphi\\ &+\sin(54.7°)[\cos\Xi\cos\varphi\cos(\omega t)\\ &+\sin\varphi\sin(\omega t)] \qquad (7)\end{aligned}$$

where Ξ and φ are the polar angles locating the z_{EFG} axis in the MAS frame (Fig. 1c) and ω is the sample spinning frequency.

Therefore, the shifts on the spin-1/2 line can be calculated as follows. For a particular orientation given by Ξ and φ, the required functions of θ and ϕ are obtained through eqns. 6 and 7, and the dipolar shift through eqn. 5. This is repeated for many equally spaced values of ωt in the range 0–2π, and the results are averaged over one cycle of ωt, yielding the desired shifts $\Delta\nu_m$ associated with the orientation (Ξ,φ). These calculations are repeated for 500 × 200 different pairs of values of Ξ and φ, the intensities are scaled according to $\sin\Xi$, and are finally stored in matrix form, as is usual in the computation of powder patterns. A microcomputer program (available on request) has been written which calculates the line shapes according to the above scheme.

Results and discussion

Fig. 2 shows the results obtained with the exact approach when $\beta^D = 0$, and when only dipolar coupling is considered as a mechanism of transmission of quadrupolar effects to the MAS NMR lines of the spin-1/2 nucleus. In this figure, the four line positions are plotted (in units of D) as a function of the ratio (χ/ν_S) for a positive quadrupole coupling constant (reversing its sign reverses all line positions). The points shown in Fig. 2 are actually the centers of mass of "Pake-like" powder patterns, with the sole exception of one of the lines obtained when (χ/ν_S) = 4, which gives rise to a single spin-1/2 resonance for all orientations. For small values of (χ/ν_S) first-order conditions are seen to be met, and approximate straight lines with slope ±0.3 are obtained. When all four lines are subjected to a Gaussian broadening of 0.5 units of D, a nearly symmetric doublet is obtained up to (χ/ν_S) ≈ 3. Beyond this point, the line shape is an asymmetric 2:1:1 triplet, and for (χ/ν_S) > 5, a distorted quartet is obtained. It should be noticed that since both the triplet and the quartet are asymmetric; they are in principle a source of information on the sign of χ.

In the case of the recently observed ^{13}C,^{35,37}Cl coupling in chlorine-containing organic compounds [24–26], the quadrupole coupling con-

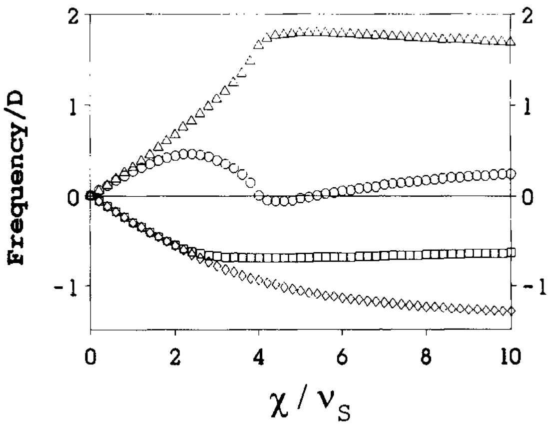

Fig. 2. Line positions (in units of D) of a spin-1/2 nucleus dipolar coupled to a spin-3/2 nucleus as a function of the ratio (χ/ν_S), as obtained by full-matrix diagonalization of the Zeeman–quadrupole Hamiltonian for positive χ and $\beta^D = 0$.

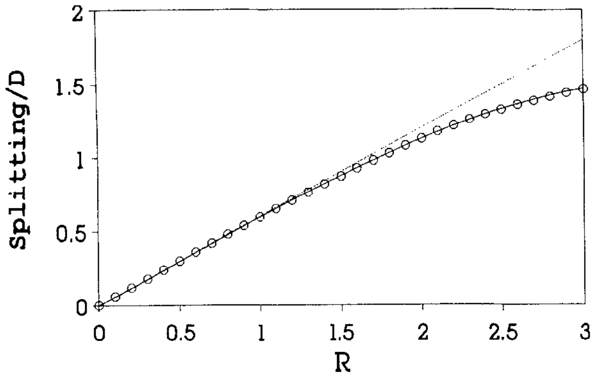

Fig. 3. Symmetric splitting (in units of D) caused by spin-3/2 nuclei on spin-1/2 MAS NMR lines, as a function of the ratio $R = |\chi/\nu_S|$. Circles: values obtained by the exact calculations. Full line: values given by eqn. 8. Dotted straight line: result predicted by first-order theory.

stant for the major ^{35}Cl isotope is *ca.* −70 MHz [27], whereas the experimental resonance frequencies ν_S at the studied fields [24–26] are 19.6, 29.4, 39.2 and 49.0 MHz at 4.7, 7.05, 9.4 and 11.7 T, respectively (^{1}H NMR frequencies are 200, 300, 400 and 500 MHz). Thus the values of $|\chi/\nu_S|$ are 3.6, 2.4, 1.8 and 1.4, respectively, and a broad triplet is expected at 4.7 T, whereas at the higher fields symmetric doublets are predicted (Fig. 2). Even for these latter cases, first-order theory is not strictly applicable, since in all of them $|\chi/\nu_S| > 1$. Fig. 3 compares the exact splittings with those given by first-order theory (again for $\beta^D = 0$). The exact splitting has been obtained by taking the centers of mass of the four lines, separately averaging those corresponding to $m = \pm 3/2$ and $m = \pm 1/2$, and subtracting them. As seen in Fig. 3, deviations towards smaller splittings result when $R = |\chi/\nu_S|$ increases. The deviation is less than 5% for $R < 0.8$. Least-squares fitting of the exact splittings to a cubic polynomial equation gives:

$$s = D(0.581R + 0.033R^2 - 0.021R^3) \tag{8}$$

which can be used in the range $0.8 < R < 3$. Table 1 compares the calculated centers of mass of the four lines and the values of s as given by first-order theory, by the exact approach and by eqn. 8.

Experimental examples are shown in Table 2. The agreement with first-order theory is good at the higher fields, whereas eqn. 8 better describes the experimental observations at 7.05 T. Even at the highest field, however, the observed splittings seem to be smaller than those predicted on the basis of exact calculations. However, the above discussion is centered on the effect of the major ^{35}Cl isotope (75.53%; $Q = -0.08165$ *b*) [28]. First-order theory predicts that s is proportional

TABLE 1

Centers of mass of the four lines expected for spin-1/2,spin-3/2 residual dipolar coupling (in units of D) as a function of the ratio χ/ν_S when $\beta^D = 0$

χ/ν_S	First order [a]	m				s		
		−3/2	−1/2	+1/2	+3/2	Exact	FOT	Eqn. 8
0.8	±0.24	−0.24	0.26	0.22	−0.24	0.48	0.48	0.48
1.0	±0.30	−0.30	0.32	0.27	−0.30	0.59	0.60	0.59
1.2	±0.36	−0.35	0.39	0.31	−0.35	0.71	0.72	0.71
1.4	±0.42	−0.41	0.46	0.35	−0.41	0.82	0.84	0.82
1.6	±0.48	−0.46	0.54	0.39	−0.46	0.92	0.96	0.93
1.8	±0.54	−0.51	0.61	0.42	−0.51	1.03	1.08	1.03
2.0	±0.60	−0.56	0.68	0.44	−0.56	1.12	1.20	1.13
2.2	±0.66	−0.61	0.76	0.46	−0.60	1.21	1.32	1.21
2.4	±0.72	−0.66	0.83	0.46	−0.63	1.29	1.44	1.29
2.6	±0.78	−0.70	0.91	0.45	−0.65	1.36	1.56	1.35
2.8	±0.84	−0.74	0.99	0.43	−0.67	1.41	1.68	1.42
3.0	±0.90	−0.78	1.07	0.39	−0.68	1.46	1.80	1.47

[a] Line positions as given by first-order theory (FOT). The positive sign corresponds to the position of the ±1/2 states; the negative to ±3/2 states.

TABLE 2

Experimental results on ^{13}C,^{35,37}Cl residual dipolar coupling

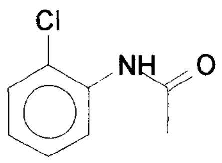

1

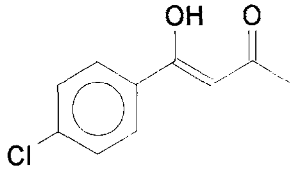

2

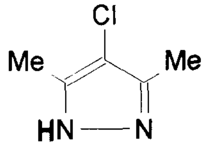

3

Compound	R	B_0/T	s_{exp} (kHz)	Ref.	s_{calc} [a] (kHz)	
					First order	Eqn. 8
1	2.38	7.05	0.59	52	0.81	0.73
1	1.43	11.7	0.41	52	0.49	0.47
2	2.38	7.05	0.69	53	0.81	0.73
3	1.79	9.4	0.50	51	0.61	0.58

[a] In all cases, $r_{C-Cl} = 1.73$ Å, $D = 0.57$ kHz and $|\chi| = 70$ MHz has been used.

to the combined factor $(D\chi/\nu_S)$, which is independent of γ_S. Thus the effect of the minor ^{37}Cl isotope (24.47%; $Q = -0.06435$ *b*) [28] is expected to be a reduction of the splitting by *ca.* 5%. It should be noted that the measurement of the ^{13}C lines are subjected to errors of *ca.* ±50 Hz.

As discussed above, the expected line shape at 4.7 T is a broad 2:1:1 triplet. Approximate second-order shifts given by the exact approach (Fig. 2) for $(\chi/\nu_S) = 3.6$ are -0.78 (average of two lines), $+0.27$ and $+1.30$ D (-8.4, $+3.0$ and $+14.7$ ppm for ^{13}C, using $D = 0.57$ kHz for $r_{C-Cl} = 1.73$ Å). These values correspond to positive quadrupole coupling constants. For χ negative, which seems to be the case for ^{35}Cl [27], they reverse their signs, and the central peak of the triplet appears on the low frequency side, measured from the center of the high-field doublets. This result is also in agreement with the experiments [24,25].

In the case of the ^{31}P,^{63,65}Cu spin pair, an indirect J interaction also occurs, leading to distorted J quartets [12–22]. Only the effect of the major (69.1%) ^{63}Cu isotope will be considered here. First-order theory predicts the following line positions (see eqn. 1):

$$\Delta\nu_{-3/2} = (3/2)J + d \tag{9}$$

$$\Delta\nu_{-1/2} = (1/2)J - d \tag{10}$$

$$\Delta\nu_{1/2} = -(1/2)J - d \tag{11}$$

$$\Delta\nu_{3/2} = -(3/2)J + d \tag{12}$$

We will call the four line positions given by eqns. 9–12 ν_1, ν_2, ν_3 and ν_4 in the order of increasing frequencies, the spacings as $\Delta\nu_{21} = \nu_2 - \nu_1$, $\Delta\nu_{32} = \nu_3 - \nu_2$, $\Delta\nu_{43} = \nu_4 - \nu_3$, and the differences between these line spacings as $\Delta\Delta\nu_{321} = \Delta\nu_{32} - \Delta\nu_{21}$, $\Delta\Delta\nu_{432} = \Delta\nu_{43} - \Delta\nu_{32}$ and $\Delta\Delta\nu_{4321} = \Delta\nu_{43} - \Delta\nu_{21}$.

When first-order conditions are no longer met, not only the quadrupole-induced distortion deviates from the expected value of d, but also the isotropic indirect contribution is not simply given by $-mJ$. Fig. 4 shows the changes in the line positions for the spin-1/2 nucleus as a function of (χ/ν_S) when only J coupling occurs (*i.e.*, $D = \Delta J = 0$). To study these deviations in the general case, where J coupling effects are combined with

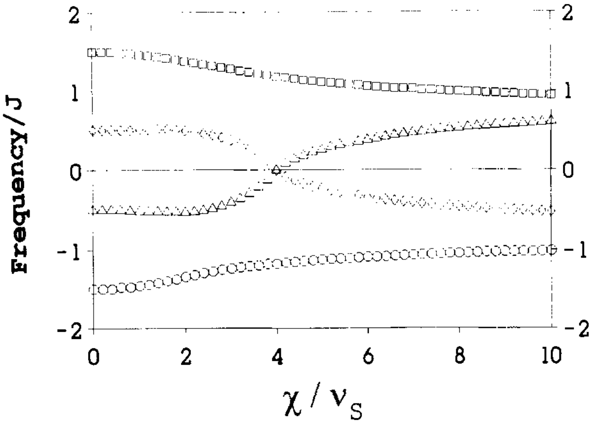

Fig. 4. Line positions (in units of J) of a spin-1/2 nucleus indirect coupled to a spin-3/2 nucleus as a function of the ratio (χ/ν_S), as obtained by full-matrix diagonalization of the Zeeman–quadrupole Hamiltonian for positive χ.

dipolar coupling, the exact approach was separately applied to the indirect and (effective) dipolar interactions, in the latter case for relevant values of the angle β^D (0, 30, 60 and 90°), up to $R = 3$. It was found that only a single set of coefficients for a cubic equation was needed in order to cover these cases, provided the factor $(3\cos^2\beta^D - 1)/2$ is included within the dipolar contribution. Thus the form of the cubic equation is:

$$\begin{aligned}\Delta\nu_m = {} & J\left[{}^J a(m) + {}^J b(m)R + {}^J c(m)R^2 + {}^J d(m)R^3\right] + D'\left[(3\cos^2\beta^D - 1)/2\right] \\ & \times\left[{}^D b(m)R + {}^D c(m)R^2 + {}^D d(m)R^3\right] \qquad (13)\end{aligned}$$

where $R = |\chi/\nu_S|$.

The coefficients ${}^J a(m)$, ${}^{J,D}b(m)$, ${}^{J,D}c(m)$ and ${}^{J,D}d(m)$ are given in Table 3. Reversing the sign of χ reverses all the line positions, thus reversing the sign of all coefficients. Table 4 shows the individual line positions for selected values of the ratio χ/ν_S when only the isotropic J coupling is involved, as compared to those given by eqn. 13.

As already discussed, the sense of the distortion d provides information about the sign of χ [22]. It has been argued that, even when first-order theory is not strictly applicable to these cases, d can still be obtained as $d = \Delta\Delta\nu_{4321}/4$ [22], and important information concerning the sign of χ and the value and sign of ΔJ can be obtained [22]. However, first-order theory is unable to provide the sign of J, since eqns. 9–12 predict that the line spacings are $\Delta\nu_{21} = |J| - 2d$, $\Delta\nu_{32} = |J|$, $\Delta\nu_{43} = |J| + 2d$ (provided that $|d|$ is smaller than $|J|$ so that no cross-over of lines takes place). An interesting outcome of the deviations from the first-order regime which are accounted for by eqn. 13 is the possibility of determining the sign of J. In the case of phosphine–copper–halide complexes, R lies in the range 0.2–0.9 at 7.05 T [22]. For comparison of the first-order results with those given by eqn. 13 when $J = \pm D'$, $D' > 0$, $\beta^D = 0$, $R = 1$, $\gamma_I > 0$, $\gamma_S > 0$, see Table 5. Notice that the columns for $J > 0$ and $J < 0$ are interchanged if either γ_I or γ_S are negative, whereas those for positive and negative χ are interchanged if (a) the factor $(3\cos^2\beta^D - 1)$ is negative or (b) the parameter D' becomes negative as a result of large ΔJ effects. Several interesting conclusions can be drawn. The value of $\Delta\Delta\nu_{4321}/4$ is an excellent approximation for d, as expected [22]. It can also be concluded that when first-order theory is not applicable, the sign of J can be gathered from the relation between $\Delta\Delta\nu_{321}$

TABLE 3

Coefficients corresponding to the cubic eqn. 13. These coefficients were derived assuming a positive value for χ. For negative χ, all coefficients change their signs.

m	${}^J a(m)$	${}^J b(m)$	${}^J c(m)$	${}^J d(m)$	${}^D b(m)$	${}^D c(m)$	${}^D d(m)$
−3/2	1.501	0.002	−0.045	0.006	−0.301	0.002	0.004
−1/2	0.501	−0.017	0.038	−0.016	0.308	0.017	0
1/2	−0.505	0.045	−0.072	0.022	0.272	0.017	−0.021
3/2	−1.497	−0.029	0.077	−0.013	−0.280	−0.034	0.017

TABLE 4

Centers of mass of the four lines expected for spin-1/2,spin-3/2 scalar coupling (in units of J) as a function of the ratio χ/ν_S

χ/ν_S	m [a]			
	−3/2	−1/2	+1/2	+3/2
0	+1.50	+0.50	−0.50	−1.50
1.4	+1.44+1.43	+0.51+0.51	−0.51−0.52	−1.44−1.42
1.6	+1.42+1.41	+0.51+0.51	−0.52−0.53	−1.40−1.40
1.8	+1.40+1.39	+0.50+0.50	−0.52−0.53	−1.39−1.38
2.0	+1.38+1.37	+0.50+0.49	−0.52−0.53	−1.35−1.35
2.2	+1.36+1.35	+0.48+0.48	−0.52−0.52	−1.32−1.33
2.4	+1.34+1.33	+0.46+0.46	−0.50−0.51	−1.30−1.30
2.6	+1.32+1.31	+0.44+0.43	−0.48−0.49	−1.28−1.28
2.8	+1.30+1.29	+0.41+0.40	−0.45−0.46	−1.26−1.26
3.0	+1.28+1.26	+0.37+0.36	−0.41−0.42	−1.24−1.24

[a] For each value of m, the first entry is the value computed using the exact approach, the second is that calculated using eqn. 13.

and $\Delta\Delta\nu_{432}$, provided that the sign of χ is known. For example, when $\chi/\nu_S = +1$, $|\Delta\Delta\nu_{432}| > |\Delta\Delta\nu_{321}|$ for positive values of J and *vice versa*. This simple relationship has been found to hold for several values of $|J|$ in the range $0.5D'$–$2D'$ and for β^D having the relevant values 0, 30 and 90°, which are typical of P,Cu complexes [13–22]. In all complexes studied so far the distortion d was found to be negative, implying positive values of χ for $\beta^D = 0$ and negative values when $\beta^D = 90°$ [22]. Since ΔJ effects are smaller than D, the effective constant D' is positive. Experimental line spacings (Table 6) for several different complexes provide evidence ($|\Delta\Delta\nu_{432}| > |\Delta\Delta\nu_{321}|$, compare with Table 5), that J is, in all cases,

TABLE 5

Line positions and spacings (in units of D') for a spin-1/2 nucleus coupled to a spin-3/2 nucleus, when $J = \pm D'$, $D' > 0$, $\beta^D = 0$ and $R = 1$

	First-order theory		Exact [a]			
			$J>0$	$J<0$	$J>0$	$J<0$
(χ/ν_S)	+1	−1	+1	+1	−1	−1
ν_1	−1.80	−1.20	−1.76	−1.76	−1.17	−1.16
ν_2	−0.20	−0.80	−0.24	−0.18	−0.83	−0.78
ν_3	0.80	0.20	0.83	0.78	0.24	0.18
ν_4	1.20	1.80	1.17	1.16	1.76	1.76
$\Delta\nu_{21}$	1.60	0.40	1.52	1.58	0.34	0.39
$\Delta\nu_{32}$	1.00	1.00	1.07	0.96	1.07	0.96
$\Delta\nu_{43}$	0.40	1.60	0.34	0.39	1.52	1.58
$\Delta\Delta\nu_{4321}/4$	−0.30	0.30	−0.30	−0.30	0.30	0.30
$\langle\Delta\nu\rangle$ [b]	1.00	1.00	0.98	0.98	0.98	0.98
$\Delta\Delta\nu_{321}$	−0.60	0.60	−0.45	−0.62	0.73	0.57
$\Delta\Delta\nu_{432}$	−0.60	0.60	−0.73	−0.57	0.45	0.62

[a] The line positions were calculated for a positive γ_I (see the text).

[b] $\langle\Delta\nu\rangle = (\Delta\nu_{21} + \Delta\nu_{32} + \Delta\nu_{43})/3$.

TABLE 6

Literature ^{31}P line spacings (in kHz) for several copper–phosphine–halide complexes

Complex [a]	$\Delta\nu_{43}$	$\Delta\nu_{32}$	$\Delta\nu_{21}$	$\Delta\Delta\nu_{432}$	$\Delta\Delta\nu_{321}$	$\langle\Delta\nu\rangle$ [b]	$\|J\|$ [c]
$(PCuCl)_4$ (c)	1.72	1.99	2.12	−0.27	−0.13	1.94	1.95
	1.68	1.98	2.11	−0.30	−0.13	1.92	1.93
$(PCuBr)_4$ (c)	1.71	1.91	2.00	−0.20	−0.09	1.87	1.88
	1.69	1.91	2.03	−0.22	−0.12	1.88	1.88
$(PCuI)_4$	1.41	1.57	1.69	−0.16	−0.12	1.56	1.56
	1.47	1.70	1.71	−0.23	−0.01	1.63	1.63
PCuCl	1.40	2.21	2.50	−0.81	−0.29	2.04	2.06
PCuBr	1.48	2.17	2.43	−0.69	−0.26	2.03	2.08
$(PCuBr)_4$ (s)	1.65	1.86	1.99	−0.21	−0.13		
	1.43	1.87	2.06	−0.44	−0.19		
$(PCuI)_4$ (s)	1.34	1.68	1.88	−0.34	−0.20		
	1.35	1.69	1.75	−0.34	−0.06		
$P_3Cu_2Cl_2$	1.49	1.91	2.08	−0.42	−0.17		
$P_3Cu_2I_2$	1.23	1.62	1.75	−0.39	−0.13		
$P_3Cu_2Br_2^-$	1.37	1.69	1.92	−0.32	−0.23		
$P_3Cu_2I_2^-$	1.08	1.20	1.23	−0.12	−0.03		
P_2CuCl	0.94	1.27	1.43	−0.33	−0.16		
P_2CuBr	0.88	1.28	1.44	−0.40	−0.16		
P_2CuI	0.88	1.20	1.43	−0.32	−0.23		

[a] P = Triphenylphosphine and derivatives; c = cube; s = step; experimental data from refs. 13–21.

[b] See Table 5.

[c] The values of $|J|$ have been obtained by fitting the three experimental line spacings to eqn. 13, with χ taken from ref. 22.

TABLE 7

Literature ^{119}Sn line spacings (in kHz) for Sn,Cl compounds

Compound	B_0/T	$\Delta\nu_{43}$	$\Delta\nu_{32}$	$\Delta\nu_{21}$	$\Delta\Delta\nu_{432}$	$\Delta\Delta\nu_{321}$	$\langle\Delta\nu\rangle$ [a]	$\vert J\vert$ [b]
Ph_3SnCl [c]	7.05	0.42	0.26	0.11	0.17	0.15	0.26	0.27
Ph_3SnCl [c]	4.7	0.50	0.24	0	0.26	0.24	0.25	0.27
Bz_3SnCl	4.7	0.48	0.23	0	0.25	0.23	0.24	0.26

[a] See Table 5.

[b] As in Table 6, with values of χ taken from refs. 9–11.

[c] Average of two non-equivalent crystal sites.

positive. Since both $\gamma(^{31}P)$ and $\gamma(^{63}Cu)$ are positive, it follows that $K(^{31}P,^{63}Cu)$ is positive. This latter result is in line with other cases of one-bond indirect coupling between ^{31}P and spin-1/2 transition metals [29]. Finally, one should note that the value of $|J|$ cannot be simply obtained from inspection of the spectra (see Table 5). A good approximation to the magnitude of the isotropic value of the indirect coupling constant can be obtained by applying eqn. 13. In the case of the tetrahedral copper sites in "cube" $(PCuX)_4$ complexes and in the linear PCuX complexes, $\beta^D = 0$ and the EFG at ^{63,65}Cu is axially symmetric, as required by the site symmetry in crystals [22]. Using the known (or derived) value of χ (with sign) and adjusting the line spacings to eqn. 13, J can be obtained (as shown in Table 6). As can be seen, the values of J are very close to the average of the three spacings, as previously suggested [13–21].

Similar arguments apply to the ^{119}Sn,^{35,37}Cl spin pair, where both J and D' effects are manifested in the ^{119}Sn MAS NMR spectra in the solid state [9–11]. Table 7 shows experimental values for Sn,Cl compounds at two different fields. Consideration of the relative line positions shows that in this case d is positive (in contrast to the P,Cu case), as a result of the combination of $\beta^D = 0$, $D' > 0$ and $\chi < 0$ [11]. Comparison of $\Delta\Delta\nu_{321}$ and $\Delta\Delta\nu_{432}$ (Table 7) with the results shown in Table 5 for χ/ν_S negative indicates that J is positive for the ^{119}Sn,^{35}Cl spin pair in these compounds $[\gamma(^{119}Sn) < 0]$. Therefore, the value of $K(^{119}Sn,^{35}Cl)$ is negative, again in agreement with signs of one-bond K values measured for pairs of nuclei of groups IV and VII of the periodic table [29]. As before, the value of $|J|$ (shown in Table 7) can be obtained by applying eqn. 13 and using the known value of χ for the major ^{35}Cl isotope.

It should be noticed that the relationship $|\Delta\Delta\nu_{432}| > |\Delta\Delta\nu_{321}|$ for positive J (and *vice versa*) has been restricted to cases where $D' > 0$, $\beta^D = 0$, 30 and 90° and $|J|$ in the range 0.5–2 D' which are applicable to the experimental observations in the ^{31}P,^{63,65}Cu and ^{119}Sn,^{35,37}Cl couplings. In other cases, one should resort to eqn. 13 in order to establish the sign of J.

In conclusion, equations have been developed which can be used to calculate the multiplet splittings of spin-1/2 MAS NMR lines when coupling to spin-3/2 nuclei occurs. These equations are suitable for a range of quadrupole coupling constants outside the validity of first-order theory, and take into account the existence of dipolar and scalar (both iso- and anisotropic) interactions. Additionally, the possibility of determining the sign of the isotropic indirect coupling constant is discussed.

Acknowledgements

A.C.O. and S.H.A. are grateful to the University of Rosario, to CONICET (Consejo Nacional de Investigaciones Cientificas) and to Fundacion Antorchas for financial support. S.H.A. thanks CONICET for a fellowship. R.K.H. acknowledges Research Grant GR/H30175 from the UK Science and Engineering Research Council, with access to the National Solid-State NMR Service.

References

1 R.K. Harris and A.C. Olivieri, *Prog. Nucl. Magn. Reson. Spectrosc.*, 24 (1992) 435.

2 K. Eichele, R.E. Wasylishen, J.F. Corrigan, S. Doherty, Y. Sun and A.J. Carty, *Inorg. Chem.*, 32 (1993) 121.

3 K. Eichele and R.E. Wasylishen, *Angew. Chem. Int. Ed. Engl.*, 31 (1992) 1222.

4 A.C. Olivieri, L. Frydman and L.E. Diaz, *J. Magn. Reson.*, 75 (1987) 50.

5 A.C. Olivieri, *J. Magn. Reson.*, 81 (1989) 201.

6 A.C. Olivieri, L. Frydman, M. Grasselli and L.E. Diaz, *Magn. Reson. Chem.*, 26 (1988) 615.

7 A.C. Olivieri, *J. Magn. Reson.*, 101A (1993) 313.

8 A.C. Olivieri, *Solid State Nucl. Magn. Reson.*, 1 (1992) 345.

9 R.K. Harris, A. Sebald, D. Furlani and G. Tagliavini, *Organometallics*, 7 (1988) 388.

10 R.K. Harris, *J. Magn. Reson.*, 78 (1988) 389.

11 D.C. Apperley, H. Bai and R.K. Harris, *Molec. Phys.*, 68 (1989) 1277.

12 E.M. Menger and W.S. Veeman, *J. Magn. Reson.*, 46 (1982) 257.

13 J.W. Diesveld, E.M. Menger, H.T. Edzes and W.S. Veeman, *J. Am. Chem. Soc.*, 102 (1980) 7935.

14 G. A. Bowmaker, J.C. Dyason, P.C. Healy, L.M. Engelhardt, C. Pakawatchai and A.H. White, *J. Chem. Soc. Dalton Trans.*, (1987) 1089.

15 P.F. Barron, J.C. Dyason, P.C. Healy, L.M. Engelhardt, C. Pakawatchai, V.A. Patick and A.H. White, *J. Chem. Soc. Dalton Trans.*, (1987) 1099.

16 G.A. Bowmaker, L.M. Engelhardt, P.C. Healy, J.D. Kildea, R.I. Papasergio and A.H. White, *Inorg. Chem.*, 26 (1987) 3533.

17 G.A. Bowmaker, J.D. Cotton, P.C. Healy, J.D. Kildea, S.B. Silong, B.W. Skelton and A.H. White, *Inorg. Chem.*, 28 (1989) 1462.

18 G.A. Bowmaker, A. Camus, P.C. Healy, B.W. Skelton and A.H. White, *Inorg. Chem.*, 28 (1989) 3883.

19 P.C. Healy, J.V. Hanna, J.D. Kildea, B.W. Skelton and A.H. White, *Austr. J. Chem.*, 44 (1991) 427.

20 P.C. Healy, A.K. Whittaker, J.D. Kildea, B.W. Skelton and A.H. White, *Austr. J. Chem.*, 44 (1991) 729.

21 B. Mohr, E.E. Brooks, N. Rath and E. Deutsch, *Inorg. Chem.*, 30 (1991) 4541.

22 A.C. Olivieri, *J. Am. Chem. Soc.*, 114 (1992) 5758.

23 V. Mlynárik, *Prog. Nucl. Magn. Reson. Spectrosc.*, 18 (1986) 277.

24 A.C. Olivieri, P. Cabildo; R.M. Claramunt and J.E. Elguero, *J. Phys. Chem.*, submitted for publication.

25 R.K. Harris, M. Sunnetcioglu, K.S. Cameron and F.G. Riddell, *Magn. Reson. Chem.*, submitted for publication.

26 R.M. Cravero, C. Fernandez, M. Gonzalez-Sierra and A.C. Olivieri, *J. Chem. Soc. Chem. Commun.*, (1993) 1253.

27 E.A.C. Lucken, *Nuclear Quadrupole Coupling Constants*, Academic Press, London, 1969, p. 187.

28 P. Pyykko, *Z. Naturforsch. A: Phys. Sci.*, 47 (1992) 189.

29 C.J. Jameson, in J. Mason (Ed.), *Multinuclear NMR*, Plenum Press, New York, NY, 1987, Ch. 4.

Structural Information from Quadrupolar Nuclei in Solid State NMR

SHARON E. ASHBROOK,[1] MELINDA J. DUER[2]

[1] *School of Chemistry and EaStChem, University of St. Andrews, North Haugh, St. Andrews, KY16 9ST, United Kingdom*
[2] *Department of Chemistry, University of Cambridge, Lensfield Road, Cambridge, CB2 1EW, United Kingdom*

ABSTRACT: Solid-state NMR has become the method of choice for determining details of molecular-level structure in heterogeneous systems. Though spin-1/2 nuclei still form the core of most such studies, quadrupolar nuclei are increasingly being used. This review assesses what is currently possible, from achieving high-resolution spectra for quadrupolar nuclei (a prerequisite for most structure determination work), to forming correlation spectra which give qualitative details of spatial proximity of nuclei and the determination of internuclear distances, between quadrupolar spins and quadrupolar and spin-1/2 nuclei. Examples are given of each method discussed, and the advantages and disadvantages of the various experiments for different possible applications are assessed. © 2006 Wiley Periodicals, Inc. Concepts Magn Reson Part A 28A: 183–248, 2006

KEY WORDS: solid-state NMR; quadrupole coupling; quadrupolar nuclei; structure determination; magic-angle spinning; double rotation; dynamic-angle spinning; correlation spectroscopy; multiple-quantum magic-angle spinning; satellite-transition magic-angle spinning; multiple quantum; rotational resonance; rotational-echo double resonance; J-coupling; scalar coupling; computation/calculation of NMR parameters.

1. INTRODUCTION

1.1 Why Use Quadrupolar Nuclei?

Most solution-state NMR spectroscopists have an inbuilt horror of quadrupolar nuclei. They are "impossible" to use spectroscopically and often have unpleasant side effects on otherwise well-behaved spin-1/2 nuclei and their spectra. The situation has never been this bad in solid-state NMR. For a start, the excessively short relaxation times that occur for quadrupolar nuclei in solution and that lead to excessive line broadening do not occur to the same extent in the solid state. Fast relaxation requires a large time-dependent nuclear spin interaction, the time dependence usually arising from molecular motion. In the solid state, the molecular motion, and thus the time-dependent element, is often greatly reduced, and so the relaxation times experienced by quadrupolar nuclei in the solid state, though often still fast, are not so fast that they lead to (more) line broadening. Since 1995,

Received 5 September 2005; revised 20 December 2005; accepted 22 December 2005

Correspondence to: Dr. Melinda Duer; E-mail: mjd13@cam.ac.uk

Concepts in Magnetic Resonance Part A, Vol. 28A(3) 183–248 (2006)

there has been an easily accessible technique for obtaining high-resolution spectra of quadrupolar nuclei in the solid state. There is no doubt that the interest in using quadrupolar nuclei to study molecular structure in solids has received a huge boost from the introduction of the multiple-quantum magic-angle-spinning (MQMAS) method (*1*). But there remains the question of why we should wish to use quadrupolar nuclei in any structural study when, despite the high-resolution methods for quadrupolar nuclei, there is no doubt that spin-1/2 nuclei are still much easier to handle.

The answer is simple: 75% of NMR-active nuclei are quadrupolar (and of these, the vast majority are half-integer). Thus, for many materials that we may wish to examine, we have no choice but to use quadrupolar nuclei in our study. Even if there are convenient spin-1/2 nuclei present, we cannot hope to obtain a full structural picture if we ignore all the atomic species that have quadrupolar nuclei. Beyond this, there is the further consideration that many otherwise useful spin-1/2 nuclei have inconveniently low natural abundances—for example, ^{13}C (1.1% natural abundance) and ^{15}N (0.37%). So if we wish to study the structure of a naturally occurring solid protein, we have the option of using these low-abundance nuclei or ^{1}H if we restrict ourselves to using spin-1/2 nuclei. The strong dipolar couplings within the network of abundant ^{1}H in a solid protein means that ^{1}H NMR spectra consist of broad, featureless lines unless rather sophisticated methods are employed. How much easier life would be if we could use instead the near-100% abundant ^{14}N quadrupolar ($I = 1$) nucleus in our study. To this end, there have been experiments developed that use ^{14}N overtone spectroscopy and measure the ^{14}N overtone spectrum directly, indirectly, and via cross-polarization, which brings us closer to this goal (*2–4*).

1.2 What Is Quadrupolar Coupling?

So-called quadrupolar nuclei (i.e., those with $I > ½$) possess an electric quadrupole moment in addition to the magnetic dipole moment that all NMR-active nuclei must have. Electric quadrupole moments interact with electric field gradients, which in turn arise from the particular distribution of electrons and other nuclei around the nucleus in question, unless that nucleus is at a crystallographic site of cubic symmetry. The nuclear electric quadrupole moment/electric field gradient interaction can be rather large, causing powder patterns of megahertz in width for solid samples consisting of large numbers of randomly oriented crystallites (i.e., powders). The size of the interaction depends on the size of the nuclear electric quadrupole moment, a constant that is tabulated in many places (*5*), and the size of the electric field gradient, which is determined by the molecular and electronic structure around the nucleus. The nuclear electric quadrupole moment/electric field gradient interaction can be described by the Hamiltonian in Eq. [1.1]:

$$\hat{H}_Q = \frac{eQ}{6I(2I-1)\hbar}\,\hat{\mathbf{I}}\cdot\mathbf{V}\cdot\hat{\mathbf{I}} \qquad [1.1]$$

where eQ is the nuclear electric quadrupole moment and $\mathbf{V}$ is a second-rank Cartesian tensor describing the electric field gradient. Such a tensor can be represented by a 3 × 3 matrix (Eq. [1.2]) in which a component $V_{\alpha\beta}$, α, $\beta = x, y, z$, is the α-component of the electric field gradient where the applied magnetic field of the NMR experiment is in the direction β of the defining frame of reference (the relevance of the applied magnetic field for an electric interaction will become clear shortly).

$$\mathbf{V} = \begin{pmatrix} V_{xx} & V_{xy} & V_{xz} \\ V_{yx} & V_{yy} & V_{yz} \\ V_{zx} & V_{zy} & V_{zz} \end{pmatrix} \qquad [1.2]$$

As already implied, such a tensor can be expressed with respect to any Cartesian axis frame. One frame of particular relevance is the principal axis frame (PAF), which is the reference frame in which the tensor is diagonal, with components V_{xx}, V_{yy}, and V_{zz}, which are often expressed as the anisotropy and asymmetry:

$$eq = V_{zz}^{PAF}, \qquad \eta_Q = \frac{V_{xx}^{PAF} - V_{yy}^{PAF}}{V_{zz}^{PAF}} \qquad [1.3]$$

where eq is the anisotropy of the electric field gradient tensor and η_Q its asymmetry. The trace of the electric field gradient tensor is always zero.

In a large magnetic field, the Zeeman interaction with the nuclear magnetic dipole moment is the dominant interaction, and the applied magnetic field in such a case acts as the quantization axis for the nuclear spins. Thus the magnetic dipole moment is oriented by the applied magnetic field, and with it (because it is part of the same nucleus) the nuclear electric quadrupole moment, even though the latter has no interaction with the applied field (Fig. 1.1).

The electric field gradient tensor meanwhile is determined purely by the molecular structure around the nucleus and thus has an orientation that is fixed with respect to a molecular frame of reference. The interaction between the nuclear electric quadrupole

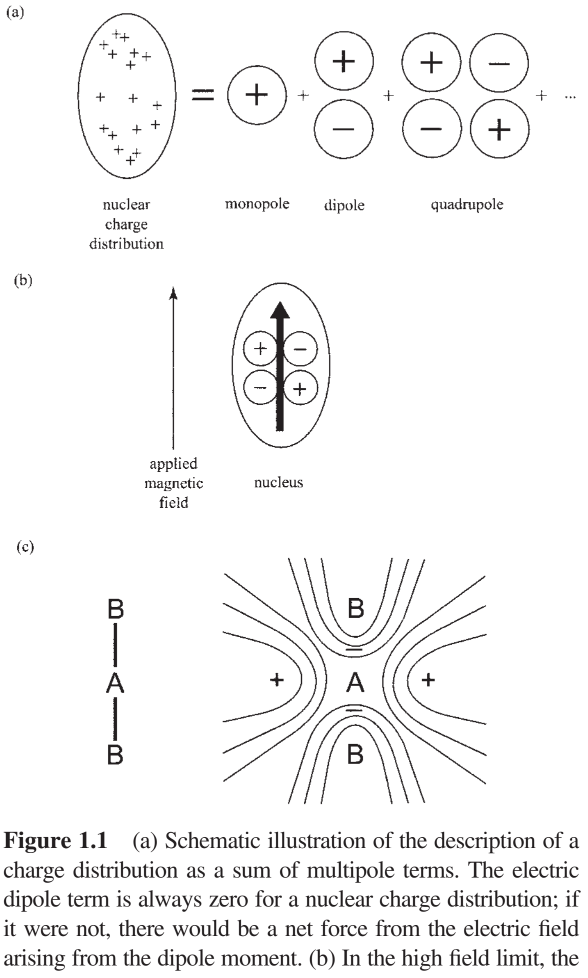

Figure 1.1 (a) Schematic illustration of the description of a charge distribution as a sum of multipole terms. The electric dipole term is always zero for a nuclear charge distribution; if it were not, there would be a net force from the electric field arising from the dipole moment. (b) In the high field limit, the magnetic dipole moment (represented by the bold arrow) is oriented by the applied magnetic field in the NMR experiment. The nuclear electric quadrupole moment associated with the nucleus is thus also oriented with respect to the applied field, although it has no interaction with it. (c) A molecule (AB_2) with bonds in geometry shown on the left will give rise to an electric field gradient of the form shown on the right by virtue of the bond electron distribution. (There will also be an electric field gradient arising from the core electrons of all atoms.) Such an electric field gradient will interact with any nuclear electric quadrupole moment.

moment then depends on its orientation with respect to the molecule, which in turn is determined by the direction of the applied field. In other words, the strength of the nuclear electric quadrupole moment/electric field gradient interaction depends on the orientation of the molecule (or more precisely, the electric field gradient tensor arising from it) with respect to the applied magnetic field, and so is termed anisotropic (i.e., the interaction strength depends on molecular orientation).

The principal axis frame of the electric field gradient tensor is a property of the molecular structure; the orientation of the electric field gradient is generally described by the orientation of its principal axis frame with respect to the applied magnetic field or, equivalently, with respect to a laboratory frame in which, by convention, the applied magnetic field lies along *z*.

The effect of the quadrupole coupling Hamiltonian of Eq. [1.1] can then be approximated in this high field case using average Hamiltonian theory or, equivalently, perturbation theory. Both these approaches express the quadrupole interaction Hamiltonian as a sum of contributions of successively higher order in the applied magnetic field; the level of approximation required for any given case then depends on the size of the quadrupole coupling interaction relative to the Zeeman interaction. The first- and second-order contributions to the quadrupole coupling Hamiltonian are given by Eqs. [1.4] and [1.5] (*6*):

$$\hat{H}_Q^{(1)} = \sqrt{6}\,\frac{e^2qQ}{4I(2I-1)}\,W_{20}^Q\hat{T}_{20}^Q \qquad [1.4]$$

$$\hat{H}_Q^{(2)} = -\left(\frac{e^2qQ}{4I(2I-1)}\right)^2 \frac{1}{\omega_0}\frac{2}{5} \times \left\{\begin{array}{l} (-3\sqrt{10}\,\hat{T}_{30}^Q + \hat{T}_{10}^Q(3-4I(I+1)))V_{00}^Q \\ +\,(-12\sqrt{10}\,\hat{T}_{30}^Q - \hat{T}_{10}^Q(3-4I(I+1)))V_{20}^Q \\ +\,(-34\sqrt{10}\,\hat{T}_{30}^Q + 3\hat{T}_{10}^Q(3-4I(I+1)))V_{40}^Q \end{array}\right\} \qquad [1.5]$$

where the spherical tensor operators $\hat{T}_{k0}^Q$ are given by

$$\hat{T}_{10}^Q = \hat{I}_z, \qquad \hat{T}_{20}^Q = \sqrt{\frac{1}{6}}\,(3\hat{I}_z^2 - I(I+1)),$$

$$\hat{T}_{30}^Q = \sqrt{\frac{1}{10}}\,(5\hat{I}_z^2 - 3I(I+1)+1)\hat{I}_z \qquad [1.6]$$

The W_{20}^Q parameters that contain all the geometrical terms for the first-order term are given by

$$W_{20}^Q = \sum_{n=0,\pm2} D_{n0}^2(\alpha, \beta, \gamma)\,B_{2n} \qquad [1.7]$$

ith

$$_{20} = 1 \quad B_{2\pm2} = \frac{1}{\sqrt{6}}\,\eta_Q \qquad [1.8]$$

and the V_{k0}^Q parameters containing all the geometrical terms for the second-order term are given by

$$V_{k0}^Q = \sum_n D_{n0}^k(\alpha, \beta, \gamma)\,A_{kn} \qquad [1.9]$$

with

$$A_{00} = -\frac{1}{5}(3 + \eta_Q^2)$$

$$A_{20} = \frac{1}{14}(\eta_Q^2 - 3) \qquad A_{2\pm2} = \frac{1}{7}\sqrt{\frac{3}{2}}\,\eta_Q$$

$$A_{40} = \frac{1}{140}(18 + \eta_Q^2) \quad A_{4\pm2} = \frac{3}{70}\sqrt{\frac{5}{2}}\,\eta_Q \quad A_{4\pm4} = \frac{1}{4\sqrt{70}}\,\eta_Q^2 \qquad [1.10]$$

In Eqs. [1.4], [1.5], [1.7], and [1.9], the angles (α, β, γ) are the Euler angles (see ref. [*6*] for a definition of Euler angles), which rotate the electric field gradient tensor principal axis frame into the laboratory frame, and the $D_{n0}^k(\alpha,\ \beta,\ \gamma)$ are Wigner rotation matrix elements for the rotation matrices connecting the two frames.

Equations [1.4] and [1.5] can be used to derive the transition frequencies expected for a quadrupolar spin I between levels $m \rightarrow m + 1$, where m denotes the magnetic quantum number. The first- and second-order contributions to the transition frequencies so derived are given by Eqs. [1.11] and [1.12]:

$$\Delta\omega_Q^{(1)} = \frac{3e^2qQ}{4I(2I-1)}(2m+1)W_{20}^Q \qquad [1.11]$$

$$\Delta\omega_Q^{(2)} = -\left(\frac{e^2qQ}{4I(2I-1)}\right)^2 \frac{2}{\omega_0} \times \left\{ \begin{array}{l} (I(I+1) - 9m(m+1) - 3)V_{00}^Q \\ +\ (8I(I+1) - 36m(m+1) - 15)V_{20}^Q \\ +\ 3(6I(I+1) - 34m(m+1) - 13)V_{40}^Q \end{array} \right\} \qquad [1.12]$$

Two other terms are frequently used when discussing quadrupolar nuclei: the quadrupole coupling constant, C_Q, which is given by (e^2qQ/h) in units of hertz or, equivalently, χ, which is $(e^2qQ/\hbar)$ and so is in units of rad s^{-1} and the quadrupole coupling tensor, $\boldsymbol{\chi}$, which is given by $\boldsymbol{\chi} = (eQ/\hbar)\,\mathbf{V}$.

Quadrupole coupling constants are often of the order of megahertz or even tens of megahertz for quadrupolar spins in sites of noncubic symmetry. In these cases, the second-order (and possibly higher-order) contributions to the transition frequency are significant. Both first- and second-order contributions have a molecular orientation dependence (see Eqs [1.11] and [1.12]), and thus we can identify the cause of the dramatic linebroadening seen in solid-state NMR spectra of quadrupolar nuclei from powder samples as arising from this anisotropy in the interaction.

There is one important point to note from Eq. [1.11], however, as regards line broadening: for half-integer spins, the so-called central transition $+1/2 \rightarrow -1/2$ has a transition frequency that to first order is independent of molecular orientation. Thus, to first order, this transition is not broadened by the quadrupolar coupling. The second-order contribution to the transition frequencies has an isotropic component (proportional to V_{00}^Q). This will feature in the NMR spectrum of the nucleus in addition to any isotropic chemical shift that may be present.

1.3 Brief Overview

The huge line broadening discussed in section 1.2, which is inevitable in the solid-state NMR spectra of most quadrupolar spins, would make the situation seem hopeless as far as their use in structure determination is concerned. However, this is far from the case. A prerequisite is clearly to obtain resolution between the signals from chemically different sites, and we discuss this in the next section. Excellent and straightforward methods now exist to perform such resolution efficiently. In sections 4–6, we examine current and emerging methods designed as tools for molecular and solid-state structure determination using quadrupolar nuclei. Here we find an increasingly vast array of methods that can provide quantitative internuclear distance information and more qualitative spatial correlation methods.

2. METHODS FOR OBTAINING HIGH-RESOLUTION SPECTRA OF QUADRUPOLAR NUCLEI

It is not the intention of this review to give a comprehensive account of all the methods available for obtaining high-resolution spectra of quadrupolar nuclei in the solid state and, in particular, all their refinements. However, as mentioned previously, an essential prerequisite to using quadrupolar nuclei to study molecular structure is that we can somehow resolve signals from different chemical sites. Thus, it is appropriate here to say a few words on resolution methods and their relative efficacy. For a more comprehensive review of these methods, the reader is referred to (*7*). In the discussion that follows, we focus exclusively on half-integer quadrupolar spins. There are at present no general techniques for obtaining high-resolution spectra for integer spin quadrupolar nuclei when the quadrupole coupling is large. There are, however, only two such nuclei that chemists are ever likely to be concerned with and those are ^{14}N and ^{2}H, both spin-1.

2.1 Magic-Angle Spinning

Rapid magic-angle spinning (or MAS) will average to zero the W_{20}^{Q} term of the first-order contribution to the quadrupolar spin transition frequencies (see Eq. [1.11]) and the V_{20}^{Q} term of the second-order contribution (Eq. [1.12]). In practice, it is often not possible to spin the sample rapidly enough to completely average the first-order term (the spinning rate needs to be significantly larger than the size of the W_{20}^{Q} term and its associated coefficients in Eq. [1.11]), i.e., potentially several megahertz. Where the spinning rate does not satisfy this condition, spinning sidebands will result. The first-order term for the central transition ($+1/2 \rightarrow -1/2$) is zero (see Eq. [1.11]), so this transition is unaffected to first order by magic-angle spinning. The satellite transitions ($m \rightarrow (m + 1)$, where $m \neq 1/2$), however, are affected, and magic-angle spinning will cause otherwise broad and hence low-intensity powder patterns arising from these transitions to break up into (usually more easily observable) spinning sideband patterns. However, for larger quadrupole couplings, the spinning sidebands from the satellite transitions are spread over such a large frequency range that their individual intensities are so low that they are sometimes still not observable above the noise in the spectrum. Moreover, their intensity is understandably highly dependent on the spinning angle, and any slight deviation from the magic angle, with such large anisotropies involved, will broaden (and hence lower the maximum intensity of) the spinning sidebands into scaled powder patterns. They will then be difficult, if not impossible, to observe above the noise.

To second order (and higher even orders), all transitions are affected by the quadrupole coupling and so are affected by magic-angle spinning. As already stated, magic-angle spinning will average to zero the V_{20}^{Q} term of the second-order contribution (Eq. [1.12]), so removing the effects of this term from the NMR spectrum providing the rate of sample spinning is sufficiently rapid. It must be significantly larger than the size of the V_{20}^{Q} term and its associated coefficients in Eq. [1.12]. If the rate of spinning is not sufficient, spinning sidebands will again result. Magic-angle spinning will also have an averaging effect on the V_{40}^{Q} term in the second-order contribution to the transition frequency (Eq. [1.12]), but the resultant average will not be zero; thus, effects of this term will remain in the NMR spectrum, albeit scaled.

This effect is easily quantified: the transition frequencies under magic-angle spinning are those given in Eqs. [1.11] and [1.12] but with the W_{20}^{Q} and V_{k0}^{Q} parameters of Eqs. [1.7] and [1.9] replaced by

$$W_{20}^{Q} = \sum_{m} D_{m0}^{2}(-\omega_R t, \theta_R, 0) \sum_{n} D_{nm}^{2}(\alpha, \beta, \gamma) B_{2n} \tag{2.1}$$

$$V_{k0}^{Q} = \sum_{m} D_{m0}^{k}(-\omega_R t, \theta_R, 0) \sum_{n} D_{nm}^{k}(\alpha, \beta, \gamma) A_{kn} \tag{2.2}$$

where θ_R is the sample spinning angle with respect to the applied magnetic field and ω_R is the sample spinning rate.

Figure 2.1 shows the effect of magic-angle spinning on the central transition of a spin $I = 3/2$ nucleus; the transition is clearly narrowed by the technique, but a powder pattern caused by the V_{40}^{Q} component of the second-order transition frequency remains.

In summary, magic-angle spinning assists resolution but does not completely remove anisotropic broadening if the quadrupolar interaction is large.

2.2 Multiple-Quantum Magic-Angle Spinning (MQMAS)

In 1995, Frydman and Harwood (*1*) proposed a new method for obtaining high-resolution NMR spectra of half-integer quadrupolar nuclei. The method involves recording a two-dimensional spectrum under magic-angle spinning, a straightforward proposition in comparison with previous methods (see sections 2.4 and 2.5). It is no exaggeration to say that the invention of this technique completely changed the attitude of the spectroscopist toward quadrupolar nuclei for serious structural studies. Prior to 1995, use of quadrupolar

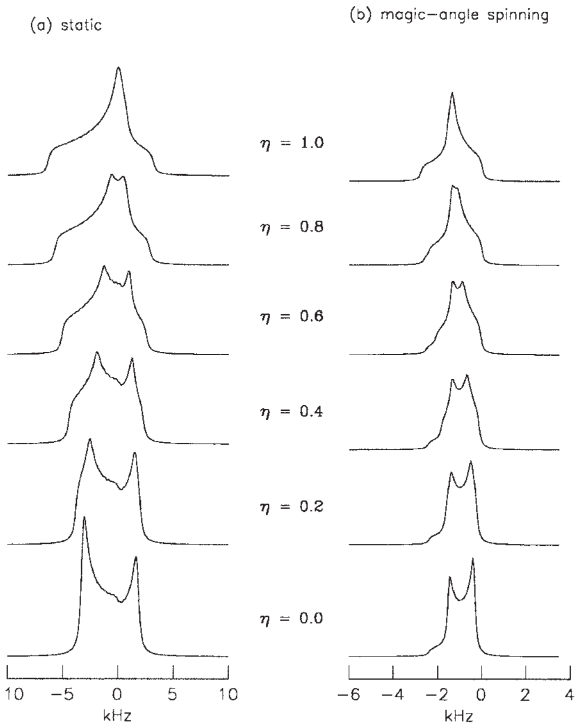

Figure 2.1 (a) Static, i.e., nonspinning and (b) magic-angle spinning (MAS) central-transition second-order quadrupolar powder pattern lineshapes, plotted as a function of the asymmetry parameter, η. The excitation pulses producing each spectrum are assumed to be ideal, i.e., $\omega_1 \gg \omega_Q$, and the spinning speed in the MAS spectra is assumed to be much larger than ω_Q.

nuclei in such studies was restricted largely to a few dedicated specialists. Since 1995, there have been too many studies to enumerate here. MQMAS began the drive for new techniques to use quadrupolar nuclei to determine structural information.

The MQMAS experiment (Fig. 2.2(a)) proceeds by initial excitation of a symmetric ($+m \rightarrow -m$) multiple-quantum coherence associated with the quadrupolar spin under study, while spinning the sample at the magic angle, as shown in Fig. 2.2(a) for $m = 3/2$. The quadrupolar contribution to the evolution frequency of such a coherence in the rotating frame can be deduced from Eqs. [1.4] and [1.5]. The first-order contribution from Eq. [1.4] is zero, leaving just a second-order contribution of

$$\Delta\omega_{m,-m} = -\left(\frac{e^2qQ}{4I(2I-1)}\right)^2 \frac{4}{\omega_0} m \times \left\{ \begin{array}{l} (I(I+1)-3m^2)V_{00}^Q + \\ (8I(I+1)-12m^2-3)V_{20}^Q + \\ (18I(I+1)-34m^2-5)V_{40}^Q \end{array} \right\} \qquad [2.3]$$

where the V_{k0}^Q parameters are given by Eq. [2.2], as this experiment is performed under magic-angle spinning. Under MAS, the V_{20}^Q or second-rank term in the evolution frequency averages to zero, so that during the t_1 period of the two-dimensional experiment, the $2m$ multiple-quantum coherence evolves under just

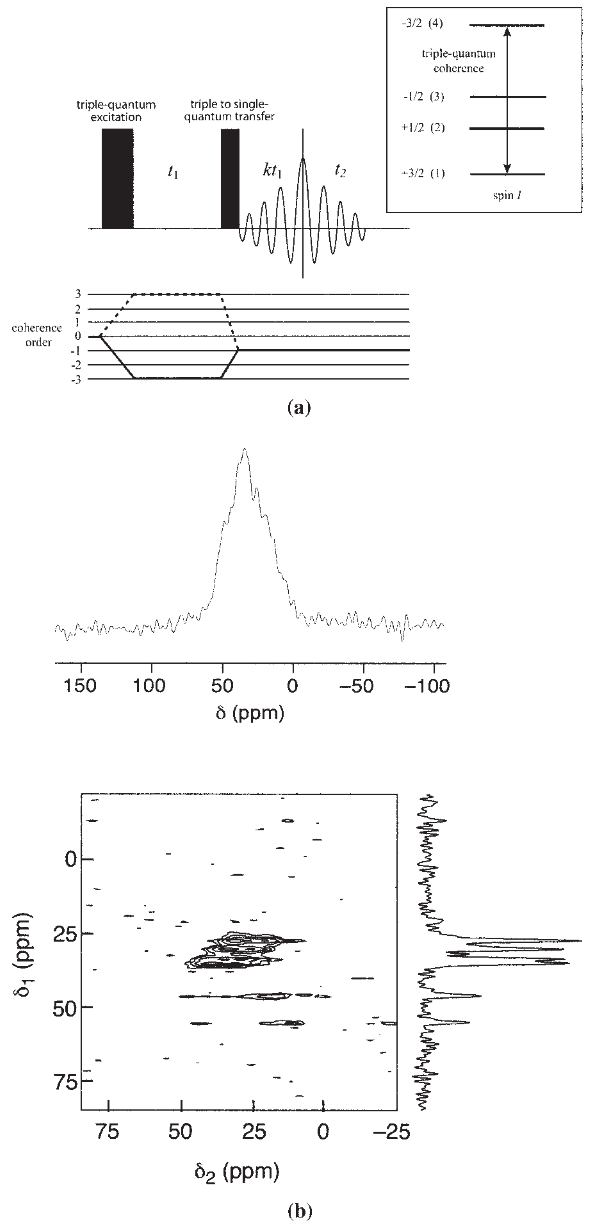

Figure 2.2 (a) Pulse sequence and coherence transfer pathway diagram for a basic triple-quantum MAS experiment (*1*). Phase cycling should be used to select the solid coherence pathway for $I = 3/2$, and the dashed pathway for $I > 3/2$. If pure-phase lineshapes are desired, further pulses are required (*12, 14, 15*). See text for further details. (b) ^{17}O (54.3 MHz) NMR of orthoenstatite ($MgSiO_3$), including a conventional MAS spectrum, a two-dimensional triple-quantum MAS spectrum, recorded using a split-t_1 sequence (*15*), and corresponding isotropic projection (*8*).

the zeroth- (isotropic) and fourth-rank terms of Eq. [2.3].

At the end of t_1 the multiple-quantum coherence is then transferred to single-quantum coherence associated with the central transition $+1/2 \rightarrow -1/2$. The frequency of evolution of this coherence has no first-order quadrupolar dependence and a second-order dependence of (from Eq. [1.12])

$$\Delta\omega_{(1/2),-(1/2)} = -\left(\frac{e^2qQ}{4I(2I-1)}\right)^2 \frac{1}{\omega_0}(3 - 4I(I+1)) \times \left\{\frac{1}{2}V_{00}^Q + 4V_{20}^Q + 9V_{40}^Q\right\} \quad [2.4]$$

Once again, the second-rank V_{20}^Q term is averaged to zero by the magic-angle spinning, leaving the evolution frequency of the single-quantum coherence governed by an isotropic term and another fourth-rank term. These fourth-rank terms cause line broadening, through their orientation dependence, and it is these that the MQMAS experiment neatly eradicates.

The single-quantum central-transition coherence is allowed to evolve for a time $\tau = k\,t_1$, where k is equal to the ratio of the fourth-rank terms in the multiple-quantum coherence evolution frequency and the single-quantum evolution frequency (i.e., from Eqs. [2.3] and [2.4]):

$$k = 4m\left(\frac{18I(I+1) - 34m^2 - 5}{9(3 - 4I(I+1))}\right) \quad [2.5]$$

for an experiment in which the multiple-quantum coherence is between the $+m$ and $-m$ levels. With this setting for k, the evolution of the multiple-quantum coherence under the fourth-rank terms of its evolution frequency is undone or refocused by the evolution of the single-quantum coherence under the fourth-rank terms of its evolution frequency during the t_1 period, which occurs at the end of kt_1 (see Fig. 2.2(a)). Thus, at the end of the time $t_1 + kt_1$, the net evolution of the remaining central-transition coherence is governed only by the isotropic quadrupolar terms acting on the evolution of the multiple-quantum coherence in t_1 and the single-quantum coherence in kt_1.

Finally, in the MQMAS experiment, an FID of the central-transition single-quantum coherence is collected in t_2. Subsequent processing of the two-dimensional dataset involves Fourier transformation with respect to t_2 to produce a normal single-quantum spectrum of the central transition and a second Fourier transformation with respect to t_1' where $t_1' = t_1 + k\,t_1$. Some extra work is required to produce pure-absorption lineshapes, but the end result is an isotropic spectrum in f_1' with signals at frequencies

$$\omega_1^{iso} = \frac{1}{k+1}(2m\omega_{iso} + \omega_{m,-m}^{iso}) + \frac{k}{k+1}(\omega_{iso} + \omega_{(1/2),-(1/2)}^{iso}) \quad [2.6]$$

where ω_{iso} is the isotropic chemical shift and

$$\omega_{(1/2),-(1/2)}^{iso} = \left(\frac{e^2qQ}{4I(2I-1)}\right)^2 \frac{1}{10\omega_0}(3 - 4I(I+1)) \times \{3 + \eta^2\} \quad [2.7]$$

is the isotropic quadrupolar component of the evolution frequency of the single-quantum central-transition coherence, and

$$\omega_{m,-m}^{iso} = \left(\frac{e^2qQ}{4I(2I-1)}\right)^2 \frac{4}{\omega_0} m(I(I+1) - 3m^2) \quad [2.8]$$

is the isotropic quadrupolar component of the evolution frequency of the $2m$ multiple-quantum coherence.

The signals in f_1' are correlated with powder patterns in f_2 corresponding to the central transition for each site. This can be seen in Fig. 2.2(b), a ^{17}O triple-quantum MAS spectrum (54.3 MHz) of orthoenstatite ($MgSiO_3$), a chain silicate (*8*). The f_1' projection shows six sharp resonances corresponding to the six distinct O species in this material, while cross-sections parallel to f_2 yield anisotropically broadened MAS lineshapes. Simulation of these powder patterns in f_2 allows the quadrupole coupling constants, C_Q, and asymmetry, η_Q, to be obtained for each site. As we discuss in section 3, this information can be valuable in structure determination studies. Furthermore, the position of the center of gravity of the lineshapes within the two-dimensional spectrum allows the isotropic quadrupolar and chemical shifts to be evaluated (*9*). Both of these affect the position of a resonance in the MAS spectrum for quadrupolar nuclei, with the result that the isotropic chemical shift cannot be simply determined in a normal one-dimensional spectrum. As in spin-1/2 NMR, however, the isotropic chemical shift is extremely useful for spectral assignment and structural studies.

MQMAS works by virtue of selecting different coherences to evolve in the initial t_1 period and the subsequent kt_1 period and selecting for these periods coherences whose evolution frequencies both depend on the awkward anisotropic terms we wish to eliminate from our spectrum, but which have a different dependence in each case. Under such circumstances, it will always be possible to arrange for the evolution in one period to be refocused in the next with proper arrangement of the time periods for each evolution. For spin $I > 3/2$ nuclei, there is a choice of multiple-quantum coherence available for the MQMAS experiment. In many cases, triple-quantum coherences remain the coherence of choice owing to the increased efficiency, relative to higher-order coherences, with which they can be created and converted to single-quantum coherence or a population state (*10*). In some cases, a resolution enhancement in the isotropic spectrum may be obtained when a higher-order multiple-quantum coherence is used; however, the magnitude of this increase depends on the nature of the line broadening (i.e. homogeneous or inhomogeneous) present in the isotropic spectrum. Inhomogeneous interactions scale with $2m$, the order of the multiple-quantum coherence excited, and so result in a similar line broadening whichever coherence is employed (*9*).

Since its original invention in 1995, many modifications have been suggested to the basic MQMAS experiment (*1*, *11*). Various methods have been proposed for obtaining pure-absorption lineshapes, and key amongst these is the concept of acquiring an echo or shifted echo FID in t_2 and the use of a z-filter when acquiring data in the hypercomplex manner, both of which require straightforward additions to the simple pulse sequence in Fig. 2.2(a) and have been reviewed in much more detail elsewhere (*12–14*). Other approaches increase the ease with which an isotropic or high-resolution spectrum may be acquired, using a "split-t_1" approach (*15*). Many modifications have focused on sensitivity enhancement (*16–23*) owing to the inherently poor sensitivity associated with the excitation and conversion of multiple-quantum coherences. Many authors have attempted to improve the efficiency of triple- to single-quantum conversion, with fast-amplitude modulation (FAM) pulses (*16*), soft-pulse added mixing (SPAM) (*23*), and double-frequency sweeps (DFS) (*17*) being some of the more promising approaches. Other methods aim to improve either the efficiency or quantitation of multiple-quantum coherence excitation, notably the combination of rotor-assisted population transfer (RAPT) and rotation-induced coherence transfer (RIACT) (*18*, *19*), or FASTER-MQMAS (*20*), which exploits the increase in triple-quantum excitation associated with rotary resonance effects. In addition, the relative merits of one- and two-pulse excitation of multiple-quantum coherences have been considered, as indeed has the use of composite pulses (*21*, *22*). It is not the purpose of this work to review or discuss these further, and the list of references given is not intended to be complete but rather to exemplify the type of improvements which have been made.

2.3 Satellite-Transition Magic-Angle Spinning (STMAS)

The satellite transition magic-angle spinning (STMAS) experiment, shown in Fig. 2.3(a), follows the same basic principles as the MQMAS experiment in section 2.2 (*24*, *25*). It affords resolution in a two-dimensional experiment by using magic-angle spinning to eliminate line broadening from second-rank terms in the evolution frequencies for different coherences, as in MQMAS, and employs refocusing of evolution of coherences due to fourth-rank terms by switching between different coherences in the initial t_1 period and a subsequent kt_1 period. The difference between STMAS and MQMAS is that whereas MQMAS selects a symmetric $+m \rightarrow -m$ multiple-quantum coherence in t_1, STMAS selects coherences associated with single-quantum satellite transitions, i.e., $m = \pm n - 1/2 \leftrightarrow m = \pm n + 1/2$, $n = 1, 2, \ldots, (I - 1/2)$. As with the MQMAS experiment, this coherence is converted at the end of t_1 into single-quantum coherence associated with the central transition of the observed spin.

The satellite-transition evolution frequency (appropriate for the t_1 period of the two-dimensional experiment) has first- and second-order quadrupolar contributions (see Eqs. [1.11] and [1.12]), unlike the multiple-quantum coherences employed in MQMAS. Clearly, if the quadrupole coupling constant is of the order of megahertz, the first-order term represented by Eq. [1.11] will be substantial and lead to vast numbers of spinning sidebands in the f_1 dimension of the final two-dimensional spectrum. This is avoided in practice by synchronizing the t_1 data collection with the sample spinning—that is, the increment in t_1 in the two-dimensional dataset collection must be τ_R, the rotor period (or $n\tau_R$ where n is an integer). The first t_1 increment must be set correctly to take into account finite pulse effects (*24*, *26*). In this way, evolution of the satellite-transition coherence under any second-rank terms in the evolution frequency is avoided in the t_1 dataset. Thus, the effects of the first-order quadrupole term are eliminated entirely (Eq. [1.11]), as are the second-rank terms of the second-order quadrupole term (Eq. [1.12]), in addition to any chemical shift anisotropy or dipole–dipole coupling terms.

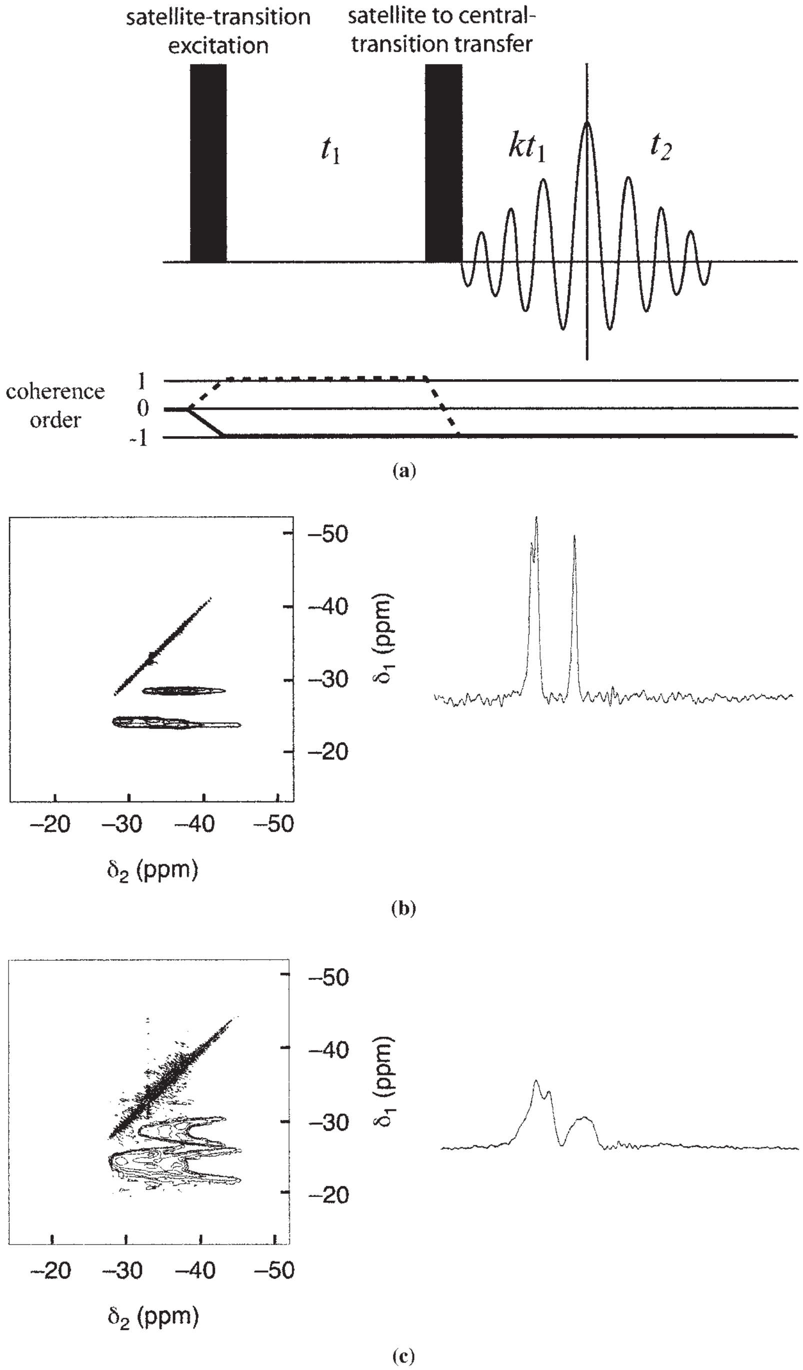

Figure 2.3 (a) Pulse sequence and coherence transfer pathway diagram for a satellite-transition MAS experiment (*24*). Phase cycling should be used to select the solid coherence pathway for $I = 3/2$, and the dashed pathway for $I > 3/2$. If pure-phase lineshapes are desired, further pulses are required (*24, 25*). See text for further details. (b, c) Two-dimensional ^{87}Rb (130.9 MHz) STMAS NMR spectra of $RbNO_3$, recorded using a split-t_1 experiment (*25*). In (c), the magic angle is misset by 0.03°, severely compromising the sensitivity and resolution.

The satellite-transition coherence then evolves in t_1 purely under the effects of the fourth-rank terms in the second-order quadrupolar contribution to the evolution frequency and isotropic terms arising from the second-order quadrupole coupling effects and chemical shift.

In the subsequent kt_1 period, the evolution frequency of the central-transition coherence is given by Eq. [2.4]. If k is set to the ratio of the coefficients of the fourth-rank quadrupolar terms in the evolution frequencies of the satellite-transition coherence and the central-transition coherence, i.e.,

$$k = \frac{2}{3}\left(\frac{6I(I+1) - 34m(m+1) - 13}{3 - 4I(I+1)}\right) \qquad [2.9]$$

for transitions m to $m + 1$, the evolution under the fourth rank terms during t_1 is refocused by the evolution under the fourth-rank terms during the subsequent kt_1 period. As in MQMAS, this allows the complete removal of the quadrupolar interaction and the acquisition of an isotropic or high-resolution spectrum, as shown in Fig. 2.3(b), a two-dimensional ^{87}Rb (130.9 MHz) STMAS spectrum of $RbNO_3$ (*25*).

For half-integer spins with $I > 3/2$, more than one satellite transition is available. In general, all satellite transitions may be excited, at least to some extent, and thus may affect the final spectrum (*24*, *27*). Obviously, the value of k can only be set to refocus one of the satellite transition evolutions. The other satellite transitions will appear in the final two-dimensional STMAS spectrum as ridgelike correlations between the satellite transitions and central transition, with slopes depending on the coefficient of the fourth-rank term in the evolution frequency for the particular satellite transition and the value of k chosen for the experiment. The relative amounts of each satellite transition depend crucially on the pulse durations employed for excitation and conversion of the satellite-transition coherences (*25*, *27*). In many cases, it is possible to adjust pulse durations to minimize the undesirable transfer while leaving the efficiency of the desired transfer almost unaffected. Finally, there is the question of which satellite transition coherence should be used. Simulations suggest that the transfer of coherence from satellites to the central transition is most efficient for the innermost satellite transitions that share an energy level with the central transition (*24*, *27*). However, the use of higher-order satellite-transition coherences may increase the resolution of the experiment, although once again this depends on the nature (homogeneous or inhomogeneous) of the broadening observed in the isotropic spectrum.

As with the MQMAS experiment, some consideration needs to be given to obtaining pure-absorption spectra from this experiment using either a z-filter (*24*) or a shifted echo (*25*), but once this is achieved, quadrupole coupling constants and isotropic chemical shifts can be extracted from the two-dimensional spectrum following the same principles as for the MQMAS experiment.

The advantage of the STMAS experiment over MQMAS is that it involves excitation of single-quantum coherences only, which is more efficient than the excitation of multiple-quantum coherences in MQMAS. This sensitivity advantage is greatest at lower Larmor frequencies and, in particular, at fast MAS rates, where the efficiency of multiple-quantum filtration is significantly reduced (*25*). In contrast, there appears to be little change to the efficiency of STMAS as the MAS rate is increased. In addition, the excitation efficiency of the satellite transitions appears to have a weaker dependence on the quadrupole coupling constant than does the multiple-quantum coherence in MQMAS. Coupled with the overall sensitivity advantage of STMAS, there is much to be gained from implementing this experiment over MQMAS when quadrupolar coupling constants are large. Furthermore, the signal intensities arising in the isotropic dimension of an STMAS spectrum may often be closer to being proportional to the number of spins contributing to the signal than those arising from the MQMAS experiment.

There are, however, disadvantages to the STMAS experiment. The presence of the large first-order broadening in the satellite transitions results in stringent practical requirements for accurate spinning angle adjustment and rotor synchronization (*24*, *25*). Any slight missetting in the magic angle will reintroduce first-order quadrupolar broadening into the satellite transitions, which, although scaled, is still of sufficient magnitude to result in a substantial broadening or splitting of the isotropic spectrum. As shown in Fig. 2.3(c), an ^{87}Rb (130.9 MHz) STMAS spectrum of $RbNO_3$ where the magic angle is misset by only 0.03°, this severely compromises the sensitivity and resolution of STMAS (*25*). It can be estimated that the magic angle must be set with an accuracy of $\sim$0.002° or better if good high-resolution spectra are to be achieved. Recent work has resulted in the development of an STMAS experiment that is self-compensating for any angle misset (SCAM-STMAS), substantially easing the implementation of STMAS but often resulting in a loss in sensitivity (*25*, *28*). In STMAS and SCAM-STMAS, the spinning rate must be stable to within a few hertz for accurate rotor synchronization.

Second, the fact that several satellite transitions may contribute to the spectrum for spins with $I > 3/2$ can lead to resolution problems, especially in samples where there are several different chemical sites (*24*, *25*). In addition, the STMAS experiment, as described originally (*24*), cannot avoid a central transition-cen-

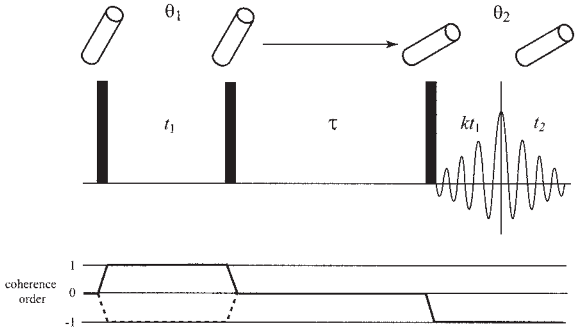

Figure 2.4 Pulse sequence and coherence transfer pathway diagram for a dynamic angle spinning (DAS) experiment (*30*) showing the change in sample rotation angle from θ_1 in t_1 to θ_2 in t_2, during which the magnetization is stored along the applied field. See text for further details.

tral transition autocorrelation ridge in the spectrum, as its production involves the same coherence transfer pathway as for a satellite transition-central transition correlation. This can be seen clearly in Fig. 2.3(b), where a strong narrow ridge is observed in addition to the ridges parallel to f_2. However, the recent implementation of a double-quantum filter within the STMAS experiment has enabled the removal of this autocorrelation signal with, in many cases, little loss of sensitivity (*29*). The excitation of double-quantum coherences using a selective central-transition inversion pulse also avoids the presence of higher-order satellite transitions in the STMAS spectrum, unless the quadrupolar interaction is particularly small.

In summary, some superb results have been obtained with STMAS, and for samples where sensitivity is an issue or where there are likely to be sites with widely differing quadrupole coupling constants, STMAS may be the experiment of choice.

2.4 Dynamic-Angle Spinning (DAS)

The dynamic-angle spinning (DAS) experiment is another refocusing experiment (Fig. 2.4), and though it produces spectra that often look similar to MQMAS and STMAS, it does exploit an inherently different principle to achieve high resolution (*30*). The DAS experiment takes advantage of the fact that the evolution frequency of a coherence depends on the sample spinning angle. The previous experiments we have described are all carried out on samples spinning at the magic angle. In the DAS experiment, the sample spinning angle is changed between different periods of the experiment to achieve changes in coherence evolution frequency.

The experiment (see Fig. 2.4) begins by the excitation of single-quantum coherence associated with the central transition of the observed spin with a selective 90° pulse (see ref. (*6*) for a discussion of selective pulses for quadrupolar nuclei). This coherence is then allowed to evolve for a time t_1 while the sample is rotated at an angle θ_1. The evolution frequency of the central-transition coherence is given by Eqs. [2.2] and [2.4], with $\theta_R = \theta_1$ in Eq. [2.2] during this period. At the end of t_1, another selective 90° pulse stores the magnetization along the applied magnetic field while the sample spinning angle is changed to an angle θ_2. The stored magnetization is then returned to the transverse plane with another selective 90° pulse and allowed to evolve for a period kt_1 while the sample is spinning at angle θ_2. The evolution frequency of the magnetization/central-transition coherence during this period is given again by Eqs. [2.2] and [2.4], but with $\theta_R = \theta_2$. At the end of the kt_1 period, an FID is collected in t_2 in the normal way.

Subsequent processing of the final two-dimensional dataset, involving Fourier transformation with respect to t_2 and t_1' where $t_1' = t_1 + kt_1$ yields an isotropic spectrum in f_1' and powder patterns in f_2 corresponding to those expected for the central transition for a sample spun at angle θ_2.

There are many pairs of spinning angles that allow this refocusing effect; for the combination $\theta_1 = 37.38°$, $\theta_2 = 79.19°$, $k = 1$, so that the refocusing period is equal in length to the initial evolution period (*30*). One problem with this experiment is that no pair of spinning angles includes one of the angles being the magic angle. Thus, the effects of dipolar coupling and chemical shift anisotropy remain in the two-dimensional spectrum, in both dimensions. This can lead to a lack of resolution in the isotropic dimension for some samples. A further change in spinning angle to 54.7° may be added to the experiment before detection of the FID under MAS.

A further problem with this experiment is the need to change sample spinning angles during the experiment. Not only is this technically difficult, it must be performed in a time that is short compared with the spin-lattice relaxation time for the observed spins, or the stored magnetization simply relaxes back to equilibrium during the angle change. Because quadrupolar nuclei can have short relaxation times, even in the solid state, this is a real restriction on this experiment, particularly if the additional change to the magic angle is also performed. In addition, the storage step while the angle is changed results in the loss of half the signal compared with a single pulse experiment, because only one component of the transverse magnetization (x or y) can be stored. These difficulties with the experiment and the requirement for a specialist probehead to perform the angle change means

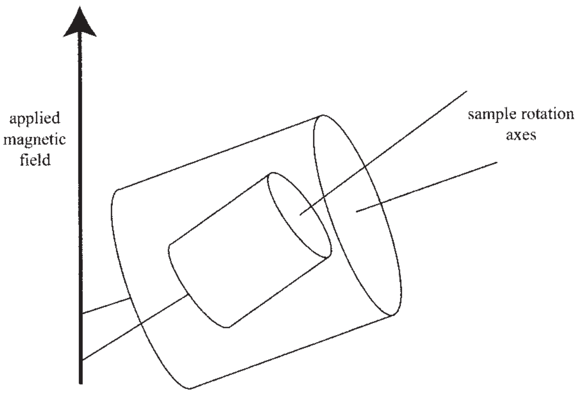

Figure 2.5 Schematic of a double rotor as used in DOR to remove the effects of quadrupolar broadening in a one-dimensional NMR experiment (*31*). Two rotors are used, one inside the other, rotating at angles of either 30.6° or 70.1° and 54.736°, respectively, averaging fourth- and second-rank quadrupolar broadening.

that DAS tends to be performed rarely compared with the commonly used MQMAS experiment.

2.5 Double Rotation (DOR)

As explained in section 1, the central transition of a half-integer quadrupolar spin is unaffected by the quadrupole coupling to first order. To second order, the evolution frequency of the coherence associated with the central transition is given by Eqs. [2.2] and [2.4]; it consists of a sum of terms that depend, respectively, on zeroth-, second-, and fourth-rank rotation matrices. As discussed in section 2.1, the effects of terms depending on second-rank rotation matrices can be averaged to zero by spinning the sample at the magic angle. In a similar way, it can be shown that the effects of terms containing fourth-rank rotation matrices can be averaged to zero by spinning the sample at an angle of 30.6° or 70.1° with respect to the applied field. The double rotation experiment (DOR) takes advantage of this fact and achieves an isotropic spectrum by simultaneously spinning the sample at the magic angle and at 30.6° or 70.1° (usually the latter, as higher rf field strengths are achievable) (*31*, *32*).

This conceptually simple technique results in an isotropic spectrum in a "pulse-acquire" one-dimensional experiment. By appropriate choice of excitation pulse, the resulting spectrum gives near-quantitative signal intensities, the only high-resolution experiment for quadrupolar nuclei which does so. Of course this comes at a price; the technical difficulties of spinning a sample rapidly about two angles simultaneously is not to be underestimated. It is achieved in practice (Fig. 2.5) by having two rotors, one inside the other with one spinning at the magic angle and one at 30.6° or 70.1°. The problem in the past has been to spin both rotors at rates fast enough to achieve sufficient averaging. When the rate of spinning is smaller than the anisotropy associated with the term in the evolution frequency that is being averaged, spinning sidebands result, and these may overlap with signals from other sites in the sample, leading to poor resolution. However, modern probe designs have made the DOR experiment a real proposition. Furthermore, as NMR experiments are performed at higher and higher fields, the magnitude of the second-order quadrupole coupling reduces, and so the spinning rate required to produce sideband-free spectra is also reduced.

After the introduction of the MQMAS experiment, DOR seemed set to become obsolete. However, because it can be made quantitative, that it relies only on single-quantum coherence from the central transition and is a one-dimensional experiment may make it set for a revival, especially for higher-field instruments and modern probeheads.

Recently, technical improvements to the double-rotation technique have meant that much better spinning stability has been achieved (*33*). This means that longer two-dimensional experiments are now possible, and this feature has been used in a double-rotation version of the MQMAS experiment. The so-called MQDOR experiment results in the correlation of an isotropic, multiple-quantum spectrum with an isotropic, single-quantum central transition spectrum (*33*, *34*). Signals occur at frequency $\delta_{\mathrm{iso}} + \delta_{\mathrm{Q,\ iso}}$ in the single-quantum dimension and at $M(\delta_{\mathrm{iso}} + c\delta_{\mathrm{Q,\ iso}})$ where M is the order of the multiple-quantum coherence used in the experiment and c is -1, ¼, 3/5, ¾ for $I = 3/2, 5/2, 7/2, 9/2$ respectively. Thus, simply measuring the signal positions in both dimensions of the spectrum allows one to determine the isotropic chemical shift and $P_Q = C_Q\,(1 + \eta_Q^2/3)^{1/2}$ immediately. This is likely to be particularly useful for samples exhibiting a distribution of isotropic chemical shifts and/or quadrupole couplings, such as γ-$\mathrm{Al_2O_3}$.

2.6 Relaxation Methods

In cases where the nuclei suffer large quadrupole couplings (relative to the Larmor frequency), it may be that none of the experiments described in sections 2.2–2.5 will be useful for resolving signals from different sites. The multiple-quantum coherence needed in the MQMAS experiment becomes increasingly difficult to excite evenly over a powder sample as the quadrupole coupling becomes larger. The sensitivity of the STMAS experiment to spinning angle misset-

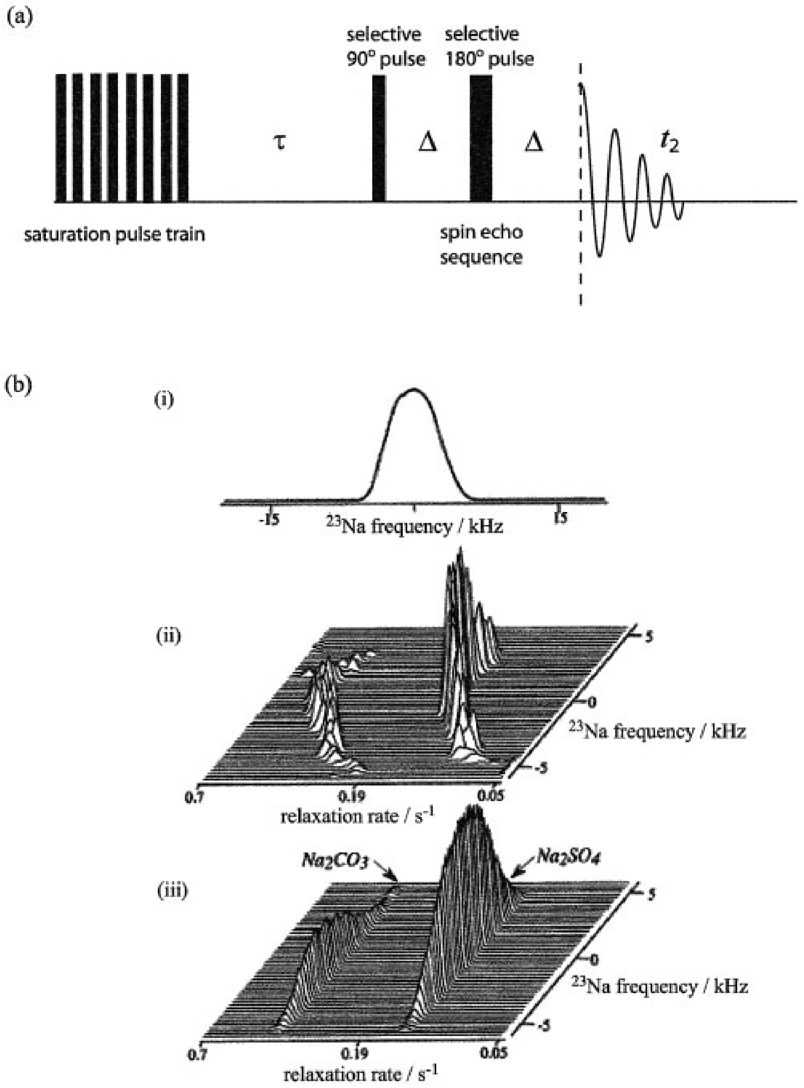

Figure 2.6 (a) Pulse sequence for a two-dimensional relaxation experiment that separates quadrupolar lineshapes according to their characteristic T_1 relaxation time constant (*35*). The spin echo pulses are applied with a low radiofrequency field strength so they are selective for the central transition of the half-integer quadrupolar nucleus. (b) ^{23}Na NMR of a mixture of Na_2SO_4 and Na_2CO_3 under static conditions (*35*), (i) conventional one-dimensional spectrum, (ii) two-dimensional relaxation spectrum, showing two curved ridges corresponding to the ^{23}Na sites in Na_2SO_4 and Na_2CO_3, respectively, (iii) two-dimensional relaxation spectrum where the curved ridges are replaced by skyline projections in which the average relaxation rate for each signal is plotted.

ting increases with the size of the first-order quadrupole coupling, resulting in incomplete refocusing of the t_1 coherence, and so a decreased intensity in the signal measured in t_2. For large quadrupole couplings, it may not be possible to set the magic angle sufficiently accurately.

Similar problems will arise with DAS for samples with large quadrupole couplings; the sensitivity of the experiment to angle missetting increases with the size of the second-order quadrupole coupling, resulting in incomplete refocusing of the evolutions of magnetization in t_1 and kt_1 and a concomitant loss of signal going into t_2. As for DOR, the number of spinning sidebands in the spectrum increases as the second-order quadrupole coupling increases (for a constant spinning rate), and for large quadrupole couplings, this will prohibit spectral resolution of signals from different sites.

Thus, in the case of large quadrupole couplings, it becomes necessary to use different strategies to achieve spectral resolution. One method that has proved useful exploits the differences in spin-lattice relaxation times, T_1, for different signals in the spectrum to achieve their separation in a two-dimensional experiment (*35*). The basic pulse sequence for the experiment is shown in Fig. 2.6(a). This technique has to date been applied solely to half-integer spins, where it is the relaxation of the central transition that is studied. However, there is nothing in principle to prevent it from being applied also to integer spins.

A two-dimensional dataset is collected as a function of a time τ in the experiment, during which spin-lattice relaxation is allowed to occur, and a time t_2, during which a conventional FID of the restored z-magnetization (associated with the central transition for half-integer spins) is recorded. Saturation is generally used to form the initial nonequilibrium state from which relaxation then occurs. The other option is inversion of the equilibrium magnetization, but this is often not favored owing to the difficulty of achieving uniform inversion across the entire central-transition powder pattern.

The experiment may be carried out under magic-angle spinning or static conditions. For samples for which sensitivity is not an issue (i.e., moderate- or high-γ nuclei), 100% or near 100% abundance, and for which the observed nuclei does not suffer large quadrupole couplings, there are some advantages to using magic-angle spinning. Whether static or magic-angle spinning conditions are used, the FID associated with the central transition, which is collected in t_2 of the experiment, is collected after a spin echo, as shown in Fig. 2.6(a), to prevent any distortion of the central-transition lineshape.

For low-γ nuclei, or elsewhere where sensitivity is an issue, it is possible to replace the spin echo in Fig. 2.6(a) with a CPMG echo train. Multiple echoes are then collected in t_2. Prior to data processing, these are separated and added together to form a single t_2 FID, which greatly improves the signal to noise (although at the expense of resolution). CPMG sequences work best under static sample conditions; if magic-angle spinning is used, the echo periods are restricted to being multiples of the rotor period, which, for large quadrupole couplings, is unnecessarily long, and any small variations in sample spinning rate will result in significant loss of intensity in the echoes as the echo train proceeds. Figure 2.6(b) shows the results of using this pulse sequence for ^{23}Na in a mixture of Na_2SO_4 and Na_2CO_3.

A key point in this experiment is in the data processing. The two-dimensional time-domain dataset has the form

$$S(\tau, t_2) = \int\int I(\nu, R)\exp(i\nu t_2)G(R, \tau)dRd\tau \quad [2.10]$$

where $\exp(i\nu t_2)$ describes the t_2 FID, for a component in the central-transition spectrum that evolves at frequency ν. R is the relaxation rate constant (T_1^{-1}) governing the relaxation in the τ period of the experiment, and $G(R, \tau)$ describes the relaxation process that occurs during τ or, more specifically, the proportion of the magnetization that has recovered during τ, i.e., $G(\tau) = 1 - \exp(-R\tau)$ for a saturation recovery process. $I(\nu, R)$ is the intensity of signal at frequency ν whose relaxation is described by a rate constant R. In other words, a two-dimensional plot of $I(\nu, R)$ as a function of ν and R separates frequency spectra in the ν dimension according to their characteristic relaxation rate constant R. Thus, $I(\nu, R)$ is the two-dimensional "spectrum" we need to extract from the two-dimensional time-domain dataset. A Fourier transform with respect to t_2 yields the frequency dimension ν. We then need to perform an inverse Laplace transform on the τ data to obtain the R dimension. The Laplace transform has the form

$$S(\tau) = \int_{-\infty}^{+\infty} I(R)\exp(-iR\tau)dR \quad [2.11]$$

where $I(R)$ is the amplitude of the exponential function $\exp(-iR\tau)$ in the function $S(\tau)$. Inverse Laplace transforms to extract the $I(R)$ amplitudes from experimental data, which can be assumed to derive from sums of exponential functions, are generally performed by fitting sums of exponentials to the experimental data. Such a process is notoriously unstable and highly dependent on the noise in the dataset. However, in the relaxation-assisted separation of quadrupolar lineshapes, the goal is not highly accurate relaxation rate constants but merely separation of the differently relaxing components. This can be realistically achieved for up to three components from an experimental dataset with a reasonable level of signal to noise (100:1 or better), providing the relaxation rate constants are reasonably different.

3. DETERMINING STRUCTURE FROM QUADRUPOLAR AND CHEMICAL SHIFT PARAMETERS

The acquisition of high-resolution spectra (as described in the previous section) is often a vital pre-

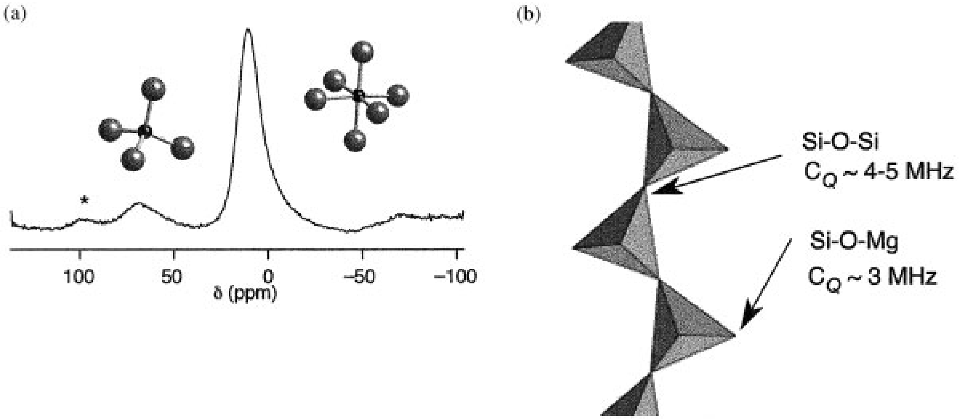

Figure 3.1 (a) ^{27}Al (104.3 MHz) MAS NMR spectrum of γ-Al_2O_3, demonstrating the dependence of chemical shift upon coordination number (*36*). (b) Schematic representation of a silicate chain in orthoenstatite ($MgSiO_3$), indicating the differences in quadrupolar coupling constant, C_Q, for bridging (Si–O–Si) and nonbridging (Si–O–Mg) oxygen species (*8*).

requisite for the extraction of any structural information (either qualitative or quantitative) for quadrupolar nuclei. The removal of anisotropic broadening allows simple information, such as the number of crystallographically distinct species and their relative populations, to be determined. Even this can provide structural insight, limiting the number of possible space groups and therefore structures which need, or are able, to be considered. Usually, from high-resolution spectra it is then also possible to extract accurate values for the quadrupolar and chemical shift interaction parameters, primarily C_Q (or χ), η_Q and δ_{iso}, and in some cases the chemical shift anisotropy. These parameters are determined by the local structure and environment, and their knowledge, therefore, can provide structural insight. For example, the quadrupolar interaction, as described in section 1, is the interaction between the nuclear electric quadrupole moment of the nucleus, *eQ*, and any electric field gradient at the nucleus arising from the particular arrangement of electrons and nuclei which surround it. The electric field gradient component of this interaction depends therefore on the surrounding molecular structure, with a significant contribution from the electrons in the bonds around the nucleus in question, as the core electron density is generally more symmetrically arranged. Similarly, the chemical shift depends on the electron density and so crucially on the number and nature of chemical bonds present. Although many complex factors (e.g., coordination number and atom, bond distances and angles, and covalency) determine the exact values of quadrupole and chemical shift parameters, sometimes a particularly strong dependence or correlation may enable structural information to be extracted from merely a single measurement or series or measurements on related compounds.

For example, the isotropic chemical shift for a particular nucleus often shows a strong dependence on the number and type of coordinating species. For nuclei where the shift range is reasonably large, different species may be well separated in NMR spectra, and indeed the determination of the chemical shift then provides a direct indication of the coordination number. This is often the case for ^{27}Al, where Al in tetrahedral (60–80 ppm) or octahedral (0–20 ppm) coordination environments are usually easily distinguished (*36*), as shown in Fig. 3.1(a), a ^{27}Al MAS NMR spectrum of γ-Al_2O_3. Here, the two resonances, corresponding to four and six coordinating atoms, can be clearly resolved even under MAS. Distinct shift ranges for ^{17}O in various coordination environments in titanates have also been observed (for OTi_x 650–850 ppm for $x = 2$, 450–650 ppm for $x = 3$, 250–450 for $x = 4$, and <250 ppm for $x = 5$) (*36*). In addition, the isotropic chemical shift also exhibits a distinct dependence (albeit usually of smaller magnitude) on structural parameters such as bond distances or bond angles, and much work has been undertaken to provide mathematical descriptions. For example, for ^{27}Al the isotropic shift in a series of framework aluminosilicates (with tetrahedrally coordinated Al) has been shown to depend on the Al–O–Si bond angle (α), with $\delta_{iso} = -0.5\alpha + 132$ (ppm) (*37*), whereas in ^{17}O NMR, a strong correlation of δ_{iso} with Si–O bond distance has been demonstrated for a range of silicate minerals (*8*). However, the dependence of the chemical shift on such a large number of structural parameters ensures that such correlations rarely have universal use, although they may be useful when studying a series of related materials.

Similarly, there has been much study of the dependence of the quadrupolar coupling on structure. For ^{17}O, for example, early work determined that C_Q displays a strong dependence on the covalency of the M–O bond (*38*):

$$C_Q \text{ (in MHz)} = -0.203I(\%) + 14.78 \quad [3.1]$$

where I is the ionicity and is defined in terms of the Pauling electronegativities

$$I(\%) = 100[EN(O) - EN(M)]/EN(O) \quad [3.2]$$

a relationship that appears to hold for a wide range of compounds. This has been of particular use in the study of silicates where so-called bridging oxygens (Si–O–Si) and nonbridging oxygens (Si–O–Mg, for example) display different C_Q values of (4–6 MHz and 2–3 MHz, respectively). Measurement of C_Q, therefore, can instantly provide information on the structural moieties present. For example, the ^{17}O C_Q values for the six oxygen species in the MQMAS spectrum of $MgSiO_3$ previously shown in Fig. 2.2(b) fall into two distinct groups, four around ~3 MHz (corresponding to nonbridging oxygens) and two much higher, 4–5 MHz, (bridging species). This indicates $MgSiO_3$ is a chain silicate, as shown schematically in Fig. 3.1(b) (*8*). Similar correlations are known for many other nuclei, including ^{11}B, where tetrahedral and trigonal B species can be easily discriminated with C_Q values of 0–0.5 MHz and 2.3–2.5 MHz, respectively (*36*). However, as with the chemical shift the many empirical correlations present in the literature must be regarded with care if general application is required, rather than within a series of related materials.

3.1 Ab Initio Calculations of NMR Parameters

More recently, the development of computational methods has provided an alternative, more flexible, and perhaps ultimately more detailed approach to the study of the dependence of quadrupolar and chemical shift parameters on structure. The calculation of NMR parameters may aid in the interpretation of complex spectra but, more generally, provides a means for following the direct dependence of a particular interaction upon a structural parameter, such as a bond length or bond angle, in a detailed manner that may be difficult to achieve experimentally. The quantum-mechanical determination of NMR parameters, involving a detailed description of the electrons and nuclei and the way they respond to the presence of a magnetic field, is a complex, many-body problem that is unable to be solved without some approximations (*39*). One approach is Hartree-Fock (HF) theory, where each electron is assumed to move independently in the mean field generated by the other electrons. An alternative is density functional theory (DFT), where the energy is considered as a functional of the total charge density, thereby reducing significantly the dimensionality of the problem. However, this does require additional approximations when considering the form of the functional used to describe the electron exchange and correlation. Nevertheless, DFT has been used with great success, enabling calculations to be performed on large systems at a fraction of the computational cost.

The details of how to calculate the chemical shielding and quadrupole coupling tensors from electronic wavefunctions are the subjects of extensive reviews elsewhere (*40*), so only a brief outline of each will be given here.

3.1.1 Chemical Shielding Tensor. The net chemical shielding tensor, $\boldsymbol{\sigma}$, is given by the sum of the diamagnetic and paramagnetic terms (*5*, *6*)

$$\boldsymbol{\sigma} = \boldsymbol{\sigma}^d + \boldsymbol{\sigma}^p \quad [3.3]$$

where components of the constituent tensors are given by:

$$\sigma^d_{\gamma\gamma} = \frac{\mu_0}{4\pi}\frac{e^2}{2m_e}\left\langle \Psi_0 \middle| \sum_i \frac{\alpha_i^2 + \beta_i^2}{r_i^3} \middle| \Psi_0 \right\rangle \quad [3.4]$$

and

$$\sigma^p_{\alpha\beta} = -\frac{\mu_0}{4\pi}\frac{e^2}{2m_e} \sum_{k\neq 0}\left[\frac{\langle\Psi_0|\Sigma_i\,\hat{l}_{i\alpha}|\Psi_k\rangle\left\langle\Psi_k\middle|\Sigma_i\,\frac{\hat{l}_{i\beta}}{r_i^3}\middle|\Psi_0\right\rangle + \text{c.c}}{\mathrm{E_k}-\mathrm{E_0}}\right] \quad [3.5]$$

when the gauge origin (i.e., the origin from which the electron distances r_i are measured) is at the nucleus in question. α, β, γ denote Cartesian axes. The Ψ are electronic wavefunctions; the suffix i denotes the ith electron. The ground electronic state is denoted 0, and an excited electronic state, by k. r_i is the distance of the ith electron from the nucleus, and α_i, β_i its coordinates along the α and β directions respectively. $\hat{l}_{i\alpha}$,

$\hat{l}_{i\beta}$ are components of the electronic orbital angular momentum operator, $\hat{l}_i$ for the ith electron. "c.c" denotes the complex conjugate of the first term in the summation of Eq. [3.5].

The diamagnetic term (Eq. [3.4]) depends only on the ground electronic state, making it straightforward to calculate from an ab initio or first-principles electronic structure calculation. Its dependence on r_i^{-3} means that it is very much a local contribution, arising largely from the core electrons surrounding the nucleus.

The paramagnetic term (Eq. [3.5]) provides more of a commentary on bonding, so is the part that the calculation must focus on getting right. Unfortunately, it depends on integrals involving components of the electronic orbital angular momentum operator, $\hat{l}_\alpha$, the ground electronic state, and various excited electronic states. The requirement that excited electronic states must be calculated means that the calculation is considerably more time-consuming. Excited states are also notoriously more difficult to calculate accurately.

3.1.2 Quadrupole Coupling Tensor. The definitions of the quadrupole coupling parameters were given in section 1 but are repeated here for convenience:

$$\chi = \frac{e^2qQ}{h} = \frac{eQ}{h} V_{zz}^{PAF}, \qquad \eta_Q = \frac{V_{xx}^{PAF} - V_{yy}^{PAF}}{V_{zz}^{PAF}} \quad [3.6]$$

where $V_{\alpha\alpha}^{PAF}$ are components of the second-rank tensor describing the electric field gradient at the nucleus of interest in its principal axis frame, and eQ is the nuclear electric quadrupole moment. Thus, the problem of calculating the quadrupole coupling constant and asymmetry for a nucleus is really one of calculating the electric field gradient tensor $\mathbf{V}^{PAF}$ at the nucleus.

Classically, the electric field gradient is the second derivative of the electric potential V arising from the distribution of charges around the nucleus. The potential V at the origin due to a point charge C a distance r away is

$$V = \frac{C}{4\pi\varepsilon_0 r} \quad [3.7]$$

where ε_0 is the permittivity of free space. Expressing V in Eq. [3.7] in terms of Cartesian coordinates x, y, z, the second derivatives with respect to those x, y, z, i.e., the electric field gradient at the origin, can be easily determined to be for the zz component; for instance (*41*):

$$V_{zz} = e\,\frac{3z^2 - r^2}{r^5} \quad [3.8]$$

or in terms of spherical tensor coordinates:

$$V_{zz} = e\,\frac{3\cos^2\theta - 1}{r^3} \quad [3.9]$$

Equation [3.9] represents the classical expression for the zz component of the electric field gradient tensor. The quantum mechanical operator for V_{zz} is thus Eq. [3.9] with each term replaced by the appropriate quantum mechanical operator, i.e.,

$$\hat{V}_{zz} = e\,\frac{3\cos^2\theta - 1}{r^3} \quad [3.10]$$

Similar expressions may be found for all the other components $V_{\alpha\beta}$ of the electric field gradient tensor.

In a molecule or compound, the distribution of electrons is described by a wavefunction, ψ_e (for convenience expressed such that the origin is at the nucleus of interest and normalized). The expectation value of the zz component of the electric field gradient due to this electron distribution, $\langle V_{zz}\rangle_e$ is then given in the normal way:

$$\begin{aligned}\langle V_{zz}\rangle_e &= \langle\psi_e|\hat{V}_{zz}|\psi_e\rangle \\ &= e\int \psi_e{}^*\,\frac{3\cos^2\theta - 1}{r^3}\,\psi_e r^2 \sin\theta\, dr\, d\theta\, d\phi \quad [3.11]\end{aligned}$$

where $r^2\sin\theta dr d\theta d\phi$ is the integration volume element.

The contribution to V_{zz} from the distribution of nuclei around the nucleus of interest $\langle V_{zz}\rangle_n$ is determined by assuming the surrounding nuclei act like point charges, and using Eqs. [3.8] or [3.9]. The other components $V_{\alpha\beta}$ of the electric field gradient tensor can be calculated in a similar manner and the complete electric field gradient tensor formed by summing the electronic and nuclear contributions for each component. It is then a simple matter to diagonalize the resulting tensor to find the electric field gradient in its principle axis frame, V^{PAF}, and its components used to calculate the quadrupole coupling constant and asymmetry according to Eq. [3.6].

The electronic wavefunction ψ_e needed for calculating the electric field gradient tensor V^{PAF} can be determined using ab initio electronic structure calculations. The electric field gradient depends only on the ground state electronic structure and arrangement of nuclei in the molecule, and so it should be possible to obtain much more accurate calculations of it than of the chemical shift for instance, which, as described above, depends on excited electronic states in addition to the ground electronic state, and these are significantly more costly to calculate with any degree of accuracy.

One potential difficulty with ab initio calculations of the quadrupole coupling constant χ is that it depends on the nuclear electric quadrupole moment, Q, which although a constant for a given nuclear isotope, is for many nuclei, not accurately known. Generally speaking, it is difficult to measure the sign of the quadrupole coupling constant experimentally, and often, only its magnitude is reported. This could mean that several molecular structures yield calculated quadrupole coupling constants whose magnitude agrees with the empirically derived value. Further useful information could be obtained if the principal axis frame of the quadrupole coupling tensor (or equivalently, the electric field gradient tensor on which it depends) could be determined experimentally, as this information is necessarily calculated in any *ab initio* calculation of the quadrupole coupling parameters. One obvious, if experimentally tedious, way to do this is by employing single crystal studies. There are other methods now being developed that are discussed in later sections.

The simplest calculations of NMR parameters, using either Hartree-Fock or DFT approaches, are for molecules, often with localized basis sets such as the atomic orbitals. An infinite periodic solid is approximated only as a cluster, with the nucleus of interest at its center (*39*), and terminated (at a chosen distance) with nuclei such as ^{1}H. As the cluster size increases, the calculated values approach those expected for an infinite solid, but correspondingly the cost increases. The observation that NMR parameters are essentially local properties, dominated by the bonding in the first few coordination spheres is the justification for such an approach. However, many calculations are then necessary if the system is large, with each species in turn positioned at the cluster center. Even so, it can often be difficult (and costly) to achieve sufficiently large clusters and basis sets, restricting the accuracy of the calculation in many nonmolecular solids (*39*). Despite these limitations, the emerging importance of NMR for the study of local structure has resulted in many investigations using this type of approach, a few examples of which are described in the next section. Qualitative results may be produced easily and are often sufficient for structural assignment of simple spectra, whereas the variation of NMR parameters with the local structural environment, determined for well-ordered crystalline materials, can then be applied to the interpretation of more complex, disordered solids.

However, in some cases the level of accuracy achieved by cluster methods is not sufficient for complete spectral assignment. Alternative approaches to the calculation of infinite solids often involve the use of periodic boundary conditions, exploiting the high translational symmetry of solids (*39*). This approach formally applies only to perfect crystals, but aperiodicity may be considered through the use of super cells. Many such codes use plane waves as basis sets. Although a large number of waves may be required to accurately represent complex wavefunctions, plane waves provide an orthonormal basis set which is computationally simple and cheap. The WIEN (*42*) package (a linearized augmented plane wave code or LAPW) has enabled the accurate determination of electric field gradient tensors in many periodic crystals with great accuracy, aiding spectral assignment. The approach used by WIEN, an all-electron approach, is accurate but may be time-consuming and it is currently only applicable for the calculation of the quadrupolar parameters and not the chemical shift. More recently, Pickard and Mauri (*39*) introduced a plane wave pseudopotential method for calculating NMR parameters, where the core and valence electrons are considered separately, an approximation that works well for many cases. This considerably improves the efficiency of the calculation, allowing more complex systems to be calculated on reasonable timescales. An extension of this theory, the gauge-including projector-augmented wave (GIPAW) method (*43*), reintroduces the core electrons, allowing parameters dependent upon them, such as the chemical shift, to be determined. Since its introduction, the accuracy of this approach has been demonstrated in a variety of applications, examples of which are described in the next section.

3.2 Experimental Correlations of Quadrupole Coupling Parameters with Structural Features

Despite the limitations in the calculations of NMR parameters described in the previous section, excellent results have been achieved in several areas, most notably in work on ^{17}O in silicate glasses and related crystalline analogues. Tossell and colleagues (*44–46*) pioneered the early application of calculations using simple cluster models of the environment around the bridging oxygen linkage in such materials and ab initio calculations using coupled Hartree-Fock perturbation theory with large Gaussian basis sets to predict simple trends for the ^{17}O quadrupole coupling parameters with Si–O–Si bond angle. These trends were later confirmed by Grandinetti and colleagues (*47*) in an ^{17}O DAS study of the SiO_2 polymorph coesite.

Since then, there have been many studies that have further refined the ab initio calculations and predicted further trends in the ^{17}O quadrupole coupling parameters with different structural features. For instance, Clark and Grandinetti (*48*) have determined how the Si–O bridging oxygen distance affects the quadrupole coupling constant, and the Si–O–Si bond angle, the quadrupole asymmetry parameter with *ab initio* calculations using GAUSSIAN 94 on a model $(OH)_3Si–O–Si(OH)_3$ cluster. Similar work has also examined how these trends are modified by alkali metal cations (important for silicate glasses containing network modifier cations) located in the vicinity of the bridging Si–O–Si (*49*) and shown that while the effect of a single coordinating cation is significant, the effect of a second cation is less so. More importantly perhaps is the confirmation that the orientation of the bridging oxygen-cation vector is important in determining the quadrupole coupling parameters. More recently, these authors have employed a combined approach using both cluster methods and the LAPW WIEN code for the study of bridging oxygens in alkali silicates (*50*). Good agreement was obtained between the two methods, and similar trends observed.

Grandinetti's work has shown (*48–50*) that the ^{17}O quadrupole coupling parameters in M–O–M units depend largely on the first coordination sphere surrounding the oxygen. Xue and Kanzaki (*51*) have performed calculations with clusters extending out to two to four coordination spheres and confirmed that indeed both the quadrupole coupling constant and asymmetry are largely reproduced by considering just the first coordination sphere, with little improvement in the calculation if the structure is considered beyond the second coordination sphere. It is worth noting that a significantly larger coordination sphere is required for reliable calculation of chemical shifts, and hence that calculation of quadrupole coupling parameters are a considerably more economical mode of structure determination.

Other studies that use the quadrupole coupling parameters to examine structural details use experimental correlations between particular bond angles or bond lengths and quadrupole coupling parameters. For instance, the C–Li–C bond angle in organolithium compounds (found from X-ray diffraction studies) has been correlated with the ^{7}Li quadrupole coupling constant (*52*) and a linear relationship found between the two:

$$\chi(^7\mathrm{Li}) = (3.9 \pm 0.4)[\angle \mathrm{C} - \mathrm{Li} - \mathrm{C}] - (215.2 \pm 55.6) \quad [3.12]$$

A similar relationship was found between the N–Li–N bond angles in lithiated amines:

$$\chi(^7\mathrm{Li}) = (4.1 \pm 0.5)[\angle \mathrm{N} - \mathrm{Li} - \mathrm{N}] - (110.8 \pm 69) \quad [3.13]$$

The similarity in the slope of the two correlations means that the angular dependence of the ^{7}Li quadrupole coupling constant depends purely on geometrical factors (and not electronic factors). This supports the idea that Li–C and Li–N bonds are largely ionic (*52*).

The differences in the intercepts between the two correlations reflect the fact that the ^{7}Li quadrupole coupling constants are significantly larger for the amides, which in turn arises from the different charge separations in the Li–C and Li–N bonds. N, being more electronegative than C has a significantly larger negative charge than C in their respective bonds with Li, and Li, in consequence, is significantly more positively charged in its bonds with N. Indeed, ab initio calculations show that the positive charge on Li involved in an Li–C bond is typically 0.82–0.83, whereas in an Li–N bond, it is 0.90–0.92.

As discussed previously, the use of a cluster approach does have limitations, particularly when used for calculation of chemical shifts. This was demonstrated by Profeta and colleagues (*53*) who employed the PARATEC/CASTEP GIPAW code (*43*) for the determination of ^{17}O quadrupole and chemical shift parameters in a series of SiO_2 polymorphs. The use of this method with a plane wave basis set enables fully converged computationally efficient calculations to be performed on structures containing up to 144 atoms in the unit cell. Excellent agreement was obtained with experiment but no simple correlations between C_Q and δ_{iso} and Si–O–Si were observed in this series of compounds, although a distinct correlation of η_Q with this angle was established. The authors were then able to extend this approach to assign the 10 distinct ^{17}O resonances in the spectrum of the zeolite ferrierite, a spectrum that had not been able to be assigned in a study using a cluster approach (*53*). Charpentier and colleagues (*54*) have also used this method for the study of ^{17}O, ^{29}Si, and ^{23}Na NMR parameters in a series of sodium silicate crystalline materials. The dependence of the NMR parameters on structural features obtained was then used in the study of silicate glasses, where much less information about the structure is available.

4. STRUCTURAL INFORMATION FROM HETERONUCLEAR DIPOLAR COUPLING

The dipolar coupling interaction is perhaps the obvious choice for use in structural measurements. Its direct internuclear distance dependence (r^{-3}) means that it can be used to measure internuclear distances, potentially with great accuracy, and its known orientation dependence (the dipolar coupling tensor always has axial symmetry with the unique tensor principal axis along the internuclear vector) enables it to be used to measure the orientation of other nuclear spin interaction tensors with respect to the molecular frame.

Unfortunately, the often large quadrupole couplings present for quadrupolar nuclei mean that the much smaller dipolar coupling is easily obscured, and many experiments that are effective at measuring dipolar couplings between spin-1/2 nuclei are not useful for quadrupolar spins. Nevertheless, the dipolar coupling between quadrupolar nuclei and either spin-1/2 nuclei or other quadrupolar nuclei has been successfully exploited in structural studies. This section focuses primarily on those methods that have so far proved useful in employing dipolar couplings between quadrupolar spins and spin-1/2 nuclei, illustrating this discussion with representative examples from the literature.

4.1 Cross-Polarization

Cross-polarization is used almost ubiquitously in NMR of spin-1/2 nuclei, principally as a means of enhancing signal to noise (*55*, *56*). However, it is also a valuable spectral editing tool and can be used effectively to determine which spins are in close spatial proximity. It is primarily in this context that it has found use for quadrupolar nuclei.

The basic cross-polarization experiment is shown in Fig. 4.1 (*56*) for two dipolar-coupled nuclei *I* and *S*. It consists of an initial 90°_x pulse applied, conventionally, to the *I* spin, creating transverse magnetization, which is then spin-locked (retains a constant amplitude of magnetization as a function of time) by a contact pulse applied along the rotating frame *y* axis. Simultaneously, a contact pulse is also applied to the *S* spin nucleus to spin-lock emerging *S* spin magnetization. If the rf amplitudes of these contact pulses, ω_{1I} and ω_{1S}, are chosen such that they match a characteristic nutation frequency of the other spin (i.e., ω_{1I} must be set equal to a characteristic frequency in the nutation spectrum of spin *S* and vice versa), magnetization will be transferred from the *I* spin to the *S* spin where it can then be detected. Thus, for cross-polarization between two spin-1/2 nuclei in a static sample, in the absence of any interactions in the rotating frame that are of similar magnitude or larger than the interaction with the rf fields, the two rf amplitudes are simply related by $\omega_{1I} = \omega_{1S}$, the nutation frequency of the *I* spin magnetization under rf irradiation being ω_{1I} and that for *S* being ω_{1S}. This relationship between ω_{1I} and ω_{1S} is known as a Hartmann-Hahn match condition (*55*). It can be shown that polarization transfer from a more abundant, high-γ *I* nucleus (often ^{1}H) will result in a signal enhancement of a less abundant, low-γ *S* nucleus (e.g., ^{13}C). The theoretical maximum gain over a conventional experiment (M_{S0}) can be shown to be (*57*)

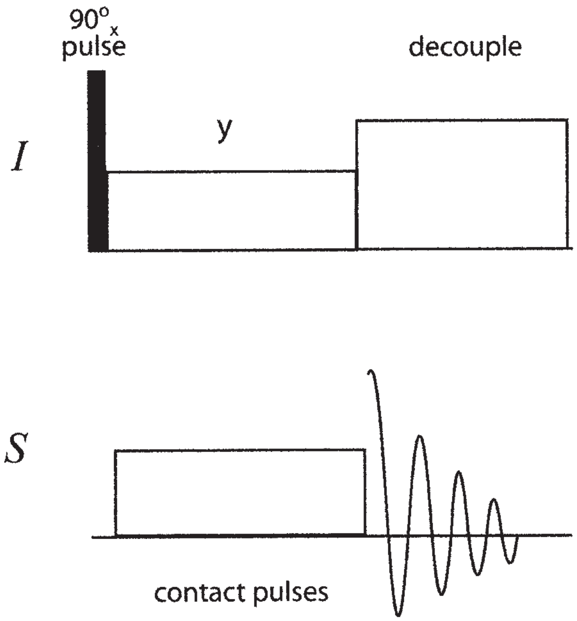

Figure 4.1 Pulse sequence for a cross-polarization experiment between two dipolar-coupled nuclei *I* and *S* (*56*). Magnetization is transferred when the Hartmann-Hahn matching condition is met. See text for details.

$$\frac{M_{S\infty}}{M_{S0}} = \frac{\gamma_I}{\gamma_S}\frac{1}{1+\varepsilon} \qquad [4.1]$$

where ε is given by $S(S+1)N_S/I(I+1)N_I$, with N_S and N_I the number of *S* and *I* spins, respectively. For the case described above, where *I* is an abundant spin and *S* much less abundant, this is frequently approximated as γ_I/γ_S, predicting a considerable gain in sensitivity. This transfer, however, will only take place when a dipolar interaction connects the two nuclei, resulting in a "spectral editing" where only the *S* nuclei that are close in space to an *I* nucleus are observed in the final *S* spin spectrum.

Although the application of MAS during cross-polarization may be desired for the acquisition of spin-1/2 high-resolution spectra, sample rotation will introduce a time dependence into the dipolar interaction that mediates the polarization transfer (*58*). Consequently, optimum transfer is no longer obtained at the Hartmann-Hahn match but at a modified condition, $\omega_{1I} = \omega_{1S} \pm n\omega_R$, where ω_R is the spinning frequency and n is an integer, usually 1 or 2. There may often be little intensity found at the $\omega_{1I} = \omega_{1S}$ match condition, particularly as the spinning rate is increased.

4.1.1 Theory of Cross-Polarization for Quadrupolar Spins: Static Case. Cross-polarization to or from a quadrupolar nucleus is a more complex process, the dynamics of which are still poorly understood (*59–61*). In particular, signal enhancements are rarely observed for many quadrupolar nuclei, although the application of cross-polarization to quadrupolar systems still holds great potential as a spectral editing tool for the elucidation of spatial relationships.

Although there is a unique Hartman-Hahn matching condition for cross-polarization between spin-1/2 nuclei, no such simple condition exists when one (or both) spins are quadrupolar. To determine the matching conditions expected in this case it is necessary to consider the rotating frame Hamiltonian for I and S spins during the application of rf pulses. We begin by considering the static case (with $I = 1/2$), with no sample rotation. Here,

$$\hat{H}_1 = \omega_{1I}\hat{I}_x \qquad [4.2]$$

$$\hat{H}_S = \omega_{1S}\hat{S}_x + \omega_Q(\hat{S}_z^2 - S(S+1)/3) \qquad [4.3]$$

with

$$\omega_Q = \frac{3e^2qQ}{4S(2S-1)\hbar}(1/2) \cdot (3\cos^2\theta - 1 + \eta_Q \sin^2\theta \cos 2\phi) \qquad [4.4]$$

where θ and ϕ describe the orientation of the principal axis frame of the S spin quadrupole tensor in the laboratory frame. The quadrupolar interaction perturbs the eigenstates of $\omega_{1S}S_x$ with the result that there are several S spin nutation rates, some or all of which may be available to match in a cross-polarization experiment. To calculate these values, first we must determine a unitary transformation V that will diagonalize the S spin Hamiltonian such that (*59*, *62*)

$$\hat{H}_S^D = V\hat{H}_S V^{-1} \qquad [4.5]$$

This can be determined either analytically or numerically. In the eigenbasis of the spin-locking Hamiltonian, the energy levels of the S nucleus are given by the diagonal elements of $\hat{H}_S^D$. The S spin nutation rates may then be determined from the differences of these elements

$$\omega_{a,b} = (\hat{H}_S^D)_{b,b} - (\hat{H}_S^D)_{a,a} \qquad [4.6]$$

resulting in $S(2S+1)$ nutation rates.

However, matching of an S spin nutation rate does not necessarily lead to magnetization transfer. For cross-polarization to take place, there must also exist an element in the dipolar Hamiltonian that connects the I and S spin transitions (*59*). The heteronuclear dipolar Hamiltonian is given by

$$\hat{H}_{IS} = 2\omega_D\hat{I}_z\hat{S}_z \qquad [4.7]$$

becoming in the eigenbasis of the spin-locking Hamiltonian

$$\hat{H}_{IS}^D = -2\omega_D\hat{I}_x V\hat{S}_z V^{-1} \qquad [4.8]$$

where ω_D is the dipolar coupling frequency. This Hamiltonian may be described in terms of fictitious spin-1/2 operators (*63*), $\hat{S}_x^{a,b}$ and, for $S = 3/2$ (*59*),

$$\hat{H}_{IS}^D = -2\omega_D\hat{I}_x(C_{1,2}\hat{S}_x^{1,2} + C_{2,3}\hat{S}_x^{2,3} + C_{3,4}\hat{S}_x^{3,4} + C_{1,4}\hat{S}_x^{1,4}) \qquad [4.9]$$

where $C_{a,b}$ are described as dipolar coefficients. The existence of only four nonzero dipolar coefficients for $S = 3/2$ (in contrast to six nutation rates) demonstrates that cross-polarization does not result from matching of every S spin nutation rate. In general, of the $S(2S+1)$ nutation rates of a spin S nucleus only $(S+1/2)^2$ are available to match in a cross-polarization experiment, corresponding to $\omega_{a,b}$ where $b - a$ is an odd integer. It is possible, therefore, to define a general Hartmann-Hahn match condition $\omega_{1I} = \omega_{a,b}$, where $\omega_{a,b}$ is one of the available $(S+1/2)^2$ nutation rates (*59*) to determine which rotating frame coherences have been created by the nutation match within the spin-locking eigenbasis by

$$\hat{\sigma}(t) = V^{-1}\hat{\sigma}^D(t)V = V^{-1}n\hat{S}_z^{a,b}(t)V \qquad [4.10]$$

where n is a constant.

For many nuclei, the quadrupolar interaction is large, resulting in $\omega_Q \gg \omega_{1S}$. For $S = 3/2$ it can be shown that in this limit, the dipolar coefficients $C_{1,4}$ and $C_{2,3}$ are zero. In this limiting case, cross-polarization can only occur when ω_{1I} is matched to $\omega_{1,2}$ or $\omega_{3,4}$ given by

$$\omega_{1,2} = 2\omega_{1S} \qquad [4.11]$$

$$\omega_{3,4} = 3\omega_{1S}^3/8\omega_Q^2 \qquad [4.12]$$

The result is cross-polarization exclusively to rotating frame single- and triple-quantum coherences (by matching $\omega_{1,2}$ or $\omega_{3,4}$ respectively). The former condition provides a practically useful method of single-quantum cross-polarization. The latter, however, does not appear to represent a feasible method for triple-quantum cross-polarization as this nutation rate is extremely low and may be difficult, if not impossible, to match effectively for all ω_Q in a powdered sample. In contrast, outside of the limit $\omega_Q \gg \omega_{1S}$, matching of any of the S spin nutation rates will result in cross-polarization to single- and triple-quantum coherences in the rotating frame. The relative proportions of the coherences produced depend on the exact matching conditions employed. In the limit of $\omega_Q \ll \omega_{1S}$, cross-polarization is analogous to the spin-1/2 case with a single simple Hartmann-Hahn condition when $\omega_{1I} = \omega_{1S}$.

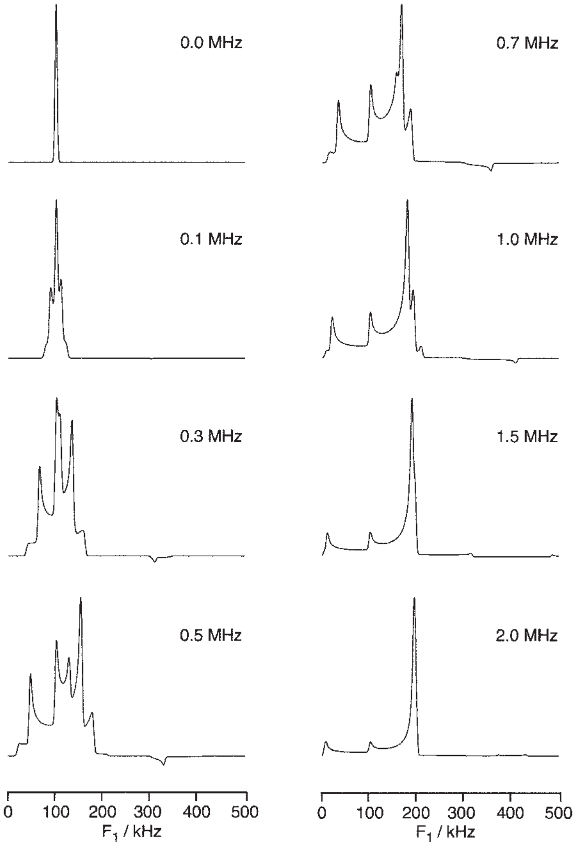

Figure 4.2 Simulated $S = 3/2$ ($\eta_Q = 0$) single-quantum nutation spectra (*59, 65*) (i.e., f_1 projections from a two-dimensional nutation spectrum) for powdered samples where the effect of increasing C_Q is considered, with $\omega_{1S}/2\pi = 100$ kHz. When C_Q is small there is a single dominant nutation rate with a frequency ω_{1S}. As the quadrupolar interaction increases, the presence of more than one nutation rate is apparent, resulting in a powder-averaged spectrum spread over a range of frequencies. For very large values of C_Q, there is once again a dominant nutation rate, now with a frequency 2 ω_{1S} (or more generally $(S + 1/2)\omega_{1S}$), although significant intensity is also observed at lower frequencies.

The range of ω_Q in a powdered sample (present as a result of the dependence upon crystallite orientation; see Eq. [4.4]) results in complex nutation behavior, with a broad distribution of nutation frequencies expected. It is possible to measure this spread of nutation frequencies using a two-dimensional quadrupolar nutation experiment (*64*, *65*). For the nutation of single-quantum coherence, this involves applying a pulse for a nutation/evolution time t_1 before acquiring a signal in an acquisition time t_2. For multiple-quantum nutation, a second pulse is required before acquisition to convert the multiple-quantum coherences created by the first pulse into observable single-quantum coherence (*59*). In either case, the two-dimensional spectrum produced contains a conventional dimension, f_2, including the static quadrupolar-broadened lineshape, and an f_1 dimension, including information on the nutation frequencies of the observed coherences. Figure 4.2 shows a series of simulated spin $S = 3/2$ ($\eta_Q = 0$) single-quantum nutation spectra (i.e., f_1 projections) for powdered samples where the effect of increasing C_Q is considered with ω_{1S} constant. When C_Q is small there is a single dominant nutation rate with a frequency ω_{1S}. As the strength of the quadrupolar interaction increases, the presence of more than one nutation rate is apparent, resulting in a powder averaged spectrum spread over a range of nutation frequencies. For large values of C_Q, there is once again a dominant nutation rate, with a frequency 2 ω_{1S} (or more generally $(S + 1/2)$ ω_{1S}), although significant intensity is also observed for lower nutation frequencies.

If we once again consider cross-polarization, the orientational dependence of ω_Q within a powdered sample results in many crystallites outside the limit $\omega_Q \gg \omega_{1S}$, even when the quadrupole coupling constant is large, offering the possibility of substantial cross-polarization directly to single- and multiple-quantum coherences. The use of cross-polarization to both types of coherence has been exploited in many of the more complex two-dimensional experiments, which are described later in this section.

4.1.2 Theory of Cross Polarization for Quadrupolar Spins: Magic-Angle Spinning Case. Although cross-polarization under magic-angle spinning is widely used for spin-1/2 nuclei, when S is a quadrupolar nucleus, the application of MAS, while increasing the spectral resolution, has important and complex consequences for the cross-polarization dynamics. Sample rotation introduces a time dependence into not only the dipolar interaction, which mediates the polarization transfer (as previously described for $I = 1/2$), but also into the quadrupolar interaction. For the limiting case where the quadrupolar interaction is large, the nominal Hartmann-Hahn matching condition has no dependence on ω_Q, and therefore it has been proposed it would become

$$\omega_{1I} = (S + 1/2)\omega_{1S} \pm n\omega_R \qquad [4.13]$$

as a result of the time-dependent dipolar interaction (*66*). However, even for systems where the quadrupolar interaction is large, in a powder sample undergoing MAS, all crystallites will have $\omega_Q < \omega_{1S}$ at some point in the rotor period, considerably complicating the cross-polarization dynamics.

The time dependence introduced into the quadrupolar interaction has important consequences for cross-polarization under MAS conditions. The eigenstates and eigenvalues (and correspondingly the nutation rates of coherences given by differences between appropriate eigenvalues) are determined by the magnitude of the quadrupolar interaction (*62*). Under sample rotation, the quadrupolar interaction experienced by each crystallite varies with time, resulting in a change in the energies of the eigenstates of the constituent nuclei. Figure 4.3 shows the variation with ω_Q of the eigenvalues of on-resonance $S = 3/2$ and 5/2 spin-locking Hamiltonians, i.e., the energies of the eigenstates of the spins under conditions of rf irradiation with $\omega_1 \ll C_Q$, the quadrupole coupling constant. Thus, the time dependence of the quadrupolar interaction results in time-dependent nutation rates and complex cross-polarization matching conditions.

In addition to the factors mentioned previously, the efficiency of cross-polarization also depends on the extent to which spin-locking can be maintained. Although spin-locking may be achieved easily for a spin $S = 1/2$ nucleus, the spin-locking of a quadrupolar nucleus is often nontrivial in the presence of MAS (*66*, *67*). Not only does sample rotation result in a time-dependent modulation of the eigenstates of the spin-locking Hamiltonian as described above, but the exact nature of the eigenstates also changes (*62*). For example, eigenstates that correspond to single-quantum coherences in the rotating frame when $\omega_Q < 0$ correspond to rotating frame triple-quantum coherences when $\omega_Q > 0$ for $S = 3/2$ and rotating frame five-quantum coherences when $\omega_Q > 0$ for $S = 5/2$, with avoided crossings when $\omega_Q \approx 0$, as shown in Fig. 4.3. There are two limiting cases that describe what happens to the populations of these eigenstates as the sample rotates. If the zero crossing of ω_Q (i.e., passage of the system through $\omega_Q = 0$) occurs adiabatically (i.e., slowly) the original population distribution across the eigenstates is maintained. This results in an interconversion of rotating frame single- and triple- ($S = 3/2$) or single- and five-quantum ($S = 5/2$) coherences. This rotor-driven interconversion is the basis of the RIACT phenomenon used to excite and convert multiple-quantum coherences in MQMAS (*19*, *68*). Alternatively, if the zero crossing occurs suddenly (i.e., rapidly), the populations of the individual eigenstates are conserved. In this case, rotating frame single-quantum coherences would remain as rotating frame single-quantum coherences throughout the rotor period.

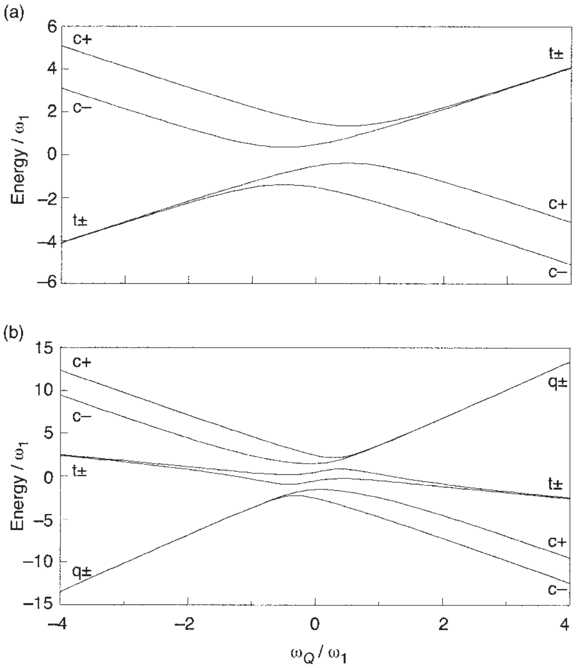

Figure 4.3 Eigenvalues and eigenstates of an on-resonance (a) $S = 3/2$ and (b) $S = 5/2$ Hamiltonian, consisting of a first-order quadrupolar term and a radiofrequency term, as a function of ω_Q/ω_1 (*62*). The eigenstates, when populated, correspond to rotating-frame central-transition ($c\pm$), triple- ($t\pm$), and five quantum ($q\pm$) coherences. See text for details.

In both of these limiting cases, it is found that spin-locking is maintained efficiently. Vega (*66*, *67*) proposed a parameter, α, as a practical definition of whether the rotor-driven interconversion takes place suddenly or adiabatically. Using $\omega_Q = 3e^2qQ/(4S(2S-1)\hbar$ for single-quantum spin-locking

$$\alpha = \frac{\omega_{1S}^2}{2\omega_Q\omega_R} \qquad [4.14]$$

If $\alpha \gg 1$, the zero crossings occur adiabatically, whereas if $\alpha \ll 1$, crossings are predicted to be sudden. In the intermediate regime, zero crossings will convert population differences into a range of different coherences and populations, some of which are not able to be efficiently spin-locked. These will dephase, and spin-locking efficiency will decrease (*69*). In a powdered sample, a range of ω_Q values are present and a range of spin-locking behavior is expected. It may be that some crystallites in the sample undergo fast passage under MAS, others adiabatic passage, and still others are somewhere in between. Thus, only a proportion of the spins in the sample can ever be described as spin-locked, reducing the overall spin-locking efficiency still further.

The combination of a range of possible nutation rates, the orientation dependence of ω_Q, the time dependence introduced into the quadrupolar Hamiltonian and, correspondingly, the nutation rates by MAS and the complex spin-locking behavior ensure that cross-polarization of quadrupolar nuclei is nontrivial, particularly under MAS. Moreover, when added to the fact that many quadrupolar nuclei have high natural abundances and reasonable gyromagnetic ratios, it is not difficult to see why signal enhancements are rarely obtained. Figure 4.4(a) shows ^{27}Al (104.3 MHz) single-quantum MAS and CP (^{1}H(^{27}Al)) MAS NMR spectra of aluminum acetylacetonate. In comparison with the conventional spectrum, the cross-polarized spectra (recorded using two different match conditions) have a much reduced intensity, and both show substantial distortions from the ideal quadrupolar broadened powder lineshape resulting from the orientational dependence of the nutation rates and spin-locking efficiencies. Similarly for triple-quantum cross-polarization, the CP spectra (again recorded using two different match conditions) show a decrease in intensity when compared with a triple-quantum filtered spectrum, although the decrease in intensity is less than that observed for the single-quantum, cross-polarized spectra (*70*). As in the conventional case, the spectra show distorted lineshapes and, significantly, at the two different match conditions the amplitudes of the signals are of opposite sign.

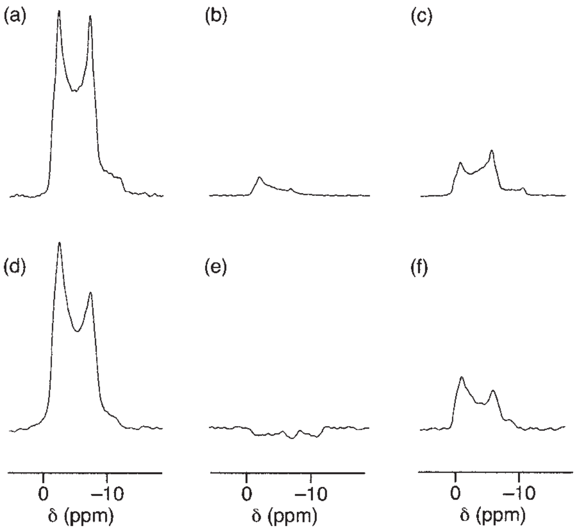

Figure 4.4 (a) Conventional, (b, c) single-quantum cross polarized (from ^{1}H), (d) triple-quantum filtered, and (e, f) triple-quantum cross-polarized (from ^{1}H) ^{27}Al (104.3 MHz) MAS NMR spectra of aluminum acetylacetonate recorded using different matching conditions (*70*).

4.1.3 Uses of Cross-Polarization. The complexity of cross-polarization for quadrupolar nuclei as described above often results in little or no signal enhancement, particularly under MAS conditions. In some cases, however, signal enhancements may be possible, and may even enable the acquisition of spectra not possible in the absence of cross-polarization. For example, cross-polarization (from ^{1}H) has been employed to acquire natural abundance (~0.037%) ^{17}O NMR spectra of static samples, as shown in Fig. 4.5 for brucite (Mg(OH)$_2$) (*71*). The reasonably large quadrupolar interaction and use of a low rf field strength result in a dominant nutation rate, which may be matched for most crystallites simultaneously. The lack of MAS ensures high spin-locking efficiency, whereas the low natural abundance results in a large gain in signal intensity. Similar enhancements have been found in α-alumina using ^{27}Al to ^{17}O cross-polarization, also in a static sample (*72*). Lipton and colleagues (*73*) demonstrated the use of cross-polarization (from ^{1}H) to enhance the signal intensity of dilute and insensitive nuclei, such as ^{67}Zn and ^{25}Mg, in static samples. They used low temperatures to enhance the Boltzmann population difference and then employed cross-polarization, exploiting not only the inherent gain from magnetization transfer but also the decrease in the relaxation time of the experiment. The use of a "flip back" pulse for ^{1}H also enabled a faster repetition of the experiment (*74*).

For spin-1/2 nuclei, it is well known that the efficiency of magnetization transfer can be improved if a

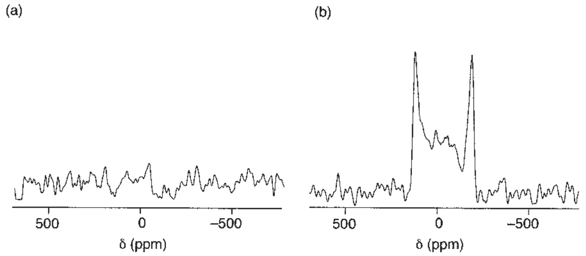

Figure 4.5 Natural abundance (~0.037%) (a) spin echo and (b) cross-polarized (from ^{1}H) spin echo ^{17}O (67.8 MHz) NMR spectra of a static sample of brucite ($Mg(OH)_2$), recorded in 12 hours (*71*).

"ramped" cross-polarization experiment is used (*75*). This involves a linear increase in the rf field strength of one (or sometimes both) of the spin-locking pulses, widening the match condition. The use of a ramped cross-polarization pulse on the *I* (i.e., nonquadrupolar) spin has been demonstrated to increase the sensitivity for cross-polarization to quadrupolar nuclei also (*68*, *76*, *77*). Alternatively, for cross-polarization from a quadrupolar nucleus, Eden and colleagues (*77*) have also recently demonstrated a sensitivity enhancement in a sialon phase, using cross-polarization from a quadrupolar nucleus (in this case ^{27}Al) to a spin-1/2 nucleus (^{29}Si) by the use of RAPT before the cross-polarization step.

So what structural information is it possible to obtain from cross-polarization experiments? The signal enhancement that the technique can offer in certain circumstances may simply allow the determination of NMR parameters, such as the quadrupolar and chemical shift tensors for materials where this may have been difficult otherwise (e.g., in natural samples where synthetic isotopic enrichment is not possible). The measurement of these values may provide structural information either by consideration of empirical correlations or ab initio calculations as described in section 3. On the simplest level, the detection of a cross-polarization signal indicates a spatial proximity (i.e., a significant nonzero dipolar coupling) between two heteronuclei. For example, the demonstration of cross-polarization from ^{23}Na to all three types of ^{31}P nuclei (Q^1, Q^2, and Q^3) in a sodium phosphate glass by Prabakar and colleagues (*78*) indicates the association of Na^+ cations with the nonbridging oxygen of the Q^1 and Q^2 species (as would be expected) and, perhaps more unexpectedly, with the double-bonded O of the Q^3 phosphorous.

When more than one type of species is present, cross-polarization may be used as a spectral editing technique, differentiating species on the basis of their spatial proximity to a heteronucleus. This can provide useful structural information even in the absence of any signal enhancement. For example, ^{1}H to ^{17}O cross-polarization has been to used to identify the Al–O–Al and Al–O–H oxygens in boehmite (AlO(OH)) (*79*, *80*). Two resonances are observed in the conventional MAS spectrum, whereas only one (Al–O–H) is present in the CP MAS spectrum, as shown in Fig. 4.6 (*79*). Similarly, only one of the three resonances in the ^{17}O spectrum of talc is observed when cross-polarization (from ^{1}H) is employed, selectively exciting the hydroxyl oxygen (*80*). This selectivity may be exploited either for assignment of complicated spectra, for example, or perhaps for the observation of hydrated surfaces in a bulk material, as demonstrated by Morris and Ellis (*81*) on aluminas. Kirkpatrick (*82*) followed the hydration of albite by ^{27}Al NMR, using cross-polarization to select the hydration products from the starting materials.

The observation of cross-polarization signal indicates spatial proximity, but the strong distance dependence of the dipolar coupling should, in principle, enable the quantitative determination of the *I*-*S* distance. For pairs of spin-1/2 nuclei, this is easily achieved by performing a variable contact time experiment. The signal intensity obtained from cross-polarization varies as a function of the length of the two contact pulses, the contact time. As this is incremented, the cross-polarization signal builds up from zero, increasing to a maximum before decaying. The exact form of the signal is determined by the time constants for the relaxation of the spin-locked magnetization during the contact pulses on both spins, $T_{1\rho I}$ and $T_{1\rho S}$, each of which may be determined separately, and upon a cross-polarization time constant T_{IS}, which has a direct dependence on the dipolar coupling between the *I* and *S* spins and so on the internuclear distance (*83*). This distance, therefore, can be determined from the variation of signal intensity with contact time. However, once again, the cross-polarization dynamics are considerably more complex for quadrupolar nuclei, and a simple analysis is often no longer valid. Variable contact time experiments may still provide useful qualitative information with the build up of signal intensity increasing at faster rate when internuclear distances are smaller or when strong dipolar couplings to a larger number of heteronuclei are present (*79*, *80*).

In certain circumstances, quantitative information may be obtained from variable contact time experiments. Mali and Kaucic (*84*) were able to determine H–Al distances in aluminophosphate framework systems (AlPO) using ^{1}H to ^{27}Al cross-polarization experiments with weak rf field strengths. In this limit, efficient spin-locking even under MAS during the

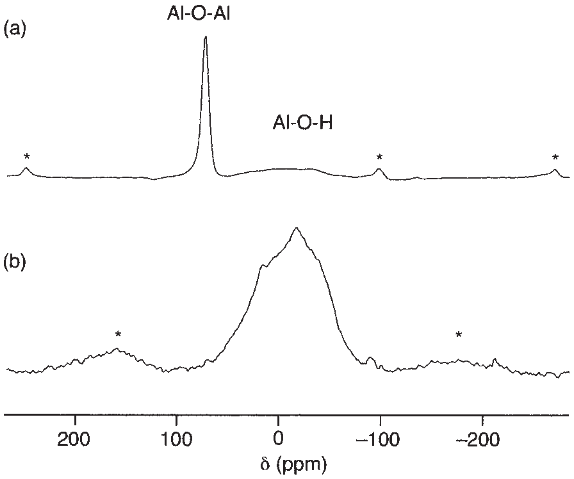

Figure 4.6 (a) Conventional and (b) cross-polarized (from ^{1}H) ^{17}O (54.2 MHz) MAS NMR spectra of boehmite (AlO(OH)), identifying the Al–O–Al and Al–O–H oxygen species. Spinning sidebands are marked with an asterisk (*79, 80*).

contact pulses is ensured and selectivity of individual *I-S* pairs is obtained using a variable resonance offset. Also, with only a few assumptions, the cross-polarization dynamics in this regime may be described in terms of fictitious spin-1/2 operators, and a simplified analysis of variable contact time experiments is therefore possible (*62*, *85*, *86*). Variable contact time experiments have also been used to great effect by Fyfe and colleagues (*87*, *88*) to assign ^{27}Al and ^{29}Si resonances in the aluminophosphates VPI-5 and AlPO-8 and ^{27}Al and ^{29}Si resonances in zeolite frameworks.

4.1.4 High-Resolution Experiments. In many cases, the spectral resolution achieved merely by MAS is not sufficient to enable accurate determination of site-specific structural information. The high-resolution methods described previously must therefore be employed to improve resolution and then combined in some way with the spectral editing power of cross-polarization.

Perhaps the simplest approach to high-resolution cross-polarization experiments is through the use of DOR. Here, a conventional cross-polarization pulse sequence can be employed while spinning around two angles simultaneously (*89*). As with cross-polarization under MAS the rotor-driven modulation of the eigenstates in DOR does decrease the efficiency of cross-polarization and complicate the dynamics, although the spinning frequencies employed are often limited to a few kilohertz by the technical complexity of DOR, as described in section 2.5.

Alternatively, cross-polarization can be combined with DAS in a two-dimensional experiment (*90*). As DAS may be performed with a continuous range of possible angle pairs (see section 2.4), it is possible to choose a pair where the first angle, θ_1, is 0°. Excellent cross-polarization efficiency is obtained at a spinning angle of 0° as there is no rotor-driven modulation of the spin-locking eigenstates. To fully refocus the quadrupolar evolution under θ_1 of 0°, the second angle, θ_2, must be 63.4° (with $k = 5$).

Perhaps the most commonly used approach is the combination of MQMAS with cross-polarization. As this experiment relies on the use of multiple-quantum coherences to refocus the quadrupolar broadening in the t_1 period, the combination of the two techniques may be performed in a number of ways. The initial method proposed (termed CP-MQMAS) is shown in Fig. 4.7(a) (*91*). It involves cross-polarization from *I* to the quadrupolar *S* spin single-quantum central-transition coherences. These are then converted (by the use of a central-transition selective 90° pulse) into a population difference across the Zeeman $m_S = \pm 1/2$ eigenstates from which multiple-quantum coherence is then generated for the following MQMAS experiment. This ensures that multiple-quantum coherences are generated only for spins that have a dipolar coupling to *I* (i.e., an editing of the spectrum occurs). The MQMAS experiment that follows was originally described as a z-filtered experiment (*91*), but could be replaced by the MQMAS variation of choice. If cross-polarization is performed in the limit $\omega_Q \gg \omega_{1I}$ with the use of low *S* spin rf field strengths to improve spin-locking during the contact time, the efficiency of the cross-polarization step may be fairly high. However, the large number of coherence transfer steps involved in the total experiment will decrease the overall efficiency. Furthermore, a conventional MQMAS experiment excites triple-quantum coherences by acting on a population difference across the triple-quantum energy levels, whereas in this approach the population difference is across $m_S = \pm 1/2$, the central-transition levels, a process which will be inefficient unless a high rf field strength is used, or perhaps a RIACT (*19*) excitation is employed.

Alternatively, it has been proposed to reduce the number of coherence transfer steps required in the experiment by converting the single-quantum coherences created by cross-polarization directly to multiple-quantum coherences for MQMAS, as shown in Fig. 4.7(b), in a manner analogous to two-pulse excitation of multiple-quantum coherences (*92*). If both the dotted and solid coherence pathways in Fig. 4.7(b) are selected, pure-phase lineshapes are not observed and there are additional distortions present. These

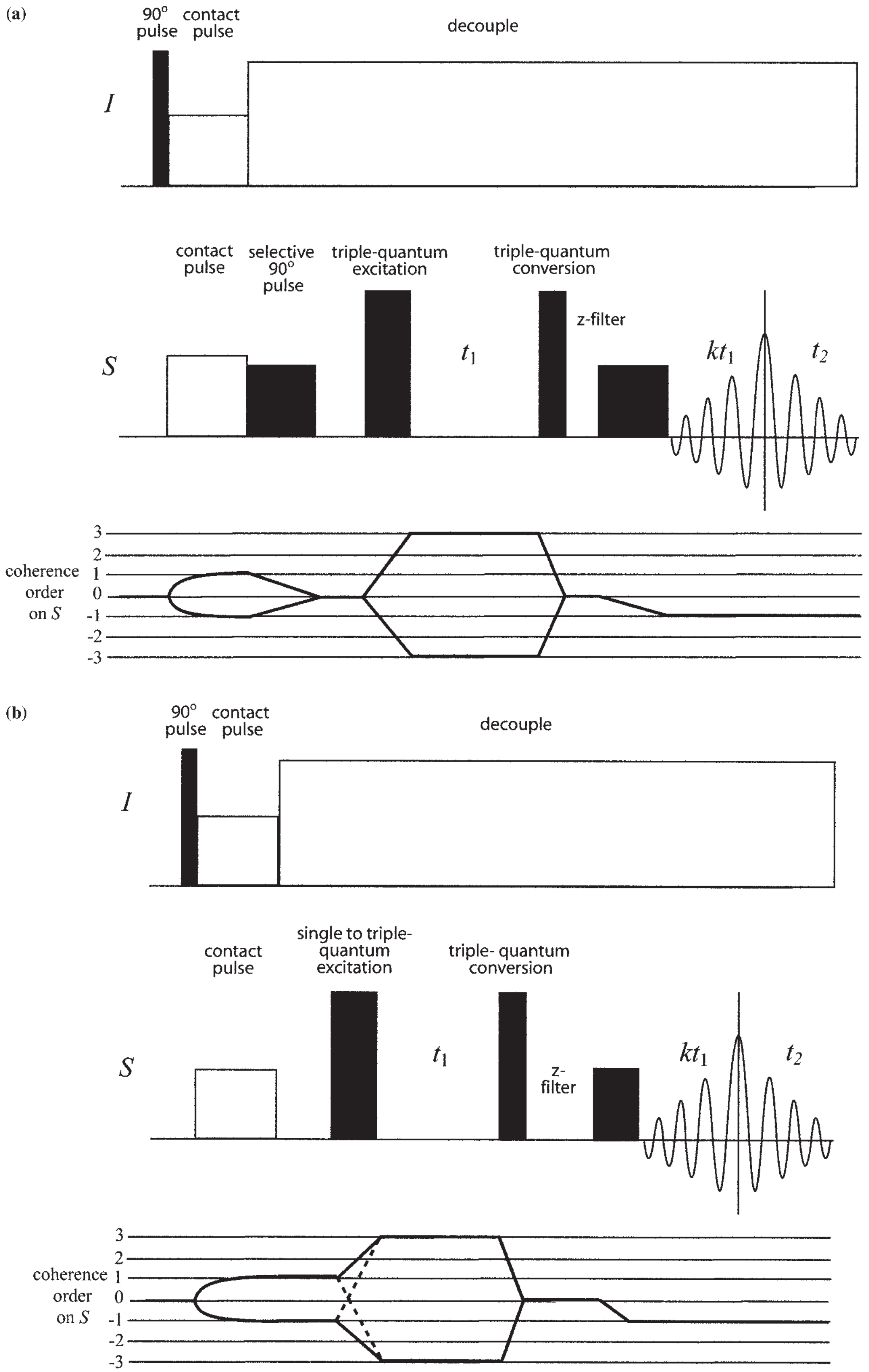

Figure 4.7 Pulse sequences and coherence transfer pathway diagrams for various experiments that combine cross-polarization and MQMAS. (a) Single-quantum cross-polarized amplitude-modulated z-filter of Fernandez et al. (*91*), (b) single-quantum cross-polarized amplitude-modulated z-filter of Ashbrook et al. (*92*) with direct single- to triple-quantum transfer, (c) phase-modulated "reverse split-t_1" variant of (b) (*92*) (shown for $I = 3/2$), and (d) triple-quantum cross-polarized amplitude-modulated z-filter of Ashbrook et al. (*70*). See text for further details.

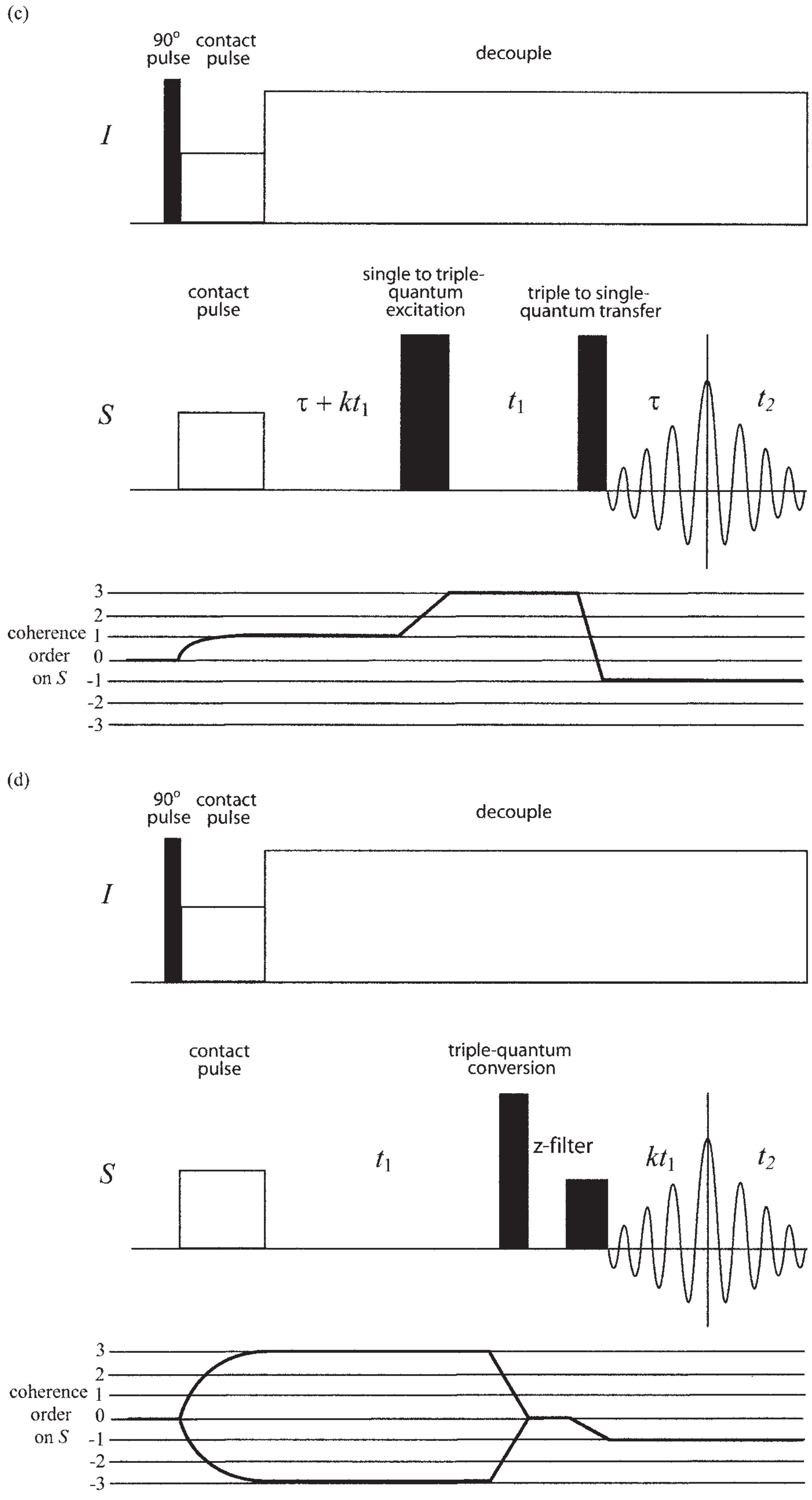

Figure 4.7 (Continued)

distortions result from triple-quantum coherences being created directly by cross-polarization and the failure of the phase cycle to reject these. Modification of the phase cycle to select only the solid coherence pathways removes the possibility of this direct triple-quantum cross-polarization and pure-phase spectra result. Alternatively, a phase-modulated MQMAS experiment may be employed (as shown in Fig. 4.7(c)) with the selection of only a single coherence transfer pathway and the use of a whole echo to obtain pure-phase lineshapes (*92*). This experiment is easily modified to enable straightforward acquisition of the isotropic spectrum (in a "reverse split-t_1" approach). This three-pulse sequence offers a simple approach to cross-polarized high-resolution spectra with few coherence transfer steps.

A different approach, proposed by Ashbrook and colleagues (*70*), exploits the potential for cross-polarization directly to the multiple-quantum coherences of a quadrupolar nucleus, which are then used directly in an MQMAS experiment, as shown in Fig. 4.7(d). Phase cycling may be used to cross-polarize to either $p = \pm 3$ coherences (as shown in Fig. 4.7(d)) in an amplitude-modulated (z-filtered) experiment, or to select $p = +3$ coherences only, as in a phase-modulated split-t_1 experiment. This results in an experiment with few coherence transfer steps. Cross-polarization conditions are chosen to maximize transfer to triple-quantum coherences (*59*, *70*, *76*), or indeed to allow a RIACT-like mechanism to take place (*68*). Experiments involving higher-order coherences are also possible in a similar approach.

In all cases, whether through DOR, DAS, or MQMAS, the acquisition of a high-resolution cross-polarized spectrum then allows site-specific structural information to be obtained. This is seen in Fig. 4.8, a five-quantum cross-polarized MQMAS spectrum, where a ^{1}H-^{27}Al dipolar coupling is observed between all three tetrahedrally coordinated Al species in AlMePO-β, a novel microporous material, information which is unavailable from the conventional MAS spectrum (*80*). Once resolution has been achieved, more information can be obtained, from variable contact time experiments for example. These methods have been exploited to study many materials, in particular ^{1}H/^{27}Al, ^{19}F/^{27}Al, and ^{31}P/^{27}Al NMR of aluminophosphate materials (*80*, *91*, *92*), and ^{1}H/^{23}Na and ^{19}F/^{23}Na cross-polarization of inorganic solids (*60*, *76*, *80*).

4.2 SEDOR, REDOR, and TEDOR

The family of multiple resonance experiments that includes spin echo double-resonance (SEDOR), rotational echo double-resonance (REDOR), and transferred echo double-resonance (TEDOR) exploit the dipolar coupling between two nuclei, *I* and *S*, to obtain structural information (*93, 94*, *95*). These related methods are, as their names suggest, based on a form of echo experiment in which the heteronuclear dipolar coupling would normally be refocused, but this is prevented by the application of rf pulses to the dipolar-coupled partner. As with cross-polarization, this type of experiment is commonly used for the study of spin-1/2 nuclei, but becomes more complex when quadrupolar nuclei are involved. For simplicity, the use of these techniques is briefly outlined for the spin-1/2 case before their applications to quadrupolar systems are discussed.

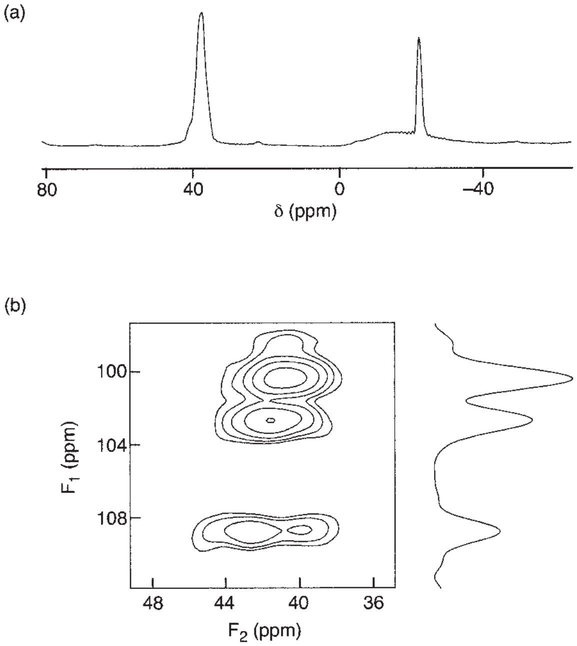

Figure 4.8 A five-quantum cross-polarized MQMAS spectrum, where a ^{1}H–^{27}Al dipolar coupling is observed between all three tetrahedrally coordinated Al species in AlMePO-β, a novel microporous material (*80*).

The simplest approach of this type is spin echo double-resonance or SEDOR (*93*). Although easy to implement, the low resolution of this technique, even for spin-1/2 nuclei, results in its infrequent use. Nonetheless, it provides the simplest, and perhaps most useful, explanation of this genre of experiment. The experiment, performed on a static sample, involves the application of a spin echo (90°-τ-180°-τ) sequence to one of the dipolar-coupled spins, *I* for example, as shown in Fig. 4.9(a), which, if applied in isolation, would refocus the heteronuclear dipolar interaction and the chemical shift anisotropy. If, however, a 180°

pulse is also applied to a dipolar-coupled partner, *S*, at the same time as that applied to *I*, proper refocusing of the heteronuclear dipolar interaction is prevented and, consequently, the echo intensity at time $t = 2\tau$ is diminished. The amount of intensity lost is a function of the echo time τ and the strength of the *I*–*S* dipolar coupling. Any loss of intensity provides qualitative structural information (i.e., on the spatial proximity of *I* and *S*). To obtain quantitative information, a "SEDOR curve" can be measured, following echo intensity, usually as a function of echo time τ. A reference experiment, without any *S* spin irradiation, is also acquired to take into account T_2 relaxation effects during τ. The difference in intensity of signals between the reference *I* spin spectrum and the SEDOR *I* spin spectrum, the so-called "SEDOR fraction," has a form that depends only on the *I*–*S* dipolar coupling, allowing the *I*–*S* distance to be determined.

The lack of resolution available from SEDOR led to the development of the related rotational echo double-resonance or REDOR experiment (*94*). In principle, REDOR involves the use of a SEDOR-like echo experiment under MAS conditions, increasing spectral resolution and sensitivity. There are a few possible types of REDOR experiments, but a typical pulse sequence is shown in Fig. 4.9(b). As in SEDOR, a spin echo is applied on the *I* spin, whereas now a series of rotor-synchronized 180° pulses are applied on the *S* spin. These prevent refocusing of the heteronuclear dipolar interaction (which would normally be achieved under MAS by the rotational echoes in addition to that achieved by the spin echo) and so again lead to dephasing of the *I* spin magnetization. Two pulses are applied per rotor period (usually at $\tau_R/2$ and τ_R) to ensure the sign of the dipolar coupling is the same at the start of each rotor period. As in SEDOR, two experiments are recorded, with and without the 180° pulses, and the REDOR difference signal intensity determined. A plot of this against echo time τ yields a curve which depends only upon the dipolar coupling and so the *I*–*S* distance may be extracted. The practical problems that may be caused by imperfect 180° pulses may be minimized by varying the phases of these pulses on the dephasing spin, using for example the XY-4 "cycle" or related supercycles (*96*).

REDOR is ideal for the measurement of dipolar couplings between a hundred and a few thousand hertz. For larger dipolar couplings, dephasing is rapid and the signal often disappears after echo times of only a few rotor periods, whereas for smaller couplings the dephasing is often too small to be significant in comparison with intensity variations due to noise. Quantitative distance information is only accurately obtained when an isolated *I*–*S* spin pair is present (often necessitating selective isotopic enrichment of materials). The interpretation of results is much more complex when multi-spin systems, such as I–S_2 and I–S_3, are present, with the observed dephasing dependent on the orientation of all internuclear vectors, and also influenced by *S*–*S* homonuclear dipolar couplings. There have been a few approaches in the literature to solving this problem, including θ-REDOR and FS-REDOR (*97*, *98*). The first of these involves the use of a so-called θ pulse in place of the *I* spin 180° (or π) pulse in Fig. 4.9(b). If θ is chosen to be small, the likelihood of all *S* spins in the multispin systems inverting is also small, essentially creating a series of isolated *I*–*S* spin pairs. The *I* spin signal is then the result of dephasing by a sum of *n I*–*S* dipolar interactions, with the additional advantage that the dependence on relative orientation of these interactions is eliminated. The use of only a small flip angle pulse may lead to a loss of sensitivity. The second approach, frequency-selective or (FS) REDOR, involves an *I* spin frequency-selective spin echo generated by the application of a pair of selective 180° pulses applied simultaneously to *I* and *S* spins in the center of the REDOR dephasing period. Selectivity is achieved through the use of Gaussian-shaped pulses with varying resonance offset, allowing individual dipolar couplings to then be probed separately.

Finally, the transferred echo double resonance (or TEDOR) experiment involves transferring magnetization between two heteronuclear spins (*95*). It consists of two sequential REDOR sequences, one on *I* one on *S*, with a transfer of magnetization between the two spins through the application of a simultaneous 90° pulses (Fig. 4.10). Signal loss on the *I* spin is no longer measured, but instead the gain in *S* spin signal intensity is observed. Quantitative information is once again obtained from a variation of the *S* spin signal as a function of the dephasing time, now either of the *I* or *S* spins. TEDOR is less efficient than REDOR (owing to the transfer step) but has the advantage of being easily converted in a two-dimensional correlation experiment (as will be described later).

4.2.1 REDOR and TEDOR for Quadrupolar Nuclei.

It is generally accepted that experiments such as REDOR and TEDOR are much more difficult to perform and analyze in a quantitative manner when one or both of the *I* and/or *S* spins is quadrupolar. These methods rely on an ability to accurately invert the spins through the use of 180° (π) pulses. For quadrupolar nuclei, this is often difficult, if not impossible, owing to the range of nutation rates present and the magnitude of the quadrupolar broadening. It can be

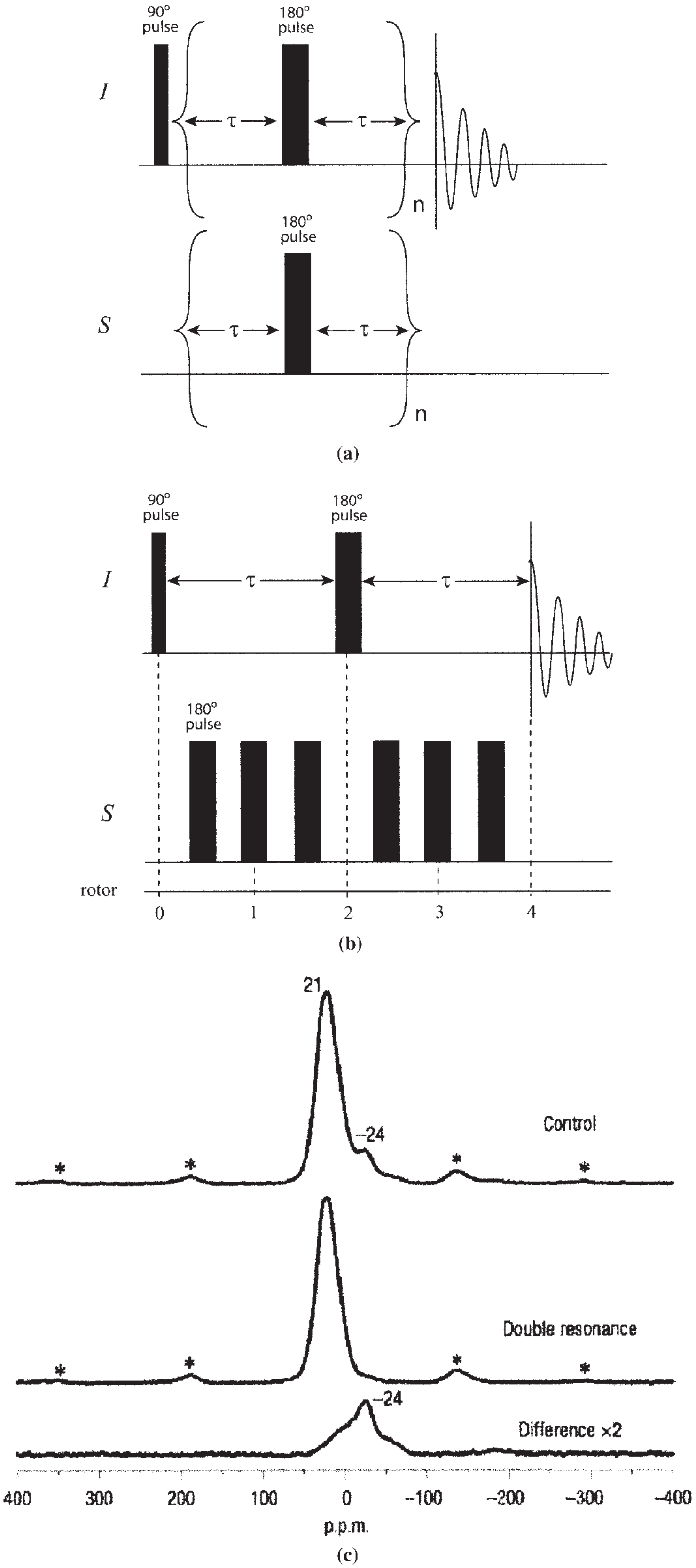

Figure 4.9 (a) SEDOR pulse sequence for measuring the dipolar coupling between two heteronuclear spins *I* and *S* in static samples (*93*). (b) A typical REDOR pulse sequence for measuring the dipolar coupling between two heteronuclear spins *I* and *S* in samples spinning at the magic angle (*94*). (c) ^{1}H–^{17}O REDOR experiment on zeolite HY identifying the Brønsted acid site (*103*).

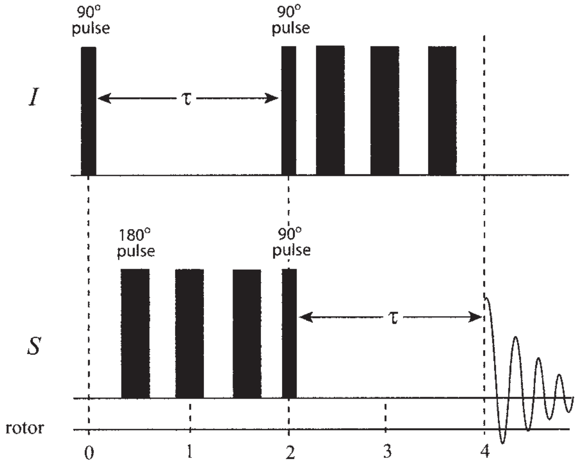

Figure 4.10 TEDOR pulse sequence, transferring magnetization between two dipolar-coupled heteronuclear spins *I* and *S* under MAS (*95*). A two-dimensional correlation experiment may be acquired through the insertion of a t_1 period in place of the initial τ duration (*109*).

seen, therefore, that for the best results in REDOR experiments where only one of the spins involved is quadrupolar, the quadrupolar spin should be chosen as the *I* spin (the observed spin), and the long train of dephasing 180° pulses applied to the $S = 1/2$ nucleus. This will also yield the additional advantage that the repetition rate of the experiment will depend on the quadrupolar (*I*) spin T_1 relaxation time, which can often be significantly faster than for spin-1/2 nuclei. The problem of accurate spin inversion is exacerbated in TEDOR as dephasing pulses are applied to both *I* and *S* spins. For qualitative TEDOR measurements, the choice of the nucleus on which to begin the experiment is usually governed by the relative T_1 values. To extract distance information, it is preferable to vary the REDOR section in which dephasing pulses are applied to the spin-1/2 system. For the case where both *I* and *S* are quadrupolar, care must be taken with both REDOR and TEDOR measurements, and any information obtained is likely to be qualitative only.

Nonetheless, REDOR and TEDOR experiments have been used to great effect in many types of quadrupolar systems, providing qualitative and sometimes quantitative structural information on spatial proximities. There has been much interest in the use of ^{2}H REDOR experiments, primarily owing to the selectivity and specificity that isotopic labeling can offer. The quadrupolar interaction for ^{2}H is often small (50–500 kHz) even for nonmotionally averaged species. However, as ^{2}H is a $I = 1$ nucleus, the MAS spectrum usually consists of a broad envelope of spinning sidebands. For finite rf field strengths, the efficiency of a ^{2}H 180° pulse is often less than ideal, with only a fraction of spins making the desired transitions (*99*). To overcome this, θ-REDOR-type experiments, using a smaller pulse flip angle, have been proposed and have been demonstrated to outperform REDOR experiments when the ^{2}H quadrupolar coupling is fairly large (*100*). In both cases, however, the dipolar dephasing can be difficult to describe analytically and quantitative information is best obtained by comparison with numerical simulations. Alternatively, it has been demonstrated that the use of a composite 180° pulse for ^{2}H can significantly improve the inversion efficiency. For example, the use of the composite 90°-180°-90° inversion sequence has enabled measurement of ^{2}H-^{15}N distances in amino acids (*101*). The PM5 ($90°_y$-$90°_x$-$90°_y$-$90°_x$-$90°_y$) composite inversion pulse was used to detect weak ^{13}C-^{2}H couplings in REDOR experiments on alanine and to determine the torsion angle in ethylmalonic acid by measuring the dipolar dephasing curves for two different ^{13}C species (*101*).

Useful structural information may also be obtained from REDOR and TEDOR experiments on quadrupolar nuclei with half-integer spin. The presence of dephasing (REDOR) or of signal (TEDOR) indicates spatial proximity and qualitative conclusions are easily drawn. These experiments have been used to great effect by Fyfe and colleagues (*102*) for the study of the aluminophosphate VPI-5 and ALPO-8 frameworks. Both ^{27}Al and ^{31}P dephasing experiments are possible in these systems, although analysis is complicated by the presence of *I*-S_4 multispin systems (arising from the tetrahedral network). For the case where dephasing pulses are applied to ^{31}P, both ^{27}Al sites (tetrahedrally and octahedrally coordinated) appear close to ^{31}P, but the REDOR difference curves show few oscillations, as expected from a multispin system. For the case of dephasing pulses applied to ^{27}Al, the situation is more complex. Although each ^{31}P resonance may be considered individually (owing to resolution in the MAS spectrum), the large quadrupolar coupling of ^{27}Al results in a 180° pulse, which is selective for the central transition only. In this case, only a fraction of the Al nuclei are inverted. Although this can provide a convenient route to achieving isolated *I*-*S* pairs, as in θ-REDOR, it can be difficult to determine the effective size of the spin system and so quantitative analysis is further complicated. However, qualitative structural information obtained by REDOR and TEDOR in this work, and also in the study of other systems, has proved vital for the spectral assignment of these framework structures. Recently, ^{1}H–^{17}O REDOR has enabled the detection of the

Brønsted acid site (Si–(OH)–Al) in the zeolite HY, observed only as a shoulder on a broad resonance in the conventional MAS spectrum, as shown in Fig. 4.9(c) (*103*).

An alternative approach to obtaining quantitative distance information from REDOR and TEDOR has been demonstrated by Strojek and colleagues (*104*). They exploit the fact that although REDOR dephasing curves in multispin systems differ from those of the simple two-spin case, the initial rate of dephasing (i.e., that at small echo times) is the same, affected only by a scaling factor derived from the magnitude of the quadrupolar interaction and not by any additional geometrical constraints. Any further effects, including spinning rate or rf amplitude, can be taken into account by comparison with numerical simulations of this initial part of the REDOR curve. This type of analysis was used to differentiate the different Q^n ^{31}P moieties in glassy sodium phosphates and to demonstrate an increase in ^{23}Na-^{31}P dipolar coupling with an increase in charge of the phosphate moiety. Although many assumptions are made and this method does require a priori knowledge of the I spin quadrupolar couplings, it may provide useful information for complex systems such as glasses.

The use of frequency-selective (FS) REDOR for I–S_n systems where I is a quadrupolar nucleus has also been successfully demonstrated for ^{27}Al observe ^{31}P dephase REDOR for VPI-5 (*105*). As in the spin-1/2 case, a Gaussian (frequency selective) pulse is applied to the ^{31}P nuclei, in the center of the train of dephasing pulses. By varying the frequency of this pulse, dipolar interactions with each ^{31}P may be measured separately for ^{27}Al species, which are resolved in the MAS spectrum. The results achieved are in excellent agreement (to within $\sim$1%) with those obtained by X-ray diffraction.

Finally, for REDOR (or FS-REDOR) involving quadrupolar nuclei, significant distortions of the quadrupolar lineshapes are observed as a function of the echo delay τ in Fig. 4.9(b). These do not affect the intensity of the REDOR signal (and hence the accuracy of the distance measurements). However, these distorted lineshapes do offer information on the relative orientation of the dipolar and quadrupolar tensors. This has been used to provide information on the relative orientation of the ^{17}O quadrupolar and ^{17}O/^{31}P dipolar tensors for the nonbridging oxygens in a phosphate glass (*106*).

4.2.2 High-Resolution REDOR/TEDOR Experiments. Once again, although REDOR can provide either qualitative or quantitative distance information, the lack of resolution in MAS NMR spectra of quadrupolar nuclei may hinder the extraction of this information. As with cross-polarization, it is possible to combine REDOR with methods to increase the spectral resolution. In particular, the combination of REDOR and MQMAS has proved popular, with different variations of the experiment proposed. The initial approach (now termed MQ-t_2-REDOR) (*107*) involves the application of a REDOR dephasing sequence after a (z-filtered) MQMAS experiment. The phase cycling of the 90° pulse after the selection of population states in the z-filter is altered to select $p = +1$ rather than $p = -1$ coherences as in conventional MQMAS. A spin echo is then performed while dephasing pulses are applied to the dipolar-coupled spin. The increase in resolution afforded by MQMAS can then allow the site-specific observation of REDOR signal (and indeed measurement of dipolar couplings and bond lengths in favorable circumstances) for resonances that may be overlapped in the conventional MAS spectrum. This was demonstrated using ^{19}F dephasing of the ^{27}Al MQMAS spectrum for a fluorinated aluminium phosphate, although a spin pair approximation was assumed when calculating bond lengths (*108*). Note that for any quantitative information, a series of two-dimensional experiments (along with the corresponding reference two-dimensional spectra with no dephasing pulses applied) is required, resulting in a long total experiment time.

Alternatively, it is possible to use a REDOR-like dephasing in the t_1 (or triple-quantum) dimension of the MQMAS experiment, in a method termed MQ-t_1-REDOR (*108*). Here, an initial pulse creates triple-quantum coherences, which are allowed to evolve for a time t_1. A REDOR dephasing train of pulses is applied to the heteronuclear dipolar partner, before an I spin 180° pulse inverts the triple-quantum coherences. The second dephasing train is then applied, after which the triple-quantum coherences are converted via a population state using a z-filter, to observable single-quantum magnetization. The use of REDOR in the triple-quantum evolution period has the advantage that the dipolar coupling is enhanced by a factor of 3, allowing the observation (and measurement) of couplings that may be too small to accurately measure in a single-quantum technique. However, the inversion of triple-quantum coherences (a six-quantum step) is particularly inefficient, reducing the signal intensity by a factor of $\sim$5. This reduction may still allow the acquisition of spectra in systems where sensitivity is not a problem, but may limit the use of MQ-t_1-REDOR elsewhere (*109*).

The combination of MQMAS and TEDOR is also possible (in an analogous manner to that of MQMAS and cross-polarization) (*109*). A TEDOR experiment is performed transferring magnetization from an initial spin to the quadrupolar spin. The single-quantum coherences created are then converted to triple-quantum coherences before a (z-filtered) MQMAS experiment is carried out. In this way, the high-resolution spectrum produced contains signal only from those species that possess a significant dipolar coupling to the initial spin.

A related approach that may offer qualitative information is the use of dipolar dephasing (*110*). This involves the application of a train of *S* spin dephasing pulses, as in REDOR, to dephase any evolving *I* spin signal which has a contribution in its evolution frequency from dipolar coupling. In contrast to REDOR, dipolar connectivity is demonstrated by the significant broadening or the absence of a resonance. Though useful for qualitative measurements, the lack of resolution resulting from the broadening of resonances may make any additional interpretation difficult. Dipolar dephasing has also been combined with MQMAS (DD-MQMAS) (*111*), with the train of *S* spin dephasing pulses applied during the triple-quantum t_1 evolution period of a conventional z-filtered MQMAS experiment, and used to study fluorinated aluminophosphate framework materials (*111*).

4.3 REAPDOR and TRAPDOR

Although SEDOR, REDOR, and TEDOR have successfully been applied to systems where one or other of the dipolar-coupled nuclei is quadrupolar, the spin dynamics associated with the experiment become much more complicated than those for the simple two spin-1/2 case, and the experiment itself may become somewhat inefficient. In contrast, the rotational echo adiabatic passage double-resonance (REAPDOR) (*112*) and transfer of population in double-resonance (TRAPDOR) (*113*) experiments are designed specifically to study dipolar interactions involving quadrupolar nuclei. These sequences (shown in Fig. 4.11) are similar to REDOR in their philosophy, preventing the refocusing of the dipolar interaction under MAS, but where REDOR achieves this using trains of 180° pulses REAPDOR and TRAPDOR both use adiabatic pulses on the quadrupolar spin.

TRAPDOR (see Fig. 4.11(a)) is perhaps the simplest of the two to implement, comprising of a spin echo on an observe spin *I*, which is usually, although not necessarily, spin-1/2 (*114*). During either or both of the echo time periods, τ, a dipolar-coupled quadrupolar *S* spin partner is continuously irradiated. This irradiation causes a rotor-driven modulation of the quadrupolar eigenstates (as described previously for cross-polarization and spin locking) altering, therefore, the dipolar coupling of these states to the *I* spin, as this coupling depends on the spin state of both spins (*6*). This prevents refocusing of the dipolar interaction and leads to a dephasing of the *I* spin spectrum. As in REDOR, a reference experiment (with no *S* spin irradiation) is required to take into account any effects of T_2 relaxation. The "TRAPDOR difference" curve, the difference in intensities of signals between the reference experiment and that where the *S* spin is irradiated, can once again be plotted as a function of echo time τ to obtain a "TRAPDOR curve," dependent on the dipolar coupling. There is a significant phase change between the TRAPDOR and reference signals. This is due to a phase accumulation from the TRAPDOR effect itself, and also to a Bloch-Siegert shift resulting from long irradiation periods (*113*, *114*).

The amount of TRAPDOR dephasing depends crucially on the adiabaticity parameter, α, described previously. If α is small, no dephasing occurs, whereas the maximum dephasing is obtained when $\alpha \gg 1$. In a powdered sample, this adiabatic condition will not hold for all crystallites simultaneously, and some may not participate in the dephasing at all. Furthermore, unlike REDOR, the transfer does not occur concomitantly in the rotor period for each spin, but depends significantly on the crystallite orientation. The key problem in the quantitative interpretation of TRAPDOR is the determination of the fraction of crystallites, which need to be considered, and the calculation of the timings of their adiabatic passages (*115*). This has resulted in the use of TRAPDOR often in a more qualitative sense, particularly if multispin systems are involved, where an analytical approach is impossible and even numerical analysis difficult. However, in contrast to REDOR, where only dipolar couplings to the $m_S \pm 1/2$ levels are considered, in TRAPDOR dipolar couplings to all quadrupolar spin states are used, resulting in a much larger dephasing effect.

Although TRAPDOR often provides only semi-quantitative distance information, it has been used to great effect in various chemical problems. For example, $^1H/^{27}Al$ and $^1H/^{23}Na$ TRAPDOR have been used to distinguish different water environments within zeolite frameworks (*115*) and to determine the structural position of these water molecules based upon their TRAPDOR dephasing. Similarly, $^{31}P/^{27}Al$ TRAPDOR has been used to distinguish the bulk alumina from Al species close to ^{31}P in phosphorous impregnated γ-Al_2O_3 (*116*). An interesting application of TRAPDOR experiments has been the measurement of large quadrupolar couplings. The TRAPDOR effect only occurs when the irradiation is applied at a frequency within the first-order quadrupolar line

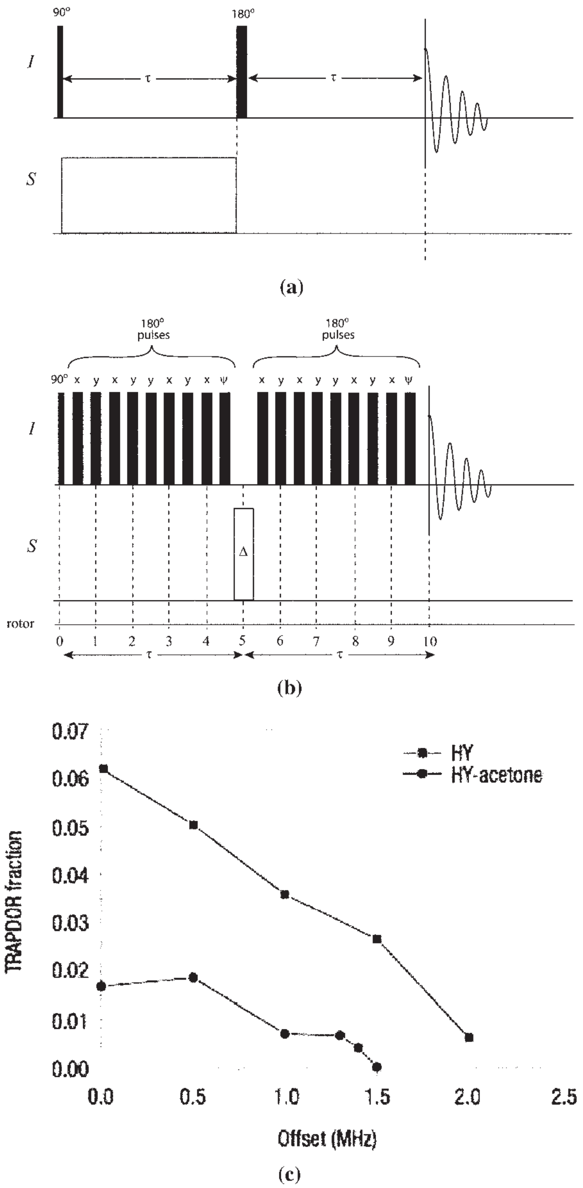

Figure 4.11 (A) TRAPDOR experiment for measuring the dipolar coupling between a quadrupolar spin *S* and (usually) a spin-1/2 *I* under MAS (*113*). The long *S* spin pulse produces a rotor-driven modulation of the quadrupolar eigenstates, reintroducing the *I*–*S* dipolar coupling. (b) REAPDOR experiment for measuring the dipolar coupling between a quadrupolar spin *S* and a spin-1/2 *I* under MAS (*112*). (c) Plot of ^{1}H–^{27}Al TRAPDOR fraction as a function of offset for zeolite HY, demonstrating the change in quadrupolar coupling constant on the interaction of acetone with the Brønsted acid site (*103*).

width. Variation of the irradiation frequency until no TRAPDOR effect is observed can, therefore, define the extent of the line and the magnitude of the quadrupolar coupling. This effect has been used to determine large ^{14}N (*115*) and ^{27}Al (*117*) quadrupolar couplings that are difficult if not impossible to observe directly. TRAPDOR (^{1}H–^{17}O) has also been employed in this way the study of the Brønsted acid site in zeolite HY (in combination with REDOR, as described earlier) (*103*). On reaction with acetone, known to interact with the zeolite framework via the Brønsted site, a significant decrease in the C_Q (from 6.6 to 5 MHz) was observed by TRAPDOR, as shown in Fig. 4.11(c), ascribed to a lengthening of the O–H bond length from 0.97 to 1.02 Å.

REAPDOR (or rotational echo adiabatic passage double resonance) (see Fig. 4.11(b)) is similar to TRAPDOR in using an adiabatic pulse on the quadrupolar *S* spin, but is also much more similar to REDOR with a train of pulses applied to the observe spin *I*, which again is usually spin-1/2 (*112*, *118*). Figure 4.11(b) shows that the experiment begins with a 90° pulse on the *I* spin, which is followed by a rotor-synchronized train of 180° pulses, separated by $\tau_R/2$, or half a rotor period. The pulse in the center of the train is omitted, resulting in a dephasing of the *I* spin signal in the first half of the experiment (due to both dipolar and chemical shift anisotropy interactions) and a refocusing in the second half of the experiment. The introduction of an adiabatic *S* spin pulse in the center of the dephasing train, applied for length Δ where $0 < \Delta < \tau_R$, changes the spin state of the quadrupolar nucleus through a modulation of the *S* spin eigenstates, changing the dipolar coupling to *I* and preventing complete refocusing of the dipolar interaction. As in REDOR, the difference in signal intensities compared with a reference experiment is determined and plotted, usually, against echo duration τ to obtain a REAPDOR curve, which then depends on the dipolar coupling. When compared with TRAPDOR, REAPDOR has the advantage of a much smaller period of *S* spin irradiation, reducing the strain on the probe and, in addition, results in a much smaller phase difference of the REAPDOR signal from the reference signal (*113*, *119*). It is, however, a more demanding *I* spin experiment than TRAPDOR. As with TRAPDOR, dipolar interactions to all quadrupolar spin states are considered and the amount of dephasing is considerably greater than that obtained by REDOR.

The analysis of a REAPDOR dephasing curve is more complex than that for spin-1/2 REDOR as the dipolar evolution depends on many parameters, and full density matrix calculations need to be performed to for accurate distance information to be extracted (*119*). This has been performed for many systems, including ^{23}Na/^{29}Si (*120*, *121*) and ^{1}H/^{27}Al in zeolites (*122*) and ^{29}Si/^{11}B (*123*) in ceramic materials. It can be shown, however, that in certain limits it is possible to describe a "universal" curve, depending principally on the dipolar coupling and with minimal dependence on the MAS rate, the rf field strength, the quadrupolar asymmetry, or the relative orientations of the quadrupole and dipole tensors. The main requirement for this simple analysis is that the adiabaticity parameter, α (section 4.1.2) is large. This technique has been proven to be particularly effective for $I = 1/2$, $S = 1$ systems such as ^{2}H/^{13}C and ^{14}N/^{13}C (*120*) and has also been demonstrated for $I = 1/2$, $S = 5/2$ pairs, such as ^{13}C/^{17}O (*124*). These analyses, as in REDOR, rely on the presence of isolated spin pairs, with the quantitative analysis of multispin systems a computationally more challenging problem.

4.4 Two-Dimensional Correlation Experiments

Heteronuclear correlation spectroscopy has been widely used in solid-state NMR to provide information on the spatial proximity of different nuclei in complex spin systems (*125*). When more than one distinct I and/or S spin species is present, a two-dimensional correlation experiment enables the detection of dipolar couplings between specific distinct I–S pairs. Typically, the experiment consists of a 90° pulse to create transverse I spin magnetization, which evolves for a time t_1 before it is transferred to spin S, usually via cross-polarization. The S spin FID is then detected in t_2. Two-dimensional Fourier transformation yields a two-dimensional spectrum, with the appearance of cross peaks between individual I and S resonances from spins which are dipolar coupled. It is also possible to achieve magnetization transfer through a TEDOR-like mechanism through the introduction of a t_1 period in the TEDOR experiment shown previously in Fig. 4.10.

It has been demonstrated that these two-dimensional heteronuclear experiments, generally termed HETCOR experiments, are also feasible when either I or S is a half-integer quadrupolar nucleus, using either cross-polarization (*126*) or TEDOR (*127*) transfer. In both cases, the spectra are able to provide information unavailable by one-dimensional methods owing to the increase in resolution obtained from the presence of a second spectral dimension. For example, ^{27}Al to ^{31}P cross-polarization transfer was used in a HETCOR experiment to confirm that all three ^{31}P resonances exhibit a dipolar coupling to tetrahedrally and octahedrally coordinated Al species in the microporous material VPI-5 (*127*).

For quadrupolar nuclei, the problems of obtaining optimum sensitivity in cross-polarization or TEDOR transfer once again may limit the quantitative information available, as may the time-consuming acquisition of a series of two-dimensional experiments. In general, therefore, it is usual to begin a HETCOR experiment with pulses on the quadrupolar nucleus, enabling a faster repetition rate owing to the (usually) faster quadrupolar T_1 relaxation. Moreover, techniques for increasing sensitivity can also be employed. In particular, the use of RAPT prior to the excitation of transverse magnetization on a quadrupolar S spin has been used to great effect in ^{27}Al/^{29}Si HETCOR experiments (*77*).

Although resolution in HETCOR experiments compared to one-dimensional spectra has been increased through the use of a second dimension, the presence of second-order quadrupolar broadening in the spectrum of the quadrupolar nucleus may limit the information available. The combination of a high-resolution technique, such as DAS or MQMAS, with HETCOR is the obvious choice to alleviate this problem. Jarvie and colleagues (*128*) have demonstrated a ^{23}Na/^{31}P high-resolution HETCOR spectrum of sodium trimetaphosphate, utilizing the resolution achieved in DAS. A DAS experiment is first performed on the quadrupolar spin, using the 79.19°/37.38° angle pair. A further rotor angle change to 0° for optimum cross-polarization follows before finally acquisition of a ^{31}P FID under MAS (at 54.736°). Though this experiment gives high resolution in both dimensions, it requires three changes of rotor axis and so is not particularly useful for species systems limited by efficient T_1 relaxation.

An alternative approach introduced by Wang and colleagues (*129*) used MQMAS to achieve a high resolution spectrum, again in a ^{23}Na/^{31}P high-resolution HETCOR spectrum of sodium trimetaphosphate. This was achieved using the pulse sequence shown in Fig. 4.12(a), where triple-quantum ^{23}Na coherences are excited (for a time t_1) and converted to single-quantum coherences of the same sign, which evolve for a time kt_1, before transfer, via cross-polarization, to ^{31}P. The use of a split-t_1 period enables the quadrupolar broadening to be refocused before t_2 producing a high-resolution ^{23}Na spectrum, as shown in Fig. 4.12(b). In principle, the experiment could be applied in reverse, i.e., from ^{31}P to ^{23}Na, but this approach does have a few disadvantages. First, a three-dimensional experiment is then required to obtain a correlation spectrum that is high-resolution in both dimensions. Second, the experiment no longer exploits the short ^{23}Na T_1, further increasing the total experiment time.

Correlations involving z-filtered MQMAS experiments have also been proposed, where conventional cross-polarization transfer occurs after the selection of population states (*130*) or, alternatively, after a kt_1 single-quantum evolution period (*131*, *132*). Although a z-filter is perhaps the easiest MQMAS experiment to perform, it is often not suited to use in a HETCOR experiment, as pointed out by Fernandez and colleagues (*133*). The presence of echo and antiecho pathways (i.e., $p = \pm 3$ coherences in t_1) results in severe distortions in the HETCOR spectrum and the presence of "ghost" peaks that do not result from true magnetization transfer. The use of a phase-modulated experiment, with correlation of triple- and single-quantum coherences of the same or opposite sign as determined by the sign of the MQMAS ratio, however, alleviates these problems (*134*), as does the original amplitude-modulated experiment of Wang and colleagues, owing to its split-t_1 nature (*129*).

The high-resolution TEDOR experiment of Amoureux and colleagues (*109*) described previously can be easily adapted to provide a two-dimensional correlation spectrum through the insertion of a t_1 evolution period before magnetization transfer.

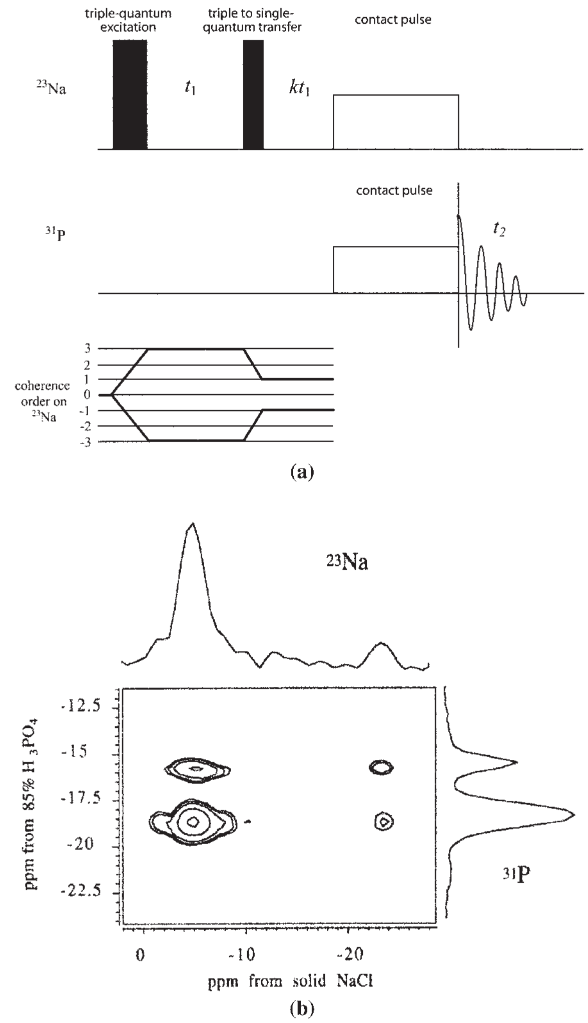

Figure 4.12 (a) Pulse sequence and coherence transfer pathway diagram for an MQMAS-based heternouclear correlation (HETCOR) experiment, shown for the correlation of ^{23}Na and ^{31}P. The use of a split-t_1 MQMAS sequence enables the acquisition and correlation of high-resolution ^{23}Na NMR spectra (*25*). (b) ^{23}Na–^{31}P two-dimensional multiple-quantum HETCOR spectrum of sodium trimetaphosphate (*129*).

4.5 Other Techniques

In addition to the more commonly used techniques described so far, many different experiments have been proposed to exploit the information that the dipolar coupling may offer. Although it would be impossible to detail all of these, some of the more promising approaches are described in this section.

Lupulescu and colleagues (*135*) have used a REDOR-like series of pulses within the triple-quantum evolution period of a MQMAS experiment to reintroduce the dipolar interaction between the quadrupole and a proximate spin-1/2 nucleus. This allows the creation (and selection by phase cycling) of a heteronuclear multiple-quantum (either two- or four-quantum) coherence, comprising of triple-quantum coherences on the quadrupole and single-quantum coherence on the spin-1/2 nucleus, which evolves in a time t_1. This leads to so-called rotor-encoded spinning sideband patterns (*136*) in the indirect dimension (f_1) of the resulting two-dimensional spectrum, which depend on recoupling time, the quadrupolar and dipolar coupling, and the relative orientation of the quadrupolar and dipolar tensors. The experiment has been demonstrated on dibasic sodium phosphate with heteronuclear multiple-quantum ^{23}Na-^{1}H coherences generated. Sideband patterns simulated for an I–S_2 (Na-H$_2$) spin system agree well with the experimental data for the Na(2) species and were sensitive to the angle between the two internuclear I–S vectors, demonstrated to deviate 10° from linearity. The sideband pattern for the Na(1) species could only be described properly when the ^{23}Na chemical shift anisotropy was also included in the simulations.

An alternative approach has been used by Levitt and colleagues (*137*) to recouple the heteronuclear dipolar interaction between a quadrupole and a spin-1/2 nucleus, specifically ^{17}O and ^{1}H, which is otherwise removed by MAS. This recoupling is achieved by the application of a symmetry-based recoupling sequence (*138*), which in this case can be described by $R18_1^7$, enabling recoupling of the heteronuclear dipolar interaction but decoupling of the homonuclear dipolar coupling and the isotropic interactions. This experiment, termed PRESTO (or phase-shifted recoupling engenders a straightforward transfer of order), has been successfully applied to L-valine.HCl, increasing the sensitivity of the spectrum (by a factor of 2) and to $Mg(OH)_2$ (brucite). It is possible to obtain information on the dipolar coupling and hence the *I-S* internuclear distance by observing signal intensity as a function of recoupling time. A two-dimensional spectrum can also be obtained by Fourier transforming this series of spectra, providing a correlation of quadrupolar and dipolar interactions. The shape of the cross-peak obtained is sensitive to the relative orientation of the quadrupolar and dipolar tensors, which may be extracted if the magnitude of these have been determined previously.

A similar correlation is obtained using the separated local field experiment described by van Eck and Smith (*139*). This was used to ascertain the orientation of quadrupole and dipole tensors of hydroxyl groups by recording a series of cross-polarized spectra as a function of the contact time and applying a subsequent two-dimensional Fourier transformation. This provides a spectrum correlating the quadrupole and dipole tensors, with cross-peak shapes sensitive to their relative orientation. As with PRESTO, this can be determined if the magnitude of both interactions can be measured independently. Unlike PRESTO, however, this experiment was applied to static samples (of brucite and $Mg(OH)_x(OCH_3)_{2-x}$) (*139*). The application of Lee-Goldburg decoupling in the t_1 dimension was shown to improve the resolution by removing homonuclear dipolar interactions.

Finally, an interesting experiment has been developed that uses ^{14}N and allows the determination of the orientation of the ^{14}N quadrupole coupling tensor with respect to ^{14}N-^{13}C vectors (*140*). This is achieved by observing the effect of dipolar coupling between ^{14}N and ^{13}C on the evolution of ^{13}C double-quantum coherence.

5. STRUCTURAL INFORMATION FROM HOMONUCLEAR DIPOLAR COUPLING

The difficulties measuring or even using dipolar couplings between heteronuclei, where one nucleus is a quadrupolar nucleus, detailed in section 4, become magnified when dealing with a homonuclear quadrupolar spin pair. The majority of techniques available for spin-1/2 nuclei will not give meaningful results for a homonuclear quadrupolar spin pair. As in the heteronuclear case, the quadrupole coupling generally far exceeds the dipolar coupling, which results in a major challenge when designing experiments to observe the much smaller dipole coupling. In addition, unlike the situation for a heteronuclear spin pair where only one nucleus is quadrupolar, there is now no convenient spin-1/2 nucleus for direct observation on, and the situation might appear hopeless. This is far from being the case, however, and a number of methods have been developed that successfully exploit the homonuclear dipolar coupling in quadrupolar spin systems. Only recently has this work extended in any general sense to quantitative measurement of dipolar couplings, for reasons that will become clear. Correlation experiments affording qualitative structural information are, however, highly achievable. This section summarizes what is currently possible. Details are given of how homonuclear dipolar recoupling under magic-angle spinning is achieved in each case, as this is generally the most challenging part of any such experiment.

5.1 Two-Dimensional Correlation Experiments

Correlation experiments on homonuclear spin systems allow qualitative assessment of which spins are close in space, just as for the analogous heteronuclear correlation experiments. Typically, they are two-dimensional experiments in which transverse magnetization is first created in the homonuclear spin system of interest and allowed to evolve for a time t_1 under its characteristic frequency, which for quadrupolar spins usually (but not always) is a sum of chemical shift and quadrupole coupling terms. The transverse magnetization is then transferred by some means between spins that have a significant dipolar coupling—how significant is determined by the details of the experiment, so that transverse magnetization that originated on one spin in the homonuclear spin system ends up on another nearby spin. The resulting transferred transverse magnetization then evolves in t_2, while an FID is recorded. Recording such experiments for a series of incremental t_1 time ends up with a two-dimensional dataset, which, after processing, displays in the projections in f_1 and f_2, spectra corresponding to the interactions present in the time periods t_1 and t_2 respectively. Cross-peaks between signals in f_1 and f_2 occur in the two-dimensional spectrum where the spins giving rise to those signals are close enough in space to have a significant dipolar coupling between them.

Under magic-angle spinning, the dipolar coupling between spins is, of course, averaged to zero, making the magnetization transfer involved in such a correlation spectrum challenging. For spin-1/2 systems, many methods exist for recoupling the dipolar interaction under magic-angle spinning (i.e., preventing the averaging to zero of the interaction). For quadrupolar nuclei suffering a large quadrupole coupling interaction, most of these methods will not work at all or will be highly inefficient. Thus one of the first challenges in producing homonuclear correlation spectra for quadrupolar nuclei is to recouple the dipolar coupling under the magic-angle spinning, which will almost certainly be required for resolution in the experiment.

This brings us to the second challenge: resolution. As section 2 showed, achieving high-resolution spectra for quadrupolar nuclei can be done, but it is not trivial. Resolution to some degree will usually be required in correlation spectra if they are to be interpreted to give useful structural information.

There have been a variety of ingenious approaches to both these challenges and more continue to be developed. Those developed to date are described in the remainder of this section. It begins with the use of rotational resonance, widely used for spin-1/2 systems, and then continues with various multiple-quantum approaches, which again, mirror to some extent an approach prevalent in spin-1/2 spectroscopy. Finally, there are a series of methods based on the MQMAS experiment which confer the much-needed resolution on the experiment and also, as will be explored, yield other useful structural information.

5.1.1 Rotational Resonance Methods for Correlation Spectroscopy. Rotational resonance has been used effectively for spin-1/2 nuclei as a means to provide quantitative structural information. In essence, it relies on the fact that the dipolar coupling between nuclei, which is normally averaged to zero by magic-angle spinning, does not average to zero when the spinning rate is a specific multiple of the isotropic chemical shift difference between the two dipolar-coupled spins. When the chemical shift anisotropy of both spins is negligible in comparison with the spinning rate, the so-called rotational resonance condition is

$$m\omega_R = \Delta\omega_{iso} \quad m = \pm 1, \pm 2 \qquad [5.1]$$

where $\Delta\omega_{iso}$ is the difference in isotropic chemical shift between the spins.

The beauty of the rotational resonance effect is that it can be used to select a specific spin pair to study the dipolar coupling between, simply by adjusting the spinning rate, thereby adjusting which spin pairs come into rotational resonance by virtue of their chemical shift difference. For this reason as much as any other, the rotational resonance experiment has been used to great effect to measure quantitative internuclear distances in many compounds. The form of experiment used varies, but all generally employ a mixing time during which the rotational resonance effect is allowed to operate. Under rotational resonance, spin polarization is transferred between the two dipolar-coupled spins that meet the rotational resonance condition. The polarization transfer is an oscillatory process, in the absence of relaxation effects, with the oscillation frequency directly dependent on the dipolar coupling constant. Thus by arranging the experiment to observe the polarization transfer as a function of time and suitable simulations, the dipolar coupling constant for the spin pair may be extracted.

Rotational resonance has been applied to half-integer quadrupolar nuclei for the purposes of forming a two-dimensional correlation experiment in which those nuclei that are close in space show a cross-peak between their respective signals. Rotational resonance has not, as yet, been used to measure quantitative internuclear distances between half-integer quadrupolar spins with any appreciable size of quadrupole coupling constant. The reasons for this will become clear as we consider a simple theoretical analysis of the rotational resonance effect for half-integer quadrupolar nuclei.

Theoretical Analysis of the Rotational Resonance Effect for Half-Integer Quadrupolar Nuclei. The complete Hamiltonian for a homonuclear pair *IS* of half-integer quadrupolar nuclei is (for simplicity, neglecting the effects of chemical shift anisotropy) (*141*)

$$\hat{H} = \hat{H}_{iso,I} + \hat{H}_{iso,S} + \hat{H}^{(1)}_{Q,I} + \hat{H}^{(1)}_{Q,S} + \hat{H}^{(2)}_{Q,I} + \hat{H}^{(2)}_{Q,S} + \hat{H}_{IS} \qquad [5.2]$$

where $\hat{H}_{iso,I}$ describes the isotropic chemical shift, $\hat{H}^{(1)}_{Q,I}$, the first-order quadrupole coupling contribution, and $\hat{H}^{(2)}_{Q,I}$, the second-order quadrupole coupling contribution for spin *I* in each case, with similar terms for spin *S*. The term of greatest importance to this discussion is the last one—namely, $\hat{H}_{IS}$, which is the secular part of the dipolar coupling between spins *I* and *S*:

$$\hat{H}_{IS} = 2\omega_D(t)\left(\hat{I}_z\hat{S}_z + \frac{1}{4}\,(\hat{I}_+\hat{S}_- + \hat{I}_-\hat{S}_+)\right) \qquad [5.3]$$

where $\omega_D(t)$ is the dipolar coupling frequency, time dependent due to the magic-angle spinning of the sample.

Rotational resonance is induced by the so-called “flip-flop” term, the last term, of Eq. [5.3], linking Zeeman levels of the form

$$(m_I, m_S) \leftrightarrow (m_I + 1, m_S - 1)$$

The corresponding matrix element of $\hat{H}_{IS}$ is

$$H_{IS}(m_I, m_S; t) = c_{m_I m_S} \omega_D(t)$$

$$= c_{m_I m_S} \sum_{m=-2}^{+2} \omega_D^{(m)} \exp(im\omega_R t) \qquad [5.4]$$

where

$$c_{m_I m_S} = \frac{1}{2} \langle m_I m_S | \hat{I}_+ \hat{S}_- + \hat{I}_- \hat{S}_+ | m_I + 1, m_S - 1 \rangle \qquad [5.5]$$

and where in Eq. [5.4] we have expressed the (periodic) time dependence of the dipolar coupling frequency in terms of its Fourier components. To see the effect of dipolar coupling most easily, we need to form a first-order average Hamiltonian in a frame in which the other terms in the total Hamiltonian (Eq. [5.2]) that do not commute with the dipolar coupling Hamiltonian, $\hat{H}_{IS}$, are removed. In such a circumstance, the so-formed first-order average Hamiltonian is a good approximation of the true, untruncated average Hamiltonian (see section 5.2 and ref. (*6*) for more details on average Hamiltonians). Thus we need to express the matrix element above in Eq. [5.4] in a frame where the isotropic chemical shift, and first- and second-order quadrupole coupling contributions to the $(m_I m_S) \leftrightarrow (m_I + 1, m_S - 1)$ transition frequency are zero. This is accomplished by the following transformation:[1]

$$\tilde{H}_{IS}(m_I, m_S; t)$$

$$= c_{m_I m_S} \sum_{m=-2}^{+2} \omega_D^{(m)} \exp(im\omega_R t) \cdot \exp\{i[(\omega_{iso,I} - \omega_{iso,S})t$$

$$+ \int_0^t (\omega_{Q,I}^{(1)}(\alpha, \beta, \gamma; t') - \omega_{Q,S}^{(1)}(\alpha, \beta, \gamma; t'))dt'$$

$$+ \int_0^t (\omega_{Q,I}^{(2)}(\alpha, \beta, \gamma; t') - \omega_{Q,S}^{(2)}(\alpha, \beta, \gamma; t'))dt'] \qquad [5.6]$$

where $(\omega_{Q,I}^{(1)}(\alpha, \beta, \gamma; t') - \omega_{Q,S}^{(1)}(\alpha, \beta, \gamma; t'))$ is the first-order quadrupolar contribution under MAS to the $(m_I m_S) \leftrightarrow (m_I + 1, m_S - 1)$ transition frequency, and $(\omega_{Q,I}^{(2)}(\alpha, \beta, \gamma; t') - \omega_{Q,S}^{(2)}(\alpha, \beta, \gamma; t'))$ is the corresponding second-order quadrupolar contribution. It is worth noting (as is clear from an examination of Eqs. [1.11] and [1.12] in section 1.2 and Eqs. [2.1] and [2.2] in section 2.1) that both quadrupolar contributions depend on molecular orientation. The significance of this for the rotational resonance effect becomes clear later.

Defining

$$\Delta\omega_{iso} = \omega_{iso,I} - \omega_{iso,S} \qquad [5.7]$$

$$\Delta\omega_Q^{(1)}(\alpha, \beta, \gamma; t') = \omega_{Q,I}^{(1)}(\alpha, \beta, \gamma; t') - \omega_{Q,S}^{(1)}(\alpha, \beta, \gamma; t') \qquad [5.8]$$

and

$$\Delta\omega_Q^{(2)}(\alpha, \beta, \gamma; t') = \omega_{Q,I}^{(2)}(\alpha, \beta, \gamma; t') - \omega_{Q,S}^{(2)}(\alpha, \beta, \gamma; t') \qquad [5.9]$$

we can rewrite Eq. [5.6] more succinctly as

$$\tilde{H}_{IS}(m_I, m_S; t)$$

$$= c_{m_I m_S} \sum_{m=-2}^{+2} \omega_D^{(m)} \exp(im\omega_R t) \cdot \exp\left\{ i[\Delta\omega_{iso} t + \int_0^t \Delta\omega_Q^{(1)}(\alpha, \beta, \gamma; t')dt' + \int_0^t \Delta\omega_Q^{(2)}(\alpha, \beta, \gamma; t')dt'] \right\} \qquad [5.10]$$

It is useful at this point to express the periodic functions $(i \int_0^t \Delta\omega_Q^{(1)}(\alpha, \beta, \gamma; t')dt')$ and $\exp(i \int_0^t \Delta\omega_Q^{(2)}(\alpha, \beta, \gamma; t')dt')$ in terms of their Fourier components:

---

[1] The only nonzero term in the matrix element of the dipolar coupling Hamiltonian H_{IS} arises from the $\hat{I}_-\hat{S}_+$ component. Under a rotation of the *I* spin operator about z at the *I* spin transition frequency (i.e., frequency of the $m_I \leftrightarrow m_I + 1$ transition) and a rotation of the *S* spin operator about z at the *S* spin transition frequency (i.e., frequency of the $m_S \leftrightarrow m_S - 1$ transition), this operator is transformed to $\hat{I}_- \exp(+i \int_o^t \omega_{m_I}(t')dt') \hat{S}_+ \exp(-i \int_o^t \omega_{m_S}(t')dt') = \hat{I}_- \hat{S}_+ \exp(+i \int_o^t \omega_{m_I}(t') - \omega_{m_S}(t')dt')$ after time t where $\omega_{m_I}(t')$ is the *I* spin transition frequency. Hence, matrix elements of this operator are modified by the factor $\exp(+i \int_o^t \omega_{m_I}(t') - \omega_{m_S}(t')dt')$.

$$\exp\left(i\int_0^t \Delta\omega_Q^{(1)}(\alpha,\beta,\gamma;t')dt'\right) = \sum_{k=-\infty}^{+\infty} A^{(k)}_{m_Im_S}(\alpha,\beta,\gamma)\exp(ik\omega_R t) \qquad [5.11]$$

The term arising from the second-order quadrupole contribution is best expressed as

$$\exp\left(i\int_0^t \Delta\omega_Q^{(2)}(\alpha,\beta,\gamma;t')dt'\right) = \exp\{i\Delta\omega^{(2)}_{Q,m_Im_S}(\alpha,\beta,\gamma)t\} \sum_{q=-\infty}^{+\infty} B^{(q)}_{m_Im_S}(\alpha,\beta,\gamma)\exp(iq\omega_R t) \qquad [5.12]$$

where $\Delta\omega^{(2)}_{Q,m_Im_S}(\alpha, \beta, \gamma)$ expresses the rotational average under MAS of the second-order quadrupolar frequency shift of the $(m_Im_S) \leftrightarrow (m_I + 1, m_S - 1)$ transition. It is easily seen from Eqs. [1.12] and [2.2] in sections 1.2 and 2.1, respectively, that this rotational average is nonzero (there is an isotropic component, Eq. [1.12]); the fourth-rank terms of Eq. [1.12] expresses the molecular orientation dependence of the second-order quadrupolar contribution to the transition frequency that do not average to zero under MAS, but to some finite value that depends on the Euler angles describing molecular orientation (α, β, γ), as described in section 2.1.

We are now in a position to determine the matrix element arising from the first-order average Hamiltonian formed from the transformed dipolar Hamiltonian of Eq. [5.10]. The matrix element we require is $\bar{H}_{IS}(m_I, m_S)$, which from the definition of the first-order average Hamiltonian (see, e.g., section 5.1.2 or reference (*6*) for a discussion of average Hamiltonians) is simply

$$\bar{H}_{IS}(m_I, m_S) = \frac{1}{\tau_R}\int_0^{\tau_R} \tilde{H}_{IS}(m_I, m_S; t)dt \qquad [5.13]$$

Substituting from Eq. [5.6] for $\tilde{H}_{IS}(m_I, m_S; t)$, and using the Fourier expansions of the first- and second-order quadrupolar coupling contributions to the $(m_Im_S) \leftrightarrow (m_I + 1, m_S - 1)$ transition frequency from Eqs. [5.11] and [5.12], we have the required matrix element:

$$\bar{H}_{IS}(m_I, m_S) = \frac{1}{\tau_R} c_{m_Im_S} \sum_{m=-2}^{+2} \omega_D^{(m)} \sum_{k=-\infty}^{+\infty} \sum_{q=-\infty}^{+\infty} A^{(k)}_{m_Im_S}(\alpha,\beta,\gamma) B^{(k)}_{m_Im_S}(\alpha,\beta,\gamma) \int_0^{\tau_R} \exp\{i[(m+k+q)\omega_R + \Delta\omega_{iso} + \Delta\omega^{(2)}_{Q,m_Im_S}(\alpha,\beta,\gamma)]t\}dt \qquad [5.14]$$

The integral in Eq. [5.14] is zero unless the argument of the exponential function is zero. In other words, the net dipolar coupling contribution over one rotor period to the $(m_Im_S) \leftrightarrow (m_I + 1, m_S - 1)$ transition, represented by Eq. [5.4], is nil unless this condition is satisfied. This is the source of the rotational resonance effect, for when the condition, the rotational resonance condition, is satisfied, the matrix element of Eq. [5.14] is nonzero and equal to

$$\bar{H}_{IS}(m_I, m_S) = c_{m_Im_S} \sum_{m=-2}^{+2} \omega_D^{(m)} \sum_{k=-\infty}^{+\infty} \sum_{q=-\infty}^{+\infty} A^{(k)}_{m_Im_S}(\alpha,\beta,\gamma) B^{(k)}_{m_Im_S}(\alpha,\beta,\gamma) \qquad [5.15]$$

This nonzero matrix element (Eq. [5.15]) represents the transition moment for the $(m_Im_S) \leftrightarrow (m_I + 1, m_S - 1)$ transition (i.e., the rate of spin polarization transfer between spins *I* and *S*). As can be seen from Eq. [5.15], this rate depends not only on the dipolar coupling through $\omega_D^{(m)}$ (as for the spin-1/2 case) but also on the first- and second-order quadrupolar coupling through $A^{(k)}_{m_Im_S}(\alpha, \beta, \gamma)$ and $B^{(k)}_{m_Im_S}(\alpha, \beta, \gamma)$ respectively.

It is partly for this reason that the rotational resonance effect has not been used to determine quantitative internuclear distances for half-integer quadrupolar spin pairs; the dependence on the quadrupole coupling is too great and masks the comparatively small dipolar effect. Nevertheless, as outlined previously, the rotational resonance effect can be used to perform spatial correlation experiments.

We can identify two regimes in which we can define the rotational resonance condition:

(i) *$C_Q \ll \omega_R$ for one or both spins.* When the spinning rate is much greater than the quadrupole coupling constant, the only Fourier component of the first-order quadrupole coupling component of the $(m_Im_S) \leftrightarrow (m_I + 1, m_S - 1)$ transition frequency that has a significant nonzero amplitude is the $k = 0$ component (and likewise for the second-order quadrupole coupling, $q = 0$ is the only significant component, but the second-order quadrupole coupling will in any case be small in this regime), i.e., only the centerband of any transitions with a first-order quadrupole coupling component appears in the spectrum. Thus for $\bar{H}_{IS}(m_I, m_S)$ to be nonzero, we have (neglecting the second-order quadrupole coupling contribution in this regime) as the rotational resonance condition

$$m\omega_R + \Delta\omega_{iso} = 0 \qquad [5.16]$$

or

$$m\omega_R = \Delta\omega_{iso} \quad \text{where } m = \pm 1, \pm 2 \text{ only} \qquad [5.17]$$

as for the spin-1/2 case.

(ii) $C_Q \gg \omega_R$ *for one or both spins*. When the quadrupole coupling constant is much larger than the spinning rate, there will be significant components of the first-order quadrupole coupling contribution to the $(m_I m_S) \leftrightarrow (m_I + 1, m_S - 1)$ transition frequency for many values of $k > 0$; that is, many sidebands appear in the spectrum because of the first-order quadrupole coupling component of the transition frequency. Even for those transitions for which there is no first-order quadrupole coupling contribution, such as central transitions $(-1/2, +1/2) \leftrightarrow (+1/2, -1/2)$, if the quadrupole coupling is large compared with the spinning rate, then the second-order quadrupolar contribution to this transition frequency will have significant Fourier components with $q > 0$. The condition for $\bar{H}_{IS}(m_I, m_S)$ to be nonzero now; that is, the appropriate rotational resonance condition is

$$(m + k + q)\omega_R + \Delta\omega_{iso} + \Delta\omega^{(2)}_{Q,m_I m_S}(\alpha, \beta, \gamma) = 0$$
$$\text{where } m = \pm 1, \pm 2 \quad \text{and}$$
$$k, q = 0, \pm 1, \pm 2, \pm 3, \cdots$$

or

$$n\omega_R = \Delta\omega_{iso} + \Delta\omega^{(2)}_{Q,m_I m_S}(\alpha, \beta, \gamma) \quad \text{where}$$
$$n = 0, \pm 1, \pm 2, \pm 3, \cdots \qquad [5.18]$$

There are several points to notice here. First, there are many rotational resonance conditions, most notably one for $n = 0$, which has no spinning rate dependence. Second, each rotational resonance condition depends on the isotropic chemical shift difference between I and S as expected from the spin-1/2 case and also on the rotational average of the second-order quadrupole contribution to the transition frequency, which is dependent on molecular orientation and hence varies over a powder sample.

This highlights the other reason that rotational resonance is not used to make quantitative internuclear distance measurements; for a constant spinning rate, the rotational resonance condition is only met by a fraction of the crystallites. The width of the rotational resonance condition is determined by the dipolar coupling, as for spin-1/2 nuclei, but in general, this will be insufficient to cover the entire frequency range of the $(m_I m_S) \leftrightarrow (m_I + 1, m_S - 1)$ transition, especially when the quadrupole coupling constant for one or more of the spins is large (compared with the dipolar coupling).

For spinning rates and quadrupole coupling constants between these limiting cases, the rotational resonance conditions will be as for the $C_Q \gg \omega_R$ case but with progressively weaker spin polarization transfer rates for the $C_Q \gg \omega_R$ rotational resonance conditions, as the $k, q > 0$ Fourier components of the quadrupole coupling contributions to the $(m_I m_S) \leftrightarrow (m_I + 1, m_S - 1)$ transition frequency decrease in amplitude.

Nijman and colleagues (*141*) have performed an elegant and detailed analysis of the rotational resonance phenomenon for half-integer quadrupolar nuclei using a Floquet formalism. Using this analysis, they have shown that the most significant transitions involved in the rotational resonance process are as follows:

For

$C_Q \gg \omega_R$, $(\mp 1/2, \pm 1/2) \leftrightarrow (\pm 1/2, \mp 1/2)$
$C_Q \ll \omega_R$, all transitions contribute
$C_{Q,I} \gg \omega_R$ and
$C_{Q,S} \ll \omega_R$, $(\mp 1/2, \pm 1/2) \leftrightarrow (\pm 1/2, \mp 1/2)$ dominates but $(m_I, -1/2) \leftrightarrow (m_I - 1, +1/2)$ also contributes.

Experimental Implementation of Correlation Experiments Using the Rotational Resonance Effect. Nijman and colleagues (*141*) provided a nice demonstration of a 2D correlation experiment using the ^{27}Al ($I = 5/2$) resonances of yttrium aluminium garnet (YAG) with the pulse sequence shown in Fig. 5.1 and a swept spinning frequency during the mixing time in which the rotational resonance condition was required. Sweeping the spinning rate ensures that most, if not all, crystallites in the powder sample come into a rotational resonance condition at some time during the mixing period. Their results from experiments using a mixing time of 1.15 s while sweeping the spinning rate from 4.5 kHz to 8 kHz in a linear fashion showed projections in the two dimensions of the two-dimensional spectrum (Fig. 5.2), which agreed well with the expected second-order

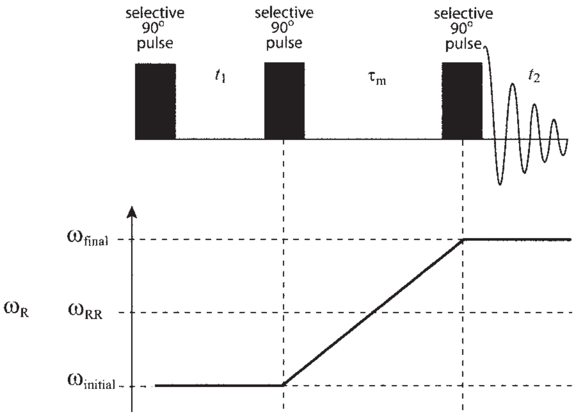

Figure 5.1 Pulse sequence used to generate two-dimensional homonuclear correlation spectra for half-integer quadrupolar nuclei via a mixing period that employs rotational resonance conditions (*141*). The sample spinning frequency is swept during the mixing time, τ_m, where the rotational resonance condition is required, ensuring that most, if not all, crystallites in the powder sample come into a rotational resonance condition at some time during this period.

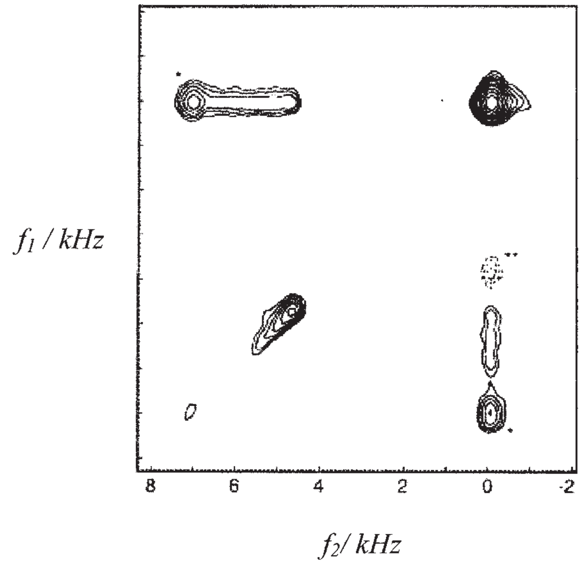

Figure 5.2 Two-dimensional ^{27}Al homonuclear correlation spectrum of yttrium aluminum garnet (YAG) using the rotational resonance pulse sequence shown in Fig. 5.1 (*141*).

quadrupole powder patterns arising from the central transitions of the two ^{27}Al sites in YAG ($C_{Q,I} \sim 600$ kHz and $C_{Q,S} \sim 6$ MHz). The cross-peak in the two-dimensional spectrum shows that these two ^{27}Al sites are close in space, with a dipolar coupling between them sufficiently large enough to allow significant magnetization transfer between the spins during the particular rotational resonance mixing time used in the experiment.

Other Effects Arising from Rotational Resonance. Kwak and colleagues (*142*) have observed an interesting effect in simple one-dimensional spin echo spectra that may be ascribed to the effects of rotational resonance. They point out that for $C_Q \gg \omega_R$ for one or both nuclei, the rotational resonance conditions are $n = 0, \pm 1, \pm 2, \pm 3, \ldots$ as described above. They also show that these rotational resonance conditions are extremely sensitive to missetting of the magic angle (in a way similar to that experienced by STMAS experiments described in section 2.3). If the sample is rotated away from the magic angle, then the first-order quadrupole coupling contribution to the $(m_I m_S) \leftrightarrow (m_I + 1, m_S - 1)$ transition frequency does not average to zero, as assumed in the previous analysis (Eq. [5.11]). Rather, it averages to some finite value $\Delta\omega^{(1)}_{Q,m_I} m_S(\alpha, \beta, \gamma) P_2(\cos\theta_R)$, where θ_R is the sample spinning angle. Working through the previous theoretical analysis with this addition to Eq. [5.11] for the decomposition of the first-order quadrupole coupling contribution to the $(m_I m_S) \leftrightarrow (m_I + 1, m_S - 1)$ transition frequency, we obtain a new rotational resonance condition for the sample spinning at a general angle θ_R:

$$n\omega_R = \Delta\omega_{iso} + \Delta\omega^{(1)}_{Q,m_I m_S}(\alpha, \beta, \gamma) P_2(\cos\theta_R) + \Delta\omega^{(2)}_{Q,m_I m_S}(\alpha, \beta, \gamma, \theta_R) \quad [5.19]$$

The second-order quadrupole coupling contribution to the $(m_I m_S) \leftrightarrow (m_I + 1, m_S - 1)$ transition frequency in the above equation will also be modified according to the orientation of the sample rotation axis, as indicated by the inclusion of the θ_R in the parameter list for $\Delta\omega^{(2)}_{Q,m_I m_S}(\alpha, \beta, \gamma)$. The point, however, is that the first-order quadrupole coupling is so large that even for a small mismatch of the magic angle, the term $\Delta\omega^{(1)}_{Q,m_I m_S}(\alpha, \beta, \gamma) P_2(\cos\theta_R)$ can be large and make a significant change to the rotational resonance condition, even for the $(\mp 1/2, \pm 1/2) \leftrightarrow (\pm 1/2, \mp 1/2)$ transition, which of course has no first-order contribution.

Furthermore, rotational resonance involving inner satellite transitions may affect the $(\mp 1/2, \pm 1/2) \leftrightarrow (\pm 1/2, \mp 1/2)$ transition, as it perturbs the populations of levels involved in the central transitions. From the analysis of Kwak and colleagues (*142*), it is clear that rotational resonance effects can manifest themselves in many experiments, including MQMAS, often without the experimenter's intention!

5.1.2 Double-Quantum (DQ) Methods for Correlation Spectroscopy. For spin-1/2 nuclei, double-quantum (DQ) spectroscopy, where a homonuclear double-quantum coherence is excited between a pair of dipolar-coupled nuclei (Fig. 5.3(a)), is a popular method of demonstrating spatial proximity of the two nuclei. Such coherence can only be excited with any significant amplitude if the dipolar coupling between the spins is significant (i.e., they are close in space). The experiments are generally conducted under MAS with the dipolar coupling between the spins being recoupled by various rf pulse sequences and other methods (*6*), including, of course, the rotational resonance discussed in the previous section. The same principle can be applied to quadrupolar nuclei, with the double quantum coherence in this case being that between the central transitions of dipolar-coupled spins (see Fig. 5.3(b)). The question remains, however, how to recouple the dipolar coupling under the MAS, which is needed for spectral resolution. The pulse sequences applied to spin-1/2 nuclei will not work for a multitude of reasons, the most important being that the quadrupole coupling is generally strong compared with any rf field amplitude. Thus, the spin system will evolve under the quadrupole coupling as we attempt to perturb it by the rf pulse sequence and, moreover, will evolve faster due to the quadrupole coupling than our pulse sequence. The result is not so much recoupling as a rather large mess, with coherence appearing in every part of the density matrix.Fortunately, there are methods, akin to some used for spin-1/2 nuclei, that are appropriate. The most commonly used takes advantage of a rotary resonance condition and is described below.

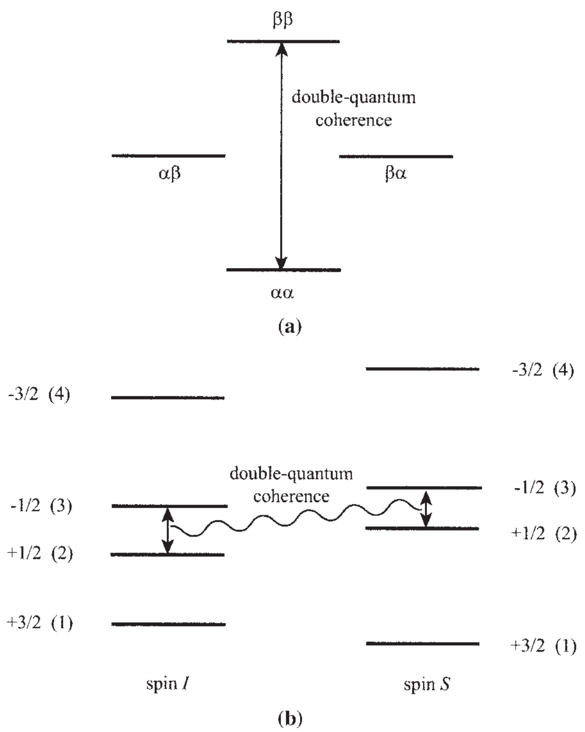

Figure 5.3 Schematic energy level diagrams showing (a) the formation of DQ coherence from a dipolar-coupled pair of spin-1/2 nuclei and (b) the formation of the equivalent DQ coherence for a pair of spin-3/2 nuclei. Here, the DQ coherence involves the two central transitions (2–3) of the nuclei.

Theory of Double-Quantum Excitation between Dipolar-Coupled Half-Integer Quadrupolar Spins

The double-quantum excitation takes place under spin-lock conditions (*143*, *144*), that is

(i) $0.1 < (\omega_1/\omega_R) < 0.3$

where ω_1 is the amplitude of the rf irradiation applied to the homonuclear spin system and

(ii) $\omega_1 >$ the anisotropic chemical shift and quadrupole terms affecting the central-transition frequency of either spin.

Under these conditions, we can reasonably assume that the rf field only affects the central transition of the quadrupolar spins (providing it is applied close to resonance) for both spins. We shall assume for this analysis that we are dealing with a homonuclear spin-3/2 pair, with the Zeeman levels of each spin labeled 1, 2, 3, and 4, as in Fig. 5.3(b). Thus the central transition involves coherences between levels 2 and 3 for each spin. For simplicity of notation, we consider only those terms in the Hamiltonian affecting the spin system that pertain to the 2–3 subspace of the complete Zeeman basis. Moreover, when we consider the dipolar coupling terms, we shall restrict ourselves to consideration of those terms that couple the 2–3 subspace of each spin. This is not to say that the other terms of either the dipolar coupling operator or the complete Hamiltonian for the system are irrelevant. Unfortunately, this is far from the case. As we shall see later, such terms do operate on the system, causing evolution in ways that we do not desire, in addition to the way we shall derive. These unwanted terms serve to reduce the efficiency of the double-quantum excitation and also yield some unwanted double-quantum terms that are difficult to remove. However, we ignore these difficulties for the present and return to them later, once we have discussed the principle of how to excite the double-quantum coherence that we do want.

The Hamiltonian affecting the 2–3 subspace is

$$\hat{H} = \hat{H}_{rf} + \hat{H}_{IS} + \hat{H}_{\Omega} \qquad [5.20]$$

$$\hat{H}_{rf} = 2\omega_1(\hat{I}_x^{2-3} + \hat{S}_x^{2-3})$$

$$\hat{H}_{IS} = 2\omega_D(t)(\hat{I}_z^{2-3}\hat{S}_z^{2-3} - 2\hat{I}_x^{2-3}\hat{S}_x^{2-3} - 2\hat{I}_y^{2-3}\hat{S}_y^{2-3})$$

$$\hat{H}_{\Omega} = (\Omega_{I,CS}^{2-3} + \Omega_{I,Q}^{2-3}(\alpha,\ \beta))\hat{I}_z^{2-3} + (\Omega_{S,CS}^{2-3} + \Omega_{S,Q}^{2-3}(\alpha,\ \beta))\hat{S}_z^{2-3} \qquad [5.21]$$

Under the conditions of spin-locking defined above, this is a reasonable approximation for the total Hamiltonian for the system; its flaw is that there are other quadrupole terms that under MAS conditions are still relevant.

The $\hat{\Lambda}_{\alpha}^{2-3}$ operators ($\Lambda = I,\ S$) are fictitious spin-1/2 operators, which are essentially akin to the usual Cartesian spin operators I_{α} and S_{α}, but which act (in this case) only within the 2–3 subspace (*86*). The terms $(\Omega_{I,CS}^{2-3} + \Omega_{I,Q}^{2-3}(\alpha,\ \beta))$ and $(\Omega_{S,CS}^{2-3} + \Omega_{S,Q}^{2-3}(\alpha,\ \beta))$ represent the net chemical shift and quadrupole terms affecting the central-transition frequency, referred to above in the definition of the spin-lock conditions. The $\Omega_{I,CS}^{2-3}$ is the isotropic chemical shift for spin *I* and similarly for spin *S* (any chemical shiftanisotropy is assumed to be averaged to zero by magic-angle spinning). The $\Omega_{I,Q}^{2-3}(\alpha,\ \beta)$ term represents the residual (under MAS) second-order quadrupolar coupling affecting the central 2–3 transition for spin *I* and similarly for spin *S*. This coupling is of course molecular orientation dependent, as identified here by the dependence of the term on the Euler angles α, β.

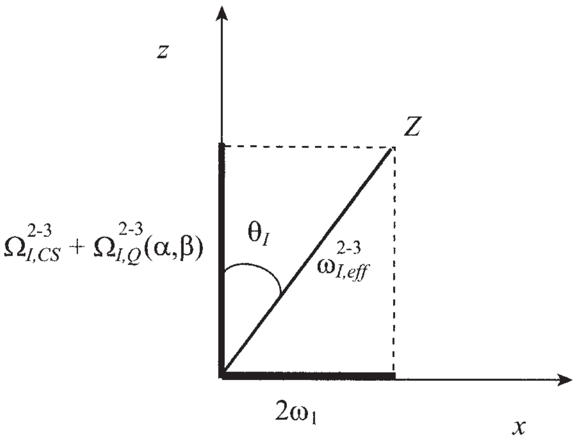

Figure 5.4 Representation of the fields acting on the 2–3 subspace of the *I* spin in the dipolar-coupled *IS* spin pair of spin-3/2 nuclei referred to in text. There is a "field" along *z* due to the combined effects of isotropic chemical shift and second-order quadrupole coupling acting on the *I* spin central transition (2–3) and a field along *x* due to the rf. The net effective field, the vectorial sum of these along *x* and *z*, is also shown.

If we ignore, for the moment, the dipolar coupling (represented by $\hat{H}_{IS}$, and time dependent due to MAS), then we see that within the 2–3 subspace, we have a term of magnitude $2\omega_1$ acting on spin *I* along *x* due to the rf field and also acting on spin *I*, a term of magnitude $(\Omega_{I,CS}^{2-3} + \Omega_{I,Q}^{2-3}(\alpha,\ \beta))$ along *z*. The equivalent *S* spin terms are present also. The situation is summarized in Fig. 5.4. Thus, the net term acting on spin *I* is the vectorial sum of the *x* and *z* fields, shown in Fig. 5.4 as the effective interaction term with amplitude $\omega_{I,eff}^{2-3}$ and direction labeled *Z*, and similarly for spin *S*.

To assess the effect of the Hamiltonian of Eq. [5.20] on the *IS* spin system, it is useful to form an average Hamiltonian. The average Hamiltonian at a point in time *tp* is defined as

$$\bar{H}(t_p) = \bar{H}^{(0)} + \bar{H}^{(1)} + \bar{H}^{(2)} + \cdots \qquad [5.22]$$

where

$$\bar{H}^{(0)} = \frac{1}{t_p}\{\hat{H}_1 t_1 + \hat{H}_2 t_2 + \cdots + \hat{H}_n t_n\}$$

$$\bar{H}^{(1)} = -\frac{i}{2t_p}\{[\hat{H}_2 t_2, \hat{H}_1 t_1] + [\hat{H}_3 t_3, \hat{H}_1 t_1] + [\hat{H}_2 t_2, \hat{H}_3 t_3] + \cdots\}$$

$$\bar{H}^{(2)} = -\frac{1}{6t_p}\left\{[\hat{H}_3 t_3, [\hat{H}_2 t_2, \hat{H}_1 t_1]] + [[\hat{H}_3 t_3, \hat{H}_2 t_2], \hat{H}_1 t_1] + \frac{1}{2}[\hat{H}_2 t_2, [\hat{H}_2 t_2, \hat{H}_1 t_1]] + \frac{1}{2}[[\hat{H}_2 t_2, \hat{H}_1 t_1], \hat{H}_1 t_1] + \cdots\right\} \qquad [5.23]$$

and so on, where the Hamiltonians $\hat{H}_1, \hat{H}_2, \ldots, \hat{H}_n$ operate piecewise for periods $t_1, t_2, \ldots, t_n$ respectively, such that $t_1 + t_2 + \ldots + t_n = t_p$. If the full summation series, Eq. [5.22], for the average Hamiltonian is used, this gives the same effect on the spin system at the point t_p as the full Hamiltonian. The use of the average Hamiltonian approach, however, is to avoid having to use the complete summation series, and to approximate the series with, preferably, just the first term in Eqs. [5.22] and [5.23]. Obviously, this is only a good approximation if the Hamiltonians acting during t_p largely commute with one another (the higher-order terms of Eq. [5.23] all involve commutators between the Hamiltonians acting at different time periods). This can often be arranged by transforming the frame of reference in which the Hamiltonian is defined. In particular, we transform to a rotating frame of reference that mimics the evolution of the density operator for the spin system has under the (noncommuting) terms of the Hamiltonian, such that in the new frame there is no evolution due to these terms; that is, these terms of the Hamiltonian are transformed away (zeroed) in the new frame of reference.

In the case of the Hamiltonian of Eqs. [5.21] and [5.22], the I_x^{2-3} and I_z^{2-3} terms do not commute, and likewise for the corresponding terms for spin S. We can remove the effects of both these terms for spins I and S by transforming to a new frame of reference that for spin I rotates at a rate $\omega_{I,eff}^{2-3} = \sqrt{(\Omega_{I,CS}^{2-3} + \Omega_{I,Q}^{2-3}(\alpha, \beta))^2 + (2\omega_1)^2}$, that is, the effective interaction strength acting on the 2–3 subspace of spin I, as defined in Fig. 5.4, and rotates about the effective interaction axis (Z), as defined in Fig. 5.4 also. This rotation is that which the $\hat{H}_{rf}$ and $\hat{H}_\Omega$ terms of the Hamiltonian in Eq. [5.21] would effect on the I spin part of the density operator describing the spin system. The effects of the equivalent S spin terms are removed by an analogous rotation involving the S spin operators. Thus, in our new frames of reference for the I and S spin operators, the effects of the $\hat{H}_{rf}$ and $\hat{H}_\Omega$ terms are removed, and we only have to consider the frame-transformed dipolar coupling term $\hat{H}_{IS}$ in the formation of our required average Hamiltonian.

To recap, the dipolar coupling term in the original frame of reference (the usual rotating frame of reference in which all NMR experiments are conducted) is

$$\hat{H}_{IS} = 2\omega_D(t)(\hat{I}_z^{2-3}\hat{S}_z^{2-3} - 2\hat{I}_x^{2-3}\hat{S}_x^{2-3} - 2\hat{I}_y^{2-3}\hat{S}_y^{2-3}) \qquad [5.24]$$

where $\omega_D\,(t)$ is given by a Fourier expansion (*6*):

$$\omega_D(t) = \sum_{m=-2}^{+2} \exp(im\omega_R t)\omega_D^{(m)} \qquad [5.25]$$

and the $\omega_D^{(m)}$ are constants derived from the dipolar coupling constant for the *IS* spin system. Their exact form is not important in this analysis, and as they are given elsewhere (*6*), we do not muddy the waters any further by deriving them again here. We now need to transform the dipolar operator of Eq. [5.24] into the new rotating tilted frame defined above for spins I and S and in Fig. 5.4. Rotation about the Z axis at rate $\omega_{I,eff}^{2-3}$ for spin I operators (($\omega_{I,eff}^{2-3}$ is defined above) and $\omega_{S,eff}^{2-3}$ for spin S operators introduces an extra time dependence for the dipolar coupling operator of $\exp(i\omega_{I,eff}^{2-3}t)\ \exp(i\omega_{S,eff}^{2-3}t)$. (*6*, *143*). The frame transformation (which we do not need to perform in detail here) yields a number of terms, amongst them a double-quantum term (*143*):

$$\hat{H}_{DQ}(t) = \exp(i\omega_{I,eff}^{2-3}t)\exp(i\omega_{S,eff}^{2-3}t)\omega_D(t)F(\theta_I, \theta_S) \times (\hat{I}_+^{2-3}\hat{S}_+^{2-3} + \hat{I}_-^{2-3}\hat{S}_-^{2-3}) \qquad [5.26]$$

where

$$F(\theta_I, \theta_S) = 1 - 2\cos\theta_I\cos\theta_S + 2\sin\theta_I\sin\theta_S \qquad [5.27]$$

and the raising and lowering operators are defined in the usual way:

$$\hat{\Lambda}_\pm^{2-3} = \hat{\Lambda}_x^{2-3} \pm i\hat{\Lambda}_y^{2-3} \qquad [5.28]$$

When we form the first-order average double-quantum Hamiltonian pertaining to the system using Eq. [5.23], i.e.,

$$\bar{H}^{(0)} = \frac{1}{t_p}\{\hat{H}_1 t_1 + \hat{H}_2 t_2 + \cdots + \hat{H}_n t_n\} = \frac{1}{\tau_R}\int_0^{\tau_R} \hat{H}_{DQ}(t)dt \qquad [5.29]$$

In this case, it is the time dependence of the double-quantum term which matters, as in general, it causes the integral of Eq. [5.29] to be zero, and thus no double-quantum term survives. The double-quantum term only survives averaging over a rotor period, that is survives being averaged to zero by the MAS, if the time dependence of some part of the $\hat{H}_{DQ}(t)$ double-quantum operator is zero.

Expanding the $\omega_D(t)$ term of Eq. [5.26], we see the full-time dependence of the double-quantum operator becomes:

$$\hat{H}_{DQ}(t)$$

$$= \sum_{m=-2}^{+2} \exp(i\omega_{I,eff}^{2-3}t)\exp(i\omega_{S,eff}^{2-3}t)\exp(im\omega_R t)\omega_{IS}^{m}F(\theta_I, \theta_S$$

$$\cdot (\hat{I}_+^{2-3}\hat{S}_+^{2-3} + \hat{I}_-^{2-3}\hat{S}_-^{2-3}) \qquad [5.30]$$

Clearly, the time dependence of Eq. [5.30] vanishes when

$$\omega_{I,eff}^{2-3} + \omega_{S,eff}^{2-3} = m\omega_R \qquad [5.31]$$

This is a rotary resonance condition; under this condition, the double-quantum operator arising from the dipolar coupling between spins I and S is not averaged to zero by MAS.

To summarize, we can excite double-quantum coherences between the central transitions of two dipolar-coupled half-integer quadrupolar spins if we (i) have an rf irradiation such that the spin-lock conditions defined previously apply and (ii) ensure that the sum of the effective nutation frequencies for the central transitions of the two dipolar-coupled spins is equal to ω_R or $2\omega_R$.

Experimental Implementation of Double-Quantum Correlation Experiments. The knowledge derived above on how to excite double-quantum coherence under MAS conditions is used in the double-quantum–single-quantum (DQ–SQ) correlation experiment shown in Fig. 5.5. It has also been used to derive single-quantum–single-quantum (SQ–SQ) correlation spectra, via a double-quantum mixing period (*144*).

There are potential problems with such experiments:

(i) It is impossible to satisfy the rotary resonance condition of Eq. [5.31] for all crystallites in the sample, as the condition necessarily depends on crystallite orientation within the sample rotor as defined by the Euler angles α, β. This restriction can be somewhat alleviated by the use of rf amplitude modulation (so that ω_1 varies throughout the excitation). Tangential amplitude modulation shapes have been found effective (*143*).

(ii) It may be impossible to satisfy the spin-lock conditions defined above, while irradiating both spins close to resonance *and* ensuring that ω_1 is greater than the isotropic chemical shift and second-order quadrupolar coupling effects acting on the central transition of both spins (so that the complete central-transition powder pattern of each spin is uniformly irradiated).

If either or both of these situations arise, they result in additional terms in the average Hamiltonian, some of which may be large. One particularly problematic term is another double-quantum term, but one that arises solely from the quadrupole coupling and connects Zeeman levels on the same spin, which differ by 2 in their magnetic quantum number (i.e., creates double-quantum coherence on a single spin). This term increases with the magnitude of ω_1, and as it depends on the first-order quadrupole coupling, which is generally of MHz in size, this may be a large term, and for even moderate rf field strengths may dominate over the required double-quantum term connecting the central transitions of dipolar-coupled spins.

The effect of this term in a single-quantum/single-quantum correlation spectrum is to produce diagonal autocorrelation peaks, regardless of the spatial correlation of spins, and in a double-quantum/single-quantum correlation spectrum to produce vast numbers of spinning sidebands in the f_1 dimension of the two-dimensional spectrum, corresponding to the various double-quantum transitions possible on a single spin in the system (i.e., $+3/2 \rightarrow -1/2$ and $+1/2 \rightarrow -3/2$ for a spin-3/2). Though these sidebands are not in themselves a problem, they may obscure genuine correlation peaks in the spectrum, and in adverse circumstances, may have a net intensity that is considerably greater than that of the desired correlation peaks.

There is no obvious way to avoid this situation; one is caught between the proverbial rock and hard place, requiring large rf amplitude to ensure that ω_1 is larger than the chemical shift and second-order quadrupole terms associated with the central transitions of both spins, and also to ensure both spins are irradiated as close as possible to on-resonance, while at the same time requiring ω_1 to be as small as possible to ensure that $0.1 < (\omega_1/\omega_R) < 0.3$.

Another method, based on the same rotary resonance principle, has been proposed for the excitation of the requisite double-quantum coherence (*145*, *146*). The method includes a way of discriminating between the desired two-spin double-quantum coherence and the unwanted single-spin double-quantum coherence, namely by applying a 180° pulse after the excitation of the double-quantum coherence, which is selective for the central transition for both spins. Such a pulse has almost no effect on the single-spin double-quantum coherence but inverts the sign of the two-spin double-quantum coherence. Thus the two components may be separated by phase cycling. The fact remains, however, that if such techniques are needed,

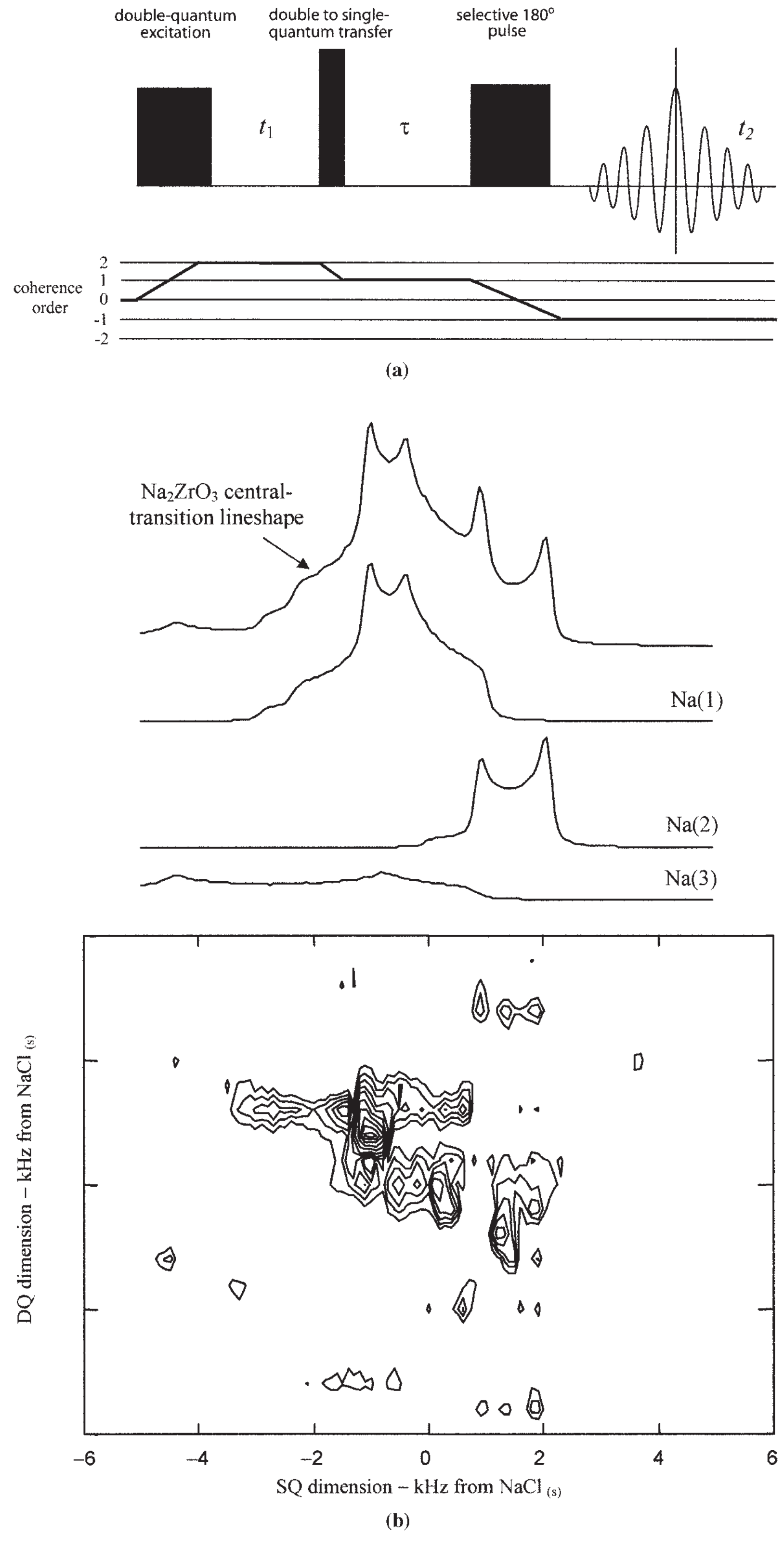

Figure 5.5 (a) Pulse sequence and coherence transfer pathway diagram for a phase-modulated double-quantum experiment to correlate half-integer quadrupolar nuclei (*144*). The double-quantum excitation pulse is a low-amplitude rf pulse, such that a rotary resonance condition is satisfied. See text for details. (b) A two-dimensional DQ–SQ ^{23}Na correlation spectrum for Na_2ZrO_3 obtained using the pulse sequence in (a) for a sample spinning at 10 kHz (*144*).

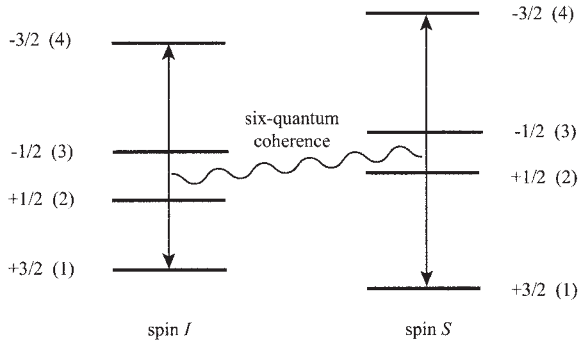

Figure 5.6 The formation of 6Q coherence for a pair of spin-3/2 nuclei. The coherence involves the correlation of the triple-quantum coherences for each spin.

it necessarily means that the excitation efficiency of the desired coherence is compromised, as the excitation sequence is producing undesired coherences with a greater amplitude than the desired ones (*144*).

5.1.3 4I-Quantum Methods for Correlation Spectroscopy. Exciting a 4*I*-quantum coherence represents an alternative to exciting double-quantum coherence for a spin-*I* pair. Such a coherence can only arise via the agency of dipolar coupling (or *J* coupling) between the two spins (Fig. 5.6), unlike the case of double-quantum coherence, which can arise on a single spin for $I > ½$.

Six-quantum (6Q) coherence has been used in a 6Q-SQ correlation experiment to identify which ^{23}Na spins are close in space in sodium zirconate (Na_2ZrO_3) (*147*). The pulse sequence used is shown in Fig. 5.7(a), and the corresponding 6Q-SQ correlation spectrum is shown in Fig. 5.7(b). The drawback of such an experiment, however, is that the excitation efficiency of the 4*I*-quantum coherence is low, and so many transients need to be averaged to obtain spectra suitable for analysis. The 6Q coherence for a spin-3/2 pair, for instance, effectively consists of a triple-quantum transition on both spins, produced coherently via the mutual dipolar coupling between the spins. As we have seen in section 5.1.2, the required dipolar coupling between two quadrupolar spins is not averaged by MAS, providing the irradiating rf amplitude is low and spin-lock conditions are achieved. The excitation of triple-quantum coherence on a quadrupolar spin, in contrast, generally requires as large an rf amplitude as can be achieved by the NMR spectrometer, provided the quadrupolar coupling is large. Thus, there is no happy solution for the production of 6Q coherence.

It is, however, worth noting that the 6Q experiment (*147*) may also be used to determine relative quadrupole tensor orientations. The 6Q lineshapes that arise from the experiment in the f_1 dimension of the 2D spectrum depend strongly on the relative orientation of the quadrupole coupling tensors. Recording the 6Q lineshape as a function of the length of time for which the 6Q coherence is excited allows the relative orientation of the two quadrupole coupling tensors to be determined by simulation of the lineshapes, as shown in Fig. 5.8.

Finally, the concept of the 6Q experiment has been neatly combined with a double-quantum experiment by Mali and Kaucic (*148*) to give a high-resolution, two-dimensional correlation spectrum with impressive sensitivity. The form of the experiment is shown in Fig. 5.9(a) for spin $I = 3/2$ nuclei. In essence, the t_1 period of the experiment consists of a double-quantum MQMAS experiment: double-quantum coherences in the first 7/16 t_1 part are transferred into 6Q coherences for the remaining 9/16 t_1, with the result that for the coherence remaining at the end of t_1, all evolution due to the fourth-rank terms of the second-order quadrupole coupling is refocused and all evolution due to second-rank terms is refocused by the magic-angle spinning (with the proviso that the MAS rate is large enough; if it is not, spinning sidebands remain in the corresponding f_1 dimension of the resulting 2D spectrum). Thus the coherence at the end of t_1 has only net evolution due to isotopic chemical shift and isotropic second-order quadrupolar terms, and only coherence arising from dipolar-coupled spin pairs is present (as this is the only way that 6Q coherence in the last part of t_1 can be formed). Hence, the f_1 dimension of the spectrum has a projection that is a high-resolution 2Q/6Q correlated spectrum. The f_2 dimension consists of the central-transition (single-quantum) powder lineshapes for the dipolar-coupled spins, or in the case of the spectrum in Fig. 5.9(b), of a series of sidebands arising from those powder patterns, as in this case, the t_2 FID was recorded using a CPMG pulse sequence (*149*) to improve the signal to noise. The sequence may also optionally use a RAPT sequence prior to the rest of the sequence, to enhance sensitivity (*16*, *150*).

5.1.4 MQMAS-Based Methods for Correlation Spectroscopy. As discussed in section 3, the principal values and the orientation of the quadrupole coupling tensor's principal axis frame contains valuable information about molecular structure. Several useful techniques now exist to measure the relative orientation of homonuclear quadrupole coupling tensors for this purpose, via two-dimensional homonuclear correlation experiments. As ever, the challenge in these experiments is to recouple the dipolar coupling be-

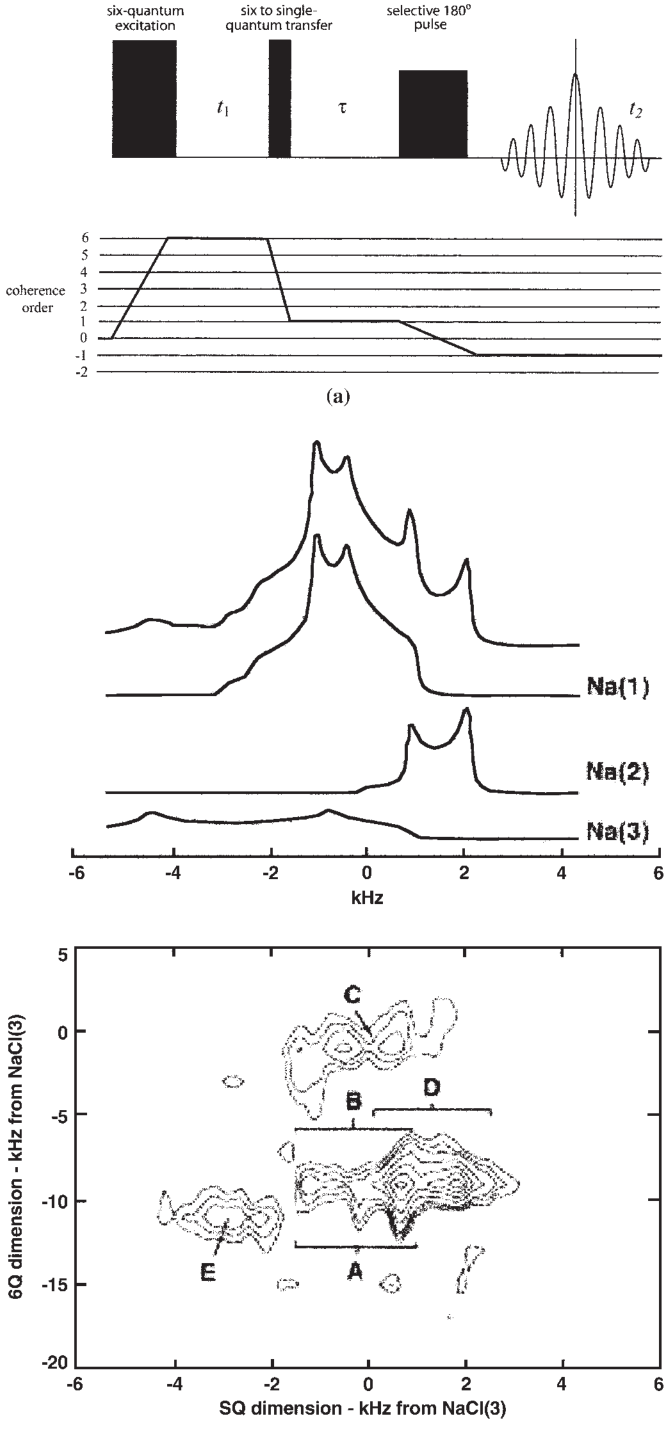

(a)

(b)

Figure 5.7 (a) Pulse sequence and coherence transfer pathway diagram for a six-quantum experiment to correlate half-integer quadrupolar nuclei (*147*). (b) A ^{23}Na 6Q–SQ correlation spectrum for sodium zirconate recorded using the pulse sequence in (a) (*147*). There are three ^{23}Na sites in this material, whose simulated central transition powder lineshapes are shown above the 2D spectrum. The correlations peaks A and E correspond to correlations between Na(1) and Na(3); B and D to correlations between Na(2) and Na(3), and C to autocorrelations between Na(1) spins.

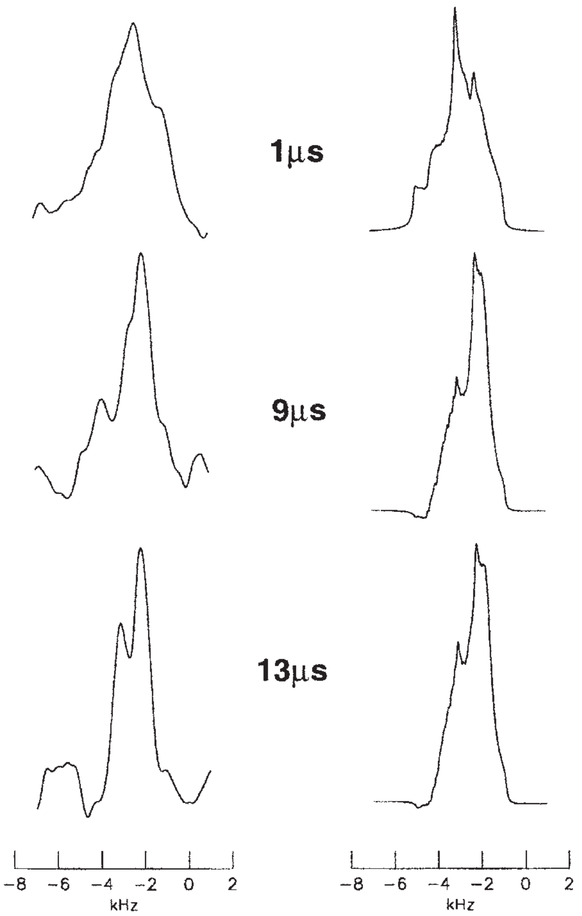

Figure 5.8 (Left) The ^{23}Na 6Q lineshapes arising in the f_1 dimension of a two-dimensional ^{23}Na 6Q–SQ correlation spectrum for Na_2SO_4 obtained using the pulse sequence in Fig. 5.7(a) for different 6Q excitation times, as indicated in the figure. The 6Q lineshape depends on the relative orientation of the quadrupole coupling tensors of the two ^{23}Na spins involved in the 6Q coherence. From the crystal structure of Na_2SO_4, the tensors should be related by the Euler angles (0°, 23.4°, 0°) and the simulations of the 6Q lineshapes, shown on the right, assuming this geometrical relationship.

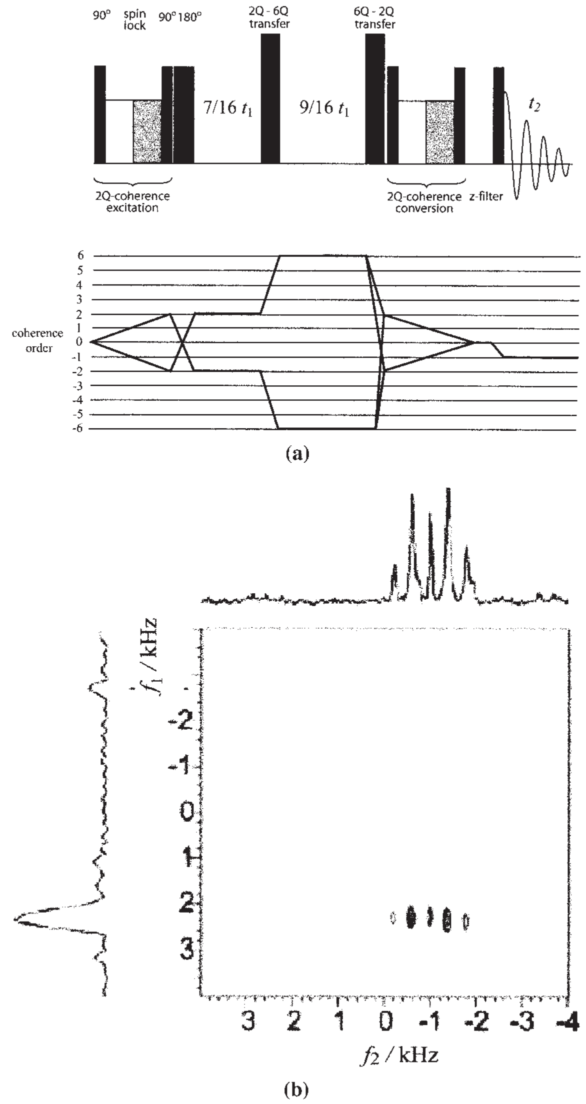

Figure 5.9 Pulse sequence and coherence transfer pathway diagram for a 6Q–2Q correlation experiment which correlates half-integer quadrupolar nuclei and allows a high-resolution spectral dimension and is shown here for $I = 3/2$ (*148*). (b) A ^{23}Na 6Q–2Q spectrum for Na_2SO_4 obtained using the pulse sequence in (a) (*143*). The spectrum is recorded with the aid of CPMG in t_2, and thus the f_2 projection consists of a series of sidebands arising from the ^{23}Na central transition powder pattern, rather than the powder pattern itself.

tween the quadrupolar spins under study. Different approaches are taken in the different experiments, as described below, and some are likely to have more general utility than others. A further advantage of these types of experiment is that in addition to spatial correlation information, they yield quantitative information on the relative orientation of the correlated quadrupole coupling tensors.

All the methods are based on the MQMAS experiment described in section 2.2. A typical experiment is shown in Fig. 5.10(a) (*151*, *152*). The experiment proceeds as per a normal MQMAS experiment, except that between the multiple-quantum evolution in t_1 and the single-quantum detection in t_2, there is a mixing period, τ_m, where the coherence is stored as longitudinal magnetization (associated with populations of the central transition levels of the quadrupolar nuclei under study). In a compound where there are ^{1}H available, exchange of the longitudinal magnetization may take place most efficiently via the agency of spin diffusion through the ^{1}H dipolar-coupled net-

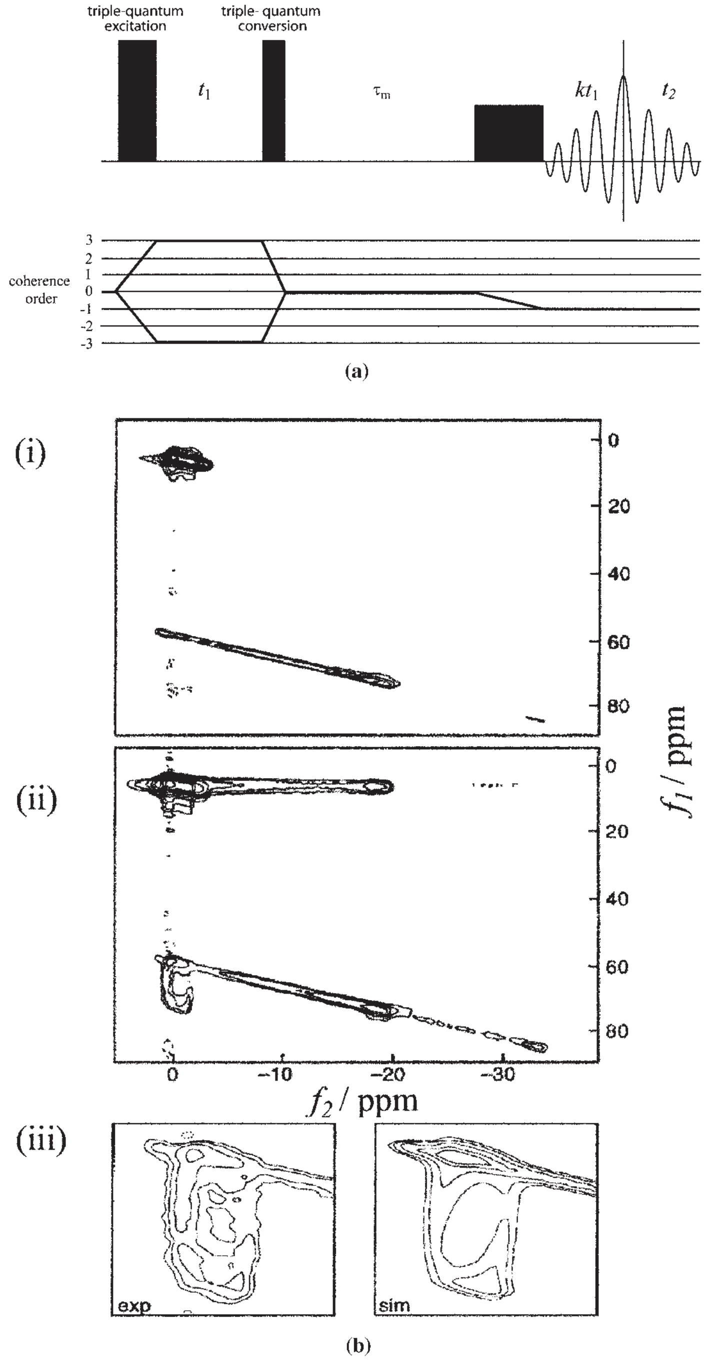

Figure 5.10 (a) Pulse sequence and coherence transfer pathway diagram for an MQMAS-based exchange experiment (*151, 152*). (b) ^{23}Na MAS NMR spectra of $Na_2MoO_4 \cdot 2H_2O$ recorded using the pulse sequence in (a); (i) triple-quantum MAS spectrum showing the two distinct Na sites, (ii) similar spectrum recorded using τ_m of 200 ms showing cross-peaks between the two Na species, (iii) left: expansion of the low-field cross-peak in (ii) and right: corresponding simulation of the cross-peak assuming the relative orientation of the two quadrupole coupling tensors is given by $\alpha = 90°$, $\beta = 24°$, and $\gamma = 15°$ (*151, 152*).

work, if no ^{1}H decoupling is performed. Where ^{1}H spins are present, this is an efficient way of driving the transfer of magnetization between the quadrupolar spins, even under MAS. In the absence of ^{1}H, this magnetisation transfer in the experiment could proceed via the homonuclear dipolar coupling between the two quadrupolar spins. Figure 5.10(b) shows the form of the cross-correlation peaks obtained by this experiment (^{23}Na NMR of $Na_2MoO_4.2H_2O$) along with a simulation that allows the relative orientation of the two ^{23}Na quadrupolar tensors to be determined. Obviously, such an experiment could be performed by exciting single-quantum coherence initially and letting that evolve in t_1 rather than the multiple-quantum coherence used in the experiment of Fig. 5.10. The advantage of using multiple-quantum coherence is one of resolution; the signals in an N-quantum spectrum are separated by N times the chemical shift differences that are present in the single-quantum spectrum (in addition to the quadrupolar isotropic shift, which is also magnified in a multiple-quantum spectrum).

Eden and colleagues (*153*) proposed a similar experiment (using in this particular case direct dipolar coupling between the quadrupolar spins rather than via a ^{1}H network) but extended the approach to three dimensions to obtain an isotropic spectral dimension with the cross-correlation peaks appearing in two-dimensional slices correlated with the isotropic peaks in f_1'. The form of the experiment is shown in Fig. 5.11(a) (*153*). Initial multiple-quantum evolution for a time t_1 is followed by a single-quantum refocusing period kt_1, during which evolution under fourth-rank terms of the second-order quadrupole Hamiltonian is refocused. There then follows a period of evolution, t_2, of central-transition single-quantum coherence under the second-order quadrupole coupling before a mixing period where the magnetization is stored along the axis of the applied field. During the mixing period, there is exchange of magnetization between the quadrupolar spins by virtue of the residual dipolar coupling (arising from a second-order dipole-quadrupole cross-term in the average Hamiltonian) that is not removed under MAS (*154*) and MAS-driven recoupling through modulation of the first-order quadrupole coupling as described in section 5.1.1 in the discussion of rotational resonance (*155*). Finally, the single-quantum spectrum pertaining to the central transition is acquired in t_3. The experiment results in a three-dimensional spectrum with a high-resolution f_1 dimension in which signals are correlated with cross-correlation patterns arising from correlation between the central-transition powder patterns of dipolar-coupled nuclei, as shown in Fig. 5.11(b).

Figure 5.12(a) shows the pulse sequence used in two further MQMAS-based methods for correlating half-integer quadrupolar nuclei that use different methods for recoupling the dipolar coupling between the quadrupolar spins (*156*, *157*). In each case, dipolar recoupling is achieved simply by spinning the sample at some angle other than the magic angle with respect to the applied field so that the dipolar coupling is not averaged to zero as it would be under magic-angle spinning.

In the MQP$_4$MAS experiment, the sample is spun continuously at 70.1° to the applied field (*156*, *157*). Spinning at this angle averages to zero the fourth-rank terms in the second-order quadrupole coupling average Hamiltonian (Eq. [1.5]), while leaving the second-rank ones and the dipolar coupling (and chemical shift anisotropy) to be averaged to some finite, nonzero value. Thus, in the MQP$_4$MAS experiment for dipolar-coupled spin-3/2, initial triple-quantum coherence is excited and this is then transferred at the end of t_1 to zero-quantum longitudinal magnetization for a period τ_m, during which magnetization exchange takes place between spins via the agency of the (nonzero) dipolar coupling between them. Finally, a selective 90° pulse (selective for the central transitions of the spins under study) yields -1-quantum coherence for observation. After a period $k't_1$ of evolution of the -1Q coherence, the evolution (of the triple-quantum coherence) under the second-rank terms of the second-order quadrupole coupling that takes place in the t_1 period of the experiment is refocused.

After appropriate processing of the time domain data, one achieves a high-resolution projection in the effective f_1' dimension exactly as in a conventional MQMAS experiment (see section 2.2), except for the effects of any chemical shift anisotropy (CSA). CSA and dipolar couplings are not averaged to zero by spinning at 70.1°, of course, and so their effects remain in both dimensions of the spectrum, which can cause a problem in resolving signals for some samples.

The f_2 dimension will contain powder patterns corresponding to the central-transition powder pattern due to the second-rank terms of the second-order quadrupole coupling and chemical shift anisotropy of the nuclei under study. The two-dimensional plane will show cross-peaks between resonances for which exchange of magnetization occurred via dipolar coupling during the mixing period τ_m. Figure 5.12(b) shows the application of this method to ^{23}Na in Na_2SO_3, which has three inequivalent ^{23}Na sites. The MQP$_4$MAS spectrum (*156*, *157*) shows distinctive correlations between two of the ^{23}Na sites, even for short mixing times of $\tau_m = 10$ μs, showing that the residual dipolar coupling at the spinning angle of 70.1° is sufficient to introduce exchange between spins.

In the MQOMAS method (*157*), the same pulse sequence is used as for MQP$_4$MAS (see Fig. 5.12(a)), but the sample is rotated at the magic angle during all

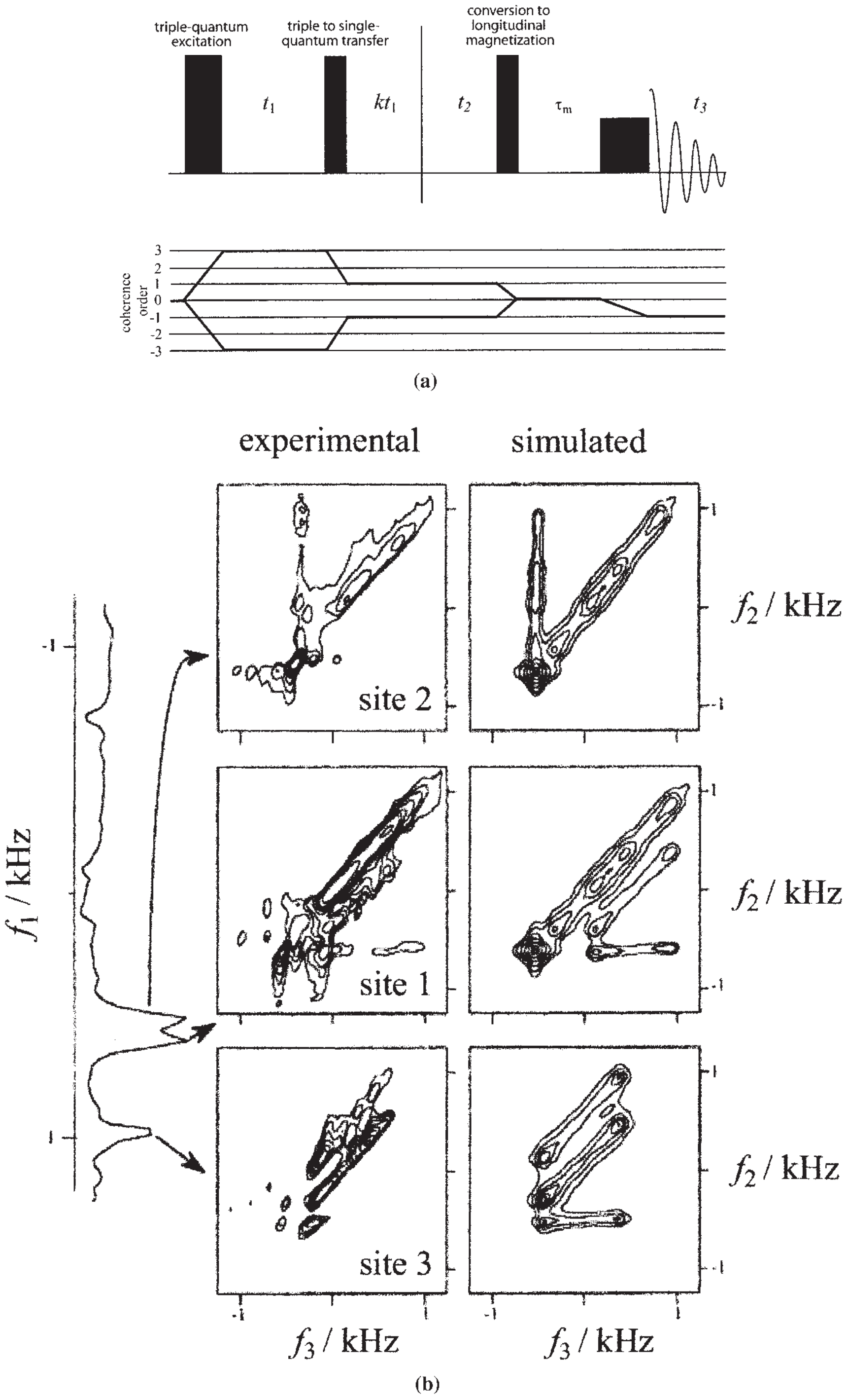

Figure 5.11 (a) Pulse sequence and coherence transfer pathway diagram for a three-dimensional MQMAS-based exchange experiment (*153*) The use of a split-t_1 period enables the anisotropic broadening to refocus before t_2 and an isotropic spectral dimension to be obtained. (b) High-resolution 3D exchange spectrum of Na_2SO_3, illustrating the 2D exchange slices at the indicated frequencies (*153*).

periods except for the mixing period, τ_m, during which rotation at 45° is used, so that the dipolar coupling is not averaged to zero by the sample spinning. The result is a spectrum that is similar to an MQP_4MAS spectrum but without the unwanted effects of chemical shift anisotropy (and of course a

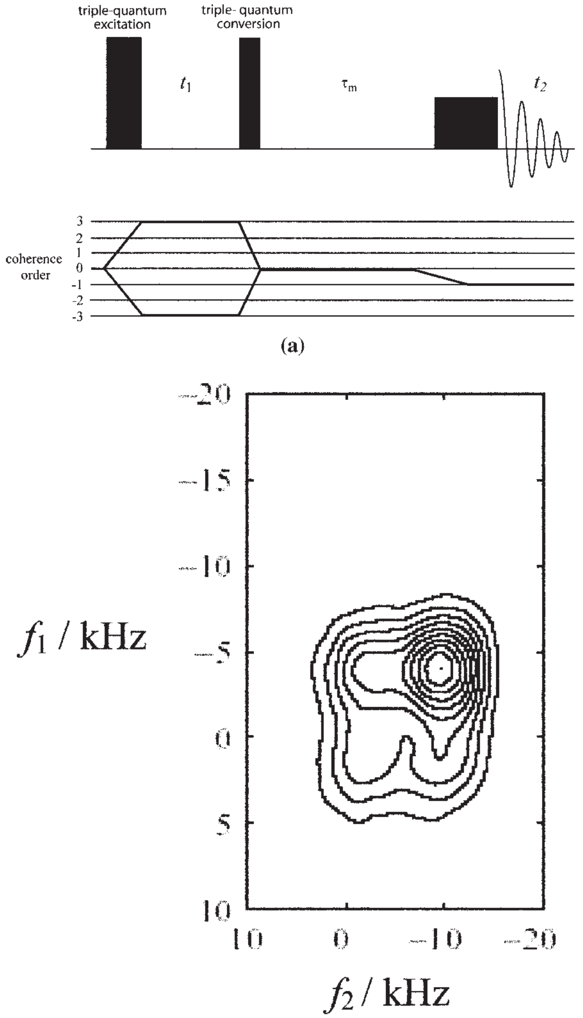

(a)

(b)

Figure 5.12 (a) Pulse sequence and coherence transfer pathway diagram for the MQP$_4$MAS and MQOMAS exchange experiments (*156, 157*). In MQP$_4$MAS, the sample is rotated at an angle of 70.1° throughout the experiment, while in MQOMAS, the sample is rotated at the magic angle at all times except during τ_m, when the sample is rotated at 45°, ensuring the dipolar coupling is not removed. (b) MQP$_4$MAS NMR exchange spectrum of Na$_2$SO$_3$, demonstrating the presence of cross-peaks between some of the Na resonances that are able to be resolved (*156, 157*).

different quadrupolar lineshape in the anisotropic dimension as the second- not the fourth-rank terms are now removed by sample rotation). This experiment, though technically more demanding due to the angle switching, provides a general way to recouple dipolar coupling for quadrupolar nuclei, which should be applicable to the vast majority of samples. It is, of course, directly related to the exchange experiment demonstrated in Fig. 5.10 (*152*, *153*), but enables a more efficient magnetization transfer during the mixing time.

The same work (*157*) compares the MQP$_4$MAS and MQOMAS methods with a DAS exchange experiment (a DAS experiment as in section 2.4 and Fig. 2.4, with a mixing period τ_m included in the delay τ before the spinning angle is switched). The DAS exchange experiment has limited resolution, as the DAS experiment itself does, due to dipolar broadenings in both dimensions.

5.2 Measuring Homonuclear Dipolar Couplings between Quadrupolar Nuclei

As discussed in the introduction to this section, there is no generally useful way to measure homonuclear dipolar couplings between quadrupolar nuclei with large quadrupolar couplings, although some techniques have appeared in the literature, which have proved efficacious, at least in some cases.

In MQMAS spectra, the high-resolution, multiple-quantum/single-quantum f_1' dimension often contains spinning sidebands, and these have a significant contribution from dipolar coupling effects where present (*158*). The effect of dipolar coupling during the multiple-quantum evolution is multiplied by N, the order of the multiple-quantum coherence (*159*), ensuring that even small dipolar couplings have a significant effect. The sideband pattern in the f_1' dimension may then be simulated and the dipolar coupling information retrieved. This method should be generally applicable, providing that chemical shift anisotropy is negligible and that the multiple-quantum excitation and transfer back to single-quantum coherence are dealt with carefully. The molecular orientation dependence of both processes means that rotor-encoded spinning sidebands will also appear in the f_1' dimension of the spectrum (*160*). These will be convoluted with the sidebands arising from dipolar coupling and so will tend to extend the effect of the dipolar spinning sidebands. The effect of rotor-encoding is easily taken into account in the simulation of the sidebands, but nevertheless, it is prudent to ensure that such sidebands do not dominate the sideband spectrum. The easiest way to achieve this is to keep both excitation and transfer pulse sequences as short as possible. If chemical shift anisotropy is not negligible, then the sideband pattern in f_1 will also contain a contribution from that interaction, making it significantly more difficult to uniquely extract the dipolar coupling information. Figure 5.13 shows an example where this approach has been used for the dipolar coupling between ^{23}Na spins in Na$_2$SO$_4$.

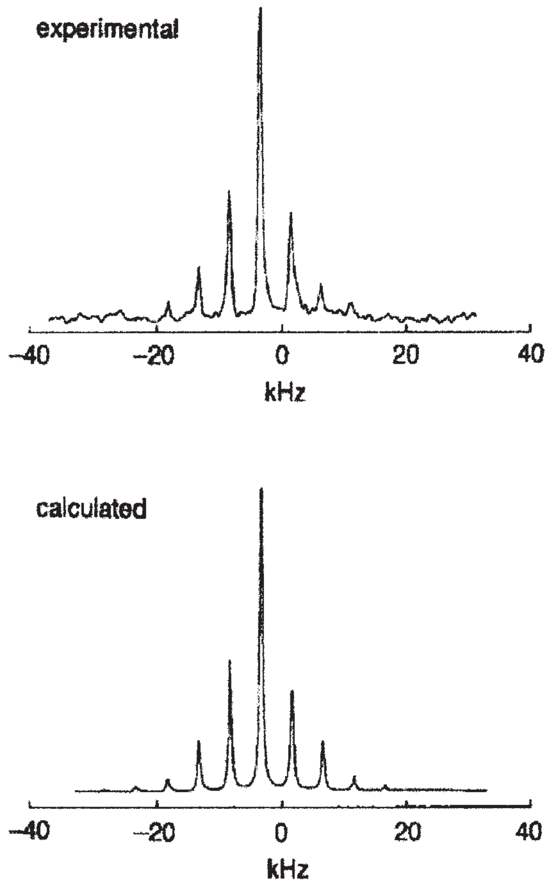

Figure 5.13 The spinning sideband pattern in the f_1 isotropic dimension of a ^{23}Na MQMAS spectrum of Na_2SO_4 that principally arises from dipolar coupling between the ^{23}Na spins. The simulation of the sideband pattern according to the known dipolar coupling in this compound (determined from its crystal structure) is shown below.

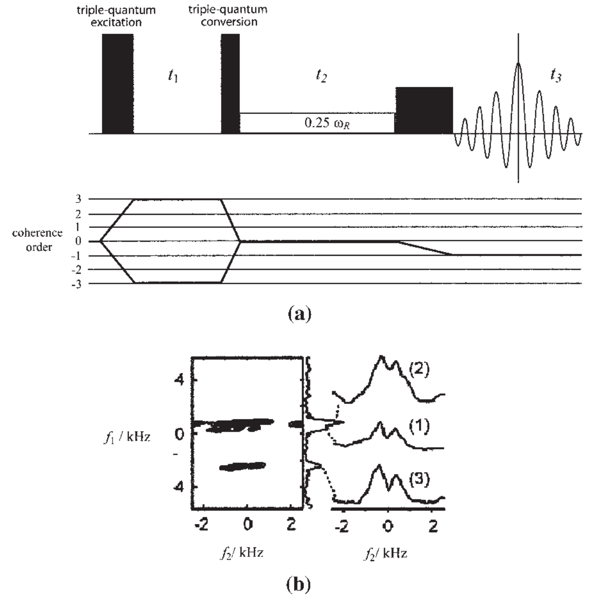

Figure 5.14 (a) Pulse sequence and coherence transfer pathway diagram used in the three-dimensional exchange experiment of Pines et al. (*161*). Recoupling is promoted in τ_m through the use of a HORROR coupling condition, where a radiofrequency field strength of 0.25 ω_R is applied. (b) A two-dimensional slice extracted from such an experiment for ^{23}Na in Na_2HPO_4. this slice shows powder patterns due to dipolar coupling in the f_2 dimension, correlated with a high-resolution dimension f_1 (*161*).

More recently, a three-dimensional experiment has been developed to measure dipolar couplings between quadrupolar nuclei more directly (*161*). This approach is promising, the only drawback being its 3D nature and somewhat long experimental time. The form of the experiment is shown in Fig. 5.14(a). It is based on a typical MQMAS experiment, with the addition of a variable time period (t_2 in Fig. 5.14(a)) between the triple-quantum coherence evolution and the subsequent observation of single-quantum coherence (in t_3 in Fig. 5.14(a)), during which homonuclear dipolar coupling is recoupled. The dipolar recoupling is simply achieved in this case using the equivalent of the spin-1/2 HORROR condition (*162*). The HORROR condition for spin-1/2 nuclei is a rotary resonance condition, described in detail in (*162*), under which homonuclear dipolar coupling is recoupled under rf irradiation when $\omega_1 = 0.5\ \omega_R$, that is, the nutation rate of the spin-1/2 magnetization under rf irradiation (ω_{rf}) equal to half the sample spinning rate. For a spin-3/2 nucleus, for rf irradiation applied to the central transition such that $\omega_1 \ll \omega_Q$, where ω_Q is the quadrupole splitting defined in Eq. [4.4], the nutation frequency of the central-transition magnetization under the rf irradiation is 2 ω_1 as shown in detail in (*6*) and references therein. Thus the equivalent HORROR condition for dipolar recoupling involving the central transitions of spin-3/2 nuclei is $\omega_1 = 0.25\ \omega_R$,[2] and this is applied in the experiment of (*161*). In this experiment, the dipolar recoupling is applied to longitudinal magnetization associated with the central transition. This has the advantage that such magneti-

---

[2] This result can also be derived from the analysis in section 5.1.2 for the recoupling of dipolar coupling for the purposes of generating double-quantum coherence between spins. In this analysis, for the present purposes, all terms in $\hat{I}_z$ and $\hat{S}_z$ and $(\hat{I}_z + \hat{S}_z)$ can be ignored as they have no effect on a density operator, which is proportional to $(\hat{I}_z + \hat{S}_z)$ and so the only effective field acting is that due to the rf irradiation along x, described by Eq. [5.20] ($\hat{H}_{rf} = 2\omega_1(\hat{I}_x^{2-3} + \hat{S}_x^{2-3})$). Thus the rotary resonance condition of Eq. [5.31] ($\omega_{I,eff}^{2-3} + \omega_{S,eff}^{2-3} = m\omega_R$; $m = \pm 1, \pm 2$) simply becomes $4\omega_1 = m\omega_R$.. The condition $\omega_1 = 0.5\omega_R$ also recouples chemical shift, heteronuclear dipolar coupling, and second-order quadrupole coupling terms and so is not so useful.

zation suffers no evolution under quadrupole coupling, heteronuclear dipolar coupling, or chemical shifts, as these interactions impart only rotations about z and so have no effect on magnetization stored along z. Only the recoupled homonuclear dipolar coupling imparts non-z rotations and so has a net effect on the stored longitudinal magnetization. Figure 5.14(b) shows an example of the use of this method for ^{23}Na in Na_2HPO_4 (*161*).

5.3 Spin Counting

In spin-1/2 NMR spectroscopy, the number of spins in a cluster may be counted by examining (a) what orders of multiple-quantum coherence may be excited within the cluster, with order $2N$ (where N is the number of spins in the cluster) being the maximum possible and (b) the amplitude of each coherence order excited as a function of the length of multiple-quantum excitation. Such methods have been used in static and spinning samples and provide a useful structural tool (see ref. [*6*] and references therein for a more complete discussion of the spin-1/2 case). Such a tool would be invaluable for quadrupolar nuclei also. Unfortunately, however, the strong quadrupole coupling found in many systems renders this impossible (*163*). For systems with small quadrupole couplings, notably ^{7}Li, conventional spin-1/2 methods may be used with some success (*163*, *164*).

6. STRUCTURAL INFORMATION FROM SCALAR (J) COUPLING

The scalar coupling, or J coupling, which provides so much useful information in liquid-state NMR, is often overlooked in solid-state NMR as it is much smaller in magnitude (~10–50 Hz) than the anisotropic broadening resulting from dipolar, CSA, and quadrupolar interactions. However, this through-bond coupling can provide insight on the local bonding network, topology, and connectivity, and aid spectral assignment. Experiments involving coherence transfer through the J coupling are highly selective and, unlike those based on the through space dipolar interaction, usually display little orientational dependence and a low sensitivity to molecular motion, often enabling a simple interpretation. In the simplest case, the presence of a J coupling to a remote spin S can be directly observed by a multiplet splitting (of $2S + 1$ lines) in the I spin spectrum, from which the J coupling can be extracted directly. This indicates a direct link of I and S through a number of chemical bonds, usually only between one and three, unlike the dipolar coupling, which indicates only spatial proximity. For example, a two-bond J coupling of 64 Hz between ^{29}Si and ^{93}Nb observed in the ^{29}Si MAS spectrum of $Rb_4(NbO)_2(Si_8O_{21})$, results in a 10-line multiplet structure (*165*). In many cases, the direct observation of a J coupling in the spectrum of a quadrupolar nucleus is difficult if significant second-order quadrupolar broadening is present. The removal of this broadening with MQMAS (or an alternative high-resolution approach) may be able to resolve a J coupling, as demonstrated by Wu and colleagues (*166*) where a 85-Hz ^{11}B-^{31}P J coupling was observed in the isotropic spectrum of $(PhO)_3P\text{-}BH_3$. The magnitude of a J coupling usually decreases with the number of chemical bonds connecting the two nuclei, but is also dependent to some extent on other geometrical factors, such as bond angles and exact relationships (e.g., cis or trans) to other functional groups.

Many of the experiments used in solution-state NMR designed to either measure a J coupling or simply demonstrate a through-bond connection have been successfully applied to solid-state NMR of spin-1/2 nuclei, including homonuclear methods such as COSY and INADEQUATE (*167*), and heteronuclear methods such as INEPT, DEPT, J-resolved spectroscopy, J-HSQC, and J-HMQC (*168–170*). These approaches often result in spectral simplification and increased resolution, allowing assignment and the extraction of site-specific structural information. Despite the presence of larger anisotropic interactions, which often render the actual multiplet splitting resulting from the scalar coupling unresolvable, experiments that use this coupling to mediate coherence transfer are still possible.

The use of experiments exploiting the J coupling to or from a quadrupolar nucleus are much less common, and perhaps offer an area of untapped potential. However, Fyfe and colleagues (*171*) have demonstrated that coherence transfer from a quadrupolar nucleus with noninteger spin to a spin-1/2 nucleus is possible by INEPT (insensitive nuclei enhanced by polarization transfer) (*172*) refocused INEPT (*173*) and DEPT (distortionless enhancement by polarization transfer) (*174*) transfers. The standard one-dimensional INEPT experiment is shown in Fig. 6.1(a), with coherence transfer occurring through the J coupling with the final 90° pulses converting $2I_xS_z$ to $2I_zS_y$. (The refocused INEPT experiment employs an additional echo before acquisition, allowing the S spin antiphase vectors to come back into alignment, converting $2I_zS_y$ into $-S_x$.) Fyfe and colleagues (*171*) used these techniques for detection of ^{27}Al/^{29}Si and ^{23}Na/^{29}Si J couplings in microcline and albite, respectively.

The use of INEPT to extract structural information was also demonstrated by Kao and Grey (*175*), who studied a trimethyphosphine bound to a Lewis acid site in dehydroxylated HY zeolite, investigating the presence of host-guest interactions within these microporous materials. A full investigation of ^{27}Al-^{31}P INEPT transfer was undertaken also by Kao and Grey (*176*) on a $(CH_3)_3P$-$AlCl_3$ complex, once again within a zeolite, now NaX. For short pulse durations (θ and 2θ), the ^{31}P spectrum showed only coupling to the ^{27}Al central transition ($m_I = \pm 1/2$) levels. As the pulse duration increased, J coupling to the $m_I = \pm 3/2$ and ±5/2 levels was also observed. However, if the INEPT pulses were applied in a rotor-synchronized manner, the full multiplet structure was observed for all pulse durations. INEPT transfer was chosen from ^{27}Al to ^{31}P on the basis of the relative relaxation times.

An alternative approach, that of J-resolved spectroscopy, for the measurement of J couplings was used by Massiot and colleagues (*177*). A simple ^{27}Al spin echo pulse sequence is adapted with an additional ^{31}P 180° pulse applied simultaneously with that for ^{27}Al. This pulse modulates the obtained signal, M(τ), by the Al–O–P scalar coupling such that

$$M(\tau) = \prod_n \cos(2\pi J_n \tau)\exp(-2\tau/T_2') \qquad [6.1]$$

where J_n is the scalar coupling and T_2' the relaxation time corresponding to the nonrefocusable line width. Incrementation of τ and subsequent Fourier transformation leads to a so-called J-resolved spectrum in the indirect dimension, which can be modeled to extract the various J couplings. The presence of two distinct J couplings in the Al–$(OP)_4$ tetrahedron of $AlPO_4$ berlinite (of 26 and 19.4 Hz, respectively) has been demonstrated using this method (*177*). Although simple to perform, this technique is limited to cases where T_2' is ample to provide sufficient coherence lifetimes.

The Al–O–P coupling was further used to generate a heteronuclear J-HMQC correlation experiment (*177*). This derives directly from the J-resolved experiment, splitting the ^{31}P 180° pulse into two 90° pulses placed symmetrically around the ^{27}Al 180° pulse and separated by an incremented $t_1/2$ evolution period, as shown in Fig. 6.2(a). Phase cycling selects double-quantum coherences that evolve under the ^{31}P chemical shift in t_1. This experiment uses the isotropic part of the J coupling that is independent of crystallite orientation, yielding undistorted quadrupolar lineshapes, which are correlated with the ^{31}P lineshapes connected through chemical bonding, as shown in Fig. 6.2(b), a two-dimensional J-HMQC (^{27}Al/^{31}P) spectrum of $AlPO_4$ berlinite, demonstrating through-bond connectivity of Al and P. The through-bond correlation of Al and P resonances in hydrated VPI-5 was also studied using this technique (*177*). Although connectivity of all three Al species to all three ^{31}P resonances was observed, the intensity of the cross-peaks show clear differences, reflecting the different magnitude of the J couplings. Recently, a modified J-HMQC experiment has been performed using the J coupling between two quadrupolar nuclei for the first time (*178*). This work used the J coupling between ^{27}Al and ^{17}O in crystalline $CaAl_2O_7$ (grossite) with 30% ^{17}O enrichment and a glass, $CaAl_2O_4$, also with 30% ^{17}O enrichment.

The simple one-dimensional INEPT sequence described above may also be converted into a two-dimensional correlation experiment, through the incrementation of the initial τ delay as a t_1 period. Subsequent two-dimensional Fourier transformation results in a two-dimensional spectrum where cross-peaks appear between *I* and *S* spin resonances, which are connected through chemical bonds. Such a spectrum is shown in Fig. 6.1(b), a two-dimensional ^{27}Al/^{31}P INEPT spectrum of $AlPO_4$-14. As has been the case for many methods described thus far, the second-order quadrupolar broadening present in the spectrum of the quadrupolar spin may often hinder the observation of cross peaks or the measurement of a J coupling. Wiench and Pruski (*179*) have introduced a series of experiments that combine two-dimensional heteronuclear correlation through the J coupling with the high resolution offered by MQMAS. These involve a initial triple-quantum ($p = +3$) excitation on a quadrupolar *I* spin and subsequent conversion to single-quantum ($p = -1$) coherence, in this case through the use of a composite FAM-type pulse. This coherence is then used in a correlation experiment, using either INEPT (*172*), INEPTR (*173*), INEPT+ (*180*), or DEPT (*174*) transfers. The refocused INEPT (INEPTR) experiment produces multiplets that are in phase, as opposed to the antiphase multiplets of INEPT. Further refinement using INEPT+ reduces phase and multiplet anomalies, although a longer experiment (i.e., more T_2' dependant) results. This is also the problem with the DEPT sequence, where time periods are significantly longer. Excellent resolution and sensitivity were shown for ^{27}Al-^{31}P INEPTR transfer in $AlPO_4$-14 (with an isopropylamine template) (*179*), where correlation of Al1 and Al3 to P1, P3, and P4; Al2 to P1, P2, and P4; and Al4 to P2, P3, and P4 is observed. The increase in resolution over the conventional INEPT experiment significantly eases the spectral assignment. However, incomplete

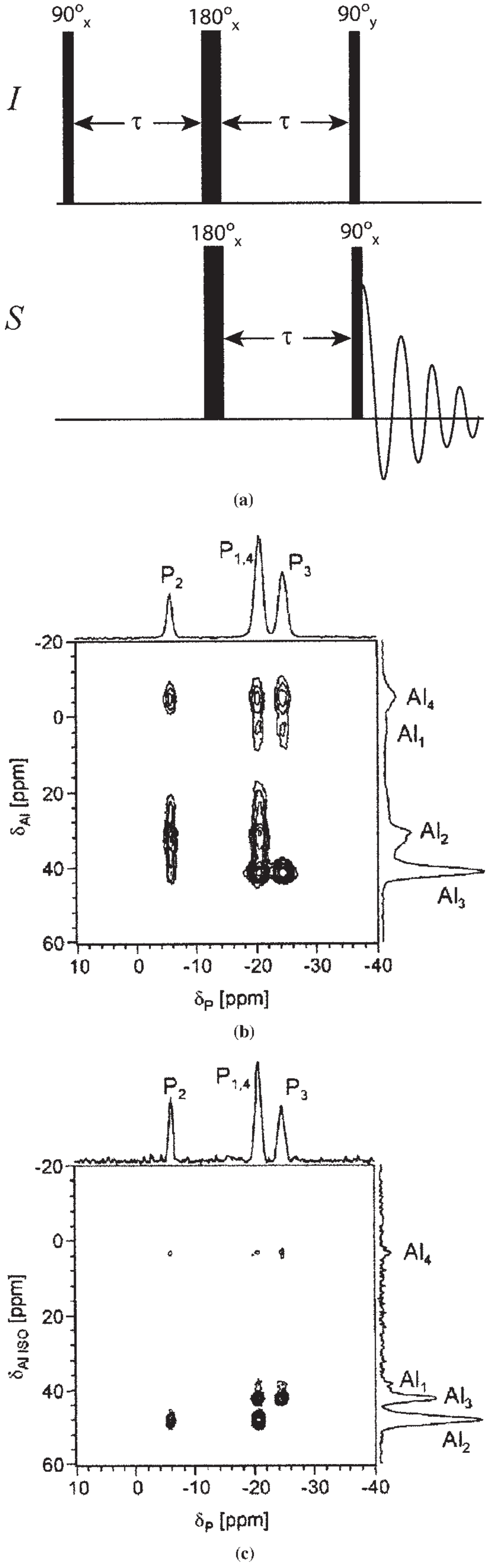

Figure 6.1 (a) Pulse sequence for a one-dimensional INEPT (*172*) experiment where magnetization is transferred from *I* to *S* via a through-bond scalar or J coupling. Incrementation of the initial τ duration enables the acquisition of a two-dimensional correlation spectrum. An additional echo may also be employed before acquisition on the *S* spin (a refocused INEPT experiment) (*173*). (b) Two-dimensional ^{27}Al/^{31}P INEPT and MQ-INEPT spectra of AlPO$_4$-14 (with an isopropylamine template) (*179*). Note the increase in resolution in the ^{27}Al dimension when the MQ experiment is used.

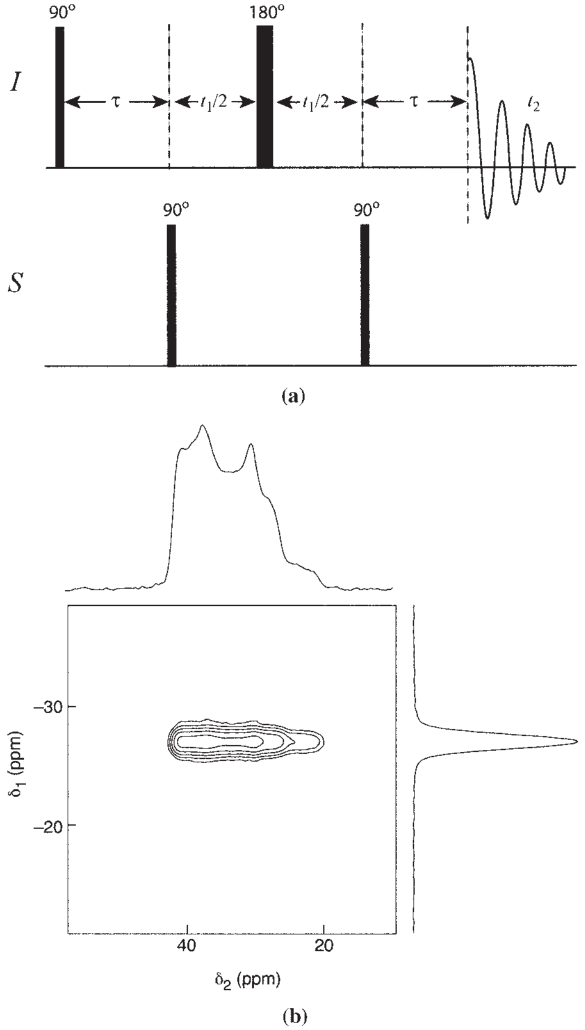

Figure 6.2 (a) Pulse sequence and coherence transfer pathway diagram for a J-HMQC experiment (*177*). Phase cycling selects double-quantum coherences that evolve under the ^{31}P chemical shift in t_1, producing a two-dimensional correlation spectrum. (b) J-HMQC (^{27}Al/^{31}P) of AlPO$_4$ berlinite, demonstrating through-bond connectivity of Al and P.

refocusing of the second-order quadrupolar interaction may affect the relative cross-peak intensities.

The presence of one or more *I-S* heteronuclear J couplings may also affect measurements of the *I-S* dipolar coupling through experiments such as REDOR. Trebosc and colleagues (*105*) have shown that a frequency-selective REDOR experiment on a SI_n multispin system is affected by J_{IS} scalar couplings. These J couplings can, however, be determined (by least-squares fitting) from this experiment, and spatial and through-bond information obtained simultaneously.

7. SUMMARY

Solid-state NMR provides an element-specific nondestructive probe for the examination of the local structural environment in crystalline and amorphous materials. It has the potential to provide detailed structural information, qualitative and quantitative in nature, through the many interactions (chemical shielding and dipolar, quadrupolar, and scalar couplings) that affect NMR spectra. Although much of this potential is currently being exploited for nuclei with spin $I = 1/2$, with structural information on complex materials such as peptides and proteins almost routine, the more complex spin dynamics associated with quadrupolar spins, coupled with the presence of large anisotropic broadenings, have resulted in many fewer studies, despite the fact that over 75% of NMR-active nuclei possess spin $I > 1/2$, including many chemically, industrially, and geologically relevant species. The recent advances in high-resolution NMR, particularly for half-integer spins, have enabled a fresh perspective on the use of such nuclei for structural studies and a resurgence of interest and work in the literature. In many ways, structural studies using quadrupolar spins still trail behind those used routinely in spin-1/2 NMR, with often only qualitative information available and the highly desirable quantitative measurements still difficult or impossible. The potential information and benefits of obtaining this quality of information from quadrupolar nuclei still drives much research.

Finally, a thought on where this area is, or perhaps should be, headed in future. Although a vast amount of information is present in a solid-state NMR spectrum, high resolution (and with good sensitivity) is usually required for accurate measurements. Continuing research in this area, improving the sensitivity and ease of acquisition of high-resolution spectra is therefore of great importance, particularly when such spectra are not the ultimate aim but only a single small part of a much more complicated experiment. Improvements to old experiments and new techniques are still being introduced, and perhaps when the determination of structural information is more widely considered as the goal, new and different approaches may be found. In many cases, current methods provide only qualitative results and, as is often the case for quadrupolar nuclei, more theoretical work is required to understand more deeply the nature of the coherence transfers occurring and whether they may be better controlled or directed. Although out of the scope of this current work, there is also much to be gained from the consideration of molecular motion. NMR is particularly sensitive to the presence of motion or dynamics within a system on a range of timescales through exchange experiments (s), lineshape perturbations (ms-μs) to relaxation times (ns). Not only can information on rates or activation energies be extracted, but often the symmetry or orientation relationships of various nuclei or moieties can also be determined. Lastly, the growing use of ab initio calculations to aid with spectral assignment, study the dependence of NMR parameters upon structural features, and to assist with the study of complex disordered or amorphous materials potential also offers for future development and expansion.

REFERENCES

1. Frydman L, Harwood JS. 1995. Isotropic spectra of half-integer quadrupolar spins from bidimensional magic-angle-spinning NMR. J Am Chem Soc 177: 5367–5368.
2. Tycko R, Opella SJ. 1986. High-resolution 14N overtone spectroscopy: an approach to natural abundance nitrogen NMR of oriented and polycrystalline systems. J Am Chem Soc 108:3531–3532.
3. Wi S, Frydman L. 2001. Heteronuclear recoupling in solid-state magic-angle-spinning NMR via overtone radiation. J Am Chem Soc 123:10354–10361.
4. Lee DK, Ramamoorthy A. 1998. Cross polarization in 14N overtone NMR spectroscopy of solids. Chem Phys Lett 286:398–402.
5. Harris RK. 1993. Nuclear magnetic resonance spectroscopy. Harlow, United Kingdom: Longman Scientific and Technical.
6. Duer MJ. 2004. Introduction to solid-state NMR spectroscopy. Oxford: Blackwell Science.
7. Smith ME, van Eck ERH. 1999. Recent advances in experimental solid state NMR methodology for half-integer spin quadrupolar nuclei. Prog Nucl Magn Reson Spectrosc 34:159–201.
8. Ashbrook SE, Berry AJ, Wimperis S. 2002. 17O multiple-quantum MAS NMR study of pyroxenes. J Phys Chem B 106:773–778.

9. Pike KJ, Malde RP, Ashbrook SE, et al. 2000. Multiple-quantum MAS NMR of quadrupolar nuclei. Do five-, seven- and nine-quantum experiments yield higher resolution than the three-quantum experiment? Solid State Nucl Magn Reson 16:203–215.
10. Amoureux JP, Fernandez C, Frydman L. 1996. Optimized multiple-quantum magic-angle spinning NMR experiments on half-integer quadrupoles. Chem Phys Lett 259:347–355.
11. Medek A, Harwood JS, Frydman L. 1995. Multiple-quantum magic-angle spinning NMR: a new method for the study of quadrupolar nuclei in solids. J Am Chem Soc 117:12779–12787.
12. Massiot D, Touzo B, Trumeau D, et al. 1996. Two-dimensional magic-angle spinning isotropic reconstruction sequences for quadrupolar nuclei. Solid State Nucl Magn Reson 6:73–83.
13. Sorensen OW, Rance M, Ernst RR. 1984. Z-filters for purging phase-distorted or multiplet-distorted spectra. J Magn Reson 56:527–534.
14. Amoureux JP, Fernandez C, Steuernagel S. 1996. Z filtering in MQMAS NMR. J Magn Reson A 123: 116–118.
15. Brown SP, Wimperis S. 1997. Two-dimensional multiple-quantum MAS NMR of quadrupolar nuclei. Acquisition of the whole echo. J Magn Reson 124:279–285.
16. Madhu PK, Goldbourt A, Frydman L, et al. 1999. Sensitivity enhancement of the MQMAS NMR experiment by fast amplitude modulation of the pulses. Chem Phys Lett 307:41–47.
17. Kentgens APM, Verhagen R. 1999. Advantages of double frequency sweeps in static, MAS and MQMAS NMR of spin I = 3/2 nuclei. Chem Phys Lett 300: 435–443.
18. Kwak HT, Prasad S, Yao Z, et al. 2001. Enhanced sensitivity in RIACT/MQ-MAS NMR experiments using rotor assisted population transfer. J Magn Reson 150:71–80.
19. Wu G, Rovnyak D, Griffin RG. 1996. Quantitative multiple-quantum magic-angle-spinning NMR spectroscopy of quadrupolar nuclei in solids. J Am Chem Soc 118:9326–9332.
20. Vosegaard T, Florian P, Massiot D, et al. 2001. Multiple quantum magic-angle spinning using rotary resonance excitation. J Chem Phys 114:4618–4624.
21. Duer MJ, Stourton C. 1997. Further developments in MQMAS NMR spectroscopy for spin-3/2 nuclei. J Magn Reson 124:189–199.
22. Marinelli L, Medek A, Frydman L. 1998. Composite pulse excitation schemes for MQMAS NMR of half-integer quadrupolar spins. J Magn Reson 132:88–95.
23. Gan Z, Kwak HT. 2004. Enhancing MQMAS sensitivity using signals from multiple coherence transfer pathways. J Magn Reson 168:346–351.
24. Gan Z. 2000. Isotropic NMR spectra of half-integer quadrupolar nuclei using satellite transitions and magic-angle spinning. J Am Chem Soc 122:3242–3243.
25. Ashbrook SE, Wimperis S. 2004. High-resolution NMR of quadrupolar nuclei in solids: the satellite-transition magic angle spinning (STMAS) experiment. Prog Nucl Magn Reson Spectrosc 45:53–108.
26. Ashbrook SE, Wimperis S. 2003. SCAM-STMAS: satellite-transition MAS NMR of quadrupolar nuclei with self-compensation for magic-angle misset. J Magn Reson 162:402–416.
27. Ashbrook SE, Wimperis S. 2002. Satellite-transition MAS NMR of spin I = 3/2, 5/2, 7/2, and 9/2 nuclei: sensitivity, resolution, and practical implementation. J Magn Reson 156:269–281.
28. Ashbrook SE, Wimperis S. 2002. High-resolution NMR spectroscopy of quadrupolar nuclei in solids: satellite-transition MAS with self-compensation for magic-angle misset. J Am Chem Soc 124:11602–11603.
29. Kwak HT, Gan Z. 2003. Double-quantum filtered ST-MAS. J Magn Reson 164:369–372.
30. Mueller KT, Sun BQ, Chingas GC, et al. 1990. Dynamic-angle spinning of quadrupolar nuclei. J Magn Reson 86:470–487.
31. Samoson A, Lippmaa E, Pines A. 1988. High-resolution solid-state NMR averaging of 2nd-order effects by means of a double-rotor. Mol Phys 65:1013–1018.
32. Chmelka BF, Mueller KT, Pines A, et al. 1989. O-17 NMR in solids by dynamic-angle spinning and double rotation. Nature 339:42–43.
33. Kentgens AP, Van Eck ER, Ajithkumar TG, et al. 2006. New opportunities for double-rotation NMR of half-integer quadrupolar nuclei. J Magn Reson 178: 66–78.
34. Samoson A. 1996. Two-dimensional isotropic NMR of quadrupole nuclei in solids. J Magn Reson A 121: 209–211.
35. Lupulescu A, Kotecha M, Frydman L. 2003. Relaxation-assisted separation of chemical sites in NMR spectroscopy of static solids. J Am Chem Soc 125: 3376–3383.
36. Mackenzie KJD, Smith ME. 2002. Multinuclear solid-state NMR of inorganic materials. Oxford: Pergamon.
37. Lippmaa E, Samoson A, Magi M. 1986. High-resolution Al-27 NMR of aluminosilicates. J Am Chem Soc 108:1730–1735.
38. Schramm S, Oldfield E. 1984. High-resolution O–17 NMR of solids. J Am Chem Soc 106:2502–2506.
39. Pickard CJ, Mauri F. 2004. Calculations of magnetic resonance parameters in solids and liquids using periodic boundary conditions. In: Kaupp M, Bühl M, and Malkin VG, editors. Calculation of NMR and EPR parameters: theory and applications. Weinheim, Germany: John Wiley & Sons.
40. Tossell JA, editor. 1992. Nuclear magnetic shieldings and molecular structure. NATO ASI Series, vol. 386. Dordrecht: Kluwer.
41. Slichter CP. 1992. Principles of magnetic resonance. 3rd edition. Berlin: Springer-Verlag.
42. Blaha P, Schwarz K, Herzig P. 1985. First principles

calculation of the electric-field gradient of Li3N. Phys Rev Lett 54:1192–1195.

43. Pickard CJ, Mauri F. 2001. All-electron magnetic response with pseudopotentials: NMR chemical shifts. Phys Rev B 63:245101.
44. Tossell JA, Lazzeretti P. 1987. Ab initio calculations of oxygen nuclear-quadrupole coupling-constants and oxygen and silicon NMR shielding constants in molecules containing Si-O bonds. Chem Phys 112:205–212.
45. Tossell JA, Lazzeretti P. 1988. Calculation of NMR parameters for bridging oxygens in H3Al–O–Al′H3, H3Si–O–Si′H3, H3P–O–P′ H3 linkages for oxygen in SiH3O−, SiH3OH and SiH3OMg+ and for bridging fluorine in H3SiFSiH3+. Phys Chem Miner 15:564–569.
46. Lindsay CG, Tossell JA. 1991. Abinitio calculations of O–17 and (N)T NMR parameters ((N)T=P–31, Si–29) in H3TOTH3 dimers and T3O9 trimeric rings. Phys Chem Miner 18:191–198.
47. Grandinetti PJ, Baltisberger JH, Werner U, et al. 1995. Solid-state O–17 magic-angle and dynamic-angle spinning NMR-study of the SiO2 polymorph coesite. J Phys Chem 99:12341–12348.
48. Clark TM, Grandinetti PJ. 2003. Dependence of bridging oxygen O–17 quadrupolar coupling parameters on Si–O distance and Si–O–Si angle. J Phys Cond Mat 15:S2387–S2395.
49. Vermillion KE, Florian P, Grandinetti PJ. 1998. Relationships between bridging oxygen O–17 quadrupolar coupling parameters and structure in alkali silicates. J Chem Phys 108:7274–7285.
50. Clark TM, Grandinetti PJ. 2005. Calculation of bridging oxygen O–17 quadrupolar coupling parameters in alkali silicates: a combined ab initio investigation. Solid State Nucl Magn Reson 27:233–241.
51. Xue X, Kanzaki M. 2000. An ab initio calculation of O–17 and Si–29 NMR parameters for SiO2 polymorphs. Solid State Nucl Magn Reson 16:245–259.
52. Pepels A, Gunther H, Amoureux JP, et al. 2000. Li–7 solid-state NMR of organolithium compounds: dependence of Li–7 quadrupolar coupling, chi(Li–7), on the structural angle C–Li–C. J Am Chem Soc 122:9858–9859.
53. Profeta M, Mauri F, Pickard CJ. 2003. Accurate first principles prediction of O–17 NMR parameters in SiO2: assignment of the zeolite ferrierite spectrum. J Am Chem Soc 125:541–548.
54. Charpentier T, Ispas S, Profeta M, et al. 2004. First-principles calculation of O–17, Si–29, and Na–23 NMR spectra of sodium silicate crystals and glasses. J Phys Chem B 108:4147–4161.
55. Hartmann SR, Hahn EL. 1962. Nuclear double resonance in the rotating frame. Phys Rev 128:2042–2053.
56. Pines A, Gibby MG, Waugh JS. 1972. Proton-enhanced nuclear induction spectroscopy. A method for high-resolution NMR of dilute spins in solids. J Chem Phys 56:1776–1777.
57. Pines A, Gibby MG, Waugh JS. 1973. Proton enhanced NMR of dilute spins in solids. J Chem Phys 59:569–589.
58. Stejskal EO, Schaefer J, Waugh JS. 1977. Magic-angle spinning and polarization transfer in proton-enhanced NMR. J Magn Reson 28:105–112.
59. Ashbrook SE, Wimperis S. 2000. Single- and multiple-quantum cross-polarization in NMR of quadrupolar nuclei in static samples. Mol Phys 98:1–26.
60. Lim KH, Grey CP. 1999. Triple quantum cross-polarization NMR of H–1/Al–27 and F–19/Na–23 spin systems in solids. Chem Phys Lett 312:45–56.
61. Amoureux JP, Pruski M. 2002. Theoretical and experimental assessment of single- and multiple-quantum cross-polarization in solid state NMR. Mol Phys 100: 1595–1613.
62. Vega S. 1981. Multiple-quantum cross-polarization NMR on spin systems with I = 1/2 and S = 3/2 in solids. Phys Rev A 23:3152–3173.
63. Wokaun A, Ernst RR. 1977. Selective excitation and detection in multilevel spin systems—application of single transition operators. J Chem Phys 67:1752–1758.
64. Samoson A, Lippma E. 1983. Central transition NMR excitation-spectra of half-integer quadrupole nuclei. Chem Phys Lett 100:205–208.
65. Kentgens APM. 1998. Off-resonance nutation nuclear magnetic resonance spectroscopy of half-integer quadrupolar nuclei. Prog NMR Spectrosc 32:141–164.
66. Vega AJ. 1992. CP/MAS of quadrupolar S = 3/2 nuclei. Solid State Nucl Magn Reson 1:17–32.
67. Vega AJ. 1992. MAS NMR spin locking of half-integer quadrupolar nuclei. J Magn Reson 96:50–68.
68. Rovnyak D, Baldus M, Griffin RG. 2000. Multiple-quantum cross polarization in quadrupolar spin systems during magic-angle spinning. J Magn Reson 142: 145–152.
69. Ashbrook SE, Wimperis S. 2004. Spin-locking of half-integer quadrupolar nuclei in nuclear magnetic resonance of solids: creation and evolution of coherences. J Chem Phys 120:2719–2731.
70. Ashbrook SE, Brown SP, Wimperis S. 1998. Multiple-quantum cross-polarization in MAS NMR of quadrupolar nuclei. Chem Phys Lett 288:509–517.
71. Ashbrook SE, Farnan I. 2004. Solid-state O-17 nuclear magnetic resonance spectroscopy without isotopic enrichment: direct detection of bridging oxygen in radiation damaged zircon. Solid State Nucl Magn Reson 26:105–112.
72. Haase J, Oldfield E. 1994. Aluminum to oxygen cross-polarization in α-Al2O3 (corundum). Solid State Nucl Magn Reson 3:171–175.
73. Lipton AS, Sears JA, Ellis PD. 2001. A general strategy for the NMR observation of half-integer quadrupolar nuclei in dilute environments. J Magn Reson 151:48–59.
74. Stejskal EO, Schaefer J. 1975. Removal of artifacts

from cross-polarization NMR experiments. J Magn Reson 18:560–563.

75. Metz G, Wu X, Smith SO. 1994. Ramped-amplitude cross-polarization in magic-angle-spinning NMR. J Magn Reson A110:219–227.
76. Lim KH, Grey CP. 2000. F-19/Na-23 multiple quantum cross polarization NMR in solids. J Chem Phys 112:7490–7504.
77. Eden M, Grins J, Shen Z, et al. 2004. Fast Si-29 magic-angle-spinning NMR acquisitions by RAPT-CP Al–27 → Si–29 polarization transfer. J Magn Reson 169:279–283.
78. Prabakar S, Wenslow RM, Mueller KT. 2000. Structural properties of sodium phosphate glasses from Na–23 → P–31 cross-polarization NMR. J Non-Cryst Solids 263:82–93.
79. Walter TH, Turner GL, Oldfield E. 1988. O–17 cross-polarization NMR-spectroscopy of inorganic solids. J Magn Reson 76:106–120.
80. Ashbrook SE, Wimperis S. 2000. Multiple-quantum cross-polarization and two-dimensional MQMAS NMR of quadrupolar nuclei. J Magn Reson 147:38–249.
81. Morris HD, Ellis PD. 1989. Al–27 cross polarization of aluminas—the NMR-spectroscopy of surface aluminum atoms. J Am Chem Soc 111:6405–6409.
82. Kirkpatrick RJ. 1988. MAS NMR spectroscopy of minerals and glasses. In: Hawthorne FC, editor. Spectroscopic methods in mineralogy and geology, vol. 18. Washington, DC: Mineralogical Society of America.
83. Mehring M. 1983. Principles of high-resolution NMR in solids. Berlin: Springer-Verlag.
84. Mali G, Kaucic V. 2002. Determination of distances between aluminum and spin-1/2 nuclei using cross polarization with very weak radio-frequency fields. J Chem Phys 117:3327–3339.
85. Vega S, Naor Y. 1981. Triple quantum NMR on spin systems with 1 = 3/2 in solids. J Chem Phys 75:75–86.
86. Vega S. 1978. Fictitious spin 1-2 operator formalism for multiple quantum NMR. J Chem Phys 68:5518–5527.
87. Fyfe CA, Mueller KT, Grondey H, et al. 1993. Solid-state double-resonance NMR experiments involving quadrupolar and spin 1/2 nuclei. J Phys Chem 97:13484–13495.
88. Fyfe CA, Wong-Moon KC, Huang Y, et al. 1995. Dipolar-based Al–27-Si–29 solid-state NMR connectivity experiments in zeolite molecular-sieve frameworks. J Phys Chem 99:8707–8716.
89. Wu Y, Lewis D, Frye JS, et al. 1992. Cross-polarization double-rotation NMR. J Magn Reson 100:425–430.
90. Baltisberger JH, Gann SL, Grandinetti PJ, et al. 1994. Cross-polarization dynamic-angle spinning nuclear-magnetic-resonance of quadrupolar nuclei. Mol Phys 81:1109–1124.
91. Fernandez C, Delevoye L, Amoureux JP, et al. 1997. Al–27{H–1} cross polarization triple-quantum magic angle spinning NMR. J Am Chem Soc 119:6858–6862.
92. Ashbrook SE, Wimperis S. 2001. Novel two-dimensional NMR methods that combine single-quantum cross-polarization and multiple-quantum MAS of quadrupolar nuclei. Chem Phys Lett 340:500–508.
93. Kaplan DE, Hahn EL. 1958. Experience de double irradiation enresonance magnetique par la methode d'impulsions. J Phys Radium 19:821–825.
94. Gullion T, Schaefer S. 1989. Rotational-echo double-resonance NMR. J Magn Reson 81:196–200.
95. Hing AW, Vega S, Schaefer J 1992. Transferred-echo double-resonance NMR. J Magn Reson 96:205–209.
96. Gullion T, Baker DB, Conradi MS. 1990. New, compensated Carr-Purcell sequences. J Magn Reson 89: 479–484.
97. Gullion T, Pennington C. 1998. Theta-REDOR: an MAS NMR method to simplify multiple coupled heteronuclear spin systems. Chem Phys Lett 290:88–93.
98. Jaroniec CP, Tongue BA, Herzfeld J, et al. 2001. Frequency selective heteronuclear dipolar recoupling in rotating solids: accurate C–13-N–15 distance measurements in uniformly C–13,N–15-labeled peptides. J Am Chem Soc 123:3507–3519.
99. Gullion T. 1999. A comparison between REDOR and theta-REDOR for measuring C–13-D–2 dipolar interactions in solids. J Magn Reson 139:402–407.
100. Sack I, Goldbourt A, Vega S, et al. 1999. Deuterium REDOR: principles and applications for distance measurements. J Magn Reson 138:54–65.
101. Sack I, Vega S. 2000. Efficient deuterium-carbon REDOR NMR spectroscopy. J Magn Reson 145:52–61.
102. Fyfe CA, Mueller KT, Grondey H, et al. Solid-state double-resonance NMR experiments involving quadrupolar and spin 1/2 nuclei. J Phys Chem 97:13484–13495.
103. Peng L, Liu Y, Kim N, et al. 2005. Detection of Bronsted acid sites in zeolite HY with high-field O–17-MAS–NMR techniques. Nat Mater 4:216–219.
104. Strojek W, Kalwei M, Eckert H. 2004. Dipolar NMR strategies for multispin systems involving quadrupolar nuclei: P–31{Na–23} rotational echo double resonance (REDOR) of crystalline sodium phosphates and phosphate glasses. J Phys Chem B 108:7061–7073.
105. Trebosc J, Amoureux JP, Wiench JW, et al. 2003. Simultaneous frequency-selective solid-state NMR analysis of internuclear distances and through-bond connectivities in the presence of quadrupolar nuclei. Chem Phys Lett 374:432–438.
106. Zeyer M, Montagne L, Jaeger C. 2003. Measuring oxygen-phosphorus distances and the orientation of electric field gradient tensors using O–17{P–13} REDOR in phosphate glasses. Solid State Nucl Magn Reson 23:136–144.
107. Fernandez C, Lang DP, Amoureux JP, et al. 1998. Measurement of heteronuclear dipolar interactions between quadrupolar and spin-1/2 nuclei in solids by

multiple-quantum REDOR NMR. J Am Chem Soc 120:2672–2763.

108. Pruski M, Bailly A, Lang DP, et al. 1999. Studies of heteronuclear dipolar interactions between spin-1/2 and quadrupolar nuclei by using REDOR during multiple quantum evolution. Chem Phys Lett 307:35–40.
109. Amoureux JP, Pruski M. 2002. Advances in MQMAS NMR. In: Grant DM, Harris RK, editors. Encyclopedia of nuclear magnetic resonance, vol. 9. Chichester: Wiley.
110. Opella SJ, Frey MH. 1979. Selection of non-protonated carbon resonances in solid-state nuclear magnetic-resonance. J Am Chem Soc 101:5854–5856.
111. Pruski M, Fernandez C, Lang DP, et al. 1999. Measurement of interatomic connectivities in molecular sieves using MQMAS-based methods. Catlaysis Today 49:401–409.
112. Gullion T. 1995. Measurement of dipolar interactions between spin-1/2 and quadrupolar nuclei by rotational-echo, adiabatic-passage, double-resonance NMR. Chem Phys Lett 246:325–330.
113. Grey CP, Veeman WS. 1992. The detection of weak heteronuclear coupling between spin-1 and spin-1/2 nuclei in MAS NMR— N–14/C–13/H–1 triple resonance experiments. Chem Phys Lett 192:379–385.
114. Grey CP, Veeman WS, Vega AJ. 1993. Rotational echo N–14/C–13/H–1 triple-resonance solid-state nuclear-magnetic-resonance—a probe of C–13–N–14 internuclear distances. J Chem Phys 98:7711–7724.
115. Zeng Q, Nekvasil H, Grey CP. 1999. Proton environments in hydrous aluminosilicate glasses: a H–1 MAS, H–1/Al–27, and H–1/Na–23 TRAPDOR NMR study. J Phys Chem B 103:7406–7415.
116. van Eck ERH, Kentgens APM, Kraus H, et al. 1999. A solid-state double-resonance NMR investigation of phosphorus-impregnated gamma-Al2O3 J Phys Chem 99:16080–16086.
117. Grey CP, Vega AJ. 1995. Determination of the quadrupole coupling-constant of the invisible aluminum spins in zeolite HY with H–1/Al–27 TRAPDOR NMR. J Am Chem Soc 117:8232–8242.
118. Gullion T. 1995. Detecting C–13–O–17 dipolar interactions by rotational-echo, adiabatic-passage, double-resonance NMR. J Magn Reson 117:326–329.
119. Hughes E, Gullion T, Goldbourt A, et al. 2002. Internuclear distance determination of S = 1, I = 1/2 spin pairs using REAPDOR NMR. J Magn Reson 156: 230–241.
120. Ganapathy S, Vega S. 1998. REAPDOR NMR spectroscopy and location of cations in molecular sieves. J Am Chem Soc 120:1078–1079.
121. Ganapathy S, Kumar R, Montouillout V, et al. 2004. Identification of tetrahedrally ordered Si–O–Al environments in molecular sieves by {Al–27}-Si–29 REAPDOR NMR. Chem Phys Lett 390:79–83.
122. Kalwei M, Koller H. 2002. Quantitative comparison of REAPDOR and TRAPDOR experiments by numerical simulations and determination of H–Al distances in zeolites. Solid State Nucl Magn Reson 21:145–157.
123. van Wullen L, Muller U, Jansen M. 2000. Understanding intermediate-range order in amorphous nitridic ceramics: A Si–29{B–11} REDOR/REAPDOR and B–11{Si–29} REDOR study. Chem Mater 12:2347–2353.
124. Goldbourt A, Vega S, Gullion T, et al. 2003. Interatomic distance measurement in solid-state NMR between a spin-(*1*)/(*2*) and a spin-(*5*)/(*2*) using a universal REAPDOR curve. J Am Chem Soc 125:11194–11195.
125. Ernst RR, Bodenhausen G, Wokaun A. 1987. Principles of nuclear magnetic resonance in one and two dimensions. New York: Oxford University Press.
126. Fyfe CA, Grondey H, Mueller KT, et al. 1992. Coherence transfer involving quadrupolar nuclei in solids—Al–27-reversible-arrow-P–31 cross-polarization NMR in the molecular-sieve VPI–5. J Am Chem Soc 114:5876–5878.
127. Fyfe CA, Mueller KT, Grondey H, et al. 1992. Dipolar dephasing between quadrupolar and spin-1/2 nuclei—REDOR and TEDOR NMR experiments on VPI-5. Chem Phys Lett 199:198–204.
128. Jarvie TP, Wenslow RM, Mueller KT. 1995. High-resolution solid-state heteronuclear correlation NMR for qnadrupolar and spin-1/2 nuclei. J Am Chem Soc 117:570–571.
129. Wang SH, DePaul SM, Bull LM. 1997. High-resolution heteronuclear correlation between quadrupolar and spin-1/2 nuclei using multiple-quantum magic-angle spinning. J Magn Reson 125:364–368.
130. Steuernagel S. 1998. A new sequence for the MQ-MAS/HETCOR experiment. Solid State Nucl Magn Reson 11:197–201.
131. Mali G, Amoureux JP, Kaucic V. 2000. Al–27 → P–31 3QMAS/HETCOR experiment in aluminophosphate molecular sieves. Phys Chem Chem Phys 2:5737–5742.
132. Chan JCC. 1999. High-resolution heteronuclear correlation between quadrupolar nuclei. J Magn Reson 140:487–490.
133. Fernandez, C Morais C, Pruski M. 2001. Comment on “Al–27 → P–31 3QMAS/HETCOR experiment in aluminophosphate molecular sieves.” Phys Chem Chem Phys 3:2552–2553.
134. Fernandez C, Morais C, Rocha J, et al. 2002. High-resolution heteronuclear correlation spectra between P–31 and Al–27 in microporous aluminophosphates. Solid State Nucl Magn Reson 21:61–70.
135. Lupulescu A, Brown SP, Speiss HW. 2002. Rotor-encoded heteronuclear MQ MAS NMR spectroscopy of half-integer quadrupolar and spin I = 1/2 nuclei. J Magn Reson 154:101–129.
136. Geen H, Titman JJ, Gottwald J, Spiess HW. 1995. Spinning side-band in the fast-MAS multiple-quantum spectra of protons in solids J Magn Reson A114:264–267.

137. Levitt MH. 2003. Paper presented at Third Alpine Conference on Solid-State NMR. Chamonix-Mont Blanc, France.
138. Zhao X, Eden M, Levitt MH. 2001. Recoupling of heteronuclear dipolar interactions in solid-state NMR using symmetry-based pulse sequences. Chem Phys Lett 342:353–361.
139. van Eck ERH, Smith ME. 1998. Orientation of the quadrupole and dipole tensors of hydroxyl groups by O–17 quadrupole separated local field NMR. J Chem Phys 108:5904–5912
140. Hughes CE, Pratima R, Karlsson T, et al. 2002. Double-quantum solid-state NMR of 13C spin pairs coupled to 14N. J Magn Reson 159:25–35.
141. Nijman M, Ernst M, Kentgens APM, et al. 2000. Rotational-resonance NMR experiments in half-integer quadrupolar spin systems. Mol Phys 98:161–178.
142. Kwak HT, Srinivasan P, Quine J, et al. 2003. Satellite transition rotational resonance of homonuclear quadrupolar spins: magic-angle effect on spin-echo decay and inversion recovery. Chem Phys Lett 376:75–82.
143. Baldus M, Rovnyak D, Griffin RG. 2000. Radio-frequency-mediated dipolar recoupling among half-integer quadrupolar spins. J Chem Phys 112:5902–5909.
144. Duer MJ, Painter AJ. 2002. Double-quantum-filtered nuclear magnetic resonance spectroscopy applied to quadrupolar nuclei in solids. J Chem Phys 116:710–722.
145. Mali G, Taulelle F. 2004. Detecting proximities between quadrupolar nuclei by double-quantum NMR. Chem Comm 868–869.
146. Mali G, Fink G, Taulelle F. 2004. Double-quantum homonuclear correlation magic angle sample spinning nuclear magnetic resonance spectroscopy of dipolar-coupled quadrupolar nuclei. J Chem Phys 120:2835–2845.
147. Duer MJ, Painter AJ. 1999. Correlating quadrupolar nuclear spins: a multiple-quantum NMR approach. Chem Phys Lett 313:763–770.
148. Mali G, Kaucic V. 2004. Enhancing sensitivity or resolution of homonuclear correlation experiment for half-integer quadrupolar nuclei. J Magn Reson 171: 48–56.
149. Larsen FH, Jakobsen HJ, Ellis PD, et al. 1998. QCPMG-MAS NMR of half-integer quadrupolar nuclei. J Magn Reson 131:144–147.
150. Yao Z, Kwak HT, Sakellariou D, et al. 2001. Sensitivity enhancement of the central transition NMR signal of quadrupolar nuclei under magic-angle spinning. Chem Phys Lett 327:85–90.
151. Dowell NG, Ashbrook SE, McManus J, et al. 2001. Relative orientation of quadrupole tensors from two-dimensional multiple-quantum MAS NMR. J Am Chem Soc 123:8135–8136.
152. Dowell NG, Ashbrook SE, Wimperis S. 2002. Relative orientation of quadrupole tensors from high-resolution NMR of powdered solids. J Phys Chem A 106:9470–9478.
153. Eden M, Grinshtein J, Frydman L. 2002. High resolution 3D exchange NMR spectroscopy and the mapping of connectivities between half-integer quadrupolar nuclei. J Am Chem Soc 124:9708–9709.
154. Wi S, Frydman L. 2000. Residual dipolar couplings between quadrupolar nuclei in high resolution solid state NMR: description and observations in the high-field limit. J Chem Phys 112:3248–3261.
155. Eden M, Frydman L. 2001. Quadrupolar-driven recoupling of homonuclear dipolar interactions in the nuclear magnetic resonance of rotating solids. J Chem Phys 114:4116–4123.
156. Ajithkumar TG, Kentgens APM. 2003. Homonuclear correlation experiments of half-integer quadrupolar nuclei using multiple-quantum techniques spinning at a P-4 magic angle. J Am Chem Soc 125:2398–2399.
157. Ajithkumar TG, van Eck ERH, Kentgens APM. 2004. Homonuclear correlation experiments for quadrupolar nuclei, spinning away from the magic angle. Solid State Nucl Magn Reson 26:180–186.
158. Duer MJ. 1997. Determination of structural data from multiple-quantum magic-angle spinning NMR experiments. Chem Phys Lett 277:167–174.
159. Friedrich U, Schnell I, Brown SP, et al. 1998. Spinning-sideband patterns in multiple-quantum magic-angle spinning NMR spectroscopy. Mol Phys 95:1205–1227.
160. Marinelli L, Frydman L. 1997. On the origin of spinning sidebands in MQMAS NMR experiments. Chem Phys Lett 275:188–198.
161. Wi S, Heise H, Pines A. 2004. Reintroducing anisotropic interactions in magic-angle-spinning NMR of half-integer quadrupolar nuclei: 3D MQMAS. J Am Chem Soc 124:10652–10653.
162. Nielsen NC, Bildsoe H, Jakobsen H, et al. 1994. Double-quantum homonuclear rotary resonance—efficient dipolar recovery in magic-angle-spinning nuclear-magnetic-resonance. J Chem Phys 101:1805–1812.
163. Dodd AJ, van Eck ERH. 2004. Multiple quantum spin counting techniques with quadrupolar nuclei. Solid State Nucl Magn Reson 26:121–131.
164. Tomaselli M, Meier BH, Ricco M, et al. 2001. A multiple-quantum nuclear magnetic resonance study of interstitial Li clusters in LixC60. J Chem Phys 115:472–476.
165. Kao HM, Lii KH. 2002. The first observation of heteronuclear two-bond J-coupling in the solid state: crystal structure and solid-state NMR spectroscopy of Rb–4(NbO)(2)(Si8O21). Inorgan Chem 41:5644–5646.
166. Wu G, Kroeker S, Wasylishen RE, et al. 1997. Indirect spin-spin coupling in multiple-quantum magic-angle-spinning NMR spectra of quadrupolar nuclei. J Magn Reson 124:237–239.
167. Fyfe CA, Feng Y, Grodney H, et al. 1991. One-dimensional and 2-dimensional high-resolution solid-

state NMR-studies of zeolite lattice structures. Chem Rev 91:1525–1543.

168. Kubo A, McDowell CA. 1990. One-dimensional and 2-dimensional P31 cross-polarization magic-angle-spinning nuclear-magnetic-resonance studies on 2-spin systems with homonuclear dipolar coupling and J coupling. J Chem Phys 92:7156–7170.
169. Lesage A, Sakellariou D, Steuernagel S, et al. 1998. Carbon–proton chemical shift correlation in solid-state NMR by through-bond multiple-quantum spectroscopy. J Am Chem Soc 120:13194–13201.
170. Lesage A, Emsley L. 2001. Through-bond heteronuclear single-quantum correlation spectroscopy in solid-state NMR, and comparison to other through-bond and through-space experiments. J Magn Reson 148:449–454.
171. Fyfe CA, Wong-Moon KC, Huang Y, et al. 1995. INEPT experiments in solid-state NMR. J Am Chem Soc 117:10397–10398.
172. Morris GA, Freeman R. 1979. Enhancement of nuclear magnetic-resonance signals by polarization transfer. J Am Chem Soc 101:760–762.
173. Pegg DT, Doddrell DM, Brooks WM, et al. 1981. Proton polarization transfer enhancement for a nucleus with arbitrary spin quantum number from n-scalar coupled protons for arbitrary preparation times. J Magn Reson 44:32–40.
174. Doddrell DM, Pegg DT, Bendall MR. 1982. Distortionless enhancement of NMR signals by polarization transfer. J Magn Reson 48:323–327.
175. Kao HM, Grey CP. 1997. Determination of the P–31–Al–27 J-coupling constant for trimethylphosphine bound to the Lewis acid site of zeolite HY. J Am Chem Soc 119:627–628.
176. Kao HM, Grey CP. 1998. INEPT experiments involving quadrupolar nuclei in solids. J Magn Reson 133: 313–323.
177. Massiot D, Fayon F, Alonso B, et al. 2003. Chemical bonding differences evidenced from J-coupling in solid state NMR experiments involving quadrupolar nuclei. J Magn Reson 164:160–164.
178. Iuga D, Morais C, Gan Z, et al. 2005. NMR heteronuclear correlations between quadrupolar nuclei in solids. J Am Chem Soc 127:11540–11541.
179. Wiench JW, Pruski M. 2004. Probing through bond connectivities with MQMAS NMR. Solid State Nucl Magn Reson 26:51–55.
180. Sorensen OW, Ernst RR. 1983. Elimination of spectral distortion in polarization transfer experiments—improvements and comparison of techniques. J Magn Reson 51:477–489.

BIOGRAPHY

Sharon Ashbrook graduated in chemistry from Hertford College, Oxford, where she also gained her D.Phil for work on new solid-state NMR techniques for quadrupolar nuclei. After postdoctoral research at the University of Exeter (in the group of Dr. Stephen Wimperis), she became a teaching fellow in mineral physics at the University of Cambridge. In 2003, she was awarded the Royal Society Dorothy Hodgkin Fellow at the Department of Earth Sciences, University of Cambridge, and also held the Charles and Katherine Darwin Research Fellowship at Darwin College. From October 2005, she was appointed an academic fellow in the School of Chemistry, University of St. Andrews. Currently, she is interested in the development of new techniques for solid-state NMR and their applications, particularly to mineral systems and to ceramic phases for the encapsulation of nuclear waste. She is also interested in the use of first-principles calculations for the determination of NMR parameters. In 2004, Dr. Ashbrook was awarded the Royal Society of Chemistry Harrison Prize for her contributions to solid-state NMR and has more than 35 publications in this area.

Melinda Duer is a senior lecturer in the Department of Chemistry, University of Cambridge. She graduated from the University of Cambridge in natural sciences and then went on to gain her Ph.D., also at the University of Cambridge (with Dr. Malcolm Gerloch, ScD) in theoretical inorganic chemistry. Her research for the past 15 years has concerned determination of structure and molecular dynamics in solids using NMR, frequently involving quadrupolar nuclei. She has more than 50 publications, many in the area of structure determination using quadrupolar nuclei and has written a book on the subject of solid-state NMR (*Introduction to Solid-State NMR Spectroscopy*, published by Blackwell Scientific Ltd., 2004).

AIP | Review of Scientific Instruments

Double Resonance Technique for the Elimination of Proton SpinSpin Splitting in High Resolution PMR Spectra

Reinhold Kaiser

Citation: Review of Scientific Instruments **31**, 963 (1960); doi: 10.1063/1.1717118
View online: http://dx.doi.org/10.1063/1.1717118
View Table of Contents: http://scitation.aip.org/content/aip/journal/rsi/31/9?ver=pdfcov
Published by the AIP Publishing

LVDT. In Fig. 3, a sensitivity of 10 d/cm/in. of chart paper was used. The zero-point drift over a period of 5 hr was negligible. After each run, the monolayer was swept off the trough. In each case the barrier regained its initial position to within 0.1 d/cm.

By adjusting the recorder x-axis span, a one-to-one correspondence between the position of the barrier and the projection of the recorder pen on the x axis was accomplished with an error of approximately 0.5 mm of travel of the barrier on the trough. This will usually correspond to an error in area/molecule of approximately 0.05 to 0.1 A^2/molecule, depending upon the amount of surfacant spread on the surface.

In actual use, our instrument is enclosed in a thermostat designed after that described by Harkins.[2] We are able to control closely the temperature (over a wide range) and the atmosphere of the inner chamber housing the film balance. We are able to control airborne contamination and we are easily able to keep the inner chamber saturated with respect to the substrate liquid.

We should point out that the LVDT can be adapted to a null-detection apparatus such as that described by Anderson and Evett[3] by using the output from the LVDT secondary as an error signal in a servo system. As the core passes through the null position, the output signal from the LVDT changes phase by 180°. A system designed with this principle in mind could offer an elegant way of following the change in surface area as a function of time at constant pressure. The possibilities of this system have not been explored.

ACKNOWLEDGMENT

We wish to acknowledge the excellent machine work done by Gary Wells of this Laboratory on the barrier transport mechanism.

THE REVIEW OF SCIENTIFIC INSTRUMENTS VOLUME 31, NUMBER 9 SEPTEMBER, 1960

Double Resonance Technique for the Elimination of Proton Spin-Spin Splitting in High Resolution PMR Spectra

REINHOLD KAISER
Departments of Chemistry and Physics, University of New Brunswick, Fredericton, New Brunswick, Canada

(Received May 4, 1960; and in final form, June 15, 1960)

The double resonance technique aims at removing the effect of spin-spin coupling by the application of a strong rf field at the resonance frequency of the disturbing nucleus in addition to the weak rf field used for observation of the NMR spectrum. A method is described whereby the weak rf field is obtained by a small audio frequency modulation of the magnetic field strength. This method is applicable to chemically nonequivalent groups of hydrogen nuclei to simplify the interpretation of high resolution proton magnetic resonance spectra. Two examples are given.

THE interpretation of high resolution proton magnetic resonance spectra is often made difficult by the appearance of complex multiplet patterns due to indirect spin-spin couplings in the molecule. In cases where the chemical shift is large compared to the spin coupling constant, the spin-spin splitting can be effectively removed by the application of a second rf field strong enough to scramble the spin states of the disturbing nuclei. This double resonance method was originally proposed and theoretically investigated by Bloch[1] while a simplified theory and experimental verification for the case in which the interacting nuclei have different gyromagnetic ratios were given by Bloom and Shoolery.[2] The method has recently been applied in numerous cases[3] to eliminate the effects of B^{11}, N^{14}, Al^{27}, and P^{31} nuclei on the proton spectrum. The application to chemically nonequivalent hydrogen groups should be of considerable assistance in the interpretation of complex high resolution proton magnetic resonance spectra, yet the only examples of such application appear to be those reported by Anderson.[4] This may be caused by the fact that the electronic components used by Anderson are not normally available in most high resolution spectrometer installations. It is the purpose of this paper to show how proton spin decoupling can be achieved by relatively simple means.

The method is based on the audio modulation technique[4] which is commonly employed in high resolution PMR to produce sidebands for calibration purposes. In order to collapse the spin multiplets the rf amplitude of the transmitter is adjusted to a sufficiently high value so that the zero-order v-mode spectrum, which in the following will

---

[1] F. Bloch, Phys. Rev. **102**, 104 (1956), see Sec. 7.

[2] A. L. Bloom and J. N. Shoolery, Phys. Rev. **97**, 1261 (1955).

[3] J. A. Pople, W. G. Schneider, and H. J. Bernstein, *High-Resolution Nuclear Magnetic Resonance* (McGraw-Hill Book Company, Inc., New York, 1959).

[4] W. A. Anderson, Phys. Rev. **102**, 151 (1956).

TABLE I. Relative signal intensity and mode for audio modulation technique.

		Low sideband	Center band	High sideband
dc		$J_1{}^2v$	$J_0{}^2v$	$J_1{}^2v$
af	in phase component	$-J_1(J_0+J_2)v$	0	$+J_1(J_0+J_2)v$
	quadrature component	$-J_1(J_0-J_2)u$	$+2J_0J_1u$	$-J_1(J_0-J_2)u$

u, v = slow-passage no-saturation solution of Bloch's equations for u- or v-mode display, respectively

J_0, J_1, J_2 = Bessel functions of the first kind of argument $\gamma h/\Omega$, (h = audio modulation field amplitude, Ω = audio modulation angular frequency)

be referred to as "center band," is saturated and no longer shows any fine structure due to spin-spin couplings. The disappearance of the fine structure indicates that Bloom and Shoolery's condition for the scrambling of spin states, viz.,

$$\gamma H_1 > \pi J \tag{1}$$

(γ = gyromagnetic ratio, H_1 = rotating magnetic rf field, J = spin-spin coupling constant in cycles/sec), is being met. After this adjustment has been made, a very small audio modulation signal is applied to the sweep coils, and the resulting first-order sidebands are observed with a phase-sensitive detector which is locked to the audio frequency. The reference voltage to the detector should be in phase with the audio modulation field, because in this case the detector will suppress the center band signal and will give v-mode signals for the first sidebands, one of which will be inverted. Table I, which is derived from the theory given by Anderson[4] for the audio modulation technique, shows the modes and strengths of the various signals that can be observed with small audio modulation when the rf receiver is adjusted for v-mode display. To avoid saturating the sideband signals the modulation index $\gamma h/\Omega$ must be very small to satisfy the condition

$$[J_1(J_0+J_2)\gamma H_1]^2 T_1 T_2 \ll 1, \tag{2}$$

where T_1, T_2 = longitudinal and transverse relaxation times, respectively. Because of condition (1), this inequality essentially reduces to

$$\gamma h \ll \Omega/\pi J T_2. \tag{2a}$$

If Ω is chosen to satisfy the double resonance condition

$$\Omega^2 = (\delta\times\omega\times10^{-6})^2 + \gamma^2 H_1{}^2, \tag{3}$$

where δ = chemical shift in ppm between the two groups of nonequivalent hydrogen atoms whose spins are to be decoupled, and $\omega = 2\pi f$ with f = radio frequency of the spectrometer, then either of the two interacting groups can be observed in one sideband while the other one is being irradiated by the strong center band rf field.

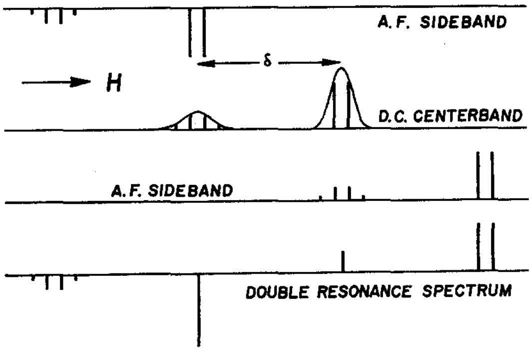

FIG. 1. Schematic composition of acetaldehyde proton double resonance spectrum.

This situation is explained in Fig. 1 which, for simplicity, has been drawn for the acetaldehyde spectrum. The acetaldehyde spectrum consists of two groups of lines: a quadruplet at low field due to the aldehyde hydrogen being split by indirect spin-spin interaction with the three methyl hydrogens, and a doublet at high field due to the equivalent methyl hydrogens being split by spin coupling with the aldehyde hydrogen. These two groups of resonances, as they would normally be recorded by the spectrometer in v-mode operation with weak rf field, are indicated by the vertical bars in the second line of Fig. 1 marked "dc center band." When the rf amplitude of the transmitter is increased to satisfy Eq. (1) (and, if necessary, the receiver gain is temporarily reduced to avoid overloading), this center band spectrum takes the appearance that is indicated in Fig. 1 by the curved "hoods." After the value of H_1 needed to saturate sufficiently the center band has thus been determined, Ω and h can be adjusted according to Eqs. (2) and (3), and the two sideband spectra indicated in the first and third lines of Fig. 1

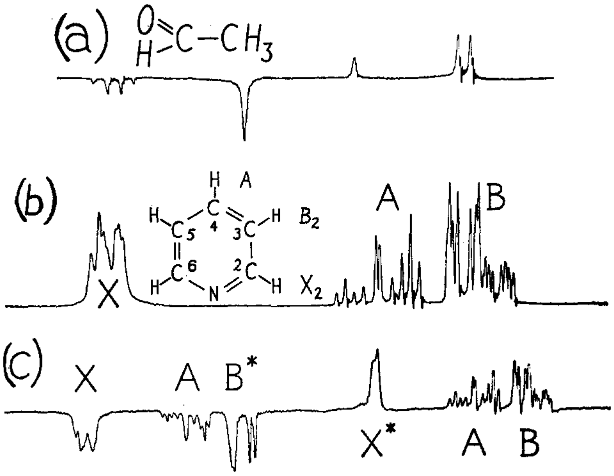

FIG. 2. (a) Proton double resonance spectrum of acetaldehyde ($\omega = 2\pi\times56.4$ Mc, $\Omega = 2\pi\times427$ cps, $H_1 \sim 10$ milligauss). Sweep speeded up between groups of lines. (b) Proton resonance spectrum of pyridine at 56.4 Mc. (c) Proton double resonance spectrum of pyridine ($\omega = 2\pi\times56.4$ Mc, $\Omega = 2\pi\times88$ cps, $H_1 \sim 3.8$ milligauss). Sweep speeded up between groups of lines.

can be observed in the output of the phase-sensitive detector. Equation (3) ensures that they are displaced to either side of the center band spectrum by an amount equal to the chemical shift δ. The center band spectrum will be suppressed by the phase detector and the sideband spectra will be in v-mode display, provided the reference voltage to the phase-sensitive detector has been adjusted to be in phase with the audio modulation field. A slow sweep of H (or ω) through the region of the spectra will then result in an output from the phase-sensitive detector of the form indicated in the bottom line of Fig. 1.

The double resonance spectrum of acetaldehyde reproduced in Fig. 2(a) shows how the spin-spin splitting is removed in the two central components. This and the following spectra were taken using the high resolution components of a Varian V 4302 spectrometer operating at 56.4 Mc and modified by the addition of a phase-sensitive detector with phase shifter, and an attenuator, as shown in the block diagram in Fig. 3. These two additional components are readily available commercially.[5] The selective amplifier[6] shown dashed in Fig. 3 is not required when working with strong signals, but is recommended for weak samples to prevent overloading the phase-sensitive detector by noise and other unwanted signals. It should be tuned to the audio frequency. It is important that the output from the rf receiver is taken from a point ahead of any response limiting network that would attenuate the audio frequency signal carrying the sideband information.

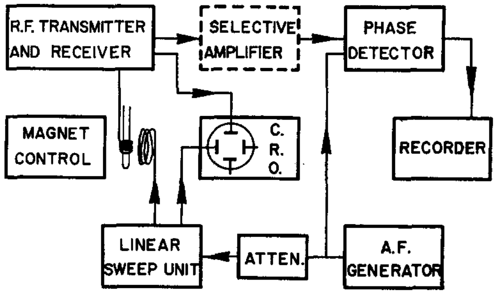

FIG. 3. Block diagram of double resonance spectrometer.

As a further example the method was applied to the pyridine spectrum shown in Fig. 2(b). This spectrum was analyzed by Schneider, Bernstein, and Pople[7] with the aid of the spectra of partially deuterated pyridines. The spectrum is of the AB_2X_2 type, the hydrogen in position 4 giving the A part, the equivalent hydrogens in positions 3 and 5 giving the B part, and those in positions 2 and 6 giving the X part at the low field end of the spectrum. The theoretical analysis shows that there are 110 lines altogether, of which 42 are due to combination transitions involving changes in spin of two or more nuclei. The intensities of these combination lines are too weak to be observed, but the analysis of the remaining 68 lines is still a formidable task. Figure 2(c) shows the double resonance spectrum of pyridine with the audio frequency adjusted to remove the B-X spin coupling. The lines marked B* constitute the B spectrum with the X hydrogens being irradiated. These lines are easily recognized as the B part of an AB_2 system. The lines marked X* constitute the X spectrum with the B hydrogens being irradiated. They form a partially resolved doublet from which the J_{AX} coupling constant can be read off directly. A similar spectrum can be taken with the audio frequency adjusted to remove the A-X spin coupling. The data reported by Schneider, Bernstein, and Pople[7] are consistent with an analysis of these double resonance spectra.

After this work had been completed the author became aware[8] of a double resonance technique developed by Itoh and Sato[9] which differs from the one described here by the fact that the sidebands are observed by their dc component (first instead of second line in Table I). This method has the advantage of added simplicity in that a phase-sensitive detector is not required, but the resonance line under investigation (and its neighborhood) appears superimposed on the broadened peak from which it is being decoupled, because the center band is not suppressed. Audio phase detection ensures a stable baseline unaffected by broadened center band lines or changes in probe balance due to the mechanical vibration of the spinning sample, etc., and this becomes important when the area under a v-mode line is to be determined.

---

[5] We use Industrial Test Equipment Company "Phazor" model 200 A phase meter with added recorder output, and Hewlett-Packard model 350 B attenuator.

[6] A Heathkit model HD-1 harmonic distortion meter can easily be modified to serve this purpose.

[7] W. G. Schneider, H. J. Bernstein, and J. A. Pople, Can. J. Chem. **35**, 65, 1060, 1487 (1957) and Ann. N. Y. Acad. Sci. **70**, 806 (1958).

[8] The author is indebted to the referee for bringing the work of Itoh and Sato to his attention.

[9] J. Itoh and S. Sato, J. Phys. Soc. Japan **14**, 851 (1959).

NUCLEAR MAGNETIC DOUBLE RESONANCE

É. T. Lippmaa

UDC 535.34.083.2

CONTENTS

1. Introduction

High-resolution nuclear magnetic resonance (NMR) has found extensive application and has become the chief method for studying the spatial and electronic structure, isomerism, and transformations of complex organic and inorganic liquids or soluble compounds. In addition to this structural information, relaxation phenomena in NMR spectra give much information, unobtainable by other methods, on the molecular motion, association, and microstructure of solutions. All these characteristics of the substance being studied are reflected in the NMR spectra in the form of the chemical shift δ, the spin-spin coupling constant J, and the relaxation parameters (relaxation times). The analysis of NMR spectra involves the determination of some or all of these quantities in order subsequently to interpret the data obtained and relate them to the spatial and electronic structure of the molecule, and sometimes also to processes of relaxation and molecular motion. In structural chemistry the first stage of this analysis plays the most important role, and the theoretical interpretation of the data is often only qualitative,

---

Tallin Cybernetics Institute, Academy of Sciences of the Estonian SSR. Translated from Zhurnal Strukturnoi Khimii, Vol. 8, No. 4, pp. 717-780, July-August 1967. Original article submitted February 17, 1967.

particularly in the case of such complex compounds as alkaloids, steroids, antibiotics, etc. Even the determination of all the constants δ and J, however, is usually a very complex task. Chemical shifts, and more particularly spin-spin coupling constants and their signs, in most cases cannot be determined from ordinary NMR spectra. Nuclear magnetic double (and sometimes triple) resonance (NMDR) opens up completely new possibilities in this field, and these methods are being used on an increasing scale for the solution of problems of structural analysis and molecular physics.

NMR acquired considerable importance for chemistry after the discovery of chemical coupling δ [63, 25] and scalar spin-spin coupling [64, 24-26] in polyatomic organic molecules. At the present time, approximately 1000 papers are published annually in this field of science. A large number of monographs [2-9, 12] have been devoted to the application of high-resolution NMR spectrometry in chemistry. Among works devoted to physical principles [1-3, 11-19] and experimental technique [10, 11, 18], Abragam's monograph [1] is particularly fundamental. The analysis of the complex spectra of organic compounds by NMR methods has been examined in detail in a number of monographs [2-4, 9, 18, 61] and in a review [62]. The first work in the field of NMDR is examined in reviews by Baldeschwieler and Randall [22] and Hoffman and Forsen [16] and also briefly in [23, 350] and in monographs by Abragam [1], Emsley, Feeney, and Sutcliffe [3], and Corio [18].

The present review examines the theory of the application and the experimental technique of double resonance between nuclear spins in the high-resolution NMR spectroscopy of liquids. Double nucleus-nucleus magnetic resonance in solids, electron-nucleus double resonance, which is also used chiefly for the study of solids, and double resonance in gas spectroscopy at superhigh frequencies are not dealt with in this review.

Let us examine the influence of two or several coherent high-frequency (hf) fields on the spin systems of the molecules of a liquid specimen. The specimen is placed in a strong magnetic field H_0, directed along the +z axis, and the hf-field acts in the xy plane. The measuring hf-field H_1 is almost always very weak, so that the amplitude of its single rotating component γH_1 is much less than the width of the spectral line at its half-height $|\gamma| H_1 < 2/T_2^*$ and does not lead to saturation of the spectral lines studied, for which it is necessary that $\gamma^2 H_1^2 T_1 T_2^* < 1$. The other hf-field (or fields) may have any amplitude within a range of almost 80 dB (differing by a factor of 10,000). The nature of the observed effects depends to a marked extent on the intensity of the perturbing hf-field H_2. We shall subsequently assume that the gyromagnetic ratio γ is positive. The magnetic nuclei being studied are designated using Pople's system [2], where ABC denotes a system of three magnetically nonequivalent strongly coupled spins. The letter X denotes a spin with a high relative chemical shift δ_{AX}, and also the spin irradiated with a strong perturbing hf-field H_2. Where necessary, the nucleus being irradiated is placed in braces and the decoupling of the spins of hydrogen nuclei from the nuclei of carbon C^{13} by the strong radiation of the latter is denoted H^1-$\{C^{31}\}$. The spin-spin coupling constants J are expressed in Hz, and the relative chemical shifts δ are expressed in Hz or in parts per million in the negative direction from the chemical shift of tetramethylsilane (TMS).

2. Effects Produced by a Perturbing hf-Field H_2 in NMR Spectra

2.1 Action of a Strong Perturbing hf-Field. If an individual spectral line is exposed to the influence of a strong hf-field H_2 under conditions when $\gamma^2 H_2^2 T_1 T_2^* \gg 1$, the line is saturated and the absorption signal can no longer be measured by means of the field H_2. The line disappears, but in spite of the saturation and the equalization of the populations of the corresponding energy levels [1, 13, 17], the interaction of the nuclear spins in the hf-field does not stop. This is manifested in the preservation of the dispersion signal and in the fact that, as a result of the coherence of the motion of the nuclear spins, two new narrow absorption lines can be detected close to the saturated spectral line in studies using a weak measuring hf-field H_1 [37, 58, 53, 85] (Fig. 1). If the angular frequency $\omega_2 = 2\pi f_2$ of the perturbing hf-field is tuned exactly in resonance, so that $\omega_2 = \omega_0 = \gamma H_0$, and the double resonance spectrum is recorded by scanning the measuring frequency ω_1, the displacement of these two new lines will be equal to the double amplitude $2\gamma H_2$ (rad/sec) of the strong hf-field [37, 58]. If the frequencies are measured in Hz, the amplitude $\gamma H_2/2\pi$ is also expressed in Hz. This phenomenon can be explained by examining the motion of the perturbed nuclear spins in a system of coordinates rotating with frequency $-\omega_2$ in which their motion involves rotation around the direction of the effective magnetic field $\gamma H_{ef} = \pm\sqrt{(\gamma H_0 - \omega_2)^2 + (\gamma H_2)^2}$. The high-frequency field γH_2 in these coordinates is also stationary, like γH_0 in laboratory coordinates, but is orientated in the xy plane. By examining the motion in laboratory coordinates, we obtain under these conditions for the nuclear spins two resonance frequencies $\omega_1 = \omega_2 \pm \sqrt{(\gamma H_0 - \omega_2)^2 + (\gamma H_2)^2}$. This phenomenon makes it possible to measure accurately the intensity of the perturbing high-frequency [10, 53, 58]. From this it also follows that with increase in the amplitude of the hf-field, the direction of the magnetization vector of the perturbed spins approaches the xy plane. Since the Hamiltonian for a system of two weakly coupled spins AX can be written in the form

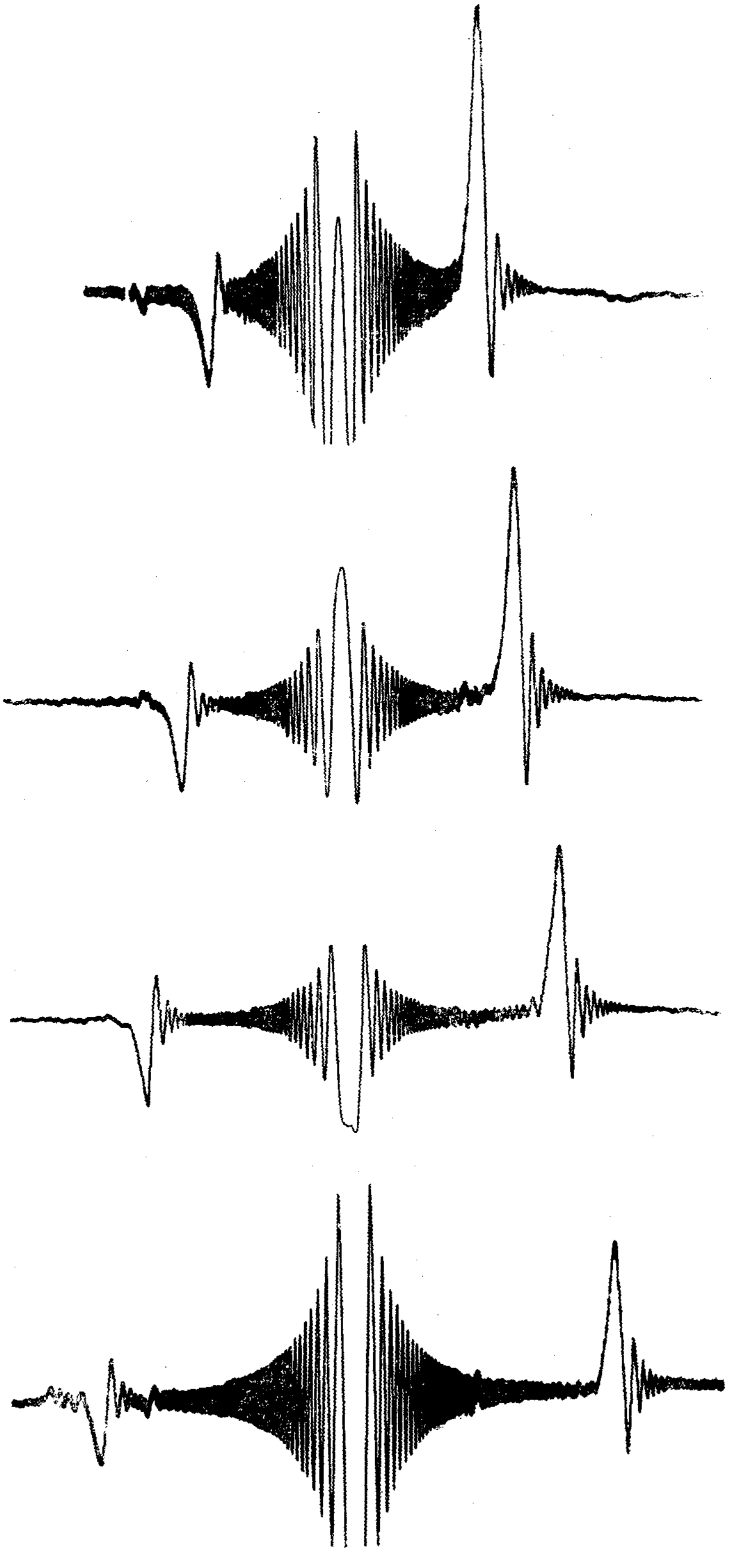

Fig. 1. Double resonance for a single spin of $^1/_2$ [53].

$$\mathcal{H}_0 = -\omega_A I_z(A) - \omega_X I_z(X) + 2\pi J_{AX} I_z(A) I_z(X), \qquad (1)$$

it may be assumed that if the strong perturbing field H_2 acts only on the X nuclei and does not act on the A nuclei, the magnetizations of the two nuclei have different directions and the directions of the quantization (or, classically, the directions of the precession axes) of the spin vectors **I**(A) and **I**(x) form a right angle, as a result of which the

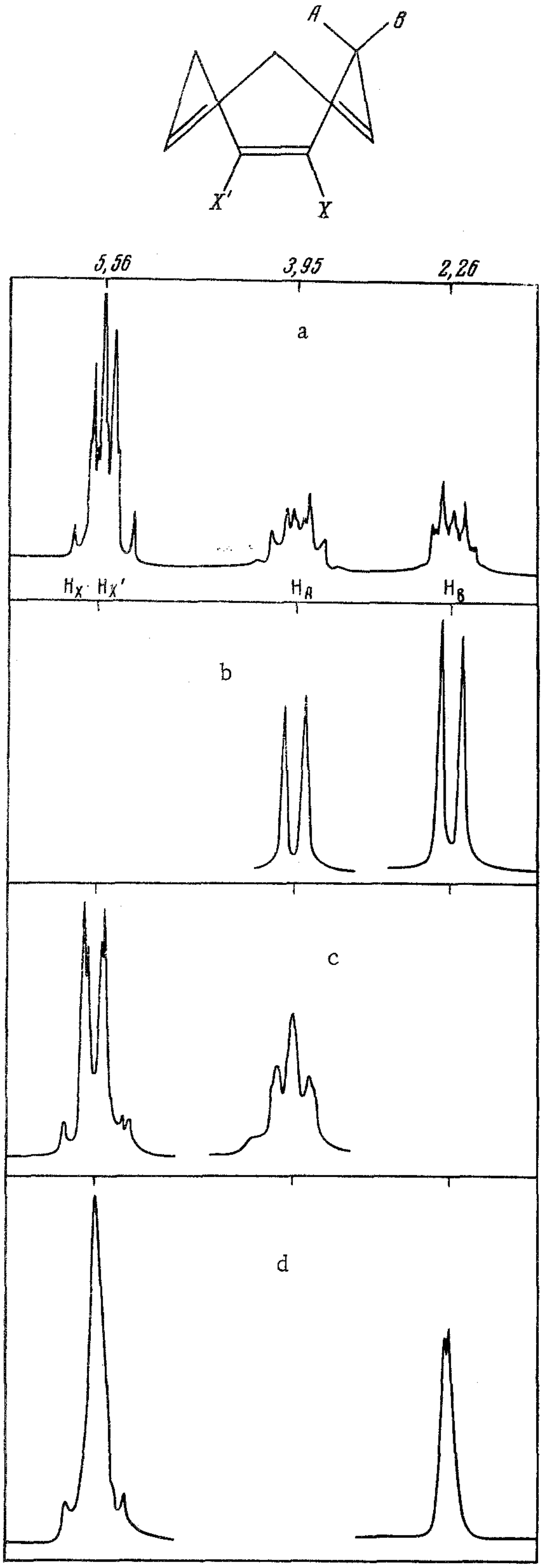

Fig. 2. Decoupling of the protons in cis, cis-1,4,7-cyclononatriene. a) Single resonance spectrum, b) perturbation of nuclei X, X'; c) perturbation of nuclei B; and d) perturbation of nuclei A [273].

scalar product in the Hamiltonian (1) is equal to zero, and the spin-spin coupling and the related doublet splitting of the signal for nucleus A disappears [11, 71]. The same result is obtained when this phenomenon is considered in rotating coordinates, where the Hamiltonian (1) acquires the form

$$\mathcal{H}_0^R = -(\omega_A - \omega_2) I_z(A) - \gamma H_2 I_x(X) - (\omega_X - \omega_2) I_z(X) + 2\pi J_{AX} I_z(A) I_z(X). \qquad (2)$$

[the term $\gamma H_2 I_X(X)$ takes account of the influence, on the spin of nucleus X, of the strong hf-field H_2, directed along the x axis]. If the field H_2 is tuned exactly in resonance with nucleus X, but does not influence nucleus A, so that $\omega_2 = \omega_X$ and $|\omega_A - \omega_2| \gg \gamma H_2$ but $\gamma H_2 \gg |2\pi J_{AX}|$, the last two terms in (2) are small and can be neglected. $I_Z(A)$ and $I_X(X)$ now precess independently, and, unlike the case described by the Hamiltonian (1), can acquire all possible values $m = I, I-1, \ldots -I+1, -I$ without mutual influence. The decoupling of the nuclear spins by the perturbing field leads to merging of the multiplet (in this case a doublet) of nucleus A to give one narrow line (collapse of the multiplet). The decoupling of nuclear spins [27-29, 58] has found very wide application in nuclear resonance. The partial or complete collapse of multiplets makes it possible to reveal the relationship between the individual multiplets in complex spectra, to find the chemical shifts for nuclei which are not observed directly (Xe^{129}, As^{75}, Si^{29}) or nuclei whose multiplets are overlapped by other strong lines in the spectrum, to determine the relative signs of spin-spin coupling constants, and finally to simplify the spectra. The spectrum of cis,cis,cis-cyclononatriene at −40°C is given in Fig. 2 [273]. From the spectra simplified by double resonance, it is immediately clear that at −40°C the compound being studied has the structure of a regular crown (and not a saddle), and the absolute values of all the chemical shifts δ and some of the spin-spin coupling constants J can be determined by simple measurement without analysis of the complex spectrum (Fig. 2a). By taking into account the dependence of J on the dihedral angle, it is possible to assign the multiplet at 2.26 ppm to proton B and the multiplet at 3.95 ppm to proton A. The usual values for the chemical shifts of these protons indicate that there is no annular current in this molecule. It is much more difficult to obtain all this information from the ordinary NMR spectrum.

The above analysis of the decoupling of nuclear spins has shown that the $I_Z(A)$ energy levels under the conditions of double resonance are independent of the X nucleus, so that all the intervals between the levels and the frequencies of these transitions will be equal, leading to merging of the multiplet (collapse).

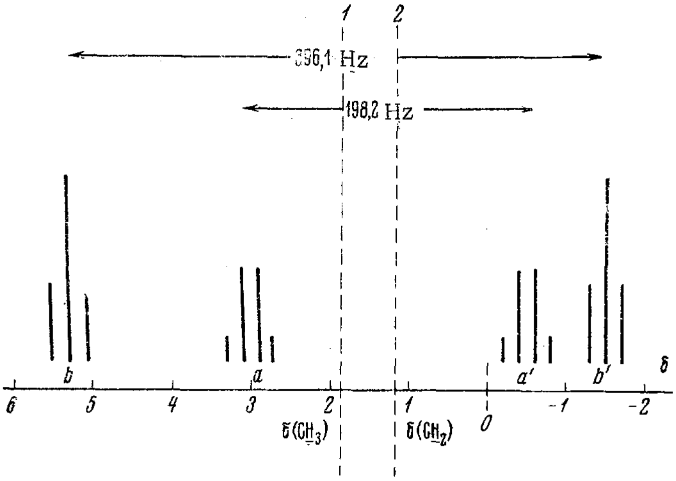

Fig. 3. Diagram of the proton spectrum of triethylthallium [82, 314].

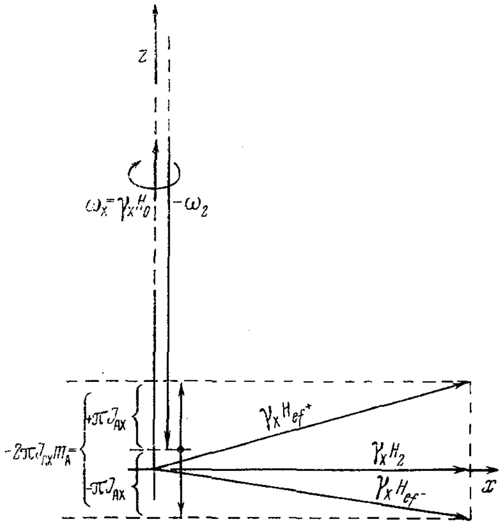

Fig. 4. Diagram of the interactions of the I(X) spin with magnetic fields in rotating coordinates [29].

Let us examine the phenomenon of collapse in a system where the values of the spin-spin coupling constants differ considerably, e.g., in triethylthallium [82, 314]. Thallium produces very marked splittings in the spectrum of the ethyl groups, and complete decoupling of the methyl protons from the methylene protons is impossible, as can be clearly seen from Fig. 3. Instead of the single triplet which is usually observed in hydrocarbons and alcohols, the methyl group in this spectrum is represented by two triplets, which correspond to different spin states of the thallium nucleus ($+^1/_2$ or α; $-^1/_2$ or β). If the triplet b' corresponds to the state α of this spin, strong perturbation of the triplet b' by the field $\gamma H_2 > 2\pi |J_{HH}|$ leads to decoupling of the methyl and methylene protons only in those molecules in which $I_z(Tl) = \alpha$, whereas γH_2 has practically no influence on other molecules. If now $J(TlCH_3)$ and $J(TlCH_2)$ have identical signs, we find that of the two quadruplets and a', quadruplet a' will correspond to the state α of the thallium spin, whereas if the signs are opposed, quadruplet a will correspond to this state. Correspondingly, collapse is produced in quadruplet a' or a. Experiment has shown [82] that the collapse of quadruplet a corresponds to the perturbation of the triplet b', and that the perturbation of triplet b leads to the merging of quadruplet a'. From this it follows that the state α of the thallium spin corresponds to different spin states of the protons of the methyl and methylene groups and that the relative signs of these spin-spin coupling constants are opposed. This experiment by itself does not make it possible to determine the absolute signs, but since J(CH) is positive in all compounds [47], it is possible by successive comparison to determine the absolute signs of all spin-spin coupling constants encountered in organic compounds. This procedure is also applicable in those cases where the coupling constants are not very large, and the only important requirement is that the spectrum should show more or less clearly defined individual multiplets for those nuclei for which it is necessary to determine the relative signs of the spin-spin coupling with another third nucleus. Unlike the case of complete decoupling of the spins under the conditions of total double resonance, in this case the perturbing field acts selectively and we are dealing with selective double resonance.

If the perturbing field acting on a system of two nuclear spins AX is weaker than in the preceding cases, we do not have complete orthogonality of I(A) and I(X), and the last term in the Hamiltonian (2) cannot be taken as equal to zero. At the same time, because of the presence of the term $-\gamma H_2 I_x(X)$, the usual selection rules $\Delta m_A = 1$ and $\Delta m_X = 0$ are inoperative, since $[I_z, I_x] \neq 0$, and it is possible to have transitions of the spin of nucleus X with simultaneous transitions of the spin A being studied, so that $\Delta m_X = 0.1 \ldots, 2I(X)$ [37, 65]. The spectrum of nucleus A is more complicated than the ordinary spectrum, and the number of spectral lines is increased.

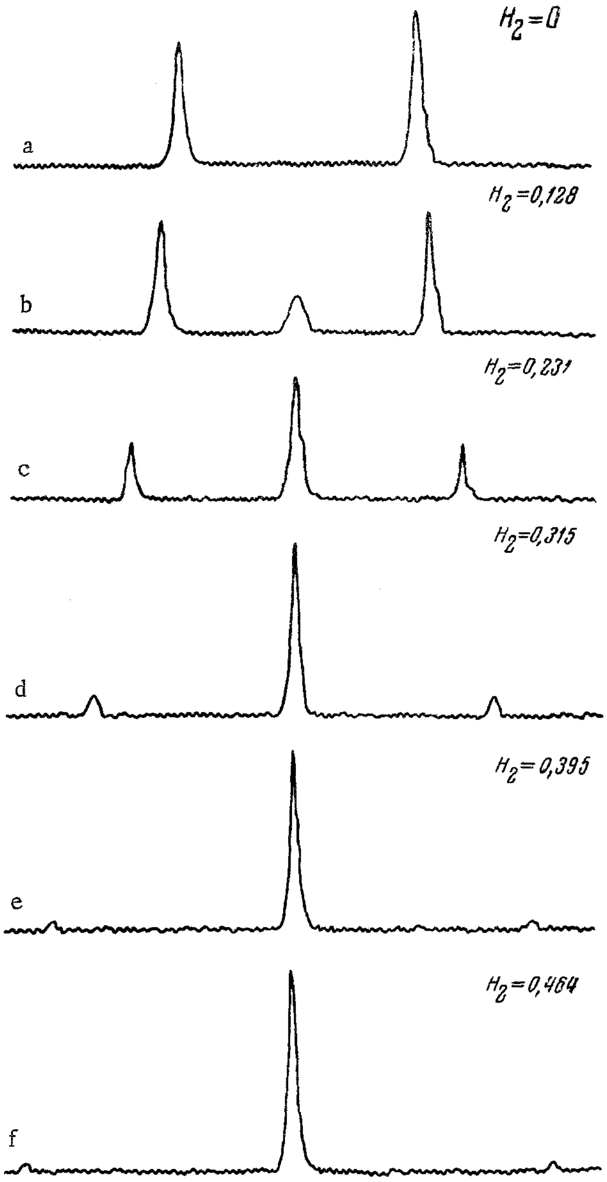

Fig. 5. Spectra of the flourine nucleus in aqueous Na_2PO_3F solution at various amplitudes of the perturbing hf-field in an experiment of the type $F^{19}-\{P^{31}\}$ [29].

Each spectral line in the multiplet of spin A is split into a submultiplet [65], whose outer components move apart and become weaker with increase in γH_2. If a perturbing field with amplitude $2/T_2^* \ll \gamma H_2 < 2\pi |J_{AX}|$ at a frequency $\omega_2 \cong \gamma_X H_0$ acts only on nucleus X and the signal from spin A is studied by means of a weak hf-field H_1 close to its resonance frequency $\omega_1 \cong \gamma_A H_0$, the I(X) spin rotating coordinates is quantized along the direction of the effective field, which now depends on the magnetic influence $-2\pi J_{AX} m_A$ of nucleus A; at the same time the quantization direction for nucleus A is, as before, the z axis [1, 29]. It is clear from Fig. 4 that the frequency of precession of nucleus X under the influence of the effective field is equal to

$$\gamma_X H_{ef} = [(\gamma_X H_0 - 2\pi J_{AX} m_A - \omega_2)^2 + (\gamma_X H_2)^2]^{1/2}, \qquad (3)$$

In spite of the fact that the quantization axes of the two nuclei are different, their energy depends on the magnetic quantum number m_A of nucleus A. If the spins of both nuclei A and X are equal to $^1/_2$, we have in the system Ax four energy levels with energies

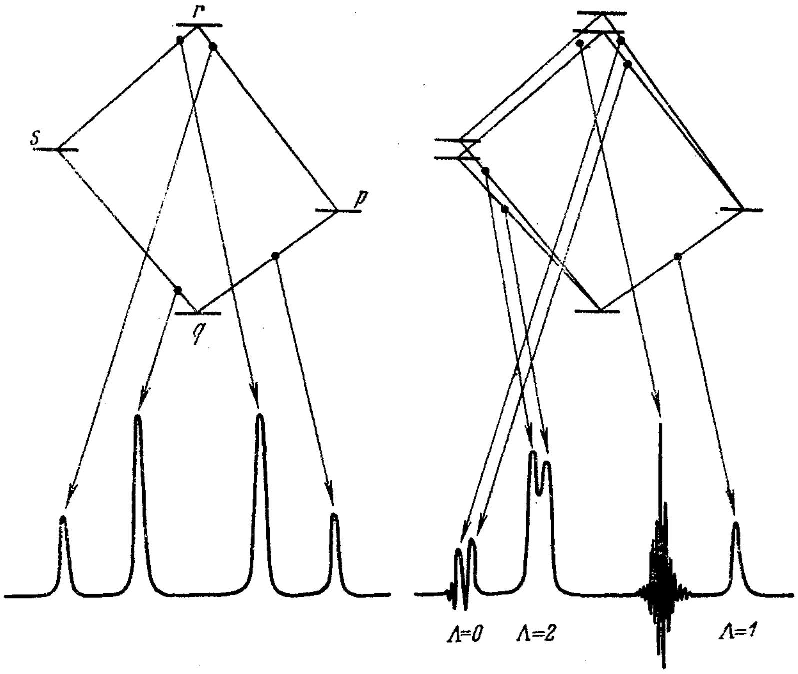

Fig. 6. Tickling in a two-spin system AB.

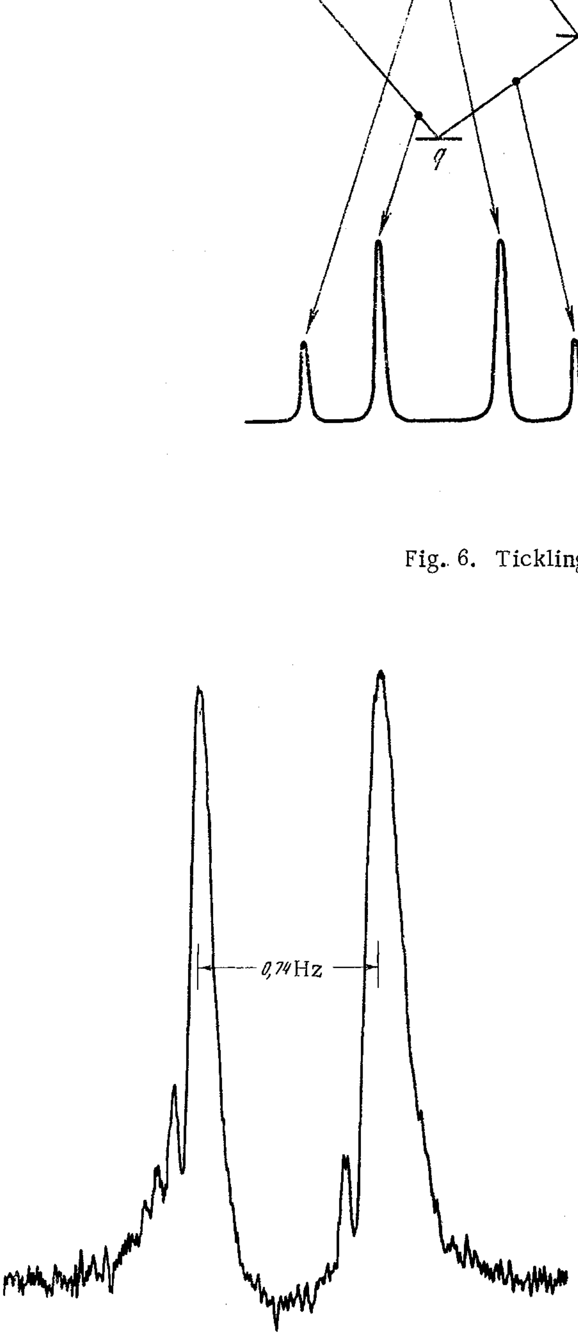

Fig. 7. Splitting of a line of type Λ = 0 in 2-bromo-5-iodothiophene [92]. Magnitude of the splitting 0.74 line width ≤ 0.17 Hz.

$$E = +\,{}^1/_2\gamma_A H_0 \pm {}^1/_2\gamma_X H_{ef+},$$
$$E = -\,{}^1/_2\gamma_A H_0 \pm {}^1/_2\gamma_X H_{ef-} \tag{4}$$

and between all these levels transitions are possible with the selection rule $\Delta m_A = 1$. In place of the doublet with splitting $2\pi J_{AX}$ in angular frequency units, which is formed if $\gamma H_2 = 0$, the spectrum of nucleus A now shows four lines at frequencies

$$\omega_1 = \gamma_A H_0 \pm ({}^1/_2\gamma_X H_{ef+}) \pm ({}^1/_2\gamma_X H_{ef-}).$$

In the case of exact resonance of the perturbing field, when $\omega_2 = \gamma_X H_0$, $H_{ef+} = H_{ef-}$, the double resonance spectrum will show only three lines at frequencies

$$\omega_1 = \gamma_A H_0 \quad \text{and} \quad \omega_1 = \gamma_A H_0 \pm \gamma_X H_{ef}. \tag{5}$$

With increase in the amplitude γH_2, the fields H_{ef+} and H_{ef-} increase, but as a result of the decrease in the angle between them the probability of simultaneous transition of the spins of both nuclei A and X and the intensities of the corresponding satellites decrease [1, 29]. When the condition $\gamma H_2 \gg 2\pi |J_{AX}|$ is satisfied, the doublet of spin A merges to form a single line. The spectra of F^{19} nuclei in aqueous Na_2PO_3F solution, recorded for various amplitudes of the resonance perturbing field, are given in Fig. 5 [29]. From analogous curves recorded at constant intensity of the frequency ω_2 relative to ω_X, it follows that the influence of the perturbing field is maximal when it is accurately tuned.

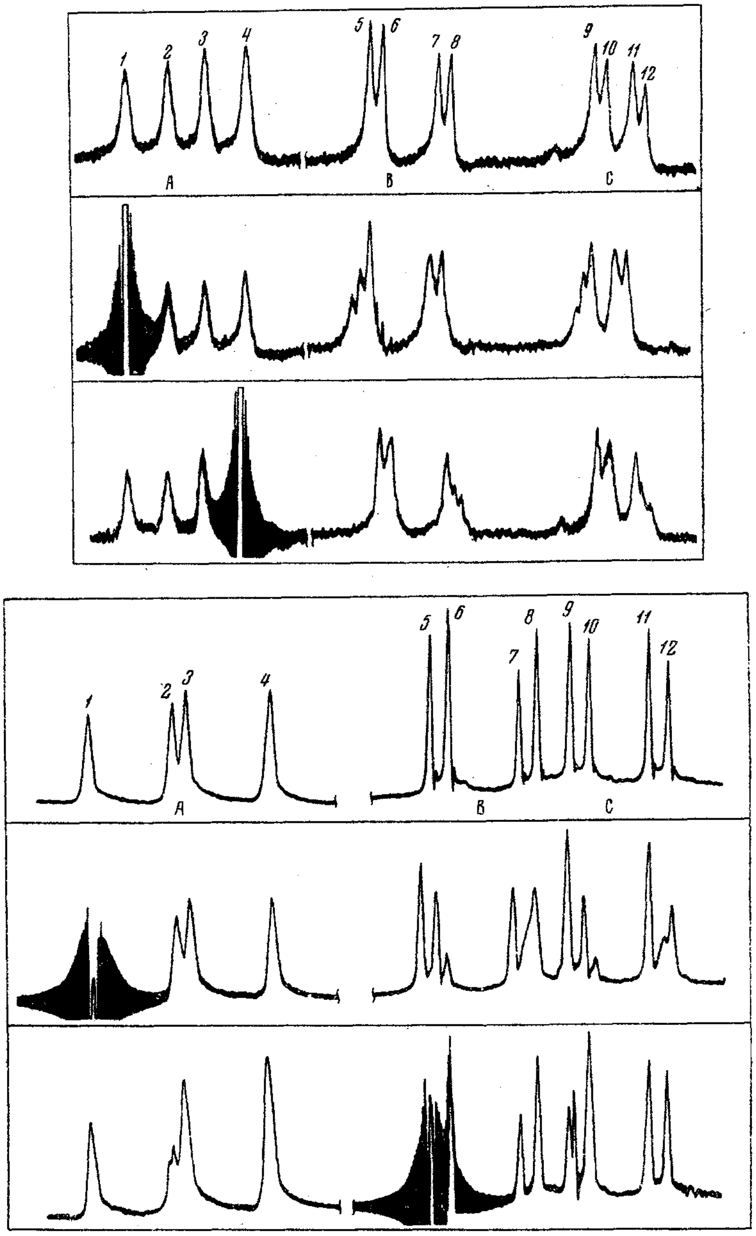

Fig. 8. Upper section: tickling in the proton spectrum of styrenimine; lower section: tickling in the proton spectrum of styrene sulfide. The constant of the geminal spin-spin coupling is negative in styrene sulfide and positive in styrenimine [367].

2.2. Action of a Weak Perturbing hf-Field. The perturbing hf-field is considered to be weak if its amplitude γH_2 is of the same order as the width of the perturbed spectral lines, and it influences only one line of the spectrum

$$2/T_2^* \cong \gamma H_2 \ll |(a'-a)|,\ |(a'-a)-(b'-b)|. \tag{6}$$

Thus a weak field H_2 influences the state of the spin system only with exact tuning on any line of the spectrum. The influence of this weak field is purely local in character and its action never leads to a decrease in the number of spectral lines. On the contrary, this field, in addition to saturation of the lines, may lead to splitting of the lines, if the lines are sufficiently narrow, so that $2/T_2^* \ll |(a'-a)-(b'-b)|$. In the examination of the action of a weak hf-field in a rotating system of coordinates (see Fig. 4), the only change is in the condition for exact tuning, in place of $\omega_2 = \gamma_X H_0$ we have $\omega_2 = \gamma_X H_0 - 2\pi J_{AX} m_A$, so that from (3) we obtain $\gamma_X H_{ef+} = \gamma_X H_2$. The energy

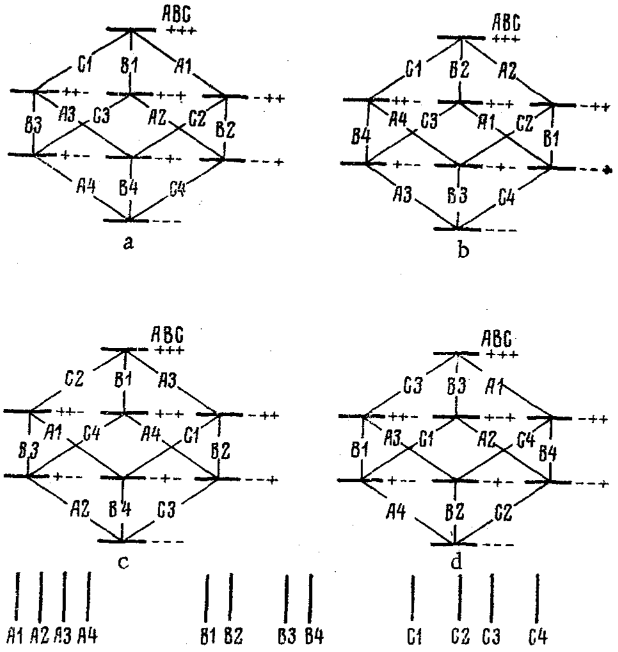

Fig. 9. Diagrams of the energy levels of systems ABC consisting of three nuclei with spin $\frac{1}{2}\gamma > 0$, but with H_0 orientated along the negative direction of the z axis $|J_{AB}| < |J_{AC}| < |J_{BC}|$ [154]. a) All the signs of the constants J the same, b) sign of J_{AB} opposed, c) sign of J_{AC} opposed, d) sign of J_{BC} opposed.

levels of nucleus A are split, in accordance with (4), by amounts $\pm\frac{1}{2}\gamma_X H_2$ and $+\frac{1}{2}2\pi J_{AX}$ respectively [291], and the spectral lines are split by $\gamma_X H_2$. Since a nuclear spin can influence the energy levels of another spin only if there is spin-spin coupling between them and the quantization of spin X along the direction of the effective field influences directly only the energy levels of this spin, the only lines which are split in the spectrum of nucleus A are those which have a common energy level with spin X. Figures 6 and 7 illustrate extremely arbitrarily the splitting of the spectral lines of the doublet of nucleus A, if γ_A, $\gamma_X > 0$ and $J_{AX} > 0$, from the Hamiltonian (1) [77]. With increase in the intensity of the perturbing field, the field will also act on another line of the doublet of nucleus X, as a result of which the central lines of the A doublet increase and approach one another, whereas the outer lines move further apart and decrease. Similar splitting of the lines is also observed in the spectra of more complex spin systems, and Fig. 8 gives in particular a picture of the splitting in spectra of the type AKM. It can be seen from the figure that the local perturbation of only one spectral line of the multiplet (tickling), like the selective decoupling of nuclear spins described above (see Fig. 3), can be used to determine the relative signs of spin-spin coupling constants. Arguments analogous to those used to explain Fig. 3 lead to the conclusion that in styrenimine (upper part of Fig. 8) the signs of the geminal and vicinal coupling constants are the same, whereas in styrene sulfide (lower part of Fig. 8) they are opposed [367]. If the relative signs of J are known, we can readily construct diagrams showing the positions of the energy levels and the transitions between them, which are necessary for an accurate iterational analysis of the complex spectra [86, 96, 261, 313]. Diagrams giving the positions of the energy levels for different relative signs of the coupling constants are given in Fig. 9. Tickling provides the chief method for the construction of the diagrams [78] and for the interpretation of the complex spectra of closely coupled spins. In degenerate systems, splitting into a larger number of components is observed [65, 78].

Tickling is always accompanied by a change in the intensities of the spectral lines. Comparison of the populations of the energy levels of the perturbed line leads to a decrease in this difference for the line $\Lambda = 0$ and to an increase in this difference for the line $\Lambda = 2$ (Fig. 10). This nuclear Overhauser effect is observed in all experiments on nuclear magnetic double resonance, so long as $\gamma_X{}^2 H_2{}^2 T_1 H_2{}^* > 1$. The first estimates of the importance of this effect [29] were apparently inaccurate.

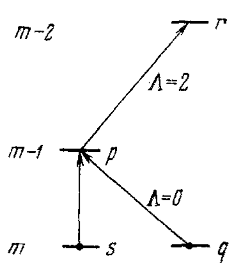

Fig. 10.

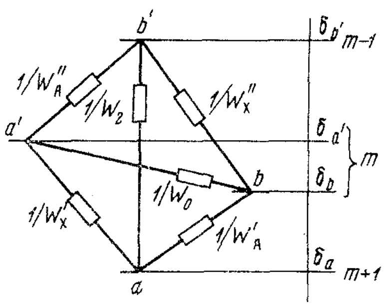

Fig. 11.

Fig. 10. Diagram of energy levels in an experiment on transition selective irradiation.

Fig. 11. Electrical analog of a two-spin system.

The intensity of a spectral line (p→r) in the NMR spectrum is proportional to the difference in the populations $(\sigma_p - \sigma_r)$ for these levels

$$L_{rp} = \gamma_A H_1 |\langle p | I_+(A) | r \rangle|^2 (\sigma_p - \sigma_r). \tag{7}$$

If the energy levels are arranged as in Fig. 10, saturation of the transition s→p leads to an increase in the intensity of the rp line and a decrease in the intensity of the pq line by approximately 50% in nondegenerate systems [87]. Since it is often possible for the conditions $\gamma_X{}^2 H_2{}^2 T_1 T_2{}^* \gg 1$ and $\gamma_X H_2 < 2/T_2{}^*$ to be satisfied simultaneously, the Overhauser effect may be observed without significant change in the wave functions, energy levels, and frequencies of the spectral lines of the perturbed spin system. Saturation or inversion of the populations on the rapid adiabatic passage of one line of the spectrum of the system AX leads to the almost instantaneous appearance of new differences in the populations different from those for thermal equilibrium, for transitions which have energy levels in common with the perturbed line. The populations of other levels acquire new values more slowly, as a result of the action of longitudinal relaxation. This difference in the rate of establishment of differences in the populations, on which the intensity of the NMR signal depends, in accordance with formula (7), forms the basis of the method of transitory selective saturation (TSS) [233] for determining the relative signs of spin-spin coupling constants and for constructing energy level diagrams.

The more effective the longitudinal relaxation, i.e., the greater the probability of relaxation transitions, the more rapidly the new equilibrium is established in the complete spin system. Longitudinal relaxation is similar to electrical conductivity in a galvanic circuit, in which the electric potentials are the analogs of the populations. If the system is linear, and the probabilities of the relaxation transitions are independent of the strength of the perturbed field (as is usually the case in liquids in the absence of chemical exchange), the analogy with electrical circuits is complete and the change in the populations is described by Kirchoff's Eqs. [37]. Figure 11 shows the electrical analog of a two-spin system, which gives correctly the dependence of the stationary states on the intensity of the perturbation and the specific values of the probabilities of the relaxation transitions W. To obtain a model of the dynamics of the process it is necessary to include capacities in the scheme [578]. It follows from Figs. 9, 10, and 11 that the magnitude and sign of the Overhauser effect depend on the relaxation mechanisms, which determine the relative values of W. From Kirchoff's laws it follows that if W_0, $W_2 \neq 0$, the greatest stationary effect will be observed on the lines which have an energy level in common with the perturbing line, and the sign of the effect depends on the nature of the transition (the position of the transition on the energy level diagram). The nuclear Overhauser effect is used to establish the mutual arrangement of the energy levels [87-90] and also to determine the relative probabilities of the transition [49, 57, 598]. Moreover, the intermolecular Overhauser effect can be used to study the microstructure of solutions of organic compounds [99]. The Overhauser effect in ethyl cinnamate is shown in Fig. 12.

3. Theory of Nuclear Magnetic Double Resonance

The qualitative description of the observed effects given above cannot serve as a theory of these phenomena and cannot give quantitative answers. The experimentally observed ordinary NMR spectra of liquids, and also the influence of a perturbing hf-field on these spin systems, are effectively described by the dynamic theory of nuclear

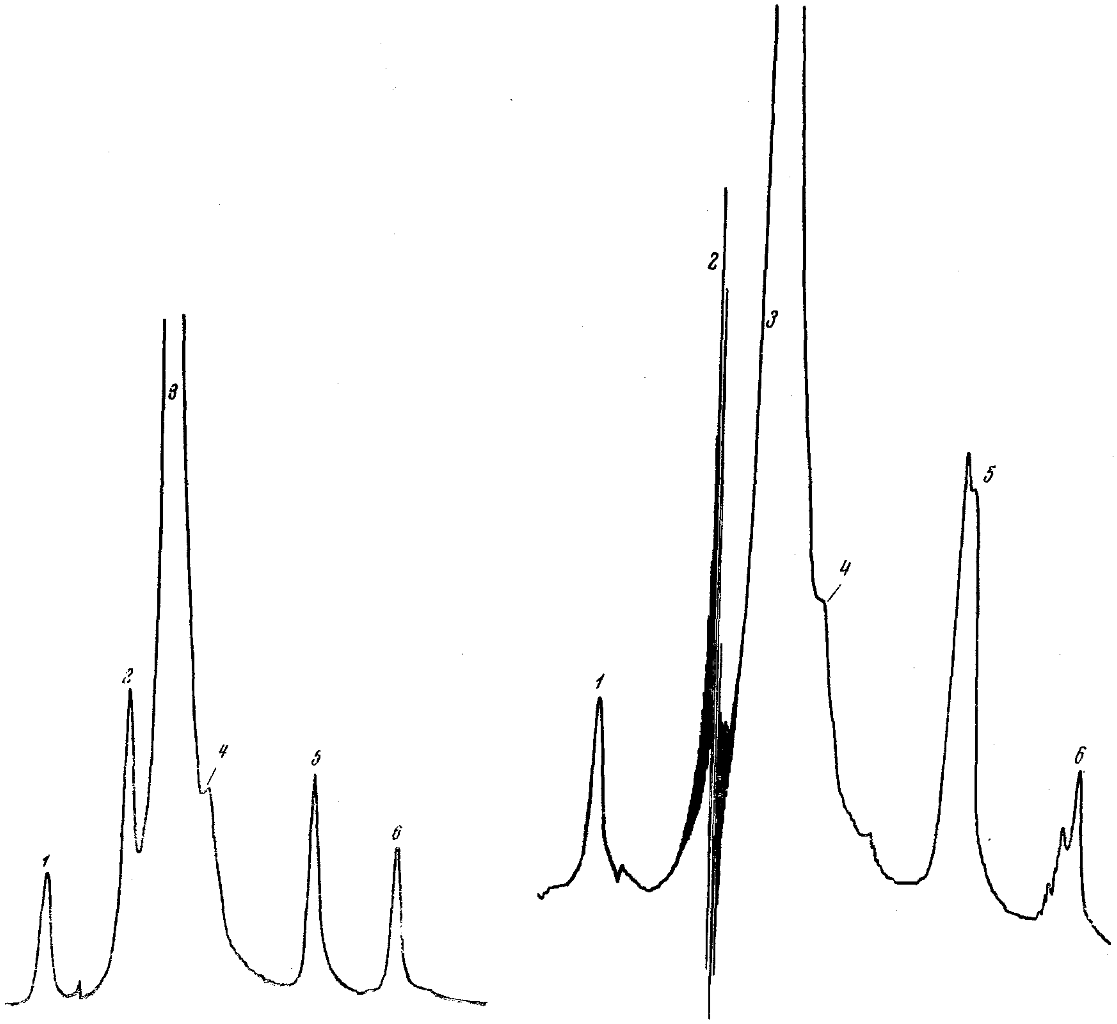

Fig. 12. Nuclear Overhauser effect in ethyl cinnamate: the single resonance spectrum is shown on the left; lines 1, 2, 5, and 6 correspond to a system AB of unsaturated protons; the perturbation of line 2 is shown on right; the intensity of line $\Lambda = 2$ (5) increases and that of the line $\Lambda = 0$ (6) decreases [93].

induction [1, 13-15, 36-39], which provides a systematic description of the behavior of all components of the macroscopic nuclear magnetization M and the changes which they undergo with time as a result of the action of relaxation processes.

3.1. The NMR Signal. The NMR signal depends on the components of the magnetization rotating in the xy plane. If a substance is acted by a constant magnetic field H_0, directed along the z axis, and a linearly oscillating hf-field with amplitude $2\gamma H$, so that

$$\begin{aligned} H_x &= 2H_1 \cos \omega_1 t + 2H_2 \cos \omega_2 t, \\ H_y &= 0, \\ H_z &= H_0, \end{aligned} \tag{8}$$

and the gyromagnetic ration of the perturbed spin $\gamma_X < 0$, this spin can be in resonance only with the component of the hf-field rotating about the z axis with an angular velocity $-\omega$. We then have

$$H = H_0 \mathbf{k} + (H_1 \cos \omega_1 t + H_2 \cos \omega_2 t)\mathbf{i} - (H_1 \sin \omega_1 t + H_2 \sin \omega_2 t)\mathbf{j}. \tag{9}$$

The oscillating components of the magnetization M_X and My and the corresponding rotating components v and u are represented in Fig. 13. The rotating components v and u are of particular importance, since it is these components which are measured by the phase detectors of NMR spectrometers; v is proportional to the absorption signal, and u is proportional to the dispersion signal [2]. In this sense even a simple diode detector is a phase detector and requires for correct operation a slight unbalance in the measuring unit, i.e., the base signal. From the geometry of Fig. 13 it follows [2, 11] that

$$\mathcal{M}_x = u \cos \omega_1 t - v \sin \omega_1 t, \tag{10}$$

$$\mathcal{M}_y = -u \sin \omega_1 t - v \cos \omega_1 t. \tag{11}$$

In Fig. 13, u is positive, so that the measuring frequency is slightly lower than the resonance frequency $\omega_1 < \gamma_A H_0$.

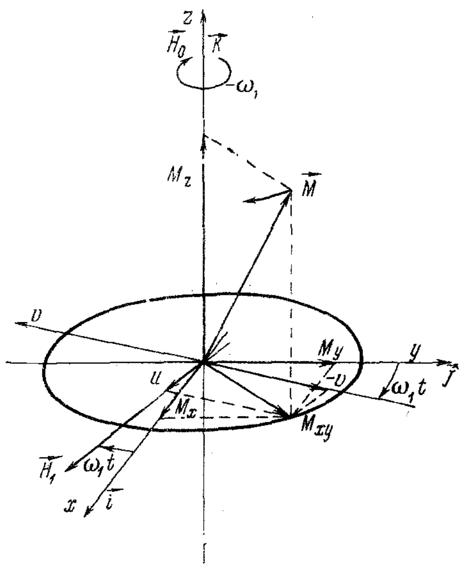

Fig. 13. Motion of the nuclear magnetization vector M.

In all experiments on double resonance, the only important measured quantity is the component of the absorption of the signal of the nuclear induction L, which is measured through M_y, if crossed coils are used and the perturbing fields are applied to the coil orientated along the x axis:

$$L = -k \frac{d}{dt} \mathcal{M}_y = k \mathcal{M}_x = k(u \cos \omega_1 t - v \sin \omega_1 t), \tag{12}$$

where all the factors associated with the apparatus are included in the instrument constant k. If the detection is carried out at a frequency ω_1, the nature of the signal obtained (u or v) depends on the choice of base voltage phase. These rotating components can be expressed by formula (19) in terms of the trace of the density matrix σ for the spin system being studied. In rotating coordinates we have

$$u = \mathrm{Sp}\,[\tilde{\sigma} M_x] \text{ and } v = \mathrm{Sp}\,[\tilde{\sigma} M_y], \tag{13}$$

where

$$M_\pm = M_x \pm i M_y = \hbar N \sum_i \gamma_i I_\pm(i) = \hbar N \sum_i \gamma_i [I_x(i) \pm i I_y(i)]. \tag{14}$$

If we take as basis the eigenfunctions a, a', of the Hamiltonian $\mathcal{H}_0$, the components of the signal corresponding to the transition a→a', for a' > a, are equal to

$$\begin{aligned} u_{a'a} &= \mathrm{Re}\,\{\langle a|\tilde{\sigma}|a'\rangle \times \langle a'|M_-|a\rangle\} = \mathrm{Re}\,\{\langle a'|\tilde{\sigma}|a\rangle \times \langle a|M_+|a'\rangle\}, \\ v_{a'a} &= -\mathrm{Im}\,\{\langle a|\tilde{\sigma}|a'\rangle \times \langle a'|M_-|a\rangle\} = -\mathrm{Im}\,\{\langle a'|\tilde{\sigma}|a\rangle \times \langle a|M_+|a'\rangle\}, \end{aligned} \tag{15}$$

and in order to obtain the complete spectrum it is necessary to take the sum of all the transitions

$$v = \sum_{a<a'} \sum v_{a'a}.$$

In a slightly different form [53, 55]

$$L = -k \frac{d}{dt} M_y = -k' \frac{d}{dt} \sum_i \gamma_i \langle I_y(i) \rangle = -\frac{k'}{2i} \frac{d}{dt} \sum_i \gamma_i \, \mathrm{Sp}\,[I_+(i)\sigma - I_-(i)\sigma]. \tag{16}$$

From the properties of the operators I_+, I_- and the trace, it follows that the magnitude of the measured signal depends on the nondiagonal elements of the density matrix σ. The fundamental problem of the dynamic theory is to find the dependence of the density matrix of the spin system on the properties of the substance and the conditions of the experiment.

3.2. The Density Matrix. If we have a set of N identical noninteracting systems, where N is the number of molecules in unit volume, and ψ^k the wave function of the system k, where k = 1.2, ..., N, and if each ψ^k can be represented by a complete set of orthonormal wave functions, we have

$$\psi^k = \sum_n c_n{}^k \phi_n. \tag{17}$$

The average value of the operator A in the system is equal to

$$A_k = \int \psi^{k*} A \psi^k d\tau, \tag{18}$$

and the average taken over the random set, which is the quantity in which we are interested, has the form

$$\langle A\rangle = \frac{1}{N}\sum_k A_k = \frac{1}{N}\sum_k \int \psi^{k*} A \psi^k d\tau = \frac{1}{N}\sum_k \sum_{m,n} c_m{}^{k*} c_n{}^k A_{mn}$$
$$= \sum_{m,n} A_{mn}\rho_{nm} = \mathrm{Sp}\,[A\rho] = \mathrm{Sp}\,[\rho A], \tag{19}$$

where the trace Sp is the diagonal sum, $A_{mn} = \int \phi_m{}^* A \phi_n d\tau$, $\rho_{mn} = \frac{1}{N}\sum_k c_n{}^{k*} c_m{}^k$, a $\langle A\rangle$ and <A> includes a twofold averaging—with respect to state and with respect to the set. The quantities $\rho_{mn} = \rho^*{}_{nm}$ are the matrix elements of the density matrix ρ and can be used to find the average values of the operators A acting on the wave functions ϕ_n over the set. The diagonal element ρ_{nn} gives the probability of finding one of the systems of the set in the state n at moment of time t. ρ can also readily be used to describe the change in <A> with time. From the Schrodinger equation

$$i\hbar \frac{d\psi^k}{dt} = \mathcal{H}\psi^k \tag{20}$$

we obtain in the ϕ_n representation:

$$i\hbar \dot{c}_n{}^k = \sum_l \mathcal{H}_{nl} c_l{}^k, \text{ where } \mathcal{H}_{nl} \equiv \langle n | \mathcal{H} | l\rangle = \int \phi_n{}^* \mathcal{H} \phi_l d\tau$$
$$i\hbar\dot{\rho}_{mn} = \sum_l (\mathcal{H}_{ml}\rho_{ln} - \rho_{ml}\mathcal{H}_{ln}),$$

or, in more compact form, if we express the Hamiltonian in units of $\hbar$

$$\frac{d\rho}{dt} = -i\,[\mathcal{H}, \rho]. \tag{21}$$

This equation of motion is similar to the Schrodinger equation; it describes the evolution with time of the quantum system being studied and makes it possible to formulate the required relationships clearly and simply [20, 34, 35, 94]. The formalism of the density matrix is widely used in the analysis of NMDR phenomena [1, 13-15, 32-57, 291].

3.3 The Kinetic Equation. In nuclear resonance, σ usually denotes the density matrix of the spin system, and ρ the density matrix describing the state of the spin system together with the lattice.

As a result of the very high heat capacity of the lattice, its state does not depend on the state of the spin system, and the lattice is always in thermal equilibrium. The fact that the equilibrium of the lattice remains unchanged is effectively illustrated by the unsuccessful attempts to detect nuclear resonance by thermal methods. The distribution of the populations of its states f is described by the Boltzmann factor

$$P(f)=\frac{e^{-hf/kT}}{\sum\limits_{f'}e^{-hf'/kT}}. \tag{22}$$

The density matrix of the spin system σ depends on the states of the lattice, and the two matrices are related by the simple expression

$$\rho(t)=P(f)\sigma(t) \tag{23}$$

or in the matrix elements

$$\langle gf|\rho(t)|g'f'\rangle=\langle g|\sigma(t)|g'\rangle P(f)\sigma_{ff'}. \tag{24}$$

It follows from (23) that the state of a spin system can be represented in terms of the matrix elements $<g|\sigma|g'>$, which also appear in the formula for the measured signal (15) and (16). The diagonal elements are proportional to the populations of the states σ_g, and the nondiagonal elements $\sigma_{g'g}$ are equal to zero for the case of thermal equilibrium of the spin system, but differ from zero in the recording of the spectrum if the resonance hf-field at a frequency $\omega = g'-g$ leads to the appearance of the matrix element $\sigma_{g'g}$. The density matrix of the spin system can be represented as the sum of the time-independent diagonal matrix σ_0, which describes the thermal-equilibrium state of the system, and the deviation matrix χ, which takes account of the departure from the equilibrium state under the influence of a strong perturbing hf-field H_2 and relaxation processes

$$\sigma=\sigma_0+\chi, \tag{25}$$

where $\mathrm{Sp}\,\sigma = 1$ and $\mathrm{Sp}\,\chi = 0$.

To take account of the influence of the weak measuring hf-field H_1 and the corresponding departure from the new equilibrium produced under the influence of H_0 and H_2, use is made of the deviation matrix η.

In this case

$$\sigma=\sigma_0+\chi+\eta. \tag{26}$$

The elements of the matrices σ, χ, and η are time-dependent, but for the sake of brevity we shall subsequently use, instead of $\sigma(t)$, the symbols adopted in (25) and (26). Since in a representation where $\mathcal{H}_0$ is diagonal the matrix σ_0 is diagonal by definition, the observed signal can depend only on the matrices χ and η. It follows from (25) that $\sigma_{g'g} = \chi_{g'g}$. If the values and time-dependence of all the elements of the matrices χ and η of the spin system being studied are known, the spectrum of this system is also known in all details. The chief task of the dynamic theory is to find the dependence of the matrices χ and η on the conditions of the experiment, on the basis of the equation of motion (21). In order to derive this kinetic equation we shall start from the Hamiltonian $\mathcal{H}$, which in units of $\hbar$ has the form

$$\mathcal{H}=E(s,t)+F(f)+G(s,f). \tag{27}$$

Here $E(s, t)$ is the Hamiltonian of the spin system (dynamic subsystem), $F(f)$ the Hamiltonian of the lattice (dissipative subsystem), and $\hbar G(s, f)$ the energy of the interaction of the spin system with the lattice. $G(s, f)$ is defined as an operator with zero trace, and first- and second-order corrections for the energy of the spin system from interaction with the lattice (electrons)—the chemical shift and the energy of the spin-spin interaction—are included in the energy of the spin system ħE(s, t) [37, 38, 42]. Since the coordinates of the lattice f are time-dependent, the operator G(s, f) may be represented as a time-dependent perturbation (G(s, t). This approach is adopted in Redfield's theory [21]. Since F ≫ E + G, the matrix ρ is always diagonal relative to the states of the dissipative subsystems, but may be nondiagonal with respect to the spin system. Thus

$$\sigma(s, t) = \mathrm{Sp}_f\,[\rho(f, s, t)]. \tag{28}$$

The change in the matrix σ(s, t) with time is determined by the interaction of the dynamic subsystem with the external magnetic field (8) and the lattice G. The latter interaction can be taken into account on the basis of quantum theory as G(s, f) [1, 13-15, 36-39] or, semiclassically, by means of an arbitrary perturbation G(s, t), different for each system of the set [1, 21, 55]. The two approaches are practically equivalent [42], but when the first version is used the physical processes of relaxation are extremely clearly seen; the practical calculations are very complex, however, as a result of which the second method is usually preferred [21, 32, 54, 55].

Equation (21) is usually solved by means of first-order and second-order perturbation theory [20, 15], using a representation of the interaction [15] in which only the slow change in the density matrix σ is preserved, while the rapid motion resulting from E(s, t) is eliminated; in this way the condition for applicability of perturbation theory—smallness of the perturbation—is satisfied [15, 36, 37, 42]. The irreversibility of the process is achieved by the absence of change in the state of the dissipative subsystem. In the time interval Δt = t−0 there is a change in the state of the spin system according to Eq. (21), after which the influence of the lattice is "included," and this restores the equilibrium state of the dynamic subsystem without change in its state. In the limit t→0 we obtain the differential equation of motion for σ. The time interval t should be long compared with the molecular motion correlation time τ_c, in order that the time interval t be sufficient for a causal change in σ to be established under the influence of G(s, t), but shorter than the Larmor period and the relaxation time T of the nuclear spin. This method of deriving the kinetic equation is not justified for the case of the large correlation times which are produced by chemical exchange and scalar relaxation [1]. The theory of these phenomena is still in the initial stage of development [43-45]. In spite of this, the kinetic equation is in fact also applicable even in these cases [21, 420, 444, 448]. For another method of deriving the kinetic equation, see [45].

To convert to the representation of the interaction it is necessary to carry out a unitary transformation over all $\mathcal{H}$ operators

$$G^*(t) = U(t)\,e^{iFt}G(s, f)\,e^{-iFt}U^{-1}(t), \tag{29}$$

$$\rho^*(t) = U(t)\,e^{iFt}\rho(s, f, t)\,e^{-iFt}U^{-1}(t), \tag{30}$$

$$\sigma^*(t) = U(t)\sigma U^{-1}(t), \tag{31}$$

where account has been taken of the fact that [F, σ] = 0.

The transformation operator U(t) [1, 13-15, 21, 38, 42, 91] satisfies the equations

$$\frac{dU(t)}{dt} = iU(t)E(t) \quad \text{и} \quad \frac{dU^{-1}(t)}{dt} = -iE(t)U^{-1}(t); \tag{32}$$
$$U(t_0, t_0) = 1; \qquad U(t, 0) = U(t); \qquad U(t)U(t-\tau, t) = U(t-\tau).$$

The equation of motion (21) in the representation of the interaction acquires the form

$$\frac{d\rho^*(t)}{dt} = -i\,[G^*(t), \rho^*(t)]. \tag{33}$$

This equation describes the slow change in ρ* (t) under the influence of only relaxation processes. If ρ* (t) at moment of time T' = 0 is known, its new value at moment of time t' + t can be written in the form of series [38] whose first two terms acquire the form

$$\frac{d\rho^*(t)}{dt} = -i[G^*(t), \rho^*(0)] - \int_0^t [G^*(t), [G^*(t-\tau), \rho^*(t)]]\, d\tau. \tag{34}$$

$G^*(t)$ is a random operator, which correlates only with itself, so that in the determination of the average density matrix of the spin system $\langle\sigma^*\rangle$ its influence is significant only in the second term

$$\frac{d\langle\sigma^*\rangle}{dt} = -\left\langle \mathrm{Sp}_f\left\{ \int_0^t [G^*(t), [G^*(t-\tau), P(f)\sigma^*(t)]]\, d\tau \right\}\right\rangle. \tag{35}$$

Subsequently, the sign for averaging over the set is not used, but σ^* is an averaged value

$$\frac{d\sigma^*}{dt} = -\mathrm{Sp}_f\left\{ U(t)\left[\frac{1}{2}\int_{-\infty}^{+\infty} [G(t), [U(t-\tau, t)G(t-\tau)U^{-1}(t-\tau, t), P(f)\sigma(t)]]\, d\tau\right]U^{-1}(t)\right\}. \tag{36}$$

To simplify the analysis, the limits of integration have been extended; this has no influence on the magnitude of the integral if $\tau_c \ll t$ [1]. If in addition we restrict ourselves to the case where according to [48]

$$E(t) = \mathcal{H}_0 + \mathcal{H}_2(t);\ \mathcal{H}_0 \gg \mathcal{H}_2(t) \text{ and } |\mathcal{H}_0|\,\tau_c \ll 1, \tag{37}$$

strong contraction takes place [1] and $U(t-\tau, t) \cong e^{-i\mathcal{H}_0\tau} \cong 1$. In this case the interaction of $\mathcal{H}_2(t)$ with the perturbing field H_2 has disappeared from Eq. (36), so that the relaxation times of the perturbed line are independent of its irradiation by a strong hf-field. The condition for strong contraction $|\mathcal{H}_0|\tau_c \ll 1$ in liquids is practically always satisfied in the absence of chemical exchange and strong scalar relaxation. Exceptions are found in nitrogen compounds, but halogens do not break down the condition $|\mathcal{H}|\tau_c \ll 1$.

The high-temperature approximation $\hbar\mathcal{H}_0/kT \ll 1$ simplifies the calculation of the trace ([1], p. 269) and gives

$$\frac{d\sigma^*}{dt} = -\frac{1}{2}U(t)\left\{\int_{-\infty}^{+\infty} [G(t), [G(t-\tau), \sigma - \sigma_0]]\, d\tau\right\}U^{-1}(t), \tag{38}$$

where in order to obtain a Boltzmann distribution of the populations of the energy levels of the spin system it is necessary to write $\sigma \rightarrow (\sigma - \sigma_0)$ even in the high-temperature approximation. This replacement does not follow naturally from the theory ([21], p. 1), but is a consequence of the fact that semiclassical examination of the lattice through $G(t)$ requires the replacement $\hbar \rightarrow 0$ in $\hbar f/kT$, which is equivalent to the requirement $T \rightarrow \infty$ [38]. It should be noted that $\sigma_0^* = \sigma_0$.

By applying the reverse transformation to (31) and taking account of the fact that as a good approximation the correlation function can be represented [55] in the form

$$\langle G(t)G(t-\tau)\rangle = \langle |G(t)|^2\rangle e^{-\frac{|\tau|}{\tau_c}}, \tag{39}$$

we obtain, after integration with respect to τ [1, 55]

$$\frac{d\sigma}{dt} = -i[E(t), \sigma] - \langle\tau_c[G(t), [G(t), \sigma - \sigma_0]]\rangle. \tag{40}$$

σ_0 is often given in the form

$$\sigma_0 \cong \frac{1}{A}\left[1-\frac{\hbar\mathcal{H}_0}{kT}\right]=\frac{1}{A}-q\mathcal{H}_0, \tag{41}$$

$$\text{where}\quad q=\frac{\hbar}{AkT} \tag{42}$$

and A is the number of $\mathcal{H}_0$ eigenfunctions. If $E(t) = \mathcal{H}_0 = -\omega_A I_z(A)$ and $G(t) = 0$, it follows from (40) that the motion of σ (and the magnetization) is a precession about the z axis with angular frequency ω_A. In the matrix elements

$$\frac{d\sigma_{aa'}}{dt}=i(a'-a)\sigma_{aa'}. \tag{43}$$

In the representation of the interaction this motion is absent by definition. From this it can be seen that the operator

$$U(t)=e^{-i\omega_A I_z(A)t}=T \tag{44}$$

denotes the transition to coordinates rotating about the z axis with frequency $-\omega_A$. These rotation operators are defined in terms of a Taylor series [13]. From the above it also follows that for the case of strong contraction the operator T does not alter the relaxation term [55]. In the presence of particularly strong perturbing fields, when $\mathcal{H}_0 \cong \mathcal{H}_2(t)$, it is expedient to give G(t) in the form of the sum

$$G(t)=\sum_r G^r e^{i\omega_r t},$$

which even in the simple case of a single spin of $^1/_2$ leads to five relaxation coefficients [38, 42]. Since nevertheless we usually have $\mathcal{H}_0 \gg H_2(t)$, there is no need to use these complicated theories. Even in a weak field at sonic frequencies, an effective qualitative description of the decoupling of the spins is provided by the ordinary theory [175].

In Redfield's theory, the approximations (39) are not made, it is assumed in (36) that $U(t-\tau, t) = e^{-i\mathcal{H}_0\tau}$, and after the reverse transformation from the representation of the interaction to the Schrodinger representation, opening of the double commutator, and integration, the relaxation term Γ of the kinetic equation can be written in terms of the spectral densities $J_{aba'b'}$ of the autocorrelation functions $G_{aba'b'}$. In the basis a, a', where $\mathcal{H}_0$ is diagonal, i.e.

$$\mathcal{H}_0\,|\,a\rangle = a\,|\,a\rangle, \tag{45}$$

we obtain

$$G_{aba'b'}=\langle\langle a|G(t)|b\rangle\times a'|G(t-\tau|b'\rangle^*\rangle; \tag{46}$$

$$J_{aba'b'}(a'-b')=\int_{-\infty}^{+\infty}G_{aba'b'}e^{-i(a'-b')\tau}\,d\tau, \tag{47}$$

where $\langle a'|G(t-\tau)|b'\rangle^* = \langle b'|G(t-\tau)|a'\rangle$.

Naturally, the greater the autocorrelation of the operator for the interaction of the spin system with the lattice in time τ, the greater the high-frequency power at a frequency (a'-b'), which is the reason for the relaxation transitions.

For the action of two hf-fields on the spin system, we have

$$E(t)=\mathcal{H}_0+\mathcal{H}_2(t)+\mathcal{H}_1(t), \tag{48}$$

where $\mathcal{H}_2(t)$ is the Hamiltonian for the interaction with a strong perturbing hf-field H_2, and $\mathcal{H}_1(t)$ is the Hamiltonian for the interaction with the measuring hf-field H_1. If $\mathcal{H} \gg \mathcal{H}_2(t)$, $\mathcal{H}_1(t)$, we obtain from (38) in matrix elements for the basis a, a'

$$\frac{d\sigma^*}{dt} = \sum_{bb'} R_{aa'bb'} e^{i[(a'-a')-(b-b')]t} (\sigma^* - \sigma_0)_{bb'}, \tag{49}$$

where

$$\begin{aligned} R_{aa'bb'} &= \frac{1}{2} J_{aba'b'}(a'-b') + \frac{1}{2} J_{aba'b'}(a-b) \\ &- \delta_{a'b'} \sum_c \frac{1}{2} J_{cbca}(c-a) - \delta_{ab} \sum_c \frac{1}{2} J_{ca'cb'}(c-b'), \end{aligned} \tag{50}$$

and the time dependence has arisen as a result of the action of the operator U. Since the time-dependent terms in (49) are related to two simultaneous transitions at different frequencies (a-a') and b-b'), their influence in the absence of overlapping lines is negligible [21]. We can refer to the experimental fact that relaxation can never be the reason for the production of coherence [1], and require that (a-a') = (b-b'). In this case Eq. (38) can be written in the general form

$$\frac{d\sigma}{dt} = -i[\mathcal{H}_0 + \mathcal{H}_2(t) + \mathcal{H}_1(t), \sigma] - \Gamma(\sigma - \sigma_0), \tag{51}$$

where

$$\Gamma(\sigma - \sigma_0)_{aa'} = -\sum_{bb'} R_{aa'bb'} (\sigma - \sigma_0)_{bb'}$$

In addition to formula (46) and (47), the approximations (39) and (40) are often used to calculate the relaxation term. From (46) and (39) we obtain

$$\langle\langle a|G(t)|b \times a'|G(t-\tau)|b'\rangle^*\rangle = \langle\langle a|G(t)|b \times a'|G(t)|b'\rangle^*\rangle\, e^{-|\tau|/\tau_c}.$$

The corresponding spectral densities are expressed through the Fourier transformations (47)

$$J_{aba'b'}(a'-b') = \frac{2\tau_c}{1+(a'-b')^2\tau_c^2} \langle\langle a|G(t)|b\rangle \langle a'|G(t)|b'\rangle^*\rangle,$$

and under conditions of strong contraction, when $\omega_{a'b'}\tau_c \ll 1$,

$$J_{aba'b'}(a'-b') = \langle\langle a|G(t)|b \times a'|G(t)|b'\rangle^*\rangle\, 2\tau_c. \tag{52}$$

This formula is widely used in specific calculations [32, 53-55] to find the spectral densities corresponding to different relaxation mechanisms. In the calculations it is expedient to take G(t) in the form [1, 55]

$$G(t) = \sum_q F^{(q)} A^{(q)}, \tag{53}$$

where $F^{(q)}$ is a random function of time, and $A^{(q)}$ an irreducible operator of the spin system. By making use of (39) and (52), we obtain, without taking account of cross terms,

$$J_{aba'b'} = 2\tau_c \sum_q \langle |F^{(q)}|^2 \times a|A^{(q)}|b \times a'|A^{(q)}|b'\rangle. \tag{54}$$

The G(t) functions for various relaxation mechanisms are given in Abragam's monograph [1] and in connection with applications in NMDR in [37] and [95]. The relaxation of a single spin under the influence of an external isotropic stochastic field is discussed in [53, 55], the relaxation in a two-spin system AX for the case of a noncorrelated external interaction is discussed in [32, 54], and correlated interaction and intramolecular dipole-dipole interaction are discussed in [32]. All these applications of the theory of nuclear spin relaxation are related to the calculation of the intensities of the spectral lines in NMDR spectra.

Bloch [37] showed that the relaxation matrix Γ acquires a particularly simple form if we have a spin system with nondegenerate states and without equal differences between the energy levels (nondegenerate system). This approximation is assumed in many papers [46, 53]. In this case

$$\Gamma(\sigma - \sigma_0)_{aa'} = -R_{aa'aa'}(\sigma - \sigma_0)_{aa'} = \frac{1}{T_{2aa'}}(\sigma - \sigma_0)_{aa'}, \tag{55}$$

$$\begin{aligned}\Gamma(\sigma - \sigma_0)_{aa} &= -\sum_b R_{aabb}(\sigma - \sigma_0)_{bb} = \sum_b W_{ab}(\sigma - \sigma_0)_{aa} - \sum_b W_{ba}(\sigma - \sigma_0)_{bb} \\ &\cong \sum_b W_{ab}\,[(\sigma - \sigma_0)_{aa} - (\sigma - \sigma_0)_{bb}].\end{aligned} \tag{56}$$

The width of the spectral line $1/\pi T_{2aa'}$ is expressed in terms of the nondiagonal element of the matrix R, and we obtain from (50)

$$\begin{aligned}R_{aa'aa'} &= J_{aaa'a'}(0) - \frac{1}{2}\sum_c \{J_{caca}(c - a) + J_{ca'ca'}(c - a')\} \\ &= J_{aaa'a'}(0) - {}^1/_2 \sum_c (W_{ac} + W_{a'c}).\end{aligned} \tag{57}$$

$R_{aa'aa'}$ is the sum of all the probabilities of transition from level a and level a' to any other energy levels of the spin system, so that it coincides with the transverse relaxation time.

The diagonal elements of the matrix R describe the process of longitudinal relaxation in the spin system. The probability of transition between the energy levels b and a is equal to

$$W_{ba} \cong W_{ab} = J_{abab}(a - b). \tag{58}$$

The quantity

$$-R_{aaaa} = \sum_b R_{bbaa} = \sum_b W_{ba} \tag{59}$$

reflects the overall rate of decrease in the population of the energy level a, and is thus equal to the reciprocal of the lifetime of this state.

3.4. Nuclear Overhauser Effect for the Action of a Weak Perturbing hf-Field. A perturbing hf-field is weak if condition (6) is satisfied. By expressing (51) in terms of the deviation matrix χ (25), we obtain

$$\frac{d\chi}{dt} = -i\,[\mathcal{H}_0 + \mathcal{H}_2(t) + \mathcal{H}_1(t), \sigma] - \Gamma(\chi). \tag{60}$$

In Baldeschwieler's notation [51, 52], where the amplitudes of the components of the magnetic field (8) are expressed in Hz, i.e.,

$$v_{0i} = -\frac{\gamma_i H_0}{2\pi}, \quad v_{2i} = -\frac{\gamma_i H_2}{2\pi}, \quad v_{1i} = -\frac{\gamma_i H_1}{2\pi}, \tag{61}$$

the Hamiltonian for a spin system of the type AB (1) acquires the form

$$\mathcal{H}_0 = 2\pi\left\{\sum_i v_{0i} I_z(i) + \sum_{i<j} J_{ij} I(i) I(j)\right\}, \tag{62}$$

and the interactions with the hf-fields are defined by the expressions

$$\mathcal{H}_2(t) = D_{2+} e^{i\omega_2 t} + D_{2-} e^{-i\omega_2 t}, \tag{63}$$

$$\mathcal{H}_1(t) = D_{1+} e^{i\omega_1 t} + D_{1-} e^{-i\omega_1 t}, \tag{64}$$

and

$$D_{k\pm} = \pi \sum_i v_{ki} I_\pm(i), \text{ where } k = 1, 2. \tag{65}$$

In the presence of only one resonance perturbing field H_2, which influences the transition $a'-a = \omega_0$, the diagonal elements of the matrix χ acquire stationary values after the transition process, but the nondiagonal elements show a periodic time dependence [37]. If $a' > a$,

$$\langle a|\chi|a\rangle = \chi_{aa} = \text{const}, \tag{66}$$

$$\langle a|\chi|a'\rangle = z_{aa'} e^{i\omega_2 t}, \quad \langle a'|\chi|a\rangle = z_{aa'}^{*} e^{-i\omega_2 t}. \tag{67}$$

From (60), (62) (63), and (41) we obtain

$$\begin{aligned}\frac{d\chi}{dt} &+ i[\mathcal{H}_0, \chi] + i[D_{2+}, \chi] e^{i\omega_2 t} + i[D_{2-}, \chi] e^{-i\omega_2 t} + \Gamma(\chi) \\ &= iq[D_{2+}, \mathcal{H}_0] e^{i\omega_2 t} + iq[D_{2-}, \mathcal{H}_0] e^{-i\omega_2 t}.\end{aligned} \tag{68}$$

To find a stationary solution of Eq. (68) it is necessary to discard $d\chi/dt$ and take the matrix elements for each term of Eq. (68) in the a, a' basis (45) [37, 53]. For the nondiagonal elements we obtain:

$$z_{aa'} = \frac{T_{2aa'} D_{2+aa'} [T_{2aa'}(\omega_2 - \omega_0) + i][q\omega_0 - (\chi_{a'a'} - \chi_{aa})]}{1 + (\omega_2 - \omega_0)^2 T^2_{2aa'}}, \tag{69}$$

$T_{2aa'} = 1/\Gamma_{aa'}$, $D_{2+aa'} = \langle a|D_{2+}|a'\rangle$, $\omega_0 = (a'-a)$. The diagonal elements χ_{aa} are expressed in terms of $z_{aa'}$ and $z^*_{aa'}$ as follows:

$$\begin{aligned}\sum_b W_{ab}(\chi_{aa} - \chi_{bb}) &= -i\{D_{2+aa'} z^*_{aa'} - z_{aa'} D^*_{2+aa'}\} \\ &= -2\,\mathrm{Im}(z_{aa'} D^*_{2+aa'}) = V[q\omega_0 - (\chi_{a'a'} - \chi_{aa})],\end{aligned} \tag{70}$$

where

$$V = \frac{2|D_{2+aa'}|^2 T_{2aa'}}{1 + (\omega_2 - \omega_0)^2 T^2_{2aa'}} \tag{71}$$

and the following system of equations is formed:

$$\begin{aligned}&\sum_b W_{ab}(\chi_{aa}-\chi_{bb})+V[q\omega_0-(\chi_{a'a'}-\chi_{aa})]=0,\\&\sum_b W_{a'b}(\chi_{a'a'}-\chi_{bb})-V[q\omega_0-(\chi_{a'a'}-\chi_{aa})]=0,\\&\sum_b W_{cb}(\chi_{cc}-\chi_{bb})=0,\qquad c\neq a,\,a',\\&\sum_b \chi_{bb}=0.\end{aligned}\tag{72}$$

There is established in the spin system a new equilibrium which is different from the thermal equilibrium and is determined by the relaxation transitions with probability W and the induced transitions a → a' under the influence of the perturbing hf-field with probability of transition $V = |D_{2+aa'}|^2 g(\omega)$, where $g(\omega)$ is a function of the form of the Lorentz line. The establishment processes are not exponential, and the longitudinal relaxation time T_1 does not exist in multispin systems. The system of equations (72) is similar to Kirchoff's laws for an electrical circuit, if it is assumed that W is the conductivity, χ the potential, and $V[q\omega_0-(\chi_{a'a'}-\chi_{aa})]$ the current, and the system can be solved by means of an electrical analog.

The solution of the system of Eq. (72) can be written according to Bloch [37] in the form

$$\chi_{cc}=T_cV[q\omega_0-(\chi_{a'a'}-\chi_{aa})]\tag{73}$$

and the difference in the populations of levels a and a' for saturation acquires the form

$$\chi_{a'a'}-\chi_{aa}=(T_{a'1}-T_{a1})V[q\omega_0-(\chi_{a'a'}-\chi_{aa})],\tag{74}$$

where

$$(T_{a'1}-T_{a1})=T_{a'a1}.\tag{75}$$

$T_{a'a_1}$ has the dimensions of time, but is not the longitudinal relaxation time. From (72), (74), and (75), we have [46, 56]:

$$\begin{aligned}&\sum_b W_{ab}T_{ba1}=1,\\&\sum_b W_{a'b}T_{ba'1}=-1,\\&\sum_b W_{cb}T_{bc1}=0\quad c\neq a,\,a',\\&\sum_b T_b=0.\end{aligned}\tag{76}$$

The difference in the populations of energy levels, on which the intensity of the signal (7) depends, are related to one another. From (73), (74), and (75), it follows that

$$\chi_{b'b'}-\chi_{bb}\,\frac{T_{b'b1}}{T_{a'a1}}\,(\chi_{a'a'}-\chi_{aa}).\tag{77}$$

From (71), (74), and (77), we obtain a formula describing the influence of saturation of the spectral line a'a on the difference in the deviations of the populations of all other energy levels of this spin system

$$\chi_{b'b'} - \chi_{bb} = \frac{T_{b'b1}}{T_{a'a1}} \cdot \frac{2|D_{2+aa'}|^2 T_{2aa'} T_{a'a1} q(a'-a)}{1 + [\omega_2 - (a'-a)^2 T^2_{2aa'} + 2|D_{2+aa'}|^2 T_{2aa'} T_{a'a1}}$$
$$= \frac{T_{b'b1}}{T_{a'a1}} \cdot Sq\,(a'-a). \tag{78}$$

The saturation factor S depends on the amplitude of the saturating field H_2, and with increase in the latter, $S \to 1$. For saturation, when $S \cong 1$, the signal a → a' disappears:

$$\sigma_{aa} - \sigma_{a'a'} = [q(a'-a) - (\chi_{a'a'} - \chi_{aa})] = q(a'-a)[1-S]. \tag{79}$$

The Overhauser effect, consisting of the change in the intensity of the spectral line b → b', is determined for saturation of the line a → a' by the expression [47-49, 56]:

$$O^{a'a}_{b'b} = \frac{I^0_{b'b} - I^{a'a}_{b'b}(0)}{I^o_{b'b}} = \frac{(\sigma_{ob} - \sigma_{ob'}) - (\sigma_b - \sigma_{b'})}{\sigma_{ob} - \sigma_{ob'}} = \frac{\chi_{b'b'} - \chi_{bb}}{\sigma_{ob'} - \sigma_{ob}} = \frac{T_{b'b1}(a'-a)}{T_{a'a1}(b'-b)}. \tag{80}$$

Here $I_{b'b}{}^0$ is the intensity of the line b → b' in the ordinary NMR spectrum in the absence of saturation, and $I^{a'a}_{b'b}(\Delta\omega_2)$ is the intensity of the line b → b' in the double resonance spectrum in the absence of saturation by the measuring field H_1 but with saturation ($S \cong 1$) of the transition a → a' by a perturbing field with frequency difference $\Delta\omega_2$. In a homonuclear system of identical spins we have $|(a'-a)| \cong |(b'-b)|$, and the change in the intensity of the line being studied, with complete saturation of the perturbed line, depends only on the constants T_1 [75]. In a heteronuclear system $(a'-a)/(b'-b) \cong \gamma_A/\gamma_B$, and the formula for the Overhauser effect acquires the form

$$Q^{a'a}_{b'b} \cong \frac{\nu_A T_{b'b1}}{\gamma_B T_{a'a1}}. \tag{81}$$

An increase in the intensity of the line b'b corresponds to a negative value of $O \leq |T_{b'b_1}/T_{a'a_1}| \leq 1$, the homonuclear Overhauser effect cannot be greater than the changes in the intensity of the line being saturated, but this effect can have any sign. Particularly marked changes in the intensities of the lines are observed in the heteronuclear case if we have saturation of spins with a large gyromagnetic ratio. This phenomenon is used to increase the sensitivity of the NMR spectrometry of carbon C^{13} by means of the double resonance $C^{13}-\{H^1\}$. In this case, $\gamma_H/\gamma_C \cong 4$.

In the system of equations (76) the coefficients T_{a_1} take the place of potentials, and it follows from Kirchhoff's law that if in Fig. 11 the line a'a is saturated, we have

$$T_{a'a} + T_{b'a} = T_{b'b} + T_{ba}. \tag{82}$$

Thus if we use the notation for spectral lines adopted in tickling (Fig. 6), we obtain from (80)

$$1 + O_2{}^{a'a} = O_1{}^{a'a} + O_0{}^{a'a}. \tag{83}$$

This relationship can be used to verify experiment, and the measured changes in the intensities of the lines can be used to calculate the relative probabilities of relaxation transitions [49]. The determination of the absolute values of relaxation coefficients requires additional experiments to establish the time scale [56]. After the perturbing hf-field has been removed, the populations of the energy levels of the system begin the process of approach to thermal equilibrium. From (68) and (56) it follows that

$$\frac{d\chi_{aa}}{dt} = \sum_b W_{ab}\chi_{bb}. \tag{84}$$

The change in the matrix elements χ_{aa} with time is described by the sum of a large number of exponents. Comparison of the calculated dynamics of this process with experiment makes it possible to determine the time scale of the process of longitudinal relaxation [56, 57].

From Eqs. (69) and (74) we obtain a formula for the signal of an individual spectral line a → a' in a complex spectrum:

$$u + iv = \mathrm{Sp}\,[\widehat{\chi}M_{+}], \tag{85}$$

$$z_{aa'} = \frac{T_{2aa'}D_{2+aa'}\,[T_{2aa'}(\omega_2 - \omega_0) + i]\,q\omega_0}{1 + (\omega_2 - \omega_0)^2 T^2_{2aa'} + 2|D_{2+aa'}|^2 T_{2aa'}T_{a'a1}}. \tag{86}$$

This expression is equivalent to the solution of Bloch's phenomenological equations, if we take $T_{2aa'} = T_2$; $T_{a'a1} = 2T_1$. By taking account of (14), (41), (61), (65), and (85), we obtain, from (86) formula (7) for the measured signal. The hf-field H_2 is used in this case as a weak measuring field, for which the inequality $2|D_{2+aa'}|^2 T_{2aa'}T_{a'a1} < 1$ must be satisfied.

3.5. Tickling. In the examination of the Overhauser nuclear effect it was assumed that the measuring field H_1 leads to only very slight perturbation of the spin system. Every real field H_1 produces a certain saturation of the lines being studied, but a much more important feature is that in the presence of two hf-fields we are dealing with double resonance and that the change in intensities is accompanied by a change in shape and by the appearance of splitting of the lines. In the case of the action (6) of a weak perturbing hf-field H_2, Eq. (60) is applicable, but Bloch's assumption [37] regarding the time-dependence of the nondiagonal elements of the matrix χ (67) requires refinement. Under these conditions the components of the nondiagonal elements of the matrix χ, with different time-dependence, become important [46], as in the analysis of multiquantum transitions [40]:

$$\overset{(\Lambda)}{\chi}_{aa'} = \overset{(\Lambda)}{z}_{aa'} \cdot e^{i\Lambda\omega_2 t}, \tag{87}$$

where $\Lambda = m_a - m_{a'} = 0, 1, 2, \ldots (2F)$.

The components of the nondiagonal matrix elements $\chi_{aa'}$ with $\Lambda \neq 1$ are different from zero for the perturbation, by hf-fields, of two transitions with a common energy level. Λ corresponds to the total change in the magnetic quantum number m in this two-quantum transition.

In order to solve Eq. (60) under the conditions of a weak perturbing hf-field and weak relaxation, it is convenient to change to coordinates rotating with a frequency $-\omega_2$ about the z axis, but to use as basis functions the same $\mathscr{H}_0$ eigenfunctions (45). In order to change to the new system of coordinates [13, 30, 37, 55] it is necessary to carry out the transformation of all operators of Eq. (60) by the operator T (44). When account is taken of the fact that $F_z = \sum_i I_z(i)$, we obtain

$$T = e^{-iF_z\omega_2 t}. \tag{88}$$

The kinetic equation acquires the form

$$\frac{d\widetilde{\chi}}{dt} + i\,[\mathscr{H}_0 + \omega_2 F_z + \widetilde{\mathscr{H}}_2 + \widetilde{\mathscr{H}}_1(t), \widetilde{\chi}] + \Gamma(\widetilde{\chi}) = -i\,[\widetilde{\mathscr{H}}_2 + \widetilde{\mathscr{H}}_1(t), \sigma_0]. \tag{89}$$

We have

$$\begin{gathered}
\widetilde{\chi} = e^{-iF_z\omega_2 t}\chi e^{iF_z\omega_2 t}, \\
\widetilde{\mathscr{H}}_0 = e^{-iF_z\omega_2 t}\mathscr{H}_0 e^{iF_z\omega_2 t} = \mathscr{H}_0, \ \text{где}\ [\mathscr{H}_0, F_z] = 0, \\
\widetilde{\mathscr{H}}_2 = e^{-iF_z\omega_2 t}\mathscr{H}_2(t)\, e^{iF_z\omega_2 t} = D_{2+} + D_{2-}, \\
\widetilde{\mathscr{H}}_1(t) = e^{-iF_z\omega_2 t}\mathscr{H}_1(t)\, e^{iF_z\omega_2 t} = D_{1+}e^{i\Omega t} + D_{1-}e^{-i\Omega t},
\end{gathered} \tag{90}$$

$$\tilde{\chi} = \tilde{\sigma} - \sigma_0, \tag{91}$$

$$\Omega = \omega_1 - \omega_2, \tag{92}$$

$$\mathscr{H}_0{}^R = \mathscr{H}_0 + \omega_2 F_z + \tilde{\mathscr{H}}_2 = 2\pi \left\{ \sum_i A_i I_z(i) + \sum_{i<j} J_{ij} \mathbf{I}(i) \mathbf{I}(j) + (D_{2+} + D_{2-}) \right\}, \tag{93}$$

$$A_i = v_{0i} + \omega_2 / 2\pi, \tag{94}$$

$$d\tilde{\sigma} / dt = - i \, [\mathscr{H}_0{}^R + \tilde{\mathscr{H}}_1(t), \tilde{\sigma}] - \Gamma(\tilde{\sigma} - \sigma_0). \tag{95}$$

In view of the harmonic time dependence of $\tilde{\mathscr{H}}_1(t)$, it is convenient to represent the stationary solution of Eq. (89) in the form of a series of n harmonics [46]:

$$\tilde{\chi} = \sum \tilde{\chi}_n e^{in\Omega t}, \tag{96}$$

where $\tilde{\chi}_n$ is weakly time dependent.

In accordance with (87), each of these harmonics consists of the components

$$\tilde{\chi}_n = \pi_n + \tilde{\chi}_n^{(0)} + \tilde{\chi}_n^{(1)} + \tilde{\chi}_n^{(2)} + \ldots + \tilde{\chi}_n^{(2F)}, \tag{97}$$

where π_n is a diagonal element of the deviation matrix, and $\tilde{\chi}_n^{(0)}$, $\tilde{\chi}_n^{(1)}$ and $\tilde{\chi}_n^{(2)}$ are the nondiagonal elements corresponding to transitions with different Λ. The signal measured at a frequency $-\omega_1$ is proportional to the element $\tilde{\chi}_1^{(1)}$. The influence of all the other components is only indirect, since they cannot be in resonance with the weak measuring field. The stationary solution of Eq. (89) under conditions of weak perturbation and weak relaxation can be found by calculating the matrix elements, rejecting $d\tilde{\chi}/dt$. The diagonal matrix elements $\tilde{\chi}_n$ are time-independent. Of the nondiagonal elements, the most important are the element $\langle c | \tilde{\chi}_0^{(1)} | c' \rangle$, produced under the influence of the perturbing hf-field H_2 at a frequency $\omega_2 \cong (c' - c)$, where $c' > c$, and the element $\langle d | \tilde{\chi}_1^{(1)} | d' \rangle$, corresponding to the measuring hf-field H_1 at a frequency $\omega_1 \cong (d' - d)$ with an accuracy equal to the line width. The other matrix elements can differ from zero only when the above elements differ from zero and the resonance condition corresponding to this element is also satisfied. The three resonance conditions can be satisfied by the two hf-fields only if the transitions $c \rightarrow c'$ and $d \rightarrow d'$ have one common energy level. This requirement restricts the possible values to $\Lambda = 0, 1, 2$ and $n = 0, 1$. In nondegenerate systems $\chi_1^{(0)}$ and $\tilde{\chi}_1^{(2)}$ may differ from zero; the production of these elements is illustrated in Fig. 14.

In the first case, when the transitions perturbed by the hf-fields H_1 and H_2 do not have common energy levels, only one value is possible, $\Lambda = 1$, $\tilde{\chi}_1^{(0)} = 0$ and $\tilde{\chi}_1^{(2)} = 0$. The matrix element $\tilde{\chi}_1^{(1)}$, which is proportional to the NMR signal, in this case depends only on the difference in the populations $\sigma_d - \sigma_{d'}$, and the field H_2 can influence this transition only through the Overhauser effect. In the other cases, when the values $\Lambda = 0$ and $\Lambda = 2$ are possible in (87), the matrix elements $\tilde{\chi}_1^{(0)} \neq 0$ and $\tilde{\chi}_1^{(2)} \neq 0$ are added. The matrix element $\tilde{\chi}_1^{(1)}$ depends on these elements and on the difference in the populations. The notation $\Lambda = 0$ and $\Lambda = 2$ are the same as those adopted by Freeman and Anders in [78]. All the necessary matrix elements can be obtained from (89) [46], and it is found that

$$\tilde{\chi}_1^{(1)} = f\{\Delta\sigma, \tilde{\chi}_1^{(0)}, \tilde{\chi}_1^{(2)}\}; \quad \tilde{\chi}_1^{(0)} = f\{\tilde{\chi}_1^{(1)}, \tilde{\chi}_0^{(1)}\}; \quad \tilde{\chi}_1^{(2)} = f\{\tilde{\chi}_1^{(1)}, \tilde{\chi}_0^{(1)}\}$$

and $\tilde{\chi}_1^{(1)}$ is expressed in matrix elements in the form of a complex formula; this formula can be written in a form which is the same for all four cases from 2 to 5 (see Fig. 14):

$$\frac{v}{\lambda} = (1 - \tau_1 S) \frac{1 + \dfrac{\nu_1 h^2}{1 + (\varkappa_1 \pm \varkappa_2)^2}}{\left[1 + \dfrac{\nu_1 h^2}{1 + (\varkappa_1 \mp \varkappa_2)^2} \right]^2 + \left[\nu_1 \varkappa_1 - \dfrac{\nu_1 h^2}{1 + (\varkappa_1 \mp \varkappa_2)^2} \right]^2} \mp$$

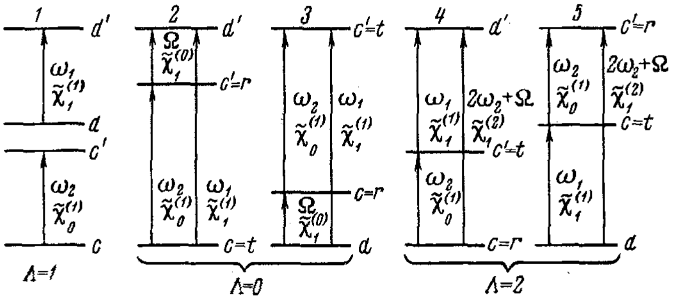

Fig. 14. Forms of arrangement of the energy levels.

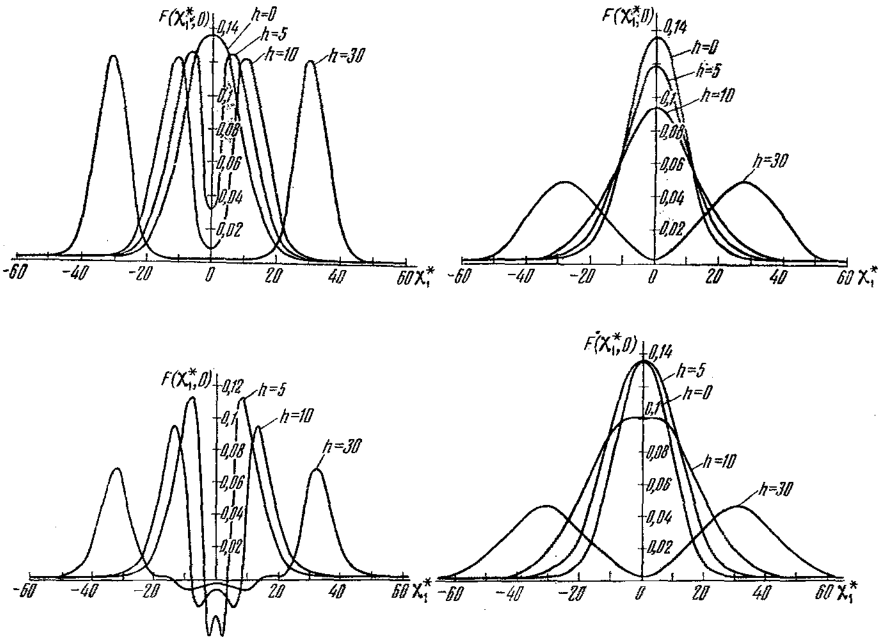

Fig. 15. Tickling: Upper diagram K > 0 (on the left Λ = 0, on the right Λ = 2); lower diagram K < 0 (on the left Λ = 0, on the right Λ = 2) [48].

$$\mp \frac{S\left[1+\nu_1 h^2-\nu_1\varkappa_1(\varkappa_1\mp\varkappa_2)\right]\pm\nu_2\varkappa_2\left[\nu_1\varkappa_1+(\varkappa_1\mp\varkappa_2)\right]}{\tau_2\left[1+\nu_1 h^2-\nu_1\varkappa_1(\varkappa_1\mp\varkappa_2)\right]^2+\left[\nu_1\varkappa_1+(\varkappa_1\mp\varkappa_2)\right]^2}, \qquad (98)$$

where the upper signs correspond to the case where Λ = 0 and the lower signs correspond to the case where Λ = 2, and the following notation is used (applicable to versions 2 and 4 in Fig. 14):

$$v = v_{td'1}$$

$$\lambda = \lambda_{td'} = \langle t|D_{+1}|d' \times d'|M_-|t\rangle T_{2d't}\, q(d'-t)$$

$$h^2 = |\langle c|D_{+2}|c'\rangle|^2 T^2_{2rd'}$$

$$\varkappa_1 = \Delta\omega_1 T_{2rd'} \quad \tau_1 = T_{d't1} / T_{c'c1} \quad \nu_1 = T_{2td'} / T_{2rd'}$$

$$\varkappa_2 = \Delta\omega_2 T_{2rd'} \quad \tau_2 = T_{c'c1} / T_{2rd'} \quad \nu_2 = T_{2cc'} / T_{2rd'} .$$

Versions 3 and 5 require changes in the indices in accordance with Fig. 14. The Overhauser effect is introduced into this formula by means of (78) and it is assumed that in the case of homonuclear tickling, i.e. $|(d'-c)| \cong |(c'-c)|$, the following equation is applicable:

$$\Delta\sigma = (\sigma_c - \sigma_{d'}) = q(d' - c)\left(1 - \frac{T_{d'c1}}{T_{c'c1}} \cdot S\right). \tag{99}$$

The intensity of the measured spectral line is equal to

$$I_{td'}^{cc'}(0) = \lambda_{td'} \int_{-\infty}^{+\infty} g(\xi) \int_{-\infty}^{+\infty} v_{td'}(\Delta^*\omega_1 - \xi, \Delta^*\omega_2 - \xi)\, d(\Delta\omega_1)\, d\xi \tag{100}$$

where $g(\xi)$ is the normalized function of the form of the line, and $\Delta^*\omega = \xi + \Delta\omega$ is the extent to which the frequency of the hf-field differs from exact resonance. Integration of formula (98) shows that the intensity of the measured spectral line depends on the first term in the right-hand side of (98), and that only the form of the line depends on the second term [48]. For saturation of the line c'c, i.e., when $S \to 1$, even for a marked change in the form of the line being studied, we have

$$\frac{I_{td'}^{cc'}(0)}{I_{td'}^{0}} = 1 \pm \tau_1, \tag{101}$$

which coincides with formula (80) obtained earlier.

The form of the line studied by the hf-field H_1 approaches the Lorentzian form if $h^2 \to 0$ and $S \to 0$. If however $h^2 > 0$, splitting of this line is produced.

A detailed analysis of this phenomenon [48] has shown that in the absence of detuning of the hf-field H_2 ($\Delta\omega_2 = 0$), symmetrical splitting is observed if in a first approximation $\gamma H_2 > 1/T_2$ or, more accurately, if

$$\left(2h^2 - \frac{\nu_1^2 + 1}{\nu_1^2}\right) K + \frac{1 + \nu_1 h^2}{\nu_1^2} \geqslant 0, \text{where } K = \frac{1 \mp (\tau_1 + 1/\tau_2) S}{1 \mp (\tau_1 - \nu_1/\tau_2) S}.$$

If for saturation $S \to 1$ of the perturbed line $K > 0$, normal splitting is observed (upper part of Fig. 15), whereas if $K < 0$, anomalous splitting is observed (lower part of Fig. 15). The condition $K < 0$ can be satisfied when intramolecular dipole relaxation predominates for the line $\Lambda = 0$, when $T_{d'c'1} < T_{2c'c'}$. The line showing anomalous splitting would be similar to Yatsiv's multiquantum maser [41]. In liquids, however, the intramolecular dipole relaxation is usually not the predominant relaxation process and the lines are split in the normal way. The magnitude of the splitting $2\Delta\omega_1$ for the case of a moderate perturbing hf-field, when $1/T_2 \ll \gamma H_2 \ll |(a'-a)-(b'-b)$, is equal to

$$2|\Delta\omega_1| = \gamma H_2 |\langle c | I_+ | c' \rangle| \tag{102}$$

with positive peak value $v(\Delta\omega_1^{\max}, 0) = \dfrac{(1 \mp \tau_1)\lambda}{1 + \nu_1}$.

It follows from (102) that perturbation of the weak lines of the spectrum leads only to slight splitting of the other lines. This feature can be used in the determination of the relative signs of the spin-spin coupling constants. It follows from (98) that the form of the measured line depends on the form and width of the perturbed line [46-48, 291].

Numerical calculation and Fig. 15 show that the regression [155] lines $\Lambda = 0$ always become narrower, whereas the progression lines $\Lambda = 2$ become broader with splitting [48, 78]. At the same time, as a result of the nuclear Overhauser effect, the intensity of the line $\Lambda = 0$ decreases and the intensity of the line $\Lambda = 2$ increases [48, 93]. The change in the intensity of the lines $\Lambda = 1$, which do not undergo splitting, may have either sign, but when the usual intermolecular relaxation processes predominate, a decrease in intensity is observed [79]. Moreover, when the extremely special conditions $T_{2dd'} \gg T_2^*$ and $T_{d't1} > 0$ are observed in a nonuniform magnetic field, weak splitting of the lines $\Lambda = 1$ may appear in a narrow range of amplitudes of the hf-field H_2 [47].

It follows from (80) and (101) that for the case of a sufficiently uniform magnetic field H_0 the relative changes in the intensities of spectral lines of all types are described by the single simple relationship

$$O^{c'c}_{d'd}/O^{c'c}_{b'b} = T_{d'd1}/T_{b'b1}. \tag{103}$$

3.6. The Overhauser Nuclear Effect for Perturbation of the Spin System by a Strong hf-Field. Marked changes take place in NMR spectra under the influence of a strong hf-field H_2. With increase in the amplitude of the hf-field, the total number of individual spectral lines in the NMDR spectrum at first increases, after which the number begins to decrease and collapse of the multiplets is observed. All these phenomena are accompanied by a change in the intensities of the lines, and the observed effects, as before, are described by the kinetic equation. In the derivation of this equation, use was made of the representation of the interaction in order to eliminate rapid time dependences. The marked time dependence of the Hamiltonian in (60) at high values of γH_2 can be eliminated by relating this equation to a system of coordinates rotating with the strong high-frequency field H_2 about the z axis with an angular velocity $-\omega_2$ (95). As a result of the marked changes in the spectrum, it is necessary to change to a new set of basis eigenfunctions (α, A') of the Hamiltonian (93):

$$\mathcal{H}_0^R\,|\alpha\rangle = \alpha\,|\alpha\rangle, \tag{104}$$

and for weakly coupled systems of the type A_mX_n a further simplification is possible. Rotation about the y axis by the angle $\theta(m)$ between the directions of H_{ef} and H_0 (Fig. 4) by the operator S

$$S = \exp[\,i\theta(m)\sum_i I_y(i)], \tag{105}$$

$$S\mathcal{H}_0^R S^{-1} = \mathcal{H}_0^S \tag{106}$$

makes it possible to use, as a new basis, simple multiplicative wave functions of the type $|\alpha\alpha\beta\alpha\ \ldots\rangle$, as in the analysis of ordinary NMR spectra. This feature follows from $[\mathcal{H}_0^S, I_z] = 0$. The properties of the operator S are given in [13, 18, 37]. In this new representation the kinetic equation acquires the form

$$\frac{d\tilde{\sigma}_S}{dt} = -i\,[\mathcal{H}_0^S + \mathcal{H}_1^S(t), \tilde{\sigma}_S] - \Gamma_S(\tilde{\sigma}_S - \sigma_{0S}), \tag{107}$$

where the relaxation term Γ_S differs from Γ in (89) and (95) [37]. To simplify the calculation of Γ_S [37], use is made of (52) [54], where

$$\tilde{G}^S(t) = G^S(t) = SG(t)S^{-1}, \tag{108}$$

and account is taken of the fact that the transformation T does not alter the relaxation term $\Gamma = \tilde{\Gamma}$ ([1], p. 492; [37, 55]) because of the equal spectral density of all frequencies for strong contraction. From (95), (93), and (25) we obtain, for the stationary state in the absence of H_1,

$$[\mathcal{H}_0^R,\ \tilde{\chi}] - i\Gamma(\tilde{\chi}) = q\,[D_{2+} + D_{2-}, \mathcal{H}_0]. \tag{109}$$

From (62), (65), and (109), taking account of the fact that the Larmor frequency is much greater than δ and J, we obtain

$$[\mathcal{H}_0^R, \tilde{\chi}] - i\Gamma(\tilde{\chi}) = -(2\pi q v_0)(\pi v_2)\sum_i [I_+(i) - I_-(i)] \tag{110}$$

or in matrix elements in the representation (104)

$$(\alpha-\alpha')\tilde{\chi}_{\alpha\alpha'}+i\sum_{\beta\beta'}R_{\alpha\alpha'\beta\beta'}\tilde{\chi}_{\beta\beta'}=-(2\pi q v_0)(\pi v_2)\sum_i[I_+(i)-I_-(i)]_{\alpha\alpha'}. \tag{111}$$

In the general case, the elements of the deviation matrix $\tilde{\chi}$ are complex. By separating the real and imaginary parts and taking account of the Hermitian character of $\tilde{\chi}$, we obtain a system of A^2 equations, where $\alpha' > \alpha$

$$\begin{aligned}(\alpha-\alpha')\operatorname{Re}(\tilde{\chi}_{\alpha\alpha'})-\sum_{\beta<\beta'}(R_{\alpha\alpha'\beta\beta'}-R_{\alpha\alpha'\beta'})\operatorname{Im}(\tilde{\chi}_{\beta\beta'})\\ =-(2\pi q v_0)(\pi v_2)\sum_i[I_+(i)-I_-(i)]_{\alpha\alpha'},\end{aligned} \tag{112}$$

$$(\alpha-\alpha')\operatorname{Im}(\tilde{\chi}_{\alpha\alpha'})+\sum_{\beta<\beta'}(R_{\alpha\alpha'\beta\beta'}+R_{\alpha\alpha'\beta'\beta})\operatorname{Re}(\tilde{\chi}_{\beta\beta'})+\sum_{\beta}R_{\alpha\alpha'\beta\beta}\tilde{\chi}_{\beta\beta}=0, \tag{113}$$

$$2\sum_{\beta<\beta'}R_{\alpha\alpha\beta\beta'}\operatorname{Re}(\tilde{\chi}_{\beta\beta'})+\sum_{\beta}R_{\alpha\alpha\beta\beta}\tilde{\chi}_{\beta\beta}=0, \tag{114}$$

$$\sum_{\beta}\tilde{\chi}_{\beta\beta}=0. \tag{115}$$

In the derivation of these equations, allowance was made for the possibility of strong relaxation, accurate tuning of ω_2 on one line of the spectrum, and simultaneous influence of the strong perturbing hf-field on several transitions.

It follows from (95) that under the conditions of weak relaxation $(\sigma_0+\tilde{\chi})$ is a diagonal matrix [37]. In actual fact, in the absence of relaxation and a measuring hf-field, in rotating coordinates, no transitions take place

$$(\sigma_0+\chi)_{\alpha\alpha'}=\frac{i\sum\limits_{\beta\beta'}R_{\alpha\alpha'\beta\beta'}\tilde{\chi}_{\beta\beta'}}{(\alpha'-\alpha)}. \tag{116}$$

In these conditions we obtain

$$\operatorname{Re}(\tilde{\chi}_{\alpha\alpha'})\gg\operatorname{Im}(\tilde{\chi}_{\alpha\alpha'}) \tag{117}$$

and the solution of the system of Eqs. (112)-(115) is simplified considerably [55]. The matrix $\tilde{\chi}$ can then be calculated from (114) and (115), from which we obtain [37, 53-55]:

$$\Gamma(\tilde{\sigma}-\sigma_0)_{\alpha\alpha}=-\sum_{\beta\beta'}R_{\alpha\alpha\beta\beta'}\tilde{\chi}_{\beta\beta'}=0. \tag{118}$$

Equation (112) is similar to formula (69), which is applicable for weak relaxation and perturbation; (113) is important only for strong relaxation, and Eqs. (114) and (115) are the analogs of the system of equations (72).

Baldeschwieler [53] emphasizes that the diagonal nature of the matrix $(\sigma_0+\tilde{\chi})$ and the system of equations (118) following from it are not observed for exact tuning of the strong perturbing hf-field H_2 with frequency $\omega_2 = (a'-a)$ on the line a'a, so that in rotating coordinates $(\alpha'-\alpha)\rightarrow 0$ and it does not follow from (116) that the nondiagonal elements of this matrix are small. In actual fact, this is not the case: under the conditions of strong perturbation we always have $|(\alpha'-\alpha)|\geq v_2$ even for exact tuning of ω_2 [52].

The system of Eqs. (112)-(115) has been used to calculate the relative intensities of the lines in the spectrum of a system of type AB under the conditions of perturbation by a very strong hf-field H_2 [32], and also for the analysis of the double resonance of a single spin $^1/_2$ [55]. The signal measured by the hf-field H_1 depends on the nondiagonal elements of the matrix η (26). Equation (89) acquires the form

$$\frac{d\tilde{\eta}}{dt} = -i[\mathscr{H}_0^R\ , \tilde{\eta}(t)] - i\,[\tilde{\mathscr{H}}_1(t), \tilde{\chi} + \tilde{\eta}(t) + \sigma_0] - \Gamma(\tilde{\eta}). \tag{119}$$

If there are no common energy levels with equal differences between these levels, and the hf-field H_1 is weak, we have [37, 55]

$$\tilde{\eta}_{\alpha\alpha'} = \overset{+}{Y}_{\alpha\alpha'} e^{i\Omega t} + \overset{-}{Y}_{\alpha\alpha'} e^{-i\Omega t}. \tag{120}$$

With allowance for the fact that $TI_{\pm}T^{-1} = e^{\pm i\omega_2 t}I_{\pm}$, we obtain from (16)

$$L = -\frac{k'}{2i}\frac{d}{dt}\sum_i \gamma_i \operatorname{Sp}[I_+(i)\,e^{-i\omega_2 t}\tilde{\sigma} - I_-(i)\,e^{i\omega_2 t}\tilde{\sigma}], \tag{121}$$

$$\overset{\pm}{L}_{\alpha\alpha'} = \mp\, k'\omega_1 \sum_i \gamma_i I_{\mp}(i)_{\alpha'\alpha} \operatorname{Im}(\overset{\pm}{Y}_{\alpha\alpha'}) \sin(\omega_2 \pm \Omega)t. \tag{122}$$

It can be seen from formula (122) that each spectral line, for perturbation by a very strong hf-field H_2, with measurement by a weak hf-field H_1, can give two signals, dependent on $\eta(t)$, at frequencies $\omega_2 \pm \Omega$ and one signal, dependent on χ, at a frequency ω_2 [55]. The two signals L^+ and L^- at frequencies ω_1 and $2\omega_2 - \omega_1$ appear because of the fact that, in rotating coordinates, as a result of the small value of the frequency Ω, both its rotating components can be simultaneously in resonance with the spin being studied [58, 85].

3.7. Double Resonance of a Single Spin of $^1/_2$. From (65) and (93) we have, for a single spin of $^1/_2$,

$$\mathscr{H}_0{}^R = 2\pi\,(AI_z + v_2 I_x). \tag{123}$$

If α and β are eigenfunctions of the Hamiltonian $\mathscr{H}_0$, the new wave functions $|1\rangle$ and $|2\rangle$ can be found by means of the operator S (105) by rotating through an angle $\theta = \arctan v_2/A$:

$$|1\rangle = \alpha\cos\theta + \beta\sin\theta, \tag{124}$$

$$|2\rangle = -\alpha\sin\theta + \beta\cos\theta, \tag{125}$$

so that the new eigenfunctions of the transformed Hamiltonian $\mathscr{H}_0{}^S$ (106) are

$$\begin{aligned} E_1 &= \pm\pi\sqrt{A^2 + v_2^2}, \\ E_2 &= \mp\pi\sqrt{A^2 + v_2^2}, \end{aligned} \tag{126}$$

The resonance frequencies in laboratory coordinates are:

$$\omega^{\pm} = \omega_2 \pm 2\pi\sqrt{A^2 + v_2^2}, \tag{127}$$

and for exact tuning of the perturbing hf-field, when A = 0,

$$\omega^+ - \omega^- = 2\gamma H_2, \tag{128}$$

which coincides with the result obtained by qualitative examination of this phenomenon. The position of these narrow [85] lines L^+ and L^- makes possible to measure the amplitude of one rotating component of the strong hf-field H_2 [37, 53, 58, 85]. Contrary to Bloch's statement [37] it is possible to avoid extrapolation and to work without detuning the perturbing field ($A = 0$) [85]. In a single experiment it is possible to record only two, but not four signals. If one of these two lines is irradiated by the measuring hf-field at a frequency ω_1, emission is observed at a frequency $2\omega_2 - \omega_1$ [60]. When isotropic dipole-dipole relaxation predominates, it is possible to calculate, from the system of Eqs. (112)-(115), the matrix $\tilde{\chi}$ and also $\tilde{\eta}(t)$, which depends on it. From (122) we obtain:

$$\frac{L_{12}{}^{+}}{L_{12}{}^{-}} = -\left\{\frac{(1+\cos 2\theta)^2}{(1-\cos 2\theta)^2}\right\}\left\{1 - \frac{2}{1-\cos 2\theta T_2{}^2 (E_1 - E_2)^2}\right\}\left\{\frac{1+4D^2_{1-12}T_2{}^2}{1+4D^2_{1+12}T_2{}^2}\right\}, \tag{129}$$

where the last term in brackets takes account of the saturation by the hf-field H_1, the middle term depends on the strength of the relaxation processes, and the first term depends on the detuning of the perturbing frequency ω_2 [55]. The first two terms coincide with the result obtained by Baldeschwieler [53], who in fact made allowance for the influence of relaxation, but not for exact tuning, on the relative intensity of the lines $L_{12}{}^+$ and $L_{12}{}^-$.

3.8. Double Resonance in Multispin Systems. The equations describing the dependence of the density matrix on the conditions of the experiment are extremely complex and often cannot be used in the examination of the more complex spin systems which are of interest in structural analysis. In these cases it is expedient to restrict oneself to the determination of the new resonance frequencies and new line intensities, following from the change in the wave function of this system, and in general to neglect relaxation processes, and also to neglect the influence of the Overhauser nuclear effect. This approach to the analysis of NMDR was very fruitfully developed by Freeman and Anderson [81, 153, 65, 78] and, in spite of the fact that it was impossible to calculate the form and width of the lines, the transition processes, the free precession, and spin echo, it has given more results of practical importance than many other NMDR theories. In this theory there is not even a place for the components of the magnetization $M_{x,y}$ and the spectral lines are obtained only as a result of the absorption of hf-energy. In this sense, this approach to the theory of NMDR is a logical development of one of the first NMR experiments [68]. The nuclear induction experiment [31, 67] and the dynamic theory [36], which uses the formalisms of the density matrix, are also related.

The resonance frequencies of spin systems for the action of a perturbing hf-field H_2 can be found as the differences in the $\mathcal{H}_0^R$ (or $\mathcal{H}_0^S$) eigenvalues in appropriate new representations. The resonance condition acquires the form $\Omega = (\alpha' - \alpha)$, and the resonance frequencies in laboratory coordinates can be obtained by adding the frequency of rotation of the coordinate system ω_2:

$$\omega_1 = (\alpha' - \alpha) + \omega_2. \tag{130}$$

Let us examine the change in the spectrum of the spin of nucleus A for perturbation, by the hf-field H_2, of only the spin of nucleus X of the two-spin system AX without any influence on the spin of nucleus A [65]. The Hamiltonian (93) of this system in a rotating system of coordinates, expressed in units of only the angular frequency ω, has the form

$$\mathcal{H}_0{}^R = -[(\omega_A - \omega_2) I_z(A) + (\omega_X - \omega_2) I_z(X) - 2\pi J_{AX} I_z(A) I_z(X) + \gamma_X H_2 I_x(X)]. \tag{131}$$

The Hamiltonian (90) of the weak measuring hf-field H_1, which acts only on spin A, acquires the form

$$\tilde{\mathcal{H}}_1(t) = -\gamma_A H_1 [I_x(A)\cos\Omega t - I_y(A)\sin\Omega t]. \tag{132}$$

The Hamiltonian (131) can be diagonalized by the transformation S (106), and we find from Fig. 4 that

$$\theta(m) = \operatorname{arctg}\frac{\gamma_x H_2}{(\omega_X - \omega_2 - 2\pi J_{AX} m)}, \tag{133}$$

where m is the eigenvalue of the operator $I_z(A)$.

$$\mathscr{H}_0^S = -[(\omega_A - \omega_2) I_z(A) + A(m) I_z(X)], \tag{134}$$

where the frequency of precession of the spin of nucleus X around the direction of the effective field H_{ef} is equal to

$$A(m) = [\omega_X - \omega_2 - 2\pi J_{AX} m)^2 + \gamma_X^2 H_2^2]^{1/2}. \tag{135}$$

Nucleus A undergoes precession about the z axis as a result of the low strength of the measuring field so that $H_{ef}(A) \parallel H_0$. The eigenvalues of the operator $\mathscr{H}_0^S$ are equal to

$$E_S(m, M) = -[(\omega_A - \omega_2) m + A(m) \cdot M], \tag{136}$$

where M is the eigenvalue of the operator $I_z(X)$.

For a weak measuring hf-field H_1 the usual selection rule $\Delta m = \pm 1$ is operative, but a strong perturbing hf-field H_2, as a result of the presence of the term $\gamma_X H_2 I_X(X)$ in the Hamiltonian (131) (as a result of which $[\mathscr{H}_0^R, I_Z(X)] \neq 0$), may produce, simultaneously with the transition $\Delta m = \pm 1$ of spin A, transitions of spin X with $\Delta M = 0, \pm 1, \pm 2, \ldots, \pm 2S$.

The resonance frequencies of spin A in the laboratory system of coordinates are equal to

$$\begin{aligned}\omega(m, M;\ m-1, M') &= E_S(m-1, M') - E_S(m, M) + \omega_2 \\ &= \omega_A + A(m)M - A(m-1)M'.\end{aligned} \tag{137}$$

Since the value of the trace in (86), (13), (16), and (121) is independent of the unitary transformations T and S, the line intensities, as before, are proportional to the squares of the matrix elements of the operators $I_\pm$ or $I_X \mid \langle a \mid I_X(A) \mid a' \rangle \mid^2$, but for the calculation of these elements the eigenfunctions U(I, m) U(S, M) of the Hamiltonian $\mathscr{H}_0^S$ must be converted back into "laboratory coordinates" by the transformation $T^{-1}S^{-1}$. We than obtain

$$\begin{aligned}|\langle a|I_x(A)|a'\rangle|^2 = |\langle U^*(I,\ m) e^{-iI_z{}^{(A)\omega_2 t}} | I_x(\mathrm{A}) | e^{iI_z{}^{(A)\omega_2 t}} U(I,\ m')\rangle \cdot \\ \langle U^*(S,\ M) | e^{-i[\theta(m')-\theta(m) I y(\mathrm{X})]} | U(S,\ M')\rangle|^2.\end{aligned} \tag{138}$$

The first term of this product gives the intensity of the corresponding line in the ordinary NMR spectrum, but the second takes account of the effects of double resonance through the matrix elements of the rotation operator S, which can be expressed according to Wigner [69]. By taking $\phi = \phi(m-1) - \theta(m)$ as the angle of rotation about the y axis, we can write (138) in a form suitable for calculation on a digital computer. The intensity of the spectral line (m, M; m−1, M') is proportional to the expression

$$L = (I - m + 1)(I + m) d^2(S, M, M', \phi), \tag{139}$$

where

$$\begin{aligned}d(S, M, M', \phi) = [(S+M)!(S-M)!(S+M')!(S-M')!]^{1/2} \\ \times \sum_k \frac{(-1)^k (\cos\phi/2)^{2S+M-M'-2k} (-\sin\phi/2)^{M'-M+2k}}{(S-M'-k)!(S+M-k)!(k+M'-M)!k!}\end{aligned} \tag{140}$$

and k is an integer such that all the factorials are positive or equal to zero. In (138), (139), and (140), the quantities I and S are the eigenvalues of the operators $I^2(A)$ and $I^2(X)$ respectively.

Relationships (137) and (138) can readily be used to calculate the dependence of the resonance frequencies and relative intensities of of the lines in the NMDR spectra of spin systems of the type AX [66], AX_2 [153], A_mX_n ($m, n \leq 3$) [65], A_3X [50], A_4X [51], AMX [52] and A_3KX_2 [266] on the relative intensity $\gamma H_2/2\pi|J|$ and relative detuning $\Delta = (\omega_2 - \omega_X)/2\pi|J|$ of the frequency of the perturbing hf-field H_2. It is convenient to represent the results

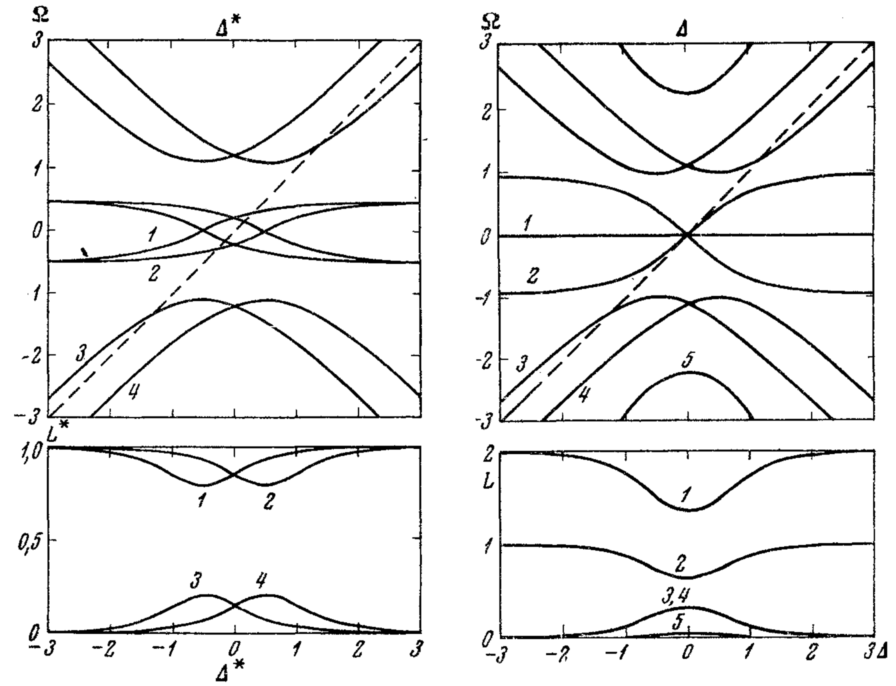

Fig. 16. Double resonance in a three-spin system: A_2X on the left, AX_2 on the right [153]; $\gamma H_2 = 2\pi J$.

graphically by means of the relative detuning of the measuring frequency $\Omega = (\omega_1-\omega_A)/2\pi|J|$ for selected constant values of the amplitude of the hf-field H_2. Usually, $\gamma H_2/2\pi = 0.2|J|$ and $\gamma H_2/2\pi = |J|$ [65]. Figure 16 gives graphs for finding the resonance frequencies and relative intensities of the lines for systems AX_2 and A_2X. Sweeping of the frequency ω_1 corresponds on these diagrams to the vertical lines for a given detuning Δ of the strong perturbing hf-field H_2 from exact resonance with the nucleus X (when $\omega_2 = \omega_X$). Sweeping of the magnetic field is equivalent to the proportional (in the case of homonuclear double resonance the almost identical) change in the frequencies ω_1 and ω_2; these experiments correspond to the line on the graphs with slope equal to 1 (45°). Maximum merging of the multiplet for nuclei A corresponds to the condition $\Delta = 0$. Sweeping of the frequency ω_2 in experiments of the INDOR type [79, 88, 89, 158] corresponds to the horizontal lines at constant detuning $\Omega = \pm{}^1/_2|J|$. Heteronuclear double resonance experiments with sweeping of the magnetic field are described by lines with slope γ_A/γ_X.

From the diagrams [65] and (137) we find that if a sufficiently weak perturbing hf-field H_2 is used and the relaxation is weak, i.e., $1/\pi T_2^* < \gamma_X H_2 \ll 2\pi|J|$, and ω_2 is tuned exactly to any line of the multiplet of nucleus X corresponding to the eigenvalue m' of the operator $I_z(A)$, so that

$$\omega_S - \omega_2 - 2\pi J_{AX} m' = 0, \qquad (141)$$

we obtain, for the frequencies of the spectral lines of nucleus A:

$$\omega(m', M';\ m'-1, M) \cong \omega_A - 2\pi J_{AX} M + \gamma_S H_2 M', \qquad (142)$$

$$\omega(m'+1, M;\ m', M') \cong \omega_A + 2\pi J_{AX} M - \gamma_S H_2 M', \qquad (143)$$

$$\omega(m'', M;\ m''-1, M) = \omega_A + 2\pi J_{AX} M, \qquad (144)$$

where in the last case m'', m'' $-1 \neq$ m'. From condition (141) it follows that the line perturbed by the hf-field H_2 in the multiplet of nucleus X and the line observed by the hf-field H_1 at a frequency ω(m', M'; M' −1, M) have, in cases (142) and (143), a common energy level corresponding to the eigenvalue m' of the operator $I_z(A)$. Under these conditions, we observe splitting of each of the 2S + 1 lines of the multiplet of nucleus A into a submultiplet of 2S + 1 lines as a result of tickling in the spin system with degenerate states ($S > {}^1/_2$). The intensity of the submultiplet is equal to the intensity of the line showing no splitting, if no account is taken of the influence of the nuclear Overhauser effect and the nonhomogeneity of H_0 [65]. In case (144) there is no common energy level and the spectral lines are not split.

3.9. Decoupling of Nuclei and Collapse. When a strong perturbing hf-field acts on nucleus X of a spin system Ax so that $\gamma_X H_2 > 2\pi |J_{AX}| I$, where I is the spin of the group A, we find, after expansion of A(m) and A(m-1) into a series $(1 + x)^{1/2} \cong 1 + {}^1/_2 x - \ldots$, from (137), that

$$\omega(m, M;\ m-1, M) \cong \omega_A - \frac{2\pi J_{AX}}{\gamma_X H_2}[\omega_X - \omega_2 - 2\pi J_{AX}(m - {}^1/_2)M]. \tag{145}$$

For perturbation under conditions corresponding to the sweeping of the frequency ω_1 of the center of the multiplet of nucleus X so that $\omega_2 = \omega_X$, all the distances between the spectral lines in the multiplet of nucleus A decrease by a factor $(2\pi J_{AX})(m - {}^1/_2)/\gamma_X H_2$. The decrease in these distances is almost the same for sweeping of the magnetic field H_0, if the additional condition $\gamma_X H_2 \gg 2\pi |J_{AX}| S$ is satisfied. Total collapse with merging of the multiplet of nucleus A into one narrow line is possible if $I = {}^1/_2$, otherwise ($I > {}^1/_2$) even when a very strong perturbing hf-field is used, the spectrum of A always preserves a certain residual splitting (Fig. 16, on the left).

The results given above are applicable only to weakly coupled systems of the type AX for the conditions of selective action of the two hf-fields. In order to examine strongly coupled systems of the type AB, when the difference in the chemical shifts compared with the spin-spin coupling constant J_{AB} and the amplitude of the perturbing hf-field $\gamma_B H_2$ is small, it is necessary to take account of the direct influence of this field on the spin of A and we obtain from (90)

$$D_{2+} + D_{2-} = H_2 \sum_i \gamma_i I_x(i) = \gamma_B H_2 I_x(\mathrm{B}) + \gamma_A H_2 I_x(\mathrm{A}).$$

In the Hamiltonian (131), where now X = B, the new term $\gamma_A H_2 I_X(A)$ appears. The diagonalization of this Hamiltonian is carried out in a fashion analogous to that described above: we first diagonalize the terms containing I(A) by the transformation

$$V = e^{i\theta_A I_y(\mathrm{A})}, \tag{146}$$

where the angle of rotation is found from the condition $\tan\theta_A = \gamma_A H_2/(\omega_A - \omega_2)$. In addition,

$$\begin{aligned}\mathscr{H}_0^V = V\mathscr{H}_0^R V^{-1} = -\{AI_z(\mathrm{A}) + [(\omega_B - \omega_2 - 2\pi J_{AB}\cos\theta_A I_z(\mathrm{A})]\, I_z(\mathrm{B})\\ + [(\gamma_A H_2 - 2\pi J_{AB}\sin\theta_A I_z(\mathrm{A})]\, I_x(\mathrm{B})\},\end{aligned} \tag{147}$$

where small terms of second order have been omitted and

$$A = [(\omega_A - \omega_2)^2 + (\gamma_A H_2)^2]^{1/2}. \tag{148}$$

The $\mathscr{H}_0^V$ terms containing the I(B) components are diagonalized by the operator W:

$$W = e^{i\theta_B(m) I_y(\mathrm{B})}, \tag{149}$$

where the angle of rotation $\theta_B(m)$ follows from the formula

$$\tan\theta_B(m) = \frac{\gamma_A H_2 - 2\pi J_{AB} m \sin\theta_A}{\omega_B - \omega_2 - 2\pi J_{AB} m \cos\theta_A}. \tag{150}$$

Thus

$$\mathcal{H}_0^W = W\mathcal{H}_0^V W^{-1} = -[AI_z(\mathrm{A}) + X(m)\,I_z(\mathrm{B})], \tag{151}$$

$$X(m) = [\omega_\mathrm{B} - \omega_2 - 2\pi J_\mathrm{AB} m \cos\theta_\mathrm{A})^2 + (\gamma_\mathrm{A} H_2 - 2\pi J_\mathrm{AB} m \sin\theta_\mathrm{A})^2]^{1/2}. \tag{152}$$

The most intense spectral lines of the spectrum of nucleus A, under the conditions of strong perturbation of nucleus B, when $\gamma H_2 \geq 2\pi\,|J_{AB}|$, correspond to the spin of nucleus A with $\Delta m = \pm 1$, $\Delta M = 0$, where M is the magnetic quantum number of the spin of nucleus B [65]. The intensities $\Delta M \neq 0$ of the lines are smaller. The resonance frequencies of the spin of nucleus A in the laboratory system of coordinates are equal to

$$\omega(m, M;\ m-1, M) = \omega_2 + A + [X(m) - X(m-1)]\,M. \tag{153}$$

After expanding A, X(m) and X(m-1) into series and taking account of the fact that $(\omega_A - \omega_2)^2 \gg (\gamma_A H_2)^2 \gg [(\omega_B - \omega_2)^2 + (2\pi J_{AB})^2 m^2]$, we obtain from (153)

$$\omega(m, M;\ m-1, M) = \omega_\mathrm{A} + \frac{(\gamma H_2)^2}{2(\omega_\mathrm{A} - \omega_2)} - \frac{2\pi J_\mathrm{AB}\cos\theta_\mathrm{A}}{\gamma H_2}[(\omega_\mathrm{B} - \omega_2) - 2\pi J_\mathrm{AB}\cos\theta_\mathrm{A}(m - {}^1/_2) + \gamma H_2 \tan\theta_\mathrm{A}]\,M. \tag{154}$$

In this equation ω_A corresponds to the chemical shift of nucleus A in the absence of spin-spin coupling with other nuclei and strong hf-fields, the second term reflects the displacement of the resonance frequency of nucleus A under the influence of the strong nonresonance hf-field, and the third represents the residual splitting. The first two terms in square brackets are analogous to the corresponding terms in (145) and disappear when $\omega_2 = \omega_B$ and $I = {}^1/_2$. The last term, however, increases with increase in γH_2 and in the limit restores the splitting $2\pi J_{BA}$, when both spins A and B are quantized along the direction of the effective field. Maximal merging of the multiplet of nucleus A corresponds to the condition

$$(\omega_\mathrm{B} - \omega_2) = \gamma H_2 \tan\theta_\mathrm{A} \cong \frac{(\gamma H_2)^2}{(\omega_\mathrm{A} - \omega_2)}, \tag{155}$$

which requires a slight displacement of the perturbing frequency from exact resonance with nucleus X. This feature is of practical importance in the indirect determination of chemical shifts from the collapse of multiplets overlapped by other lines. The correction is equal in magnitude to that which is used when the measuring hf-field H_1 is obtained from the strong perturbing hf-field H_2 by modulation of the magnetic field, but has the opposite sign. In actual fact, for large displacements of the strong hf-field H_2 from the resonance value, when it follows from (129) that only one signal appears instead of two, we obtain from (127) the resonance frequency of this signal

$$(\omega_1 - \omega_2)^2 = (\omega_\mathrm{A} - \omega_2)^2 + (\gamma H_2)^2, \tag{156}$$

where $\omega^{\pm} = \omega_1 \cong \omega_A$; $\omega_A = \gamma H_0$. Transforming this by expansion into a series, we obtain

$$\omega_1 \cong \omega_\mathrm{A} + \frac{(\gamma H_2)^2}{2(\omega_\mathrm{A} - \omega_2)}, \tag{157}$$

which coincides with the first correction in (154). Under the influence of a strong hf-field H_2, the signal of nucleus A is moved slightly from the frequency ω_2. When the measuring frequency is obtained by modulation of the hf-field H_2, the frequency of modulation necessary for resonance increases with increase in γH_2. With increase in γH_2, the difference $|\omega_1 - \omega_2|$ required for optimal decoupling of nuclei A and B decreases [65]. The corrections introduced in the form of graphs by Turner [74] should not be subtracted from the indirectly measured chemical shifts, but should be added.

With optimal decoupling, we obtain for the residual coupling in Hz

$$J_R = \frac{(2\pi J_{AB})^2 (m - 1/2)}{\gamma H_2}. \tag{158}$$

The importance of the decoupling of nuclei is not restricted to its importance as a method for the selective elimination of multiplets. In the case of rapid relaxation or exchange of nucleus X, the spin-spin coupling between nuclei A and X serves as a mechanism for the scalar relaxation of nucleus A [12]. In this case the decoupling of these nuclei has a strong influence on the relaxation times of nucleus A and leads to a decrease in the width of the spectral lines of the latter. These phenomena have been examined in detail by Bloch [37]. According to Abragam [1], as collapse of the multiplet of nucleus A is approached we have for the central line

$$\left(\frac{1}{T_A}\right)_c = \frac{1}{T_A} - \frac{\cos^2\theta}{T_X}, \tag{159}$$

and if $\gamma H_2 \gg 2\pi |J_{AX}|$, we find that $\cos^2\theta \to 0$ and the spectral lines of nucleus A will have a width due to their relaxation, which is independent of the scalar process with nucleus X.

4. Experimental Technique

All the forms of nuclear magnetic double resonance described in sections 2 and 3 require the simultaneous or (much less frequently) alternate application of two or several hf-fields, whose frequencies and amplitudes determine the nature of the observed effects. All the frequencies should be highly stable, as is always assumed in nuclear resonance, and random changes in the ratio of the frequency to the intensity of the magnetic field ω/H_0 in the study of proton spectra by the methods of homonuclear double resonance should not exceed $2 \cdot 10^{-9}$. Two methods are used to record the spectra—scanning of the magnetic field and scanning of the frequency. The first method is older, simpler, and cheaper, but it does not permit effective utilization of any of the methods described, since it is impossible to ensure prolonged preservation of the resonance of the hf-field H_2 with the perturbed nucleus. Scanning of the magnetic field is now being displaced by the more complicated scanning of the frequency, which makes it possible to achieve accurate tuning of the frequencies used on individual lines or multiplets of the spectrum and to preserve these conditions for a period of many hours.

4.1. Methods of Stabilizing the Magnetic Field and the Resonance Condition ω/H_0. The application of NMDR is very closely related to the problems and methods of stabilizing the magnetic field, so that double resonance found extensive application only after the development of effective methods of stabilization. Short-duration stability of $1 \cdot 10^{-9}$ is now the rule, and in addition to effective static stability it is also necessary to have very rapid stabilizer operation. In the case of single resonance, slowness in the stabilizer can be compensated by a high constant time before the recorder [190, 191], but this cannot be done in NMDR, since even very short-lived interference, which has almost no influence on single resonance spectra, produces unacceptable transition phenomena and noise in the observed range of the spectrum. The requirements made of the turbines are also much more severe. Irregularity of rotation and vibration lead to the appearance of strong side bands under the conditions of NMDR.

Stabilizers can be divided into two classes, with separate or common sensitive unit. A classical example of the first type is the superstabilizer with galvanometric amplifier, which does not compensate either slow drift or fast interference, and operates effectively only within an extremely narrow frequency range. At approximately the same level are the very large number of magnetic-field stabilizers based on an autodyne or bridge and ensuring a field stability not greater than 10^{-7}. Slightly more efficient operation is shown by the stabilizer of Baker and Burd [195, 196] with high-frequency amplitude modulation, but even this system is too slow [193] and bridge drift produced drift in the magnetic field. The super-regenerative stabilizer [105, 206] operates rapidly and accurately, but is unsuitable because of the very marked additional noise [193]. Spin generators with high-frequency back coupling [205, 207] rapidly follow changes in the magnetic field, but are insufficiently stable because of the drift of the sensitive unit. This drift is eliminated in spin generators on a side band [197, 210, 211, 217, 603, 604], which have found extensive application in the commercial NMR spectrometers A-60 [213], ZKR-60 [194], and PC-60 [604]. A version of the spin generator with phase-synchronized frequency modulation is also suitable for the stabilization of NMDR spectrometers [92, 189, 212, 214].

Among instruments with a single specimen, the most important is the stabilizer proposed by Primas [198], where the slow drift is eliminated by using as signal of the error in the dispersion signal a single narrow spectral

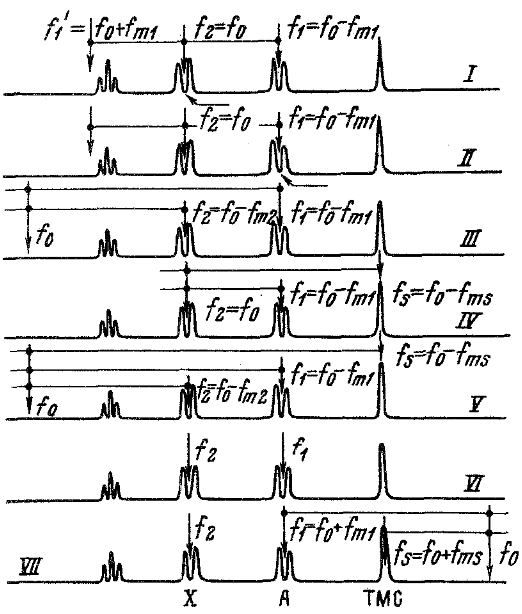

Fig. 17. Production of perturbing hf-field for double resonance.

line of the substance being studied. This system is used in most work with a weak perturbing hf-field and ensures effective long-lived stability [65, 66, 78, 81, 89, 199-202]. Spin generators can also operate with a single specimen [208, 209] and under these conditions they exhibit excellent stability, but they are unsuitable for the study of double resonance. Systems using the nuclei of another element have distinct advantages among stabilizers with a single specimen [203, 204].

4.2. Homonuclear Double Resonance Procedure. The hf-fields required for homonuclear double resonance (the measuring field H_1 at a frequency $\omega_1 = 2\pi f_1$, the perturbing field H_2 at a frequency $\omega_2 = 2\pi f_2$, necessary for the operation of internal stabilization [198]), can be obtained by modulation [10, 16, 620, 621, 622] of the magnetic field H_0 or the high frequency f_0 of an NMR spectrometer by sonic frequencies (from 20 to 10,000 cps). The relative arrangement of the side bands used is shown in Fig. 17. Version I is the simplest and has been used [103] for the decoupling of the protons in acetaldehyde. As a result of detection at a frequency f_0 the signals from the two decoupled nuclei coincided. In version II the detection is carried out at a frequency f_1 by a low-frequency phase (synchronous) detector using f_{m1} as support frequency, and signals are obtained from nuclei in resonance with frequencies f_1 and f_1' [107]. The frequency f_0 is used as perturbing frequency f_2, and the spectrum is recorded by scanning the magnetic field. The side bands are most frequently obtained by making use of modulation of the magnetic field H_0, and only rarely by amplitude [220] or frequency [105] modulation of the high frequency f_0. This procedure has been very widely used in the solution of various problems [52, 65, 73, 84, 105, 107, 108, 110, 111, 238], including the study of the decoupling of protons [65], the identification of multiplets [219, 248], and the determination of the sign of J [258]. The spectra recorded by this technique consist of two halves with different sign: in one half the nucleus A is decoupled from the nucleus X, and in the other half the opposite takes place. An elegant example of decoupling of the protons in acetaldehyde [22] was given in [110]. As a result of the fact that the frequency of modulation f_{m1} is determined by the difference in the chemical shifts δ_{AX}, in the study of more complex spectra another modulation band may fall in the spectrum and make the work impossible. This has happened in the analysis of gaillardilin [490], and version II has found application chiefly for the determination of the relative signs of J. To eliminate this marked disadvantage, in version II all the frequencies used are side bands, and use is made of sufficiently high modulation frequencies, so that f_0 and other side bands fall far outside the range of the spectrum [73, 257, 404]. To obtain the measuring frequency f_1, use is generally made of modulation of the magnetic field [257], but the perturbing frequency f_2 can be obtained by frequency modulation of f_0 [253, 254, 257]. As in version II, a low-frequency phase detector with support frequency f_{m1} is used for the detection of the NMR signal and the selection of its components (usually the absorption signal) after the high-frequency detector. Version III is usually employed with scanning of the magnetic field, but if $f_{m1} \gg \delta_{AX}$, scanning of the frequency is also possible, by means of a low-frequency generator, scanned by an electric motor [66] or sawtooth voltage [92, 404, 593]. This scanning of the measuring frequency is always accompanied by a certain change in the modulation index and phase of the modulation frequency, and in accurate work it is necessary to use a compensating filter [493]. Version III is used chiefly for the decoupling of nuclear spins in order to identify multiplets [412] in complex spectra and to determine the relative signs of spin-spin coupling constants I [253, 254, 257]. In the study of relaxation and chemical exchange [177], it is necessary to take account of the fact that a sharp change in one modulation index has a slight influence on the amplitudes of the other hf-fields used as modulation side bands [270]. Modulation of the magnetic field is unsuitable for the generation of very strong perturbing hf-fields, but an amplitude of $\gamma H_2/2\pi = 9.5$ Hz can easily be achieved [32]. The inadequate stability of ordinary spectrometers is eliminated in version V, where the use of internal stabilization makes possible the ready attainment of a long-lived stability of $1 \cdot 10^{-9}$. For this, the magnetic field H_0 is modulated by an additional frequency f_{ms}, which ensures resonance with the narrow line of an internal standard, usually 1-10% tetramethylsilane [65, 78] or C_6F_6 [357] in the study of flourine compounds. The low-frequency signal obtained from the high-frequency detector is detected after amplification in two phase detectors with support frequencies f_{m1} and f_{ms}, the phase of the latter being regulated to obtain a signal for the dispersion, which is equal to zero for exact

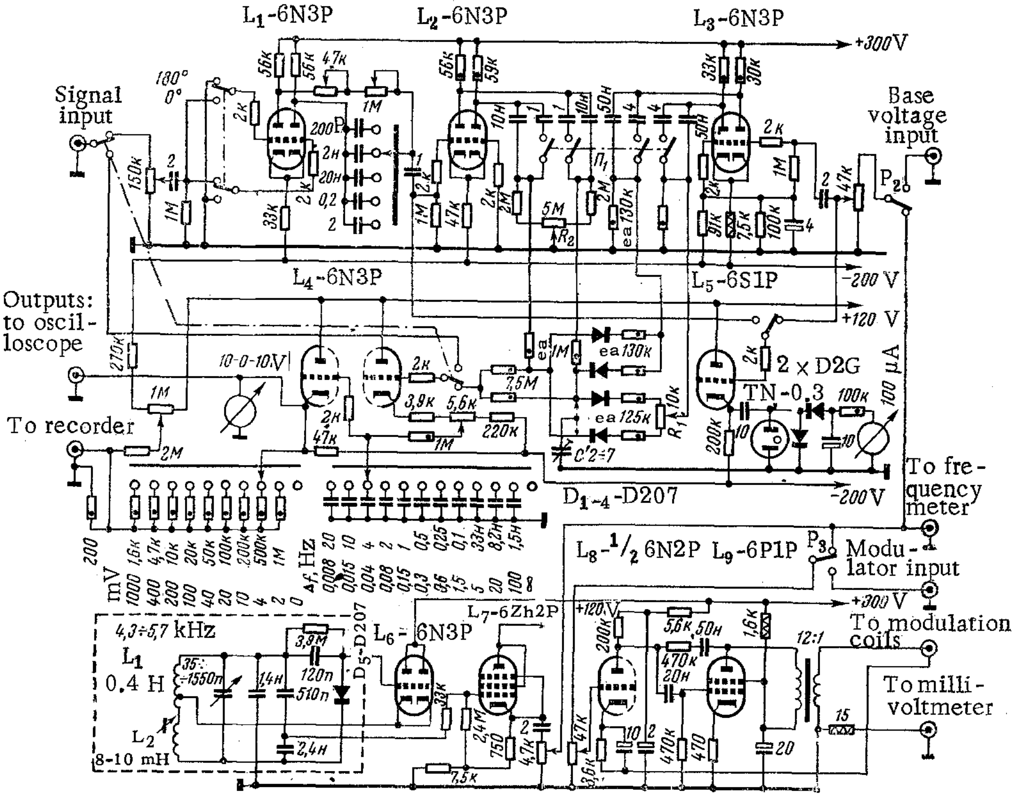

Fig. 18. Sonic frequency generator and phase detector.

Some of the following Russian abbreviations may be found in the figure: Л = tube, Д = diode, Тр = transformer, Др or др = choke, Вк = switch, в = V, М = MΩ, к = kΩ, мк = μF or μH, п = pF or pH, and н = nF or nH, ea = each.

tuning of the frequency f_s on the line and which changes sign as a result of deviations produced by interference. This signal is used to tune the magnetic field (when the superstabilizer is used) [65, 78] or the frequency [79]. Version V is the chief method of application of weak perturbing hf-field and is widely used to determine the mutual arrangement of energy levels in the interpretation of spectra [78, 139], to determine the relative signs of J by means of tickling [100] and selective double resonance, for the identification of multiplets, and for many other purposes [65, 78, 153, 344, 357, 364, 521, 565].

In the scanning of the measuring frequency f_1, f_{m1} is changed; when the INDOR spectra are recorded, f_{m1} is constant but f_{m2} is scanned; and finally, scanning of f_{ms} makes it possible to imitate scanning of the magnetic field, but with a very high stability. Version IV is a simplified form of version V and is little used, but it makes it possible to construct an instrument for double resonance as an attachment to the main spectrometer without any change in the latter [66]. In version VI the chief disadvantage of the previous versions—the change in the amplitude of the hf-field during the scanning—is eliminated. The two frequencies f_1 and f_2 are obtained by means of two quartz generators [58], by modulation of the frequency f_0 with separation of one side band [74, 83], or by synthesis of the required frequencies from the frequency f_0, stabilized by a spin generator [92, 189]. The synthesis of frequencies [58, 92, 158, 166, 189, 196, 210, 531, 555] is the most complex but also the most modern method, and makes it possible to obtain, equally readily, both weak and strong perturbing hf-fields, with amplitudes which are independent of the scanning of the frequency. Moreover, it is also readily possible to achieve additional frequency [80, 145, 216] or pulse [97, 98] modulation of the frequency f_2; this is necessary for application of the method of transfer of modulation through spin-spin coupling [80, 109, 213], for reduction of the residual splitting on decoupling of the nuclei [145], and for operation under conditions of time separation of one side band [74] is simpler than the circuit for the synthesis of frequencies, but it requires the use of a very special low-frequency generator with two output voltages with a phase displacement of 90°, which are produced to study the amplitude-phase characteristics of automatic control systems with a limited frequency range. An interesting feature is that the first experiments [58] on homonuclear decoupling $H_1-\{H^1\}$ were carried out by Anderson using synthesis of frequencies. With very severe stability requirements [79] it is still necessary to use the method of internal stabilization (version VIII).

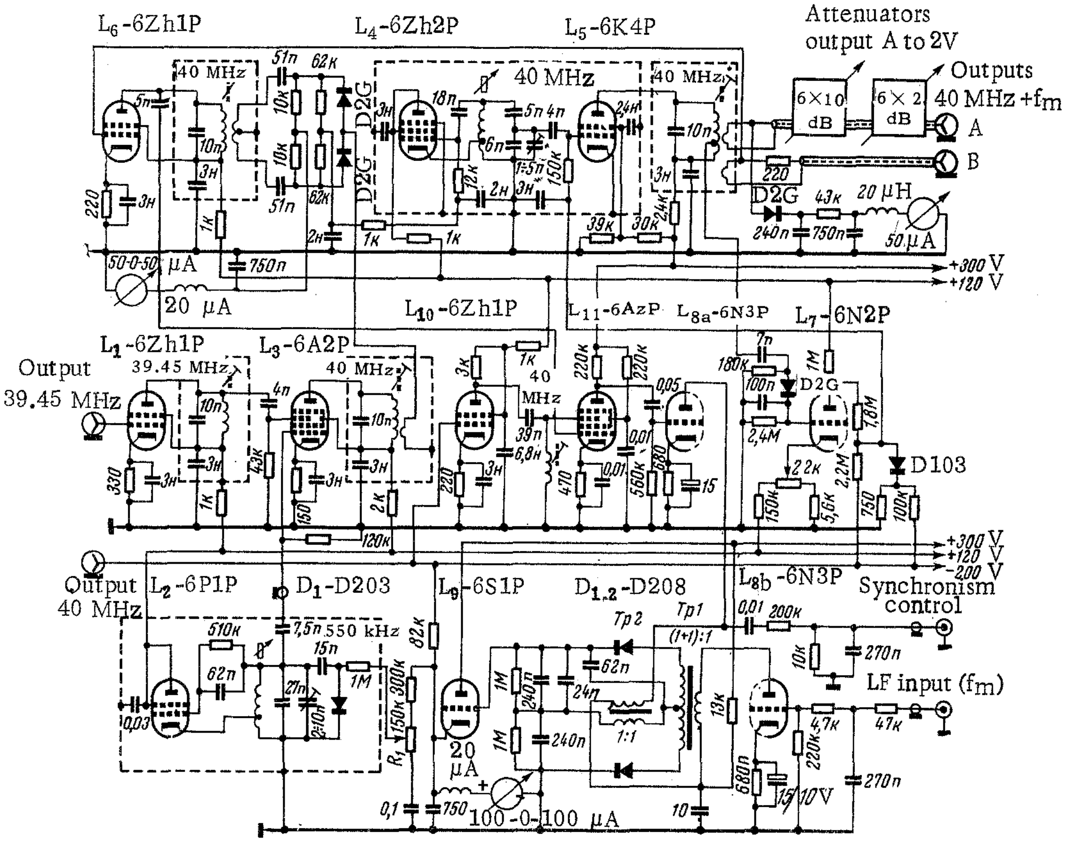

Fig. 19. Frequency synthesizer. (See note to Fig. 18.)

In spite of the fact that amplitude modulation of the magnetic field H_0 and freqiency modulation of the high frequency are theoretically equivalent [10, 197, 413, 564, 620-622], modulation of the magnetic field has in practice considerable advantages, since the influence of drift of the bridge equilibrium or the crossed coils on the spectrum is eliminated. In the case where a strong perturbing field is used, this thermal drift may be considerable. Thus the measuring hf-field H_1 in experiments on NMDR is almost always obtained by modulation of the magnetic field. The sonic frequency generators employed should be highly stable, and the drift in the course of the experiment should be less than 0.1 Hz [259, 392]. Most laboratory generators do not satisfy these requirements. Figure 18 gives the circuit of a sonic frequency generator with a range from 4.3 to 5.7 kHz, whose drift does not exceed 0.03 Hz per hour. The coil L_1 = 0.4 H is an air coil and is wound on a form with a low coefficient of thermal expansion, and the entire circuit is enclosed in a massive aluminum screen. The diode D_5 decreases considerably the dependence of the frequency on change in the emission properties of the valve L_6 and ensures a change in the amplitude of less than 1.5% in the entire working range. Phase detectors are absolutely necessary in the study of NMDR spectra, and a large number of suitable circuits have been published [10, 22, 66, 73, 104, 105, 108]. The phase detector of the integrator of NMR spectrometers from the firm of Varian have been most frequently employed [10]. These simple instruments (see also L_8 in Fig. 19) can be used sucessfully to study qualitative aspects of NMDR spectra, and for stabilization according to [198], but they will be sensitive to undetectable frequencies and harmonics, they operate only within a narrow frequency range, and they are not free from drift. Figure 18 gives the circuit (L_1-L_5) of a phase detector for operation in the frequency range from 0.5 Hz to 20 kHz, suitable for all experiments on NMDR. For operation at very low frequency from 0.5 to 30 Hz, P_1 is closed. R_1, R_2, and C' make it possible to eliminate the influence of the strong undetectable signal (e.g., beats of f_1 and f_2 in experiments with scanning of the frequency) on the output voltage. D_{1-4} are selected according to the back current ≤ 0.01 μA at 200 V; the resistances marked by a point have an accuracy of ±2%.

In experiments using a very strong perturbing hf-field on the resonance frequency of protons, synthesis of the frequency f_2 employed has distinct advantages. Figure 19 gives a circuit for obtaining, from the frequency f_2, a frequency $f_0 + f_m$ with a high stability and purity of signal, and Fig. 20 gives a corresponding power amplifier, suitable for operation under pulse conditions with attenuation of the signal in the closed period by ≥130 dB. The valves

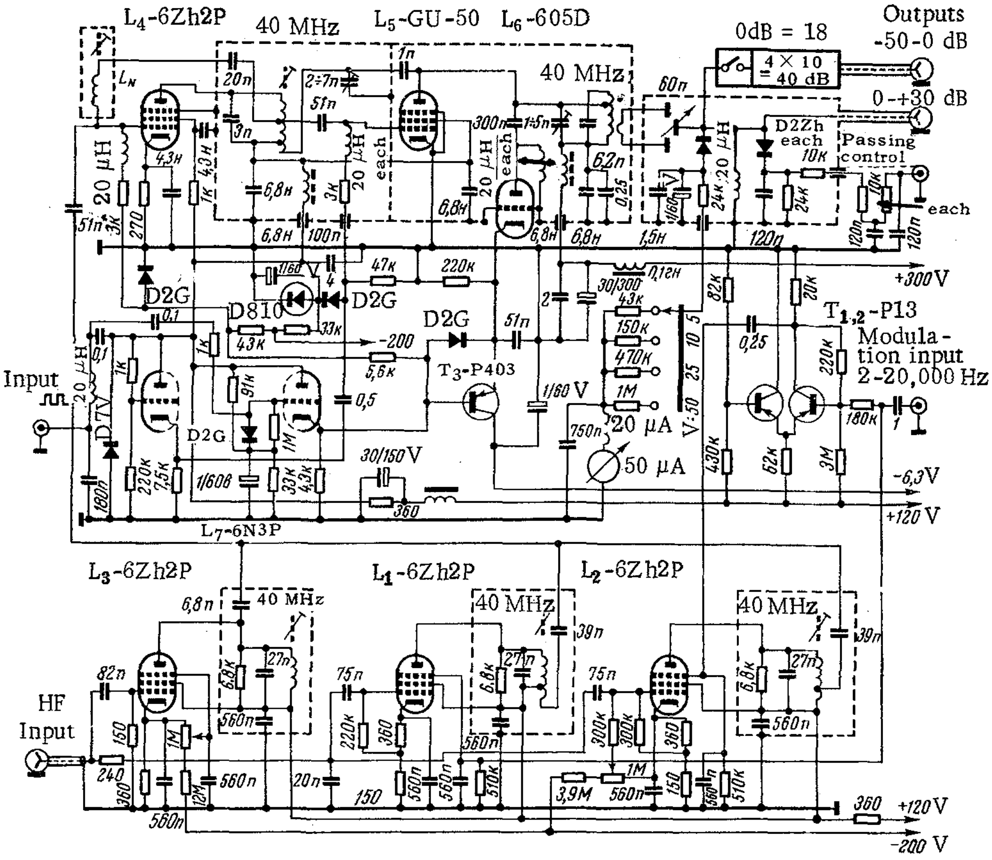

Fig. 20. Modulator and output stage. (See note to Fig. 18.)

L_{1-3} make it possible to use "pseudofrequency modulation" of the hf-field H_2 [216]. All the circuits given [92, 189] can readily operate on other frequencies, e.g., for the application of the various versions of heteronuclear double resonance.

When internal stabilization according to Primas [65, 78] is used, it is necessary to have a highly stable sonic frequency generator, e.g., a tuning generator or the generator shown in Fig. 18. The phase detector may be simple, of the type used in the integrator [10], although in this case a strong perturbing field influences the operation of the stabilizer if $f_{m2} - f_{ms} < 200$-300 Hz [252, 364]. It is therefore desirable to use a selective amplifier of low frequency in the stabilizer channel [200, 364], but this decreases slightly the rate of operation of the regulator. Detailed circuits for these stabilizers are given in [199-200].

For proton-proton double resonance it is possible to use the sensitive units designed for NMR—bridges and crossed coils—with the condition that there is sufficiently stable balance and nonvibrational rotation of the turbine. The use of magnetic-field modulation or time separation [98] is necessary in order to eliminate drift.

Accurate calibration of the amplitude of the perturbing hf-field is often necessary for the successful application of NMDR. This is particularly important in the determination of the signs of spin-spin coupling constants by selective double resonance, where the use of a hf-field which is too strong may lead to incorrect results. For the calibration it is possible to use the double resonance of an individual line according to formula (128), nutation vibrations according to (162) or the corresponding Bloch—Siegert displacement of the resonance frequency of this line according to formula (157). From (102) we find that the splitting $\mathscr{S}$ of the observed line for tickling in the system AX is approximately as follows:

$$\mathscr{S} \simeq \gamma_X H_2/2\pi, \qquad (160)$$

where γ_X is the gyromagnetic ratio of the nucleus X perturbed by the weak hf-field H_2 and $\mathscr{S} \ll |J_{AX}|$ [97, 493]. This method of calibration is particularly important in experiments using heteronuclear double resonance [97].

4.3. Heteronuclear Double Resonance Procedure. An important application of heteronuclear double resonance is the decoupling of nuclei in order to simplify the spectrum or for the indirect determination of chemical shifts [28]. In this connection, sufficiently powerful nonstabilized hf-generators can often be used [76, 125, 133, 296, 374, 483, 504, 591]. The stability of the spectrometer is improved when use is made of quartz generators, whose frequency can be changed within narrow ranges (from 2 kHz [29] to the record value of 8 kHz [201]) by a condenser connected in parallel with the quartz. These ranges are usually insufficient, and the required frequencies are obtained by amplitude modulation of a quartz generator [316] or the subsequent stages of the high-frequency amplifier [51, 521]. Frequency scanning can readily be achieved by changing the modulation frequency [316]. A more universal method of generating the frequency f_2 is by synthesis of the frequencies [51, 163], which makes it possible to couple the resonance frequencies of the nuclei being studied with the resonance frequency of individual groups of protons or other nuclei, e.g., F^{19} [158], in the same molecule [102, 139, 302, 303, 321]. The two frequencies employed f_1 and f_2 are obtained by multiple transformation of the frequency of the single stable generator. This method has been used to measure the chemical shifts of N^{14} [102] and C^{13} [28, 139, 158, 302, 303, 474, 624] with very high accuracy. The error in the measurement of the chemical shifts of the C^{13} in the carbonyl group of substituted benzaldehydes did not exceed 0.08 ppm (±2 Hz) [474]. These measurements, and also the tickling of satellites in the proton spectra by perturbation of C^{13} nuclei [139, 600] require the use of spin stabilization [139, 158, 321]. Additional frequency modulation [109, 145, 216], "pseudofrequency" modulation [80, 216], or pulse modulation [97, 201] of the perturbing hf-field are sometimes used to study the satellites from C^{13} in proton spectra, to improve the decoupling of nuclei, and to study relaxation processes. Very strong perturbation of the hf-field is necessary for complete decoupling of nuclei with broad lines and for the transfer of modulation through spin-spin coupling. A hf-field H_2 with an amplitude of 1.2 G (with forced cooling of the specimen) has been used for the complete decoupling of the protons in formamide [374], and a field with an amplitude up to 0.7 G has been used in the study of the double resonance $H^1-\{C^{13}\}$ [216]. The sensitive units of spectrometers designed for heteronuclear double resonance are always fitted with circuits with double tuning on both frequencies employed [51, 139, 201, 216, 374].

4.4. Commercial Instruments for Double Resonance. All modern NMR spectrometers are equipped with spin stabilization, and versions V (HA-100 and JNM-4H-100 spectrometers) and VI (A-60A spectrometer) are most frequently employed. To achieve any version of NMDR on these instruments it is necessary to have one additional stable low-frequency generator for modulation of the magnetic field, a numerical frequency counter (preferably a printing recorder), and a phase detector. The early types of NMR spectrometer, equipped only with magnetic-field scanning and stabilized by means of a superstabilizer can readily be used for the identification of multiplets and the determination of the signs of spin-spin coupling constants according to versions III and II [404], but for the application of tickling and the nuclear Overhauser effect it is desirable to use internal stabilization V [200].

Many firms produce special attachments for double resonance. The most important types are the PD-60, and SD-60 instruments for homonuclear and heteronuclear double resonance between all possible combinations of nuclei [605]. They operate according to a single-side modulation scheme, make it possible to carry out experiments using a strong (10 W) or weak perturbing hf-field, and are very widely employed, in particular, for experiments of the type $H^1-\{H^1\}$ [337, 338, 371, 546], $H^1-\{D^2\}$ [165, 315, 381, 383, 400, 410, 438], $H^1-\{B^{11}\}$ [409, 450, 505], $H^1-\{C^{13}\}$ [150, 458, 600], $H^1-\{F^{19}\}$ [192], $H^1-\{P^{31}\}$ [288, 320], $H^1-\{Tl^{203}, Tl^{205}\}$ [319], and also $B^{11}-\{H^1\}$ [475], $C^{13}-\{H^1\}$ [225, 623], $F^{19}-\{H^1\}$ [369], and even $F^{19}-\{B^{11}\}$ [409] and $P^{31}-\{P^{31}\}$ [293]. A modulator with separation of one side band [256, 346, 454, 606] and blocks for the decoupling of nuclear spins, produced together with spectrometers by Varian [125, 302, 303, 425, 447, 521] and Perkin-Elmer [376, 497, 547] are less widely employed. Use is often made of the XUA frequency synthesizer produced by the firm of Rode and Schwarz (Munich), which has a very high stability and accuracy [97, 179, 301, 325, 453, 485]. Similar instruments are also produced by "VEB Messelektronik," Berlin.

5. Applications of Nuclear Magnetic Double Resonance

5.1. The Overhauser Nuclear Effect. The possibility of a strong increase in nuclear polarization by saturation of the electronic transitions in metals, where there is strong scalar coupling between the electronic and nuclear spins, was predicted by Overhauser [594] and generalized for the case of dipole-dipole interaction by Abragam [595]. This phenomenon is widely used in electronic-nuclear double resonance, where a considerable increase in the NMR signal in a positive or negative direction is achieved, depending on the relaxation mechanism predominating [1, 464, 535, 536]. The opposite experiment with saturation of the nuclear spins is used chiefly in the study of solids and is often realized by the ENDOR metnod [596], which has recently found application for the study of free radicals in solutions [408, 424]. These experiments make it possible to determine the signs of the constants of the hyperfine splitting in EPR spectra from the known sign of the constant of the dipole-dipole coupling between nuclear spins [431]. The change in the intensities of the spectral lines in double resonance is a completely general phenomenon and is encountered in gas spectroscopy [215, 584], where saturation of mocrowave transitions make it possible to study relaxation processes [278] and to identify spectral lines [215].

The nuclear-nuclear Overhauser effect is smaller by two orders of magnitude than the electronic-nuclear effect, but in spite of this it has been widely applied. The stationary effect is used to determine the mutual arrangement of the energy levels of spin systems [56, 89, 90], often by the INDOR method [79, 88, 97, 158, 166, 271, 321, 531], to determine the chemical shift of hidden or overlapping spectral lines [319], and to study relaxation processes [49, 56, 57, 386, 466]. It follows from the system of Eq. (72) and the electrical analog (Fig. 11) that the effect is greatest on lines which have a common energy level with the line being perturbed, but it is not restricted to these lines [56, 79, 139]. There is a particularly marked change in the intensity of the line with $\Lambda = 1$ in the spectrum of type AX [79] and the lines with analogous positions in more complex spectra; this feature has been used for the determination of such lines [319]. If the relaxation time of a nucleus X coupled with the nucleus A being studied is much shorter (Tl^{203} and Tl^{205} compared with H^1 [319]), a marked decrease in the intensity of the lines $\Lambda = 1$ is observed for the case where intermolecular dipole-dipole relaxation predominates [56, 225, 319, 418, 558]. This phenomenon is used in the NMR spectrometry of C^{13} in order to determine how the spectral lines belong to the multiplets. If two (or more) lines in the spectrum of C^{13} form a multiplet, the second line is always less than the first line for rapid adiabatic passage, irrespective of the direction of scanning. If the neighboring lines in these spectra correspond to noncoupled transitions, rapid adiabatic passage of the first does not alter the intensity of the second. When intramolecular dipole-dipole relaxation predominates (in gaseous HD diluted with CO_2 [420]), an increase in the intensity of these lines is observed. The Overhauser effect between lines with different symmetries of the corresponding wave functions is usually small [90], but there are exceptions to this rule [56]. For the above reasons, the Overhauser effect cannot be taken as a reliable basis for the compilation of energy level diagrams, although this has been suggested [89, 90] and has found application [357].

In INDOR spectra, where the frequency of a very weak nonsaturating hf-field ω_1 is tuned exactly on to any line and recordings are made of the changes in the intensity of this line for passage of the spectrum under conditions of scanning of the frequency ω_2 by a weak but saturating hf-field H_2, the signal/noise ratio is much worse, and the Overhauser effect is in fact manifested first of all on the lines which have a common energy level with the line being perturbed [89]. This procedure is of practical importance in those cases where tickling is inapplicable because of the relaxation broadening of the spectral lines being studied (the α-protons of pyridine derivatives) [88], but it requires a very accurate selection of γH_2, since tickling leads to marked distortion of the form of the lines in the INDOR spectrum.

The use of the dynamic Overhauser effect in the analysis of the spectra gives more reliable results. The saturation of any transition in the NMR spectrum takes place rapidly, with constant time T [493, 562]

$$\frac{1}{T}=\frac{1}{2}\left[\frac{1}{T_1}+\frac{1}{T_2{}^*}\right] \tag{161}$$

and immediately after saturation the differences in the populations of only the directly coupled transitions are found to be changed. The other populations change much more slowly ($T^1 > T^2*$) under the influence of longitudinal relaxation. Although these processes are not exponential, here and in subsequent sections T^1 is used to denote the order of magnitude of this rate. If the frequency ω_1 of a relatively strong (saturating) measuring hf-field H_1 is tuned exactly on a single line of the spectrum, passage of the spectrum by another saturating hf-field H_2 with change in the populations of the energy levels of the transition being studied by the hf-field H_1 leads to the production of nutation vibrations with frequency Ω' [493]

$$\Omega' = \gamma H_{ef} = [\gamma^2 H_1{}^2 \lambda_{pq}{}^2 + (\omega_0 - \omega_1)^2]^{1/2}, \tag{162}$$

where $\lambda_{pq} = \langle p | I_x | q \rangle$.

The first surge of vibrations is directed in the positive direction for saturation of the progressive transition $\Lambda = 2$ and is directed in the negative direction for saturation of the regressive transition $\Lambda = 0$. Both hf-fields should be saturating, for which $\gamma^2 H^2 \lambda^2_{pq} T_1 T_2* \gg 1$; moreover, for the hf-field H_2 the condition of rapid adiabatic passage should be satisfied:

$$\gamma H_2\lambda_{qr} \gg \frac{1}{H_2\lambda_{qr}}\cdot\frac{dH_0}{dt}. \tag{163}$$

The transition processes are of short duration; both the nutation vibrations and the tickling (which appears if the hf-field H_1 is weak) disappear with a constant time close to $T_2{}^*$ [87, 97, 98], whereas the nonstationary values of the differences in the populations of the same transitions are preserved for a much longer period. This feature is used in the method of transition selective irradiation (saturation) TSI [87, 154, 233, 265] for the compilation of energy level diagrams [154] and the determination of the relative signs of spin-spin coupling constants. In this procedure the spectra are recorded by scanning the magnetic field, but the frequency difference $(\omega_2-\omega_1)/2\pi = f_{m2}-f_{m1}$ selected is a fraction of 1 Hz (0.2 Hz) smaller then the difference in the resonance frequencies of the perturbed and measured spectral lines. This ensures that the intensity of the line studied by the hf-field H_1 is measured not later than 1 sec after the adiabatic passage of the perturbed line [265]. A sharp change in the frequency f_{m2} before the passage of the line being studied can also be used for the same purpose [154]. The intensities of the lines $\Lambda = 2$ in the spectrum increase and the $\Lambda = 0$ lines decrease, the change being very marked in degenerate systems [265]. In more complex cases, selective transition irradiation of two lines having common energy levels with the spectral line being studied is possible. This procedure can be used to determine the relative signs of the coupling constants in three-spin systems of the type ABC, where one of these constants is too small for measurement [265].

The Overhauser effect accompanying the collapse of the multiplet is used in the spectrometry of C^{13}, Sn^{119}, and other nuclei. As a result of the fact that $\gamma_H/\gamma_X \gg 1$, the intensities of the lines of these nuclei increase for saturation of the corresponding lines of the proton spectrum by a factor of several times [22, 137, 227, 302, 303, 606], a marked positive effect being observed even in the strongly associated [440] purines [369]. In rare cases nuclear and electronic-nuclear Overhauser effects are used together in order to increase the intensity of the weak spectral lines of C^{13} and P^{31} [464, 535]. In general the Overhauser effect appears in all NMDR experiments, although it was not noticed by the earliest workers [29, 51]. Anderson and Freeman describe the redistribution of the intensities of the lines inside the multiplets, but without change in the over-all intensity [65]. Such changes do in fact take place, e.g., in toluene [99], dimethylformamide, and β,β-dimethylacrylic acid [442], and are particularly marked in compounds with a rigid endo-, endo-hemicellular structure [441] and in ginkgolides and many aromatic compounds containing a tert-butyl group [608, 614, 615]. A positive effect equal to 45% [422] and even 56% [608] has been measured in these compounds between protons which are spatially very close but which are not linked by spin-spin coupling (six bonds without zigzag configuration).

The Overhauser effect is widely used to study relaxation phenomena. This work is examined in section 5.6.

5.2. Tickling and Selective Double Resonance. The splitting of the spectral lines, described by formula (102) and (165) and shown in Figs. 6, 7, and 8, provides the chief method for compiling energy level diagrams of spin systems [78, 100, 146, 152, 156]. In the study of spectra consisting of narrow lines, tickling is free from the many complications associated with the use of changes in the intensities of the lines. The possibility of splitting lines without common energy levels [47] is in fact very small. Figure 8 illustrates clearly the possibility of using tickling (and also the Overhauser effect) for the determination of the relative signs of spin-spin coupling constants [100, 146, 150, 179, 283, 321, 367, 453, 485, 556, 567]. The nature of the splitting (see Fig. 15) makes it possible to determine the type of transition being studied. The lines $\Lambda = 0$ are split much more effectively than the lines $\Lambda = 2$ [78]; in the last case, splitting may sometimes even be absent. Nevertheless, this assignment of the lines to types is not always unambiguous [155] and in spectra recorded by scanning the magnetic field the splitting of the lines $\Lambda = 2$ is even more distinct than the splitting of the lines $\Lambda = 0$ [257]. Scanning of the magnetic field [150] is of course rarely used to study tickling. Scanning of the frequency is almost always used [78]. Tickling also provides a very successful method for measuring the resonance frequencies of spectral lines which overlap or which are not directly detectable on a given spectrometer, particularly the lines of the C^{13} nuclei, by means of corresponding satellites in the proton spectra [150, 600, 624]. This makes it possible to measure C^{13} chemical shifts with a very high accuracy [321], which even reaches 0.01 Hz [179].

In the derivation of formula (98) splitting was regarded as a change in the form of the line. Another approach to this phenomenon makes it possible to describe it as the appearance of new lines as the spectrum is complicated by the hf-field. The addition of one nucleus B to a two-spin system AX leads to the appearance of nondiagonal elements $^1/_2J_{AB}$ in the matrix of the Hamiltonian of this system, and under suitable conditions to splitting of the quantity $|J_{AB}|$ in the spectrum of nucleus X [599]. By a close analogy, nondiagonal elements $\gamma H_2/4\pi$ appear in the matrix of the Hamiltonian of this two-spin system AX under the influence of a resonance hf-field H_2 [599].

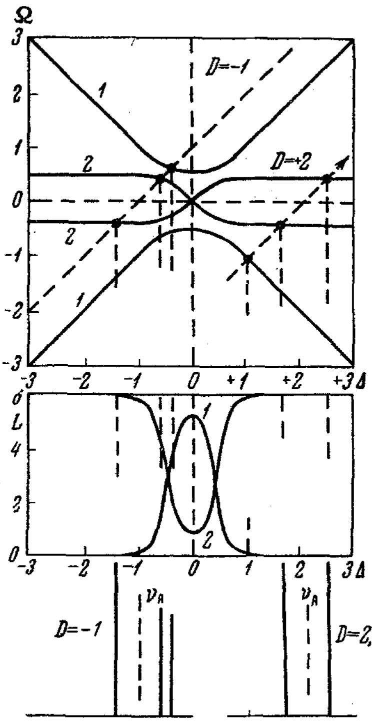

Fig. 21. Spectra of nucleus A of a two-spin system AX, recorded by scanning the magnetic field H_0; $\gamma H_2 = 0.4\pi J$.

By diagonalizing the Hamiltonian by the usual methods employed in the analysis of NMR spectra, we obtain new values of the energy for both levels of the perturbed transition [78] (see Fig. 6):

$$E = \frac{(2E_r - \omega_{rs} + \omega_2)}{2} \pm \sqrt{\frac{(\omega_2 - \omega_{rs})^2}{4} + \frac{h_{rs}^2}{4}}, \qquad (164)$$

where $h_{rs} = 2\lambda_{rs}$ and $\lambda_{rs} = \langle r | I_x(X) | s \rangle$, and for local action on only one line rs of the doublet of nucleus X we obtain an expression for both new resonance frequencies of the line rp being split in the spectrum of nucleus A:

$$\omega_1 = \omega_{rp} + \frac{(\omega_2 - \omega_{rs})}{2} \pm \frac{1}{2}\sqrt{(\omega_2 - \omega_{rs})^2 + h_{rs}^2}. \qquad (165)$$

It follows from (165) that the splitting of the line rp depends on the intensity of the perturbed line, which is proportional to h_{rs}^2 [78]. When a slightly stronger hf-field H_2 with a frequency close to the mean of ω_{pq} and ω_{rs} acts on both lines rs and pq of nucleus X, all the energy levels are split, and the values of all the square roots in expressions of type (164), with the condition that the intensities of the two lines of nucleus X are the same, show identical dependences on H_2, as a result of which two lines of the four in the spectrum of nucleus A coincide. Their intensities increase with increase in H_2, whereas the two remaining lines are reduced and move further apart (see Fig. 5). Selective collapse is produced, affecting only one "pseudo-Ax-system" of the more complex spectrum. For example, the perturbation of lines B1 and B2 by a frequency $\omega_2 = (\omega_{B1} + \omega_{B2})/2$ leads to merging of the doublet A1, A2 in the spectrum of nucleus A (Fig. 9a) if J_{AC} and J_{BC} have the same sign, and to merging of the doublet A3, A4 if the signs are opposite (Fig. 9c). This selective double resonance has found very extensive application in the identification of multiplets and the determination of the relative signs of spin-spin coupling constants in complex spectra [62, 81, 82, 149]. If however the frequency of the perturbing hf-field H_2 is tuned in a "pseudo-AX-system" with different intensities for the two lines of the doublet of nucleus X on a frequency ω_2 outside the doublet on the side of the weaker line, it is found that as a result of the difference in the splitting of the two lines of the doublet of nucleus A the distance between the most intense lines of the four lines which appear will not decrease, but increase [16, 352, 373]. This phenomenon has been used to determine the sign of a very small spin-spin coupling constant, whose magnitude was less than the resolving power of the instrument (0.3 Hz) [352]. Unfortunately, this method is not universal. Increase in the splitting from 0.15 to 0.45 Hz required a perturbing hf-field H_2 with an amplitude of 7 Hz, which is too strong for most spectra. Double tickling [259] is more universal. If in a system ABC we have $J_{AB} \cong 0$, it follows that A1 = A2; A3 = A4 and B1 = B2; B3 = B4 (Fig. 9a) and the spectrum now shows doublets consisting of two degenerate lines instead of quadruplets, whose irradiation does not lead to tickling for the reasons described above. This interfering degeneracy can be removed by additional perturbation of a single spectral line of nucleus C. With perturbation of the transition C1, the lines A1, A3, B1, and B3 are split to form doublets, the remaining lines of the spectrum remain unchanged, and as a result the degenerate lines of the spectrum are split to form triplets, which can be used for the determination of the signs of J by means of tickling. This method has been used to determine the sign of the very small coupling constant $J < 0.2$ Hz in 3-bromothiophenaldehyde-2 [259].

5.3. Action of a Perturbing Field of Intermediate Strength. The form of the spectrum recorded under those conditions can readily be found from Freeman's diagrams [65, 66, 153]: Figs. 16 and 21. The diagrams for three-spin systems of the type AKX consist of the superpositions of two diagrams for the system AX. If K = X, these are superposition diagrams with shift $\Delta = J_{AX}$ along the x axis; if $K \neq X$, then in addition to the shift J_{KX}/J_{AX} along this axis we add a vertical shift by J_{AK}/J_{AX}; and in the case of systems of the type $A_mK_nX_r$ additional shifts are added [266]. Comparison of these diagrams with the experimental spectra makes it possible to determine the relative signs of the spin-spin coupling constants [52, 216, 266]. The method requires the compilation of individual diagrams, so that it has not found extensive application except in those cases where the use of a strong perturbing hf-field is unavoidable, particularly in the study of modulation transfer [216].

The spectra recorded by scanning the magnetic field at intermediate values of the amplitude of the hf-field H_2 are symmetrical only with exact tuning of the frequency ω_2 of this field in resonance with the nucleus being perturbed. This can be shown analytically [284, 568-570], but it is also very clearly illustrated by Fig. 16. In the study of the ammonium ion by the experiment $H_1-\{N^{14}\}$, detuning of the frequency of the perturbed hf-field by 0.5 Hz led to appreciable asymmetry in the proton spectrum [51], and this made it possible to determine the chemical shift of the nitrogen very accurately. These spectra have also been used to determine the amplitude of the perturbing hf-field, but this procedure has no practical importance. At the present time the spectra recorded at intermediate values of the amplitude of the perturbing field are not used for structural analysis, but they are used for the study of relaxation processes [95, 420].

5.4. Decoupling of Nuclei and Collapse. The decoupling of nuclei with complete or partial merging of the corresponding multiplets is the most common application of NMDR. The spectra of the decoupled nuclei can be recorded under the most varied experimental conditions, with scanning of the frequency or the magnetic field and with slow or rapid adiabatic passage of the spectrum [225]. The intensity of the magnetic field H_0 als is not critical, and decoupling can be achieved even at sonic frequencies in a weak field [175]. For the decoupling of the very broad multiplets encountered in flourine compounds, it is necessary to use scanning of the frequency [189, 357] of the measuring hf-field. Only this procedure makes it possible to preserve the resonance of the hf-field H_2 with the perturbed spectral lines independently of the scanning. Additional frequency modulation of the perturbing high-frequency can be used to decrease the residual splitting (145) produced even in a spectrum of the type A_2X (see Fig. 16) [145]. In systems of the type A_3X, A_2KX, and AK_2X consisting of nuclei with spin $I = {}^1\!/_2$, the frequency of precession of the spin X about the direction of the effective field in rotating coordinates can in accordance with (135) have four values. For exact tuning of the perturbing frequency $\omega_2 = \omega_X$ $A({}^3\!/_2) = A(-{}^3\!/_2)$ and $A({}^1\!/_2) = A(-{}^1\!/_2)$, but $A({}^3\!/_2) \neq A({}^1\!/_2)$ and the residual splitting is produced as a result of this difference. If however we select the frequency of modulation in such a way that $\omega_m = {}^1\!/_2[A({}^3\!/_2) + A({}^1\!/_2)]$, we find that in the doubly rotating system of coordinates the rate of precession of nucleus X is no longer dependent on mA and this nucleus can be completely decoupled from the remaining nuclei. Unfortunately, the necessary modulation frequencies are fairly high (30 Hz for complete decoupling of the methylene protons from the methyl protons in ethyl alcohol), so that this procedure can be used primarily for heteronuclear spin decoupling, which can be further improved by the use of an infinite number of modulation frequencies, i.e., noise modulation [190, 237, 557]. Frequency noise modulation with a small modulation index is used in these experiments. Gradual increase in the power of the perturbing hf-field H_2 leads to disappearance of the multiplets; no new spectral lines are produced, and the nature of the process resembles the increase in the rate of relaxation or chemical exchange of the coupling nuclei. In actual fact, the introduction of stochastic interaction with the external hf-field H_2 in the kinetic equation leads to the appearance of a term whose form resembles that of the relaxation term Γ [557]. The analogy with relaxation is not complete; because of the spatial coherence of the perturbing hf-field, transfer of the noise modulation to the spectral lines being measured takes place and in order to achieve a good signal/noise ratio it is necessary to use slow scanning with effective filtrations of the signal. As a result of the broad frequency spectrum, decoupling is achieved even under conditions of considerable detuning of the frequency ω_2, and this method is particularly suitable for the decoupling of fluorine nuclei $H^1-\{F^{19}\}$, where the width of the spectrum of the nuclei being decoupled may reach 2 kHz.

Irradiation of the spin being decoupled by resonance pulses with definite frequency of repetition, duration, and intensity also makes it possible to save high-frequency power by comparison with the usual continuous action [351]. A nonresonance frequency-modulated strong hf-field H_2 with an amplitude of all components such that at least two of these interact with one spectral line of the nucleus being perturbed produces changes in the quantum state of this spin in time with the modulation. These changes are transferred by means of the spin-spin coupling to all other coupled spins of the molecule. Transfer of modulation has now been achieved in the systems $H_1-\{C^{13}\}$ [109, 216] and $H^1-\{N^{14}\}$ [80] and provides an excellent method for the selective isolation, in proton spectra, of only those lines (satellites) which have common energy levels with the lines of the nuclei being perturbed.

Decoupling of nuclei is widely used to simplify spectra. In some cases the simplified spectra make it possible to determine immediately all the required characteristics of the compound [119, 273, 369] or polymer [339-343] being studied, but usually, collapse is only the first stage in the analysis of the complex spectrum [257, 307, 369] or the determination of the signs of the spin-spin coupling constants by other double resonance methods [253, 254, 257, 331, 357, 540]. Decoupling of nuclei leads to the decrease in the width of the spectral lines required for many measurements. In this connection, the decoupling $H^1-\{D^2\}$ is used in all studies of the conformation of cyclic deuterated hydrocarbons [298, 315, 400, 438, 519] and was used before the determination of the rate of chemical exchange from the characteristic width of the line [262].

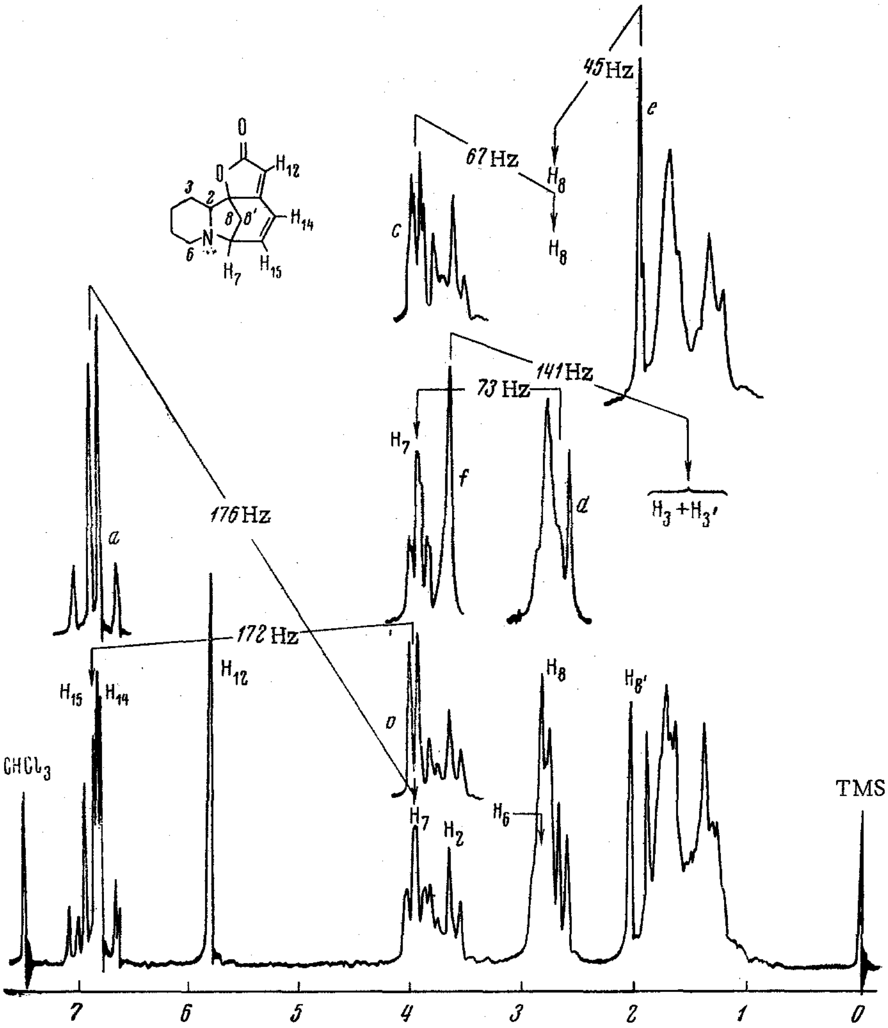

Fig. 22. Identification of the multiplets in the proton spectrum of phyllochrysene [182].

The most important and most common application of the decoupling of nuclei is for the identification of the multiplets in complex spectra. The study of spin-spin coupling makes it possible to determine which of the protons or other nuclei are coupled with one another and hence are either spatially close to one another or are present in quite difinite geometric relationships (Fig 22). In order to obtain this information all more or less effectively separated multiplets are perturbed by a hf-field H_2 and the changes produced in the spectrum are observed [23, 181-183, 310, 349, 544]. These methods also make it possible to determine the chemical shifts of multiplets which cannot be observed directly [83, 223, 443] or of other nuclei, e.g., C^{13} [28, 216, 283, 303, 304, 321, 368, 474, 522], N^{14} [51, 75, 76, 102, 132, 163, 230, 351], P^{31} [29, 288, 483] amd Xe^{129} [224, 232]. The indirect determination of chemical shifts is particularly important in the analysis of carbohydrates, where the multiplets of various protons show considerable overlap [293, 484, 524]. Of particular interest is the application of this method with the simultaneous use of dimethyl sulphoxide as solvent. This solvent forms particularly strong hydrogen bonds with the hydroxyl groups [449], the chemical exchange of the protons is prevented, and the NMR spectrum shows the individual doublets of the hydroxyl protons of the carbohydrate being studied. The collapse of these doublets readily makes it possible to find the chemical shifts of the corresponding protons of the skeleton [486].

The use of the decoupling of protons for the identification of multiplets has given particularly good results in the analysis of the alkaloids [23, 182, 223], and also steroids [5, 181], terpenes [543], and other compounds [310]. Sometimes, for low values of the coupling constant, decoupling of the nuclei is accompanied only by an increase in the peak value and a decrease in the width of certain lines of the spectrum [395, 473, 496]; a typical example is provided by the collapse of the lines due to the angular methyl group in 5-cyclodecenones [545] and steroids [242, 456].

In the analysis of particularly complex spectra, multiple decoupling of one nucleus (or group) from several others is necessary. This is achieved by using one very strong perturbing hf-field [106] or by using several, usually two, perturbing fields. In the last case there exists a narrow range of amplitudes of these fields in which the form of the spectrum under the conditions of triple resonance can be calculated, assuming that the coupling constants between the decoupled nuclei are equal to zero [252]. Triple resonance has been used to identify the multiplets in the complex spectra of norbornene derivatives [304], the nonbornadiene cation [246], chromomycinone [310], dihydropleiadened [496], steroids [181], and other compounds [445, 574], including polymers [238]. Quadruple resonance has been used to determine the structure of the product of the addition of thallium triacetate to norbornadiend [319]. Homonuclear and heteronuclear decoupling can be used simultaneously [239, 576].

Rapid relaxation of the spin coupled with the nucleus being studied leads to the disappearance of the multiplet character [37], which is similar to the decoupling of nuclei by a strong hf-field with noise modulation, but in this case the perturbing field is noncoherent. This phenomenon is always observed in compounds of the halogens, Hg^{201} [258], and Xe^{131} [224]. Nitrogen compounds occupy an intermediate position [125-131], and complete decoupling of H^1 nuclei is achieved only by irradiating the N^{14} nuclei with a strong hf-field H_2 [22, 70, 125, 138, 374]. In particular cases, partial disappearance of the multiplet in the proton spectrum is observed even as a result of the rapid relaxation of B [505] and F^{19} [160, 597, 611]. Merging of a multiplet may also take place under the influence of selectively operating paramagnetic ions [72, 170, 171]. The addition of Cu^{2+} ions to ethyl alcohol leads to broadening of the line of the hydroxyl proton and merging of the quadruplet of the methylene protons [170, 171]. Study of the influence of the paramagnetic ions Mn^{2+}, Ni^{2+}, and Co^{2+} on the spectra of adenosine-triphosphoric acid has made it possible to confirm [172] Szent-Gyorgyi's guess regarding he arrangement of the metal ions in nucleosides [173]. The "decoupling" of the H^1 nuclei from the action of paramagnetic ions [39, 482] requires the use of a very strong hf-field (>1000 G) and is practically unattainable.

5.5. Multiquantum Transitions. With a very high amplitude of the measuring hf-field H_1, new lines appear in the spectrum, corresponding to multiquantum transitions, chiefly two-quantum transitions [40, 41, 58, 140, 141, 143, 144, 159]. Two-quantum transitions take place between the extreme energy levels of transitions $\Lambda = 2$ at a frequency $2\omega \cong \omega_1 + \omega_2$ (versions 4 and 5 of Fig. 14). A new line appears between the lines of nuclei A and B with resonance frequencies ω_1 and ω_2, but with a slight shift [40, 155] towards the more intense line. These spectral lines can also be used to compile energy level diagrams [155] and to determine the signs of spin-spin coupling constants [144, 167]. The two-quantum lines are saturated readily, in proportion to $\gamma^3 H_1^3$, and the determination of all the new lines requires the use of a large number of spectra [155, 167]. The intensity of the two-quantum transitions increases when two hf-fields, tuned on frequencies ω_1 and ω_2 respectively, are used instead of one strong hf-field. These hf-fields can be obtained by modulation methods [40, 142]. Since the measuring field required in order to observe the two-quantum transitions is on the average 50 times stronger than the usual field [144], the spectra obtained are of poor quality, with strong side bands due to the rotation of the turbine. For this reason, multiquantum transitions have not found application in the analysis of complex compounds.

5.6. Study of the Relaxation of Nuclear Spins by Double Resonance Methods. The chief aim of all these studies is to determine the predominating mechanisms of the relaxation of spins and the details of molecular motion in liquids and gases. In view of the complexity of the relaxation of even simple molecules, the solution of these problems is only beginning. A large amount of information for simple molecules has also been obtained by NMR pulse methods. This work is not considered here.

Solomon [128] was the first to use NMDR to study the relaxation of the spins of H^1 and F^{19} in anhydrous HF, where, as a result of rapid chemical exchange, both nuclei are represented by a single spectral line. We find from Fig. 23 that the magnetizations of the individual nuclear spins are proportional:

$$k\langle I_z\rangle = k\{\langle I_z{}^+\rangle + \langle I_z{}^-\rangle\} = (N_{++} - N_{-+}) + (N_{+-} - N_{--}), \tag{166}$$

$$k\langle S_z\rangle = k\{\langle S_z{}^+\rangle + \langle S_z{}^-\rangle\} = (N_{++} - N_{+-}) + (N_{-+} - N_{--}). \tag{167}$$

The rates of the change in these magnetizations under the influence of longitudinal relaxation are determined by the expressions

$$\frac{d\langle I_z\rangle}{dt} = -(W_0 + 2W_I + W_2)\{\langle I_z\rangle - I_0\} - (W_2 - W_0)\{\langle S_z\rangle - S_0\}, \tag{168}$$

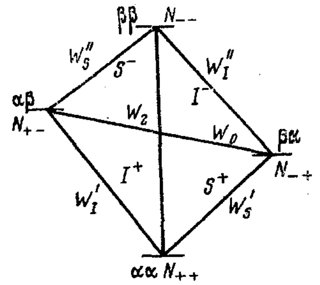

Fig. 23. Population and magnetization in a two-spin system.

$$\frac{d\langle S_z\rangle}{dt} = -(W_2 - W_0)\{\langle I_z\rangle - I_0\} - (W_0 + 2W_S + W_2)\{\langle S_z\rangle - S_0\}. \quad (169)$$

These processes themselves are not exponential, but the change in the difference in the magnetizations with time is exponential [77]:

$$\frac{d}{dt}(\langle I_z{}^+\rangle - \langle I_z{}^-\rangle) = -2(W_S + W_I)\{\langle I_z{}^+\rangle - \langle I_z{}^-\rangle\}, \quad (170)$$

$$\frac{d}{dt}(\langle S_z{}^+\rangle - \langle S_z{}^-\rangle) = -2(W_S + W_I)\{\langle S_z{}^+\rangle - \langle S_z{}^-\rangle\}. \quad (171)$$

In most cases it may be assumed that $W_S' = W_S'' = W_S$, anisotropy S of the chemical shift of the nucleus $W_S' \neq W_S''$ [528]. From (168) we obtain for the stationary value ([1], p. 313):

$$\langle I_z\rangle = I_0 + \frac{W_2 - W_0}{W_2 + 2W_I + W_0} \cdot S_0 = I_0 + \frac{\sigma}{\rho} S_0. \quad (172)$$

Under the conditions of strong contraction, we obtain for the dipole-dipole relaxation [1, 10, 59] $\sigma/\rho = {}^1\!/_2$, and for scalar relaxation [1] $\sigma/\rho = 1$ [1, 128]. The experimental value $\sigma/\rho = {}^1\!/_2$ showed that in HF both mechanisms operate, the intensity of the scalar relaxation depending to a marked extent on the moisture content. Solomon neglected intermolecular relaxation processes. In order to take account of the influence of dipole-dipole interaction between the molecules, Solomon's analysis was extended to a system of four spins AXA'X' [386, 465] with 16 energy levels. The equations derived are similar to Eqs. (168)-(171), the time dependence of the differences in the magnetizations (170, 171) being different for intramolecular and intermolecular dipole-dipole relaxation. Study of the $CHFCl_2$ molecule [386, 528, 561] showed that at low temperatures the dipole-dipole relaxation and the relaxation produced by the anisotropy of the chemical shift of fluorine predominate, so that $W_S' \neq W_S''$. The appearance of cross terms in the relaxation matrix made it possible to relate the sign of the spin-spin coupling constant J (HF) to the sign of the anisotropy of the chemical shift, and the determination of this sign [581] made it possible to determine the absolute (positive) sign of this constant. At higher temperatures the intense spin-rotational relaxation of fluorine is added, and the intramolecular and intermolecular dipole-dipole relaxations [19, 59] play approximately equal roles with little dependence on dilution [561].

Study of the relaxation of the protons of formic acid and acetaldehyde by the same methods [598] showed that dipole-dipole interaction between the formyl and carboxyl protons is the important mechanism of relaxation in this molecule. For the relaxation of the protons of the methyl group of acetaldehyde, the processes inside this group were found to be more important. The work cited gives a clear discussion and derivation of the modified equations of Solomon.

In order to measure the dynamics of the change in the intensities of the signals in [386, 528, 561, 598], use was made of repeated passage of the spectral line being studied by a weak measuring hf-field after rapid adiabatic passage or saturation of the perturbed line. The same procedure was used in [57, 466] to study proton relaxation in 2,3-dibromothiophene. In order to determine the relative probabilities of transition, the authors cited used the simple system of Eq. (72) instead of the much more complex Eqs. (112-115), describing accurately the influence of the perturbation of several spectral lines by a strong hf-field on the populations of the energy levels. Comparison with experiment [466] showed that (84) describes satisfactorily the change in the populations of the spin system with time under the influence of longitudinal relaxation at moments of time $t \gg T_2{}^*$ after the removal of the perturbing hf-field H_2, if account is taken of the influence of this field on all the transitions of the system being studied by means of formula (71). The relative values of the probabilities of the transition W, calculated from the populations, determined by extrapolation to moment of time $t = 0$, show that in this molecule both intramolecular and intermolecular dipole-dipole relaxations operate, the influence of the external fields being to a large extent correlated [57]. Direct measurement of the intensities of the spectral lines is difficult. In [56] a clearly inadequate accuracy of ±10% was achieved. Because of the intermolecular Overhauser effect [99, 101], the use of an internal standard does not give a high experimental accuracy either. In attempts to measure the Overhauser effect by slow pulses

[201, 294], spectra were obtained with a surprisingly poor signal/noise ratio. Thus all other work on the study of the mechanisms of nuclear relaxation by NMDR methods has given qualitative rather than quantitative results. It has been possible to show that in 2-chloro-5-bromothiophene the correlated intermolecular dipole-dipole relaxation of the proton predominates, with a very small contribution from intramolecular dipole-dipole relaxation [32]. In difluoroethylenes [56, 387, 597, 611], the influence of the spin-rotational relaxation of fluorine is found to show a marked dependence on the structure of the molecule. Relaxation transitions between energy levels corresponding to wave functions with different symmetry took place only in 1,1-difluoroethylene, but did not take place in cis- and trans-1,2-difluoroethylenes [56]. These compounds also did not show the influence of cross terms in the relaxation matrix, but in other cases these terms appeared [420] and were even used to determine the absolute sign of +J(HF) [528]. Study of the proton spectrum of CH_3CHF_2 in the gaseous phase showed that the probability of transition between the singlet and triplet states of the group of two fluorine nuclei is very low [160], as was assumed by Bloch in the derivation of the kinetic equation [37].

The theory of nuclear relaxation in multispin system is developed in [419, 421]. In contrast to earlier work concerned with the study of relaxation processes, Rao [420] studied the nature of the collision of gaseous HD molecules, on the basis of the theory of weak [55] and strong collisions [33]. The model with strong collisions (i.e., associated with a change in the rotational quantum number) gave better agreement with experiment.

Until now we have examined methods of studying nuclear relaxation with the action of saturating and measuring hf-fields on the same molecule. This is unimportant for dipole-dipole relaxation, however. Saturation of the signal of one of the interacting spins S influences the magnetization of the other spin I in accordance with Eq. (168), even if the nuclei are present in different molecules, but intermolecular dipole-dipole relaxation is predominant. Such effects were first observed by Nagumo and Kakiuchi [112] and were studied in more detail in [99, 101, 418]. Saturation of the signal from the protons of one molecule leads to an increase in the signal from the protons of another molecule by 10-40% [99, 101, 608]. Here, a small number of magnetic nuclei in the compound being studied is not essential. Marked effects were achieved in mixtures of chloroform [101], benzene, nitrobenzene, toluene, acetone, methanol, and other compounds with cyclohexane, dioxane, etc. [99]. With the appearance of stable associates, the effect may decrease and there is no measurable effect between the cyclohexane and benzene rings of cyclohexylbenzene in the pure liquid, whereas saturation of the signal from cyclohexane increases the signal from the benzene protons by 31%. In the study of the saturation of sodium hypophosphite in a mixture of water and dimethylformamide, saturation of the protons of the water leads to an increase in the signal from the protons of the hypophosphite, whereas saturation of the larger number of protons of the methyl groups of the dimethylformamide does not have this effect. All these data indicate the possibility of existence of an ordered microstructure in many liquids. These results, together with [566, 602], show that intermolecular dipole-dipole relaxation plays an important part even in large molecules.

Chemical exchange in alcohols is the reason for the strong scalar relaxation of the protons of functional groups adjoining the hydroxyl group. On saturation of the signal of the hydroxyl protons, the signals from neighboring groups of protons decrease to almost zero [99], since in this case $\sigma/\rho = -1$. With sufficiently rapid passage, similar effects appear even in the single resonance spectra [117].

5.7. Study of Chemical Exchange. If the nucleus X can occupy two (or three) [270] positions A and B, saturation of B leads to a decrease in the signal from A, with the obvious condition that the lifetimes τ_A and τ_B be sufficiently large (this condition is satisfied, for example, in a mixture of salicylaldehyde and 2-hydroxyacetophenone [177]. In this case we have [177, 178, 243]:

$$\frac{dM_z^A}{dt} = \frac{M_0^A}{T_{1A}} - \frac{M_z^A}{\tau_{1A}} \tag{173}$$

where M_0^A is the equilibrium magnetization of nuclei X in position A, $1/\tau_{1A} = 1/\tau_A + 1/T_{1A}$ and $1/\tau_{2A} = 1/\tau_A + 1/T_{2A}$, the signal from nuclei X in position A ν_A and the magnetization N_z^A proportional to this signal can be determined by repeated passage of A by a weak measuring hf-field H_1. After the instantaneous saturation of the signal from B at moment of time t = 0, the magnetization M_z^A will exponentially approach the new equilibrium value

$$M_z^A = M_0^A \left[\frac{\tau_{1A}}{\tau_A} e^{-t/\tau_{1A}} + \frac{\tau_{1A}}{T_{1A}} \right] \tag{174}$$

and after a sufficiently long period ($t \to \infty$)

$$M_z^A(t \to \infty) = M_0^A \left(\frac{\tau_{1A}}{T_{1A}}\right). \qquad (175)$$

From the graph giving the dependence $\log [M_z^A(t) - M_z^A(t \to \infty)]$ on t we can readily determine τ_{1A}, and from the change in the stationary value of the signal from (175) we can determine T_{1A}. From another symmetrically arranged experiment we can determine τ_B and T_{1B}. In order to satisfy the condition $\tau_{2A} \ll \tau_{1A}$ and achieve sufficiently rapid saturation of B it is necessary to work with a fairly nonhomogeneous field H_0 so that the width of the spectral lines amounts to 2-3 Hz [177].

6. Study of the Structure of Organic Compounds

For a complete analysis of the spectrum with determination of all the chemical shifts and spin-spin coupling constants, use is made of methods associated with weak perturbation of the spin system (tickling and the Overhauser effect). After compilation of the energy level diagrams [86] in the form of a cube [78, 86] or "four-dimensional" tesseract [531], use is made of iterational methods [16, 96, 261, 313] to find the required spectral constants [2-9, 12]. This systematic analysis is possible, however, only in rare cases. Usually, it is necessary to restrict oneself to a partial analysis of the spectrum, for which all the NMDR methods described above can be used. Partial analysis of the NMR spectrum provides a very powerful method of studying the structure of complex molecules and usually makes it possible to determine the constants required for the interpretation even in the case of spin systems of 20-30 different protons [310, 363]. The exact analysis of these systems is quite impossible. Particularly good results are given by the use of double resonance combined with the use of various solvents which have a selective action on the individual chemical shifts (benzene, acetone, CF_3COOH) [156, 362, 467, 599, 628], particularly since complex spectra are usually complicated by virtual coupling [393, 451, 452, 457, 629] between the nuclei or, on the other hand, since certain spin-spin couplings may be masked ("apparent simplicity" of the spectrum) [362, 367, 394, 529]. These phenomena can be used for the analysis of spectra [458, 599], but usually they interfere. Equal splitting of two multiplets in a complex spectrum is not a reliable sign of spin-spin coupling between them [111, 393]. Double resonance provides the chief method for studying these spectra. All versions of NMDR can be used together in various combinations. Figure 22 gives an example of the application of the decoupling of protons for the identification of multiplets in the spectrum of phyllochrysine [182].

From the spectrum of the solution of this alkaloid in $CDCl_3$ it is possible to determine directly only the chemical shift $\delta(H_{12}) = 5.74$ ppm. The use of another solvent, CF_3COOH, made it possible to identify and determine approximately the chemical shifts of the H_2, H_6, and H_7 protons adjoining the nitrogen. Decoupling of the H_7 nucleus led to the appearance of the quadruplet of the AB system of protons H_{24} and H_{15} and made it possible to determine $J(H_{14}H_{15}) = 9.3$ Hz and $|\delta(H_{15}) - \delta(H_{14})| = 0.18$ ppm; simultaneously, the H_8 quadruplet merged to form a doublet, from which $\delta(H_8) = 2.64$ ppm and $J(H_8H_{8'}) = 9.2$ Hz. Decoupling of the H_8 nucleus leads to merging of the H_8, doublet and the appearance of a quadruplet from the H_7 nucleus, from which $\delta(H_{8'}) = 1.90$ ppm, $\delta(H_7) = 3.90$ ppm, $J(H_7H_{14}) = 1.1$ Hz, and $J(H_7H_{15}) = 4.5$ Hz. Simultaneous irradiation by a perturbing hf-field H_2 of the protons H_{14} and H_{15}, H_3 and $H_{3'}$, or H_5 and $H_{5'}$ leads to the appearance of a doublet from the H_7 nucleus and individual lines from the H_2 and $H_{6,6'}$ nuclei. Thus $J(H_7H_8) = 4.5$ Hz. The last experiments leads to the values $\delta(H_2) = 3.67$ ppm and $\delta(H_6) = 2;88$ ppm; the chemical shifts of the overlapping lines of nuclei H_3 and H_5 are equal to $\delta(H_3) = 1.32$ ppm and $\delta(H_5) = 1.80$ ppm respectively.

6.1. Applications of Homonuclear Double Resonance. Proton-proton double resonance is used for the study of almost all classes of organic compounds. Among natural compounds, the following classes have been studied:

1. Alkaloids: Phyllochrysine, securinine and virosecurinine [182, 183], α-, β-, and γ-lumicolchicine [219], strychnospermine and spermostrychnine [223], C-fluorocurine, C-mavacurine, pleiocarpamine, normavacurine [275], dihydrotoxiferin, curarine I, calebassine, toxiferin I, C-alkaloid A, C-alkaloid E [396], picralin [349], krigeine, albomaculine, neronine, nerinine, homolycorine [355], hemanthamine, crinamine, buphanidrine, criwelline, tazettine [356], senkirkine, retusamine [363], ribalinium salts [394, 500], 6-hydroxycrinamine, hemanthidine [435], retronecine, heliotridine [436], taxinin [473], clivonine and clivimine [616], and the aspidosperma alkaloids [525].

2. Carbohydrates: Derivatives of glucose [109, 111, 299, 359, 480, 486, 628], galactose [267], fructose [293], ribose [544], xylose [551], mannose [432], and other carbohydrates [308, 393, 484]; deoxyhexoses [360, 524], 2,6-dideoxyhexoses (chromoses) [310, 547], and osazones [318, 347].

3. Terpenes and terpenoids: Derivatives of betulin [254], isorosenolic acid [276], derivatives of thujane [285, 478], sulfurenic acid [317], ovatodiolide [395], gaillardine [490], gedunin [491], linderine [492], freelingyne [509], grandifolione [539], fastigilin, hispidulin, mikanolide [543], and various hydroxyterpenes [543].

4. Steroids and hormones: 1-oxo-$\Delta^{1,5}$-steroids [428], 11-oxosteroids [456], 12α-ketosteroids [242], derivatives of cholestane [548], androstane [108], pregnadienone [514], dichlorocholesterine [488], dichloroestrone [241], and also their decomposition products and model substances [545].

5. Antibiotics: Puromucin [247], tylosin [309], intermediate products of the biosynthesis of penicillin [329], tricothecolone [462], ergoxanthine and ergoflavin [546].

6. Nucleotides: 1-methylcytosine [256] and purines [368].

7. Various natural compounds: chlorophyll and bacteriochlorophyll [248, 523, 524], chromose A [234], ichthyothereol [439], leucofisetinidin [517], and many others [249, 255, 295, 310, 338, 375, 384, 397, 405, 437, 446, 457, 459, 477, 502, 614, 615, 617].

In the study of the products of chemical synthesis, NMDR has found equally conjugated polycyclic systems. NMDR methods have been used to study the following:

1. Aliphatic oxygen-containing compounds [58, 66, 73, 74, 81, 84, 103, 106, 107, 457, 480].

2. Amines and amides [390, 403, 427, 472, 507].

3. Unsaturated compounds [81, 84, 106, 110, 273, 274, 361, 414, 416, 527].

4. Carbocyclic compounds [174, 305, 388, 389, 416, 426, 515, 613].

5. Conjugated polycyclic compounds: derivatives of norbornene and norbornadiend [246, 286, 304, 319, 380, 412, 417, 481, 540, 554, 589, 610], bicyclo[3.2.1]octene [366, 422], tricyclo[2,1,1,$0^{5,6}$]hexane [396], tricyclo[3.3.0.$0^{2,8}$]octene-3 [286, 506], tricyclo[2.2.0.$0^{2,6}$]hexane [463], and tetracyclo[5.4.0.$0^{2,4}0^{3,6}$]undeca-1(7), 8,10-triene [554], and also azabibyblo[3.2.2]nonene [434, 437, 453], and other heterocyclic [326, 499] and carbocyclic [110, 336, 402, 441, 476, 511, 515, 553, 619] systems. Problems of valence isomerism were examined in [402].

6. Heterocyclic nitrogen compounds [52, 83, 109, 250, 289, 290, 311, 323, 327, 329, 376, 379, 398, 455, 460, 461, 487, 508, 549, 629].

7. Heterocyclic oxygen compounds [120, 333, 334, 362, 364, 385, 401, 461, 468, 627].

8. Organoelemental compounds [332, 425, 426, 457, 503, 521].

6.2. Applications of Heteronuclear Double Resonance. Heteronuclear double resonance is used chiefly for the decoupling of the nuclei D^2, P^{31}, N^{14}, B^{11} and F^{19} from protons and for the decoupling of hydrogen nuclei from C^{13}. Weak perturbation of the transitions of the C^{13} nucleus is widely used for the determination of the relative signs of spin-spin coupling constants. These experiments are described in the following papers $H^1-\{D^2\}$ [119, 165, 315, 335, 380, 381, 383, 388, 400, 410, 519, 523]; $H^1-\{B^{11}\}$ [70, 120, 123, 124, 133, 269, 292, 312, 312, 353, 409, 450, 494, 505]; $H^1-\{C^{13}\}$ [28, 97, 109, 137, 145, 176, 179, 180, 216, 321, 453, 458, 474, 485, 522, 556, 612, 624]; $H^1-\{N^{14}\}$ [51, 76, 102, 125, 126, 128, 131, 132, 138, 158, 163, 175, 230, 282, 351, 374, 376, 537, 538]; $H^1-\{N^{15}\}$ [176, 277, 453, 591]; $H^1-\{F^{19}\}$ [160, 192, 201, 291, 307, 387]; $H^1-\{Al^{27}\}$ [133]; $H^1-\{Si^{29}\}$ [158, 325, 371]; $H^1-\{P^{31}\}$ [22, 29, 184, 185, 288, 290, 296, 301, 320, 324, 330, 332, 457, 483, 510, 518, 521, 601, 609, 612]; $H^1-\{Sn^{119}\}$ [22, 563]; $H^1-\{Hg^{199}\}$ [179, 258]; $H^1-\{Tl^{203}\}$ [319]; $H^1-\{Pb^{207}\}$ [134]; $F^{19}-\{F^{19}\}$ [168, 186, 565]; $F^{19}-\{H^1\}$ [281, 411]; $F^{19}-\{D^2\}$ [410]; $F^{19}-\{B^{11}\}$ [292, 409]; $F^{19}-\{C^{13}\}$ [158]; $F^{19}-\{N^{14}\}$ [136]; $F^{19}-\{Si^{29}\}$ [325]; $F^{19}-\{P^{31}\}$ [29, 268, 601]; $F^{19}-\{Xe^{129}\}$ [224, 232]; $B^{11}-\{B^{10}\}$ [135, 406, 504]; $B^{11}-\{H^1\}$ [406, 475]; $C^{13}-\{H^1\}$ [22, 137, 302, 303, 368, 447, 464, 497, 535, 607, 623, 625, 626]; $P^{31}-\{P^{31}\}$ [293].

Simplification of the spectrum by the method of heteronuclear coupling is particularly important in the study of the weak spectra of C^{13}, where an almost sixfold increase in the peak of the signal [302, 607] as a result of collapse and the Overhauser effect is achieved simultaneously, and in the study of boron compounds, for which the chemical shifts and spin-spin interaction constants often have values of the same order of magnitude [450], but the lines are broad [3]. The methods of double resonance have been used to prove the bridged structure [121, 122] of diborane and the pyramidal structure of pentaborane-9 [70, 123]. The spectrum of tetraborane-11 consists of a triplet and doublet. In [407] it was suggested that the fine structure of the doublet is due to spin-spin coupling between the boron atoms $J(B^{10}B^{11})$. In [406] it was concluded from a $B^{11}-\{H^1\}$ experiment that this assumption is

Absolute Signs of the Most Important Spin-Spin Coupling Constants

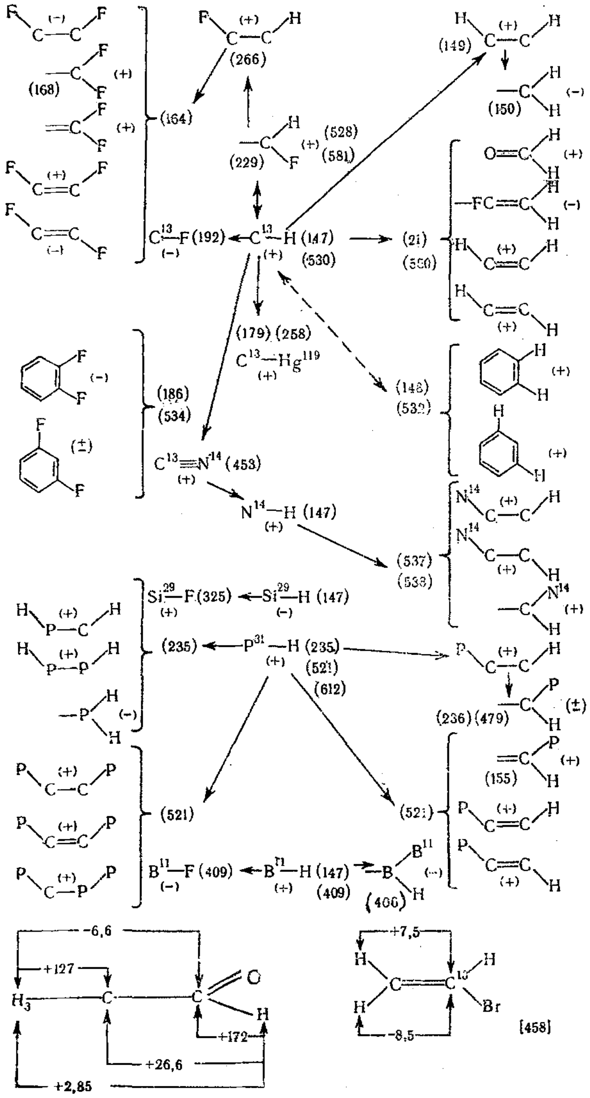

incorrect and that the fine structure is due to interaction with hydrogen nuclei. More detailed study [504] of the problem by means of the experiment $B^{11}-\{B^{10}\}$ showed, however, that the first assumption [407] was correct.

Interesting results were obtained in a study of o-, m-, and p-carboranes (barenes) in a superconducting solenoid [449] and by double resonance [450]. It is found that the carbon in these compounds produces a diamagnetic shift of the resonance frequency of the neighboring boron atoms, which is the opposite of what is expected on the basis of electronegativities. The study of boron compounds demonstrates the importance of the direct determination of the chemical shifts of other nuclei in addition to H^1 and F^{19} and even the application of double resonance between these nuclei. Unfortunately, such methods are as yet little used, although they might give very good results in the study of organoelemental compounds.

6.3. Determination of the Signs of Spin-Spin Coupling Constants. For the determination of the relative signs of J it is possible to use, in addition to the analysis of strongly coupled spectra [62, 116, 118, 136], all the methods of double resonance, e.g., selective double resonance in weakly coupled systems [81, 82, 108, 146, 149, 153, 253], and strongly coupled systems [84, 115, 220, 479], tickling [78, 100, 146, 150, 176, 179, 180, 409, 612], double tickling [259], and tickling with increase in the splitting [352], transition selective irradiation [154, 265, 280], INDOR [88, 89, 158], the complete analysis of double resonance spectra [52, 174, 266], and two-quantum transitions [144, 159]. Tickling is the best method for the study of weak long-range coupling and spin-spin coupling between different nuclei (Fig. 8). Relaxation [387, 597, 611] in gases and the effects of solvents [533-599] can also be used for the determination of the relative signs of spin-spin coupling constants. With increase in the dielectric constant of the solvent, all the geminal coupling constants between protons acquire more negative values [533]. All the relative signs are related to two absolute standards, whose absolute signs have been determined completely reliably, namely $+J(C^{13}H)$ [147, 530] and $+J(HCF)$ [528, 581], and also relative to the "secondary standard" $+J(HH_{vic})$ [149]. The determination of the sign $+J(HH_{ortho})$ in p-nitrotoluene [148] cannot be regarded as absolute after the re-examination of this work by Hahn [532] using a more sensitive method [218]. The table gives some of the most important spin-spin coupling constants whose signs have been determined by the methods of double resonance.

As a result of the negative gyromagnetic ratio γ of the nuclei N^{15} and Si^{29}, the spin-spin coupling constants $J(N^{15}H)$ and $J(Si^{29}H)$ are negative [325, 348, 371, 453], but the reduced constants [575] $K = 2\pi J_{ij}/\hbar\gamma_i\gamma_j$ are positive, in accordance with the theory of Karplus [114]. The contradiction with theory, where a positive sign was obtained for $J(HH_{gem})$ [113, 151, 583], has now been eliminated by more accurate calculation according to the theory of Pople [345, 575]. Satellites in the proton spectra are used to determine the relative signs of the constants for the spin-spin coupling of C^{13} with hydrogen. Double resonance of the type $H^1-\{H^1\}$ makes it possible to determine the relative signs of the two constants $J(C^{13}H_A)$ and $J(C^{13}H_B)$, and perturbation of the carbon nucleus $H^1-\{C^{13}\}$ gives the relative signs of the constants $J(H_AH_B)$ and $J(C^{13}H)$ [149, 458].

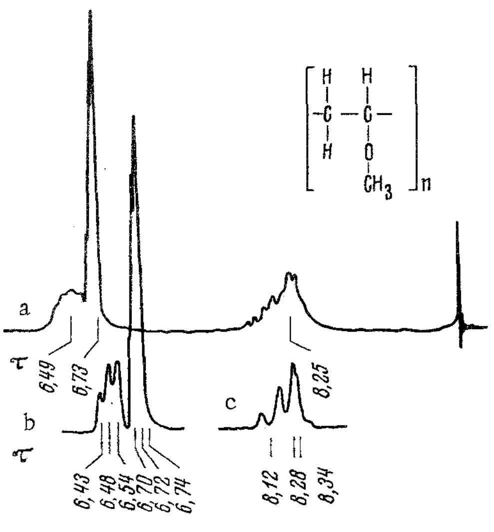

Fig. 24. Spectra of polyvinyl methyl ether [300]: a) Single resonance spectrum, identification of most of the lines of the spectrum practically impossible, b) spectrum with decoupling of the α-protons, c) spectrum with decoupling of the β-protons; the last two spectra make it possible to identify the chemical shifts of individual stereoregular triads.

Of particular importance are the signs of the geminal constants of the spin-spin coupling between protons, whose sign shows an extremely complicated dependence on structure [550]. A knowledge of the absolute value alone does make it possible in the more complex cases to reach well-founded conclusions regarding the structure of a substance.

The long-range spin-spin coupling constants [577] in conjugated molecules are acquiring ever-increasing importance. The zigzag rule [21] is obeyed exactly and can provide a more reliable method for the determination of the structure of molecules than estimation of the magnetic anisotropy of bonds and rings. Study of the decoupling of the protons of benzonorbornene [481] showed that the earlier assignment of the signals [582] was incorrect and that the 7_{syn} proton resonates in a narrower field than the 7_{anti} proton, in spite of the proximity of the benzene ring! This agrees with the zigzag rule. Zigzag may take place through a heteroatom [392, 434, 499, 510], and the effect becomes stronger in compounds with two zigzags between coupled protons [540]. In exactly the same way, the signal from equatorial protons is not always in a narrower field than the signal from axial protons [393].

The relative signs of spin-spin coupling constants were first determined by the method of selective double resonance by Maher and Evans [82]; their method was extended by Freeman to homonuclear weakly coupled systems protons [81, 84] and was later used for the study of more closely coupled systems of nuclear spins [84, 167].

Experiments on the determination of the relative signs of spin-spin coupling constants by various NMDR methods have been described in many papers [52, 62, 78, 81, 82, 84, 88, 89, 100, 108, 115, 116, 136, 144, 146-150, 155, 158, 159, 164, 167, 168, 174, 176, 179, 180, 185-188, 192, 220, 222, 228, 229, 231, 235, 236, 253, 254, 258, 260, 266, 272, 277, 291, 307, 314, 322, 325, 326, 337, 344, 348, 354, 357, 365, 367, 371, 409, 425, 453, 458, 479, 485, 489, 521, 530, 532-534, 537, 538, 567, 571, 572, 581, 592, 629]. The determination of the signs of long-range coupling constants is discussed in [87, 154, 157, 169, 233, 240, 241, 253, 259, 265, 280, 328, 331, 352, 371, 372, 373, 379, 392, 399, 401, 412, 469, 470, 526, 579, 590, 610, 627].

6.4. Study of the Stereoregularity of Polymers. Stereoregular polymers are acquiring ever increasing technical importance. The regularity of the polymer chain leads to closer packing and crystallization of the polymer, and hence to an increase in the melting point and improved mechanical properties. The NMR spectra of polymer solutions can be used to determine the concentration of isotactic (ddd or lll), syndiotactic (dld or ldl), and heterotactic (dll or ldd) triads [586, 587], but the dependence of the relative chemical shifts on the stereoregularity is slight—of the order of magnitude of the spin-spin coupling constants. Thus in order to obtain sufficiently clearly defined spectra it is necessary to make use of the decoupling of nuclei. Figure 24 gives the NMDR spectrum of polyvinyl methyl ether, where the chemical shifts in units of $\tau = (10 - \delta) = 6.43$, 6.48, and 6.54 correspond to syndiotactic, heterotactic, and isotactic structures.

Homonuclear decoupling of protons has been used to study the stereoregularity of polyvinyl chloride [238, 342, 358, 429, 512, 513, 516], polyvinyl fluoride [238, 377], polyvinyl alcohol [339, 378, 430], polyvinyl methyl ether [238, 300, 573], polyvinyl ethyl ether, polyvinyl isopropyl ether, and polyvinyl tert-butyl ether [391], polyvinyl acetate [340, 516], polyvinyl trifluoroacetate [339], polymethyl acrylate [415], polyisopropyl acrylate [423], polydimethyl-α-α'-dimethyl glutarate [415], polyvinylidene chloride [429], polyvinylidene fluoride [377], polyacetaldehyde [264, 343], polypropylene [341], polyoxypropylene [279], polystyrene [383], and even copolymers [429, 516, 618].

The structural similarity between the isotatic structure and the mesostructure is used to determine the dependence of the chemical shifts of protons on stereoregularity. Model substances were studied in [342, 383, 552, 585]. The conformation of isotatic polyalkyl acrylates in solution was studied in [495].

6.5 Various Applications of NMDR in Organic Chemistry. NMDR has been used to study the nature of the bonding in the tricarbonyls of iron and chromium with unsaturated compounds [471, 498, 522], and also to study various complex compounds formed by metals and boron with phosphorus compounds [244, 292, 433, 479].

The structure and conformation of organic ions has been studied in [246, 256, 271, 369, 454].

NMDR has proved to be an invaluable method for the study of complex cyclic compounds formed on photoisometization [219, 263, 286, 380, 401, 428, 443, 499, 506, 554, 619] and has been used in the study of tautomerism and isomerism [256, 318, 376, 435, 445, 541].

The temperature dependence of the NMR spectra of nonplanar cyclic compounds makes it possible to study the conformational changes in these compounds. Decoupling of individual groups of nuclei, usually combined with deuteration, is used to simplify the spectrum [165, 221, 262, 273, 281, 287, 297, 298, 315, 369, 370, 400, 410, 411, 438, 496, 497, 501, 519, 520].

Methods for the determination of the rates of chemical exchange [177, 270, 346] are of limited value, but saturation of the spectral line of the protons of water has been used for the qualitative determination of phenolic hydroxyl groups [559].

Reversible changes in structure without intermolecular exchange of nuclei lead to analogous phenomena. On saturation of the signal from the internal protons of [18]-annulene at −20° the signal from the external protons also disappears (and vice versa); this is a consequence of the rapid structural changes undergone by this compound [613].

Finally, the decoupling of deuterium nuclei in bacterial chlorophyll has made it possible to study the processes involved in the biosynthesis of this compound [523, 524].

LITERATURE CITED

1. A. Abragam, Principles of Nuclear Magnetism [Russian translation], IL, Moscow (1963).
2. J. A. Pople, W. G. Schneider, and H. J. Bernstein, High-Resolution Nuclear Magnetic Resonance [Russian translation], IL, Moscow (1962).
3. J. W. Emsley, J. Feeney, and L. H. Sutcliffe, High Resolution Nuclear Magnetic Resonance Spectroscopy, 1 and 2, Pergamon Press, London (1965).
4. H. Suhr, Anwendungen der kernmagnetischen Resonanz in der organishchen Chemie, Springer, Berlin (1965).
5. N. S. Bhacca and D. H. Williams, Applications of NMR Spectroscopy in Organic Chemistry [Russian translation], Izd-vo "Mir," Moscow (1966).
6. L. M. Jackman, Applications of Nuclear Magnetic Resonance Spectroscopy in Organic Chemistry, Pergamon Press, London (1959).
7. E. Fluck, Die kernmagnetische Resonanz und ihre Anwendung in der anorganischen Chemie, Springer, Berlin (1963).
8. R. D. Bible, Interpretation of NMR Spectra, Plenum Press, New York (1965).
9. J. D. Roberts, Nuclear Magnetic Resonance [Russian translation], IL, Moscow (1962).
10. NMR and ESR Spectroscopy [in Russian], Izd-vo "Mir," Moscow (1964),
11. A. Lauchet, Nuclear Induction [Russian translation], IL, Moscow (1963).
12. G. Mavel, Theories moleculaires de la resonance magnetique nucleaire—applications a la chimie structurale, Dunod, Paris (1966).
13. C. P. Slichter, Principles of Magnetic Resonance, Harper & Row, New York (1963).
14. I. V. Aleksandrov, Theory of Nuclear Magnetic Resonance [in Russian], Izd-vo "Nauka," Moscow (1964).
15. V. M. Fain and Ya. I. Khanin, Quantum Radiophysics [in Russian], Izd-vo "Sovetskoe Radio," Moscow (1965).
16. J. W. Emsley, J. Feeney, and L. H. Sutcliffe (editors), Progress in Nuclear Magnetic Resonance Spectroscopy, 1, Pergamon Press, London (1966).
17. E. R. Andrew, Nuclear Magnetic Resonance [Russian translation], IL, Moscow (1962).
18. P. L. Corio, Structure of High-Resolution NMP Spectra, Academic Press, New York (1966).
19. N. Bloembergen, Nuclear Magnetic Relaxation, W. A. Benjamin, New York (1961).
20. P. A. Dirac, Principles of Quantum Mechanics [Russian translation], IL, Moscow (1960).
21. J. S. Waugh (editor), Advances in Magnetic Resonance, 1, Academic Press, New York (1965).
22. J. D. Baldeschwieler and E. W. Randall, Chem. Rev., 63, 81 (1963).
23. J. Parello, Bull. Soc. Chim. France, 2033 (1964).
24. H. S. Gutowsky, D. W. McCall, and C. P. Slichter, J. Chem. Phys., 21, 279 (1953).
25. N. F. Ramsey and E. M. Purcell, Phys. Rev., 85, 143 (1952).

26. N. F. Ramsey, Phys. Rev., 91, 303 (1953).
27. F. Bloch, Phys. Rev., 93, 944 (1954).
28. V. Royden, Phys. Rev., 96, 543 (1954).
29. A. L. Bloom and J. N. Shoolery, Phys. Rev., 97, 1261 (1955).
30. I. I. Babi, N. F. Ramsey, and J. Schwinger, Rev. Mod. Phys., 26, 167 (1954).
31. F. Bloch, Phys. Rev., 69, 680 (1946).
32. B. D. Nageswara Rao, J. D. Baldeschwieler, and J. M. Anderson, Phys. Rev., 137, A 1477 (1965).
33. J. Freed, J. Chem. Phys., 41, 7 (1964).
34. R. C. Tolman, Principles of Statistical Mechanics, Oxford (1930).
35. U. Fano, Rev. Mod. Phys., 29, 74 (1957).
36. R. K. Wangness and F. Bloch, Phys. Rev., 89, 728 (1953).
37. F. Bloch, Phys. Rev., 102, 104 (1956).
38. F. Bloch, Phys. Rev., 105, 1206 (1957).
39. F. Bloch, Phys. Rev., 111, 841 (1958).
40. S. Yatsiv, Phys. Rev., 113, 1522 (1959).
41. S. Yatsiv, Phys. Rev., 113, 1538 (1959).
42. P. S. Hubbard, Rev. Mod. Phys., 33, 249 (1961).
43. R. L. Fulton, J. Chem. Phys., 41, 2876 (1964).
44. P. N. Argyres and P. L. Kelley, Phys. Rev., 134, A 98 (1964).
45. S. Stenholm and D. TerHaar, Physica, 32, 1361 (1966).
46. V. Sinivee and E. Lippmaa, Izv. AN ÉstSSR, ser. fiz.-matem. i tekhn. nauk, 14, 258 (1965).
47. V. Sinivee and E. Lippmaa, Izv. AN ÉstSSR, ser. fiz.-matem. i tekhn. nauk, 14, 564 (1965).
48. V. Sinivee and E. Lippmaa, Izv. AN ÉstSSR, ser. fiz.-matem. i tekhn. nauk, 15, 64 (1966).
49. V. Sinivee, Izv. AN ÉstSSR, ser. fiz.-matem. i tekhn. nauk, 15, 182 (1966).
50. J. D. Baldeschwieler, J. Chem. Phys., 34, 718 (1961).
51. J. D. Baldeschwieler, J. Chem. Phys., 36, 152 (1962).
52. B. D. Nageswara Rao and J. D. Baldeschwieler, J. Chem. Phys., 37, 2473 (1962).
53. J. D. Baldeschwieler, J. Chem. Phys., 40, 459 (1964).
54. M. Barfield and J. D. Baldeschwieler, J. Chem. Phys., 41, 2633 (1964).
55. B. D. Nageswara Rao, Phys, Rev., 137, A 467 (1965).
56. K. F. Kuhlmann and J. D. Baldeschwieler, J. Chem. Phys., 43, 572 (1965).
57. J. H. Noggle, J. Chem. Phys, 43, 3304 (1965).
58. W. A. Anderson, Phys. Rev., 102, 151 (1956).
59. N. Bloembergen, E. M. Purcell, and R. V. Pound, Phys. Rev., 73, 679 (1948).
60. L. R. Anders and J. D. Baldeschwieler, J. Chem. Phys., 43, 2147 (1965).
61. K. B. Wiberg and B. J. Nist, Interpretation of NMR Spectra, W. A. Benjamin, New York (1962).
62. P. L. Corio, Chem. Rev., 60, 363 (1960).
63. W. G. Proctor and F. C. Yu., Phys. Rev., 77, 717 (1950).
64. W. G. Proctor and F. C. Yu., Phys. Rev., 78, 471 (1950).
65. W. A. Anderson and R. Freeman, J. Chem. Phys., 37, 85 (1962).
66. R. Freeman and D. H. Whiffen, Proc. Phys. Soc., 79, 794 (1962).
67. F. Bloch, W. W. Hansen, and M. Packard, Phys. Rev., 69, 127 (1946).
68. E. M. Purcell, H. C. Torrey, and R. V. Pound, Phys. Rev., 69, 37 (1946).
69. M. E. Rose, Elementary Theory of Angular Momentum, Wiley-Chapman, New York (1957).
70. J. N. Shoolery, Disc. Faraday Soc., 19, 215 (1955).
71. J. G. Powles, Reports Progr. Phys., 22, 433 (1959).
72. W. N. Lipscomb and A. Kaczmarczyk, Proc. Natl. Acad. Sci., 47, 1796 (1961).
73. R. Freeman, Mol. Phys., 3, 435 (1960).
74. D. W. Turner, J. Chem. Soc., 847 (1962).
75. J. D. Baldeschwieler, J. H. Noggle, and C. B. Colburn, J. Chem. Phys., 37, 182 (1962).
76. E. W. Randall and J. D. Baldeschwieler, J. Chem. Soc., 303 (1961).
77. H. Shimizu and S. Fujiwara, J. Chem. Phys., 34, 1501 (1961).
78. R. Freeman and W. A. Anderson, J. Chem. Phys., 37, 2053 (1962).
79. E. Lippmaa, Yu. Puskar, and M. Alla, Izv. AN ÉstSSR, ser. fiz.-matem. i tekhn. nauk, 14, 487 (1965).
80. E. Lippmaa and M. Alla, Izv. AN ÉSTSSR, ser. fiz.-matem. i tekhn. Nauk, 15, 620 (1966).
81. R. Freeman and D. H. Whiffen, Mol. Phys., 4, 321 (1961).

82. J. P. Maher and D. F. Evans, Proc. Chem. Soc., 208 (1961).
83. J. A. Elvidge and L. M. Jackman, J. Chem. Soc., 859 (1961).
84. R. Freeman, Mol. Phys., 4, 385 (1961).
85. S. L. Gordon, J. Chem. Phys., 45, 1145 (1966).
86. E. F. Friedman and H. S. Gutowsky, J. Chem. Phys., 45, 3158 (1966).
87. R. A. Hoffman, B. Gestblom, and S. Forsen, J. Chem. Phys., 40, 3734 (1964).
88. V. J. Kowalewski, D. G. de Kowalewski, and E. C. Ferra, J. Molec. Spectr., 20, 203 (1966).
89. R. Kaiser, J. Chem. Phys., 39, 2435 (1963).
90. K. Kuhlmann and J. D. Baldeschwieler, J. Amer. Chem. Soc., 85, 1010 (1963).
91. F. J. Dyson, Phys. Rev., 75, 486 (1949).
92. A. Syugis and E. Lippmaa, Izv. AN ÉstSSR, ser. fiz.-matem. i tekhn. nauk, 16, 81 (1967).
93. E. Lippmaa, Yu. Puskar, M. Alla, and A. Syugis, Izv. AN ÉstSSR, ser. fiz.-matem. i tekhn. nauk, 14, 306 (1965).
94. J. von Neumann, Mathematische Grundlagen der Quantenmechanik [Russian translation], Izd-vo "Nauka," Moscow (1964).
95. M. Matusoka and Y, Kakiuchi, J. Phys. Soc., 20, 1174, Japan (1965).
96. J. D. Swalen and C. A. Reilly, J. Chem. Phys., 37, 21 (1962).
97. R. Freeman, J. Chem. Phys., 43, 3087 (1965).
98. E. Lippmaa, Ya. Past, Yu. Puskar, M. Alla, and A. Syugis, Izv. AN ÉstSSR, ser. fiz.-matem. i tekhn. nauk, 15, 51 (1966).
99. E. Lippmaa and M. Alla, Izv. AN ÉstSSR, ser. fiz.-matem. i tekhn. nauk, 15, 476 (1966).
100. R. Freeman and N. S. Bhacca, J. Chem. Phys., 38, 1088 (1963).
101. R. Kaiser, J. Chem. Phys., 42, 1838 (1965).
102. J. A. Glasel, L. M. Jackman, and D. W. Turner, Proc. Chem. Soc., 426 (1961).
103. J. Itoh and S. Sato, J. Phys. Soc., 14, 851, Japan (1959).
104. R. V. Pound, Rev. Sci. Instr., 28, 966 (1957).
105. R. Freeman and R. V. Pound, Rev. Sci. Instr., 31, 96, 103 (1960).
106. E. Lippmaa, S. Rang, O. Eizen, and Yu. Puskar, Izv. AN ÉstSSR, ser. fiz.-matem. i tekhn. nauk, 15, 615 (1966).
107. R. Kaiser, Rev. Sci. Instr., 31, 963 (1960).
108. D. D. Elleman and S. L. Manatt, J. Chem. Phys., 36, 2346 (1962).
109. W. A. Anderson, J. Chem. Phys., 37, 1373 (1962).
110. S. L. Manatt and D. D. Elleman, J. Amer. Chem. Soc., 83, 4095 (1961).
111. R. J. Abraham, R. Freeman, K. A. McLauchlan, and L. D. Hall, J. Chem. Soc., 2080 (1962).
112. M. Nagumo and Y. Kakiuchi, J. Phys. Soc., 14, 679, Japan (1959).
113. M. Karplus, J. Chem. Phys., 30, 11 (1959).
114. M. Karplus, J. Chem. Phys., 33, 1842 (1960).
115. S. L. Manatt and D. D. Elleman, J. Amer. Chem. Soc., 84, 1579 (1962).
116. J. A. Pople and T. Schaefer, Mol. Phys., 3, 547 (1960).
117. J. E. Wertz, P. L. Jain, and R. L. Batdorf, Phys. Rev., 102, 920 (1956).
118. V. J. Kowalewski and D. G. de Kowalewski, J. Chem. Phys., 33, 1794 (1960).
119. B. Bak, J. N. Shoolery, and G. A. Williams, J. Mol. Spectr., 2, 525 (1958).
120. P. K. Korver, P. J. van der Haak, H. Steinberg, and T. J. de Boer, Rec. trav. chim., 84, 129 (1965).
121. K. Hedberg and V. Schomaker, J. Amer. Chem. Soc., 73, 1482 (1951).
122. W. C. Price, J. Chem. Phys., 16, 894 (1948).
123. R. Schaeffer, J. N. Shoolery, and R. Jones, J. Amer. Chem. Soc., 79, 4606 (1957).
124. R. E. Williams and I. Shapiro, J. Chem. Phys., 29, 677 (1958).
125. L. H. Piette, J. D. Ray, and R. A. Ogg, J. Mol. Spectr., 2, 66 (1958).
126. E. W. Randall and J. D. Baldeschwieler, J. Mol. Spectr., 8, 365 (1962).
127. B. Sunners, L. H. Piette, and W. G. Schneider, Can. J. Chem., 38, 681 (1960).
128. I. Solomon, Phys. Rev., 99, 559 (1955).
129. W. G. Schneider, H. J. Bernstein, and J. A. Pople, Ann. N. Y. Acad. Sci., 70, 806 (1958).
130. W. G. Schneider, H. J. Bernstein, and J. A. Pople, Canad. J. Chem., 35, 1487 (1957).
131. J. A. Happe, J. Phys. Chem., 65, 72 (1961).
132. L. W. Anderson, F. M. Pipkin, and J. C. Baird, Phys. Rev., 116, 87 (1959).
133. R. A. Ogg and J. D. Ray, Disc. Faraday Soc., 19, 239 (1955).
134. E. B. Baker, J. Chem. Phys., 26, 960 (1957).

135. R. E. Williams, S. G. Gibbins, and I. Shapiro, J. Amer. Chem. Soc., 81, 6164 (1959).
136. H. Finegold, Proc. Chem. Soc., 213 (1962).
137. T. D. Alger, D. M. Grant, and E. G. Paul., J. Amer. Chem. Soc., 88, 5397 (1966).
138. J. B. Merry and J. H. Goldstein, J. Amer. Chem. Soc., 88, 5560 (1966).
139. R. Freeman and W. A. Anderson, J. Chem. Phys., 39, 806 (1963).
140. W. A. Anderson, Phys. Rev., 104, 850 (1956).
141. J. I. Kaplan and S. Meiboom, Phys. Rev., 106, 499 (1957).
142. A. D. Cohen and D. H. Whiffen, Mol. Phys., 7, 449 (1964).
143. J. I. Musher, J. Chem. Phys., 40, 983 (1964).
144. K. A. McLauchlan and D. H. Whiffen, Proc. Chem. Soc., 144 (1962).
145. W. A. Anderson and F. A. Nelson, J. Chem. Phys., 39, 183 (1963).
146. R. Freeman, N. S. Bhacca, and C. A. Reilly, J. Chem. Phys., 38, 293 (1963).
147. M. Karplus, J. Amer. Chem. Soc., 84, 2458 (1962).
148. A. D. Buckingham and K. A. McLauchlan, Proc. Chem. Soc., 144 (1963).
149. P. C. Lauterbur and R. J. Kurland, J. Amer. Chem., Soc., 84, 3405 (1962).
150. F. A. L. Anet, J. Amer. Chem. Soc., 84, 3767 (1962).
151. H. S. Gutowsky, M. Karplus, and D. M. Grant, J. Chem. Phys., 31, 1278 (1959).
152. R. Freeman, J. Chem. Phys., 40, 3571 (1964).
153. R. Freeman, Mol. Phys., 5, 499 (1962).
154. R. A. Hoffman, B. Gestblom, and S. Forsen, J. Mol. Spectr., 13, 221 (1964).
155. W. A. Anderson, R. Freeman, and C. A. Reilly, J. Chem. Phys., 39, 1518 (1963).
156. T. L. Brown and K. Stark, J. Phys. Chem., 69, 2679 (1965).
157. M. Shimizu and H. Shimizu, J. Chem. Phys., 41, 2329 (1964).
158. E. B. Baker, J. Chem. Phys., 37, 911 (1962).
159. B. Dischler and G. Englert, Z. Naturforschung, 16a, 1180 (1961).
160. G. W. Flynn and J. D. Baldeschwieler, J. Chem. Phys., 37, 2907 (1962).
161. A. P. McCann, F. Smith, I. A. S. Smith, and I. D. Thwaites, J. Sci. Instr., 39, 349 (1962).
162. J. B. Leane, R. E. Richards, and T. P. Schaefer, J. Sci. Instr., 36, 230 (1959).
163. D. Kummer and J. D. Baldeschwieler, J. Phys. Chem., 67, 98 (1963).
164. D. F. Evans, S. L. Manatt, and D. D. Elleman, J. Amer. Chem. Soc., 85, 238 (1963).
165. F. A. L. Anet and J. S. Hartman, J. Amer. Chem. Soc., 85, 1204 (1963).
166. E. B. Baker, L. W. Burd, and G. N. Root, Rev. Sci. Instr., 34, 243 (1962).
167. A. D. Cohen and K. A. McLauchlan, Disc. Faraday Soc., 34, 132 (1962).
168. D. F. Evans, Disc. Faraday Soc., 34, 139 (1962).
169. J. P. Maher and D. F. Evans, Proc. Chem. Soc., 176 (1963).
170. M. Freymann, R. Freymann, and C. Geissner-Prettre, Arch. Sci., 13, fasc. special, 506 (1960).
171. M. Freymann, R. Freymann, M. Koechlin, M. Martin, and G. Mavel, Arch. Sci., 12, fasc. special, 207 (1959).
172. H. Sternlicht, R. G. Schulman, and E. W. Anderson, J. Chem. Phys., 43, 3123, 3133 (1965).
173. A. Szent-Gyorgyi, Bioenergetics, Academic Press, N. Y. (1957).
174. B. D. Nageswara Rao, J. D. Baldeschwieler, and J. I. Musher, J. Chem. Phys., 37, 2480 (1962).
175. H. Benoit and H. Ottayi, Arch. Sci., 13, fasc. special, 691 (1960).
176. W. McFarlane, Mol. Phys., 10, 603 (1966).
177. S. Forsen and R. A. Hoffman, J. Chem. Phys., 39, 2892 (1963).
178. H. M. McConnell, J. Chem. Phys., 28, 430 (1958).
179. K. A. McLauchlan, D. H. Whiffen, and L. W. Reeves, Mol. Phys., 10, 131 (1966).
180. K. A. McLauchlan, Mol. Phys., 11, 303 (1966).
181. N. Bhacca, M. E. Wolff, and R. Kwok, J. Amer. Chem. Soc., 84, 4976 (1962).
182. J. Parello, A. Melera, and R. Goutarel, Bull. Soc. Chim., 898, France (1963).
183. J. Polonsky, C. Fouquey, and A. Gaudemer, Bull. Soc. Chim., 1818, France (1964).
184. J. R. Van Wazer and S. Norval, J. Amer. Chem. Soc., 88, 4415 (1966).
185. E. Duval and E. A. C. Lucken, Mol. Phys., 10, 499 (1966).
186. D. F. Evans, Mol. Phys., 6, 179 (1963).
187. D. F. Evans, Mol. Phys., 5, 183 (1962).
188. R. Freeman, K. A. McLauchlan, J. I. Musher, and K. G. R. Pachler, Mol. Phys., 5, 321 (1962).
189. E. Lippmaa, Izv. AN ÉstSSR, ser. fiz.-matem. i tekhn. nauk, 14, 125 (1965).
190. H. Primas, R. Arndt, and R. Ernst, Z. Instrumknd., 68, 8, 55 (1960).

191. K. V. Vladimirskii and B. A. Labzov, Pribory i tekhnika éksperimenta, 4, 59 (1961).
192. G. van D. Tiers, J. Amer. Chem. Soc., 84, 3972 (1962).
193. E. Lippmaa and A. Syugis, Tr. Tallinskogo politekhn. in-ta, Ser. A, 195, 59 (1962).
194. ZKR-10, Carl Zeiss, Jena, DDR.
195. E. B. Baker and L. W. Burd, Rev. Sci. Instr., 28, 313 (1957).
196. E. B. Baker and L. W. Burd, Rev. Sci. Instr., 34, 238 (1963).
197. W. A. Anderson, Rev. Sci. Instr., 33, 1160 (1962).
198. H. Primas, Fifth European Congr. of Molec. Spectr., Amsterdam (1961).
199. K. Drescher and D. Garte, Exp. Techn. Phys., 11, 109 (1963).
200. J. H. Noggle, Rev. Sci. Instr., 35, 1166 (1964).
201. S. L. Gordon and J. D. Baldeschwieler, J. Chem. Phys., 43, 76 (1965).
202. S. A. Knight and R. L. Erskine, J. Sci. Instr., 42, 669 (1965).
203. M. Pettig, Exp. Techn. Phys., 13, 270 (1965).
204. R. R. Ernst and W. A. Anderson, Rev. Sci. Instr. 37, 93 (1966).
205. Ch. Schmelzer, Physikertagung Innsbruck, Mosbach (1954).
206. R. J. Blume and W. L. Williams, Rev. Sci. Instr., 35, 1498 (1964).
207. V. G. Veselago, Radiotekhnika i élektronika, 6, 849 (1961).
208. K. V. Vladimirsky and B. A. Labzov, Nucl. Instr. Meth., 14, 94 (1961).
209. K. V. Vladmirskii and B. A. Labzov, Pribory i tekhnika éksperimenta, 2, 103 (1962).
210. E. Lippmaa, Tr. Tallinskogo politekhn. in-ta, ser. A, 195, 65 (1962).
211. N. M. Ievskaya and R. M. Umarkhodzhaev, Elektrichestvo, 7, 57 (1965).
212. E. Lippmaa and A. Syugis, Izv. AN ÉstSSR, ser. fiz.-matem. i tekhn. nauk, 14, 129 (1965).
213. Data Sheet for A-60 Spectrometer, Varian Ass., USA (1961).
214. Data Sheet for Spin Decoupler V-6058 for A-60 and A-60-A Spectrometers, Varian Ass., USA (1965).
215. A. P. Cox, G. W. Flynn, and E. B. Wilson, J. Chem. Phys., 42, 3094 (1965).
216. R. Freeman and W. A. Anderson, J. Chem. Phys., 42, 1199 (1965).
217. R. Kaiser, Rev. Sci. Instr., 33, 495 (1962).
218. S. R. Hartmann and E. L. Hahn, Phys. Rev., 128, 2042 (1962).
219. O. L. Chapman, H. G. Smith, and R. W. King, J. Amer. Chem. Soc., 85, 803 (1963).
220. G. van D. Tiers, J. Phys. Chem., 67, 928 (1963).
221. J. Meinwald and A. Lewis, J. Amer. Chem. Soc., 87, 2119 (1965).
222. J. M. Anderson, J. D. Baldeschwieler, D. C. Dittmer, and W. D. Phillips, J. Chem. Phys., 38, 1260 (1963).
223. F. A. L. Anet, Canad. J. Chem., 41, 883 (1963).
224. T. H. Brown, E. B. Whipple, and P. H. Verdier, Science, 140, 178 (1963).
225. R. A. Friedel and H. L. Retcofsky, J. Amer. Chem. Soc., 85, 1300 (1963).
226. R. Ernst and H. Primas, Disc. Faraday Soc., 34, 43 (1962).
227. E. G. Paul and D. M. Grant, J. Amer. Chem. Soc., 85, 1701 (1963).
228. H. H. Hutton and F. Schaefer, Canad. J. Chem., 41, 1623 (1963).
229. G. van D. Tiers, J. Phys. Chem., 67, 1373 (1963).
230. E. G. Rochow, Bull. Soc. Chim., 1360, France (1963).
231. W. G. Paterson and G. Bigam, Canad. J. Chem., 41, 1841 (1963).
232. T. H. Brown, E. B. Whipple, and P. H. Verdier, J. Chem. Phys., 38, 3029 (1963).
233. R. A. Hoffman, B. Gestblom, and S. Forsen, J. Chem. Phys., 39, 486 (1963).
234. M. Miyamoto, Y. Kawamatsu, M. Shinohara, Y. Asahi, Y. Nakadaira, H. Kakisawa, K. Nakanishi, and N. S. Bhacca, Tetrahedron Letters, 693 (1963).
235. S. L. Manatt, G. L. Juvinall, and D. D. Elleman, J. Amer. Chem. Soc., 85, 2664 (1963).
236. G. M. Whitesides, J. L. Beauchamp, and J. D. Roberts, J. Amer. Chem. Soc., 85, 2665 (1963).
237. R. R. Ernst and H. Primas, Helv. Phys. Acta, 36, 583 (1963).
238. F. A. Bovey, E. W. Anderson, D. C. Douglass, and J. A. Manson, J. Chem. Phys., 39, 1199 (1963).
239. H. Agahigian, G. D. Vickers, J. Roscoe, and J. Bishop, J. Chem. Phys., 39, 1621 (1963).
240. M. J. S. Dewar and R. C. Fahey, J. Amer. Chem. Soc., 85, 2704 (1963).
241. Y. Osawa and M. Neeman, J. Amer. Chem. Soc., 85, 2856 (1963).
242. D. H. Williams and N. S. Bhacca, J. Amer. Chem. Soc., 85, 2861 (1963).
243. S. Forsen and R. A. Hoffman, Acta Chem. Scand., 17, 1787 (1963).
244. J. M. Jennins and B. L. Shaw, Proc. Chem. Soc., 279 (1963).
245. J. M. Lehn and A. Vystrcil, Tetrahedron, 19, 1733 (1963).

246. P. R. Story, L. C. Snyder, D. C. Douglass, E. W. Anderson, and R. L. Kornegay, J. Amer. Chem. Soc., 85, 3630 (1963).
247. L. F. Johnson and N. S. Bhacca, J. Amer. Chem. Soc., 85, 3700 (1963).
248. G. L. Closs, J. J. Katz, F. C. Pennington, M. R. Thomas, and H. H. Strain, J. Amer. Chem. Soc., 85, 3809 (1963).
249. K. Nakanishi, M. Kurono, and N. S. Bhacca, Tetrahedron Letters, 2161 (1963).
250. N. J. Leonard and J. V. Paukstelis, J. Org. Chem., 28, 3021 (1963).
251. C. W. Bird, D. L. Colinese, R. C. Cookson, J. Hudec, and R. O. Williams, Tetrahedron Letters, 373 (1961).
252. B. D. Nageswara Rao and J. D. Baldeschwieler, J. Molec. Spectr., 11, 440 (1963).
253. R. A. Hoffman, B. Gestblom, S. Gronowitz, and S. Forsen, J. Molec. Spectr., 11, 454 (1963).
254. W. G. Paterson and H. Spedding, Canad. J. Chem., 41, 2706 (1963).
255. R. L. Rinehart, J. R. Beck, W. W. Epstein, and L. D. Spicer, J. Amer. Chem. Soc., 85, 4035 (1963).
256. H. T. Miles, R. B. Bradley, and E. D. Becker, Science, 142, 1569 (1963).
257. E. B. Whipple and Y. Chiang, J. Chem. Phys., 40, 713 (1964).
258. A. D. Cohen and K. A. McLauchlan, Molec. Phys., 7, 11 (1963/64).
259. A. D. Cohen, R. Freeman, K. A. McLauchlan, and D. H. Whiffen, Molec. Phys., 7, 45 (1963).
260. J. Smidt (editor), Magnetic and Electric Resonance and Relaxation, North-Holland Publ. Co., Amsterdam (1963).
261. Kato Yoshifumi and A. Saika, J. Chem. Phys., 44, 2824 (1966).
262. F. A. L. Anet, J. Amer. Chem. Soc., 86, 458 (1964).
263. O. L. Chapman and E. D. Hoganson, J. Amer. Chem. Soc., 86, 498 (1964).
264. J. Brandrup and M. Goodman, J. Polym. Sci., B2, 123 (1964).
265. S. Forsen and R. A. Hoffman, Acta Chem. Scand., 18, 249 (1964).
266. M. Barfield and J. D. Baldeschwieler, J. Molec. Spectr., 12, 23 (1964).
267. B. Coxon and H. G. Fletcher, Chem. and Ind., 662 (1964).
268. M. M. Crutchfield, C. F. Callis, and J. R. van Wafer, Inorg. Chem., 31, 280 (1964).
269. E. L. Mutterties, J. H. Balthis, Y. T. Chia, W. H. Knoth, and H. C. Miller, Inorg. Chem., 3, 444 (1964).
270. S. Forsen and R. A. Hoffman, J. Chem. Phys., 40, 1189 (1964).
271. G. A. Olah, E. B. Baker, J. C. Evans, W. S. Tolgyesi, J. S. McIntyre, and I. J. Bastien, J. Amer. Chem. Soc., 1360 (1964).
272. M. Y. DeWolf and J. D. Baldechwieler, J. Mol. Spectr., 13, 344 (1964).
273. K. G. Untch and R. J. Kurland, J. Molec. Spectr., 14, 156 (1964).
274. K. G. Untch, J. Amer. Chem. Soc., 85, 346 (1963).
275. M. Hesse, W. von Philipsborn, D. Schumann, G. Spiteller, M. Spiteller-Friedmann, W. J. Taylor, H. Schmid, and P. Karrer, Helv. Chim. Acta, 47, 878 (1964).
276. A. J. Scott, D. W. Young, S. A. Hutchinson, and N. S. Bhacca, Tetrahedron Letters, 849 (1964).
277. A. J. R. Bourn and E. W. Randall, J. Molec. Spectr., 13, 29 (1964).
278. Takeshi Oka, J. Chem. Phys., 45, 752 (1966).
279. K. C. Ramey and N. D. Field, J. Polym. Sci., B2, 461 (1964).
280. S. Forsen, B. Gestblom, S. Gronowitz, and R. A. Hoffman, Acta Chem. Scand., 18, 313 (1964).
281. F. A. Bovey, E. W. Anderson, F. P. Hood, and R. L. Kornegay, J. Chem. Phys., 40, 3099 (1964).
282. J. M. Anderson and J. D. Baldeschwieler, J. Chem. Phys., 40, 3241 (1964).
283. R. Freeman, J. Chem. Phys., 40, 3571 (1964).
284. R. Ernst and J. M. Anderson, J. Chem. Phys., 40, 3737 (1964).
285. M. S. Bergqvist and T. Norin, Arkiv Kemi, 22, 137 (1964).
286. O. L. Chapman, G. W. Borden, R. W. King, and B. Winkler, J. Amer. Chem. Soc., 86, 2660 (1964).
287. R. L. Lemieux and J. W. Lown, Canad. J. Chem., 42, 967 (1964).
288. J. B. Stothers and J. R. Robinson, Canad. J. Chem., 42, 967 (1964).
289. P. J. Black and M. L. Heffernan, Australian J. Chem., 17, 558 (1964).
290. G. Ottman, H. Agahigian, H. Hooks, G. D. Vickers, E. Kober, and R. Rätz, Inorg. Chem., 3, 753 (1964).
291. R. Freeman, R. R. Ernst, and W. A. Anderson, J. Chem. Phys., 46, 1125 (1967).
292. J. G. Verkade, R.W. King, and C. W. Heitch, Inorg. Chem., 3, 884 (1964).
293. R. V. Lemieux and R. Nagarajan, Canad. J. Chem., 42, 1270 (1964).
294. S. L. Gordon and J. D. Baldeschwieler, J. Chem. Phys., 41, 571 (1964).
295. H. W. H. Schmidt and H. Neukon, Tetrahedron Letters, 2063 (1964).
296. H.–J. Köhler, Z. Phys. Chem., 226, 283 (1964).

297. F. A. L. Anet, M. Ahamad, and L. D. Hall, Proc. Chem. Soc., 145 (1964).
298. F. A. Bovey, F. P. Hood III, E. W. Anderson, and R. L. Kornegay, Proc. Chem. Soc., 146 (1964).
299. L. D. Hall and L. F. Johnson, Tetrahedron, 20, 883 (1964).
300. K. C. Ramey, N. D. Field, and I. Hasegawa, J. Polym. Sci., B2, 865 (1964).
301. H. Weitkamp and F. Korte, Z. anal. Chem., 204, 245 (1964).
302. E. G. Paul and D. M Grant, J. Amer. Chem. Soc., 86, 2977 (1964).
303. D. M. Grant and E.G. Paul, J. Amer. Chem. Soc., 86, 2984 (1964).
304. R. S. Neale and E. B. Whipple, J. Amer. Chem. Soc., 86, 3130 (1964).
305. G. E. McCasland, S. Furuta, L. F. Johnson, and J. N. Shoolery, J. Org. Chem.,29, 2354 (1964).
306. M. Grdinic, D. A. Nelson, and V. Boekelheide, J. Amer. Chem. Soc., 86, 3357 (1964).
307. J. B. Stothers, J. D. Tolman, and R. R. Fraser, Canad, J. Chem., 42, 1530 (1964).
308. B. Coxon and L. D. Hall, Tetrahedron, 20, 1685 (1964).
309. R. B. Morin and M. Gorman, Tetrahedron Letters, 2339 (1964).
310. M. Miyamoto, K. Morita, Y. Kawamatsu, S. Noguchi, R. Marumoto, K. Tanaka, S. Tatsuoka, K. Nakanishi, Y. Nakadaira, and N. S. Bhacca, Tetrahedron Letters, 2355 (1964).
311. H. P. Hamlow, S. Okuda, and N. Nakagawa, Tetrahedron Letters, 2553 (1964).
312. W. R. Hertler and M. S. Raasch, J. Amer. Chem. Soc., 86, 3661 (1964).
313. S. Castellano and J. S. Waugh, J. Chem. Phys., 34, 295 (1961).
314. J. A. S. Smith, Lab. Practice, 13, 947 (1964).
315. F. A. Bovey, F. P. Hood III, E. W. Anderson, and R. L. Kornegay, J. Chem. Phys., 41, 2041 (1964).
316. R. C. Hoplins, Rev. Sci. Instr., 35, 1495 (1964).
317. J. Foried, P. Grabowich, E. F. Sabo, and A. J. Cohen, Tetrahedron, 20, 2297 (1964).
318. L. Mester, E. Moczar, and J. Parello, Tetrahedron Letters, 3223 (1964).
319. F. A. L. Anet, Tetrahedron Letters, 3399 (1964).
320. L. D. Quin, J. A. Peters, C. E. Griffin, and M. Gordon, Tetrahedron Letters, 3698 (1964).
321. J. H. Allen, J. K. Becconsall, and D. W. Turner, J. Sci. Instr., 41, 673 (1964).
322. D. Gagnaire, A. Rousseau, and P. Servoz-Gavin, J. Chim. Phys., 61, 1207 (1964).
323. E. W. Garbisch, Chem. and Ind., 1715 (1964).
324. R. K. Harris and B. G. Hayter, Canad. J. Chem., 42, 2282 (1964).
325. S. S. Danyluk, J. Amer. Chem. Soc., 86, 4504 (1964).
326. J. J. Uebel and J. C. Martin, J. Amer. Chem. Soc., 86, 4618 (1964).
327. P. J. Black, M. L. Heffernan, L. M. Jackman, Q. N. Porter, and G. R. Underwood, Australian J. Chem., 17, 1128 (1964).
328. D. Gagnaire, E. Payo-Subiza, and A. Rousseau, J. Chim. Phys., 62, 42 (1965).
329. N. J. Lenonard and G. E. Wilson, Jr. J. Amer. Chem. Soc., 86, 5307 (1964).
330. J. H. Smalley, F. E. Dickson, and I. I. Bezman, Inorg. Chem., 3, 1780 (1964).
331. N. Gestblom and B. Mathiasson, Acta Chem. Scand., 18, 1905 (1964).
332. B. A. Arbuzov, Yu. Yu. Samitov, A. O. Vizel, and T. V. Zykova, Dokl. AN SSSR, 159, 1062 (1964).
333. M. Anteunis and F. Alderweireldt, Bull. Soc. Chim. Belge, 73, 889 (1964).
334. M. Anteunis and F. Alderweireldt, Bull. Soc. Chim. Belge, 73, 903 (1964).
335. A. G. Whittaker, D. W. Moore, and S. Siegel, J. Phys. Chem., 68, 3431 (1964).
336. C. H. de Puy, M. Isaks, K. L. Eilers, and G. F. Morris, J. Org. Chem., 29, 3503 (1964).
337. R. C. Ferguson, J. Phys, Chem., 68, 1594 (1964).
338. M. Suchy, V. Herout, F. Strom, P. De Mayo, A. N. Starrat, and J. B. Stothers, Tetrahedron Letters, 3907 (1964).
339. K. C. Ramey and N. D. Field, J. Polym. Sci., B3, 63 (1965).
340. K. C. Ramey and N. D. Field, J. Polym. Sci., B3, 69 (1965).
341. S. Ohnishi and K. Nukada, J. Polym. Sci., B3, 179 (1965).
342. S. Shiroh Satoh, J. Polym. Sci., A2, 5221 (1964).
343. E. G. Brame, Jr., R. S. Sudol, O. Vogl. J. Polym. Sci., A2, 5337 (1964).
344. D. D. Elleman, S. L. Mannat, and C. D. Pearce, J. Chem. Phys., 42, 650 (1965).
345. P. Loeve and L. Salem, J. Chem. Phys., 43, 3402 (1965).
346. M. Scheinblatt, J. Amer. Chem. Soc., 87, 572 (1965).
347. L. Mester, E. Moczar, and J. Parello, J. Amer. Chem. Soc., 87, 596 (1965).
348. A. J. Bourn and E. W. Randall, Molec. Phys., 8, 567 (1964).
349. L. J. Durham, N. Bhacca, and H. Budzikiewicz, Tetrahedron Letters, 5 (1965).
350. D. F. Evans, Lab. Practice, 14, 57 (1965).

351. R. S. Milner and D. W. Turner, Chem. Comm., 32 (1965).
352. R. A. Hoffman, B. Gestblom, S. Rodmar, and S. Forsen, J. Chem. Phys., 42, 1695 (1965).
353. W. H. Knoth, N. R. Hertler, and E. L. Muetterties, Inorg. Chem., 4, 280 (1965).
354. K. A. McLauchlan, Chem. Comm., 105 (1965).
355. W. A. Hawksworth, P. W. Jeffs, B. K. Tidd, and T. P. Toube, J. Chem. Soc., 1991 (1965).
356. R. D. Haugwitz, P. W. Jeffs, and E. Wenkert, J. Chem. Soc., 2001 (1965).
357. K. L. Servis and J. D. Roberts, J. Amer. Chem. Soc., 87, 1339 (1965).
358. T. Yoshino and J. Komiyama, J. Polym. Sci., B3, 311 (1965).
359. H. Agahigian, G. D. Vickers, M. H. von Saltza, J. Reid, A. J. Cohen, and H. Gauthier, J. Org. Chem., 30, 1085 (1965).
360. R. U. Lemieux, D. R. Lineback, M. L. Wolfrom, F. B. Moody, E. G. Wallace, and F. Komnitsky, Jr., J. Org. Chem., 30, 1092 (1965).
361. C. J. M. Stirling, J. Chem. Soc., Suppl 1, 5863 (1964).
362. P. J. Black and M. L. Heffernan, Australian J. Chem., 18, 353 (1965).
363. L. H. Briggs, R. C. Cambie, B. J. Candy, G. M. O'Donovan, R. H. Russell, and R. N. Seelye, J. Chem. Soc., 2492 (1965).
364. A. D. Cohen and K. A. McLauchlan, Molec. Phys., 9, 49 (1965).
365. W. M. S. Gil, Molec. Phys., 9, 97 (1965).
366. C. W. Jefford, B. Naegell, and K. Ramey, J. Amer. Chem. Soc., 87, 2191 (1965).
367. S. L. Manatt, D. D. Elleman, and S. J. Brois, J. Amer. Chem. Soc., 87, 2220 (1965).
368. R. J. Pugmire, D. M. Grant, R. K. Robins, and G. W. Rhodes, J. Amer. Chem. Soc., 87, 2225 (1965).
369. A. K. Colter, I. I. Schuster, and R. J. Kurland, J. Amer. Chem. Soc., 87, 2278 (1965).
370. R. J. Kurland, I. I. Schuster, and A. K. Colter, J. Amer. Chem. Soc., 87, 2279 (1965).
371. S. S. Danyluk, J. Amer. Chem. Soc., 87, 2300 (1965).
372. S. Rodmar, S. Forsen, B. Gestblom, S. Gronowitz, and R. A. Hoffman, Acta Chem. Scand., 19, 485 (1965).
373. S. Forsen, B. Gestblom, R. A. Hoffman, and S. Rodmar, Acta Chem. Scand., 19, 503 (1965).
374. H. Kamei, Jap. J. Appl. Phys., 4, 212 (1965).
375. K. L. Stevens, R. E. Lundin, and R. Teranishi, J. Org. Chem., 30, 1690 (1965).
376. W. J. Barry, I. L. Finar, and E. F. Mooney, Spectrochim. Acta, 21, 1095 (1965).
377. C. W. Wilson III and E. R. Santee, Jr., J. Polym. Sci., C8, 97 (1965).
378. J. Bargon, K.-H. Hellwege, and U. Johnsen, Makromolek. Chemie, 85, 291 (1965).
379. K. T. Potts, M. Kanaoka, T. H. Crawford, and S. W. Thomas, J. Heterocyclic Chem., 1, 297 (1965).
380. D. R. Arnold, D. J. Trecker, and E. B. Whipple, J. Amer. Chem. Soc., 87, 2596 (1965).
381. G. Fraenkel and W. Burlant, J. Chem. Phys., 42, 3724 (1965).
382. N. Muller and R. H. Birkhahn, J. Chem. Phys., 43, 4540 (1965).
383. F. A. Bovey, F. P. Hood III, E. W. Anderson, and L. C. Snyder, J. Chem. Phys., 42, 3900 (1965).
384. W. Zürcher, J. Gutzwiller, and C. Tamm, Helv, Chim. Acta, 48, 840 (1965).
385. P. Scribe, Compt. rend. Acad. Sci., 261, 160 (1965).
386. E. L. Mackor and C. MacLean, J. Chem. Phys., 42, 4254 (1965).
387. Y. Kanazawa and J. D. Baldeschwieler, J. Molec. Spectr., 16, 325 (1965).
388. S. Wolfe and P. G. Campbell, Can. J. Chem., 43, 1184 (1965).
389. A. R. Stein, Canad. J. Chem., 43, 1184 (1965).
390. H. Kamei, Bull. Chem. Soc., 38, 1212, Japan (1965).
391. K. C. Ramey, W. D. Field, and A. E. Borchert, J. Polym. Sci., A3, 2885 (1965).
392. F. Aruska, H. H. Hutton, and T. Schaefer, Canad. J. Chem., 43, 1942 (1965).
393. R. U. Lemieux and J. D. Stevens, Canad. J. Chem., 43, 2059 (1965).
394. R. A. Corral and O. O. Orazi, Tetrahedron, 21, 909 (1965).
395. H. Immer, J. Polonsky, R. Toubiana, and Ho Dac An, Tetrahedron, 21, 2117 (1965).
396. S. Masamune, Tetrahedron Letters, 945 (1965).
397. T. Irie, M. Susuki, and T. Masamune, Tetrahedron Letters, 1091 (1965).
398. K. D. Barrow and T. M. Spotswood, Tetrahedron Letters, 3325 (1965).
399. S. Forsen, T. Alm, B. Gestblom, S. Rodmar, and R. A. Hoffman, J. Molec. Spectr., 17, 13 (1965).
400. F. A. L. Anet and M. Z. Haq, J. Amer. Chem. Soc., 87, 3147 (1965).
401. L. A. Paquette, J. H. Barrett, R. P. Spitz, and R. Pitcher, J. Amer. Chem. Soc., 87, 3417 (1965).
402. G. Schröder, J. F. M. Oth, and R. Merneyi, Angew. Chem., 77, 774 (1965).
403. R. C. Neuman, Jr., and L. B. Young, J. Phys. Chem., 69, 2570 (1965).

404. G. D. Vickers, M. J. Nadel, and H. Agahigian, Rev. Sci., Instr., 36, 1258 (1965).
405. H. Hauth, D. Stauffacher, P. Niklaus, and A. Melera, Helv, Chim. Acta, 48, 1087 (1965).
406. R. C. Hopkins, J. D. Baldeschwieler, R. Schaeffer, F. N. Tebbe, and A. Norman, J. Chem. Phys., 43, 975 (1965).
407. R. E. Williams, S. G. Gibbins, and I. Shapiro, J. Amer. Chem. Soc., 81, 6164 (1959).
408. J. S. Hyde, J. Chem. Phys., 43, 1806 (1965).
409. E. B. Whipple, T. H. Brown, T. C. Farrar, and T. D. Coyle, J. J. Chem. Phys., 43, 1841 (1965).
410. J. B. Lambert and J. D. Roberts, J. Amer. Chem. Soc., 87, 3884 (1965).
411. J. B. Lambert, L. J. Durham, P. Lepoutere, and J. D. Roberts, J. Amer. Chem. Slc., 87, 3896 (1965).
412. J. C. Davis Jr. and T. V. van Auken, J. Amer. Chem. Soc., 87, 3900 (1965).
413. H. Ottavi and R. Ribotta, Compt. rend. Acad. Sci., 261, 1515 (1965).
414. M. Itoh, S. Shimokawa, A. Arase, and K. Aomura, J. Chem. Soc., 68, 1441, Japan (1965).
415. K. Matsuzaki, T. Uryu, K. Tameda, and M. Takeuchi, J. Chem. Soc., 68, 1466, Japan (1965).
416. E. W. Garbisch, J. Org. Chem., 30, 2109 (1965).
417. P. M. Subramanian, M. T. Emerson, and N. A. LeBel, J. Org. Chem., 30, 2624 (1965).
418. A. I. Polyakov and G. I. Yakovlev, Zh. éksperim. i teor. fiziki, 49, 760 (1965).
419. N. N. Korst and O. A. Nikich-Krilichevskii, Teor. i éksperim. khimiya, 1, 505 (1965).
420. B. D. Nageswara Rao and L. R. Anders, Phys. Rev., 140, A112 (1965).
421. H. Schneider, Ann. Phys., 16, 135 (1965).
422. C. W. Jefford, J. Gunsher, and K. C. Ramey, J. Amer. Chem. Soc., 87, 4384 (1965).
423. T. Yoshino and K. Kuno, J. Amer. Chem. Soc., 87, 4404 (1965).
424. J. H. Freed, J. Chem. Phys., 43, 2312 (1965).
425. A. H. Cowley and R. P. Pinnell, J. Amer. Chem. Soc., 87, 4454 (1965).
426. A. M. Aguiar and D. Daigle, J. Org. Chem., 30, 3527 (1965).
427. W. R. Anderson, Jr., and R. M. Silverstein, Anal. Chem., 37, 1417 (1965).
428. B. Nann, H. Wehrli, K. Schaggner, and O. Jeger, Helv. Chim. Acta, 48, 1680 (1965).
429. J. L. McClanahan and S. A. Previtera, J. Polym. Sci., A3, 3919 (1965).
430. R. P. Gupta, J. Polym. Sci., A3, 3951 (1965).
431. R. J. Cook and D. H. Whiffen, J. Chem. Phys., 43, 2908 (1965).
432. H. W. H. Schmidt, Tetrahedron Letters, 235 (1967).
433. E. W. Randall and D. Shaw, Mol. Phys., 10, 41 (1965).
434. J. E. Baldwin and R. A. Smith, J. Amer. Chem. Soc., 87, 4819 (1965).
435. R. W. King, C. F. Murphy, and W. C. Wildman, J. Amer. Chem. Soc., 87, 4912 (1965).
436. C. C. J. Culvenor, M. L. Heffernan, and W. G. Woods, Australian J. Chem., 18, 1605 (1965).
437. A. S. Kende, P. T. Izzo, and J. E. Lancaster, J. Amer. Chem. Soc., 87, 5044 (1965).
438. G. Bisch and J. D. Roberts, J. Amer. Chem. Soc., 87, 5157 (1965).
439. S. C. Cascon, W. B. Mors, B. M. Fursch, R. T. Aplin, and L. J. Durham, J. Amer. Chem. Soc., 87, 5237 (1965).
440. M. P. Schweizer, S. J. Chan, and P. O. P. Tso, J. Amer. Chem. Soc., 87, 5241 (1965).
441. F. A. L. Anet, A. J. R. Bourn, P. Carter, and S. Winstein, J. Amer. Chem. Soc., 87, 5249 (1965).
442. F. A. L. Anet and A. J. R. Bourn, J. Amer. Chem. Soc., 87, 5250 (1965).
443. Y. L. Chow, Canad. J. Chem., 43, 2711 (1965).
444. S. Alexander, J. Chem. Phys., 37, 967 (1962).
445. A. Fischer, M. Golding, and W. C. Tennant, J. Chem. Soc., 6032 (1965).
446. A. Eschenmaser, R. Scheffold, E. Bertele, M. Pesaro, and H. Gschwend, Proc. Roy. Soc., 288, 306 (1965).
447. T. F. Page, T. Alger, and D. M. Grant, J. Amer. Chem. Soc., 87, 5333 (1965).
448. H. S. Gutowsky, R. L. Vald, and E. J. Vells, J. Chem. Phys., 43, 4107 (1965).
449. F. A. Nelson and H. E. Weaver, Science, 146, 223 (1964).
450. G. D. Vickers, H. Agahigian, E. A. Pier, and H. Schroeder, Inorg. Chem., 5, 693 (1966).
451. F. A. L. Anet, Canad. J. Chem., 39, 2262 (1961).
452. J. I. Musher and E. J. Corey, Tetrahedron, 18, 791 (1962).
453. K. Hafner, Angew. Chem., 75, 1041 (1963).
454. E. D. Becker, H. T. Miles, and R. B. Bradley, J. Amer. Chem. Soc., 87, 5575 (1965).
455. M. D. Mehta, D. Miller, and E. F. Mooney, J. Chem. Soc., 6695 (1965).
456. G. F. H. Green, J. E. Page, and S. E. Staniforth, J. Chem. Soc., 6695 (1965).
457. C. Hewlett and R. A. Shaw, J. Chem. Soc., 56 (1966).
458. E. Sackmann and H. Dreeskamp, Spectrochim. Acta, 21, 2005 (1965).
459. H. C. Beyerman, L. Maat, A. van Veen, A. Zweistra, and W. Von Philip-sborn, Rec. trav. chim., 84, 1367 (1965).

460. J. L. Jungnickel and C. A. Reilly, Rec. trav. chim., 84, 1526 (1965).
461. K. C. Ramey and J. Messick, Tetrahedron Letters, 4423 (1965).
462. J. Gutzwiller, C. Tamm, and H. P. Sigg, Tetrahedron Letters, 4495 (1965).
463. S. Masamune and K. Fukumoto, Tetrahedron Letters, 4647 (1965).
464. J. -P. Imbaud, Compt. rend. Acad. Sci., 261, 5442 (1965).
465. E. L. Mackor and C. MacLean, J. Chem. Phys., 44, 430 (1966).
466. N. Y. DeWolf and J. H. Noggle, J. Molec. Spectr., 19, 112 (1966).
467. T. L. Brown and K. Stark, J. Phys. Chem., 69, 2679 (1965).
468. M. Rey and A. S. Dreiding, Helv. Chim. Acta, 48, 1985 (1965).
469. B. Gestblom, S. Gronowitz, R. A. Hoffman, B. M. Mathiasson, and S. Rodmar, Arkiv Kemi, 23, 483, 501 (1965).
470. B. Gestblom, S. Gronowitz, R. A. Hoffman, and B. Mathiasson, Arkiv Kemi, 23, 517 (1965).
471. W. R. Jackson, C. H. McMuller, R. Spratt, and P. Bladon, J. Organometall. Chem., 4, 392 (1965).
472. B. Lamm, Acta Chem. Scand., 19, 2316 (1965).
473. M. C. Woods, K. Nakanishi, and N. S. Bhacca, Tetrahedron, 22, 243 (1966).
474. A. Mathias, Tetrahedron, 22, 217 (1966).
475. J. A. Potenza, W. N. Lipscomb, G. D. Vickers, and H. Schroeder, J. Amer. Chem. Soc., 88, 628 (1966).
476. C. Ganter and J. D. Roberts, J. Amer. Chem. Soc., 88, 741 (1966).
477. A. Closse, R. Mauli, and H. P. Sigg, Helv. Chim. Acta, 49, 204 (1966).
478. A. Dieffenbacher and W. von Philipsborn, Helv. Chim. Acta, 49, 897 (1966).
479. J. L. Burdett and L. L. Burger, Canad. J. Chem., 44, 111 (1966).
480. D. T. Sawyer and J. R. Brannan, Anal. Chem., 38, 192 (1966).
481. K. Tori, K. Aono, Y. Hata, R. Muneyuki, T. Tsuji, and H. Tanida, Tetrahedron Letters, 9 (1966).
482. S. S. Jha, J. Phys. Soc., 21, 42, Japan (1966).
483. A. N. Pudovik, T. Kh. Gazizov, Yu. Yu. Samitov, and T. V. Zhukova, Dokl. AN SSSR, 166, 615 (1966).
484. R. V. Lemieux and J. D. Stevens, Canad. J. Chem., 44, 249 (1966).
485. K. A. McLauchlan and T. Schaefer, Canad. J. Chem., 44, 321 (1966).
486. A. S. Perlin, Canad. J. Chem., 44, 539 (1966).
487. L. F. Johnson, A. V. Robertson, W. R. J. Simpson, and B. Witkop, Australian J. Chem., 19, 115 (1966).
488. R. Jackuesy and J. Levisalles, Bull. Soc. Chim. France, 396 (1966).
489. G. Chalier, A. Rassat, and A. Rousseau, Bull. Soc. Chim., France, 428 (1966).
490. W. Herz, S. Rajappa, M. V. Laksmikantham, and J. J. Schmid, Tetrahedron, 22, 693 (1966).
491. J. D. Connolly, R. McGrindle, K. H. Overton, and J. Feeney, Tetrahedron, 22, 891 (1966).
492. K. Takeda, M. Ikuda, M. Miyawaki, and K. Tori, Tetrahedron, 22, 1159 (1966).
493. J. A. Ferretti and R. Freeman, J. Chem. Phys., 44, 2054 (1966).
494. G. D. Vickers, H. Agahigian, E. A. Pier, and H. Schroeder, Inorg. Chem., 5, 693 (1966).
495. T. Yoshino, Y. Kakiuchi, and J. Komiyama, J. Phys. Chem., 70, 1059 (1966).
496. P. T. Lansburg, J. F. Bieron, and A. J. Lacher, J. Amer. Chem. Soc., 88, 1482 (1966).
497. W. R. Woolfenden and D. M. Grant, J. Amer. Chem. Soc., 88, 1496 (1966).
498. H. G. Preston, Jr. and J. C. Davis, J. Amer. Chem. Soc., 88, 1585 (1966).
499. L. A. Paquette and J. H. Barrett, J. Amer. Chem. Soc., 88, 1718 (1966).
500. R. A. Corral and O. O. Orazi, Tetrahedron Letters, 583 (1967).
501. C. A. Kingsbury and W. B. Thornton, J. Org. Chem., 31, 1000 (1966).
502. A. Dieffenbacher, R. M. Mondelli, and W. von Philipsborn, Helv. Chim. Acta., 49, 1355 (1966).
503. J. A. Ladd, Spectrochim. Acta, 22, 1157 (1966).
504. A. D. Norman and R. Schaeffer, J. Phys. Chem., 70, 1662 (1966).
505. H. H. Lindner and T. Onak, J. Amer. Chem. Soc., 88, 1890 (1966).
506. K. E. Wilzbach and L. Kaplan, J. Amer. Chem. Soc., 88, 2066 (1966).
507. G. R. Bedford, D. Greatbanks, and D. B. Rogers, Chem. Comm., 330 (1966).
508. M. Fraser, A. Melera, and D. H. Reid, J. Chem. Soc., B483 (1966).
509. R. A. Massy-Westropp, G. D. Reynolds, and T. M. Spotswood, Tetrahedron Letters, 1939 (1966).
510. J. J. Dunand, A. Rousseau, and P. Servoz-Gavin, Compt. rend. Acad. Sci., B262, 515 (1966).
511. K. Tori, K. Aono, K. Kitahonoki, R. Muneyuki, Y. Takano, H. Tanida, and T. Tsuji, Tetrahedron Letters, 2921 (1966).
512. J. Bargon, K.-H. Hellwege, and U. Johnsen, Makromolek. Chemie, 95, 187 (1966).
513. S. Enomato, M. Asahina, and S. Satoh, J. Polym. Sci., 4A1, 1372 (1966).
514. P. Sunder-Plassmann, P. H. Nelson, L. Durham, J. A. Edwards, and J. H. Fried, Tetrahedron Letters, 653 (1967).

515. C. Jutz, I. Rommel, I. Lengyel, and J. Feeney, Tetrahedron, 22, 1809 (1966).
516. J. Schaefer, J. Phys. Chem., 70, 1775 (1966).
517. S. E. Drewes, D. G. Roux, J. Feeney, and S. H. Eggers, Chem. Comm. 368 (1966).
518. G. Shaw, J. K. Becconsall, R. M. Canadine, and R. Murray, Chem. Comm., 455 (1966).
519. F. A. L. Anet and M. S. Jackues, J. Amer. Chem. Soc., 88, 1585 (1966).
520. F. A. L. Anet and M. S. Jackues, J. Amer. Chem. Soc., 88, 2586 (1966).
521. S. L. Manatt, G. L. Juvinall, R. J. Wagner, and D. D. Elleman, J. Amer. Chem. Soc., 88, 2689 (1966).
522. H. L. Retcofsky, E. N. Frankel, and H. S. Gutowsky, J. Amer. Chem. Soc., 88, 2710 (1966).
523. R. C. Dougherty, H L. Crespi, H. H. Strain, and J. J. Katz, J. Amer. Chem. Soc., 88, 2854, 2856 (1966).
524. T. D. Inch, J. R. Plimmer, and H. G. Fletcher, Jr., J. Org. Chem., 31, 1825 (1966).
525. J. M. F. Filho, B. Gilbert, M. Kitagawa, L. A. Leme, and L. J. Durhan, J. Chem. Soc., C 1260 (1966).
526. S. Forsen and R. A. Hoffman, J. Molec. Spectr., 20, 168 (1966).
527. J. Wiemann, O. Couvert, H. Danechpejouh, and D. Lelandais, Bull. Soc. Chim. France, 1760 (1966).
528. E. L. Mackor and C. MacLean, J. Chem. Phys., 44, 64 (1966).
529. R. J. Abraham and H. J. Bernstein, Canad. J. Chem., 39, 216 (1961).
530. A. Saupe and G. Englert, Phys. Rev. Letters, 11, 462 (1963).
531. E. B. Baker, J. Chem. Phys., 45, 609 (1966).
532. R. E. Sears and E. L. Hahn, J. Chem. Phys., 45, 2753 (1966).
533. S. L. Smith and R. H. Cox, J. Chem. Phys., 45, 2848 (1966).
534. A. Peake and L. F. Thomas, Chem. Comm., 529 (1966).
535. D. F. S. Natusch and R. E. Richards, Chem. Comm., 579 (1966).
536. R. A. Dwek and R. E. Richards, Chem. Comm., 581 (1966).
537. M. Ohtsuru and K. Tori, Chem. Comm., 750 (1966).
538. J. M. Lehn and R. Seher, Chem. Comm., 847 (1966).
539. J. D. Connolly, K. L. Handa, R. McCrindle, and K. H. Overton, Chem. Comm., 867 (1966).
540. K. Tori and M. Ohtsuru, Chem. Comm., 886 (1966).
541. A. J. R. Bourn, D. G. Gillies, and E. W. Randall, Tetrahedron, 22, 1825 (1966).
542. W. Herz, S. Rajappa, S. K. Roy, I. I. Schmid, and R. N. Mirrington, Tetrahedron, 22, 1907 (1966).
543. R. M. Silverstein, J. O. Rodin, D. L. Wood, and L. E. Browne, Tetrahedron, 22, 1929 (1966).
544. B. Coxon, Tetrahedron, 22, 2281 (1966).
545. M. Lj. Mihailovic, Lj. Lorenc, M. Gasic, M. Rogic, A. Melera, and M. Stefanovic, Tetrahedron, 22, 2345 (1966).
546. D. J. Aberhart and P. de Mayo, Tetrahedron, 22, 2359 (1966).
547. M. Miyamoto, Y. Kawamatsu, M. Shinohara, Y. Nakadaira, and K. Nakanishi, Tetrahedron, 22, 2785 (1966).
548. J. W. Blunt, M. P. Hartshorn, and D. N, Kirk, Tetrahedron, 22, 3195 (1966).
549. Altaf-ur-Rahman and A. J. Boulton, Tetrahedron, Suppl., 7, 49 (1966).
550. R. C. Cookson, T. A. Crablo, I. I. Frankel, and I. Hudec, Tetrahedron, Suppl., 7, 355 (1966).
551. A. S. Perlin, Canad. J. Chem., 44, 1757 (1966).
552. S. Fujiwara, Y. Fujiwara, K. Fujii, and T. Fukuroi, J. Mol. Spectr., 19, 294 (1966).
553. A. S. Kende, P. T. Izzo, and P. T. McGregor, J. Amer. Chem. Soc., 88, 3359 (1966).
554. J. R. Edman, J. Amer. Chem. Soc., 88, 3454 (1966).
555. E. B. Baker, L. W. Burd, and G. N. Root, Rev. Sci. Instr., 36, 1495 (1965).
556. J. D. Memory, G. W. Parker, and J. C. Halsey, J. Chem. Phys., 45, 3567 (1966).
557. R. R. Ernst, J. Chem. Phys., 45, 3845 (1966).
558. É. Lippmaa, Ya. Past, A. Olivson, and T. Saluvere, Izv. AN SSSR, ser. fiz.-matem. i tekhn. nauk, 15, 63 (1966).
559. J. Feeney and A. Heinrich, Chem. Comm., 295 (1966).
560. L. van Gerven (editor), Nuclear Magnetic Resonance and Relaxation in Solids, Proceedings of the Thirteenth Colloque AMPERE, Leuven, September, 1964, North-Holland, Amsterdam (1965).
561. C. MacLean and E. L. Mackor, J. Chem. Phys., 44, 2708 (1966).
562. H. C. Torrey, Phys. Rev., 76, 1059 (1949).
563. J. J. Burke and P. C. Lauterbur, J. Chem. Phys., 83, 326 (1961).
564. J. V. Acrivos, J. Chem. Phys., 36, 1097 (1962).
565. D. D. Elleman and S. L. Manatt, J. Chem. Phys., 36, 1945 (1962).
566. G. Bonera and A. Rigamonti, J. Chem. Phys., 42, 171 (1965).
567. D. D. Elleman and S. L. Manatt, J. Mol. Spectr., 9, 477 (1962).
568. R. L. Fulton and J. D. Baldeschwieler, J. Chem. Phys., 34, 1075 (1961).

569. J. M. Anderson and J. D. Baldeschwieler, J. Chem. Phys., 37, 39 (1962).
570. J. M. Anderson and J. D. Baldeschwieler, J. Chem. Phys., 38, 570 (1963).
571. S. L. Manatt and D. D. Elleman, J. Amer. Chem. Soc., 84, 1305 (1962).
572. P. C. Lauterbur and R. J. Kurland, J. Amer. Chem. Soc., 84, 2458 (1962).
573. S. Brownstein and D. M. Wiles, J. Polym. Sci., A2, 1901 (1964).
574. L. K. Parker, Lab. Practice, 13, 965 (1964).
575. J. A. Pople and D. P. Santry, Mol. Phys., 8, 1 (1964).
576. J. N. Shoolery, Disc. Faraday Soc., 34, 104 (1962).
577. S. Sternhell, Rev. Pure Appl. Chem., 14, 15 (1964).
578. P. R. Solomon, Rev, Sci. Instr., 36, 1130 (1965).
579. S. Forsen and B. Akermark, Acta Chem. Scand., 17, 1712 (1963).
580. F. P. Johnson, A. Melera, and S. Sternell, Australian J. Chem., 19, 1523 (1966).
581. C. MacLean and E. L. Mackor, Proc. Phys. Soc., 88, 341 (1966).
582. K. Tori, Y. Hata, R. Munepuki, Y. Takano, T. Tsuji, and H. Tanids, Canad. J. Chem., 42, 928 (1964).
583. M. Karplus, J. Amer. Chem. Soc., 85, 2870 (1963).
584. R. C. Woods, A. M. Ronn, and E. B. Wilson, Rev. Sci. Instr., 37, 927 (1966).
585. Y. Abe, M. Tasumi, T. Shimanouchi, S. Satoh, and R. Chujo, J. Polym. Sci., A1, 1413 (1966).
586. F. A. Bovey and G. van D. Tiers, J. Polym. Sci., 38, 73 (1959).
587. F. A. Bovey and G. van D. Tiers, J. Polym. Sci., 44, 173 (1960).
588. T. J. Seed, Rev. Sci. Instr., 35, 473 (1964).
589. R. J. Mohrbacher, H. R. Almond, E. L. Carson, J. D. Rosenau, and G. J. Poas, J. Org. Chem., 31, 2114 (1966).
590. J. E. Franz, M. W. Dietrich, A. Henshall, and G. Osuch, J. Org. Chem., 31, 2847 (1966).
591. D. G. Gillies and E. W. Randall, J. Sci. Instr., 43, 466 (1966).
592. C. L. Bell and S. S. Danyluk, J. Amer. Chem. Soc., 88, 2344 (1966).
593. U. Rauterberg and J. Kummer, Z. angew. Physik, 20, 284 (1966).
594. A. W. Overhauser, Phys. Rev., 92, 411 (1953).
595. A. Abragam, Phys. Rev., 98, 1729 (1955).
596. G. Feher, Phys. Rev., 103, 834 (1956).
597. G. W. Flynn, M. Matsushima, J. D. Baldeschwieler, and N. C. Criag, J. Chem. Phys., 38, 2295 (1963).
598. R. A. Hoffman and S. Forsen, J. Chem. Phys., 45, 2049 (1966).
599. R. Freeman and N. S. Bhacca, J. Chem. Phys., 45, 3795 (1966).
600. E. B. Whipple, M. Ruta, V.S. Watts, and J. H. Goldstein, J. Chem. Phys., 45, 4372 (1966).
601. V. P. Lebedev and B. I. Ionin, Izv. vysh. uchebi. zaved., Priborostoenie, 10, 29 (1967).
602. J. E. Anderson and Kang-Jen Liu, J. Chem. Phys., 45, 4744 (1966).
603. W. A. Anderson, US Patent No. 3173083 (Feb. 23, 1962) and 3173084 (April 30, 1962).
604. A. N. Lyubimov, A. F. Varenik, and A. V. Kessenikh, Zh. strukt. khimii, 7, 694 (1966).
605. Nuclear Magnetic Resonance Specialities Co., Inc., Box 145, Greensbury Road, New Kensington, Pennsylvania, USA.
606. Space Avionics, Inc., Alexandria, Virginia, USA.
607. É. Lippmaa, I. Pekhk, and Ya. Past, Izv. AN EstSSR, fiz.-mat. ser., 16, 339 (1967).
608. É. Lippmaa, M. Alla, and A. Syugis, Izv. AN EstSSR, 16, 355 (1967).
609. Yu. Yu. Samitov and T. V. Zykova, Trudy KKhTI im. S. M. Kirova, 33, 9 (1964).
610. V. F. Bystrov and A. U. Stepanyants, J. Molec. Spectr., 21, 241 (1966).
611. G. W. Flynn and J. D. Baldeschwieler, J. Chem. Phys., 38, 226 (1963).
612. W. McFarlane, Chem. Comm., 58 (1967).
613. J. C. Calder, P. J. Garratt, and F. Sondheimer, Chem. Comm., 41 (1967).
614. M. C. Woods, I. Miura, Y. Nakadaira, A. Terahara, M. Maruyama, and K. Nakanishi, Tetrahedron Letters 321 (1967).
615. M. Maruyama, A. Terahara, K. Nakanishi, M. C. Woods, Y. Takagi, and Y. Nakadaira, Tetrahedron Letters, 315 (1967).
616. W. Döpke, M. Bienert, A. L. Burlingame, H. K. Schones, P. W. Jeffs, and D.S. Farrier, Tetrahedron Letters, 451 (1967).
617. A. J. Birch, C. J. Dahl, and A. Pelter, Tetrahedron Letters, 481 (1967).
618. R. J. Kern and J. Schaefer, J. Amer. Chem. Soc., 89, 150 (1967).
619. M. Jones and L. T. Scott, J. Amer. Chem. Soc., 89, 150 (1967).
620. K. V. Vladimirskii, Zh. eksperim. i teor. fiziki, 33, 529 (1957).

621. R. Karplus, Phys. Rev., 73, 1027 (1948).
622. H. Primas, Helv, Phys. Acta, 31, 17 (1958).
623. K. S. Dhami and J. B. Stothers, Canad. J. Chem., 43, 479 (1965).
624. J. K. Becconsall and P. Hampson, Mol. Phys., 10, 21 (1965).
625. R. Waack, M. A. Doran, E. B. Baker, and G. A. Olah, J. Amer. Chem. Soc., 88, 1772 (1966).
626. G. W. Buchanan, D. A. Ross, and J. B. Stothers, J. Amer. Chem. Soc., 88, 4301 (1966).
627. S. Rodmar, B. Rodmar, and Ashfaq Ali Khan, Acta Chem. Scand., 20, 2515 (1966).
628. S. Forsen, Per J. Garegg, B. Lindberg, and E. Pettersson, Acta Chem. Scand., 20, 2763 (1966).
629. Ashfaq Ali Khan, S. Rodmar, and R. A. Hoffman, Acta Chem. Scand., 21, 63 (1967).